

**Ru-mediated ring-opening metathesis polymerization for the synthesis of
complex polymer architectures**

Samantha Jillian Scannelli

Dissertation submitted to the faculty of the Virginia Polytechnic Institute and State University in
partial fulfillment of the requirements for the degree of

Doctor of Philosophy
In
Chemistry

John B. Matson Chair
Richard D. Gandour
Michael D. Schulz
Diego Troya

May 9th, 2023
Blacksburg, VA

Keywords: Livingness, Catalyst, Propagation, Termination, Rate, Monomer, Macromonomer

Copyright 2023, Samantha J. Scannelli

Ru-mediated ring-opening metathesis polymerization for the synthesis of complex polymer architectures

Samantha J. Scannelli

ABSTRACT

Ring-opening metathesis polymerization (ROMP) has gained attention over the last few decades for its versatility and robustness. Through the use of highly active metal catalysts, such as Grubbs' first-generation catalyst [G1, (PCy₃)₂(Cl)₂RuCHPh] and Grubbs' third-generation catalyst [G3, (H₂IMes)(Cl)₂(pyr)₂RuCHPh], ROMP can exhibit living characteristics for some monomer classes, most commonly substituted norbornenes. The high livingness of ROMP makes it well-suited for the synthesis of complex polymer architectures (e.g., bottlebrush polymers, star polymers, and (multi)block copolymers, among others). However, compared to other living polymerizations, quantitative studies on the kinetic factors affecting living characteristics in ROMP are lacking.

This work describes the effects of several reaction factors on the livingness in Ru-mediated ROMP of norbornene-based monomers. We performed thorough studies on the effects of the anchor group, the series of atoms directly attached to the norbornene, in the synthesis of both linear and bottlebrush polymers. Using small molecule norbornene monomers, we studied monomer HOMO energy, rate of propagation (k_p), catalyst decomposition [a proxy for the termination rate constant (k_t)], and livingness in ROMP as measured by the k_p/k_t ratio. HOMO energies were used to predict the reactivity of various monomers based on the hypothesis that high HOMO energy would lead to high monomer reactivity and high k_p values. We observed a positive correlation between the HOMO energy and k_p with both G1 and G3 catalysts, but we

observed a plateau in k_p for monomers with the highest HOMO energy when polymerized with G3 catalyst. These results suggested that above a certain level, HOMO energy no longer influenced the rate-determining step. Additionally, the anchor group had no apparent effect on catalyst decomposition with either catalyst. Therefore, when examining the livingness in ROMP of linear polymers, differences in the k_p/k_t ratios were primarily controlled by the k_p value.

When studying the synthesis of bottlebrush polymers, we found a similar positive correlation between HOMO energy and k_p for five macromonomer (MM) species. To evaluate livingness of MMs, we targeted various backbone degrees of polymerization (N_{bb}), 100–2000, and found that MMs with high $k_{p,obs}$ values reached higher conversion with lower dispersities (\mathcal{D}) at high target N_{bb} values than MMs with low $k_{p,obs}$ values. Finally, we investigated the synthesis of bottlebrush pseudo-pentablock copolymers using MMs with the highest and lowest k_p anchor groups. This study revealed higher MM conversion and lower \mathcal{D} values for each block for the MM with the highest k_p anchor group, compared to the lowest k_p MM.

Furthering the anchor group study, we synthesized a small molecule monomer and two macromonomers containing a norbornene–benzoladderene structure. We found this anchor group had a higher HOMO energy than all other (macro)monomers previously studied. However, k_p was not higher for the small molecule monomer compared to the other monomers studied, supporting the plateau in rate observed for monomers above a certain HOMO energy. The higher HOMO energy for MMs did increase k_p for one of the MM compared to other MMs previously studied, however the MM with side-chains in the *ortho* position on the anchor group had a lower k_p than expected. This low k_p was attributed to the side-chains being in closer proximity to the reactive chain end, compared to the MM with side-chains in the *meta* position, hindering addition of new MM units. Altogether, these experiments revealed how the anchor group impacts

k_p and livingness in ROMP, two factors that are essential for the synthesis of precise bottlebrush (co)polymers.

The final chapter of this dissertation evaluates the effect of reaction atmosphere on livingness in Ru-mediated ROMP. Here we envisioned that changing the atmosphere, from under air to on a Schlenk line under N_2 to in an N_2 -filled glovebox, would reduce the rate of chain termination and improve livingness in ROMP of small molecule and macromonomers. We synthesized linear or bottlebrush pseudo-pentablock copolymers to evaluate the livingness of foud (macro)monomer structures in three different atmospheres. We found better agreement between $M_{n,expected}$ and $M_{n,obs}$ as well as lower overall and apparent D values for the bottlebrush polymers polymerized in N_2 atmospheres. Interestingly, the effect was more prominent for low k_p (macro)monomers; in other words, ROMP reactions of (macro)monomers with high k_p values were successful under air, but for those with low k_p values, a glovebox was required to observe good control.

Ru-mediated ring-opening metathesis polymerization for the synthesis of complex polymer architectures

Samantha J. Scannelli

GENERAL AUDIENCE ABSTRACT

Ring-opening metathesis polymerization (ROMP) is a powerful chemical method used to make a wide variety of polymers. With use of ruthenium-based catalysts, ROMP can exhibit living characteristics for some monomer classes, making it well-suited for the synthesis of precise linear and bottlebrush polymers. However, compared to other living polymerizations, quantitative studies on the kinetic factors affecting living characteristics in ROMP are lacking.

This work describes the effects of several reaction factors on the livingness in ROMP of norbornene-based monomers. We thoroughly studied the effects of the anchor group, the series of atoms directly attached to the norbornene, in the synthesis of both linear and bottlebrush polymers. Using small molecule norbornene monomers, we studied the monomer HOMO energy, rate of propagation (k_p), catalyst decomposition, and the livingness in ROMP. We used HOMO energy to predict the reactivity of various monomers and found that high HOMO energy led to high k_p values. Additionally, the anchor group had no apparent effect on catalyst decomposition; however, the large variations in k_p meant that the anchor group influenced livingness in ROMP.

When studying the synthesis of bottlebrush polymers, we found a similar positive correlation between HOMO energy and k_p for five macromonomer (MM) species. Attaching a polymer side-chain to the norbornene decreases k_p significantly, therefore our goal was to evaluate the livingness in ROMP under conditions that experience lower k_p than linear polymers.

We targeted large bottlebrush polymers, backbone degree of polymerization (N_{bb}) up to 2000, The final portion of this dissertation evaluates the effect of reaction atmosphere on the livingness in Ru-mediated ROMP. A large factor of livingness is k_t , which in ROMP is typically decomposition of the catalyst chain end evidenced by low molecular weight tails in size exclusion chromatography traces. Here we envisioned changing the atmosphere, from air to inert, would prevent chain termination and improve the livingness in ROMP. We again used the synthesis of linear and bottlebrush pentablock copolymers to evaluate the livingness of six (macro)monomer structures in three different reaction atmospheres, air, N_2 , and in a glove box. Polymerizations under N_2 or in the glove box produced more well-defined polymers than polymerizations in air by a marginal degree. Therefore, the livingness in ROMP improves when air is removed.

Dedication

This dissertation is dedicated to my parents, Lori Ann and Jack Scannelli. I would not be where I am today without your overwhelming love and support.

Acknowledgments

First, I would like to thank my advisor Prof. John Matson. Joining the lab in 2016 as an undergraduate researcher was one of the best decisions I made. I truly fell in love with research through your excitement and engagement with your students and I am lucky to have continued my Ph.D. career under your guidance. My growth as a scientist is largely due to the immense knowledge and wisdom you have shared over the years, and I appreciate all I have learned from you. I would also like to thank my committee members Prof. Diego Troya, Prof. Richard Gandour, and Prof. Michael Schulz. Your constant curiosity and advice were greatly appreciated and improved my work immensely. Specifically, I'd like to thank Prof. Diego Troya for his generous collaboration. I believe his guidance has made me a more well-rounded scientist.

I especially want to thank my family for the overwhelming support throughout my graduate career. To my parents, I wouldn't be where I am today without your encouragement. I want to thank my mom for knowing exactly what I needed during the ups and downs of graduate school. To my dad, thank you for constantly motivating me to better myself. Your excitement throughout my schooling kept me going and I am forever grateful. I also want to thank my sisters, Lauren and Juliana, for your constant banter and laughter. Both of you make me a better person and I am incredibly thankful for your patience and guidance over the years. Also thank you again to Lauren and my new brother-in-law Jimmy for both being so understanding of the challenges of graduate school over the years. Thank you for always being there for me when I need you to be and encouraging me to keep going. To my Grandma, thank you for always being so proud of me. I cannot thank my family enough for their constant reassurance and love.

Over the years I have met so many amazing scientists and I am thankful for all of the help my mentors and peers have provided. I'd like to first thank Dr. Jeffrey Foster and Dr. Scott

Radzinski for being great undergraduate research mentors. Shockingly, working alongside you both encouraged me to pursue my Ph.D. and I am forever grateful. Thanks to Dr. Chadwick Powell for your guidance early in my graduate school time, I never would have learned proper distillation techniques without your help. I also want to thank Dr. Mohammed Alaboalirat for the immense collaboration and discussion as one of my longest coworkers. To Dr. Kearsley Dillon, thank you for your amazing friendship both in and out of the lab. I consider you one of my best friends and am so lucky to have made so many memories with you. Thank you to Jackie Zhu for our countless hours of Taylor Swift conversations. You are such an amazing and caring friend, and I am 'the luck one' for sharing this journey with you. To Dr. Ryan Carrazzone, thank you for believing in me. Your passion for science inspires me and I cannot thank you enough for your unwavering support. You truly bring out the best in me. I also want to thank the rest of the Matson lab, there are so many of you who have helped me over the years in so many ways and I am very grateful.

I also want to acknowledge fellow graduate students outside of the Matson Lab. To Dr. Mark Paradzinsky, thank you for being so willing to disconnect from science and help me decompress from all the challenges that come with graduate school. You are one of the best listeners I have ever met and talking with you was always so rewarding. To Dr. Christina Orsino, thank you for your friendship and all of the amazing memories over the years. More importantly, thank you for sharing the most perfect cat with me. To Michelle Pomatto, thank you for all of your advice and encouragement over the years and I look forward to seeing where your graduate journey takes you. To Dr. Ryan Archer and Benjamin Stovall, thank you both for working through the program with me. Your guidance was greatly appreciated, even if at times it felt like

the blind leading the blind. You both were great support systems, and I am thankful for our time together at Virginia Tech.

Lastly, I want to thank some of my lifelong friends who were always there for me when I needed them. To my earliest childhood friend Janine Riccardi, thank you for always pushing me to better myself. It is amazing to look back at our days in chemistry together in high school and see how far we both have come. To Alyssa Cohn, thank you for being so supportive through my schooling and for all of your curiosity. I am so appreciative of your interest in my research and I look forward to sharing this final dissertation with you. I also need to acknowledge my closest group of friends, my OG Hokies. Thank you all for being so incredibly understanding about my schooling. I wouldn't be the person I am today without each and every one of your friendships. Your unwavering support means so much to me and I am so excited for our long-awaited celebrations. Specifically thank you to Nicole and Reilly Giunta. The love and encouragement you've shown over the years means the world to me; I cannot thank you both enough.

Table of Contents

Dedication	vii
Acknowledgments.....	viii
Attributions	xiv
Chapter 1: Overview of grafting-through ring-opening metathesis polymerization for the synthesis of bottlebrush polymers.....	1
1.1 Authors	1
1.2 Introduction	1
1.3 Catalysts	4
1.4 Grafting-through method.....	7
1.4.1 Purity considerations	11
1.5 Bottlebrush (multi)block copolymers.....	13
1.5.1 Diblock and triblock bottlebrush copolymers	13
1.5.2 Engineered bottlebrush polymer structures	17
1.6 Reaction conditions	19
1.6.1 Temperature.....	20
1.6.2 Solvent.....	22
1.7 (Macro)monomer structure	24
1.7.1 Norbornene stereochemistry and anchor group.....	25
1.7.2 Side-chain composition and molecular weight.....	27
1.8 Conclusions	29
1.9 References	30
Chapter 2: The influence of the norbornene anchor group in Ru-mediated ring-opening metathesis polymerization: Synthesis of linear polymers.....	41
2.1 Authors	41
2.2 Abstract	41
2.3 Introduction	42
2.4 Results and Discussion.....	46
2.4.1 HOMO energy calculations.....	46
2.4.2 ¹ H NMR kinetic analysis	48
2.4.3 Chelation effect	54

2.4.4 Catalyst decomposition and livingness in ROMP	58
2.5 Conclusions	62
2.6 Acknowledgments	63
2.7 References	64
2.8 Supporting Information	69
2.9 Supporting Information References	190
Chapter 3: The influence of the norbornene anchor group in Ru-mediated ring-opening metathesis polymerization: Synthesis of bottlebrush polymers.....	193
3.1 Authors	193
3.2 Abstract	193
3.3 Introduction	194
3.4 Results and Discussion.....	198
3.4.1 HOMO energy calculations.....	199
3.4.2 Macromonomer Synthesis and Analysis	200
3.4.3 Effects of the anchor group on livingness in high target N_{bb} bottlebrush polymers	206
3.4.4 Effects of the anchor group on livingness in bottlebrush pentablock copolymer synthesis	210
3.5 Conclusions	216
3.6 Acknowledgments	217
3.7 References	218
3.8 Supporting Information	226
3.9 Supporting Information References	273
Chapter 4: Ring-opening metathesis polymerization of norbornene–benzoladderene (macro)monomers	276
4.1 Authors	276
4.2 Abstract	276
4.3 Introduction	277
4.4 Results and Discussion.....	279
4.5 Conclusions	292
4.6 Acknowledgments.....	293
4.7 References	293
4.8 Supporting Information	300

4.9 Supporting Information References	316
Chapter 5: Effects of reaction atmosphere on Ru-mediated ring-opening metathesis polymerization	317
5.1 Authors	317
5.2 Abstract	317
5.3 Introduction	318
5.4 Results and Discussion.....	320
5.4.1 Atmosphere choice	320
5.4.2 (Macro)monomer design and synthesis.....	321
5.4.3 Kinetic analysis of ROMP.....	323
5.4.4 Pentablock copolymer synthesis and analysis.....	327
5.5 Conclusions	340
5.6 Acknowledgments	342
5.7 References	342
5.8 Supporting Information	345
5.9 Supporting Information References	357
Chapter 6: Conclusions and Future Outlooks	359
Appendix A: Solution self-assembly of 30-mer homopolymers	366
Appendix B: Synthesis and polymerization of peptide and sugar monomers	369

Attributions

This work was completed with the help of several colleagues. A brief description of contributions from each person is included below:

Chapter 1: Samantha J. Scannelli (graduate student, Department of Chemistry, Virginia Tech) provided authorship and editing of this chapter. John B. Matson (Ph.D. Department of Chemistry, Virginia Tech) is the advisor and committee chair and provided writing and editing for this chapter.

Chapter 2: Samantha J. Scannelli (graduate student, Department of Chemistry, Virginia Tech) performed the calculations, synthesis, and experimental work as well as provided authorship and editing of this chapter. Anshul Paripati (undergraduate student, Department of Chemistry, Virginia Tech) assisted with polymerizations and analysis of kinetic data for this chapter. Jeffrey R. Weaver (graduate student, Department of Chemistry, Virginia Tech) provided synthetic guidance for this chapter. Mohammed Alaboalirat (Ph.D., Macromolecules Innovation Institute, Virginia Tech) provided synthetic guidance for this chapter. Diego Troya (Ph.D., Department of Chemistry, Virginia Tech) provided guidance on the HOMO energy calculations as well as performed density functional theory calculations for this chapter. John B. Matson (Ph.D. Department of Chemistry, Virginia Tech) is the advisor and committee chair and provided writing and editing for this chapter.

Chapter 3: Samantha J. Scannelli (graduate student, Department of Chemistry, Virginia Tech) performed the calculations, synthesis, and experimental work as well as provided authorship and

editing of this chapter. Mohammed Alaboalirat (Ph.D., Macromolecules Innovation Institute, Virginia Tech) performed the synthesis of all macromonomers for this chapter. Diego Troya (Ph.D., Department of Chemistry, Virginia Tech) provided guidance on the HOMO energy calculations as well as performed density functional theory calculations for this chapter. John B. Matson (Ph.D. Department of Chemistry, Virginia Tech) is the advisor and committee chair and provided writing and editing for this chapter.

Chapter 4: Samantha J. Scannelli (graduate student, Department of Chemistry, Virginia Tech) performed the synthesis and experimental work as well as provided authorship and editing of this chapter. Mohammed Alaboalirat (Ph.D., Macromolecules Innovation Institute, Virginia Tech) contributed the synthesis of macromonomers for this chapter. Diego Troya (Ph.D., Department of Chemistry, Virginia Tech) provided guidance on the HOMO energy calculations as well as performed density functional theory calculations for this chapter. John B. Matson (Ph.D. Department of Chemistry, Virginia Tech) is the advisor and committee chair and provided writing and editing for this chapter.

Chapter 5: Samantha J. Scannelli (graduate student, Department of Chemistry, Virginia Tech) performed the synthesis and experimental work as well as provided authorship and editing of this chapter. Daniela Samaniego Gonzalez (graduate student, Department of Chemistry, Virginia Tech) performed polymerizations open to air for this chapter. Clark Vu (graduate student, Macromolecules Innovation Institute, Virginia Tech) contributed the synthesis of macromonomers for this chapter. John B. Matson (Ph.D. Department of Chemistry, Virginia Tech) is the advisor and committee chair and provided writing and editing for this chapter.

Chapter 1. Overview of grafting-through ring-opening metathesis polymerization for the synthesis of bottlebrush polymers

Parts of this chapter were adapted from (Blosch, S. E.; Scannelli, S. J.; Alaboalirat, M.; Matson, J. B., Complex Polymer Architectures Using Ring-opening Metathesis Polymerization: Synthesis, Applications, and Practical Considerations. *Macromolecules* **2022**) with permission. Copyright 2022 American Chemical Society

1.1 Authors

Samantha J. Scannelli and John B. Matson

¹Department of Chemistry, Virginia Tech, Blacksburg, Virginia 24061, United States

1.2 Introduction

Bottlebrush polymers, also termed molecular brushes, are graft polymers with densely grafted side-chains attached to a linear polymer backbone.¹⁻³ Many polymerization techniques are suitable for the synthesis of bottlebrush polymer backbones, side-chains, or both. Specifically, polymerizations exhibiting living characteristics (i.e., “livingness”) are preferred due to their ability to construct well-defined polymers. Living polymerizations lack chain termination and chain transfer, as well as exhibit linear growth in molecular weight with conversion. Another characteristic of living polymerizations is they typically have a constant number of kinetic chain carriers throughout the polymerization because initiation rates (k_i) tend to be higher than propagation rates (k_p). Altogether, these characteristics provide control over

molecular weight and dispersity allowing for the synthesis of well-defined polymers, specifically useful for generating precise bottlebrush polymers.

Historically, anionic polymerization was preferred because it was the only polymerization that truly lacked chain termination.⁴ However, many polymerizations exhibiting living characteristics have been used, most commonly are the reversible deactivation radical polymerization (RDRP) techniques such as atom transfer radical polymerization (ATRP) and reversible addition fragmentation chain transfer (RAFT) polymerization. More recently, ring-opening metathesis polymerization (ROMP) has gained popularity in bottlebrush polymer synthesis due to its relative insensitivity to air and water and high functional group tolerance. Overall, the general goal is to synthesize bottlebrush polymers with tunable chemical composition, controllable and high grafting density (z), and tunable side-chain and backbone degrees of polymerization (N_{sc} and N_{bb} , respectively), in which ROMP is well-suited.

In many cases, more than one type of polymerization technique is used in the multi-step synthesis of bottlebrush polymers. There exist four general strategies to synthesize bottlebrush polymers, grafting-to, grafting-from, transfer-to, and grafting-through, which differ in how the side-chains are connected to the backbone chain.⁵ Grafting-to requires separate polymerization reactions to generate the backbone and the side-chains, followed by efficient reactions to attach the side-chains to the backbone. The grafting-from method requires the polymerization of a monomer with a pendant functional group to make the backbone chain. Next, initiation sites are attached to the backbone (if they were not already pre-installed on the monomer), which are then used in a subsequent polymerization step to initiate the synthesis of the side-chains. The transfer-to strategy is a hybrid of grafting-to and grafting-from that is less widely used. It involves the synthesis of a polymer backbone with a pendant chain transfer agent attached via the Z-group in

the case of RAFT. The side-chains are synthesized in a process where propagation occurs free in solution, and the growing side-chains return to the backbone via a chain transfer reaction.⁶ Lastly, the grafting-through method involves the synthesis of a monotelechelic polymer with a polymerizable group on one chain end, called a macromonomer (MM). Polymerization of the MM end-groups creates the bottlebrush polymer backbone in a second step. While all four methods have advantages and disadvantages and various potential side products, grafting-through holds the potential for the greatest level of control over grafting density, side-chain degree of polymerization (N_{sc}), and backbone degree of polymerization (N_{bb}). Although ROMP can be used in all four methods, it is most commonly applied in the grafting-through of MMs, with early reports from Bowden in 2004,⁷ and later Grubbs in 2009,⁸ highlighting the capability of ROMP grafting-through to make long cylindrical bottlebrush polymers. ROMP has advantages in the polymerization of MMs over the RDRP methods, which can be hampered by low equilibrium monomer concentrations under standard conditions, even using low molecular weight MMs.⁹

Although reports of interesting polymer materials made by ROMP exist, limitations remain. For example, ROMP of even moderate molecular weight MMs ($N_{sc} \sim 50$) can be challenging, as can even relatively low target N_{bb} values ($N_{bb} \sim 100$), where broadening of SEC traces compared to smaller bottlebrush polymers is regularly observed. This difficulty is amplified in bottlebrush multiblock copolymer synthesis and the construction of non-centrosymmetric structures such as tapered bottlebrush polymers. Altogether, the synthesis of complex polymer topologies while controlling parameters including N_{sc} , N_{bb} , and grafting density requires highly tuned polymerizations. Here we discuss the ROMP grafting-through

method to synthesize bottlebrush polymers and some of the elements of the ROMP reaction conditions that influence the outcome of the polymerization (Figure 1.1).

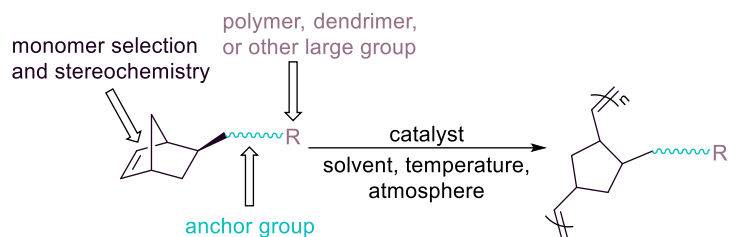


Figure 1.1. Schematic representation of the factors that influence the rate of ROMP.

1.3 Catalysts

ROMP is a polymerization method that is typically driven by the relief of ring strain in cyclic olefin monomers¹⁰ or in some cases by entropy for very large, unstrained cyclic olefins.¹¹ The most common ROMP catalysts are the Ru complexes developed by Grubbs (Figure 1.2A–D) and the primarily Mo-based catalysts introduced by Schrock (Figure 1.2E). All of these catalysts are transition metal complexes that contain a carbon-metal double bond. We note that these transition metal (pre)catalysts may be more accurately referred to as ROMP initiators in many contexts, but we use the more common term catalyst throughout for sake of ease, clarity, and in an attempt to reduce potential confusion. The main practical distinction between these two main classes of catalysts is that the Mo catalysts are somewhat more active, but they are limited by air and moisture sensitivity and react with some common functional groups. In contrast, the Grubbs' catalysts are generally bench stable and tolerate air and water. Additionally, these Ru catalysts have specificity for the C=C bond, which allows for polymerization of monomers with pendant functional groups that often cannot be polymerized by other methods (i.e., those that are sensitive to radicals or anions).

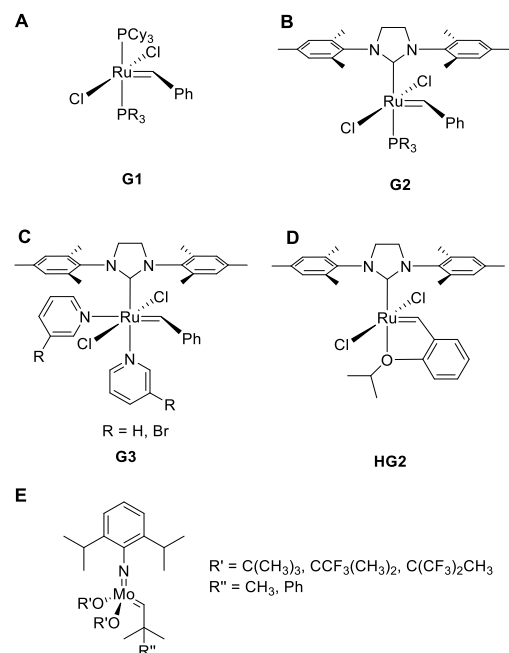


Figure 1.2. Commonly used catalysts for ROMP A) Grubbs' 1st generation (G1), B) Grubbs' 2nd generation (G2), C) Grubbs' 3rd generation (G3), D) Hoveyda–Grubbs' 2nd generation (HG2), and E) Schrock Mo-based catalysts.

Due to this high functional group tolerance and ease of handling, the Grubbs' catalysts are used widely in ROMP. Of these, Grubbs' 3rd generation catalyst [G3, (H₂IMes)(Cl)₂(pyr)₂RuCHPh] is most commonly used in the synthesis of complex polymer architectures by ROMP due to its fast initiation and propagation kinetics.¹² G3 is the catalyst used in many of the examples discussed here. Either unsubstituted pyridine ligands can be used, or they can be substituted at the 3-position with a halogen, usually Br. Here we do not distinguish between unsubstituted and halogen-substituted versions of G3, referring to both types simply as G3. The G3 catalyst can be easily prepared from commercially available Grubbs 2nd generation catalyst [G2, (H₂IMes)(Cl)₂(PCy₃)RuCHPh] by treatment with pyridine or a substituted pyridine.^{13–14} G2 is itself not typically used in ROMP when living characteristics are needed due to its slow initiation compared to propagation rate; Hoveyda–Grubbs G2 catalyst [HG2, (H₂IMes)(Cl)₂(*o*-OiPrC₆H₄)RuCHPh] exhibits similarly slow initiation.¹⁵ Grubbs 1st

generation catalyst [G1, (PCy₃)₂(Cl)₂RuCHPh] is also used to some extent to make complex polymer architectures by ROMP because it also exhibits fast initiation related to propagation, enabling living characteristics. However, G1 propagates a few orders of magnitude slower than G2/G3 catalysts.¹⁶

Beyond catalysts capable of mediating ROMP with living characteristics, there exist ROMP catalysts capable of controlling *cis/trans* stereochemistry in the resulting polymer. Some catalysts can also control tacticity in ROMP. Many of these catalysts are based on Mo or W transition metals, although some Ru-based catalysts with control over polymer microstructure have been developed. These topics were recently reviewed by Buchmeiser.¹⁷ In figures here we do not intend to imply control over backbone olefin stereochemistry.

The efficiency of ROMP relies heavily on the particular catalyst; therefore, extensive research has been done on the various catalysts as well as the invention of new catalysts to fit more specific reaction conditions. Rates of initiation and propagation dramatically influence the precision of the final polymers. The most commonly used catalysts for ROMP are the Ru-based Grubbs' catalysts. Of these, G3 catalyst (either with pyridine or bromopyridine ligands) is the most widely used catalyst, especially for norbornene species, as it has the fastest initiation and propagation rates of the common Grubbs' catalysts.^{12, 15, 18} However, G3 catalyst is less stable in solution than other ROMP catalysts and may not be the best option for polymerizations requiring reaction times of more than a few hours. G1 catalyst propagates slower than G3 catalyst by a factor of 10–100, but it also initiates quickly and lives longer in solution than G3 catalyst, making G1 catalyst still a widely used catalyst for ROMP. Unlike G1 catalyst and G3 catalyst, G2 catalyst and common variations of the G2 catalyst (e.g. HG2) rarely work well for polymerizations where living characteristics are needed, including molecular weight control and

the capacity for chain extension, because the rate of initiation is slower than the rate of propagation.¹⁹ In fact, in extreme scenarios where initiation is very slow compared with propagation, i.e., in latent catalysts at certain temperatures,²⁰ the monomer/initiator ratio plays no role in controlling molecular weight. In some cases, however, G2 catalyst can be effective for ROMP with living characteristics when monomers or MMs propagate slowly enough that control over the polymerization is maintained. In addition to the widely used Ru catalysts, Mo-based Schrock catalysts are also used in some cases due to their high activity and tacticity control,²¹ although care must be taken to avoid oxygen, water, and certain functional groups.²² Additional catalysts have been synthesized for use in more niche conditions of ROMP (e.g., aqueous ROMP), generally stemming from already published catalyst structures.

1.4 Grafting-through method

ROMP grafting-through involves the polymerization of MMs, which are made using controlled or living polymerization techniques. MMs used in ROMP grafting-through most often contain a norbornene functional group due to its high ring strain and fast polymerization by ROMP. Here we discuss norbornene-based MMs for the sake of simplicity, but other strained cyclic olefins have been used as well. The release of ring strain in the norbornene unit provides the driving force for the polymerization, and fast initiation rates and even faster propagation rates in ROMP can afford bottlebrush polymers in minutes.¹² The norbornene groups can be present during side-chain synthesis or added in a post-polymerization modification reaction, and these approaches are referred to as direct-growth and growth-then-coupling, respectively (Figure 1.3).²³

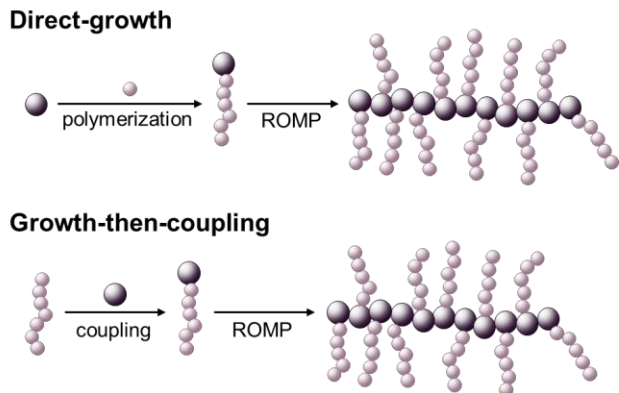


Figure 1.3. Schematic representation of bottlebrush polymer synthesis via the direct-growth and growth-then-coupling strategies.

Direct-growth is most commonly used in making bottlebrush polymers due to the more straightforward synthetic approach. This method relies on the use of a norbornene functionalized with an initiator or chain transfer agent for use in a different polymerization technique, often ring-opening polymerization (ROP) or an RDRP technique. Polymerization is carried out from this norbornene-functionalized unit to generate an MM, and then ROMP is used in the second step to form the backbone without any modification. The MM is typically isolated before the ROMP reaction, but one-pot syntheses using the direct-growth method are possible, as detailed below. Bowden and coworkers were the first to synthesize bottlebrush polymers using ROMP in the direct-growth method, achieving narrowly dispersed polymers with molecular weights exceeding 60,000 kg/mol.^{7, 24} Since then, others have successfully achieved large degrees of polymerization of the backbone using this method, although such enormous molecular weights remain difficult to access for most MMs.

RDRPs are typically used to make MMs to ensure low dispersities and the high chain end fidelity necessary for the subsequent ROMP step. Various dual-functionalized small molecules

have been made that carry a norbornene (or similar) unit and an initiator or chain-transfer agent (CTA) for the RDRP step. The RDRP techniques most commonly used to make MMs are ATRP²⁵ and RAFT.²⁶ With these techniques, MMs of polystyrene (PS), poly(methyl methacrylate) (PMMA), poly(methyl acrylate) (PMA),²⁷ poly(*tert*-butyl acrylate) (PtBA),²⁸ and poly(*N*-Isopropylacrylamide)²⁹ have been made and used to synthesize bottlebrush polymers via ROMP. In one of the first reports on this topic in 2006, Patton and Advincula showed that the direct-growth method enabled the synthesis of well-defined PS and PMMA MMs using a combination of RAFT and ROMP, with efficient ROMP to generate small bottlebrush polymers ($N_{bb} = 8$).²⁷

One important consideration in the synthesis of bottlebrush polymers by the direct-growth approach is the potential for copolymerization of the norbornene unit in the RDRP reaction. For example, some studies have shown bimodal MW distributions for the resulting bottlebrush polymers, specifically those where polyacrylates were prepared in the RDRP step.^{25, 27, 30} Xia and Grubbs noticed this problem in 2009 in the synthesis of MMs using both ATRP and RAFT of acrylates, suggesting that the norbornene can interfere with the initial polymerization of the side-chain.⁸ Keddie and coworkers recently reported a systematic study on this problem and suggest some methods to limit it, such as running RDRP reactions to low monomer conversion.³⁰ However, to avoid this problem entirely, the growth-then-coupling method can be used.

Initially used as early as 1994 by Feast and coworkers with Mo-based catalysts³¹ and later coined by Xia in 2015,²³ the growth-then-coupling method involves the synthesis of the side-chains followed by a chain end modification reaction to install the norbornene unit (Figure 1.4). Although the growth-then-coupling approach lengthens the synthesis with the addition of intermediate reactions and purification steps, it removes any interference of the side-chain

polymerization with the norbornene unit, allowing for the synthesis of well-defined bottlebrush polymers.⁸ This synthetic strategy can accommodate a broader scope of monomers and polymerization techniques than the direct-growth strategy but is limited by the intermediate modification step.

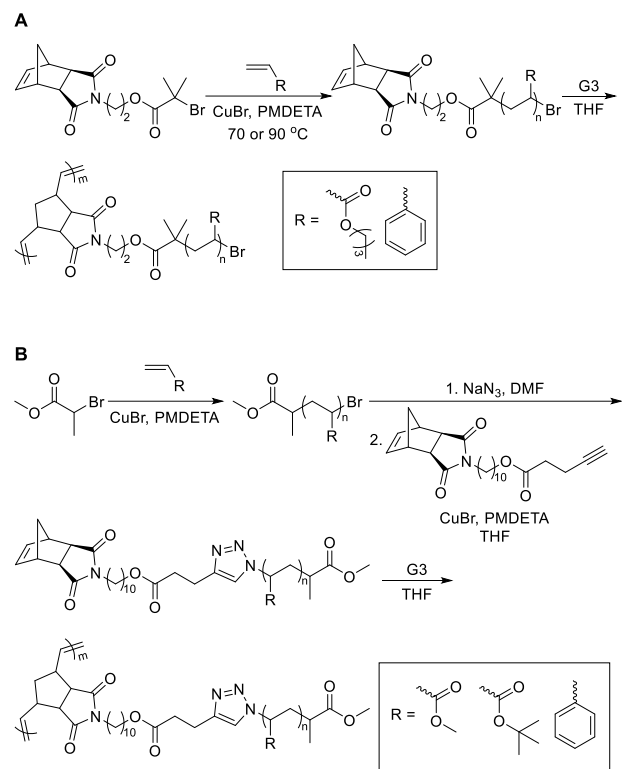


Figure 1.4. Synthesis of various MMs via the A) direct-growth and B) growth-then-coupling approaches. Adapted with permission from references^{8, 23}.

In order for the growth-then-coupling strategy to be successful, highly efficient intermediate reactions need to be used to ensure full functionalization of the side-chains, which typically include “click” reactions²³ or carbodiimide couplings.³² Anionic polymerization, RAFT, ATRP, and ROP have been used to polymerize well-defined side-chains of PMA, PtBA, PS,⁸ PMMA,²³ polycaprolactone, and poly(ethylene oxide) (PEO)³² with one end group capable of further reaction. A high-yielding coupling reaction, potentially followed by purification,

enables the synthesis of the MM. If done correctly, the growth-then-coupling strategy ensures bottlebrush polymer formation via grafting-through without branching. However, care must be taken to confirm that MMs are fully functionalized with a norbornene or similar unit; MMs lacking a polymerizable unit are simply side-chains that do not attach to the backbone in the grafting-through step. Ultimately, assuming high purity MMs in both cases, when comparing identical MMs made by the direct-growth and growth-then-coupling approaches, those made by growth-then-coupling achieve bottlebrush polymers of higher molecular weight and lower dispersity than those made by direct-growth.⁹

1.4.1 Purity Considerations

As alluded to above, an important factor to consider when performing the grafting-through method is the intermediate purification of the MM, which tends to be extensive. For direct-growth, these purifications generally include multiple precipitation steps to remove residual monomer, requiring large amounts of solvent and are tedious for polymers with low glass transition temperatures (T_g 's). If vinyl monomers are used to make the MM, exhaustive removal is usually required because even very small amounts of residual monomers such as acrylates can act as chain transfer agents or terminators in ROMP, especially when targeting large N_{bb} values or when making bottlebrush polymers using the grafting-through process.³³ In addition to precipitation steps and residual monomer removal, growth-then-coupling also requires purification after the post-polymerization modification reaction to attach the norbornene. Removal of residual impurities from previous reactions is crucial in order to achieve bottlebrush polymers of high MW and low dispersity. Even after exhaustive removal of any vinyl monomer, small amounts of other impurities (e.g., alkynes) can be detrimental in the

ROMP step due to the small amount of catalyst needed in comparison to the MM. Bang and coworkers investigated how residual impurities in MMs made via “click” reactions through the growth-then-coupling method affected ROMP.³⁴ They observed higher conversion and lower dispersities for MMs that were rigorously purified compared to MMs with residual impurities, confirming the importance of purity to produce well-defined bottlebrush polymers.

Although impurities can be detrimental to the ROMP step of the grafting-through method, several groups have avoided this problem in developing one-pot syntheses of bottlebrush polymers. One-pot processes simplify the synthesis of bottlebrush polymers by removing intermediate purification steps, although they are limited in scope. The first attempt at a one-pot bottlebrush polymer synthesis by ROMP grafting-through was in 2009 by Cheng and coworkers,³⁵ but was reported as uncontrolled with large dispersities compared to a similar grafting-from one-pot method. A successful attempt at a one-pot synthesis was performed in 2012 by Wooley and coworkers by RAFT to make a PMMA MM followed by ROMP with an intermediate cooling step to quench the RAFT reaction (Figure 1.5).³⁶ This synthesis was successful despite residual vinyl monomer because MMA does not react with Grubbs’ catalysts,³⁷ but most other vinyl monomers are metathesis active and therefore cannot be easily used in one-pot syntheses. To broaden the scope of monomers available for a one-step procedure, our group used ROP to make MMs of poly(lactic acid) (PLA) followed by ROMP. The choice of a 1,8-diazabicyclo[5.4.0]undec-7-ene (DBU) cocatalyst system for the ROP step based on its ability to maintain high end group fidelity enabled a high degree of control over the ROP, creating MMs of low dispersity and only required the addition of trifluoroacetic acid to terminate the ROP step before moving forward with the ROMP step.³⁸ Klapper and coworkers recently extended this ROP/ROMP concept to make bottlebrush polymers using a simultaneous

polymerization approach, where the ROP and ROMP steps can occur in the same pot at the same time in a hybrid of grafting-through and grafting-from.³⁹ Although one-pot synthetic procedures have proven to be successful, broadening of SEC traces at moderate N_{bb} values compared to bottlebrush polymers not synthesized via a one-pot method is regularly observed, highlighting the importance of MM purity and other reaction conditions on the livingness in ROMP.

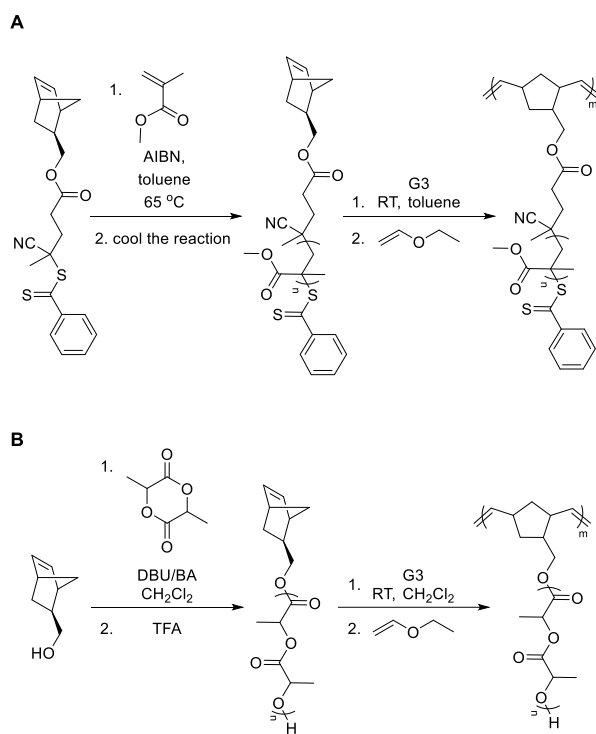


Figure 1.5. Synthesis of bottlebrush polymers with (A) PMMA side-chains and (B) PLA side-chains via a one-pot method. Adapted with permission from references ^{36, 38}.

1.5 Bottlebrush (Multi)Block Copolymers

1.5.1 Diblock and triblock bottlebrush copolymers

Along with bottlebrush homopolymers, ROMP enables the synthesis of bottlebrush block copolymers (BCPs), adding another dimension of complexity to this topology. Bowden and

coworkers reported the first synthesis of a series of BCPs that included one linear block and one bottlebrush block (i.e., linear-*block*-bottlebrush copolymers) in a pair of reports in 2007 and 2008.^{24, 40} In a large systematic study of 32 polymers, they highlighted how N_{bb} and N_{sc} of the bottlebrush component and the degree of polymerization (DP) of the linear component influenced solid-state morphology.²⁴ Grubbs and coworkers reported the first synthesis of a bottlebrush BCP with two bottlebrush blocks by ROMP in 2009.⁸ In this work, the growth-then-coupling method was used for the preparation of PS, PtBA, and poly(*n*-butyl acrylate) (PnBA) MMs, which were synthesized using ATRP followed by coupling a norbornene to the MM chain end, while a PLA MM was synthesized using the direct-growth method. A series of bottlebrush BCPs were then prepared by sequential ROMP of different combinations of two MMs (Figure 1.6A). This method enabled the synthesis of a variety of bottlebrush BCPs with variable side-chain chemistry, N_{sc} , and N_{bb} values. Small-angle X-ray scattering (SAXS) and atomic force microscopy (AFM) studies on these polymers showed self-assembly as evidenced by a bright green color due to the reflectance of light from the nanosized self-assembled domains (Figure 1.6B).

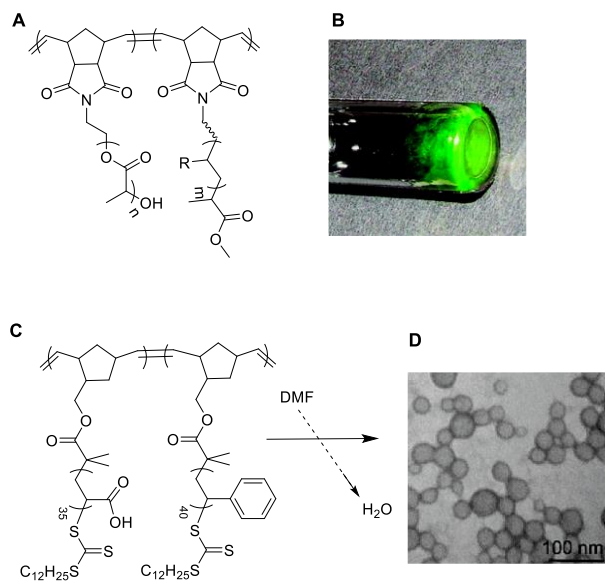


Figure 1.6. (A) Chemical structure of bottlebrush BCP based on PLA, PtBA, and PnBA side-chains. (B) Photograph of bottlebrush BCP after drying showing green color due to reflectance from the large self-assembled domains. (C) Synthesis of bottlebrush BCP based on PAA and PS side-chains. (D) TEM image of self-assembled bottlebrush BCP in aqueous solution into micelles. Adapted with permission from references ^{8,41}.

In related work, Wooley and coworkers synthesized bottlebrush BCPs using PS and PtBA MMs prepared by RAFT polymerization. Sequential ROMP afforded a bottlebrush BCP of the structure (PNb-*graft*-PS)-*block*-(PNb-*graft*-PtBA). Hydrolysis of the *tert*-butyl esters in the PtBA side-chains afforded an amphiphilic bottlebrush BCP of the structure (PNb-*graft*-PS)-*block*-(PNb-*graft*-PAA), where PAA = poly(acrylic acid) (Figure 1.6C). These polymers self-assembled in aqueous solution, forming micellar structures (Figure 1.6D).⁴¹

The versatility of ROMP grafting-through enables the preparation of bottlebrush multiblock copolymers. The same principle of using sequential polymerizations can be utilized to prepare ABA or ABC triblock or even ABCD tetrablock copolymers, where a polynorbornene (PNb) backbone is typically used while the variation occurs on the side-chains. For example, Wooley and coworkers prepared two different types of ABC bottlebrush triblock copolymers using the grafting-through method with the structures (PNb-*graft*-PEG)-*block*-(PNb-*graft*-PLA)-*block*-(PNb-*graft*-PBAEAM) (B1 and B2) and (PNb-*graft*-PEG)-*block*-(PNb-*graft*-(PHS-*co*-PNPM))-*block*-(PNb-*graft*-PBAEAM) (B3), where PBAEAM = poly(*N*-*tert*-butyloxycarbonyl-*N'*-acryl-1,2-diamino-ethane) and PHS-*co*-PNPM = poly(*p*-hydroxystyrene-*co*-*N*-phenylmaleimide) (Figure 1.7).⁴² Removal of the Boc groups on the PBAEAM side-chains afforded a cationic, water-soluble side-chain. The self-assembly of these triblock copolymers in aqueous solutions exhibited micellar or vesicular structures.

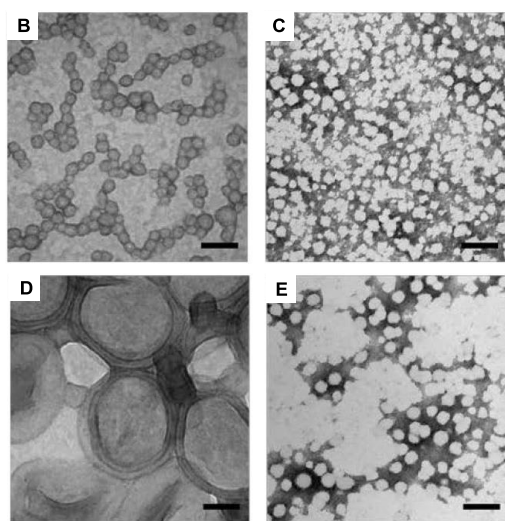
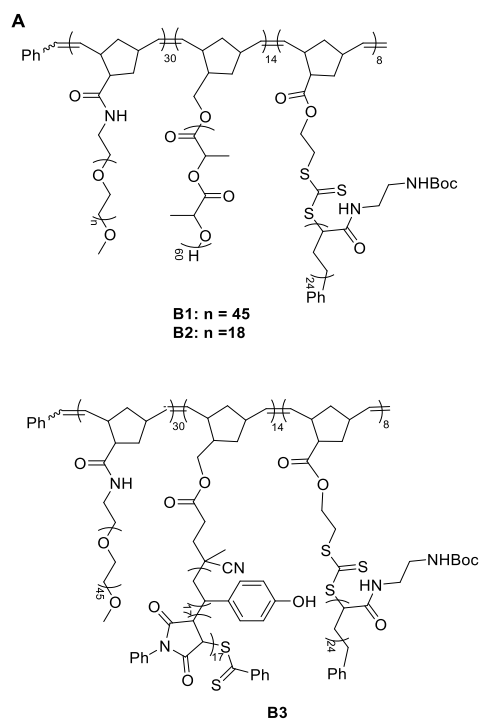


Figure 1.7. (A) Chemical structures of ABC triblock copolymers. TEM images of self-assembly in aqueous solution of (B) B1 protected with Boc (C) B1 with Boc removed (D) B2 protected with Boc (E) B2 with Boc removed. All scale bars are equal to 100 nm. Adapted with permission from reference ⁴².

1.5.2 Engineered Bottlebrush Polymer Structures

Recently, the precision that the grafting-through method by ROMP has been exploited to engineer bottlebrush polymers with non-linear and in some cases non-centrosymmetric structures. In other words, the customizability of this method enables the synthesis of bottlebrush polymers where the side-chain lengths are varied to generate a targeted shape. A comprehensive example of these types of bottlebrush polymers was demonstrated in a 2019 study published by Guironnet and coworkers where they utilized computer simulations and automated flow synthesis to feed MMs prepared *in situ* immediately into the ROMP reaction.⁴³ The MMs contained PLA and poly(valerolactone) (PVL) side-chains prepared through ROP. The authors conducted the ROP reaction in one reactor and continuously added it to another reactor containing G3 catalyst such that the side-chains increased in molecular weight along the polymer backbone, generating a cone-shaped tapered bottlebrush polymer. This methodology was also utilized in another study where PLA and polydimethylsiloxane (PDMS) were utilized as the side-chains on the MMs.⁴⁴ Further extension of the methodology allowed for even greater control over the molecular geometry of these bottlebrush polymers, with architectures including bowtie, hourglass, and football shapes (Figure 1.8A). The AFM image of the hourglass shapes is shown in Figure 1.8B.

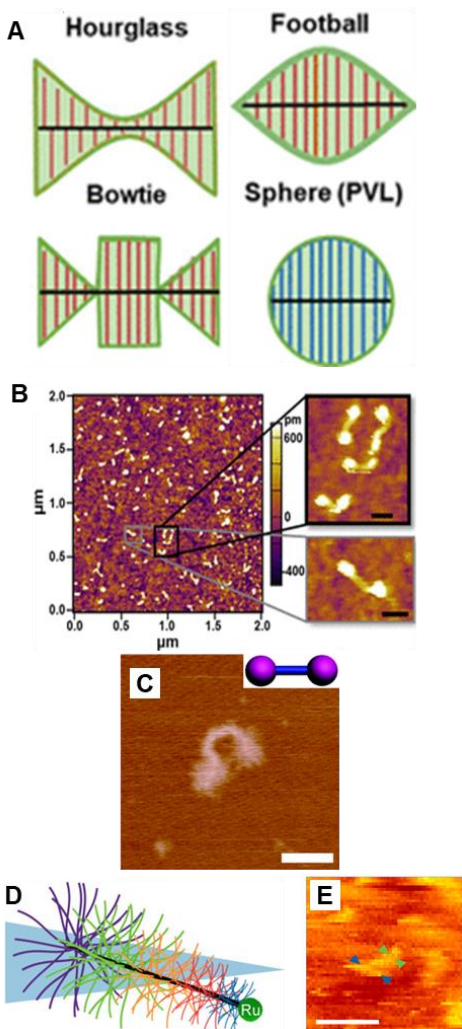


Figure 1.8. (A) Schematic illustrations of targeted engineered bottlebrush polymers architectures using a continuous flow method. (B) AFM image of hourglass shaped bottlebrush polymers (scale bar = 50 nm). (C) AFM image of dumbbell shaped bottlebrush polymers (scale bar = 50 nm). (D) Schematic illustration of cone-shaped tapered bottlebrush block copolymer and (E) AFM image of tapered bottlebrush block copolymer with PS side-chains (scale bar = 20 nm). Reproduced with permission from references ^{43, 45-46}.

The sequential addition of macromonomer ROMP (SAM-ROMP) method is another way to prepare bottlebrush polymers with non-cylindrical morphologies. This method involves the ROMP of MMs that have varied molecular weights in sequence, with the advantage that each MM can be fully characterized and purified before use in the ROMP grafting-through step. Early

work utilizing this method was carried out by Wooley and coworkers in 2012 in their synthesis of dumbbell-shaped bottlebrush polymers from an ABA triblock bottlebrush BCP where the side-chains on the first and third blocks were much longer than those on the middle block (Figure 1.8C).⁴⁵ More recently, this method was utilized by our group in 2017 to prepare tapered bottlebrush polymers that have a cone shape.⁴⁶ In this work, five PS MMs were prepared by ATRP with M_n values ranging from 1–10 kg/mol. The SAM-ROMP of the five MMs in descending order allowed for good control over the polymerizations. The cartoon shape of the tapered bottlebrush and AFM image are shown in Figures 1.8D and 1.8E, respectively.

1.6 Reaction Conditions

ROMP is a powerful method capable of producing several different complex polymer topologies. In many methods, ROMP works in tandem with other polymerization techniques, where ROMP is often the final step in the synthesis. ROMP is well-known for its functional group tolerance and ability to polymerize MMs quickly, enabling the construction of complex topologies displaying a wide variety of functional groups. However, limitations remain. For example, in bottlebrush polymer synthesis, ROMP of even moderate molecular weight MMs ($N_{sc} \sim 50$) can be challenging, as can even relatively low target N_{bb} values ($N_{bb} \sim 100$), where broadening of SEC traces compared to smaller bottlebrush polymers is regularly observed. This difficulty is amplified in bottlebrush multiblock copolymer synthesis and the construction of non-centrosymmetric structures such as tapered bottlebrush polymers. Control over grafting density may appear straightforward through copolymerization of MMs and diluent (small-molecule) monomers, but careful attention must be paid to the reactivity ratios of the two monomers types.⁴⁷ Recent advances in alternating ROMP by Xia⁴⁸ and Sampson⁴⁹ may enable

precise control over the spacing of side-chains at intervals greater than those typically achievable in ROMP of norbornene-based MMs. Altogether, the synthesis of complex polymer topologies while controlling parameters including N_{sc} , N_{bb} , and grafting density requires highly tuned polymerizations. Here we highlight some of the elements of the MM and the ROMP reaction conditions that influence the outcome of the polymerization.

Investigations into optimizing the conditions of ROMP (e.g., atmosphere, temperature, solvent, concentration) have been mostly geared toward the synthesis of bottlebrush polymers. However, lessons learned in bottlebrush polymer synthesis can be applied to a variety of the architectures discussed. As mentioned, the stability of the catalyst may determine the atmosphere needed to carry out ROMP. Although many opt for the air-stable Ru catalysts, extensive research into catalysts requiring an inert atmosphere has compelled many researchers to continue using dry and air-free conditions. This is despite many examples of ROMP reactions reaching high conversion and producing well-defined polymers while open to air using Ru catalysts. At this point, we are unaware of any systematic studies comparing ROMP carried out under air to those conducted in an inert-atmosphere glovebox. Recent work by Fogg and coworkers on ring-closing metathesis revealed AIR-dependent decomposition mechanisms,⁵⁰ but whether these would be active in ROMP is unclear because of the different propagating species (methylidene versus alkylidene). Here we discuss a variety of reaction elements that influence the rate of ROMP, such as temperature, solvent choice, and (macro)monomer structure.

1.6.1 Temperature

Choice of catalyst can determine the best temperature to use for ROMP. Most of the syntheses discussed carry out ROMP at room temperature; however, a few studies suggest that

elevated temperatures are preferable, mostly in the case of G2 and G1 catalysts. For example, G1 was used at 80 °C to synthesize a core-shell bottlebrush BCP.⁵¹ Many examples exist studying Ru catalysts derived from Grubbs' catalysts under various reaction temperatures. Lima–Neto and coworkers found higher monomer conversion when elevated temperatures were applied to the ROMP of norbornene using Ru-based catalysts containing DMSO ligands.⁵² Grubbs' and coworkers developed latent metathesis catalysts where polymerization only occurs at elevated temperatures.⁵³

In addition to elevated temperatures, low temperatures during ROMP have been used to thermodynamically drive polymerization of monomers with low ring strain.⁵⁴ Without catalyst modification, Kennemur and coworkers used G3 catalyst at temperatures up to 55°C to increase the rate of initiation for monomers with low ring strain, then the reaction mixtures were cooled in a variable temperature ROMP (VT-ROMP) process (Figure 1.9).⁵⁵ Low temperatures were required for proper propagation of cyclopentene monomers and this VT-ROMP process provided a method to achieve low dispersity polymers with accurate molecular weights from cyclopentene. Furthering this study, they found VT-ROMP useful in the synthesis of bottlebrush polymers using the grafting-from method.⁵⁶ Polymerizing cyclopentene as the bottlebrush polymer backbone provided a more flexible backbone than the traditional polynorbornene backbone.

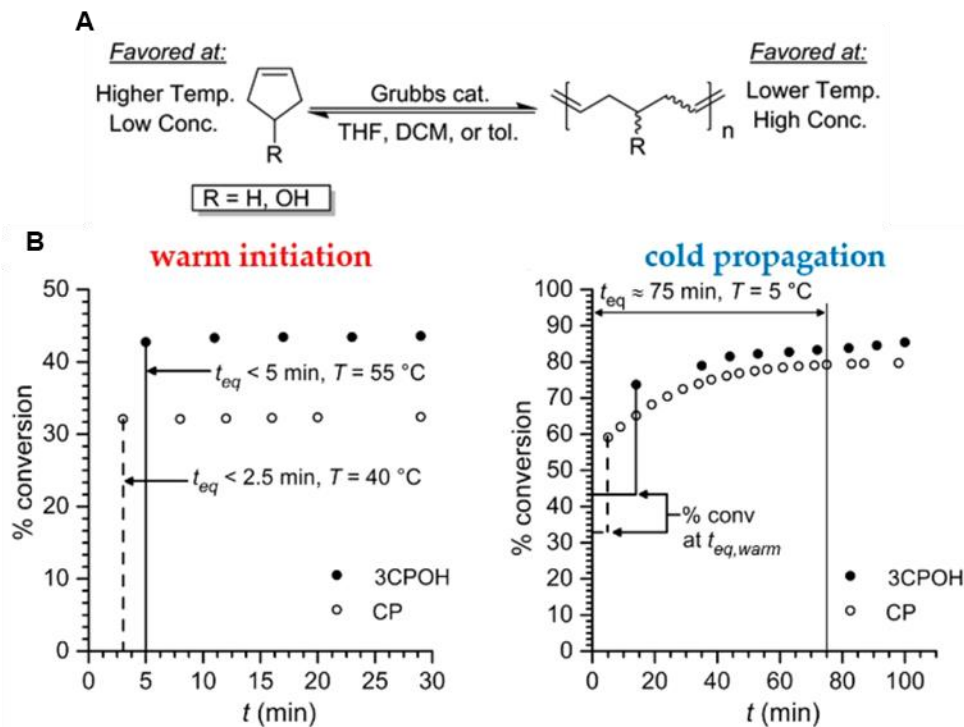


Figure 1.9. A) Equilibrium ROMP of cyclopentene (CP) and 3-cyclopenten-1-ol (3CPOH) under various conditions. B) Percent conversion versus time for initiation and propagation at different temperatures for CP (open circles, $[CP]_0 = 2.30$ M in toluene- d_8 , 0.22 mol % G2) and 3CPOH (solid circles, $[3CPOH]_0 = 2.25$ M in THF- d_8 , 0.23 mol % G2). Reproduced with permission from reference ⁵⁵.

1.6.2 Solvent

Solvent and (macro)monomer concentration have emerged as crucial variables regardless of the choice of catalyst for achieving well-defined polymers by ROMP. Studies have been conducted on both Schrock's and Grubbs' catalysts to reveal their behavior in various organic solvents. Fontanille and coworkers investigated solvent effects on a Schrock-type catalyst, finding that cyclohexane and toluene proceeded with high rates of propagation while THF formed a complex with the Mo-based catalyst decreasing the rate of propagation by over ~4-fold.⁵⁷ In terms of Grubbs' catalysts, Sanford, Love, and Grubbs found that the initiation rates of G1 and G2 were roughly proportional to the dielectric constant of the solvent.¹³ However, Percy

and coworkers measured the rate of initiation of G2 and HG-2 catalysts in nine different organic solvents and found only a slight relationship between initiation rate and solvent dielectric constant.⁵⁸ Focusing on G3, a recent study from our lab compared solvent type and purity for the synthesis of bottlebrush polymers by grafting-through ROMP studying six commonly used solvents (Figure 1.10). We found several key factors in selecting a solvent for a G3-catalyzed ROMP: First, purification of the solvent was unnecessary in most cases, although it was required for THF. Second, solvent influences the rate of propagation and the rate of catalyst decomposition, with EtOAc leading with a propagation rate ~2–4 times faster than the other tested solvents. Third, in terms of livingness, toluene was the best solvent in these studies due to its very low decomposition rate compared to all of the other solvents, but EtOAc and CH₂Cl₂ also show good living behavior during ROMP.⁵⁹ In terms of monomer concentration, we generally find that ROMP improves (i.e., highest achievable N_{bb} increases and dispersity decreases) with increasing initial MM concentration, up to a point where the reaction mixture becomes highly viscous. However, others have noted no improvement in ROMP with increased (macro)monomer concentration.⁶⁰ We speculate that the optimal concentration for a ROMP reaction depends greatly on the specific system.

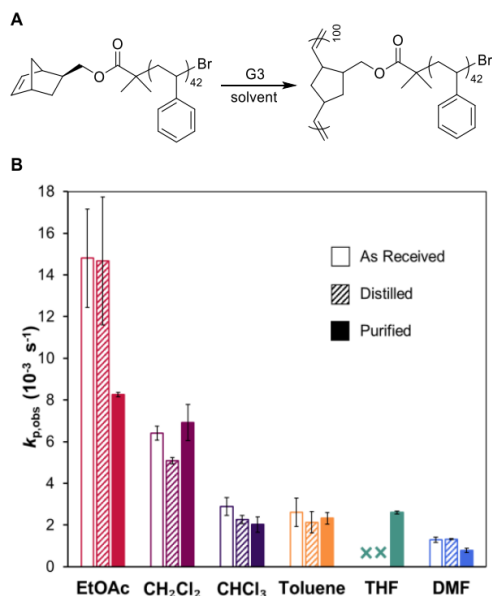


Figure 1.10. A) Reaction scheme of the ROMP grafting-through reaction used in the solvent studies. B) Measured first-order $k_{p,obs}$ values for ROMP grafting-through in six organic solvent with differing levels of purity (as received, distilled, and purified). The $k_{p,obs}$ value for ROMP in EtOAc actually decreases with purification due to removal of an acetic acid impurity. The as received and distilled THF showed <3% conversion to BB polymer, so $k_{p,obs}$ could not be determined in these two cases. Reproduced with permission from reference ⁵⁹.

1.7 (Macro)monomer Structure

Finally, the (macro)monomer structure makes a dramatic difference in the rate of propagation in ROMP and thus the “livingness” of the polymerization. Norbornenes are used widely because of their ease of synthesis and functionalization, high ring strain, and fast propagation kinetics. Oxanorbornenes are sometimes favored over norbornenes because the backbone of the resulting polymer is somewhat less hydrophobic, however, they suffer from low thermal stability due to their tendency to undergo retro-Diels–Alder reactions, generating furan.⁶¹ Therefore, we focus here on norbornene-based monomers, where the main factors are 1) the stereochemistry at the 5 and/or 6 positions (the two carbons opposite the carbon–carbon double bond), which can be either *endo* or *exo*, 2) the choice of anchor group, which describes the atoms

connecting the norbornene unit to the ‘R’ group in Figure 1.1, where R can be a biomolecule, dendron, polymer, or other units, and 3) the size of the R group.

1.7.1 Norbornene stereochemistry and anchor group

Substituted norbornenes are used widely in ROMP, specifically 5-substituted or 5,6-substituted, and the factor that influences the propagation rate the most is the *endo/exo* stereochemistry. It has been known for decades that *exo*-norbornene monomers polymerize faster than the equivalent *endo* structures by a factor of 20–100.^{62–63} This phenomenon has been validated across various catalysts, solvents, and substituents, and it is largely attributed to steric effects and the fact that Lewis basic units such as esters can coordinate to the catalyst in *endo* monomers.^{12, 64–67} A thorough study by Grubbs’ and coworkers found lower propagation and initiation rates for *endo* monomers compared to *exo* monomers, specifically caused by chelation observed for the *endo* monomers (Figure 1.11).⁶⁸ In addition to chelation, Guironnet and coworkers found higher transition state energies for the formation of the metallocyclobutane, which is the rate-determining step, with *endo*-norbornene monomers compared to *exo*-norbornene monomers, consistent with the low propagation rates typically seen for *endo* monomers.⁶⁹ Therefore, *exo* monomers are used much more widely than *endo* monomers, despite their substantially higher cost and need for extended synthetic procedures and purifications compared with the cheaper and more widely available *endo* monomers.

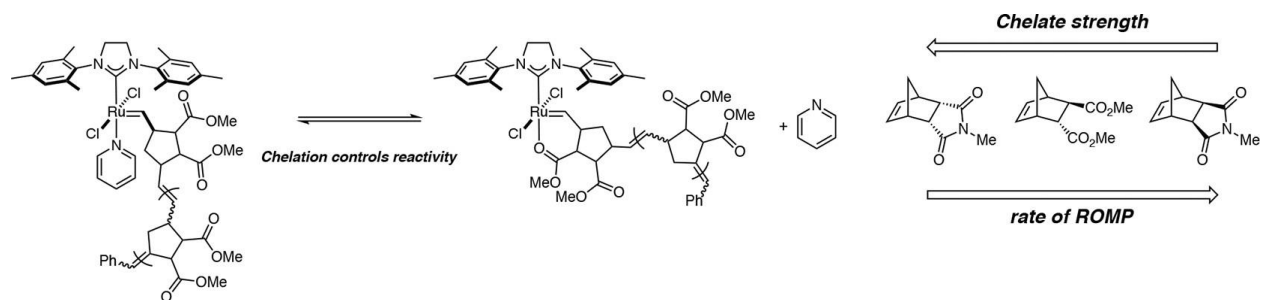


Figure 1.11. Chelation strength of various *endo*- and *exo*-norbornene monomers and the effects on ROMP. Reproduced with permission from reference ⁶⁸.

Although *exo*-norbornene monomers are favored, *endo* monomers remain useful in specific scenarios, including as diluent monomers and in cases where gradient structures are targeted.⁴⁷ Copolymerizing small molecule monomers with MMs, instead of polymerizing MMs alone, can reduce the steric bulk around the reactive catalyst center allowing for better control over molecular weights at high target N_{bb} values. Large differences in propagation rate between *endo* and *exo* monomers provides a wide scope of monomer reactivity for use as diluents.⁷⁰ Researchers have also worked on improving ROMP of the widely available *endo* monomers. Recently, Page and coworkers reported highly controlled polymerizations of *endo* monomers containing common chelating groups mediated by HG2 catalyst and found lower dispersity values and accurate molecular weight values compared to identical *exo* monomers.⁷¹

Beyond the *endo/exo* stereochemistry, our group found in 2016 that the rate of ROMP in a series of *exo* MMs depends on the choice of anchor group, a term originally coined by Slugovc,⁷² which describes the atoms connecting the norbornene unit to a functional group or polymer side-chain.⁷³ We observed a ~5-fold difference in propagation rates between different sets of three MMs with different anchor groups, and we concluded that the effect appears to be related to the HOMO energy of the (macro)monomer. The choice of anchor group dramatically

affected the ultimate N_{bb} achievable for MMs with similar molecular weights, from ~140 for an imide anchor group to >800 for a specific ester anchor group. Further investigations into the mechanism of ROMP by Guironnet confirmed that the rate-determining step is the formation of the metallocyclobutane ring when using norbornene based monomers, which further highlights the importance of monomer/anchor group choice.⁶⁹

1.7.2 Side-chain composition and molecular weight

Sterically demanding MMs and MMs containing functional groups with the ability to coordinate with the catalyst (i.e., cyclic oligosaccharides⁷⁴⁻⁷⁵ and polypeptides,⁷⁶⁻⁷⁷ respectively) typically require low target N_{bb} values for successful polymerization via ROMP grafting-through. These monomer classes are also limited by solubility as polar solvents, with low k_p values, are generally required. Protecting groups are used to improve solubility in common organic solvents, which would allow for enhanced propagation rates. Additionally, protecting groups prevent coordination of polar functional groups to the catalyst, enhancing propagation rates as well. However, protection and deprotection can be tedious. Ren and coworkers avoided protection of amino groups throughout the side-chains by introducing a spacer into the MMs.⁷⁸ Adding a PS block in between the norbornene and a poly(2-(dimethylamino)ethyl meth-acrylate) (PDMAEMA) block provided a physical barrier between the amino groups and the catalyst, preventing coordination (Figure 1.12). Thus, PDMAEMA MMs that typically experience no polymerization via ROMP, were polymerized to high conversion with relatively low dispersity values.

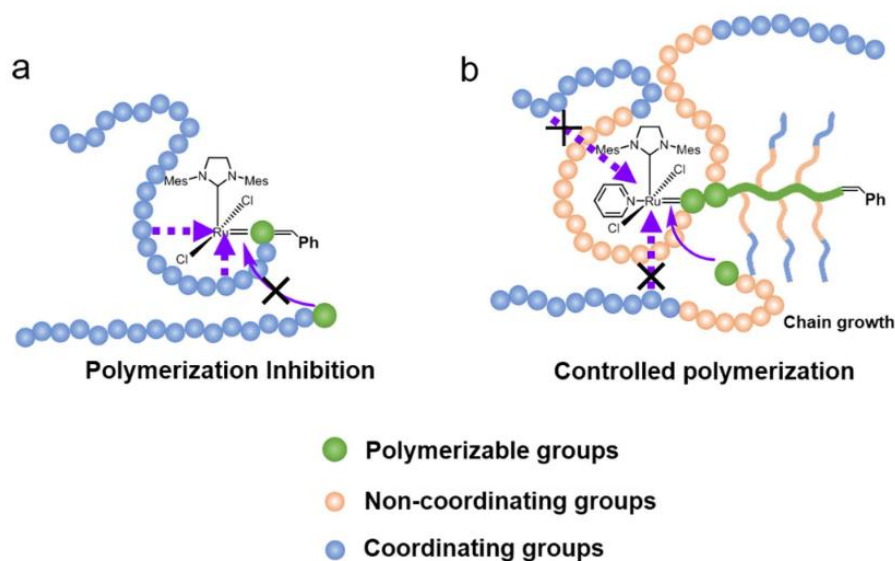


Figure 1.12. A) Polymerization inhibition caused by side-chain coordination to the catalyst. (B) Living polymerization of MMs containing a spacer chain, which prevents side-chain coordination to the catalyst. Reproduced with permission by reference ⁷⁸.

Lastly, varying the molecular weight of the monomer, specifically referring to the N_{sc} of MMs used for the synthesis of bottlebrush polymers, affects the dispersity of the resulting polymer and the maximum conversion or maximum N_{bb} under a given set of conditions. In fact, this effect was observed by Khosravi and coworkers in 1997 in a study involving ROMP of MMs using a Schrock Mo catalyst.⁷⁹ The authors noted differences in ultimate conversion for MMs of various molecular weights and suggested that there is an N_{bb} limit that varies inversely with N_{sc} . More recently, Zhu and coworkers reported a decrease in propagation rate as N_{sc} increased in ROMP of various norbornene MMs mediated by G3 catalyst.⁸⁰ They attribute these results to the growing bottlebrush segment interfering with incoming MM addition more as the molecular weight of the side-chains increases, termed the topological effect (Figure 1.13). Altogether, these results are consistent with observations in our lab and others, but the N_{bb} limit appears to depend

not only on N_{sc} but also on the other structural and reaction condition parameters discussed here. We attribute this effect to the ratio of propagation rate (k_p) to termination rate (k_t , i.e., catalyst decomposition rate), which Matyjaszewski has shown is a measure of “livingness”.⁸¹ In the case of ROMP, k_t appears to depend mostly on the specific catalyst and solvent, while k_p depends on these factors in addition to (macro)monomer structure. Therefore, optimization of structural features and reaction conditions in ROMP to achieve a high k_p/k_t ratio is needed to encourage high conversion for challenging (macro)monomers.

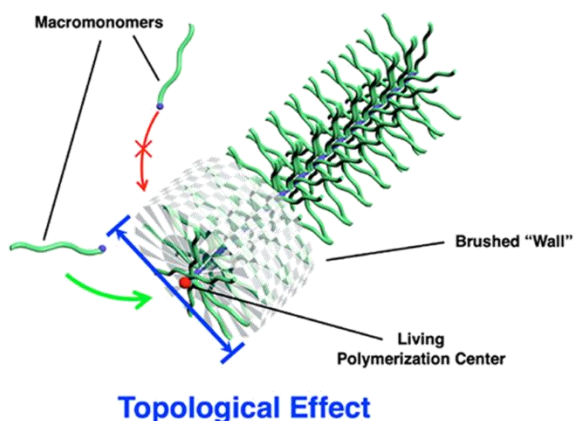


Figure 1.13. The topological effect during bottlebrush polymer synthesis hindering MMs from approaching the catalyst chain end. Reproduced with permission from reference ⁸⁰.

1.8 Conclusions

In summary, ROMP has emerged as a powerful tool over the past few decades for synthesizing complex polymer topologies. Unbound by the undesired radical–radical side reactions that limit RDRP methods and the stringent conditions and functional group restrictions imposed by anionic polymerization, ROMP in many cases provides the simplest route to bottlebrush homopolymers and BCPs. Best practices for optimizing “livingness” in ROMP

mediated by existing catalysts such as G3 continue to be discovered. For example, a handful of papers address optimizing monomer type, reaction solvent, anchor group, linker length and rigidity, or reaction conditions (concentration, temperature, atmosphere) in the construction of complex topologies by ROMP. However, few conclusions on optimal reaction conditions are derived from broad, systematic studies. In most cases, optimal conditions are empirically determined for a specific system, and it is unclear how such conditions might translate to other systems. Thus, there remains more to do and discover in order to synthesize larger (co)polymers with narrower dispersity values than currently accessible. In this respect, ROMP lags well behind other polymerization techniques such as ATRP, where many careful and thorough studies on ligands, solvents, initiators and other factors form a solid foundation of understanding. This knowledge foundation is critical for especially demanding structures such as tapered bottlebrush polymers, where the catalyst is repeatedly under monomer starved conditions. Ultimately, continued efforts will broaden the scope and size of polymers and topologies achievable by ROMP, driving fundamental studies on how polymer topology influences properties and encouraging new applications.

1.9 References

1. Wintermantel, M.; Gerle, M.; Fischer, K.; Schmidt, M.; Wataoka, I.; Urakawa, H.; Kajiwara, K.; Tsukahara, Y., Molecular bottlebrushes. *Macromolecules* **1996**, *29*, 978–983.
2. Li, Z.; Tang, M.; Liang, S.; Zhang, M.; Biesold, G. M.; He, Y.; Hao, S.-M.; Choi, W.; Liu, Y.; Peng, J.; Lin, Z., Bottlebrush polymers: From controlled synthesis, self-assembly, properties to applications. *Prog. Polym. Sci.* **2021**, *116*, 101387.

3. Verduzco, R.; Li, X.; Pesek, S. L.; Stein, G. E., Structure, function, self-assembly, and applications of bottlebrush copolymers. *Chem. Soc. Rev.* **2015**, *44*, 2405–2420.
4. Desimone, J. M.; Hellstern, A. M.; Siochi, E. J.; Smith, S. D.; Ward, T. C.; McGrath, J. E.; Gallagher, P. M.; Krukonis, V. J., Homogeneous and multiphase poly(methyl methacrylate) graft polymers via the macromonomer method. *Makromol. Chem. Macromol. Symp.* **1990**, *32*, 21–45.
5. Foster, J. C.; Varlas, S.; Couturaud, B.; Coe, Z.; O'Reilly, R. K., Getting into shape: Reflections on a new generation of cylindrical nanostructures' self-assembly using polymer building blocks. *J. Am. Chem. Soc.* **2019**, *141*, 2742–2753.
6. Foster, J. C.; Radzinski, S. C.; Matson, J. B., Graft polymer synthesis by RAFT transfer–to. *J. Polym. Sci., Part A: Polym. Chem.* **2017**, *55*, 2865–2876.
7. Jha, S.; Dutta, S.; Bowden, N. B., Synthesis of ultralarge molecular weight bottlebrush polymers using Grubbs' catalysts. *Macromolecules* **2004**, *37*, 4365–4374.
8. Xia, Y.; Kornfield, J. A.; Grubbs, R. H., Efficient synthesis of narrowly dispersed brush polymers via living ring-opening metathesis polymerization of macromonomers. *Macromolecules* **2009**, *42*, 3761–3766.
9. Cho, H. Y.; Krys, P.; Szcześniak, K.; Schroeder, H.; Park, S.; Jurga, S.; Buback, M.; Matyjaszewski, K., Synthesis of Poly(OEOMA) Using macromonomers via “grafting-through” ATRP. *Macromolecules* **2015**, *48*, 6385–6395.
10. Nuyken, O.; Pask, S. D., Ring-opening polymerization—An introductory review. *Polymers* **2013**, *5*, 361–403.

11. Pearce, A. K.; Foster, J. C.; O'Reilly, R. K., Recent developments in entropy-driven ring-opening metathesis polymerization: Mechanistic considerations, unique functionality, and sequence control. *J. Polym. Sci., Part A: Polym. Chem.* **2019**, *57*, 1621–1634.
12. Choi, T.-L.; Grubbs, R. H., Controlled living ring-opening-metathesis polymerization by a fast-initiating ruthenium catalyst. *Angew. Chem* **2003**, *42*, 1743–1746.
13. Sanford, M. S.; Love, J. A.; Grubbs, R. H., Mechanism and activity of ruthenium olefin metathesis catalysts. *J. Am. Chem. Soc.* **2001**, *123*, 6543–6554.
14. Au – Liu, J.; Au – Gao, A. X.; Au – Johnson, J. A., Particles without a box: Brush-first synthesis of photodegradable PEG star polymers under ambient conditions. *JoVE* **2013**, e50874.
15. Love, J. A.; Morgan, J. P.; Trnka, T. M.; Grubbs, R. H., A practical and highly active ruthenium-based catalyst that effects the cross metathesis of acrylonitrile. *Angew. Chem* **2002**, *41*, 4035–4037.
16. Bielawski, C. W.; Grubbs, R. H., Highly efficient ring-opening metathesis polymerization (ROMP) using new ruthenium catalysts containing N-heterocyclic carbene ligands. *Angew. Chem.* **2000**, *39*, 2903–2906.
17. Herz, K.; Elser, I.; Buchmeiser, M. R., Ring-opening metathesis polymerization: Mechanisms. In *Macromolecular Engineering*, pp 1–50.
18. Sanford, M. S.; Love, J. A.; Grubbs, R. H., A versatile precursor for the synthesis of new ruthenium olefin metathesis catalysts. *Organometallics* **2001**, *20*, 5314–5318.
19. Scholl, M.; Ding, S.; Lee, C. W.; Grubbs, R. H., Synthesis and activity of a new generation of ruthenium-based olefin metathesis catalysts coordinated with 1,3-dimesityl-4,5-dihydroimidazol-2-ylidene Ligands. *Org. Lett.* **1999**, *1*, 953–956.

20. Diesendruck, C. E.; Vidavsky, Y.; Ben-Asuly, A.; Lemcoff, N. G., A latent s-chelated ruthenium benzylidene initiator for ring-opening metathesis polymerization. *J. Polym. Sci., Part A: Polym. Chem.* **2009**, *47*, 4209–4213.
21. McConville, D. H.; Wolf, J. R.; Schrock, R. R., Synthesis of chiral molybdenum ROMP initiators and all-cis highly tactic poly(2,3-(R)₂norbornadiene) (R = CF₃ or CO₂Me). *J. Am. Chem. Soc.* **1993**, *115*, 4413–4414.
22. Bielawski, C. W.; Grubbs, R. H., Living ring-opening metathesis polymerization. *Prog. Polym. Sci.* **2007**, *32*, 1–29.
23. Teo, Y. C.; Xia, Y., Importance of macromonomer quality in the ring-opening metathesis polymerization of macromonomers. *Macromolecules* **2015**, *48*, 5656–5662.
24. Runge, M. B.; Lipscomb, C. E.; Ditzler, L. R.; Mahanthappa, M. K.; Tivanski, A. V.; Bowden, N. B., Investigation of the assembly of comb block copolymers in the solid state. *Macromolecules* **2008**, *41*, 7687–7694.
25. Cheng, C.; Khoshdel, E.; Wooley, K. L., ATRP from a norbornenyl-functionalized initiator: balancing of complementary reactivity for the preparation of α -norbornenyl macromonomers/ ω -haloalkyl macroinitiators. *Macromolecules* **2005**, *38*, 9455–9465.
26. Radzinski, S. C.; Foster, J. C.; Matson, J. B., Synthesis of bottlebrush polymers via transfer-to and grafting-through approaches using a RAFT chain transfer agent with a ROMP-active Z-group. *Polym. Chem.* **2015**, *6*, 5643–5652.
27. Patton, D. L.; Advincula, R. C., A versatile synthetic route to macromonomers via RAFT polymerization. *Macromolecules* **2006**, *39*, 8674–8683.

28. Li, Z.; Zhang, K.; Ma, J.; Cheng, C.; Wooley, K. L., Facile syntheses of cylindrical molecular brushes by a sequential RAFT and ROMP “grafting-through” methodology. *J. Polym. Sci., Part A: Polym. Chem.* **2009**, *47*, 5557–5563.
29. Li, X.; ShamsiJazeyi, H.; Pesek, S. L.; Agrawal, A.; Hammouda, B.; Verduzco, R., Thermoresponsive PNIPAAm bottlebrush polymers with tailored side-chain length and end-group structure. *Soft Matter* **2014**, *10*, 2008–2015.
30. Naguib, M.; Nixon, K. L.; Keddie, D. J., Effect of radical copolymerization of the (oxa)norbornene end-group of RAFT-prepared macromonomers on bottlebrush copolymer synthesis via ROMP. *Polym. Chem.* **2022**, *13*, 1401–1410.
31. Feast, W. J.; Gibson, V. C.; Johnson, A. F.; Khosravi, E.; Mohsin, M. A., Tailored copolymers via coupled anionic and ring opening metathesis polymerization. Synthesis and polymerization of bicyclo[2.2.1]hept-5-ene-2,3-trans-bis(polystyrylcarboxylate)s. *Polymer* **1994**, *35*, 3542–3548.
32. Zhang, H.; Zhang, Z.; Gnanou, Y.; Hadjichristidis, N., Well-defined polyethylene-based random, block, and bilayered molecular comb brushes. *Macromolecules* **2015**, *48*, 3556–3562.
33. Lexer, C.; Saf, R.; Slugovc, C., Acrylates as termination reagent for the preparation of semi-telechelic polymers made by ring opening metathesis polymerization. *J. Polym. Sci., Part A: Polym. Chem.* **2009**, *47*, 299–305.
34. Choi, J.; Kim, H.; Do, T.; Moon, J.; Choe, Y.; Kim, J. G.; Bang, J., Influence of residual impurities on ring-opening metathesis polymerization after copper(I)-catalyzed alkyne-azide cycloaddition click reaction. *J. Polym. Sci., Part A: Polym. Chem.* **2019**, *57*, 726–737.

35. Lu, H.; Wang, J.; Lin, Y.; Cheng, J., One-pot Synthesis of Brush-Like Polymers via Integrated Ring-opening Metathesis Polymerization and Polymerization of Amino Acid N-Carboxyanhydrides. *J. Am. Chem. Soc.* **2009**, *131*, 13582–13583.
36. Li, A.; Ma, J.; Sun, G.; Li, Z.; Cho, S.; Clark, C.; Wooley, K. L., One-pot, facile synthesis of well-defined molecular brush copolymers by a tandem RAFT and ROMP, “Grafting-through” strategy. *J. Polym. Sci., Part A: Polym. Chem.* **2012**, *50*, 1681–1688.
37. Chatterjee, A. K.; Choi, T.-L.; Sanders, D. P.; Grubbs, R. H., A General Model for Selectivity in Olefin Cross Metathesis. *J. Am. Chem. Soc.* **2003**, *125*, 11360–11370.
38. Radzinski, S. C.; Foster, J. C.; Matson, J. B., Preparation of Bottlebrush Polymers via a One-pot Ring-opening Polymerization (ROP) and Ring-opening Metathesis Polymerization (ROMP) Grafting-through Strategy. *Macromol. Rapid Commun.* **2016**, *37*, 616–621.
39. Kluthe, K. E. I.; Wagner, M.; Klapper, M., Simultaneous Bottlebrush Polymerization. *Macromolecules* **2021**, *54*, 1465–1477.
40. Runge, M. B.; Bowden, N. B., Synthesis of High Molecular Weight Comb Block Copolymers and Their Assembly into Ordered Morphologies in the Solid State. *J. Am. Chem. Soc.* **2007**, *129*, 10551–10560.
41. Li, Z.; Ma, J.; Cheng, C.; Zhang, K.; Wooley, K. L., Synthesis of Hetero-Grafted Amphiphilic Diblock Molecular Brushes and Their Self-Assembly in Aqueous Medium. *Macromolecules* **2010**, *43*, 1182–1184.
42. Su, L.; Heo, G. S.; Lin, Y.-N.; Dong, M.; Zhang, S.; Chen, Y.; Sun, G.; Wooley, K. L., Syntheses of triblock bottlebrush polymers through sequential ROMPs: Expanding the functionalities of molecular brushes. *J. Polym. Sci., Part A: Polym. Chem.* **2017**, *55*, 2966–2970.

43. Walsh, D. J.; Dutta, S.; Sing, C. E.; Guironnet, D., Engineering of Molecular Geometry in Bottlebrush Polymers. *Macromolecules* **2019**, *52*, 4847–4857.
44. Walsh, D. J.; Guironnet, D., Macromolecules with programmable shape, size, and chemistry. *Proc. Natl. Acad. Sci.* **2019**, *116*, 1538–1542.
45. Li, A.; Li, Z.; Zhang, S.; Sun, G.; Policarpio, D. M.; Wooley, K. L., Synthesis and Direct Visualization of Dumbbell-shaped Molecular Brushes. *ACS Macro Lett.* **2012**, *1*, 241–245.
46. Radzinski, S. C.; Foster, J. C.; Scannelli, S. J.; Weaver, J. R.; Arrington, K. J.; Matson, J. B., Tapered Bottlebrush Polymers: Cone-shaped Nanostructures by Sequential Addition of Macromonomers. *ACS Macro Lett.* **2017**, *6*, 1175–1179.
47. Lin, T.-P.; Chang, A. B.; Chen, H.-Y.; Liberman-Martin, A. L.; Bates, C. M.; Voegtle, M. J.; Bauer, C. A.; Grubbs, R. H., Control of Grafting Density and Distribution in Graft Polymers by Living Ring-opening Metathesis Copolymerization. *J. Am. Chem. Soc.* **2017**, *139*, 3896–3903.
48. Elling, B. R.; Xia, Y., Living Alternating Ring-opening Metathesis Polymerization Based on Single Monomer Additions. *J. Am. Chem. Soc.* **2015**, *137*, 9922–9926.
49. Parker, K. A.; Sampson, N. S., Precision Synthesis of Alternating Copolymers via Ring-opening Polymerization of 1-Substituted Cyclobutenes. *Acc. Chem. Res.* **2016**, *49*, 408–417.
50. Ton, S. J.; Fogg, D. E., The Impact of Oxygen on Leading and Emerging Ru-Carbene Catalysts for Olefin Metathesis: An Unanticipated Correlation Between Robustness and Metathesis Activity. *ACS Catalysis* **2019**, *9*, 11329–11334.
51. Zhang, H.; Hadjichristidis, N., Well-Defined Bilayered Molecular Cobrushes with Internal Polyethylene Blocks and ω -Hydroxyl-Functionalized Polyethylene Homobrushes. *Macromolecules* **2016**, *49*, 1590–1596.

52. Santana, S. A. A.; Carvalho Jr, V. P.; Lima-Neto, B. S., DMSO molecule as ancillary ligand in Ru-based catalysts for ring opening metathesis polymerization. *J. Brazil. Chem. Soc.* **2010**, *21*.
53. Thomas, R. M.; Fedorov, A.; Keitz, B. K.; Grubbs, R. H., Thermally Stable, Latent Olefin Metathesis Catalysts. *Organometallics* **2011**, *30*, 6713–6717.
54. Song, K.; Kim, K.; Hong, D.; Kim, J.; Heo, C. E.; Kim, H. I.; Hong, S. H., Highly active ruthenium metathesis catalysts enabling ring-opening metathesis polymerization of cyclopentadiene at low temperatures. *Nat. Commun.* **2019**, *10*, 3860.
55. Neary, W. J.; Kennemur, J. G., Variable Temperature ROMP: Leveraging Low Ring Strain Thermodynamics To Achieve Well-Defined Polypentenamers. *Macromolecules* **2017**, *50*, 4935–4941.
56. Neary, W. J.; Fultz, B. A.; Kennemur, J. G., Well-Defined and Precision-Grafted Bottlebrush Polypentenamers from Variable Temperature ROMP and ATRP. *ACS Macro Lett.* **2018**, *7*, 1080–1086.
57. Cazalis, C.; Héroguez, V.; Fontanille, M., Polymerizability of cycloalkenes in a living ring-opening metathesis polymerization initiated by Schrock complexes, 1. Effect of the solvent on the polymerization kinetics. *Macromol. Chem. Phys.* **2000**, *201*, 869–876.
58. Ashworth, I. W.; Nelson, D. J.; Percy, J. M., Solvent effects on Grubbs' pre-catalyst initiation rates. *Dalton Transactions* **2013**, *42*, 4110–4113.
59. Bloch, S. E.; Alaboalirat, M.; Eades, C. B.; Scannelli, S. J.; Matson, J. B., Solvent Effects in Grafting-through Ring-opening Metathesis Polymerization. *Macromolecules* **2022**, *55*, 3522–3532.

60. Dutertre, F.; Bang, K.-T.; Vereroudakis, E.; Loppinet, B.; Yang, S.; Kang, S.-Y.; Fytas, G.; Choi, T.-L., Conformation of Tunable Nanocylinders: Up to Sixth-generation Dendronized Polymers via Graft-Through Approach by ROMP. *Macromolecules* **2019**, *52*, 3342–3350.
61. Hillmyer, M. A.; Lepetit, C.; McGrath, D. V.; Novak, B. M.; Grubbs, R. H., Aqueous ring-opening metathesis polymerization of carboximide-functionalized 7-oxanorbornenes. *Macromolecules* **1992**, *25*, 3345–3350.
62. Rule, J. D.; Moore, J. S., ROMP Reactivity of endo- and exo-Dicyclopentadiene. *Macromolecules* **2002**, *35*, 7878–7882.
63. Ivin, K. J.; Mol, J. C., *Olefin Metathesis and Metathesis Polymerization*. Elsevier Science: 1997.
64. Pollino, J. M.; Stubbs, L. P.; Weck, M., Living ROMP of exo-norbornene Esters Possessing PdII SCS Pincer Complexes or Diaminopyridines. *Macromolecules* **2003**, *36*, 2230–2234.
65. Moatsou, D.; Hansell, C. F.; O'Reilly, R. K., Precision polymers: a kinetic approach for functional poly(norbornenes). *Chem. Sci.* **2014**, *5*, 2246–2250.
66. Pal, S.; Alizadeh, M.; Kong, P.; Kilbinger, A. F. M., Oxanorbornenes: promising new single addition monomers for the metathesis polymerization. *Chem. Sci.* **2021**, *12*, 6705–6711.
67. Miyasako, N.; Matsuoka, S.-I.; Suzuki, M., Ring-opening Metathesis Polymerization of endo- and exo-norbornene Lactones. *Macromol. Rapid Commun.* **2021**, *42*, 2000326.
68. Wolf, W. J.; Lin, T.-P.; Grubbs, R. H., Examining the Effects of Monomer and Catalyst Structure on the Mechanism of Ruthenium-catalyzed Ring-opening Metathesis Polymerization. *J. Am. Chem. Soc.* **2019**, *141*, 17796–17808.

69. Hyatt, M. G.; Walsh, D. J.; Lord, R. L.; Andino Martinez, J. G.; Guironnet, D., Mechanistic and Kinetic Studies of the Ring Opening Metathesis Polymerization of Norbornenyl Monomers by a Grubbs Third Generation Catalyst. *J. Am. Chem. Soc.* **2019**, *141*, 17918–17925.
70. Chang, A. B.; Lin, T.-P.; Thompson, N. B.; Luo, S.-X. L.; Liberman-Martin, A. L.; Chen, H.-Y.; Lee, B.; Grubbs, R. H., Design, Synthesis, and Self-Assembly of Polymers with Tailored Graft Distributions. *J. Am. Chem. Soc.* **2017**, *139*, 17683–17693.
71. Cater, H. L.; Balynska, I.; Allen, M. J.; Freeman, B. D.; Page, Z. A., User Guide to Ring-opening Metathesis Polymerization of endo-norbornene Monomers with Chelated Initiators. *Macromolecules* **2022**, *55*, 6671–6679.
72. Slugovc, C.; Demel, S.; Riegler, S.; Hobisch, J.; Stelzer, F., The Resting State Makes the Difference: The Influence of the Anchor Group in the ROMP of Norbornene Derivatives. *Macromol. Rapid Commun.* **2004**, *25*, 475–480.
73. Radzinski, S. C.; Foster, J. C.; Chapleski, R. C.; Troya, D.; Matson, J. B., Bottlebrush Polymer Synthesis by Ring-opening Metathesis Polymerization: The Significance of the Anchor Group. *J. Am. Chem. Soc.* **2016**, *138*, 6998–7004.
74. Nomura, K.; Schrock, R. R., Preparation of “Sugar-Coated” Homopolymers and Multiblock ROMP Copolymers. *Macromolecules* **1996**, *29*, 540–545.
75. Murphy, J. J.; Furusho, H.; Paton, R. M.; Nomura, K., Precise Synthesis of Poly(macromonomer)s Containing Sugars by Repetitive ROMP and Their Attachments to Poly(ethylene glycol): Synthesis, TEM Analysis and Their Properties as Amphiphilic Block Fragments. *Chemistry – A European Journal* **2007**, *13*, 8985–8997.

76. Kammeyer, J. K.; Blum, A. P.; Adamiak, L.; Hahn, M. E.; Gianneschi, N. C., Polymerization of protecting–group–free peptides via ROMP. *Polym. Chem.* **2013**, *4*, 3929–3933.
77. Sutthasupa, S.; Sanda, F.; Masuda, T., ROMP of Norbornene Monomers Carrying Nonprotected Amino Groups with Ruthenium Catalyst. *Macromolecules* **2009**, *42*, 1519–1525.
78. Zhao, T.; Zhu, K.; Yu, X.; Yuan, X.; Ren, L., From Polymerization Inhibition to Controlled Ring-opening Metathesis Polymerization of Macromonomers with Tertiary Amine Groups: The Effect of Spacer Chain†. *Chinese Journal of Chemistry* **2021**, *39*, 1927–1935.
79. Feast, W. J.; Gibson, V. C.; Johnson, A. F.; Khosravi, E.; Mohsin, M. A., Well-defined graft copolymers via coupled living anionic and living ring opening metathesis polymerisation. *J. Mol. Catal. A Chem.* **1997**, *115*, 37–42.
80. Ren, N.; Yu, C.; Zhu, X., Topological Effect on Macromonomer Polymerization. *Macromolecules* **2021**, *54*, 6101–6108.
81. Matyjaszewski, K., Ranking living systems. *Macromolecules* **1993**, *26*, 1787–1788.

Chapter 2: The influence of the norbornene anchor group in Ru-mediated ring-opening metathesis polymerization: Synthesis of linear polymers

2.1 Authors

Samantha J. Scannelli, Anshul Paripati, Jeffrey R. Weaver, Clark Vu, Mohammed Alaboalirat, Diego Troya, and John B. Matson*

Department of Chemistry, Virginia Tech, Blacksburg, VA 24061, United States

Macromolecules Innovation Institute, Virginia Tech, Blacksburg, VA 24061, United States

2.2 Abstract

Ring-opening metathesis polymerization (ROMP) mediated by Grubbs' first-generation catalyst [G1, (PCy₃)₂(Cl)₂RuCHPh] and Grubbs' third-generation catalyst [G3, (H₂IMes)(Cl)₂(pyr)₂RuCHPh] can exhibit living characteristics for some monomer classes, most commonly substituted norbornenes. Here we studied how various anchor groups, the series of atoms connecting the polymerizable norbornene unit to a functional group, affect livingness in ROMP in a series of small molecule exo-norbornene monomers. We first designed and calculated the HOMO energy of 61 monomers using density functional theory methods, finding that these energies spanned a range of 25 kcal/mol. We then performed kinetics experiments using ¹H NMR spectroscopy to measure the propagation rate constant ($k_{p,obs}$) under identical conditions for eight selected monomers with different anchor groups across the range of HOMO energies. We observed a positive correlation between the HOMO energy or the HOMO/LUMO energy gap and measured $k_{p,obs}$ values for both catalysts, revealing a 30-fold and a 10-fold

variation in $k_{p,obs}$ values across the series for G1 and G3, respectively. Interestingly, we observed a plateau for the three monomers with the highest HOMO energies for G3 catalyst, suggesting that above a certain level, HOMO energy no longer influenced the rate-determining step under the conditions studied here. Chelation studies revealed that only one of the eight monomers showed measurable binding of electron-rich groups on the monomer to the catalyst, but with no apparent effect on k_p . Finally, we utilized ^1H NMR spectroscopy to measure the rate of catalyst decomposition in the presence of each monomer, a key termination pathway in ROMP. Ultimately, we determined that the anchor group did not substantially affect catalyst decomposition, a proxy for the termination rate constant (k_t). In sum, these combined computational and experimental studies collectively demonstrate that livingness in ROMP of exo-norbornene monomers using G1 and G3 catalysts, as measured by relative k_p/k_t ratios, is primarily controlled by the k_p of the anchor group, which is correlated with HOMO energy.

2.3 Introduction

Polymerizations exhibiting living characteristics, including controllable molecular weights, narrow molecular weight distributions, and retention of chain end functionalities, have been a focus in polymer science for several decades.¹⁻² High “livingness” enables the synthesis of well-defined linear polymers including ultrahigh molecular weight polymers³⁻⁴ and (multi)block copolymers.⁵⁻⁶ Living characteristics also facilitate the construction of precise polymer structures with complex architectures, including cyclic polymers,⁷⁻⁸ star polymers,⁹ and both cylindrical¹⁰⁻¹¹ and noncylindrical¹²⁻¹⁴ bottlebrush polymers, among others. As a result, enhancing livingness across a variety of polymerization methods remains a large focus in the polymer synthesis community. Living polymerizations are defined as chain polymerizations

from which chain termination and irreversible chain transfer are absent; additionally, although not required, the rate of initiation is typically higher than that of propagation, creating a constant number of kinetic-chain carriers throughout the polymerization.¹⁵ While living anionic polymerization in the absence of air, water, or other impurities may represent the only system that fully qualifies as living,¹⁶ several other polymerization methods suppress rates of chain termination and irreversible chain transfer compared with propagation to exhibit living characteristics.^{17–18} Chief among them are the reversible-deactivation radical polymerization (RDRP) methods, including atom-transfer radical polymerization (ATRP) and reversible addition–fragmentation chain transfer (RAFT) polymerization.^{19–20} Another widely used and versatile polymerization method with living characteristics is ring-opening metathesis polymerization (ROMP).²¹ Despite extensive efforts to characterize and enhance livingness in RDRP methods, quantitative studies on the kinetic factors affecting living characteristics in ROMP are lacking.

ROMP is typically initiated and/or mediated by a transition metal catalyst and continues to increase in popularity due to its fast polymerization rates, high functional group tolerance, relative insensitivity to air and water in many cases, and ability to reach full monomer conversion without deleterious side reactions.²¹ Most ROMP syntheses with living character utilize Grubbs' 1st generation catalyst [G1, (PCy₃)₂(Cl)₂RuCHPh] or Grubbs' 3rd generation catalyst [G3, (H₂IMes)(Cl)₂(pyr)₂RuCHPh], enabling synthesis of multiblock polymers and polymers with complex topologies.²² For example, Kilbinger employed ROMP using G3 catalyst to synthesize heptablock copolymers with degradable linkages in alternating blocks,²³ and we recently synthesized decablock bottlebrush polymers to demonstrate the efficiency of a sequential addition of macromonomers (SAM) approach to ROMP.¹² Xie and coworkers

synthesized AB2 star polymers with G1 catalyst,²⁴ which has lower initiation and propagation kinetics than G3 catalyst but is simpler, cheaper, and more bench stable.²⁵ Despite these successes, close examination of the data in these and other papers reveals limits to the living character in ROMP, as evidenced by increasing dispersity values with each additional block and low molecular weight tails in the size exclusion chromatography (SEC) traces due to prematurely terminated chains. Thus, a comprehensive picture of the factors that influence living character in ROMP is critical to address these limitations, enabling synthesis of precise polymer structures to derive structure-property relationships in linear (multi)block copolymers and complex polymer topologies.

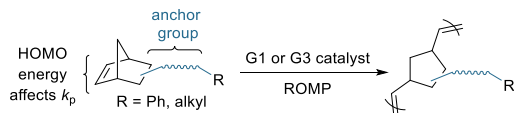
In any polymerization with living characteristics, the propagation rate, which is largely determined by the propagation rate constant (k_p), must be much higher than that of any chain-breaking reaction, i.e., chain transfer or termination (we focus here on termination, k_t). Matyjaszewski ranked the livingness of various polymerization systems by comparing k_p/k_t ratios among different polymerization systems, where higher k_p/k_t ratios indicate greater livingness.¹⁷ In the case of ROMP of substituted norbornenes initiated by G1 or G3 catalyst to make linear polymers, there is high living character due to three factors: 1) k_p is high—polymerizations are typically complete within a few minutes for G3 and several minutes to a few hours for G1; 2) chain transfer is absent; and 3) catalyst decomposition pathways, which collectively determine k_t , are relatively low.

In 2016 we hypothesized that k_p , and thus the k_p/k_t ratio, could be enhanced in ROMP by tuning monomer reactivity.²⁶ We discovered that the anchor group, the series of atoms connecting the polymerizable unit to the side-chain,²⁷ had an unexpectedly large effect on k_p . While it was already well known that *exo*-norbornene monomers underwent ROMP 10–100-fold

faster than *endo*-norbornene monomers,^{28–29} this work revealed a 5–10-fold increase in k_p among a set of three *exo*-norbornene monomers with polymerization initiated by G3 catalyst. This increase in k_p was achieved by changing the anchor group from an imide to an ester, leading to an increase in the maximum obtainable bottlebrush polymer backbone degree of polymerization from ~100 to ~800 in a pair of identical macromonomers with varying anchor groups. Computational studies in this original work indicated that the rate differences were correlated with differences in electronic structure among the various anchor groups, highlighting how rational selection of the anchor group could enable high macromonomer conversion and improve livingness in ROMP, which is vital for making precise bottlebrush polymers.

In our earlier work on the effects of the anchor group on ROMP, we studied three common anchor groups, and we observed a positive correlation between the energy of the monomer HOMO, localized on the reactive olefin, and k_p . Here we aimed to apply a combined computational/experimental approach to extensively study the effect of the anchor group in ROMP of small molecule *exo*-norbornene monomers on k_p , catalyst decomposition (a proxy for k_t), and the resulting living character of this polymerization method (Scheme 2.1). We hypothesized that computational methods could be applied to a wide range of monomer structures to suggest anchor groups with varying electronic structures, and that experimental kinetic measurements on a selected group of these monomers using both G1 and G3 catalysts would reveal how HOMO energy relates to living character in ROMP.

Scheme 2.1. Representative scheme of ROMP of monomers with various anchor groups.



2.4 Results and Discussion

To investigate the relationship between HOMO energy and k_p , we designed 61 different norbornene-based monomers with varying anchor groups (Figure S1). We then set out to 1) calculate the HOMO energy for each of them, 2) select several to synthesize across a range of HOMO energies, and 3) measure their k_p values and effects on catalyst decomposition (k_t) in ROMP using both G1 and G3 catalysts under standardized conditions. We previously showed, out of three macromonomers, that higher HOMO energies led to higher polymerization rates.²⁶ Therefore, we hypothesized that the k_p in polymerizations mediated by G1 and G3 catalysts would be commensurate with HOMO energy.

2.4.1 HOMO Energy Calculations

To obtain HOMO energies for a large number of monomers, we restricted our calculations to relatively small structures. All monomers were designed with a norbornene on one end as the polymerizable unit and a phenyl or alkyl group on the other, ensuring the differences in the HOMO energies were due to the anchor group (Figure S1). The HOMO energies were then calculated from optimized geometries of all 61 monomers using density functional theory (B3LYP method and 6–31G(d) basis set).^{30–31} Coordinates of all monomer structures and all HOMO energies are shown in the Supporting Information. The HOMO energies ranged from -161 to -136 kcal/mol. We synthesized several of these monomers, but

many precipitated out during ROMP, especially those with NH bonds. Ultimately, we selected a total of eight monomers for further experimental testing (Figure 2.1), all of which underwent ROMP without precipitation in initial tests. The selected monomers had HOMO energies ranging from -161 to -145 kcal/mol. We note that we did synthesize and ROMP some monomers in the range from -145 to -136 kcal/mol, but all precipitated during polymerization, preventing inclusion in the final study. Optimized geometries and HOMO energies of the eight selected monomers were recalculated using a higher level of theory (M06-2X method and def2-TZVP basis set)³²⁻³³ for a better understanding of their electronic structures. At this higher level of theory, the HOMO energies ranged from -197 to -186 kcal/mol. The ROMP kinetics of these monomers were then extensively studied experimentally.

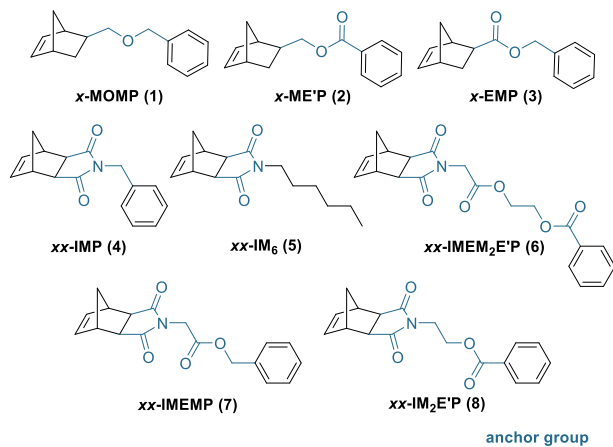


Figure 2.1. Monomers with various anchor groups (blue) synthesized and polymerized via ROMP. All monomers exhibited *exo* (*x* prefix) or *exo-Exo* (*xx* prefix) stereochemistry. Letters identify structural components of the anchor group from left to right (M = methylene/methyl, O = oxygen, P = phenyl, E = ester with carbonyl on the left, E' = ester with carbonyl on the right, I = imide). Subscripts indicate the number of times that component is repeated.

2.4.2 ¹H NMR Kinetic Analysis

All monomers were polymerized in the presence of G1 and G3 catalysts, separately, under the same conditions to investigate whether the effects of the anchor groups differed depending on the catalyst. To avoid solvent removal before NMR spectroscopic analysis, we used purified CDCl₃ as the solvent, and all polymerizations were carried out under air and at room temperature at a monomer concentration of 20 mM, targeting a degree of polymerization of 100. Aliquots were taken from the reaction mixture at pre-determined time points and injected into vials containing an excess of ethyl vinyl ether in CDCl₃ to terminate the reaction. Conversion of norbornene monomers **1–8** was monitored by ¹H NMR spectroscopy by comparing the integration of the polymer backbone olefin protons to the olefin protons of the monomer.

ROMP can be considered a pseudo-first order reaction;³⁴ therefore, these data were fit to first-order kinetic plots. Representative ¹H NMR spectra and kinetics plots are shown in Figure 2.2 for an example monomer *xx*-IM2E'P (**8**) with either G1 (A–B) or G3 (C–D) as the catalyst; plots for all other monomers can be found in the Supporting Information (Figures S20–S51). Averaged $k_{p,obs}$ and half-life values were determined over at least three kinetics runs for each monomer. After quenching the reaction following removal of the final aliquot, the reaction mixture was concentrated to obtain the final polymer. SEC analysis of the final polymers showed that molecular weights were close to expected values, and all polymers showed monomodal peaks with low dispersities (Figures S52–S67). All rate and SEC data are shown in Table 2.1.

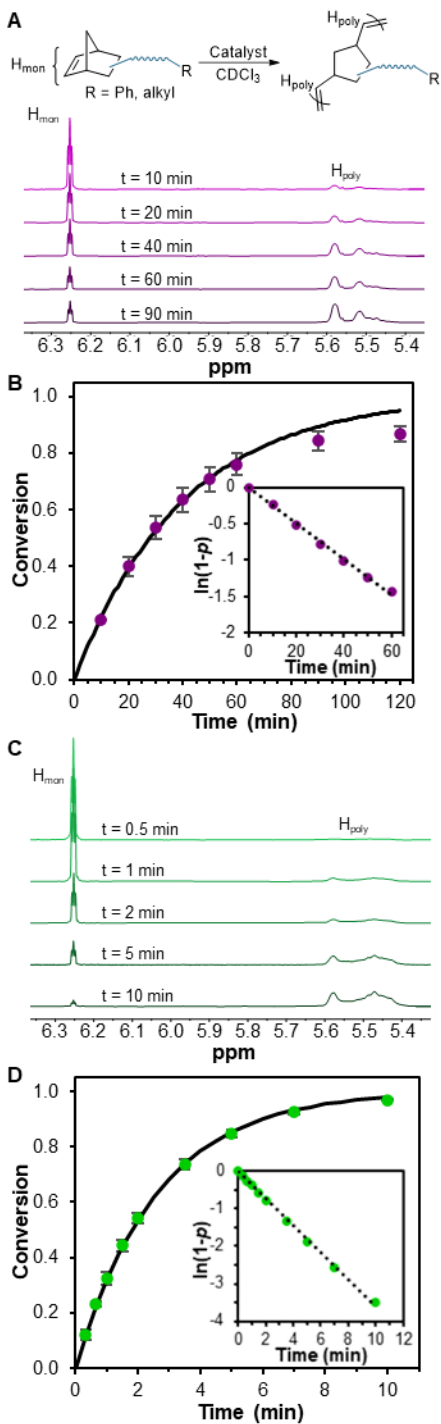


Figure 2.2. (A) Representative spectra for ^1H NMR kinetics experiment of the ROMP of monomer *xx*-IM₂E'P (**8**) with G1 catalyst. As the polymerization proceeds, the norbornene olefin resonance at ~ 6.26 ppm decreases in relative area, and the polymer backbone resonance at 5.4–5.6 ppm increases in relative area. (B) Kinetic analysis of monomer *xx*-IM₂E'P (**8**) in CDCl₃ with

G1 catalyst at a [monomer]/[G1] ratio of 100:1 and [monomer] = 20 mM. The solid line represents the fit to the averaged conversion data based on the equation $p = 1 - e^{(-k_p t)}$ where p = fractional conversion. (C) Representative spectra for ^1H NMR kinetics experiment of the ROMP of monomer $xx\text{-IM}_2\text{E}'\text{P}$ (**8**) with G3 catalyst. As the polymerization proceeds, the norbornene olefin resonance at ~ 6.26 ppm decreases in relative area, and the polymer backbone resonance at 5.4–5.6 ppm increases in relative area. (D) Kinetic analysis of monomer $xx\text{-IM}_2\text{E}'\text{P}$ (**8**) in CDCl_3 with G3 catalyst at a [monomer]/[G3] ratio of 100:1 at [monomer] = 20 mM. The solid line represents the fit of each data set generated using experimentally determined k_p values based on the equation $p = 1 - e^{(-k_p t)}$.

Table 2.1. HOMO energies, HOMO/LUMO gap energies, polymerization kinetics, and polymer characterization for ROMP of monomers **1–8**

Anchor Group	HOMO Energy ^a (kcal/mol)	HOMO/LUMO Gap ^a (kcal/mol)	Catalyst	$k_{p,\text{obs}}$ (min ⁻¹)	$t_{1/2}$ (min)	$M_{n,\text{SEC}}^b$ (kDa)	$M_{n,\text{expected}}^c$ (kDa)	D
$x\text{-MOMP}$ (1)	-186	213	G1	0.271 ± 0.008	2.6 ± 0.2	26	21	1.04
$x\text{-ME}'\text{P}$ (2)	-188	214		1.4 ± 0.1	0.51 ± 0.04	25	23	1.07
$x\text{-EMP}$ (3)	-190	211		0.055 ± 0.006	13 ± 1	19	23	1.15
$xx\text{-IMP}$ (4)	-193	215		0.049 ± 0.007	14 ± 1	22	25	1.05
$xx\text{-IM}_6$ (5)	-195	217		0.030 ± 0.007	24 ± 6	31	25	1.06
$xx\text{-IMEM}_2\text{E}'\text{P}$ (6)	-196	217		0.020 ± 0.0008	35 ± 1	48	37	1.05
$xx\text{-IMEMP}$ (7)	-196	218		0.034 ± 0.004	20 ± 3	35	31	1.05
$xx\text{-IM}_2\text{E}'\text{P}$ (8)	-197	218		0.027 ± 0.003	27 ± 4	32	31	1.04
$x\text{-MOMP}$ (1)	-186	213	G3	3.7 ± 0.3	0.19 ± 0.02	23	21	1.04
$x\text{-ME}'\text{P}$ (2)	-188	214		3.3 ± 0.6	0.22 ± 0.04	24	23	1.06
$x\text{-EMP}$ (3)	-190	211		4.8 ± 0.9	0.17 ± 0.01	28	23	1.07
$xx\text{-IMP}$ (4)	-193	215		0.54 ± 0.03	1.31 ± 0.07	22	25	1.01
$xx\text{-IM}_6$ (5)	-195	217		0.66 ± 0.05	1.06 ± 0.07	30	25	1.01
$xx\text{-IMEM}_2\text{E}'\text{P}$ (6)	-196	217		0.40 ± 0.04	1.66 ± 0.06	41	37	1.02
$xx\text{-IMEMP}$ (7)	-195	218		0.60 ± 0.04	1.15 ± 0.07	37	31	1.01
$xx\text{-IM}_2\text{E}'\text{P}$ (8)	-197	218		0.38 ± 0.02	1.8 ± 0.1	39	31	1.01

^aCalculated using M06-2X method and def2-TZVP basis set.³²⁻³³ ^bMeasured on samples

removed after the final aliquot of the kinetics run by SEC in THF at 30 °C with multiangle light scattering and refractive index detectors. ^cDetermined using the equation $M_{n,\text{expected}} = \text{monomer molar mass} * ([\text{monomer}]/[\text{catalyst}])_0$.

G1 catalyst mediates ROMP with lower k_p values than G3 catalyst,³⁵ so the rate constants observed with G1 catalyst were generally 10–20-fold lower than the rate constants observed with G3 catalyst. We noticed that some monomers, mainly those with low $k_{p,obs}$ values, did not reach full monomer conversion when polymerized with G1 catalyst. Therefore, we calculated $k_{p,obs}$ in these cases from conversion data only up to ~80% to ensure good first-order kinetics fits. Most monomers had half-lives greater than 2 min with G1 catalyst, with half-lives for imide-based monomers **4–8** in the range of 14–35 min. In contrast, all monomer half-lives were less than 2 min with G3 catalyst, with the fastest monomers showing half-lives in the range of 10 s. Additionally, the ROMP of these eight monomers with either catalyst showed at least an order of magnitude difference between the monomers with the highest and lowest $k_{p,obs}$ values; however, the spread within the series was larger for G1 catalyst (70-fold) compared with G3 catalyst (10-fold).

Our group previously found that differences in the rate of ROMP of macromonomers arose primarily from differences in electronic structure among the various anchor groups.²⁶ Additionally, investigations into the mechanism of ROMP from Guironnet and coworkers showed that the rate-determining step of ROMP with norbornene-based monomers was the formation of the metallacyclobutane (as opposed to the subsequent collapse of the metallocyclobutane to reorganize the double bonds or the coordination/decoordination of pyridine to the catalyst),³⁶ further suggesting the importance of the energy of the monomer HOMO, centered on the olefin, in determining k_p . Metallacyclobutane formation is a cycloaddition, which employs the π electrons of the olefin substrate to form a bond with the catalyst. These π electrons of the olefin correspond to the HOMO, however, other orbital interactions are possible in the rate-determining formation of the metallocyclobutane.

A detailed computational study by Suresh and Koha of frontier molecular orbitals in olefin metathesis with G1 revealed that at the transition state leading to metallocyclobutane formation, the π electrons in the olefin HOMO interact with the empty π^* and d orbitals of the Ru=C bond, but there is also a backbonding interaction of the π orbital of the Ru=C bond with the π^* orbital of the olefin (LUMO).³⁷ (We note that the π^* orbital of the olefin does not always correspond to the absolute lowest-energy unoccupied molecular orbital of the substrate. In this paper, we use LUMO to refer to the π^* orbital of the olefin.) Therefore, we examined the HOMO, LUMO, and HOMO/LUMO energy gap for our eight monomers and compared the $k_{p,obs}$ values with these calculated energies. Monomers with both high HOMO and low olefin-centered LUMO energies should facilitate the interaction with the metal carbene during the formation of the metallocyclobutane, increasing reactivity and resulting in higher $k_{p,obs}$ values than monomers with low HOMO and high olefin-centered LUMO energies.

A positive correlation between the HOMO energy and the $k_{p,obs}$ value of each monomer was found for both catalysts (Figure 2.3). An inverse correlation was found when comparing the HOMO/LUMO energy gaps and the $k_{p,obs}$ values for each monomer (Figure S68), suggesting the importance of multiple orbital interactions in the rate-determining step of ROMP. In other words, both HOMO energy and HOMO/LUMO energy gap were reasonable predictors of k_p , so we focus here on the HOMO energies. However, the trend was not completely linear for either catalyst; in fact, we observed a plateau for monomers with HOMO energies above -190 kcal/mol when G3 catalyst was used. This plateau suggests that the influence of the anchor group on the polymerization rate of monomers is lost at high HOMO energies; in other words, the anchor group may no longer influence the rate-determining step once its HOMO level exceeds this energy. However, it is possible that for ROMP with G3 catalyst under conditions that experience

low k_p such as large macromonomers³⁸ or potentially in non-ideal solvents,³⁹ a k_p difference among ester and ether-based anchor groups **1–3** may be observed. We also considered steric differences among the various monomers and their impact on metallacyclobutane formation but no significant changes in metallacyclobutane geometries were observed (Figure S69), suggesting steric constraints in the formation of this intermediate are comparable among monomers.

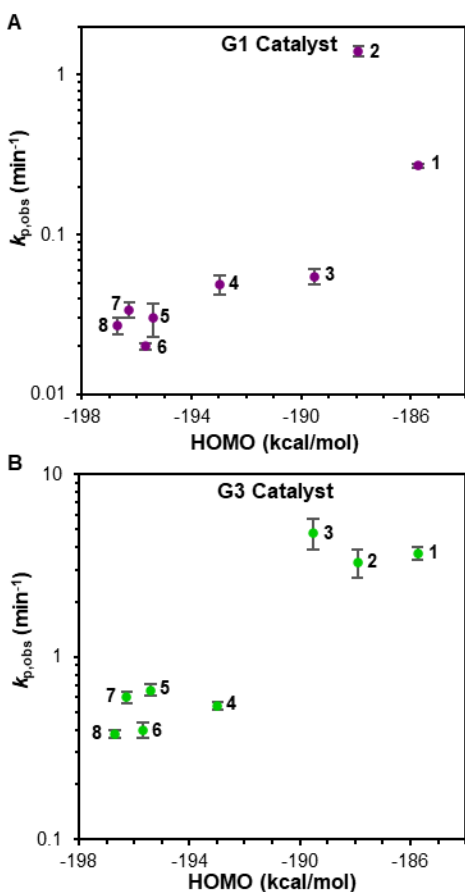


Figure 2.3. Measured $k_{p,obs}$ versus HOMO energy for monomers **1–8** with G1 catalyst (A) and G3 catalyst (B).

When using G1 catalyst, which exhibited a lower k_p for all monomers, we observed larger differences between the three monomers with HOMO energies above -190 kcal/mol (**1–3**), suggesting that the anchor group influences metallacyclobutane formation for these monomers

with G1 catalyst. Although larger rate differences among monomers **1–3** were found with G1 than with G3 catalyst, we observed an unexpectedly higher $k_{p,obs}$ in monomer *x*-ME'P (**2**) compared with monomer *x*-MOMP (**1**). The HOMO energies of *x*-MOMP (**1**) and *x*-ME'P (**2**) are likely within the accuracy of the DFT methods, but these results may also suggest additional factors that influence k_p beyond the HOMO energy. Overall, for both catalysts $k_{p,obs}$ generally increased with increasing HOMO energy.

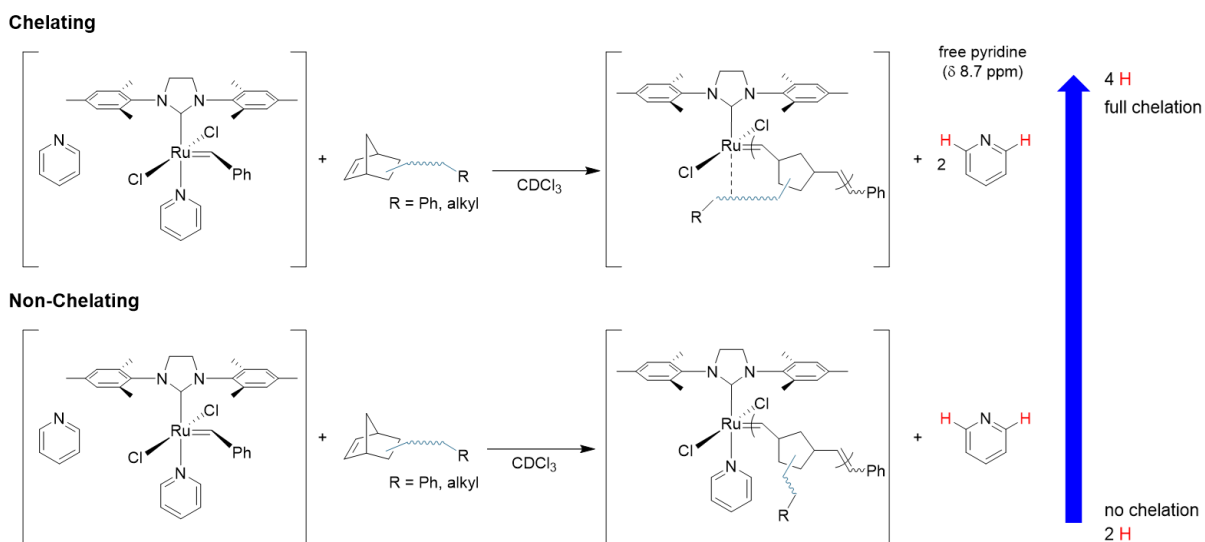
2.4.3 Chelation Effect

Certain anchor groups, mostly those containing carbonyls, may be able to chelate to Ru olefin metathesis catalysts, which can impact the polymerization rates of various monomers.³⁶ We therefore conducted ¹H NMR spectroscopy experiments, based on previously reported procedures by Grubbs and coworkers,⁴⁰ to identify the presence of chelation. These experiments rely on measuring the amount of pyridine in solution during the polymerization, a method originally established by Guirronet and coworkers.³⁴ Chelation studies were only done for G3 catalyst since G1 catalyst does not contain a pyridine ligand. However, we expect that the trends would be similar between the two catalysts due to their similar structures and reactivity profiles.⁴¹

Samples containing G3 catalyst and 10 equiv of monomers **1–8** were prepared in CDCl₃. Targeting a small degree of polymerization (10) allowed for polymerizations to reach their final propagating structure (a terminal Ru-alkylidene) prior to ¹H NMR analysis while retaining sufficient signal. All polymerizations were expected to have one pyridine free in solution, as the catalyst loses the first ligand upon dissolution.³⁴ However, the binding of the second pyridine ligand should depend on anchor group structure, where chelating anchor groups would compete

with binding of the second pyridine to the metal center, at least to some measurable degree (Scheme 2.2). Free pyridine in solution was measured by comparing the integration of the *ortho* protons of the free pyridine at about 8.7 ppm relative to the alkylidene proton of the propagating catalyst species (Ru=CH–poly) near 18.5–19.0 ppm. Therefore, in this assay, polymers without chelating anchor groups show one pyridine in solution, with an integral value of 2 for the two *ortho* protons (the other pyridine binds to the metal center). Conversely, polymers with chelating anchor groups show more than one pyridine in solution, with an integral value of more than 2 for the *ortho* protons (full chelation would show two free pyridines and therefore an integral value of 4). Monomers **1–3** have two possible regioisomers for the propagating alkylidene structure that can affect chelation; we envisioned that our experiments would reveal a mixture of chelated and nonchelated species with a free pyridine integral value near 3.

Scheme 2.2. Examples of propagating polymer chains with chelating and non-chelating anchor groups and their expected free pyridine integration values.



Because monomers *x*-ME'P (**2**), *xx*-IMEM2E'P (**6**), and *xx*-IM2E'P (**8**) experienced resonance overlap between monomer protons and the *ortho* protons of the bound pyridine, in this study we compared the relative NMR integrations of just the free pyridine to the Ru-alkylidene proton. It is worth noting that monomers **1–3** have two possible regioisomers for the propagating alkylidene structure that can affect chelation. Regardless, any form of chelation would still be observed during the experiments to reveal a mixture of chelated and nonchelated species. Out of all eight monomers tested, monomer *x*-EMP (**3**) was the only one to show any chelation of the propagating polymer structure, with a free pyridine integration value of 3.0, implying a mixture of chelated and nonchelated species during polymerization. The broad resonance also suggested the rapid and reversible chelation of the polymer chain (Figure S72). ROMP of all other monomers had free pyridine integrations close to 2, so when comparing the integration of the free pyridine to the $k_{p,obs}$ of each monomer, there was no correlation between the two variables (Figure 4). Although we did not specifically measure chelation for G1 due to a lack of pyridines on this catalyst, the chelation observed in the ROMP of monomer *x*-EMP (**3**) may explain the surprisingly low $k_{p,obs}$ found with G1 catalyst compared to G3 catalyst. The $k_{p,obs}$ of monomer *x*-EMP (**3**) more closely aligns with monomers *x*-MOMP (**1**) and *x*-ME'P (**2**) with G3 catalyst, but with imide-based monomers **4–8** with G1 catalyst, despite the structural similarities between monomers *x*-MOMP (**1**), *x*-ME'P (**2**), and *x*-EMP (**3**). Therefore, we speculate based on these results that the chelating anchor group of monomer *x*-EMP (**3**) affects k_p with G1 more than with G3 catalyst, decreasing the rate compared with a hypothetical non-chelating monomer with the same HOMO energy. Regardless, we found no correlation between chelation and $k_{p,obs}$ across all monomers in this study, which further emphasizes the relationship between HOMO energy and propagation rate.

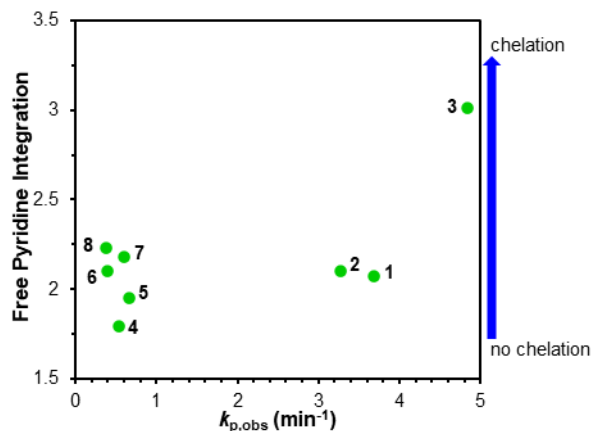


Figure 2.4. Free pyridine ¹H NMR integration values versus $k_{p,obs}$ of each monomer after polymerization with G3 catalyst. Error bars on integral values are estimated to be $\pm 10\%$ due to errors associated with integrating small peaks. Polymerizations were carried out in CDCl₃ with G3 at a [monomer]/[G3] ratio of 10:1 and [G3] = 40 mM.

Results from our chelation studies were in line with similar monomers reported by Grubbs and Guironnet.^{36, 40} Both observed no chelation in the ROMP of *exo*-norbornene imide monomers, i.e., those with anchor groups similar to monomers **4–8**. In addition, Grubbs observed no chelation in the ROMP of an ether-containing monomer with an anchor group that resembled monomer *x*-MOMP (**1**) here, and both Grubbs and Guironnet found chelation in the ROMP of monomers with ester-based anchor groups similar in structure to monomer *x*-EMP (**3**). They also did not notice any effects of chelation on k_p for *exo*-norbornene monomers. We considered the possibility that initiation rates could influence the observed propagation rate; however, Guironnet recently showed that initiation rates were similar among different *exo*-norbornene monomers.³⁶

2.4.4. Catalyst Decomposition and Livingness in ROMP

To further evaluate how the anchor group influences livingness in ROMP, we set out to estimate relative catalyst decomposition rates as a proxy for k_t values for G1 and G3 catalysts with the eight different monomers. Direct measurement of k_t during the polymerization in these samples was experimentally difficult because k_p is too fast for data collection during the polymerization by NMR spectroscopy. The earliest NMR spectrum we were able to acquire with sufficient alkyldiene signal was about 2 min into the polymerizations, which is enough time for monomer *x*-ME'P (**2**) with G1 and monomers **1–3** with G3 catalyst to reach near-complete conversion to polymer. Therefore, we were unable to measure catalyst decomposition during the polymerization for these monomers. Analysis by UV–vis was also unusable because both catalysts have featureless UV–vis spectra after initiation. Instead, we used ^1H NMR spectroscopy to estimate the % catalyst decomposition after near-complete monomer consumption. We speculate that more termination pathways are available when monomer is present because some decomposition pathways may only be accessible when the catalysts are in the metallacyclobutane form and not in the alkyldiene form.⁴² To ensure that each monomer was tested in an equal fashion, we decided to measure % catalyst decomposition after a consistent number of propagation half-lives for each catalyst: We measured all spectra after 12 propagation half-lives for G3 because it took 2 min to acquire a ^1H NMR spectrum with sufficient resolution for the fastest monomers, equivalent to 12 half-lives. For G1 catalyst, we measured all spectra after 4 half-lives because the fastest monomer with G1 [*x*-ME'P (**2**)] reaches 4 half-lives in 2 min, and 12 half-lives would have been extremely long for the slowest monomers.

Samples containing catalyst (G1 or G3) and an internal standard (phenanthrene or anthracene, respectively) were prepared in CDCl_3 . We used ^1H NMR spectroscopy to measure

the integration of the benzyldiene proton on G1 and G3 catalysts relative to an internal standard proton before monomer addition. Next, 100 equiv of monomer was added to the NMR tube, initiating the polymerization. For each monomer, we acquired a ^1H NMR spectrum after 4 propagation half-lives for G1 and 12 propagation half-lives for G3 catalyst, which allowed us to measure the decrease in the integration of the benzyldiene/alkylidene proton and to monitor catalyst decomposition over time, which we report as estimated $k_{t,\text{obs}}$ values.

We observed small differences in $k_{t,\text{obs}}$ values across all monomers with either G1 or G3 as the catalyst (Figure 2.5). For G1 catalyst, $k_{t,\text{obs}}$ values ranged from about 0.006 to 0.015 min^{-1} , while rates ranged from 0.006 to 0.018 min^{-1} for G3 catalyst. However, there were no clear trends, and the error in these measurements was fairly large due to the fairly small amounts of catalyst decomposition in these experiments and the error associated with precisely integrating small signals. To further investigate k_t , we estimated the % dead chains from the SEC traces of the final polymers. The slight variations in D values and low molecular weight tails in the SEC traces suggested different amounts of chain termination for each monomer. Therefore, we deconvoluted the low molecular weight tails of the SEC traces by assuming a Gaussian distribution,⁴³ and found little variation in the % dead chains for monomers **1–8** with both catalysts (Figures S94–109). From these results, we conclude that the anchor group did not affect $k_{t,\text{obs}}$ to a measurable extent for either catalyst. Thus, while other variables such as solvent influence k_t ,^{39, 44–45} the anchor group only significantly affects the k_p component of the k_p/k_t ratio, at least under the conditions used here. These results are consistent with HOMO localization on the reactive norbornene olefin, which would impact k_p , whereas termination events occur in the metallacyclobutane form or alkylidene form of the catalyst once the norbornene olefin has reacted.

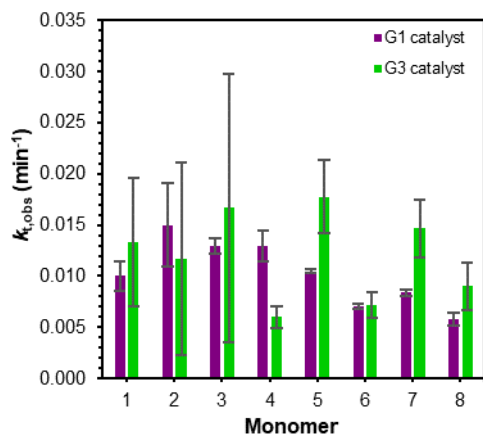


Figure 2.5. Experimentally determined $k_{t,obs}$ values for G1 (purple) and G3 (green) catalysts with different monomers. All $k_{t,obs}$ values were estimated using the equation $k_{t,obs} = (\text{fraction catalyst decomposition})(\text{time to } x \text{ propagation half-lives})^{-1}$ ($x = 4$ for G1 and 12 for G3) where decomposition was monitored using ^1H NMR spectroscopy. Polymerizations were carried out in CDCl_3 with a $[\text{monomer}]/[\text{catalyst}]$ ratio of 100:1 and $[\text{catalyst}] = 0.6 \text{ mM}$.

Using the $k_{p,obs}$ and $k_{t,obs}$ results, we were then able to generate relative k_p/k_t ratios for each monomer with both catalysts, where higher k_p/k_t ratios indicate greater living character. We used the $k_{p,obs}$ values measured from our kinetics experiments and the $k_{t,obs}$ values measured from catalyst decomposition studies to calculate the ratios, and then compared the values for each monomer. While these ratios are not true k_p/k_t ratios because $k_{p,obs}$ and $k_{t,obs}$ were measured under different conditions, they capture the relative differences between the anchor groups (Figure 2.6).

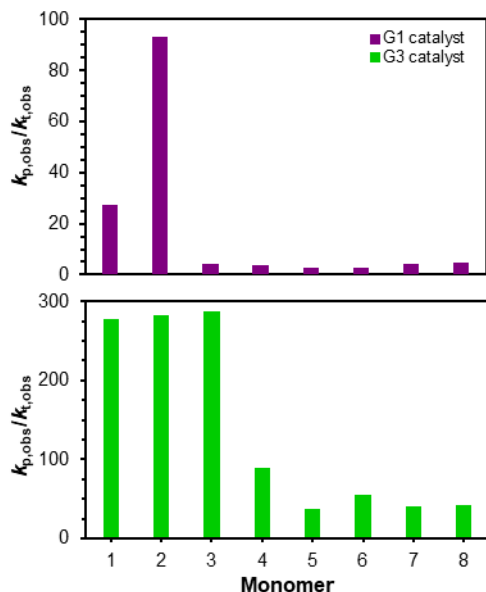


Figure 2.6. Relative k_p/k_t ratios for each monomer with either G1 (purple) or G3 (green) catalysts determined from the $k_{p,obs}$ values (measured from the kinetics studies on propagation) and the $k_{t,obs}$ values (estimated from the catalyst decomposition studies).

For polymerizations mediated by G1 catalyst, we observed at least a 10-fold difference in the k_p/k_t ratios between two groups: 1) monomers *x*-MOMP (**1**) and *x*-ME'P (**2**) with high $k_{p,obs}$ and, 2) monomers **3–8** with low $k_{p,obs}$ values. This order of magnitude difference in the k_p/k_t ratios is driven by the higher $k_{p,obs}$ values for monomers *x*-MOMP (**1**) and *x*-ME'P (**2**), as the catalyst decomposition rate was similar across all monomers. Anchor group choice is clearly crucial for polymerizations mediated by G1 catalyst, where only monomers *x*-MOMP (**1**) and *x*-ME'P (**2**) displayed a high enough k_p to maintain a high degree of livingness during ROMP to DP=100.

Polymerizations mediated by G3 catalyst showed two distinct groups as well. The high $k_{p,obs}$ monomers (**1–3**) showed at least a 4-fold higher k_p/k_t ratio compared to the monomers with lower $k_{p,obs}$ (**4–8**). The relative k_p/k_t values for monomers **1–3** were all quite similar and within

the error of the measurements. In contrast, monomer *x*-ME'P (**2**) was the most living monomer with G1 by a substantial margin. Therefore, among these anchor groups, we conclude that the ester anchor group used in monomer *x*-ME'P (**2**) is the most living for ROMP under conditions that experience low k_p (i.e., with G1 catalyst or with sterically demanding monomers). In contrast, monomers **1–3** show similar levels of livingness with G3 catalyst under higher k_p conditions utilizing small molecule monomers in a good solvent. Finally, the k_p/k_t ratios for polymerizations with G3 catalyst were 3–20-fold higher than those with G1 catalyst, consistent with the higher activity of G3 catalyst. These results suggest that while many anchor groups demonstrate a reasonably high degree of livingness for G3 catalyst, anchor group choice is more critical when using G1 catalyst, where only monomers *x*-MOMP (**1**) and *x*-ME'P (**2**) display high livingness.

2.5 Conclusions

In summary, we find that the anchor group significantly affects the propagation rate (k_p) but not the termination rate (k_t) in ROMP of small molecule *exo*-norbornene monomers. The calculated HOMO energies of monomers with various anchor groups were positively correlated with the $k_{p,obs}$ of the polymerizations initiated by either G1 or G3 catalyst, suggesting that monomers with higher HOMO energies exhibit greater reactivity in ROMP than monomers with lower HOMO energies. However, we observed an upper limit in $k_{p,obs}$ for polymerizations of this monomer set with G3 catalyst, where a plateau in rate was observed for monomers with HOMO energies above -190 kcal/mol, suggesting that the anchor group no longer affected the rate-determining step once above this limit. Chelation to G3 catalyst was also measured, but it had little impact on $k_{p,obs}$ in the eight *exo*-norbornene monomers studied here. Therefore, in the

synthesis of linear polymers by ROMP using G3 catalyst in a good solvent, anchor group choice affects k_p , but becomes inconsequential above a certain HOMO energy level.

Additionally, the anchor group had little effect on k_t for both G1 and G3 catalysts. The estimated $k_{t,obs}$ values were fairly uniform across all monomers for both catalysts, suggesting that k_t is not heavily affected by the anchor group. This result is consistent with decomposition during ROMP occurring after the norbornene olefin, where the HOMO is localized, has reacted to form a metallacyclobutane and then a propagating alkylidene. Combining $k_{t,obs}$ and $k_{p,obs}$ results, we determined that the anchor group significantly affected the k_p/k_t ratios, where higher k_p/k_t ratios indicate greater livingness. Large differences in the k_p/k_t ratios were driven by the differences in k_p because little variation was found for k_t with the different monomers. Monomers with the highest $k_{p,obs}$ values [monomer *x*-ME'P (**2**) with G1 and monomers *x*-MOMP (**1**), *x*-ME'P (**2**), and *x*-EMP (**3**) with G3] had the highest k_p/k_t ratios and therefore the highest degree of livingness. Ultimately, anchor group choice greatly influences the rate and livingness of ROMP with G1 and G3 catalysts. When synthesizing more complex topologies by ROMP, i.e., bottlebrush polymers, choice of anchor group becomes critical to reach high degrees of polymerization and achieve low dispersity polymers, a topic we are currently investigating in our laboratory.

2.6 Acknowledgments

This work was supported by a joint grant between the National Science Foundation and the Binational Science Foundation (DMR–2104602) and by GlycoMIP, a National Science Foundation Materials Innovation Platform funded through Cooperative Agreement DMR–1933525. We thank Dr. Santu Sarkar, and Tamalika Paul for critical reading of the manuscript.

We also thank Dr. Narasimhamurthy Shanaiah for helpful suggestions pertaining to our NMR experiments. The authors acknowledge Advanced Research Computing at Virginia Tech for providing computational resources and technical support that have contributed to the results reported within this paper. We also acknowledge the Virginia Tech Mass Spectrometry Research Incubator for high-resolution mass spectrometry analysis.

2.7 References

1. Szwarc, M., Living polymers. Their discovery, characterization, and properties. *J. Polym. Sci., Part A: Polym. Chem.* **1998**, *36*, IX–XV.
2. Stenzel, M. H.; Barner-Kowollik, C., The living dead – common misconceptions about reversible deactivation radical polymerization. *Mater. Horiz.* **2016**, *3*, 471–477.
3. Nicolaÿ, R.; Kwak, Y.; Matyjaszewski, K., A Green Route to Well-Defined High-Molecular-Weight (Co)polymers Using ARGET ATRP with Alkyl Pseudohalides and Copper Catalysis. *Angew. Chem* **2010**, *49*, 541–544.
4. Carmean, R. N.; Sims, M. B.; Figg, C. A.; Hurst, P. J.; Patterson, J. P.; Sumerlin, B. S., Ultrahigh Molecular Weight Hydrophobic Acrylic and Styrenic Polymers through Organic-Phase Photoiniferter-Mediated Polymerization. *ACS Macro Lett.* **2020**, *9*, 613–618.
5. Gody, G.; Maschmeyer, T.; Zetterlund, P. B.; Perrier, S., Rapid and quantitative one-pot synthesis of sequence-controlled polymers by radical polymerization. *Nat. Commun.* **2013**, *4*, 2505.
6. Steube, M.; Johann, T.; Galanos, E.; Appold, M.; Rüttiger, C.; Mezger, M.; Gallei, M.; Müller, A. H. E.; Floudas, G.; Frey, H., Isoprene/Styrene Tapered Multiblock Copolymers with

up to Ten Blocks: Synthesis, Phase Behavior, Order, and Mechanical Properties. *Macromolecules* **2018**, *51*, 10246–10258.

7. Eugene, D. M.; Grayson, S. M., Efficient Preparation of Cyclic Poly(methyl acrylate)-*block*-poly(styrene) by Combination of Atom Transfer Radical Polymerization and Click Cyclization. *Macromolecules* **2008**, *41*, 5082–5084.

8. Jia, Z.; Monteiro, M. J., Cyclic polymers: Methods and strategies. *J. Polym. Sci., Part A: Polym. Chem.* **2012**, *50*, 2085–2097.

9. Matyjaszewski, K., The synthesis of functional star copolymers as an illustration of the importance of controlling polymer structures in the design of new materials. *Polym. Int.* **2003**, *52*, 1559–1565.

10. Jha, S.; Dutta, S.; Bowden, N. B., Synthesis of Ultralarge Molecular Weight Bottlebrush Polymers Using Grubbs' Catalysts. *Macromolecules* **2004**, *37*, 4365–4374.

11. Sheiko, S. S.; Sumerlin, B. S.; Matyjaszewski, K., Cylindrical molecular brushes: Synthesis, characterization, and properties. *Prog. Polym. Sci.* **2008**, *33*, 759–785.

12. Radzinski, S. C.; Foster, J. C.; Scannelli, S. J.; Weaver, J. R.; Arrington, K. J.; Matson, J. B., Tapered Bottlebrush Polymers: Cone-shaped Nanostructures by Sequential Addition of Macromonomers. *ACS Macro Lett.* **2017**, *6*, 1175–1179.

13. Li, A.; Li, Z.; Zhang, S.; Sun, G.; Policarpio, D. M.; Wooley, K. L., Synthesis and Direct Visualization of Dumbbell-shaped Molecular Brushes. *ACS Macro Lett.* **2012**, *1*, 241–245.

14. Walsh, D. J.; Guironnet, D., Macromolecules with programmable shape, size, and chemistry. *Proc. Natl. Acad. Sci.* **2019**, *116*, 1538–1542.

15. Jenkins, A. D.; Kratochvíl, P.; Stepto, R. F. T.; Suter, U. W., Glossary of basic terms in polymer science (IUPAC Recommendations 1996). *Pure Appl. Chem.* **1996**, *68*, 2287–2311.

16. Szwarc, M., 'Living' Polymers. *Nature* **1956**, *178*, 1168–1169.
17. Matyjaszewski, K., Ranking living systems. *Macromolecules* **1993**, *26*, 1787–1788.
18. Grubbs, R. B.; Grubbs, R. H., 50th Anniversary Perspective: Living Polymerization—Emphasizing the Molecule in Macromolecules. *Macromolecules* **2017**, *50*, 6979–6997.
19. Matyjaszewski, K., Atom Transfer Radical Polymerization (ATRP): Current Status and Future Perspectives. *Macromolecules* **2012**, *45*, 4015–4039.
20. Keddie, D. J.; Moad, G.; Rizzardo, E.; Thang, S. H., RAFT Agent Design and Synthesis. *Macromolecules* **2012**, *45*, 5321–5342.
21. Bielawski, C. W.; Grubbs, R. H., Living ring-opening metathesis polymerization. *Prog. Polym. Sci.* **2007**, *32*, 1–29.
22. Bloch, S. E.; Scannelli, S. J.; Alaboalirat, M.; Matson, J. B., Complex Polymer Architectures Using Ring-opening Metathesis Polymerization: Synthesis, Applications, and Practical Considerations. *Macromolecules* **2022**, *55*, 4200–4227.
23. Hilf, S.; Kilbinger, A. F. M., Sacrificial Synthesis of Hydroxy–Telechelic Metathesis Polymers via Multiblock–Copolymers. *Macromolecules* **2009**, *42*, 1099–1106.
24. Liu, J.; Li, J.; Xie, M.; Ding, L.; Yang, D.; Zhang, L., A novel amphiphilic AB₂ star copolymer synthesized by the combination of ring-opening metathesis polymerization and atom transfer radical polymerization. *Polymer* **2009**, *50*, 5228–5235.
25. Choi, T.-L.; Grubbs, R. H., Controlled Living Ring-opening-Metathesis Polymerization by a Fast-Initiating Ruthenium Catalyst. *Angew. Chem* **2003**, *42*, 1743–1746.
26. Radzinski, S. C.; Foster, J. C.; Chapleski, R. C.; Troya, D.; Matson, J. B., Bottlebrush Polymer Synthesis by Ring-opening Metathesis Polymerization: The Significance of the Anchor Group. *J. Am. Chem. Soc.* **2016**, *138*, 6998–7004.

27. Slugovc, C.; Demel, S.; Riegler, S.; Hobisch, J.; Stelzer, F., The Resting State Makes the Difference: The Influence of the Anchor Group in the ROMP of Norbornene Derivatives. *Macromol. Rapid Commun.* **2004**, *25*, 475–480.
28. Pollino, J. M.; Stubbs, L. P.; Weck, M., Living ROMP of exo-norbornene Esters Possessing PdII SCS Pincer Complexes or Diaminopyridines. *Macromolecules* **2003**, *36*, 2230–2234.
29. Rule, J. D.; Moore, J. S., ROMP Reactivity of endo- and exo-Dicyclopentadiene. *Macromolecules* **2002**, *35*, 7878–7882.
30. Becke, A. D., Density-functional thermochemistry. III. The role of exact exchange. *J. Chem. Phys.* **1993**, *98*, 5648–5652.
31. Stephens, P. J.; Devlin, F. J.; Chabalowski, C. F.; Frisch, M. J., Ab Initio Calculation of Vibrational Absorption and Circular Dichroism Spectra Using Density Functional Force Fields. *J. Phys. Chem.* **1994**, *98*, 11623–11627.
32. Zhao, Y.; Truhlar, D. G., The M06 suite of density functionals for main group thermochemistry, thermochemical kinetics, noncovalent interactions, excited states, and transition elements: two new functionals and systematic testing of four M06-class functionals and 12 other functionals. *Theor. Chem. Acc.* **2008**, *120*, 215–241.
33. Weigend, F.; Ahlrichs, R., Balanced basis sets of split valence, triple zeta valence and quadruple zeta valence quality for H to Rn: Design and assessment of accuracy. *Phys. Chem. Chem. Phys.* **2005**, *7*, 3297–3305.
34. Walsh, D. J.; Lau, S. H.; Hyatt, M. G.; Guironnet, D., Kinetic Study of Living Ring-opening Metathesis Polymerization with Third-generation Grubbs Catalysts. *J. Am. Chem. Soc.* **2017**, *139*, 13644–13647.

35. Bielawski, C. W.; Grubbs, R. H., Highly Efficient Ring-opening Metathesis Polymerization (ROMP) Using New Ruthenium Catalysts Containing N-Heterocyclic Carbene Ligands. *Angew. Chem* **2000**, *39*, 2903–2906.
36. Hyatt, M. G.; Walsh, D. J.; Lord, R. L.; Andino Martinez, J. G.; Guironnet, D., Mechanistic and Kinetic Studies of the Ring Opening Metathesis Polymerization of Norbornenyl Monomers by a Grubbs Third Generation Catalyst. *J. Am. Chem. Soc.* **2019**, *141*, 17918–17925.
37. Suresh, C. H.; Koga, N., Orbital Interactions in the Ruthenium Olefin Metathesis Catalysts. *Organometallics* **2004**, *23*, 76–80.
38. Zografos, A.; Lynd, N. A.; Bates, F. S.; Hillmyer, M. A., Impact of Macromonomer Molar Mass and Feed Composition on Branch Distributions in Model Graft Copolymerizations. *ACS Macro Lett.* **2021**, *10*, 1622–1628.
39. Bloesch, S. E.; Alaboalirat, M.; Eades, C. B.; Scannelli, S. J.; Matson, J. B., Solvent Effects in Grafting-through Ring-opening Metathesis Polymerization. *Macromolecules* **2022**, *55*, 3522–3532.
40. Wolf, W. J.; Lin, T.-P.; Grubbs, R. H., Examining the Effects of Monomer and Catalyst Structure on the Mechanism of Ruthenium-catalyzed Ring-opening Metathesis Polymerization. *J. Am. Chem. Soc.* **2019**, *141*, 17796–17808.
41. Trnka, T. M.; Grubbs, R. H., The Development of L₂X₂RuCHR Olefin Metathesis Catalysts: An Organometallic Success Story. *Acc. Chem. Res.* **2001**, *34*, 18–29.
42. Jawiczuk, M.; Marczyk, A.; Trzaskowski, B., Decomposition of Ruthenium Olefin Metathesis Catalyst. *Catalysts* **2020**, *10*, 887.
43. O'Haver, T. *peakfit.m*, 8.2;
<https://www.mathworks.com/matlabcentral/fileexchange/23611-peakfit-M>, 2022.

44. Matos, J. M. E.; Lima–Neto, B. S., Benefits of donor solvents as additive on ROMP of norbornene catalyzed by amine Ru complexes. *J. Mol. Catal. A Chem.* **2005**, *240*, 233–238.
45. Foster, J. C.; Grocott, M. C.; Arkinstall, L. A.; Varlas, S.; Redding, M. J.; Grayson, S. M.; O'Reilly, R. K., It is Better with Salt: Aqueous Ring-opening Metathesis Polymerization at Neutral pH. *J. Am. Chem. Soc.* **2020**, *142*, 13878–13885.

2.8 Supporting Information

Materials and Methods:

All reagents and solvents were obtained from commercial vendors and used as received unless otherwise stated. CDCl₃ for all ROMPs was distilled at atmospheric pressure onto molecular sieves and was stored in a Strauss flask under nitrogen protected from light. ¹H NMR spectra for catalyst decomposition experiments were measured on either a Bruker 500 MHz spectrometer or Bruker 600 MHz spectrometer with a high ¹H sensitivity TCI Prodigy probe. The sweep width was adjusted to 8 to 22 ppm for spectra acquired on the Bruker 500 MHz spectrometer and –1 to 22 ppm for spectra acquired on the Bruker 600 MHz spectrometer for the catalyst decomposition experiments. Phenanthrene and anthracene were used as internal standards for decomposition studies of G1 and G3, respectively. NMR spectra for characterization of compounds and kinetic experiments were measured on an Agilent 400 MHz spectrometer, and spectra for chelation experiments were measured on the same Bruker 500 MHz spectrometer. ¹H and ¹³C NMR chemical shifts are reported in ppm relative to internal solvent resonances unless otherwise stated. Yields refer to compounds as isolated after requisite purification unless otherwise stated. A Biotage Selekt flash purification system was used for automated silica gel column purification.

Silica used for automated flash chromatography purifications was ZEOCHEM ZEOprep 60 HYD 40–63 μM pore size. Thin-layer chromatography (TLC) was performed on glass-backed silica plates and visualized by UV. High-resolution mass spectra were analyzed by flow injection analysis using a Shimadzu 9030 QTOF mass spectrometer interfaced with a Shimadzu 40 series UPLC. Size exclusion chromatography (SEC) was carried out in THF at 1 mL min^{-1} at $30\text{ }^\circ\text{C}$ on two Agilent PLgel $10\text{ }\mu\text{m}$ MIXED-B columns connected in series with a Wyatt Dawn Heleos 2 light scattering detector and a Wyatt Optilab Rex refractive index detector. No calibration standards were used, and dn/dc values were obtained by assuming 100% mass elution from the columns.

Preparation of Grubbs' 3rd generation catalyst (G3)

Grubbs' 3rd generation catalyst (G3) was prepared freshly and used within 2–3 days following a modified version of published methods.^{1–2} First, pyridine and pentane were purified via passage through a short column of basic alumina. A one dram vial was charged with a stir bar and 20 mg of Grubbs' 2nd generation catalyst ($\text{H}_2\text{IMes})(\text{PCy}_3)(\text{Cl})_2\text{Ru}=\text{CHPh}$). Next, purified pyridine (20 mL) was added to the vial, and the reaction mixture was stirred vigorously for 20–30 min until it had turned a vivid lime-green color. If the reaction mixture dried to a solid, additional pyridine (10 μL increments) was added, and solids were broken up manually with a spatula to allow for more stirring. Next, purified pentane (3 mL) was added to the vial to precipitate the catalyst. The pentane was decanted off and the solids were washed with additional purified pentane (3 mL). Once again, the pentane was decanted off and the remaining solids were dried by blowing air over the vial for 1 min, then transferred to a clean vial, and then dried under vacuum overnight.

Theoretical Calculations

All density functional theory calculations were performed using the Gaussian 09³ suite of software. The B3LYP functional and 6-31G(d) basis set were used to optimize the geometries of all 61 anchor groups considered, in the gas phase and with a standard integration grid. The M06-2X functional and def2-TZVP basis set were used to optimize the geometry of the 8 monomers for which measurements were carried out. The M06-2X calculations used an ultrafine integration grid and were performed using PCM solvation (chloroform). HOMO energies were obtained with the optimum structures.

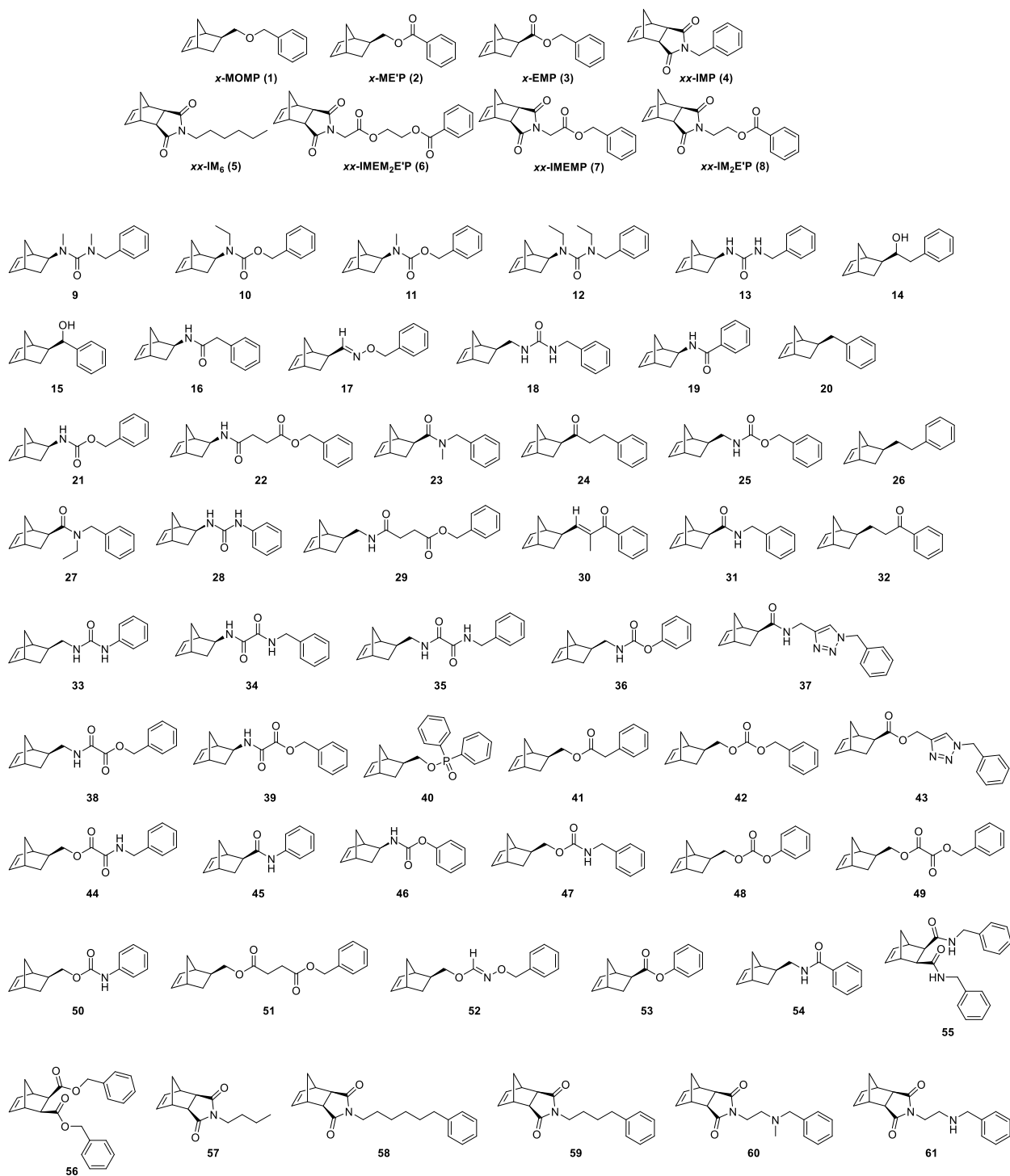
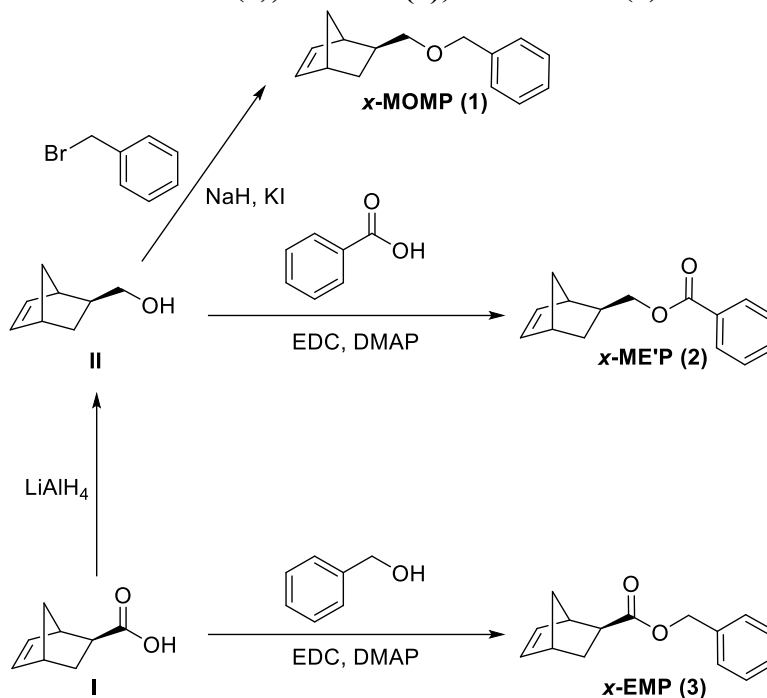


Figure S1. Chemical structures of the 61 monomers used in the HOMO energy calculations.

Table S1. HOMO energies (kcal/mol) of 61 monomers (B3LYP/6–31G* level)

Anchor Group	HOMO Energy (kcal/mol)	Anchor Group	HOMO Energy (kcal/mol)
<i>x</i> -MOMP (1)	–145	32	–146
<i>x</i> -ME'P (2)	–149	33	–147
<i>x</i> -EMP (3)	–148	34	–147
<i>xx</i> -IMP (4)	–158	35	–147
<i>xx</i> -IM ₆ (5)	–157	36	–147
<i>xx</i> -IMEM ₂ E'P (6)	–158	37	–147
<i>xx</i> -IMEMP (7)	–155	38	–147
<i>xx</i> -IM ₂ E'P (8)	–159	39	–148
9	–136	40	–148
10	–138	41	–148
11	–139	42	–148
12	–140	43	–149
13	–140	44	–149
14	–142	45	–149
15	–142	46	–149
16	–142	47	–149
17	–142	48	–149
18	–143	49	–149
19	–143	50	–149
20	–143	51	–149
21	–144	52	–150
22	–144	53	–150
23	–144	54	–150
24	–145	55	–151
25	–145	56	–151
26	–145	57	–157
27	–145	58	–157
28	–145	59	–157
29	–145	60	–158
30	–146	61	–158
31	–146		

Synthesis of Monomers *x*-MOMP (1), *x*-ME'P (2), and *x*-EMP (3)



Exo-5-norbornene-2-carboxylic acid (I)

Compound I, *exo*-5-norbornene-2-carboxylic acid was prepared according to a previously reported procedure.⁴ ¹H NMR (CDCl₃): δ 6.13 (m, 2H), 3.11 (s, 1H), 2.94 (s, 1H), 2.27 (m, 1H), 1.95 (m, 1H), 1.54 (d, *J* = 8 Hz, 1H), 1.41 (m, 2H). ¹³C NMR (CDCl₃): δ 182.77, 138.28, 135.85, 46.84, 46.54, 43.26, 41.81, 30.47. Both ¹H and ¹³C NMR spectra matched literature values.

Exo-5-norbornene-2-Methanol (II)

Compound II, *exo*-5-norbornene-2-Methanol was prepared according to a previously reported procedure.⁵ ¹H NMR (CDCl₃): δ 6.08 (m, 2H), 3.70 (m, 1H), 3.54 (m, 1H), 2.82 (s, 1H), 2.74 (s, 1H), 1.64 (m, 1H), 1.30 (m, 3H), 1.11 (m, 1H). ¹³C NMR (CDCl₃): δ 136.91, 136.57, 67.65, 45.08, 43.38, 41.99, 41.63, 29.64. Both ¹H and ¹³C NMR spectra matched literature values.

Monomer *x*-MOMP (1)

A flame-dried round-bottom flask was charged with NaH (0.106 g, 4.43 mmol), KI (66.8 mg, 0.403 mmol), and dry THF (20 mL). The flask was placed in an ice bath and stirred for 5 min to allow the reaction mixture to cool. Compound **II** (0.500 g, 4.03 mmol) was added to the round-bottom flask and allowed to dissolve for 5 min before benzyl bromide (0.717 mL, 6.04 mmol) was added. The reaction mixture was stirred overnight, allowing the ice to melt and the contents of the flask to warm to rt. The reaction was monitored by TLC (CH₂Cl₂, visualization by a potassium permanganate stain) until compound **II** was completely consumed, then the reaction mixture was placed in an ice bath again and quenched with water (10 mL). The reaction mixture was transferred to a separatory funnel, and the organic layer was separated and washed with brine (10 mL), dried over Na₂SO₄, and concentrated by rotary evaporation. The crude mixture was purified by automated flash chromatography on silica with hexanes as the mobile phase to yield a colorless oil (0.35 g, 40% yield). ¹H NMR (CDCl₃): δ 7.43–7.24 (m, 5H), 6.15–6.03 (m, 2H), 4.54 (s, 2H), 3.53 (m, 1H), 3.38 (t, *J* = 9.0 Hz, 1H), 2.79 (m, 2H), 1.79–1.69 (m, 1H), 1.36–1.22 (m, 4H), 1.17–1.09 (m, 1H). ¹³C NMR (CDCl₃): δ 138.44, 136.37, 136.35, 128.08, 127.32, 127.21, 44.76, 43.51, 41.28, 38.67, 29.48. Both ¹H and ¹³C NMR spectra matched literature values.⁶

Representative EDC Coupling (used in synthesis of monomers *x*-ME'P (2), *x*-EMP (3), *xx*-IMEM2E'P (6), *xx*-IMEMP (7), and *xx*-IM2E'P (8))

A typical EDC coupling procedure is as follows: Benzoic acid (1.28 g, 10.5 mmol) and EDC (1.63 g, 10.5 mmol) were dissolved in CH₂Cl₂ (25 mL) in a round-bottom flask equipped with a stir bar. The reaction mixture was stirred until the solids had completely dissolved (~5 min).

Meanwhile, a second flask was charged with compound **II** (1.00 g, 8.05 mmol), DMAP (0.492 g, 4.03 mmol) and CH₂Cl₂ (25 mL). This second solution was added dropwise to the flask containing the benzoic acid/EDC solution via an addition funnel while stirring. The reaction mixture was stirred at rt until complete consumption of the starting material (compound **II** here) was observed by TLC, typically around 12 h. The reaction mixture was then transferred to a separatory funnel, washed with water (2 x 20 mL) and brine (20 mL), dried over Na₂SO₄, and concentrated by rotary evaporation. Crude products were purified as detailed below.

Monomer *x*-ME'P (2)

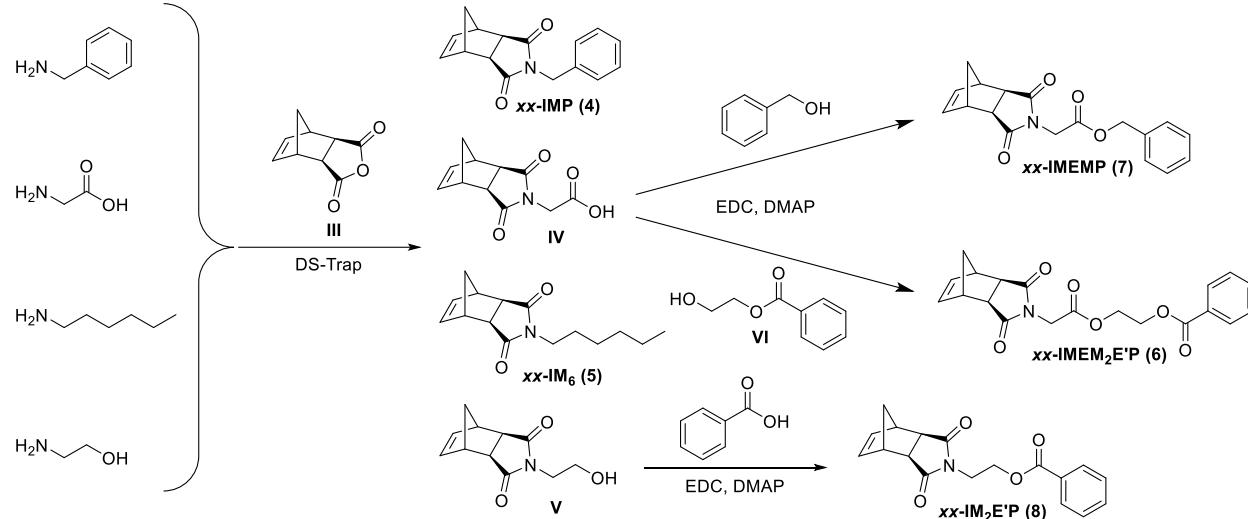
Monomer *x*-ME'P (**2**) was synthesized as described above in the Representative EDC Coupling procedure. The reaction was monitored by TLC (CH₂Cl₂, visualization by a potassium permanganate stain) until compound **II** was completely consumed. The concentrated crude product was purified by automated flash chromatography on silica, eluting with 5% EtOAc in hexanes. The product was obtained as a colorless oil (0.96 g, 52% yield). ¹H NMR (CDCl₃): δ 8.11–8.02 (m, 2H), 7.60–7.53 (m, 1H), 7.49–7.40 (m, 2H), 6.12 (m, 2H), 4.42 (m, 1H), 4.22 (m, 1H), 2.91–2.78 (m, 2H), 1.96–1.83 (m, 1H), 1.45–1.22 (m, 5H). ¹³C NMR (CDCl₃): δ 166.38, 136.72, 135.98, 132.58, 130.21, 129.31, 128.08, 68.74, 44.75, 43.46, 41.37, 37.84, 29.33. Both ¹H and ¹³C NMR spectra matched literature values.⁷

Monomer *x*-EMP (3)

Monomer *x*-EMP (**3**) was synthesized as described above in the Representative EDC Coupling procedure. The reaction was monitored by TLC (CH₂Cl₂, visualization by a potassium permanganate stain) until compound **I** was completely consumed. The concentrated crude

product was purified by automated flash chromatography on silica, eluting with 5% EtOAc in hexanes to give the pure product as a colorless oil (0.88 g, 53% yield). ^1H NMR (CDCl_3): δ 7.42–7.29 (m, 5H), 6.17–6.08 (m, 2H), 5.14 (d, $J = 0.7$ Hz, 2H), 3.08 (s, 1H), 2.93 (s, 1H), 2.33–2.26 (m, 1H), 1.96 (m, 1H), 1.55 (m, 1H), 1.44–1.34 (m, 2H). ^{13}C NMR (CDCl_3): δ 175.76, 137.82, 136.04, 135.46, 128.28, 127.81, 65.96, 46.38, 46.11, 42.92, 41.40, 30.12. Both ^1H and ^{13}C NMR spectra matched literature values.⁸

Synthesis of Monomers *xx*-IMP (4), *xx*-IMEMP (5), *xx*-IM₆ (6), *xx*-IMEM₂E'P (7), and *xx*-IM₂E'P (8)



Exo-Carbic anhydride (III)

Compound **III**, *exo*-norbornene anhydride (carbic anhydride) was prepared from *endo*-carbic anhydride according to a previously reported procedure.⁹ ^1H NMR (CDCl_3): δ 6.33 (t, $J = 1.9$ Hz, 2H), 3.26 (m, 2H), 3.06 (d, $J = 1.6$ Hz, 2H), 1.49 (m, 1H), 1.28 (m, 1H). ^{13}C NMR (CDCl_3): δ 179.02, 137.83, 49.34, 45.22, 43.01. Both ^1H and ^{13}C NMR spectra matched literature values.

Monomer *xx*-IMP (4)

A round-bottom flask was charged with compound **III** (2.00 g, 12.2 mmol), benzylamine (1.57 g, 14.6 mmol), and toluene (50 mL). The flask was affixed with a Dean–Stark trap and condenser then heated at reflux for 24 h. The reaction was monitored by TLC (50% CH₂Cl₂ in hexanes, visualization by a potassium permanganate stain) until compound **III** was completely consumed. The reaction mixture was cooled and transferred to a separatory funnel. The organic solution was diluted with additional toluene, and washed with 1N HCl (2 x 50 mL) and brine (50 mL). The organic layer was then removed and dried over Na₂SO₄, then concentrated by rotary evaporation to give the pure product as a white solid (1.86 g, 79% yield). ¹H NMR (CDCl₃): δ 7.43–7.23 (m, 5H), 6.27 (t, *J* = 1.9 Hz, 2H), 4.62 (s, 2H), 3.25 (m, 2H), 2.68 (d, *J* = 1.4 Hz, 2H), 1.44–1.38 (m, 1H), 1.06 (m, 1H). ¹³C NMR (CDCl₃): δ 177.36, 137.65, 135.68, 128.62, 128.37, 127.64, 47.53, 45.04, 42.36, 42.09. Both ¹H and ¹³C NMR spectra matched literature values.¹⁰

Compound IV

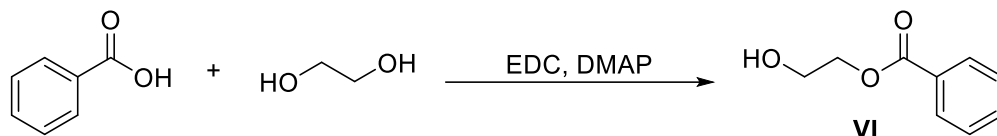
Compound **IV** was prepared according to a previously reported procedure.¹¹ ¹H NMR (CDCl₃): δ 8.80 (s, 1H), 6.30 (t, *J* = 1.9 Hz, 2H), 4.26 (s, 2H), 3.30 (m, 2H), 2.76 (d, *J* = 1.4 Hz, 2H), 1.64 – 1.57 (m, 1H), 1.50 (m, 1H). ¹³C NMR (CDCl₃): δ 177.54, 172.28, 138.32, 48.37, 45.75, 43.18, 39.45. Both ¹H and ¹³C NMR spectra matched literature values.

Compound V

Compound **V** was prepared according to a previously reported procedure.¹² ¹H NMR (CDCl₃): δ 6.27 (m, 2H), 3.74 (m, 2H), 3.67 (m, 2H), 3.25 (s, 2H), 2.69 (s, 2H), 2.45 (s, 1H), 1.49 (m, 1H),

1.33 (m, 1H). ^{13}C NMR (CDCl_3): δ 178.71, 137.76, 59.85, 47.84, 45.26, 42.79, 41.21. Both ^1H and ^{13}C NMR spectra matched literature values.

Compound VI



Compound **VI** was synthesized as described above in the Representative EDC Coupling procedure. The reaction was monitored by TLC (CH_2Cl_2 , visualization by I_2) until benzoic acid was completely consumed. The concentrated crude product was purified by automated flash chromatography on silica, eluting with 25% to 50% EtOAc in hexanes to give the pure product as a colorless oil. ^1H NMR (CDCl_3): δ 8.08–8.02 (m, 2H), 7.59–7.53 (m, 1H), 7.44 (m, 2H), 4.48–4.43 (m, 2H), 3.98–3.92 (m, 2H), 2.33 (s, 1H). ^{13}C NMR (CDCl_3): δ 167.10, 133.30, 129.97, 129.80, 128.53, 66.78, 61.51. Both ^1H and ^{13}C NMR spectra matched literature values.¹³

Monomer *xx-IM*₆ (**5**)

A round-bottom flask was charged with compound **III** (1.00 g, 6.09 mmol), hexylamine (0.97 mL, 7.31 mmol), and toluene (20 mL). The flask was affixed with a Dean–Stark trap and condenser then heated at reflux for 24 h. The reaction was monitored by TLC (50% CH_2Cl_2 in hexanes, visualization by potassium permanganate) until compound **III** was completely consumed. The reaction mixture was cooled and transferred to a separatory funnel. The organic solution was diluted with additional toluene, washed with 1N HCl (2 x 50 mL) and brine (50 mL), dried over Na_2SO_4 , and concentrated by rotary evaporation to give the pure product as a colorless oil (1.2 g, 79% yield). ^1H NMR (CDCl_3): δ 6.27 (t, $J = 1.9$ Hz, 2H), 3.48–3.39 (m, 2H),

3.26 (m, 2H), 2.66 (d, $J = 1.4$ Hz, 2H), 1.59–1.45 (m, 3H), 1.33–1.20 (m, 7H), 0.90–0.81 (m, 3H). ^{13}C NMR (CDCl_3): δ 177.80, 137.55, 47.53, 44.91, 42.42, 38.49, 31.05, 27.46, 26.35, 22.20, 13.69. Both ^1H and ^{13}C NMR spectra matched literature values.¹⁴

Monomer *xx*-IMEM₂E'P (6)

Monomer *xx*-IMEM₂E'P (6) was synthesized as described above in the Representative EDC Coupling procedure. The reaction was monitored by TLC (50% CH_2Cl_2 in hexanes, visualization by potassium permanganate) until compound **IV** was completely consumed. The concentrated crude product was purified by automated flash chromatography on silica, eluting with 2.5% EtOAc in hexanes to give the pure product as a white solid (0.73 g, 44% yield). ^1H NMR (CDCl_3): δ 8.06–8.00 (m, 2H), 7.62–7.54 (m, 1H), 7.49–7.42 (m, 2H), 6.28 (t, $J = 1.9$ Hz, 2H), 4.54–4.45 (m, 4H), 4.28 (s, 2H), 3.27 (m, 2H), 2.73 (d, $J = 1.4$ Hz, 2H), 1.67 (m, 1H), 1.48 (m, 1H). ^{13}C NMR (CDCl_3): δ 176.73, 166.56, 165.96, 137.68, 132.94, 129.52, 129.37, 128.16, 63.23, 61.99, 47.74, 45.16, 42.54, 39.06. HR-MS calculated for $\text{C}_{20}\text{H}_{19}\text{NO}_6$ $[\text{M} + \text{Na}]^+$ 392.1105; found 392.1048.

Monomer *xx*-IMEMP (7)

Monomer *xx*-IMEMP (7) was synthesized as described above in the Representative EDC Coupling procedure. The reaction was monitored by TLC (50% CH_2Cl_2 in hexanes, visualization by potassium permanganate) until compound **IV** was completely consumed. The concentrated crude product was purified by automated flash chromatography on silica, eluting with 2.5% EtOAc in hexanes to give the pure product as a colorless oil (0.38 g, 50% yield). ^1H NMR (CDCl_3): δ 7.43–7.29 (m, 5H), 6.34–6.26 (m, 2H), 5.16 (s, 2H), 4.28 (s, 2H), 3.29 (m, 2H), 2.74

(d, $J = 1.4$ Hz, 2H), 1.64 (m, 1H), 1.43 (m, 1H). ^{13}C NMR (CDCl_3): δ 176.80, 166.47, 137.69, 134.54, 128.38, 128.34, 128.20, 67.39, 47.74, 45.16, 42.54, 39.24. HR-MS calculated for $\text{C}_{18}\text{H}_{17}\text{NO}_4$ $[\text{M} + \text{H}]^+$ 312.1230; found 312.1248.

Monomer *xx*-IM₂E'P (8)

Monomer *xx*-IM₂E'P (8) was synthesized as described above in the Representative EDC Coupling procedure. The reaction was monitored by TLC (50% CH_2Cl_2 in hexanes, visualization by potassium permanganate) until compound **V** was completely consumed. The concentrated crude product was purified by flash chromatography on silica, eluting with 2.5% EtOAc in hexanes to give the pure product as a white solid (0.82g, 52% yield). ^1H NMR (CDCl_3): δ 7.99–7.94 (m, 2H), 7.58–7.52 (m, 1H), 7.43 (m, 2H), 6.27 (t, $J = 1.9$ Hz, 2H), 4.48–4.43 (m, 2H), 3.92 (m, 2H), 3.25 (m, 2H), 2.71 (d, $J = 1.4$ Hz, 2H), 1.43 (m, 1H), 1.27 (m, 1H). ^{13}C NMR (CDCl_3): δ 177.46, 165.92, 137.51, 132.85, 129.40, 128.12, 128.04, 61.25, 47.56, 44.98, 42.38, 37.22. HR-MS calculated for $\text{C}_{18}\text{H}_{17}\text{NO}_4$ $[\text{M} + \text{Na}]^+$ 334.1050; found 334.0996.

NMR Kinetic experiments on anchor group monomers

A representative synthesis is as follows: Monomer (40 mg) was dissolved in CDCl_3 in a vial equipped with a stir bar. A stock solution of **G3** in CDCl_3 was made, and 0.1 mL of this solution (to achieve 1 equiv with respect to monomer) was then added rapidly to the first vial to make the final concentration of monomer = 20 mM. Polymerizations were conducted under air with capping of the vials in between aliquot removal steps. Aliquots (0.50 mL) were withdrawn periodically via micropipette at pre-determined timepoints and added to 1.5 mL Eppendorf microcentrifuge tubes containing 0.1 mL CDCl_3 and ethyl vinyl ether (2 μL) to terminate the

polymerizations. Each aliquot was then analyzed by ^1H NMR spectroscopy. Kinetic parameters were obtained from a conversion vs. time plot.

Monomer Characterization:

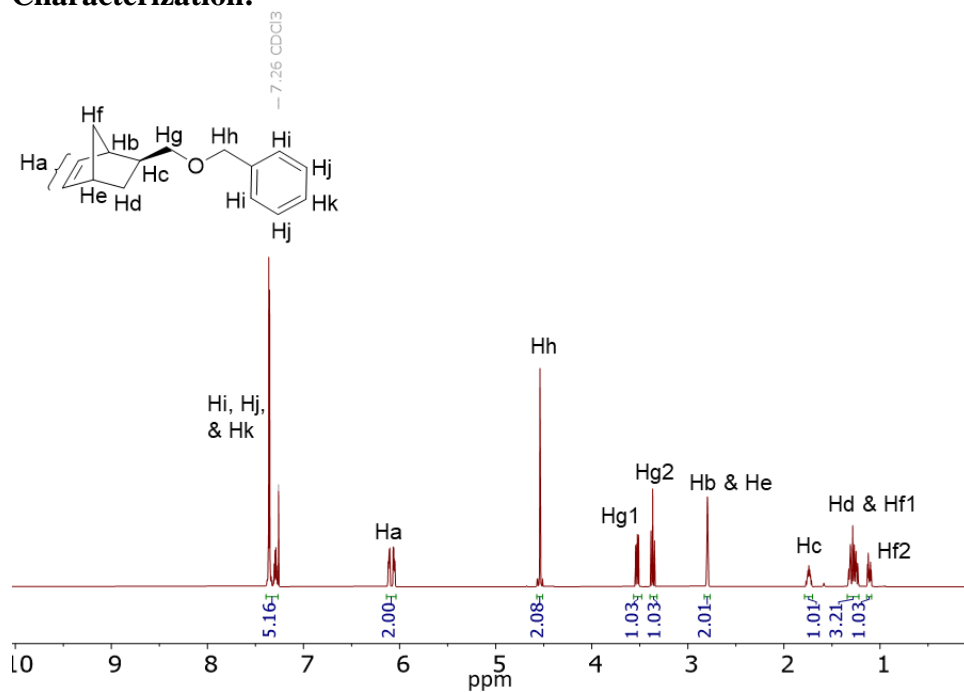


Figure S2. ^1H NMR spectrum of monomer *x*-MOMP (1).

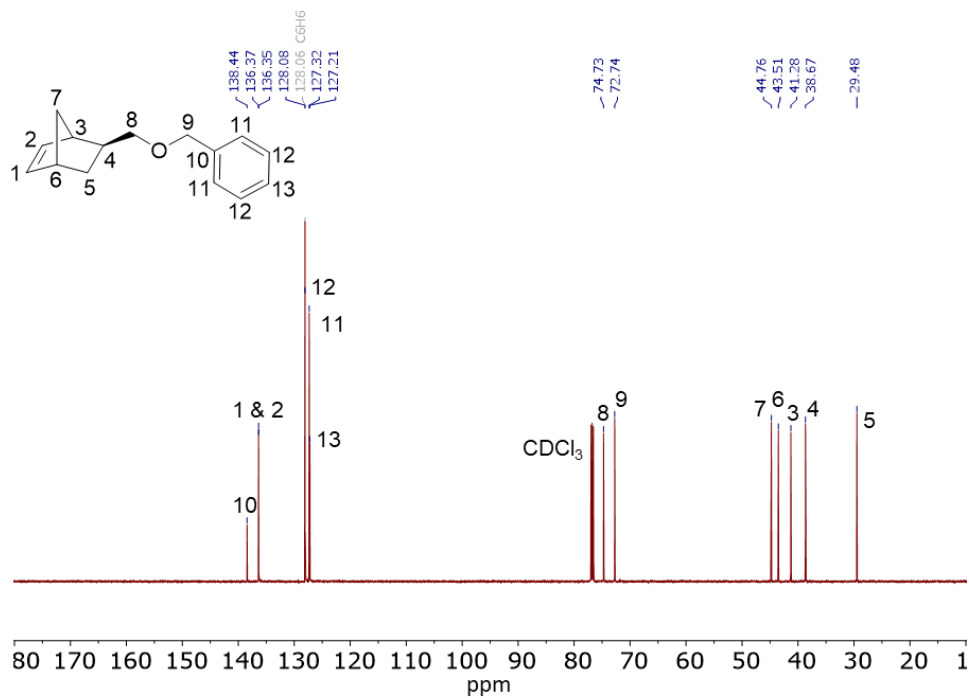


Figure S3. ¹³C NMR spectrum of monomer *x*-MOMP (1). Benzene was added as an internal standard, and the spectrum was aligned to the C₆H₆ reference peak.

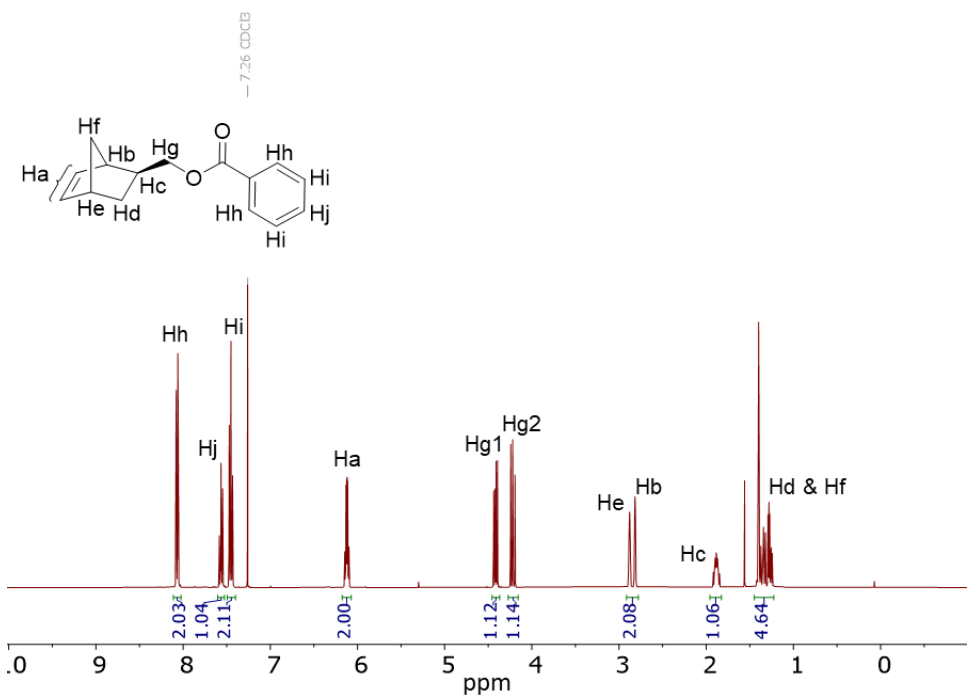


Figure S4. ¹H NMR spectrum of monomer *x*-ME'P (2).

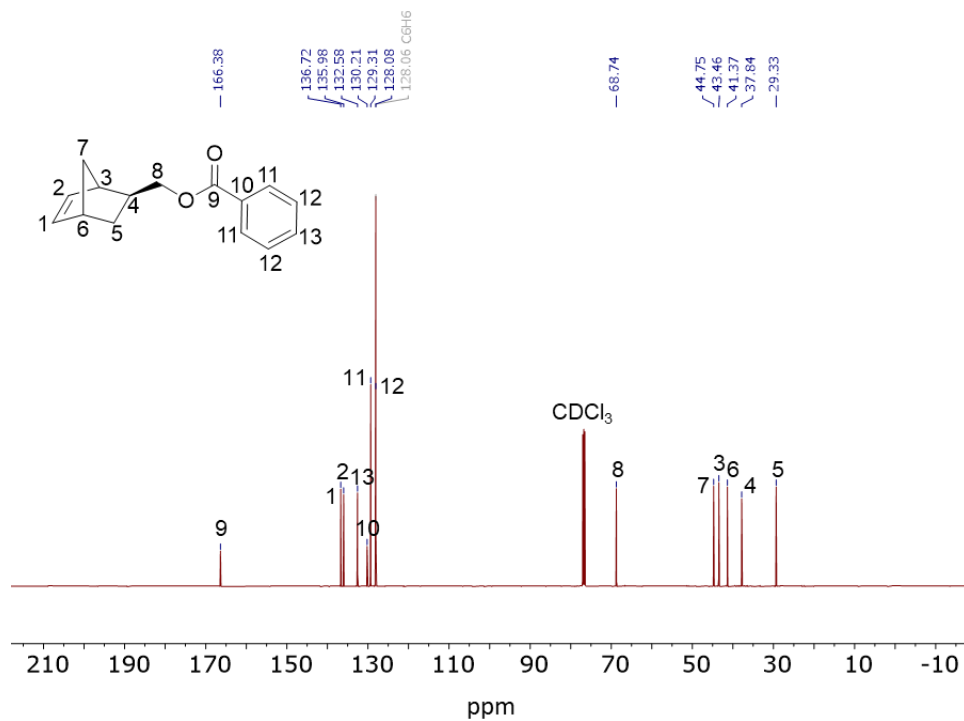


Figure S5. ¹³C NMR spectrum of monomer *x*-ME'P (2). Benzene was added as an internal standard, and the spectrum was aligned to the C₆H₆ reference peak.

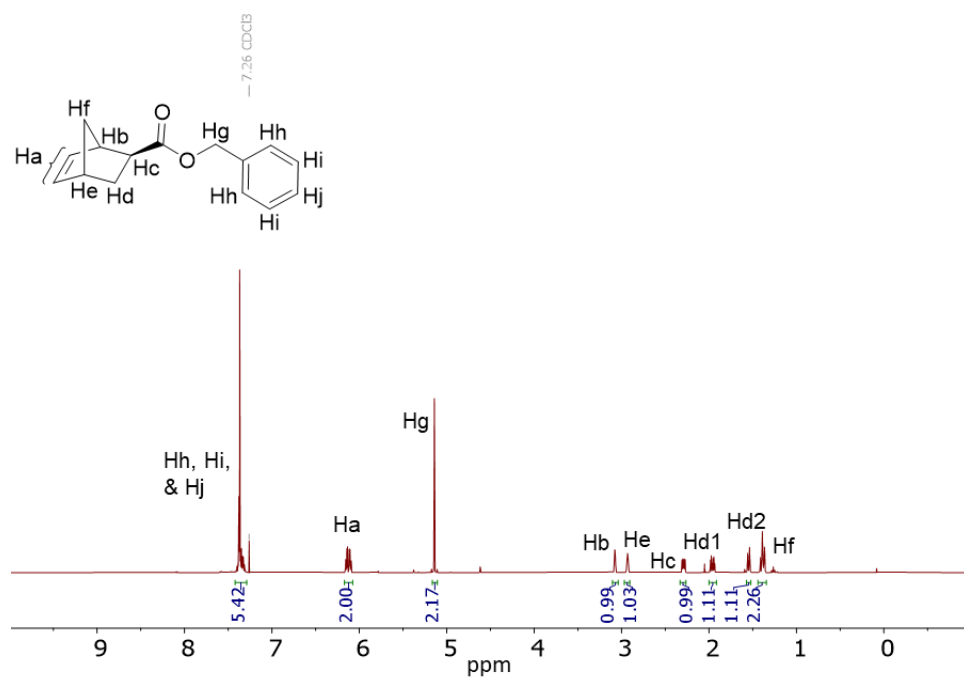


Figure S6. ¹H NMR spectrum of monomer *x*-EMP (3).

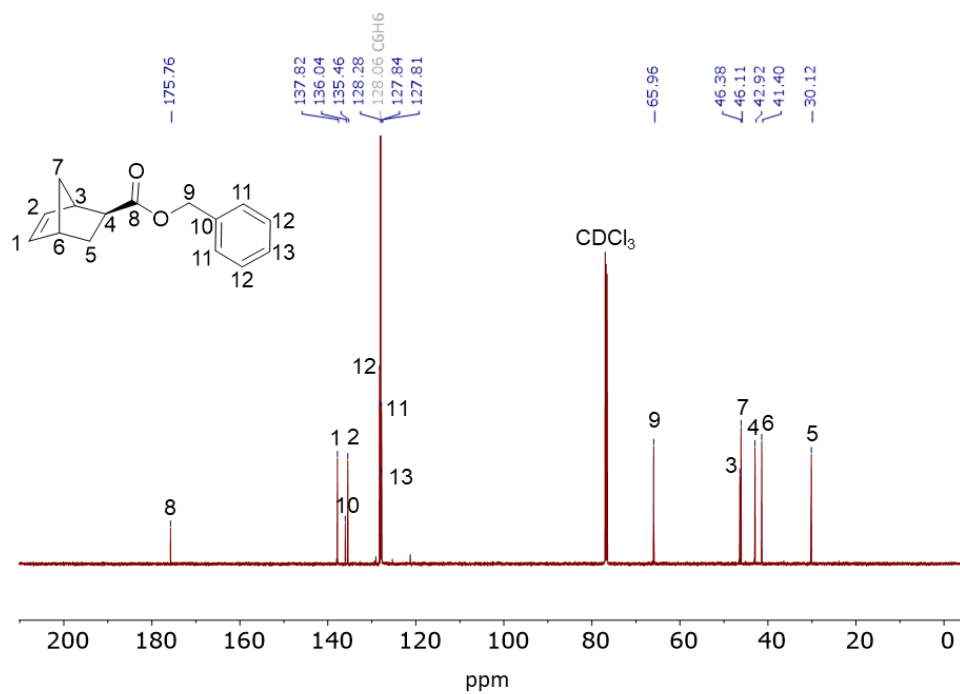


Figure S7. ¹³C NMR spectrum of monomer *x*-EMP (3). Benzene was added as an internal standard, and the spectrum was aligned to the C₆H₆ reference peak.

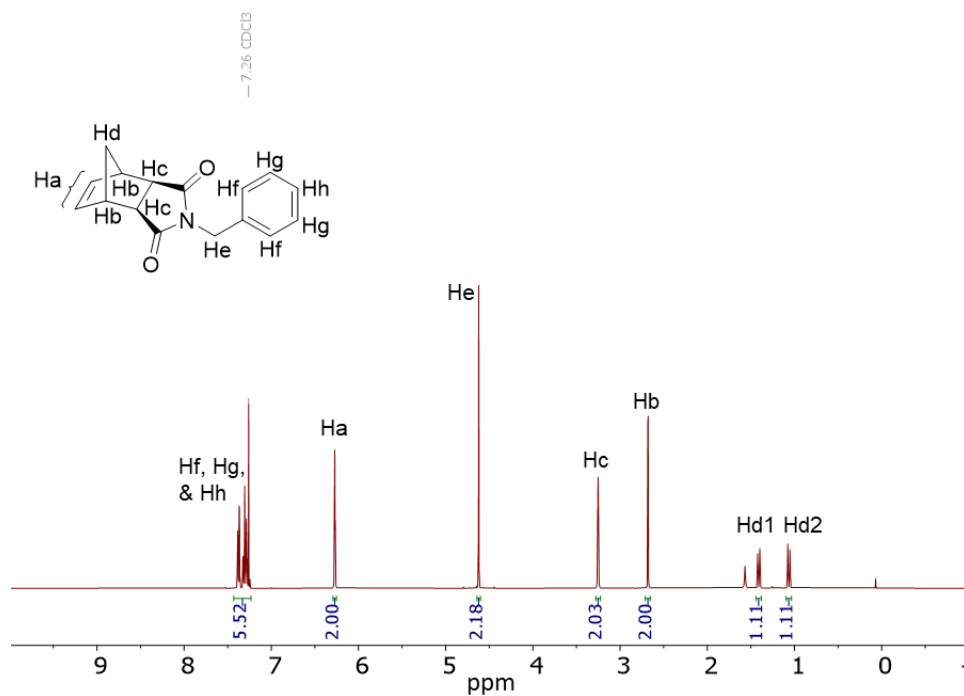


Figure S8. ¹H NMR spectrum of monomer *xx*-IMP (4).

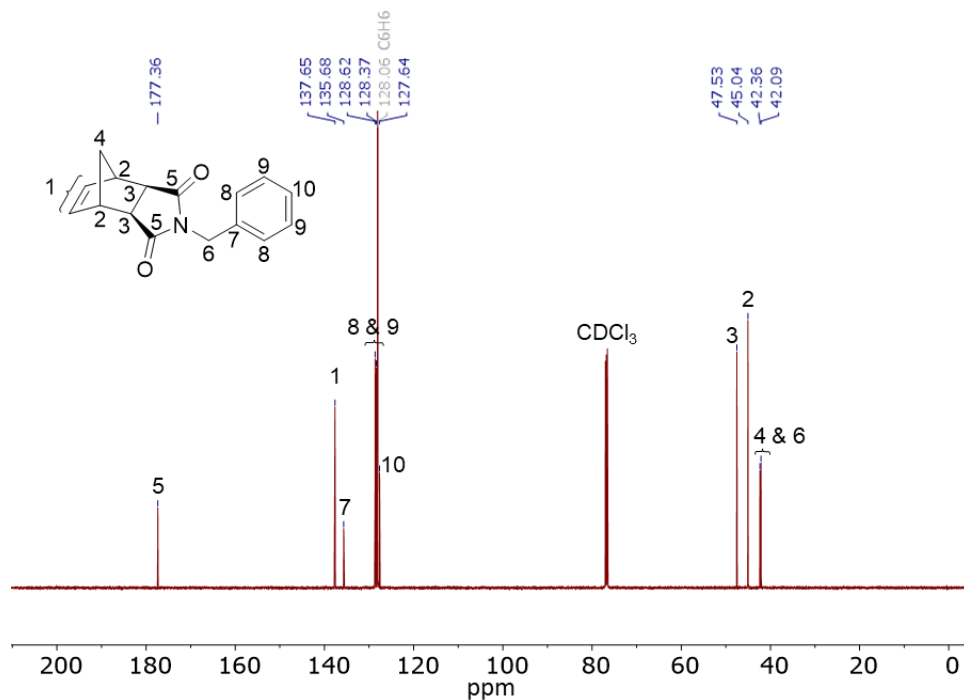


Figure S9. ^{13}C NMR spectrum of monomer *xx*-IMP (**4**). Benzene was added as an internal standard, and the spectrum was aligned to the C_6H_6 reference peak.

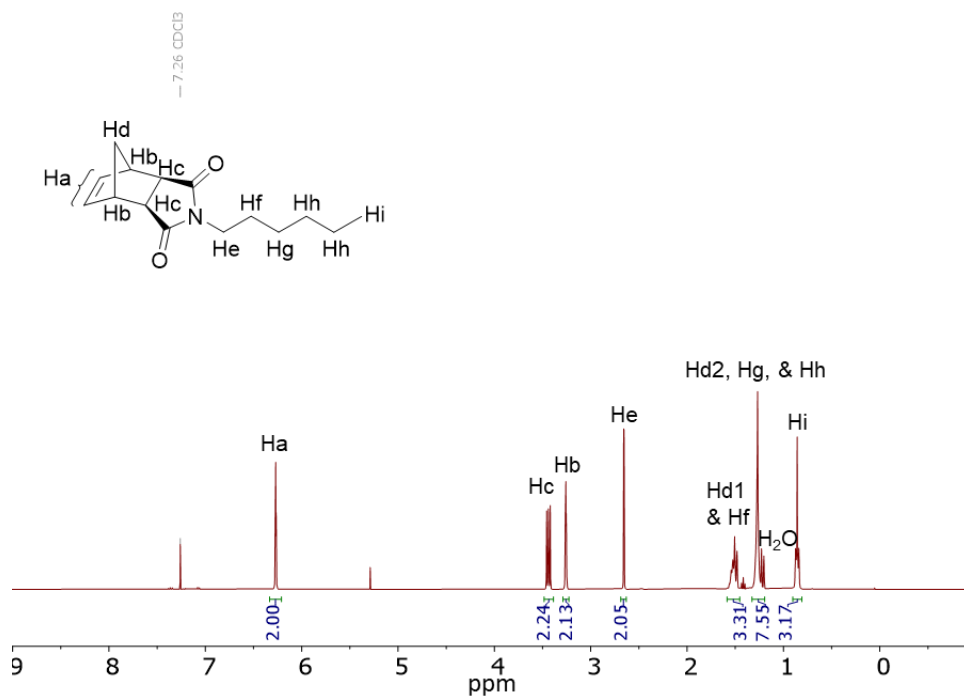


Figure S10. ^1H NMR spectrum of monomer *xx*-IM₆ (**5**).

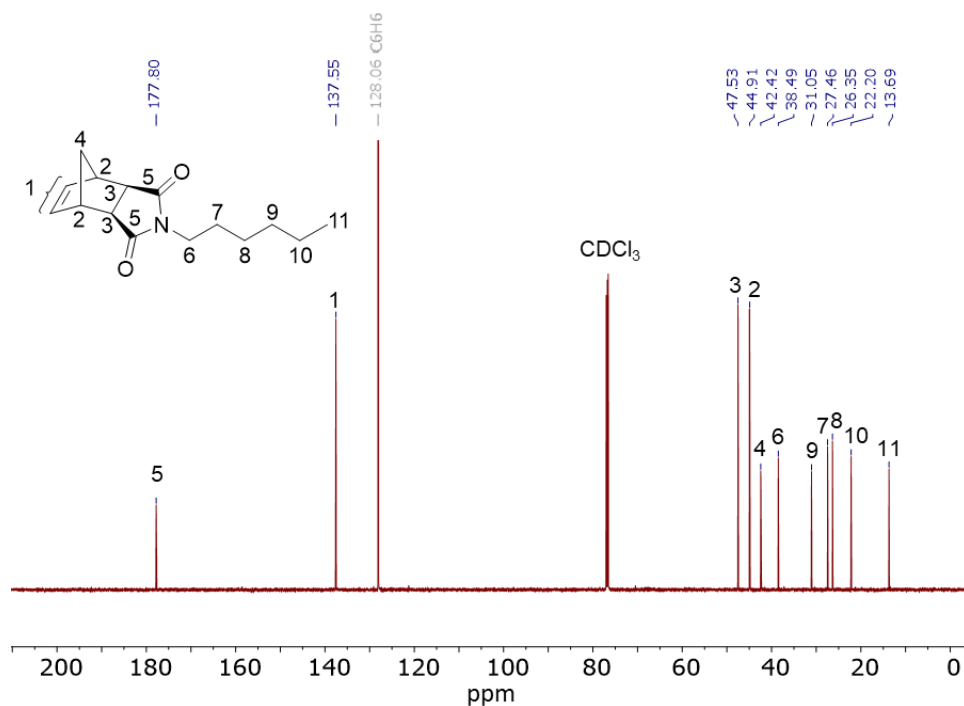


Figure S11. ¹³C NMR spectrum of monomer *xx*-IM₆ (5). Benzene was added as an internal standard, and the spectrum was aligned to the C₆H₆ reference peak.

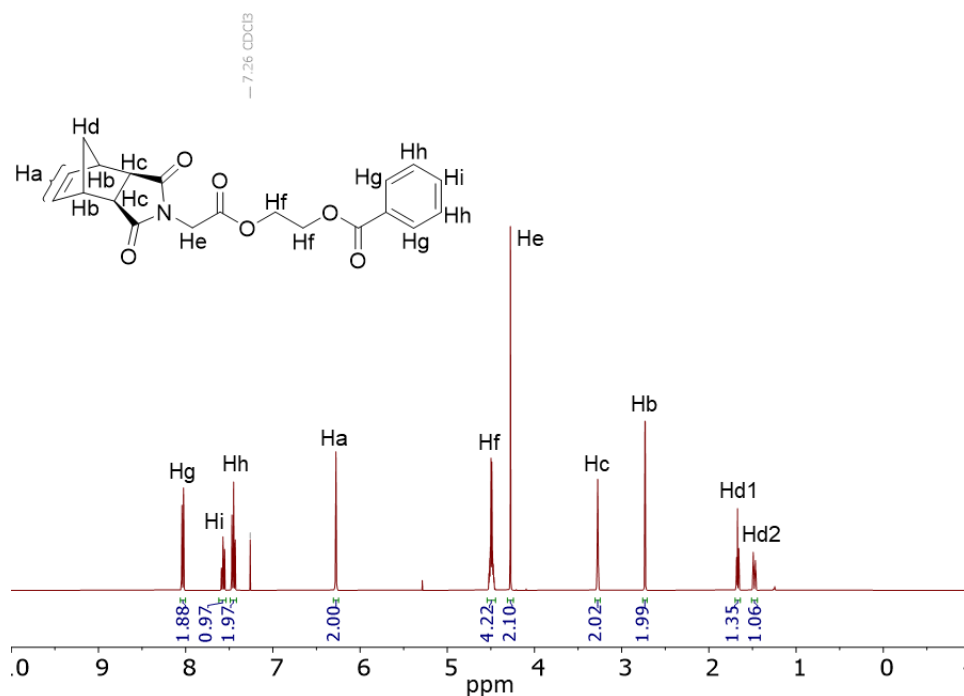
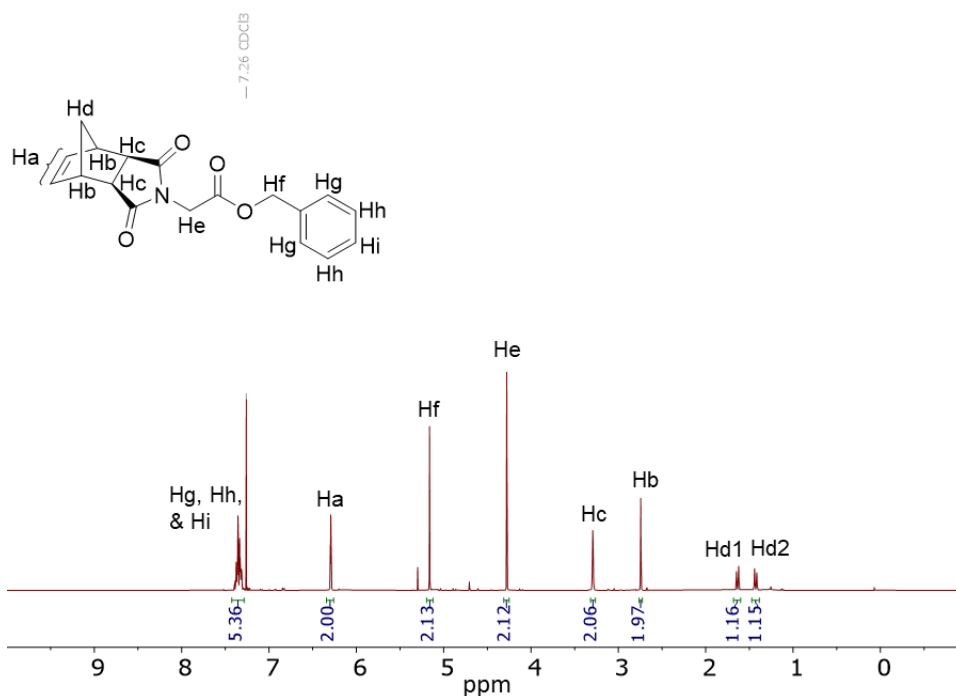
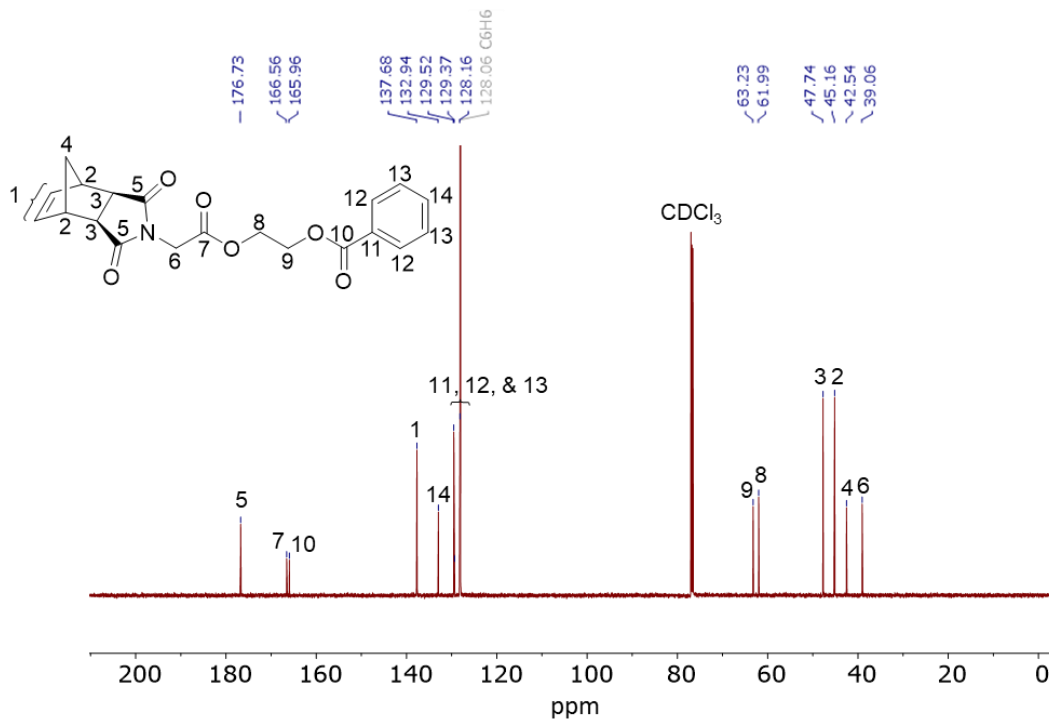


Figure S12. ¹H NMR spectrum of monomer *xx*-IMEM₂E'P (6).



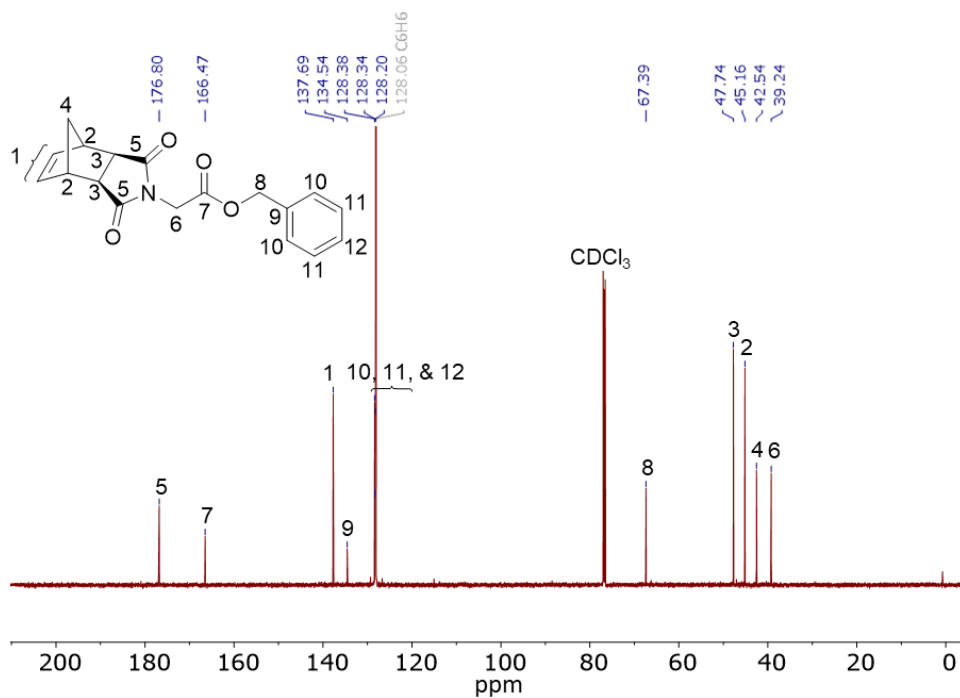


Figure S15. ¹³C NMR spectrum of monomer *xx*-IMEMP (**7**). Benzene was added as an internal standard, and the spectrum was aligned to the C₆H₆ reference peak.

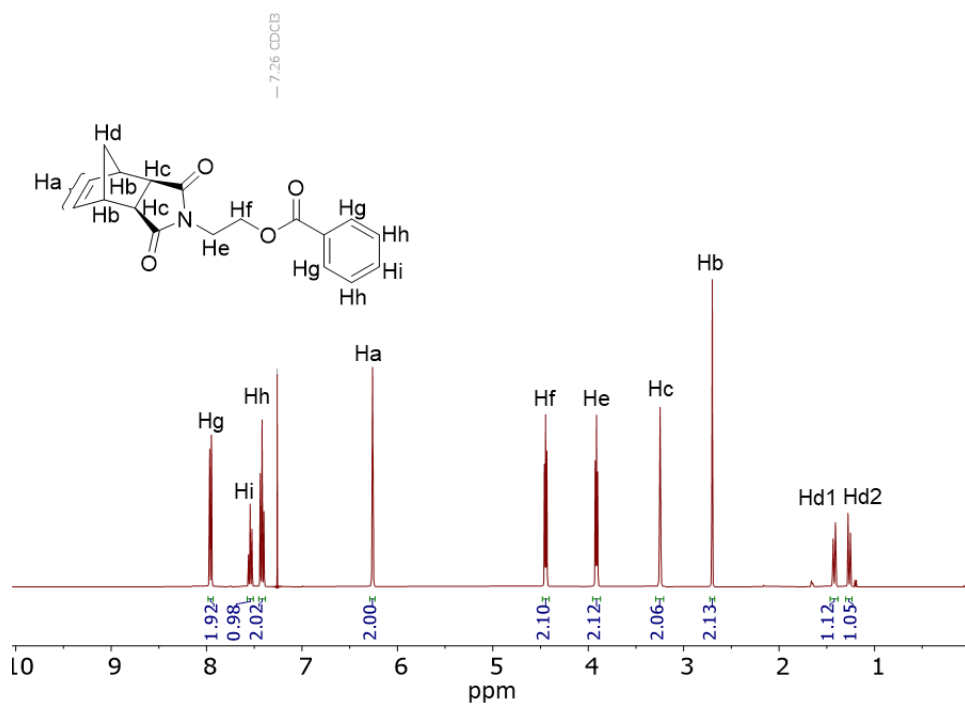


Figure S16. ¹H NMR spectrum of monomer *xx*-IM₂E'P (**8**).

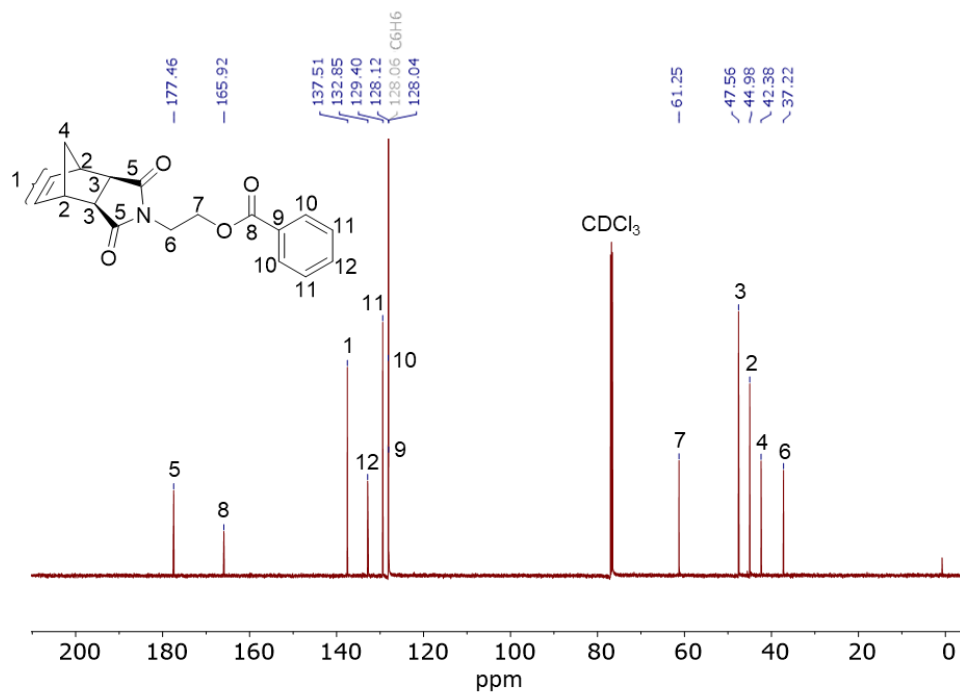


Figure S17. ¹³C NMR spectrum of monomer α -IM₂E'P (**8**). Benzene was added as an internal standard, and the spectrum was aligned to the C₆H₆ reference peak.

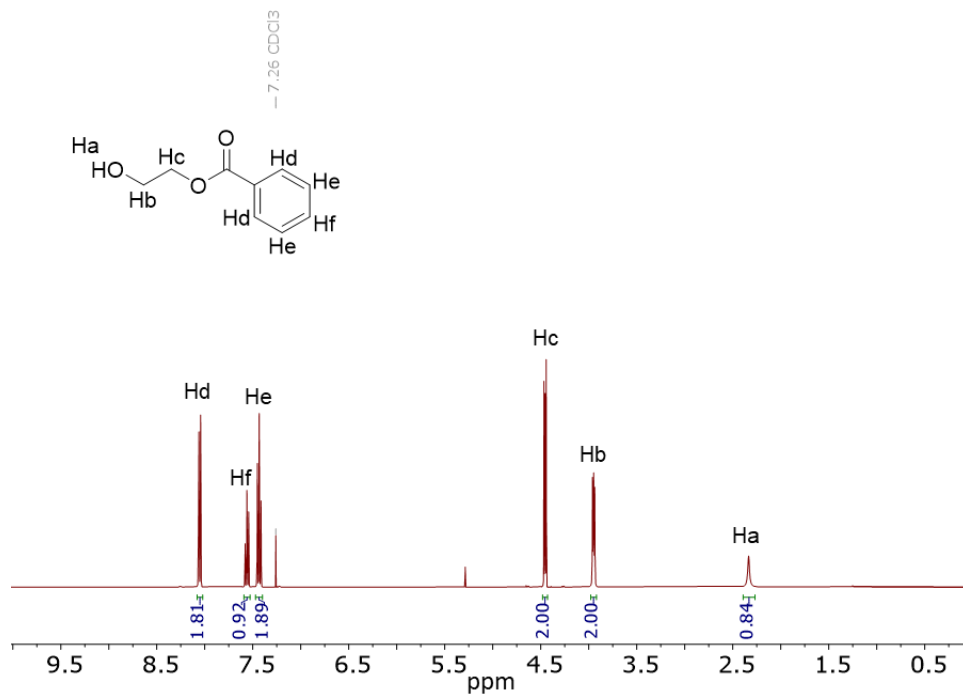


Figure S18. ¹H NMR spectrum of compound **VI**.

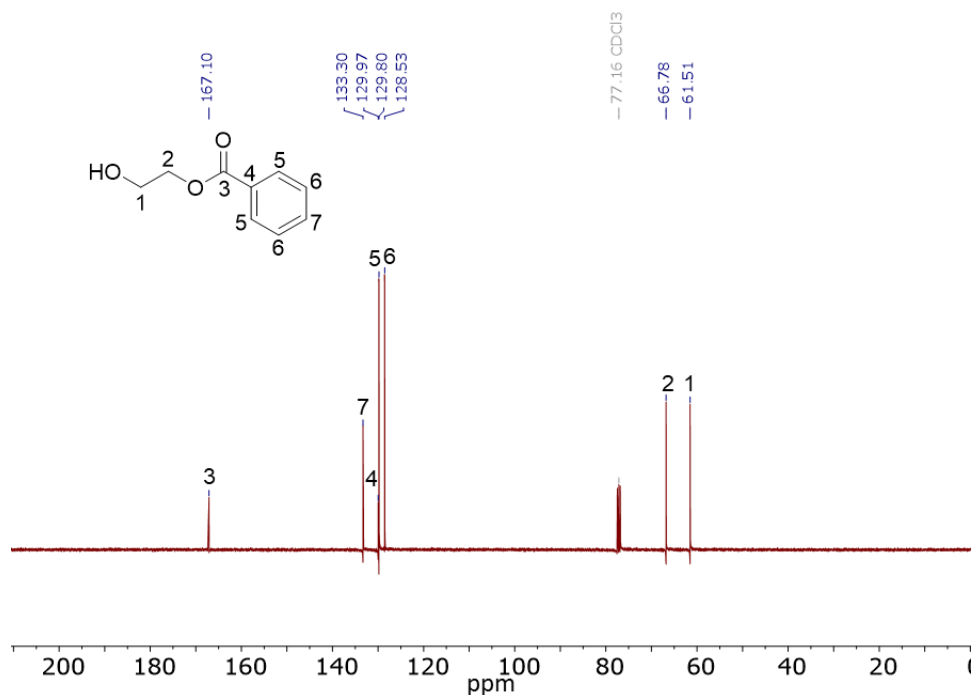


Figure S19. ^{13}C NMR spectrum of compound **VI**.

Kinetic Analysis of Anchor Groups

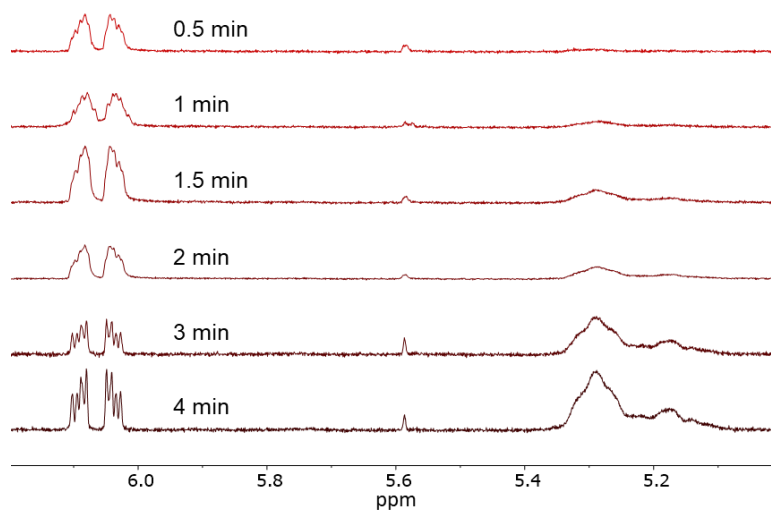


Figure S20. Representative spectra for ^1H NMR kinetics experiment of the ROMP of monomer *x*-MOMP (**1**) with G1. As the polymerization proceeds, the norbornene olefin resonance at ~6.1 ppm decreases in intensity, and the polymer backbone resonance at 5.1–5.4 ppm increases in intensity.

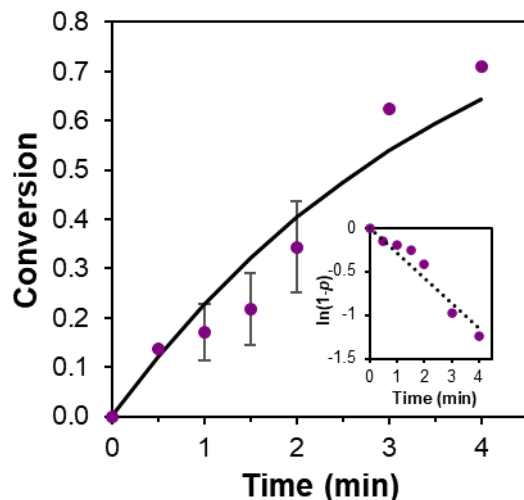


Figure S21. Kinetic analysis of monomer *x*-MOMP (**1**) in CDCl₃ with G1 at a [monomer]/[G1] ratio of 100 and [monomer] = 20 mM. The solid line represents the fit to the averaged conversion data based on the equation $p = 1 - e^{(-k_p t)}$ where p = fractional conversion.

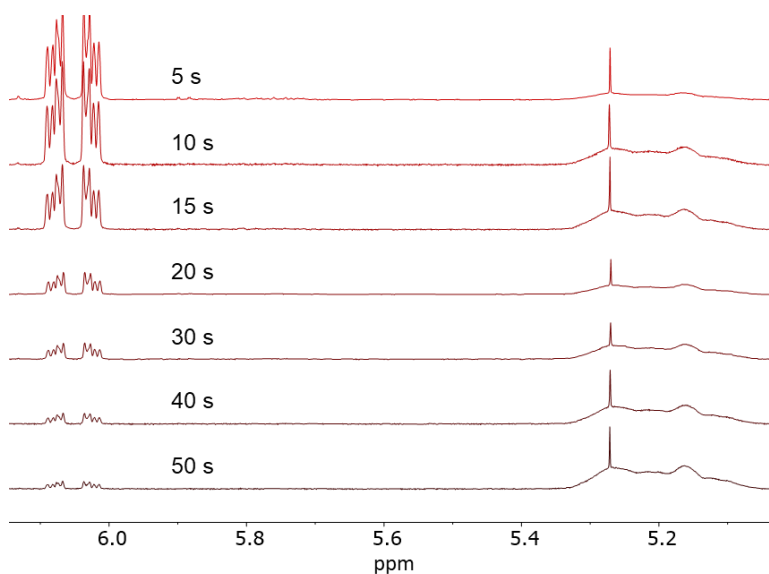


Figure S22. Representative spectra for ¹H NMR kinetics experiment of the ROMP of monomer *x*-MOMP (**1**) with G3. As the polymerization proceeds, the norbornene olefin resonance at ~6.1 ppm decreases in intensity, and the polymer backbone resonance at 5.1–5.4 ppm increases in intensity. The peak at ~5.26 ppm corresponds to residual CH₂Cl₂ in the monomer and was subtracted from the polymer backbone integration based on an estimated integration from the first aliquot.

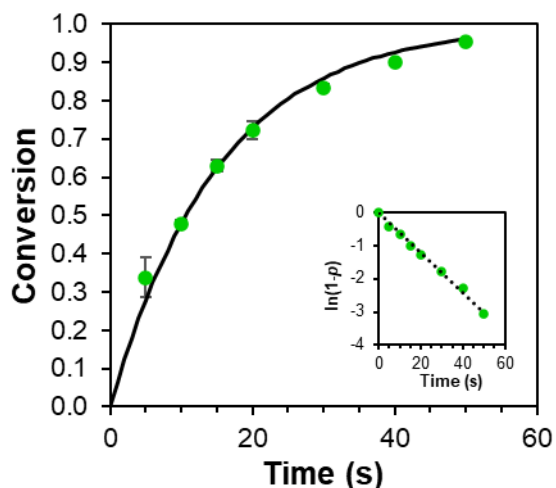


Figure S23. Kinetic analysis of monomer *x*-MOMP (**1**) in CDCl₃ with G3 at a [monomer]/[G3] ratio of 100 and [monomer] = 20 mM. The solid line represents the fit to the averaged conversion data based on the equation $p = 1 - e^{-k_p t}$ where p = fractional conversion.

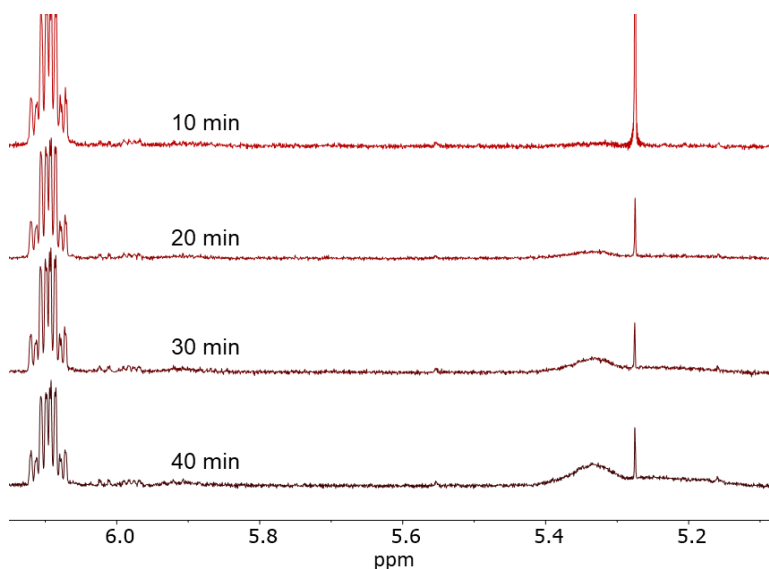


Figure S24. Representative spectra for ¹H NMR kinetics experiment of the ROMP of monomer *x*-ME'P (**2**) with G1. As the polymerization proceeds, the norbornene olefin resonance at ~6.1 ppm decreases in intensity, and the polymer backbone resonance at 5.2–5.4 ppm increases in intensity. The peak at ~5.26 ppm corresponds to residual CH₂Cl₂ in the monomer and was subtracted from the polymer backbone integration based on an estimated integration from the first aliquot.

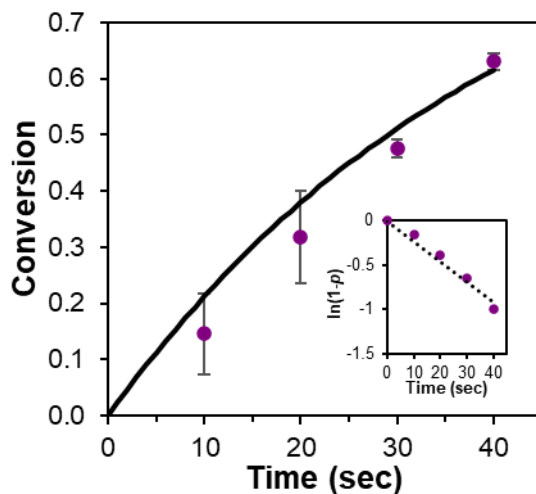


Figure S25. Kinetic analysis of monomer *x*-ME'P (**2**) in CDCl₃ with G1 at a [monomer]/[G1] ratio of 100 and [monomer] = 20 mM. The solid line represents the fit to the averaged conversion data based on the equation $p = 1 - e^{(-k_p t)}$ where p = fractional conversion.

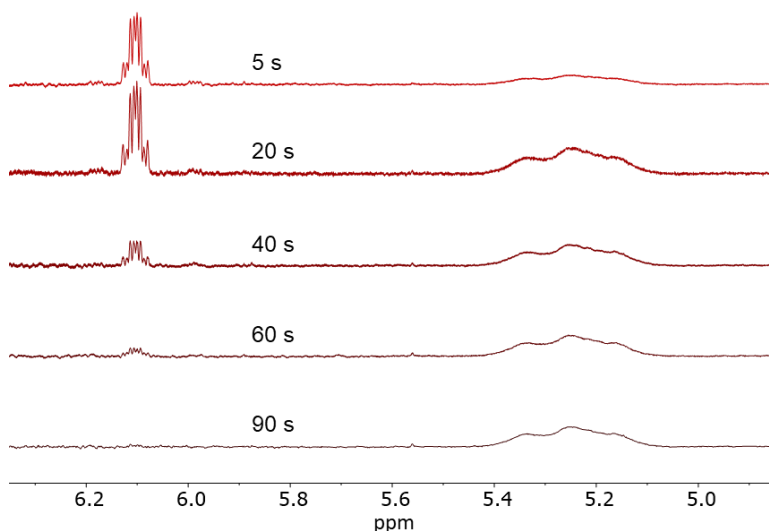


Figure S26. Representative spectra for ¹H NMR kinetics experiment of the ROMP of monomer *x*-ME'P (**2**) with G3. As the polymerization proceeds, the norbornene olefin resonance at ~6.1 ppm decreases in intensity, and the polymer backbone resonance at 5.2–5.4 ppm increases in intensity.

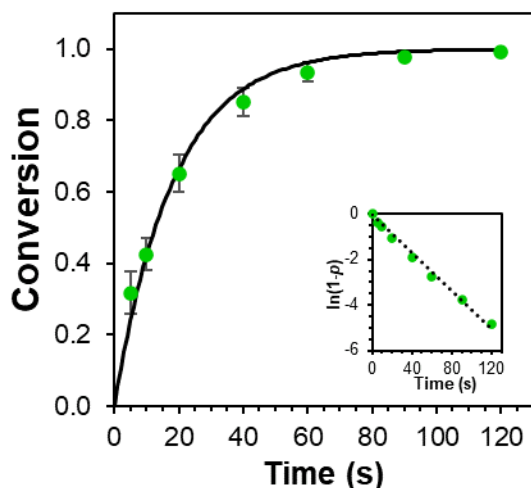


Figure S27. Kinetic analysis of monomer *x*-ME'P (**2**) in CDCl_3 with G3 at a [monomer]/[G3] ratio of 100 and [monomer] = 20 mM. The solid line represents the fit to the averaged conversion data based on the equation $p = 1 - e^{(-k_p t)}$ where p = fractional conversion.

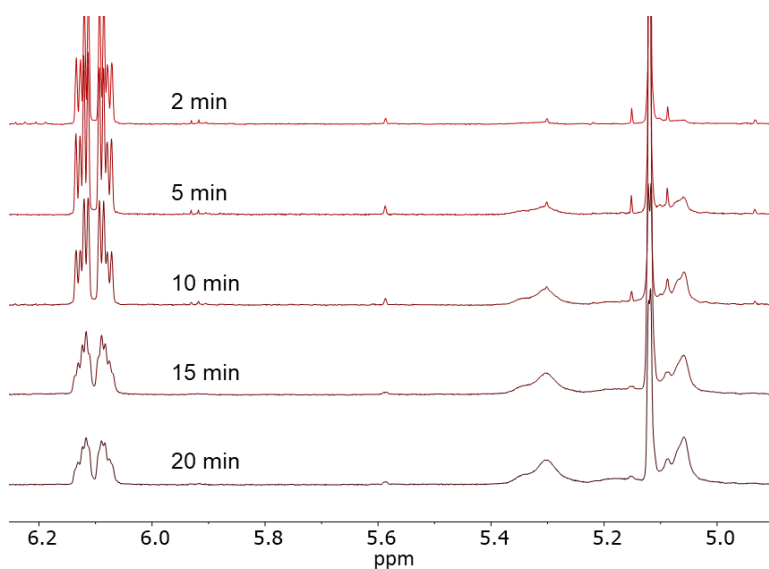


Figure S28. Representative spectra for ^1H NMR kinetics experiment of the ROMP of monomer *x*-EMP (**3**) with G1. As the polymerization proceeds, the norbornene olefin resonance at ~6.1 ppm decreases in intensity, and the polymer backbone resonance at 5.05–5.35 ppm increases in intensity. The peak at ~5.14 ppm corresponds to two monomer protons unaffected by the polymerization, therefore 2.0 was subtracted from the integration of the 5.05–5.35 ppm region for all aliquots.

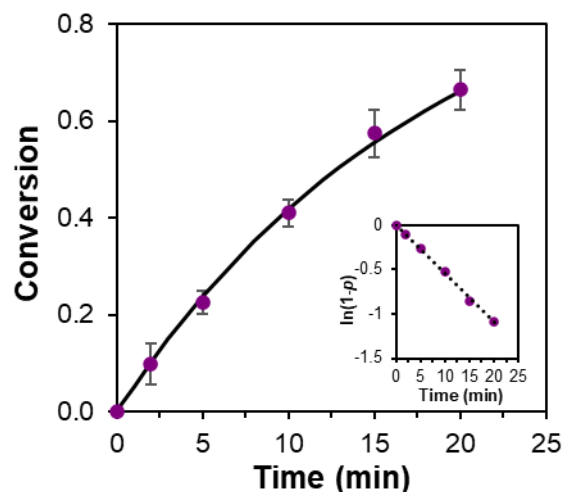


Figure S29. Kinetic analysis of monomer *x*-EMP (**3**) in CDCl₃ with G1 at a [monomer]/[G1] ratio of 100 and [monomer] = 20 mM. The solid line represents the fit to the averaged conversion data based on the equation $p = 1 - e^{(-k_p t)}$ where p = fractional conversion.

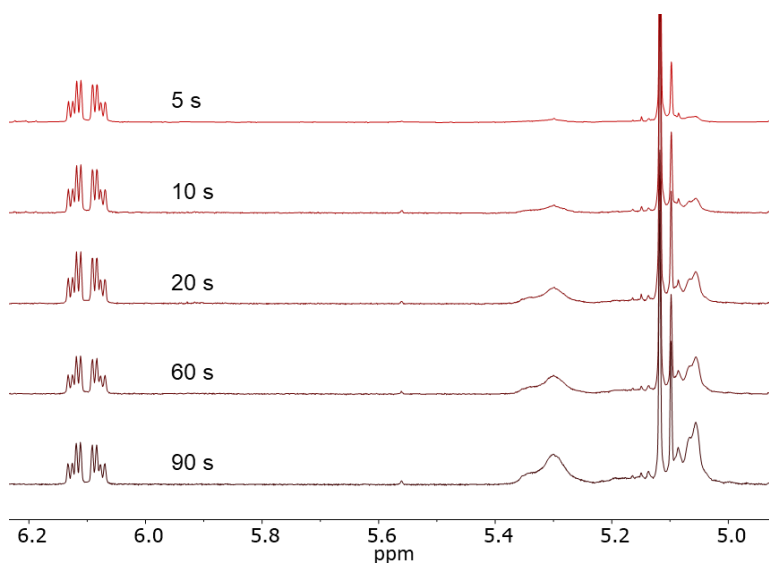


Figure S30. Representative spectra for ¹H NMR kinetics experiment of the ROMP of monomer *x*-EMP (**3**) with G3. As the polymerization proceeds, the norbornene olefin resonance at ~6.1 ppm decreases in intensity, and the polymer backbone resonance at 5.05–5.35 ppm increases in intensity. The peak at ~5.14 ppm corresponds to two monomer protons unaffected by the polymerization, therefore 2.0 was subtracted from the integration of the 5.05–5.35 ppm region for all aliquots.

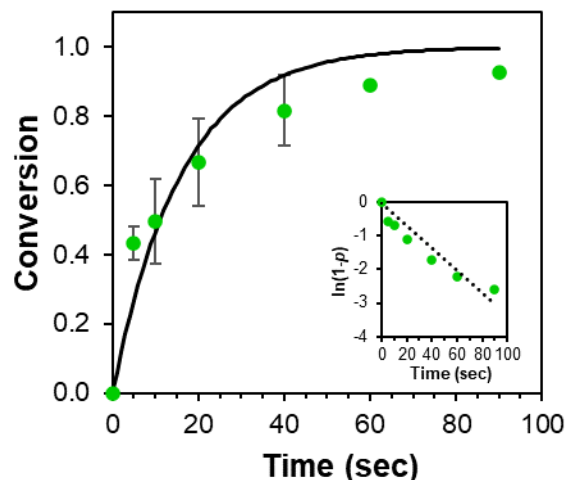


Figure S31. Kinetic analysis of monomer *x*-EMP (**3**) in CDCl_3 with G3 at a [monomer]/[G3] ratio of 100 and [monomer] = 20 mM. The solid line represents the fit to the averaged conversion data based on the equation $p = 1 - e^{(-k_p t)}$ where p = fractional conversion.

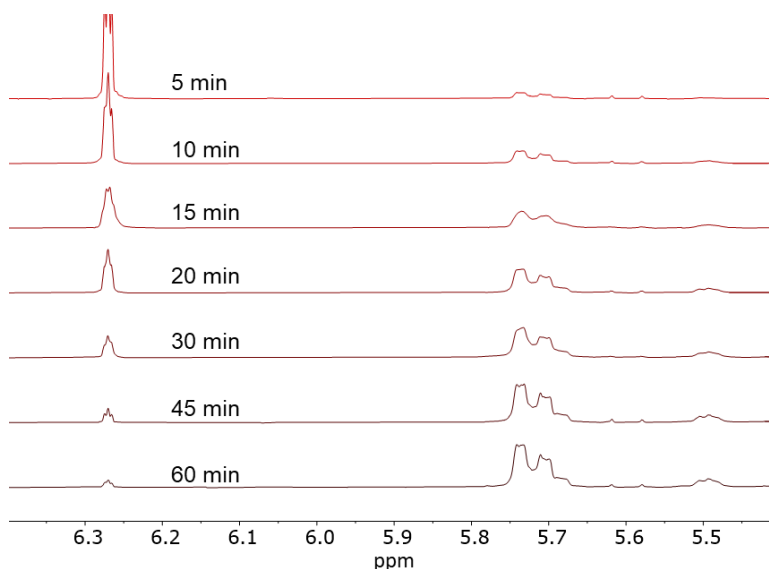


Figure S32. Representative spectra for ^1H NMR kinetics experiment of the ROMP of monomer *xx*-IMP (**4**) with G1. As the polymerization proceeds, the norbornene olefin resonance at ~ 6.28 ppm decreases in intensity, and the polymer backbone resonance at 5.4–5.75 ppm increases in intensity.

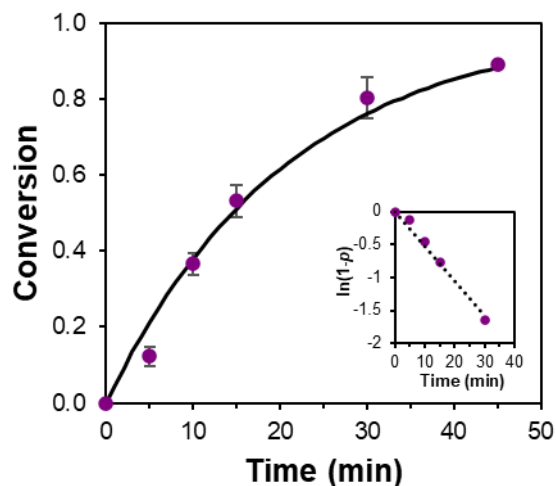


Figure S33. Kinetic analysis of monomer *xx*-IMP (**4**) in CDCl_3 with G1 at a [monomer]/[G1] ratio of 100 and [monomer] = 20 mM. The solid line represents the fit to the averaged conversion data based on the equation $p = 1 - e^{(-k_p t)}$ where p = fractional conversion.

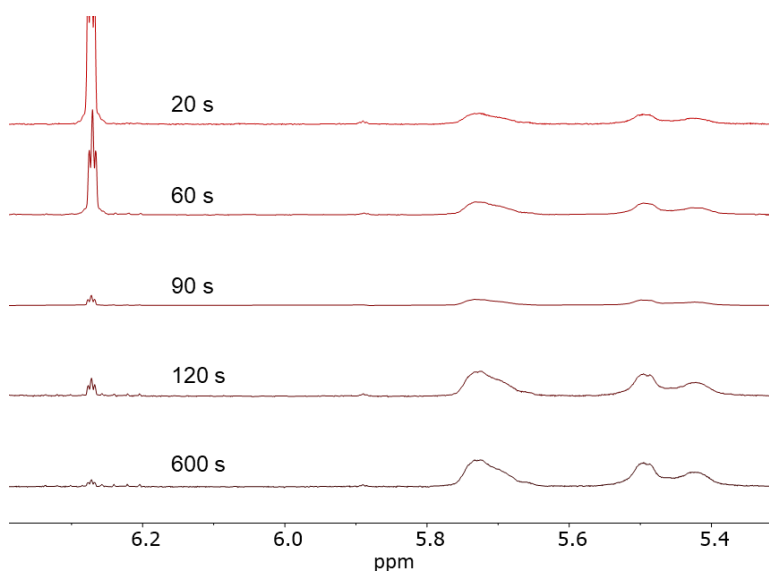


Figure S34. Representative spectra for ^1H NMR kinetics experiment of the ROMP of monomer *xx*-IMP (**4**) with G3. As the polymerization proceeds, the norbornene olefin resonance at ~ 6.28 ppm decreases in intensity, and the polymer backbone resonance at 5.4–5.75 ppm increases in intensity.

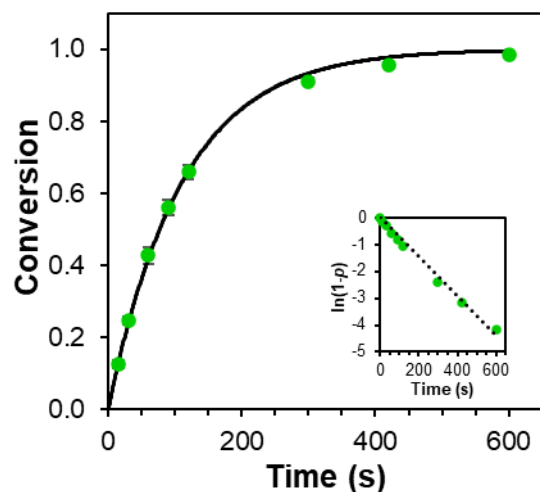


Figure S35. Kinetic analysis of monomer *xx*-IMP (**4**) in CDCl_3 with G3 at a [monomer]/[G3] ratio of 100 and [monomer] = 20 mM. The solid line represents the fit to the averaged conversion data based on the equation $p = 1 - e^{(-k_p t)}$ where p = fractional conversion.

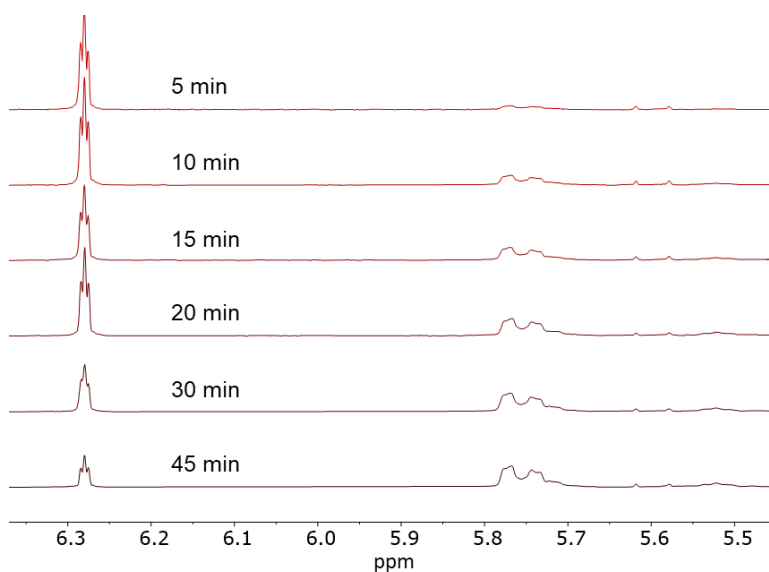


Figure S36. Representative spectra for ^1H NMR kinetics experiment of the ROMP of monomer *xx*-IM₆ (**5**) with G1. As the polymerization proceeds, the norbornene olefin resonance at ~6.28 ppm decreases in intensity, and the polymer backbone resonance at 5.4–5.8 ppm increases in intensity.

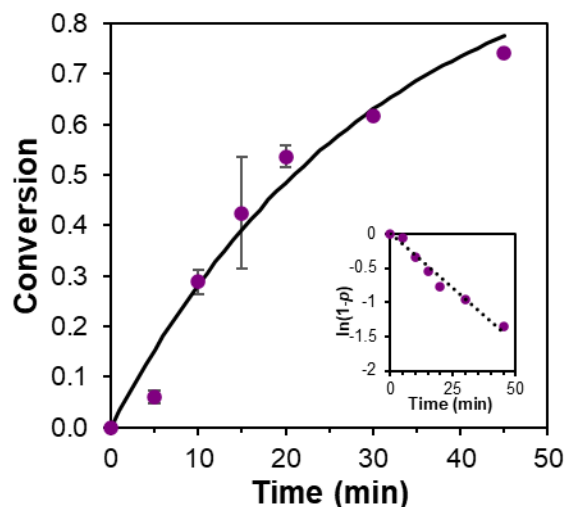


Figure S37. Kinetic analysis of monomer xx -IM₆ (**5**) in CDCl₃ with G1 at a [monomer]/[G1] ratio of 100 and [monomer] = 20 mM. The solid line represents the fit to the averaged conversion data based on the equation $p = 1 - e^{(-k_p t)}$ where p = fractional conversion.

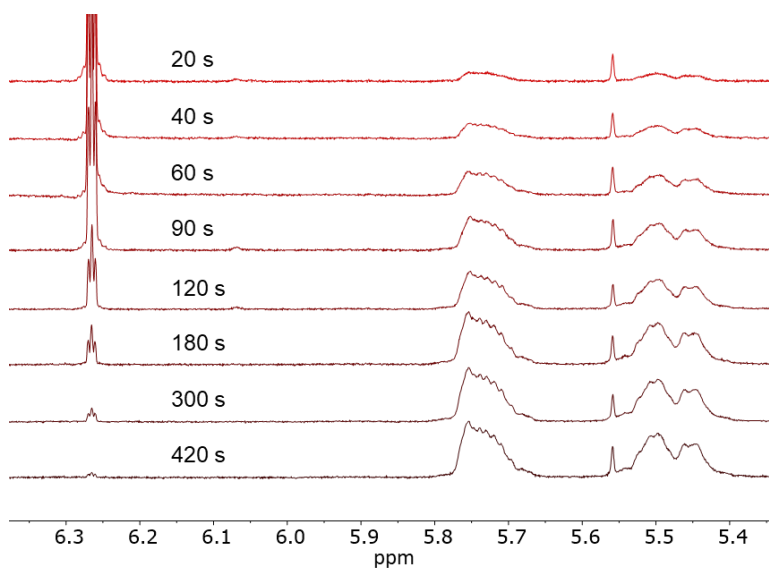


Figure S38. Representative spectra for ¹H NMR kinetics experiment of the ROMP of monomer xx -IM₆ (**5**) with G3. As the polymerization proceeds, the norbornene olefin resonance at ~6.28 ppm decreases in intensity, and the polymer backbone resonance at 5.4–5.8 ppm increases in intensity.

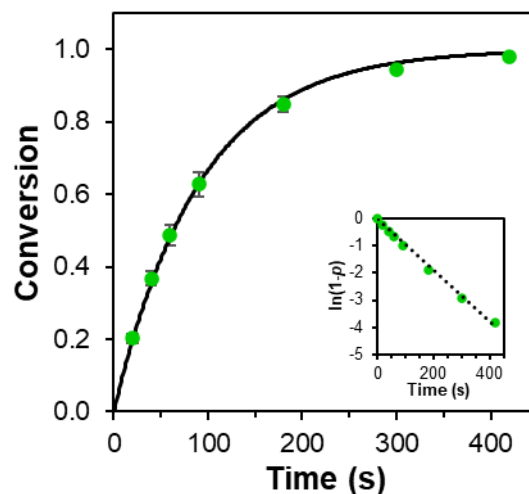


Figure S39. Kinetic analysis of monomer xx -IM₆ (**5**) in CDCl₃ with G3 at a [monomer]/[G3] ratio of 100 and [monomer] = 20 mM. The solid line represents the fit to the averaged conversion data based on the equation $p = 1 - e^{(-k_p t)}$ where p = fractional conversion.

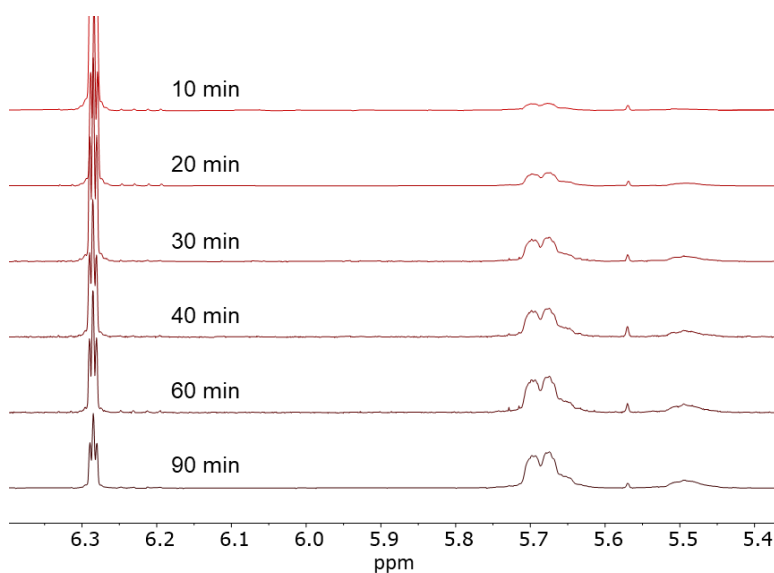


Figure S40. Representative spectra for ¹H NMR kinetics experiment of the ROMP of monomer xx -IMEM₂E'P (**6**) with G1. As the polymerization proceeds, the norbornene olefin resonance at ~6.28 ppm decreases in intensity, and the polymer backbone resonance at 5.4–5.7 ppm increases in intensity.

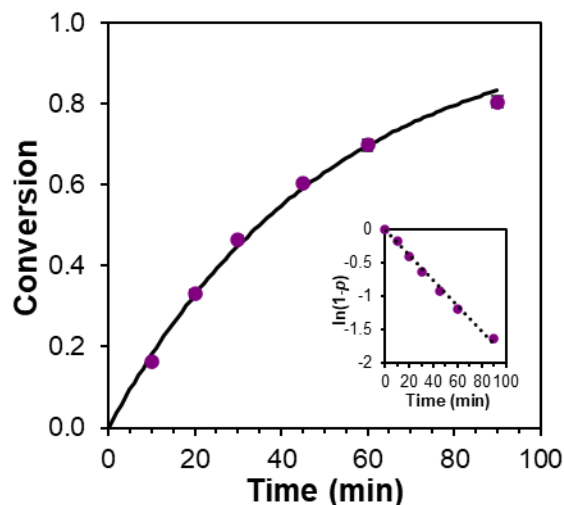


Figure S41. Kinetic analysis of monomer *xx*-IMEM₂E'P (**6**) in CDCl₃ with G1 at a [monomer]/[G1] ratio of 100 and [monomer] = 20 mM. The solid line represents the fit to the averaged conversion data based on the equation $p = 1 - e^{(-k_p t)}$ where p = fractional conversion.

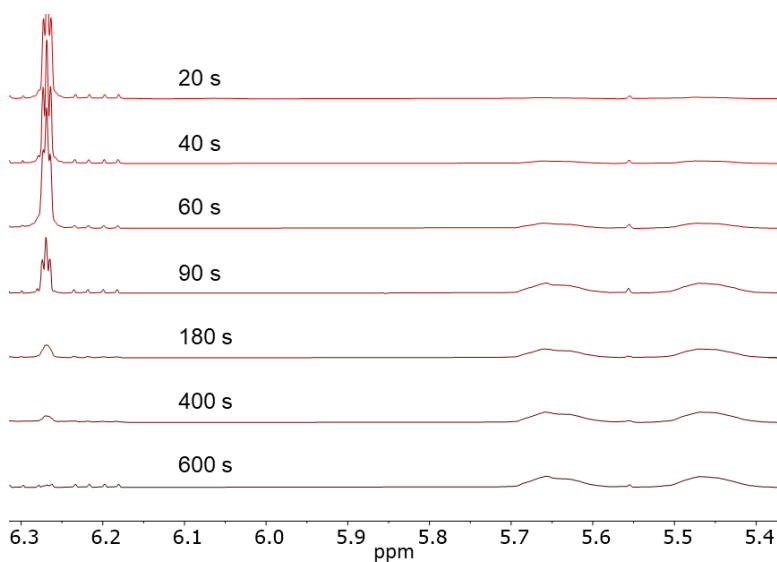


Figure S42. Representative spectra for ¹H NMR kinetics experiment of the ROMP of monomer *xx*-IMEM₂E'P (**6**) with G3. As the polymerization proceeds, the norbornene olefin resonance at ~6.28 ppm decreases in intensity, and the polymer backbone resonance at 5.4–5.7 ppm increases in intensity.

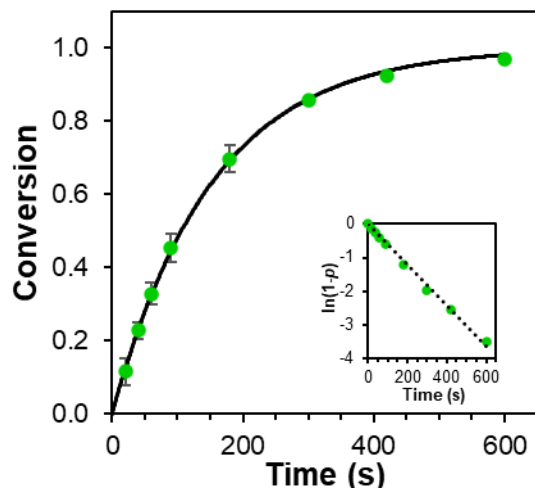


Figure S43. Kinetic analysis of monomer *xx*-IMEM₂E'P (**6**) in CDCl₃ with G3 at a [monomer]/[G3] ratio of 100 and [monomer] = 20 mM. The solid line represents the fit to the averaged conversion data based on the equation $p = 1 - e^{-k_p t}$ where p = fractional conversion.

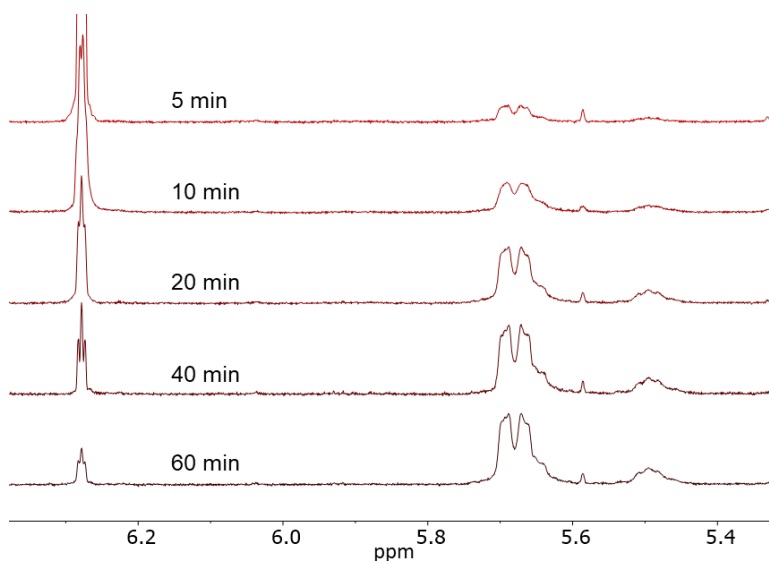


Figure S44. Representative spectra for ¹H NMR kinetics experiment of the ROMP of monomer *xx*-IMEMP (**7**) with G1. As the polymerization proceeds, the norbornene olefin resonance at ~6.28 ppm decreases in intensity, and the polymer backbone resonance at 5.4–5.7 ppm increases in intensity.

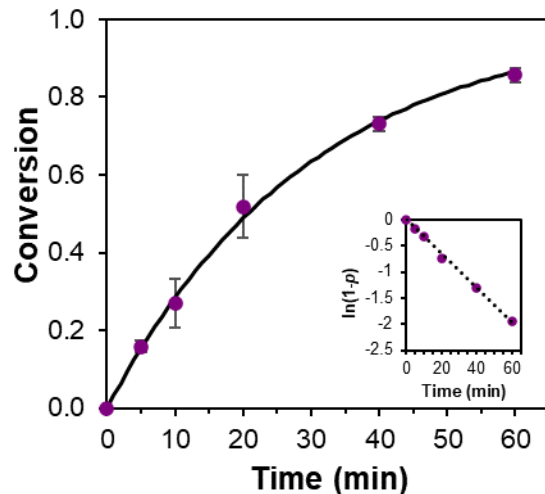


Figure S45. Kinetic analysis of monomer *xx*-IMEMP (**7**) in CDCl_3 with G1 at a [monomer]/[G1] ratio of 100 and [monomer] = 20 mM. The solid line represents the fit to the averaged conversion data based on the equation $p = 1 - e^{(-k_p t)}$ where p = fractional conversion.

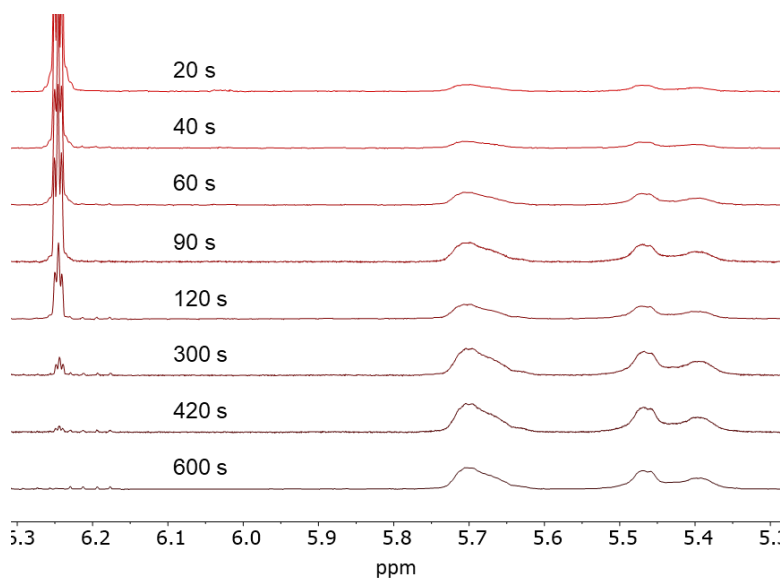


Figure S46. Representative spectra for ^1H NMR kinetics experiment of the ROMP of monomer *xx*-IMEMP (**7**) with G3. As the polymerization proceeds, the norbornene olefin resonance at ~ 6.28 ppm decreases in intensity, and the polymer backbone resonance at 5.4–5.7 ppm increases in intensity.

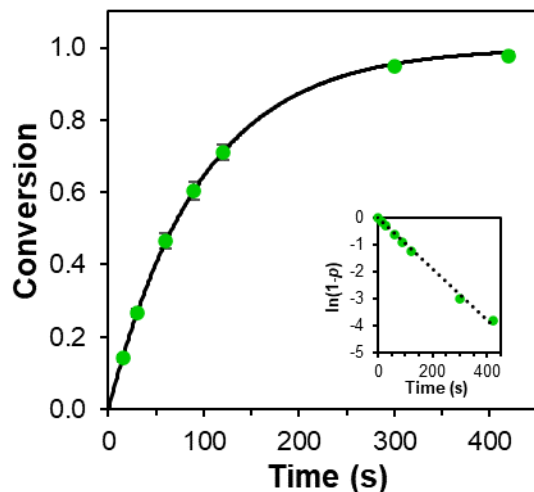


Figure S47. Kinetic analysis of monomer *xx*-IMEMP (**7**) in CDCl_3 with G3 at a [monomer]/[G3] ratio of 100 and [monomer] = 20 mM. The solid line represents the fit to the averaged conversion data based on the equation $p = 1 - e^{-k_p t}$ where p = fractional conversion.

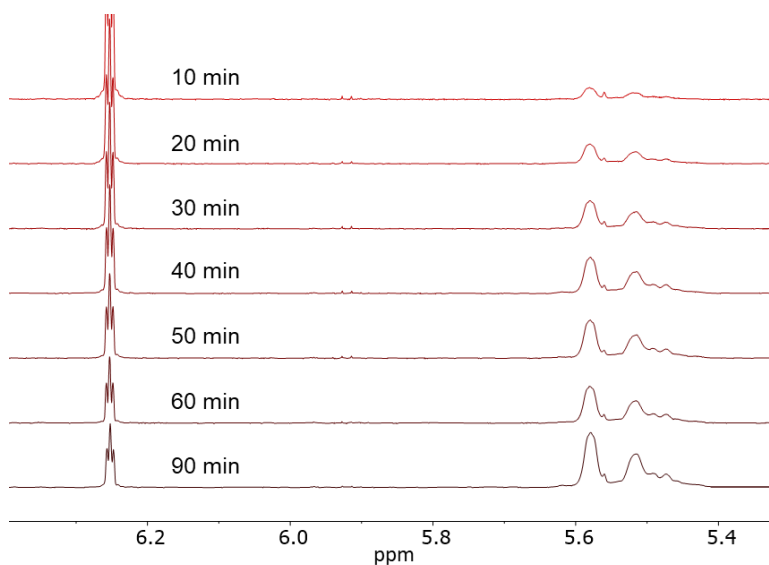


Figure S48. Representative spectra for ^1H NMR kinetics experiment of the ROMP of monomer *xx*-IM₂E'P (**8**) with G1. As the polymerization proceeds, the norbornene olefin resonance at ~6.25 ppm decreases in intensity, and the polymer backbone resonance at 5.4–5.6 ppm increases in intensity.

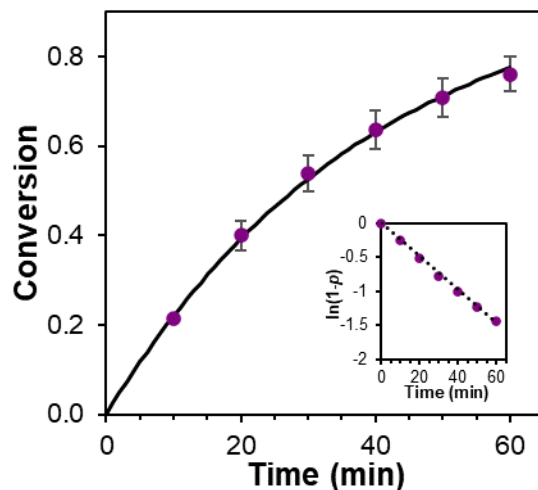


Figure S49. Kinetic analysis of monomer *xx*-IM₂E'P (**8**) in CDCl₃ with G1 at a [monomer]/[G1] ratio of 100 and [monomer] = 20 mM. The solid line represents the fit to the averaged conversion data based on the equation $p = 1 - e^{(-k_p t)}$ where p = fractional conversion.

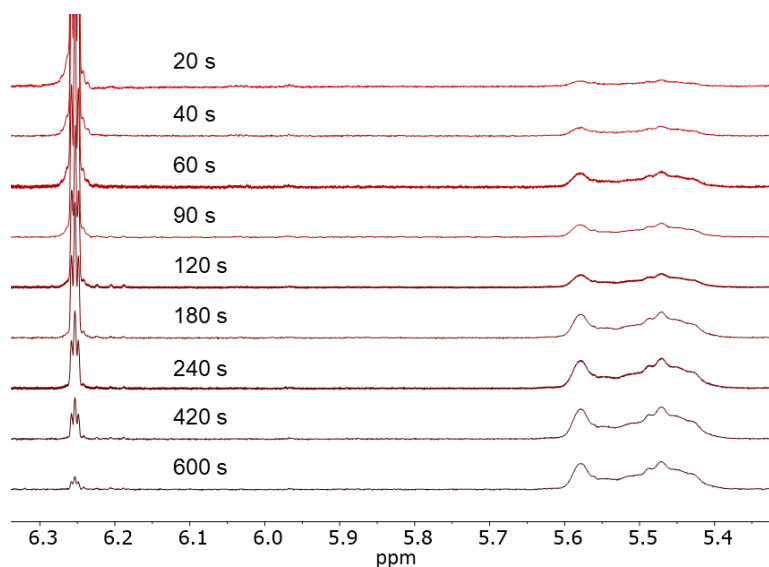


Figure S50. Representative spectra for ¹H NMR kinetics experiment of the ROMP of monomer *xx*-IM₂E'P (**8**) with G1. As the polymerization proceeds, the norbornene olefin resonance at ~6.25 ppm decreases in intensity, and the polymer backbone resonance at 5.4–5.6 ppm increases in intensity.

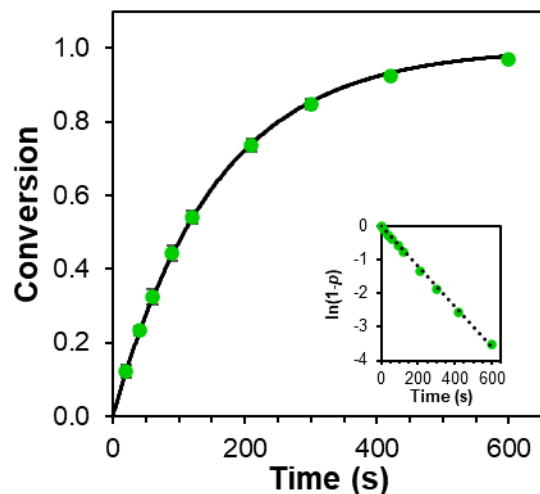


Figure S51. Kinetic analysis of monomer *xx*-IM₂E'P (**8**) in CDCl₃ with G3 at a [monomer]/[G3] ratio of 100 and [monomer] = 20 mM. The solid line represents the fit to the averaged conversion data based on the equation $p = 1 - e^{-k_p t}$ where p = fractional conversion.

GPC Traces of Linear Polymers Made by ROMP at a [Monomer]/[Catalyst] Ratio of 100

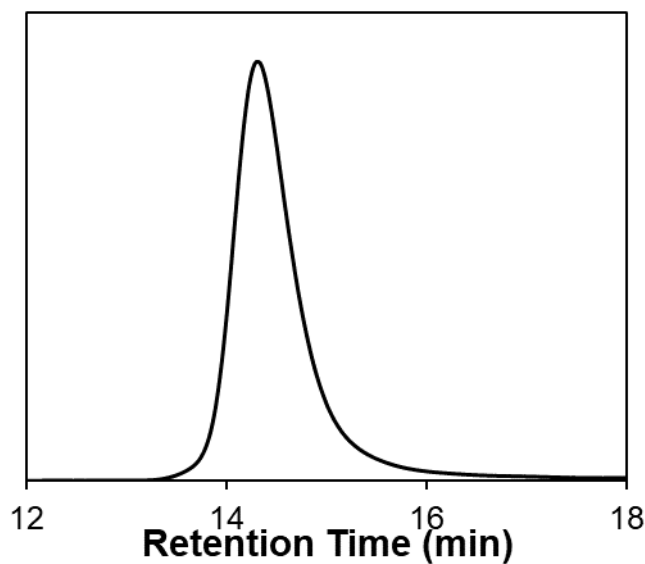


Figure S52. SEC trace of the linear polymer of monomer *x*-MOMP (**1**) with G1.

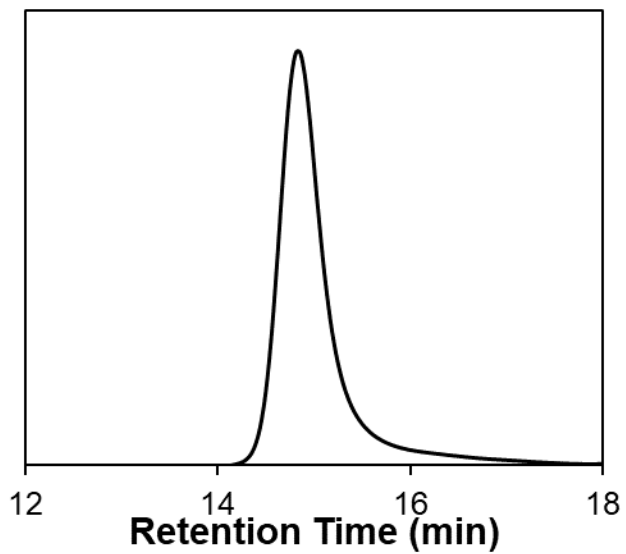


Figure S53. SEC trace of the linear polymer of monomer *x*-MOMP (**1**) with G3.

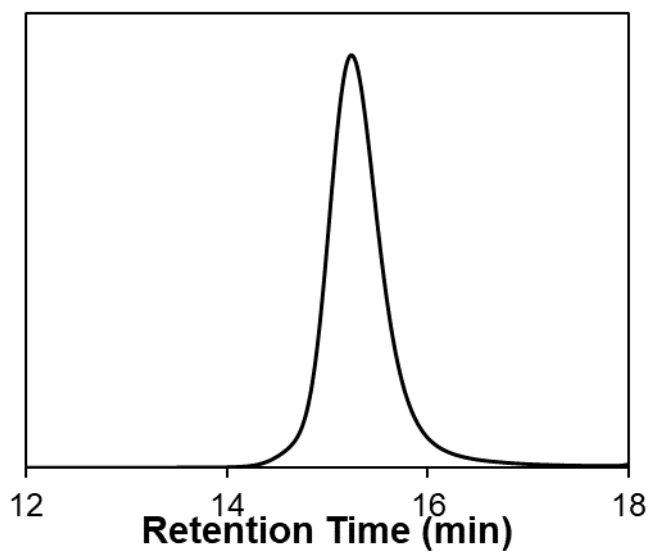


Figure S54. SEC trace of the linear polymer of monomer *x*-ME'P (**2**) with G1.

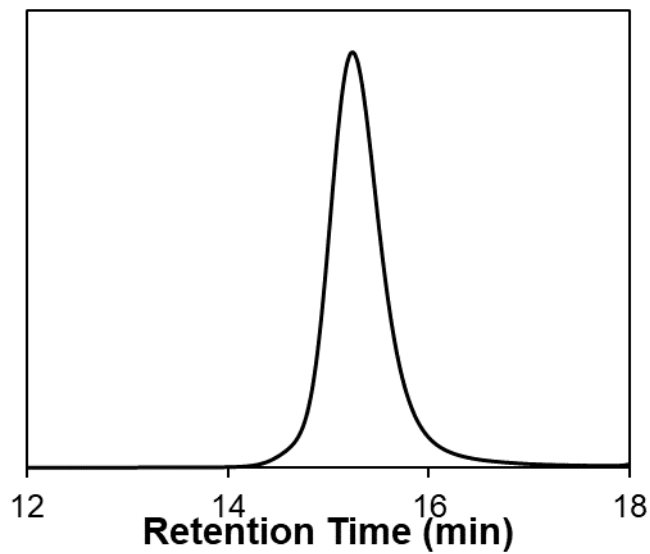


Figure S55. SEC trace of the linear polymer of monomer *x*-ME'P (**2**) with G3.

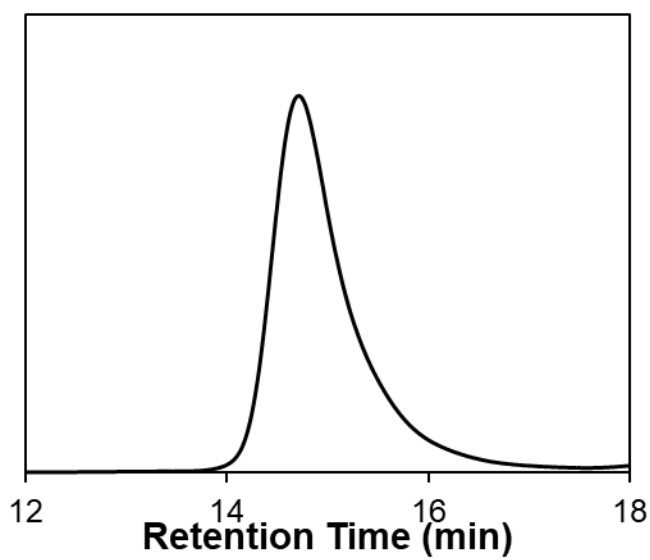


Figure S56. SEC trace of the linear polymer of monomer *x*-EMP (**3**) with G1.

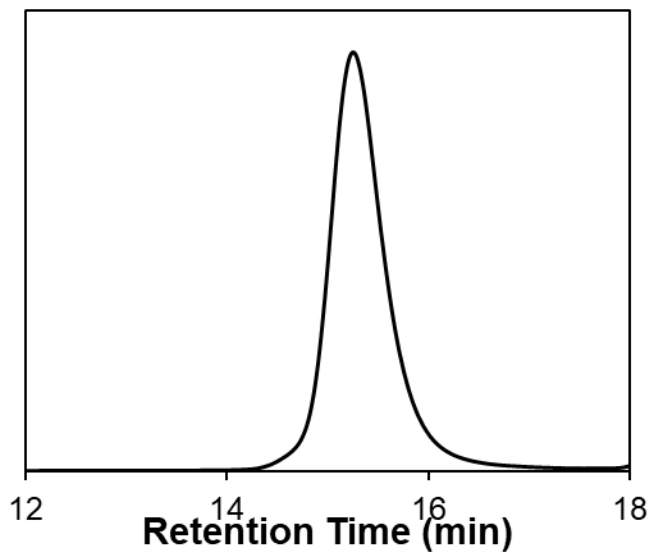


Figure S57. SEC trace of the linear polymer of monomer *x*-EMP (**3**) with G3.

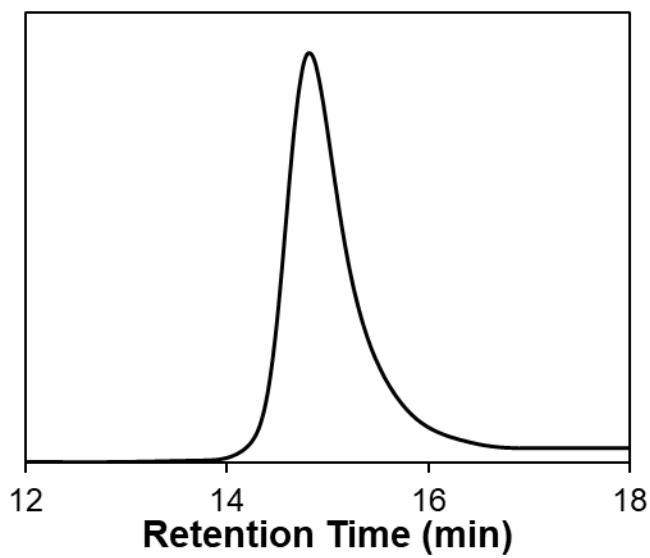


Figure S58. SEC trace of the linear polymer of monomer *xx*-IMP (**4**) with G1.

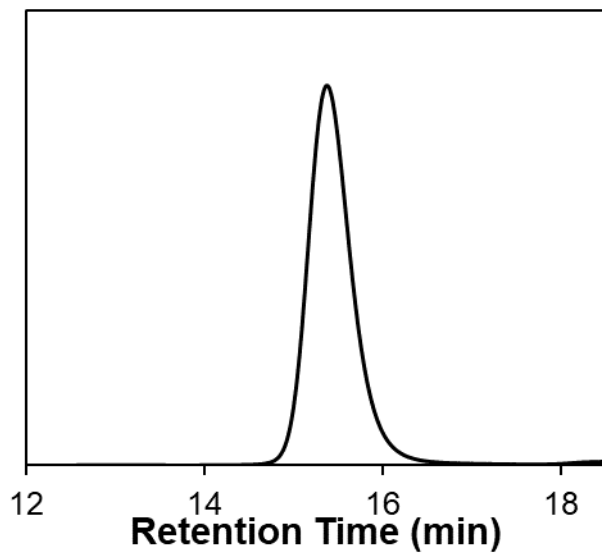


Figure S59. SEC trace of the linear polymer of monomer *xx*-IMP (**4**) with G3.

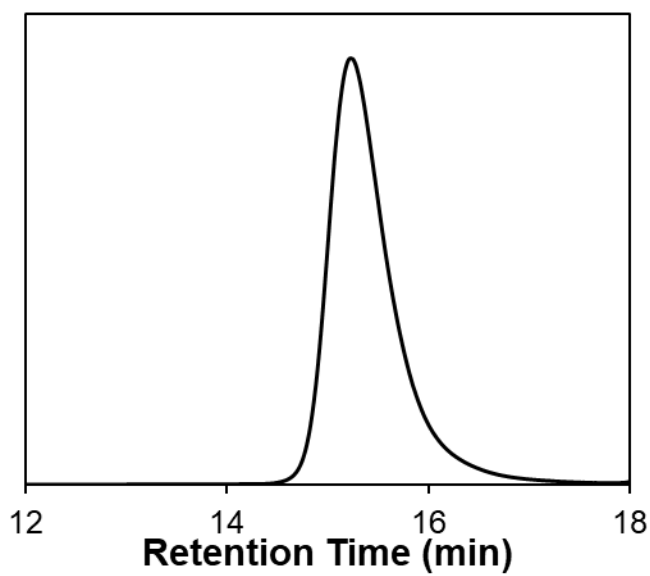


Figure S60. SEC trace of the linear polymer of monomer *xx*-IM₆ (**5**) with G1.

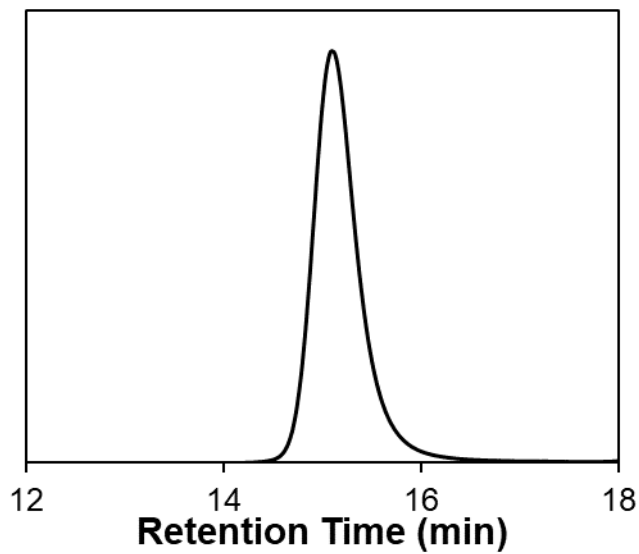


Figure S61. SEC trace of the linear polymer of monomer xx -IM₆ (**5**) with G3.

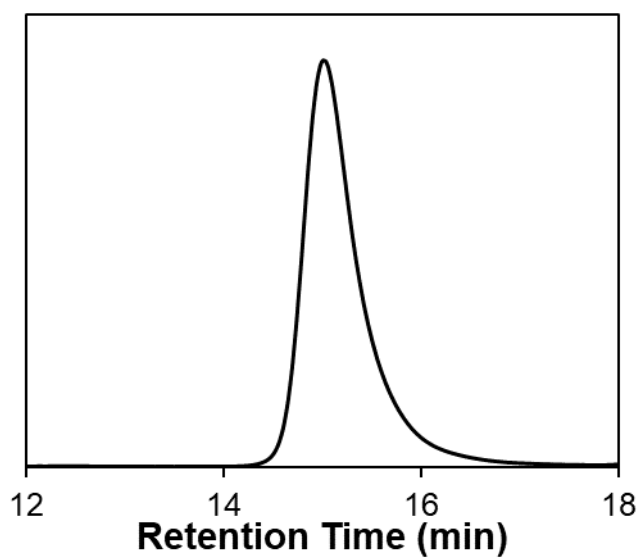


Figure S62. SEC trace of the linear polymer of monomer xx -IMEM₂E'P (**6**) with G1.

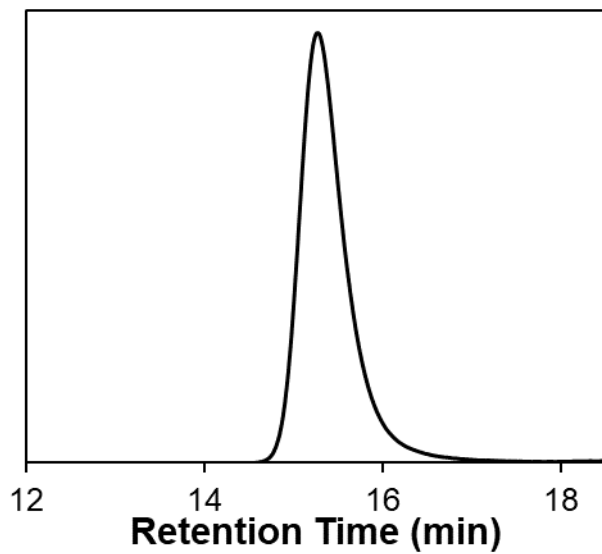


Figure S63. SEC trace of the linear polymer of monomer *xx*-IMEM₂E'P (**6**) with G3.

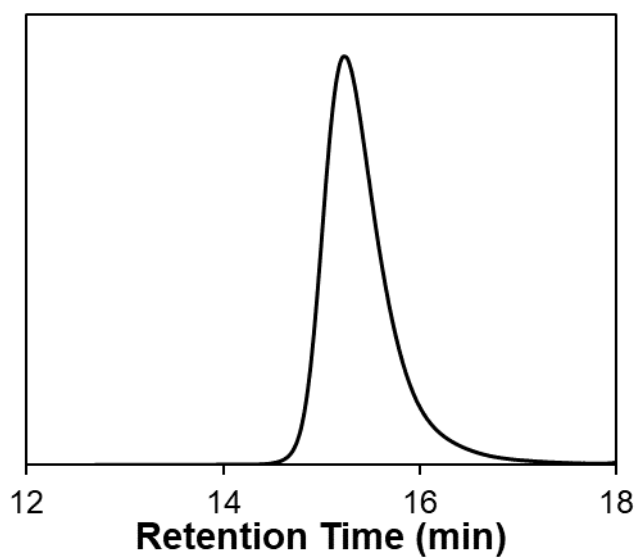


Figure S64. SEC trace of the linear polymer of monomer *xx*-IMEMP (**7**) with G1.

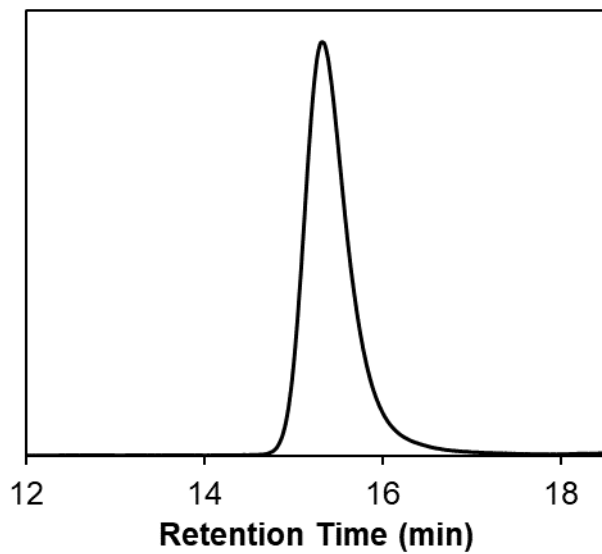


Figure S65. SEC trace of the linear polymer of monomer *xx*-IMEMP (**7**) with G3.

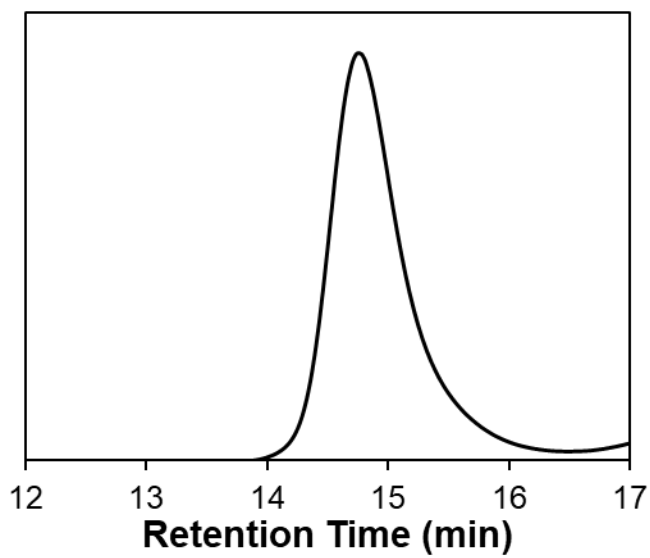


Figure S66. SEC trace of the linear polymer of monomer *xx*-IM₂E'P (**8**) with G1.

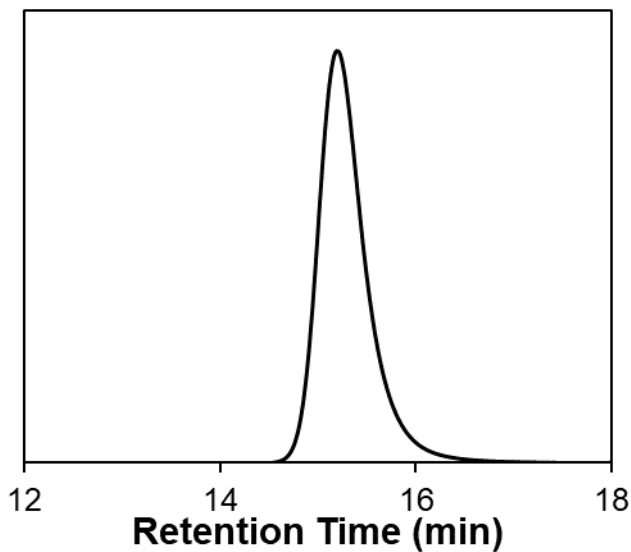


Figure S67. SEC trace of the linear polymer of monomer xx -IM₂E'P (**8**) with G3.

HOMO/LUMO Energy Gap

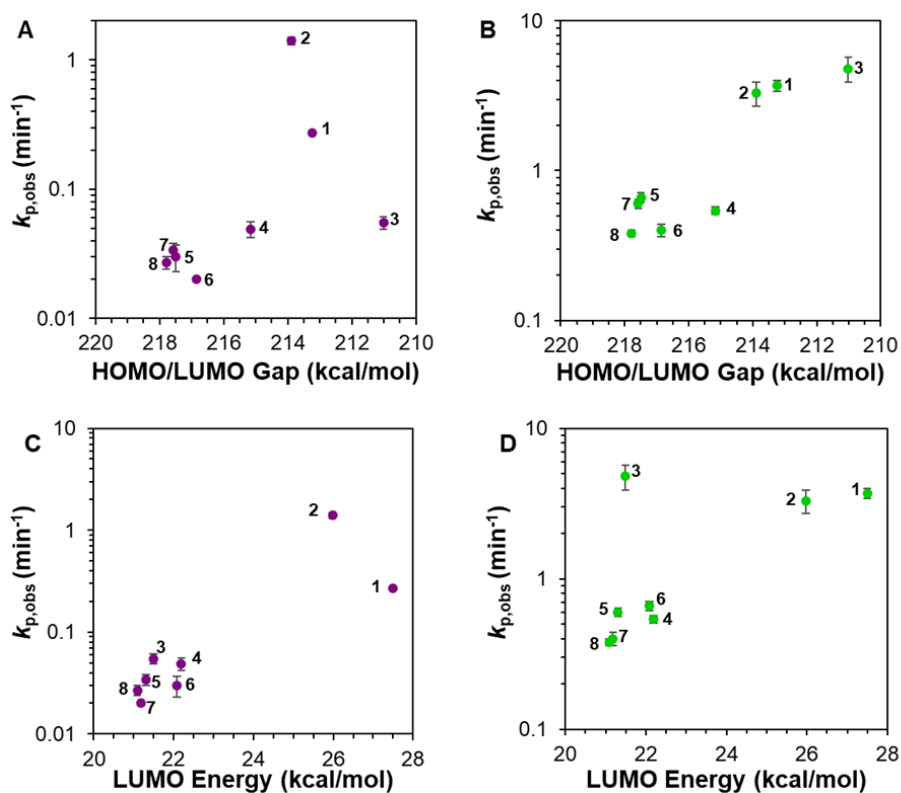


Figure S68. Measured $k_{p,obs}$ versus HOMO/LUMO energy gap for monomers **1–8** with G1 catalyst (A) and G3 catalyst (B). Measured $k_{p,obs}$ versus LUMO energy for monomers **1–8** with G1 catalyst (C) and G3 catalyst (D).

Metallocyclobutane Intermediate Calculations

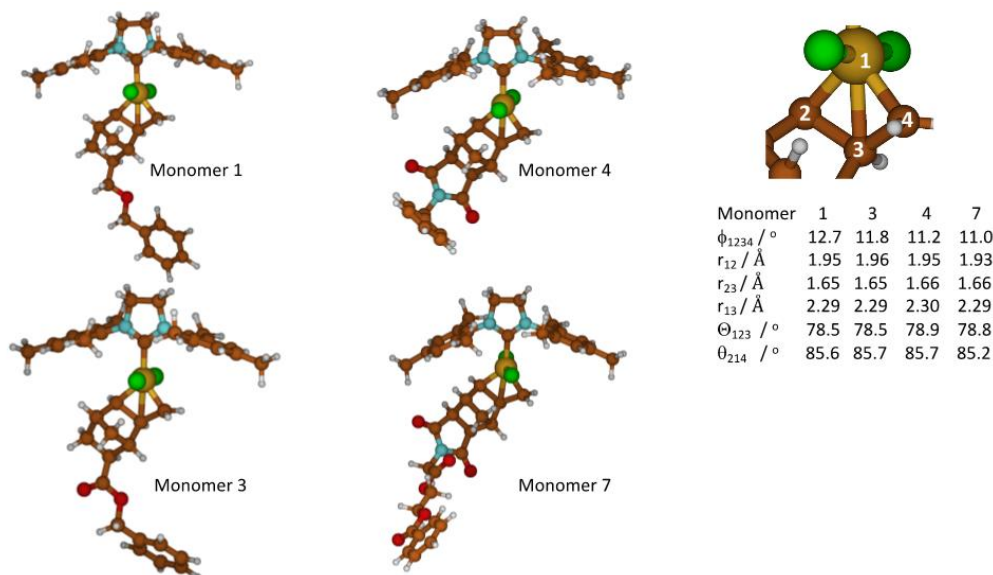


Figure S69. Geometries of the metallocyclobutane intermediates formed in the ROMP reaction of monomers 1, 3, 4, and 7 with Ru=CH₂ catalyzed by G3. The geometry of the metallocyclobutane is very similar among monomers. Color code: Ru: gold, Cl: green, C: brown, H: white, N: blue, O: red.

Monomer Chelation Analysis

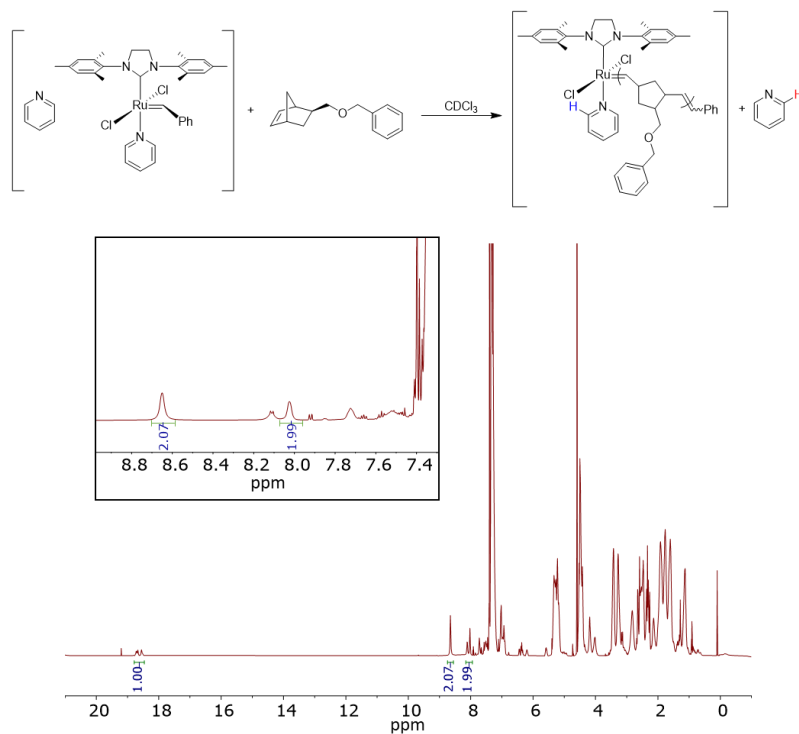


Figure S70. ^1H NMR spectrum of the poly(1) bound Ru alkylidene species.

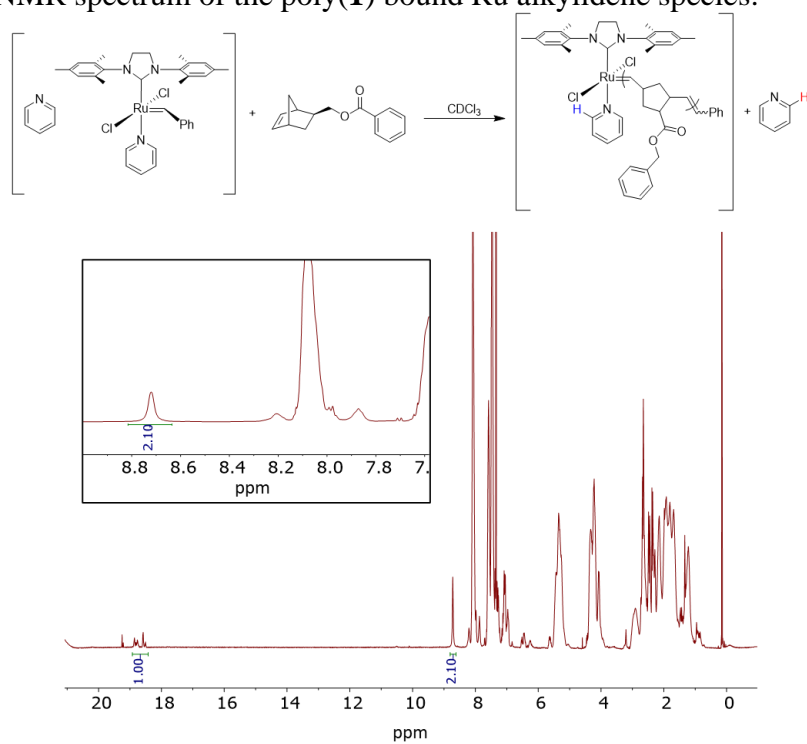


Figure S71. ^1H NMR spectrum of the poly(2) bound Ru alkylidene species.

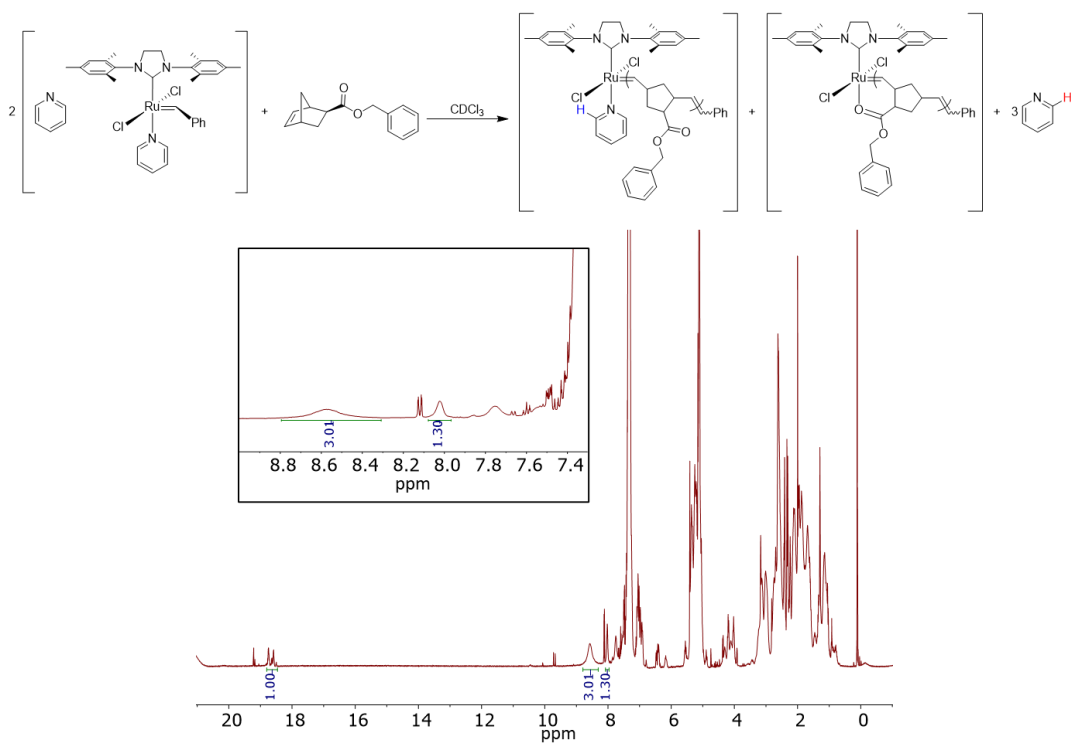


Figure S72. ^1H NMR spectrum of the poly(3) bound Ru alkylidene species.

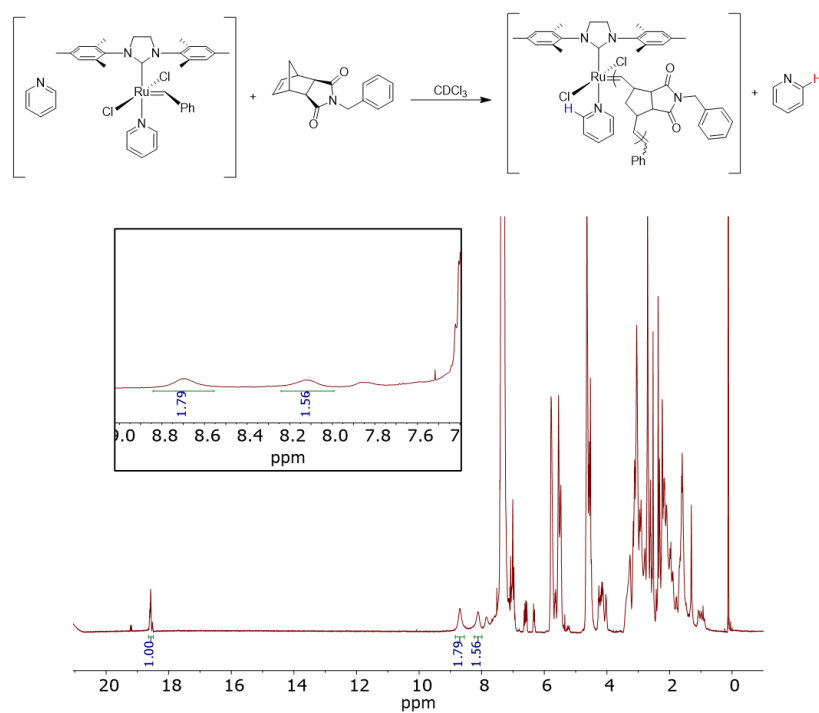


Figure S73. ^1H NMR spectrum of the poly(4) bound Ru alkylidene species.

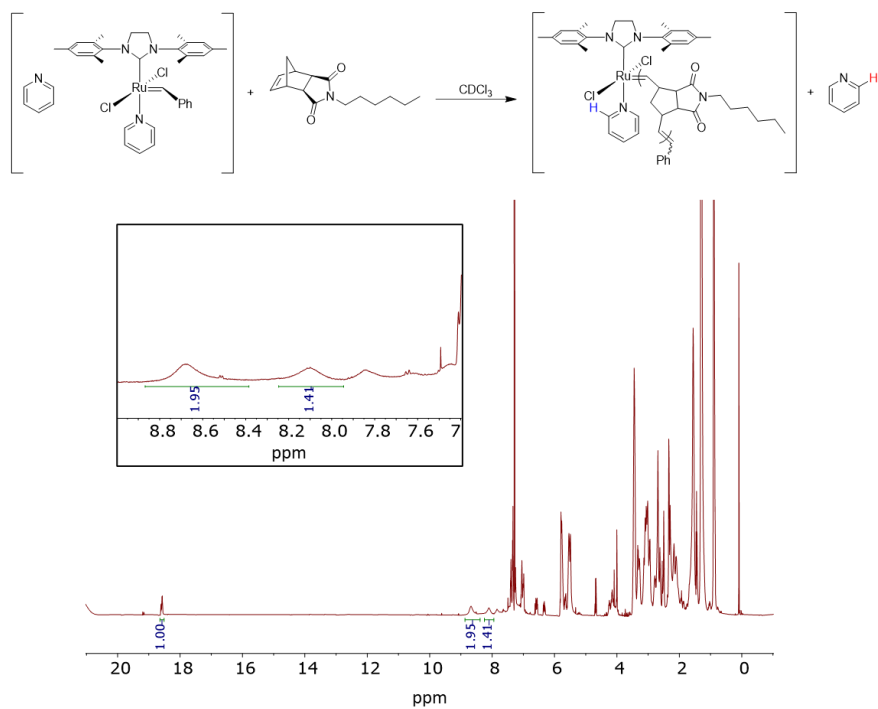


Figure S74. ^1H NMR spectrum of the poly(5) bound Ru alkylidene species.

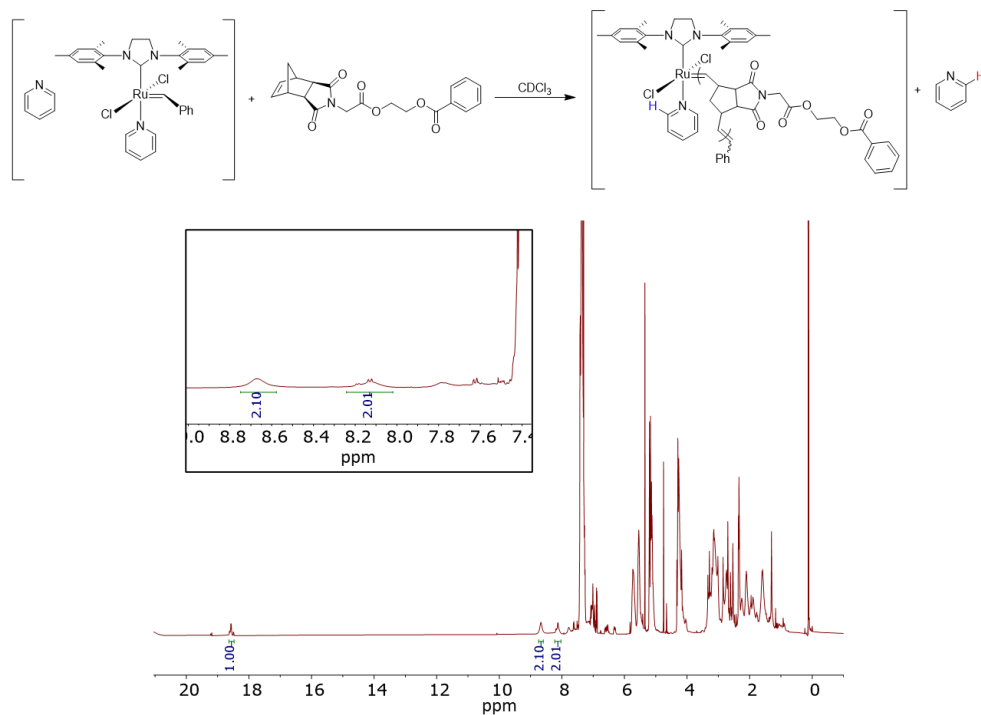


Figure S75. ¹H NMR spectrum of the poly(6) bound Ru alkylidene species.

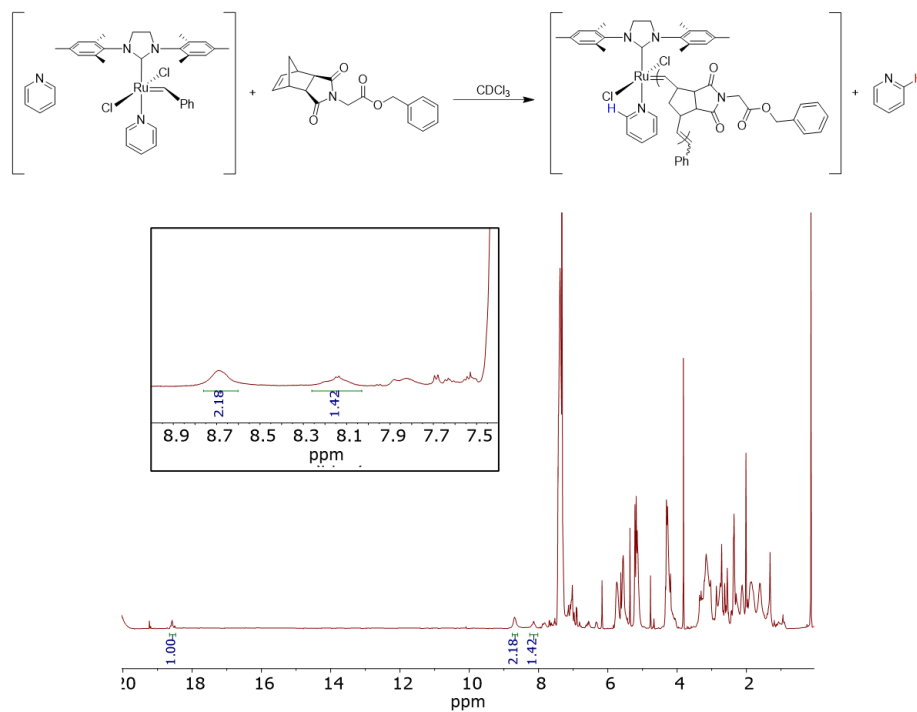


Figure S76. ¹H NMR spectrum of the poly(7) bound Ru alkylidene species.

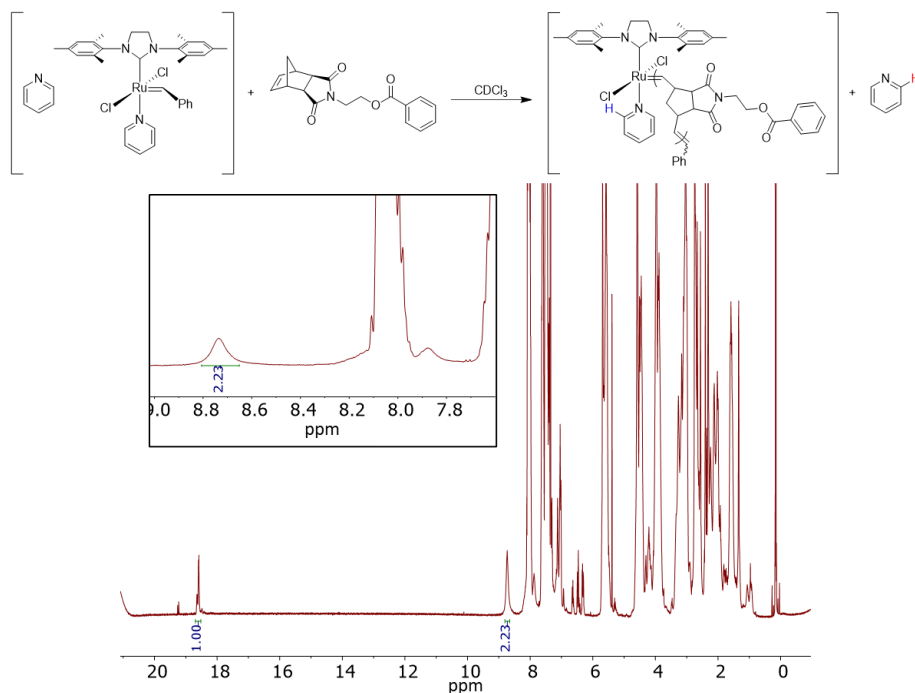


Figure S77. ¹H NMR spectrum of the poly(8) bound Ru alkylidene species.

Catalyst Decomposition Analysis

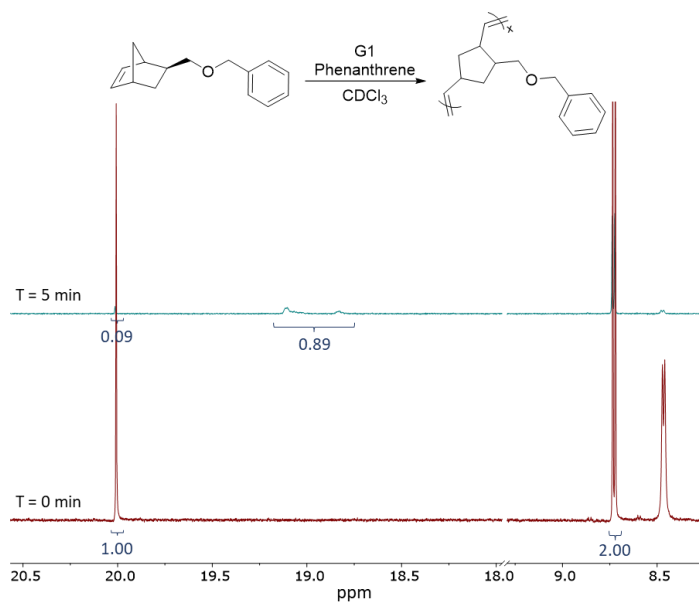


Figure S78. ¹H NMR spectrum of the benzylidene proton of G1 before initiation and the alkylidene proton at 4 propagation half-lives of monomer *x*-MOMP (**1**). Phenanthrene was used as an internal standard.

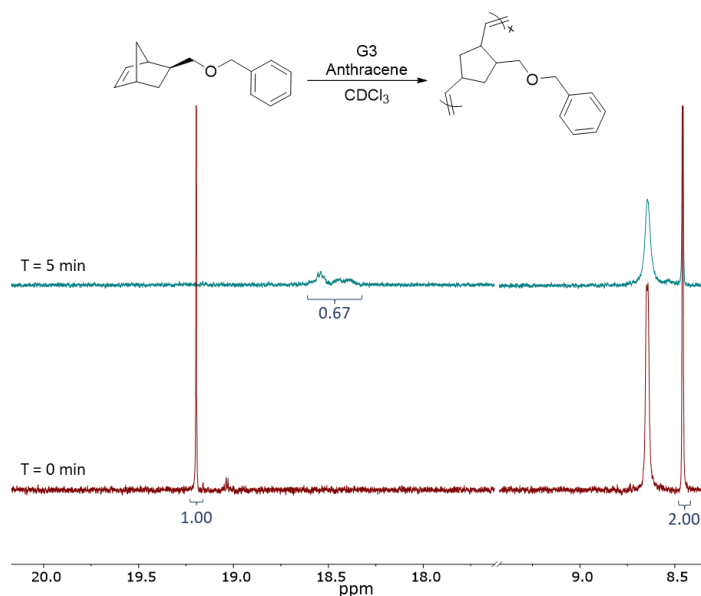


Figure S79. ^1H NMR spectrum of the benzylidene proton of G3 before initiation and the alkylidene proton at 12 propagation half-lives of monomer x -MOMP (**1**). Anthracene was used as an internal standard.

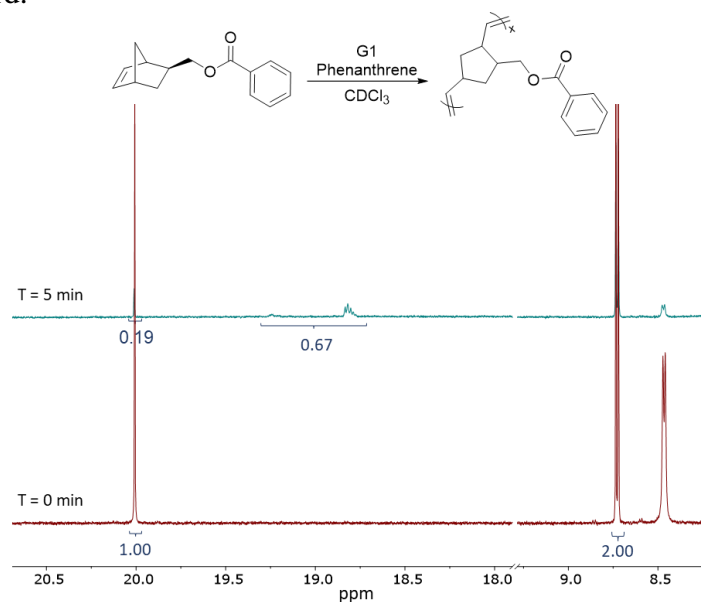


Figure S80. ^1H NMR spectrum of the benzylidene proton of G1 before initiation and the alkylidene proton at 4 propagation half-lives of monomer x -ME'P (**2**). Phenanthrene was used as an internal standard.

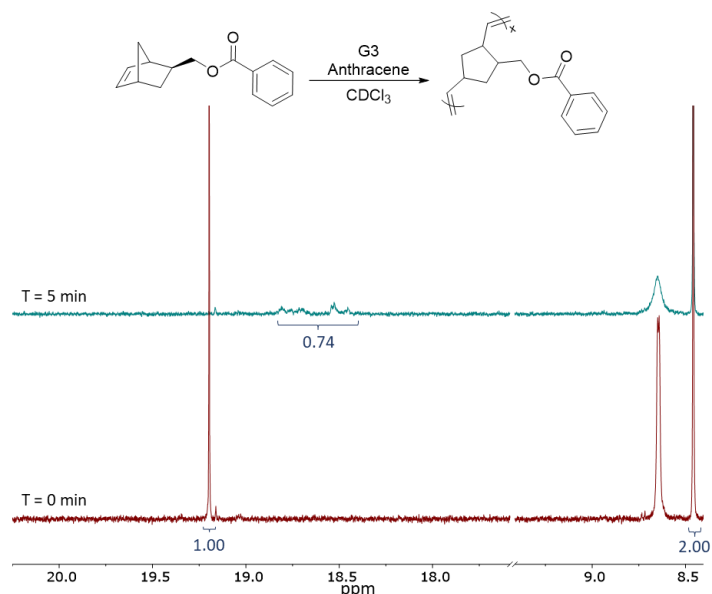


Figure S81. ^1H NMR spectrum of the benzylidene proton of G3 before initiation and the alkylidene proton at 12 propagation half-lives of monomer α -ME'P (**2**). Anthracene was used as an internal standard.

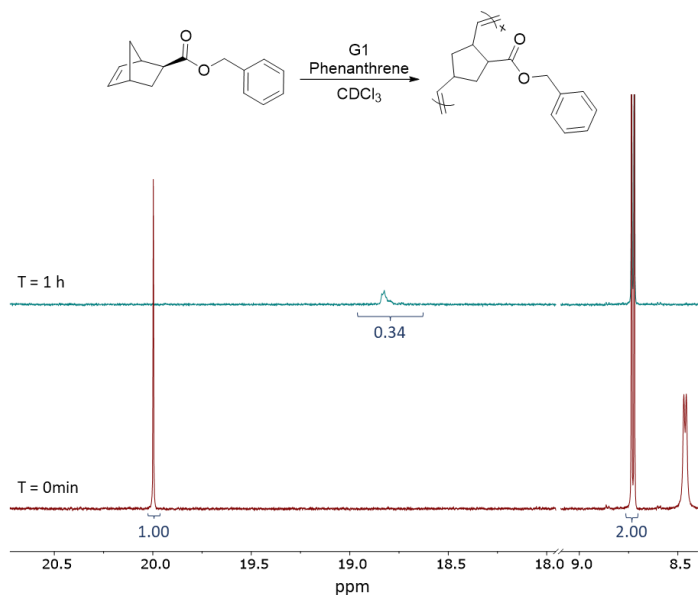


Figure S82. ^1H NMR spectrum of the benzylidene proton of G1 before initiation and the alkylidene proton at 4 propagation half-lives of monomer α -EMP (**3**). Phenanthrene was used as an internal standard.

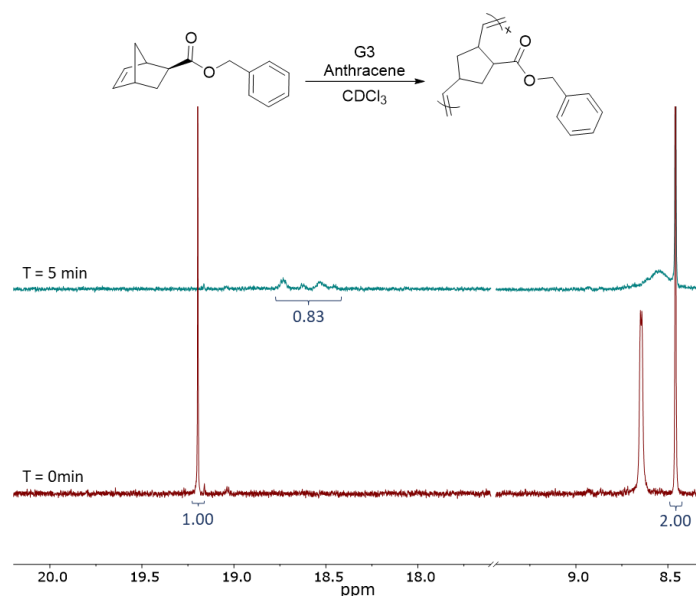


Figure S83. ^1H NMR spectrum of the benzylidene proton of G3 before initiation and the alkylidene proton at 12 propagation half-lives of monomer x -EMP (**3**). Anthracene was used as an internal standard.

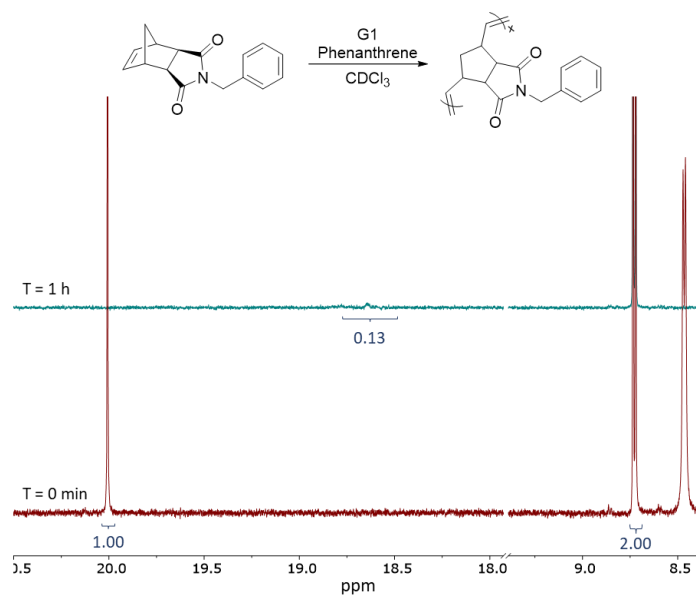


Figure S84. ^1H NMR spectrum of the benzylidene proton of G1 before initiation and the alkylidene proton at 4 propagation half-lives of monomer xx -IMP (**4**). Phenanthrene was used as an internal standard.

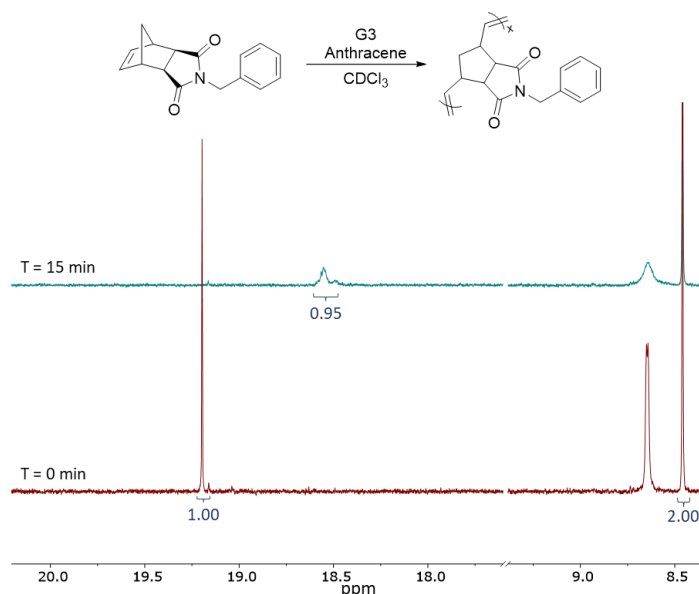


Figure S85. ^1H NMR spectrum of the benzylidene proton of G3 before initiation and the alkylidene proton at 12 propagation half-lives of monomer $xx\text{-IMP}$ (**4**). Anthracene was used as an internal standard.

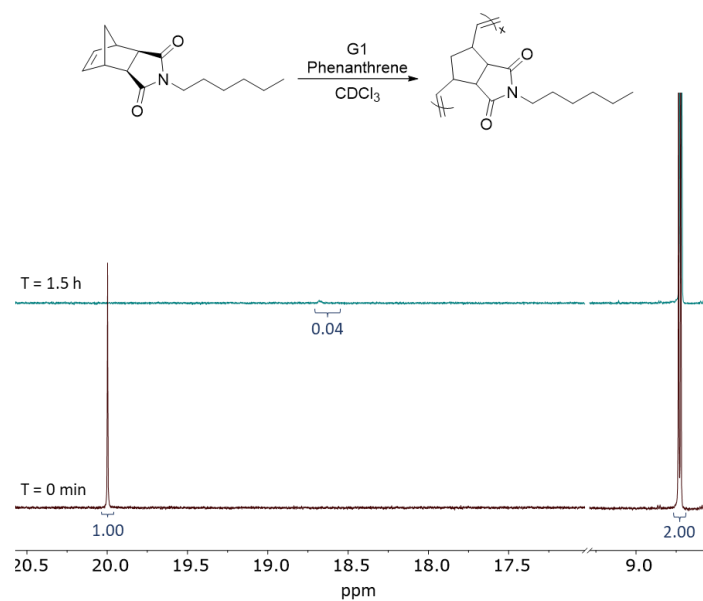


Figure S86. ^1H NMR spectrum of the benzylidene proton of G1 before initiation and the alkylidene proton at 4 propagation half-lives of monomer $xx\text{-IM}_6$ (**5**). Phenanthrene was used as an internal standard.

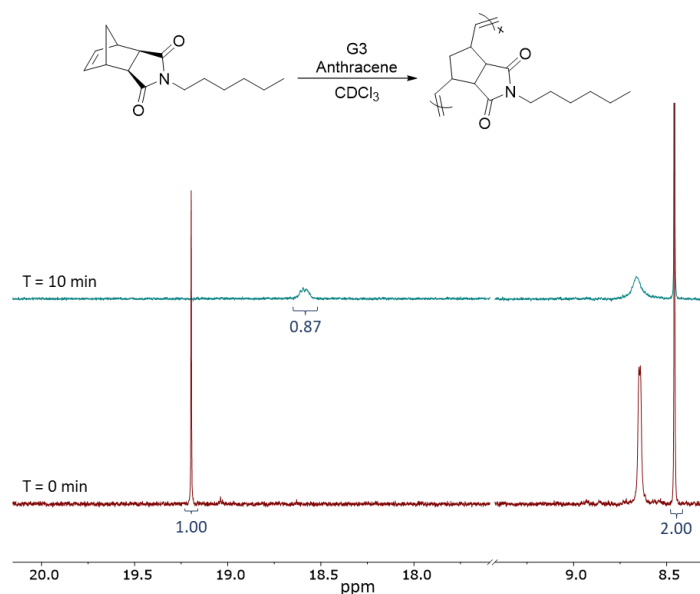


Figure S87. ¹H NMR spectrum of the benzylidene proton of G3 before initiation and the alkylidene proton at 12 propagation half-lives of monomer $\alpha\alpha$ -IM₆ (**5**). Anthracene was used as an internal standard.

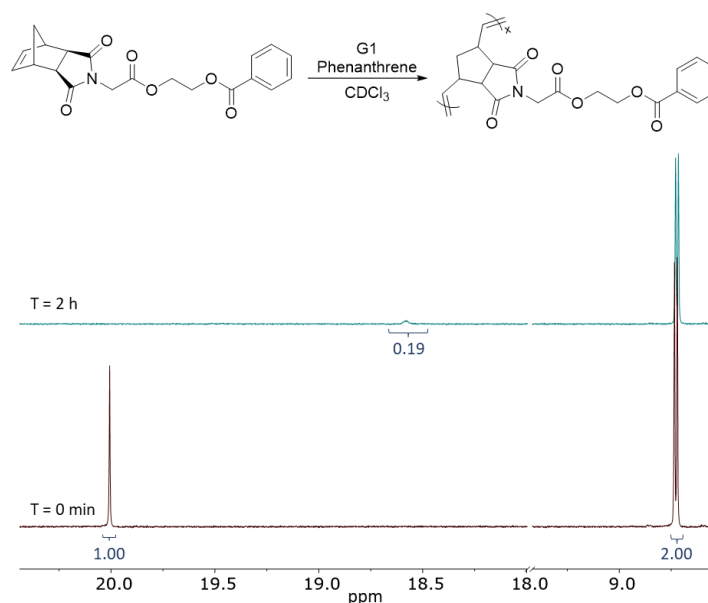


Figure S88. ¹H NMR spectrum of the benzylidene proton of G1 before initiation and the alkylidene proton at 4 propagation half-lives of monomer $\alpha\alpha$ -IMEM₂E'P (**6**). Phenanthrene was used as an internal standard.

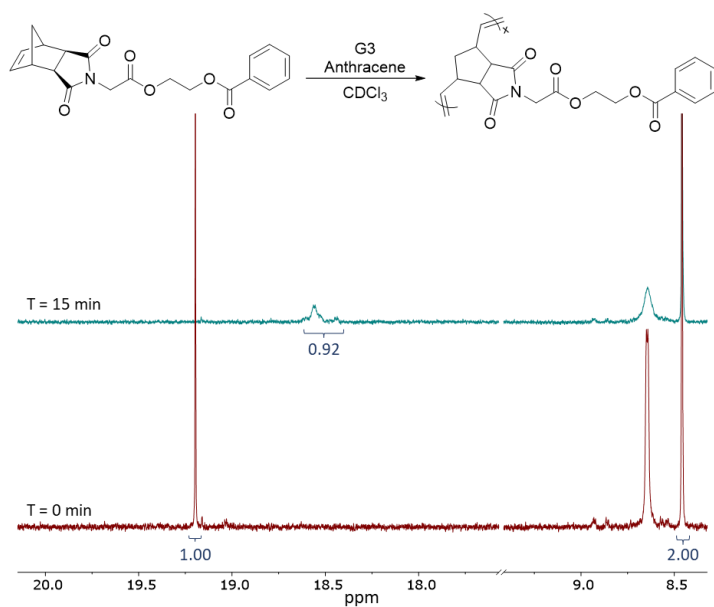


Figure S89. ^1H NMR spectrum of the benzylidene proton of G3 before initiation and the alkylidene proton at 12 propagation half-lives of monomer $xx\text{-IMEM}_2\text{E}'\text{P}$ (**6**). Anthracene was used as an internal standard.

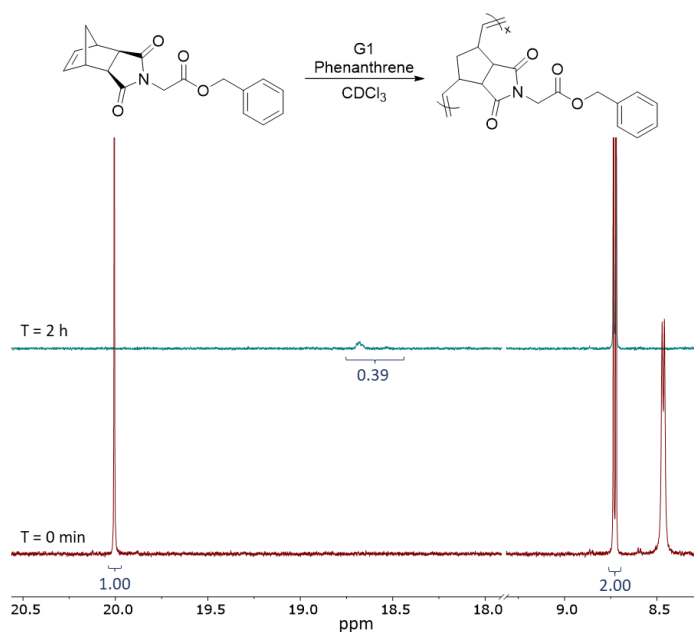


Figure S90. ^1H NMR spectrum of the benzylidene proton of G1 before initiation and the alkylidene proton at 4 propagation half-lives of monomer $xx\text{-IMEMP}$ (**7**). Phenanthrene was used as an internal standard.

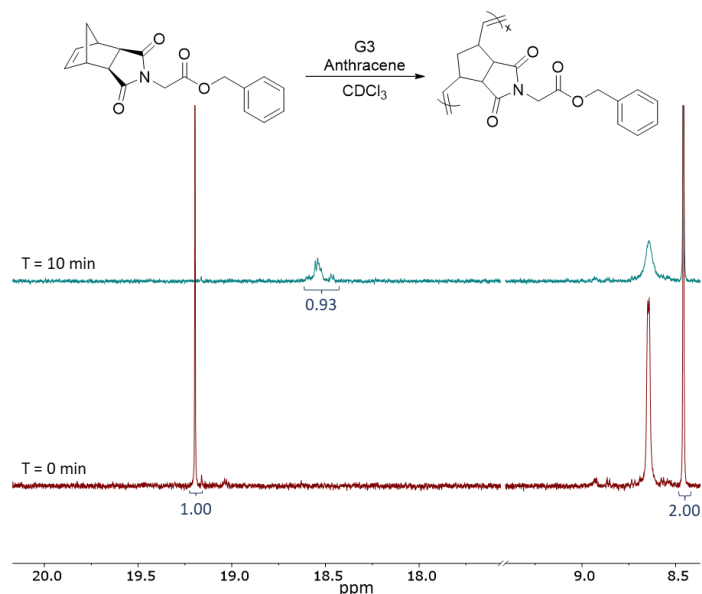


Figure S91. ^1H NMR spectrum of the benzylidene proton of G3 before initiation and the alkylidene proton at 12 propagation half-lives of monomer *xx*-IMEMP (**7**). Anthracene was used as an internal standard.

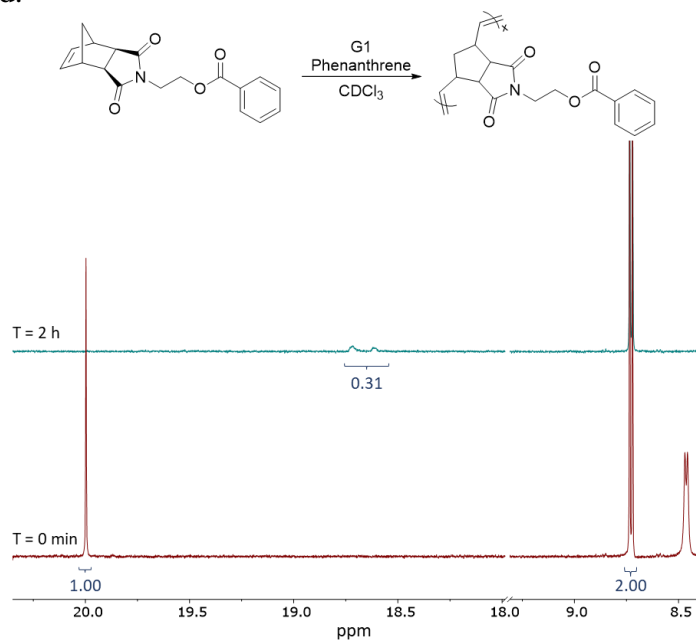


Figure S92. ^1H NMR spectrum of the benzylidene proton of G1 before initiation and the alkylidene proton at 4 propagation half-lives of monomer *xx*-IM₂E'P (**8**). Phenanthrene was used as an internal standard.

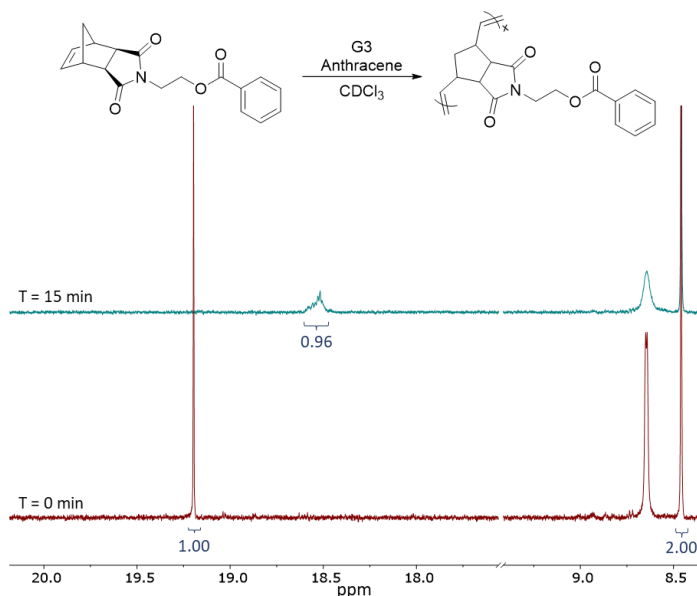


Figure S93. ^1H NMR spectrum of the benzylidene proton of G3 before initiation and the alkylidene proton at 12 propagation half-lives of monomer $\alpha\alpha\text{-IM}_2\text{E}'\text{P}$ (**8**). Anthracene was used as an internal standard.

Deconvolution of linear polymer SEC traces

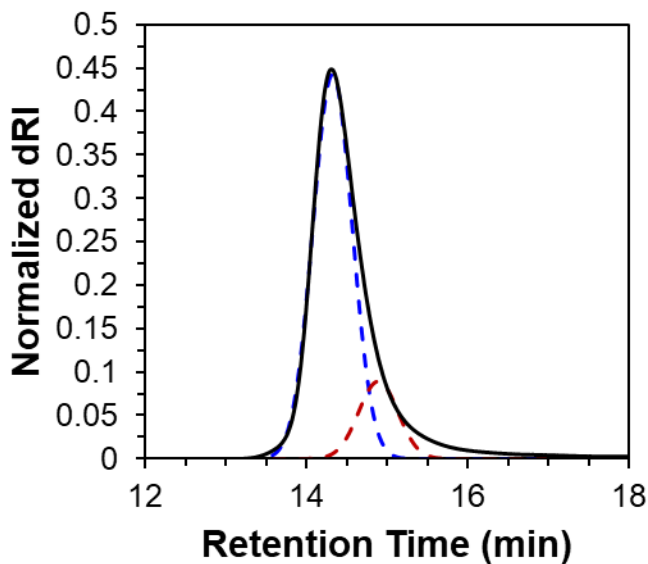


Figure S94. SEC trace (dRI signal) of the linear polymer of monomer $\alpha\alpha\text{-MOMP}$ (**1**) with G1 (solid, black), deconvoluted living linear polymer (dash, blue), and deconvoluted dead chains (dash, red).

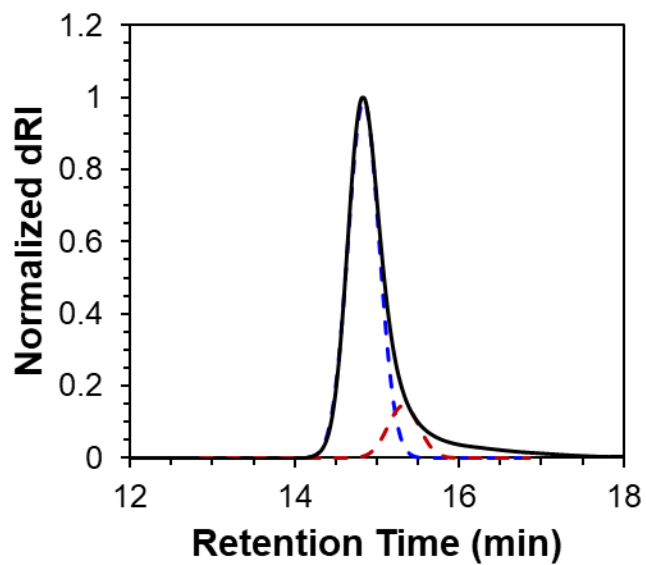


Figure S95. SEC trace (dRI signal) of the linear polymer of monomer *x*-MOMP (**1**) with G3 (solid, black), deconvoluted living linear polymer (dash, blue), and deconvoluted dead chains (dash, red).

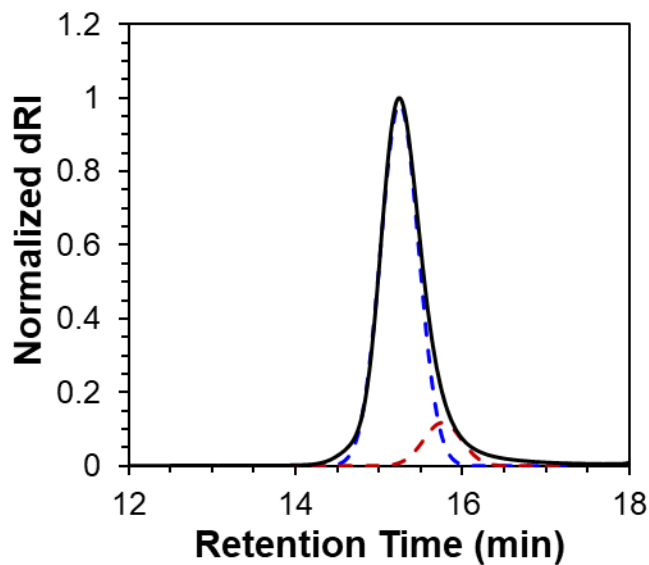


Figure S96. SEC trace (dRI signal) of the linear polymer of monomer *x*-ME'P (**2**) with G1 (solid, black), deconvoluted living linear polymer (dash, blue), and deconvoluted dead chains (dash, red).

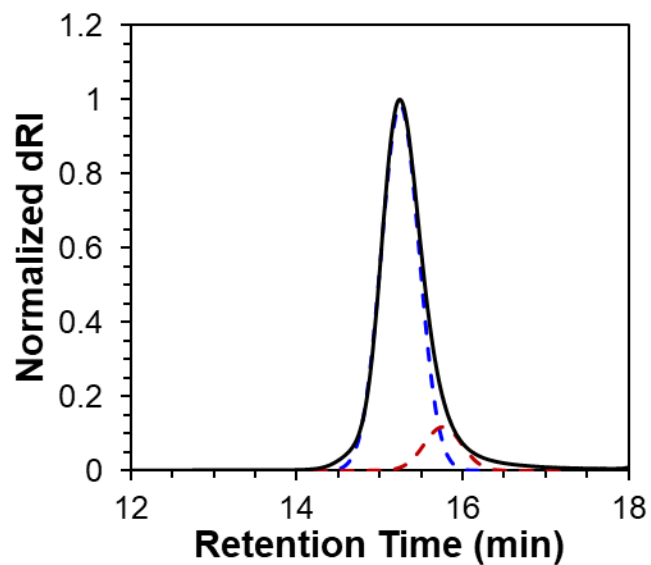


Figure S97. SEC trace (dRI signal) of the linear polymer of monomer *x*-ME'P (**2**) with G3 (solid, black), deconvoluted living linear polymer (dash, blue), and deconvoluted dead chains (dash, red).

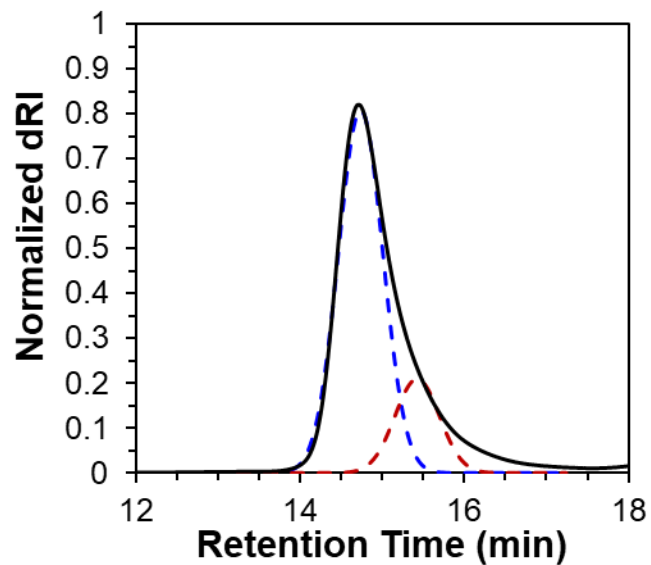


Figure S98. SEC trace (dRI signal) of the linear polymer of monomer *x*-EMP (**3**) with G1 (solid, black), deconvoluted living linear polymer (dash, blue), and deconvoluted dead chains (dash, red).

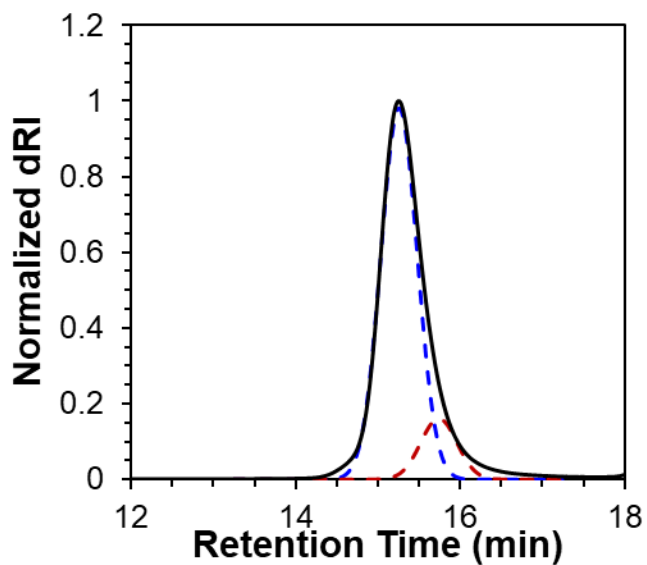


Figure S99. SEC trace (dRI signal) of the linear polymer of monomer *x*-EMP (**3**) with G3 (solid, black), deconvoluted living linear polymer (dash, blue), and deconvoluted dead chains (dash, red).

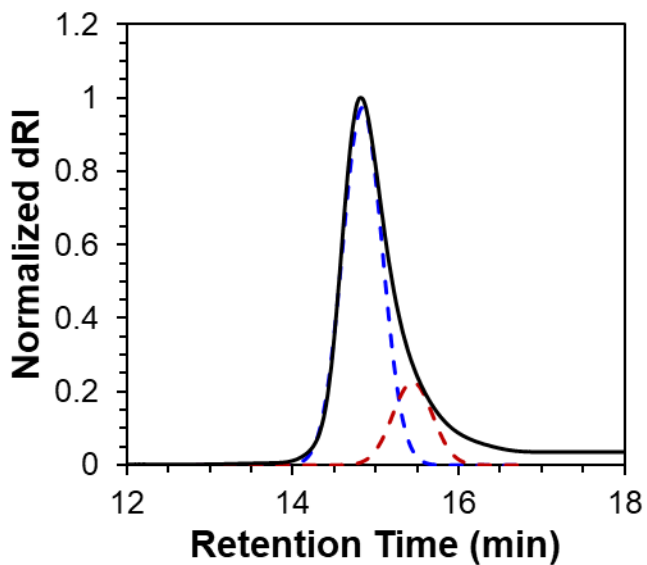


Figure S100. SEC trace (dRI signal) of the linear polymer of monomer *xx*-IMP (**4**) with G1 (solid, black), deconvoluted living linear polymer (dash, blue), and deconvoluted dead chains (dash, red).

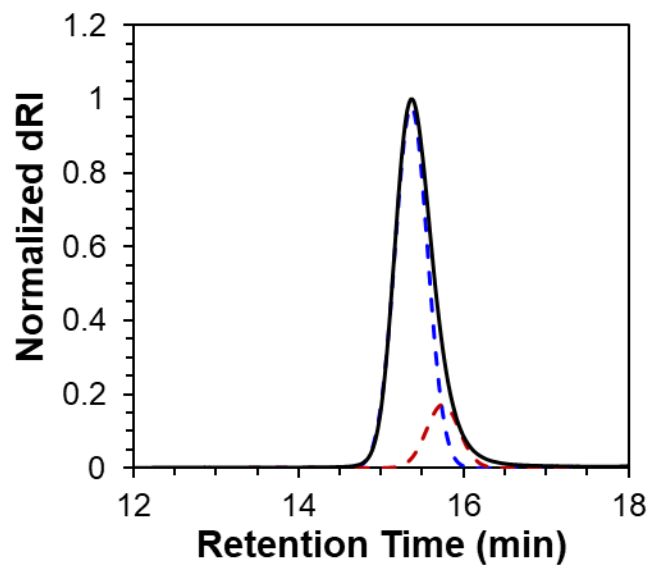


Figure S101. SEC trace (dRI signal) of the linear polymer of monomer *xx*-IMP (**4**) with G3 (solid, black), deconvoluted living linear polymer (dash, blue), and deconvoluted dead chains (dash, red).

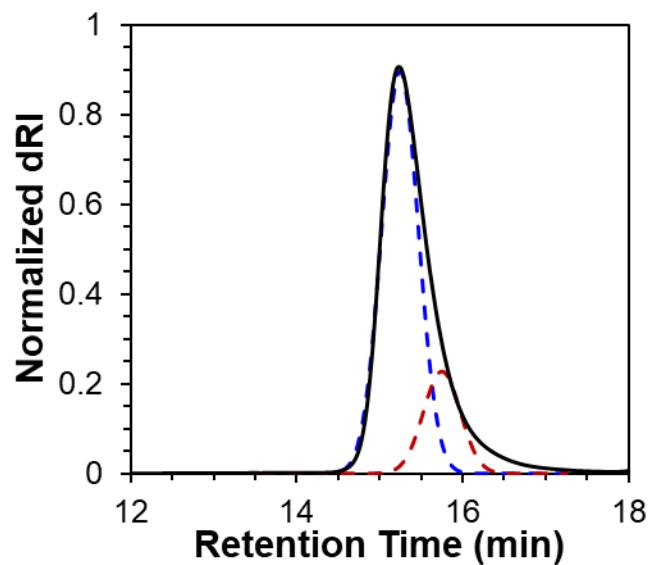


Figure S102. SEC trace (dRI signal) of the linear polymer of monomer *xx*-IM₆ (**5**) with G1 (solid, black), deconvoluted living linear polymer (dash, blue), and deconvoluted dead chains (dash, red).

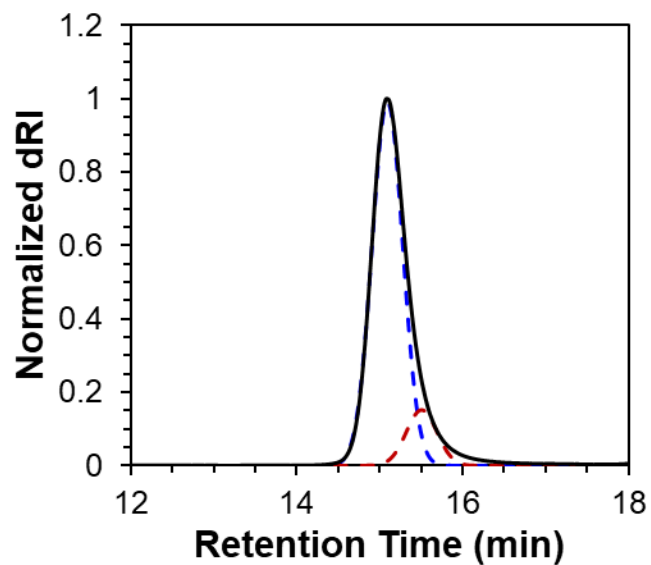


Figure S103. SEC trace (dRI signal) of the linear polymer of monomer xx -IM₆ (**5**) with G3 (solid, black), deconvoluted living linear polymer (dash, blue), and deconvoluted dead chains (dash, red).

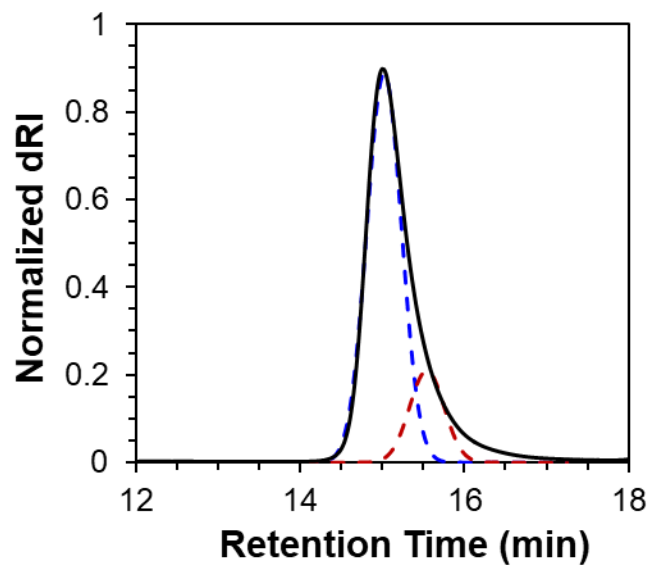


Figure S104. SEC trace (dRI signal) of the linear polymer of monomer xx -IMEM₂E'P (**6**) with G1 (solid, black), deconvoluted living linear polymer (dash, blue), and deconvoluted dead chains (dash, red).

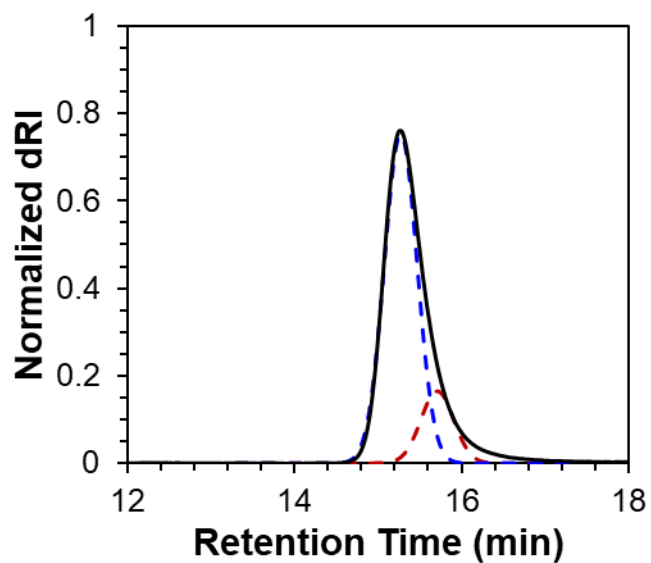


Figure S105. SEC trace (dRI signal) of the linear polymer of monomer xx -IMEM₂E'P (**6**) with G3 (solid, black), deconvoluted living linear polymer (dash, blue), and deconvoluted dead chains (dash, red).

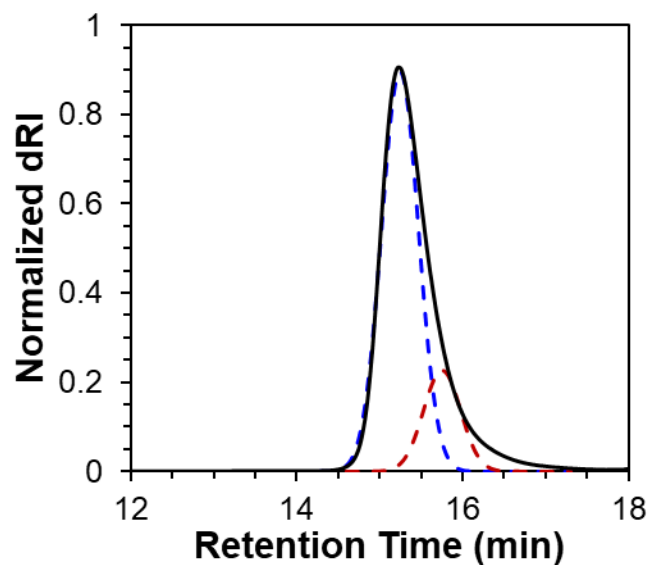


Figure S106. SEC trace (dRI signal) of the linear polymer of monomer xx -IMEMP (**7**) with G1 (solid, black), deconvoluted living linear polymer (dash, blue), and deconvoluted dead chains (dash, red).

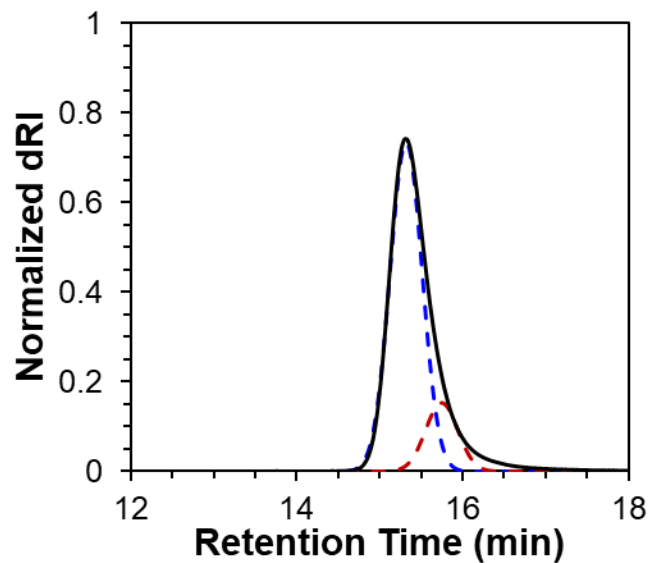


Figure S107. SEC trace (dRI signal) of the linear polymer of monomer *xx*-IMEMP (**7**) with G3 (solid, black), deconvoluted living linear polymer (dash, blue), and deconvoluted dead chains (dash, red).

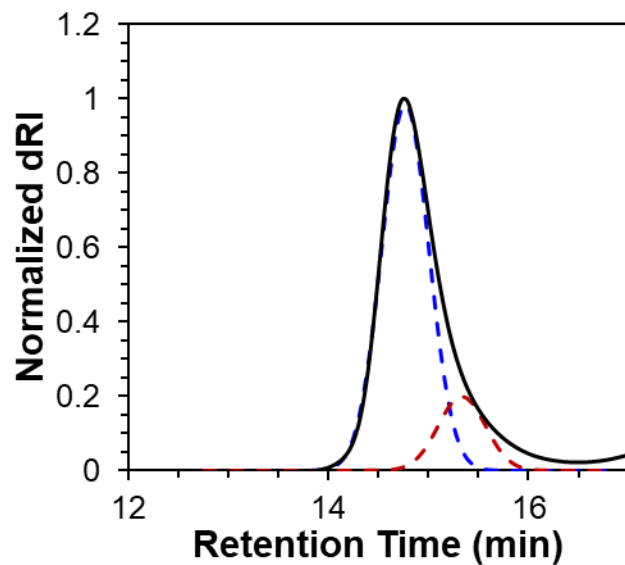


Figure S108. SEC trace (dRI signal) of the linear polymer of monomer *xx*-IM₂E'P (**8**) with G1 (solid, black), deconvoluted living linear polymer (dash, blue), and deconvoluted dead chains (dash, red).

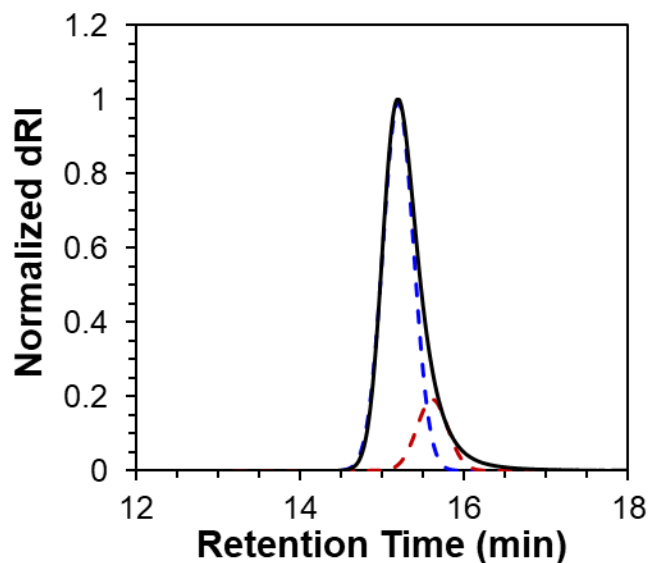


Figure S109. SEC trace (dRI signal) of the linear polymer of monomer *xx*-IM₂E'P (**8**) with G3 (solid, black), deconvoluted living linear polymer (dash, blue), and deconvoluted dead chains (dash, red).

Table S2. Percent dead chains in the ROMP of monomers **1–8** with either G1 or G3 catalyst

Anchor Group	Catalyst	% dead chains ^a
<i>x</i> -MOMP (1)	G1	18
<i>x</i> -ME'P (2)		11
<i>x</i> -EMP (3)		21
<i>xx</i> -IMP (4)		19
<i>xx</i> -IM ₆ (5)		20
<i>xx</i> -IMEM ₂ E'P (6)		19
<i>xx</i> -IMEMP (7)		20
<i>xx</i> -IM ₂ E'P (8)		17
<i>x</i> -MOMP (1)	G3	13
<i>x</i> -ME'P (2)		11
<i>x</i> -EMP (3)		15
<i>xx</i> -IMP (4)		15
<i>xx</i> -IM ₆ (5)		13
<i>xx</i> -IMEM ₂ E'P (6)		18
<i>xx</i> -IMEMP (7)		17
<i>xx</i> -IM ₂ E'P (8)		16

^aPercent dead chains calculated from the area under the deconvoluted SEC traces (dRI) of the linear polymers synthesized from monomers **1–8** with either G1 or G3 catalyst.

XYZ Coordinates (Angstrom) of B3LYP/6-31G* geometry optimizations of anchor groups

Anchor Group *x*-MOMP (1)

6 4.312510 -0.304569 0.216697
6 4.456867 1.198527 0.011966
6 3.270096 1.757129 0.287052
6 2.312981 0.636729 0.671935
6 2.028474 -0.149218 -0.663306
6 3.405681 -0.831922 -0.947532
1 3.805552 -0.580126 -1.934044
1 3.324216 -1.925691 -0.894818
6 0.886153 -1.152915 -0.551412
8 -0.319901 -0.446022 -0.311873
6 -1.449333 -1.291311 -0.206482
6 -2.707727 -0.465945 -0.058753
6 -3.814421 -0.991999 0.617212
6 -5.000864 -0.264051 0.714911
6 -5.090086 1.006915 0.144504
6 -3.986655 1.541375 -0.523613
6 -2.803789 0.808691 -0.628449
1 -1.941143 1.223021 -1.139616
1 -4.046289 2.532896 -0.965376
1 -6.010989 1.578525 0.224648
1 -5.851257 -0.685866 1.244471
1 -3.747326 -1.977493 1.074136
1 -1.520751 -1.928402 -1.107527
1 -1.342493 -1.975532 0.652710
1 0.802419 -1.738025 -1.484337
1 1.071282 -1.873490 0.264281
1 1.762111 0.555582 -1.457943
6 3.296851 -0.323795 1.382963
1 3.701447 0.095576 2.309136
1 2.882152 -1.318873 1.586107
1 1.408054 0.928373 1.207308
1 2.982487 2.795241 0.151255
1 5.338737 1.687037 -0.391190
1 5.240563 -0.866418 0.349630

Anchor Group *x*-ME'P (2)

6 -2.617336 -1.101288 0.657556
6 -3.797639 -0.631465 1.498309
6 -4.630919 0.032143 0.685347
6 -4.022468 0.012022 -0.711085
6 -3.336544 -1.374036 -0.686627
1 -4.047422 -2.203193 -0.620897
1 -2.659149 -1.541323 -1.533029

6 -2.766109 0.946548 -0.667818
6 -1.801393 0.204224 0.312918
6 -0.431368 -0.106431 -0.282541
8 0.205845 1.141246 -0.637138
6 1.459038 1.475456 -0.222718
8 1.726892 2.641697 -0.040829
6 2.485923 0.393086 -0.069649
6 3.477968 0.564864 0.906182
6 4.495971 -0.375237 1.045489
6 4.549798 -1.479908 0.191180
6 3.581420 -1.641960 -0.801409
6 2.548382 -0.713451 -0.927876
1 1.805986 -0.834753 -1.710758
1 3.631685 -2.489365 -1.479576
1 5.349602 -2.208402 0.293800
1 5.253730 -0.242354 1.812696
1 3.438471 1.443655 1.541855
1 0.186039 -0.656290 0.434389
1 -0.521674 -0.711251 -1.192340
1 -1.635372 0.793099 1.221034
1 -3.008135 1.957108 -0.329041
1 -2.318018 1.035871 -1.664021
1 -4.705329 0.217216 -1.539171
1 -5.520907 0.586749 0.966052
1 -3.862181 -0.725672 2.577861
1 -2.017561 -1.912035 1.081346

Anchor Group *x*-EMP (3)

6 -2.437354 0.625048 0.907466
6 -3.313286 1.838549 0.636003
6 -4.419349 1.403724 0.016215
6 -4.294754 -0.105690 -0.139347
6 -3.178850 -0.356813 -1.212470
6 -1.890300 0.173266 -0.517047
6 -0.813470 -0.881378 -0.356967
8 0.405695 -0.303491 -0.233568
6 1.512305 -1.213731 -0.019685
6 2.790154 -0.417076 0.009574
6 3.672761 -0.532992 1.087858
6 4.877186 0.174212 1.101543
6 5.204901 1.014219 0.037739
6 4.325011 1.141825 -1.040889
6 3.128641 0.427842 -1.056390
1 2.443703 0.531458 -1.893731
1 4.574143 1.796640 -1.871777
1 6.139381 1.568876 0.047713

1 5.553577 0.072498 1.946025
1 3.416843 -1.180793 1.923261
1 1.354383 -1.756780 0.917161
1 1.507161 -1.952183 -0.829133
8 -0.985942 -2.082254 -0.294175
1 -1.447495 1.030855 -1.028272
1 -3.382096 0.162457 -2.153228
1 -3.082306 -1.426221 -1.419442
6 -3.516187 -0.455316 1.150828
1 -3.119765 -1.475765 1.157179
1 -4.094025 -0.269018 2.061122
1 -5.221916 -0.651878 -0.328076
1 -5.214657 2.008150 -0.409224
1 -3.014935 2.866498 0.816597
1 -1.654480 0.747028 1.659181

Anchor Group *xx*-IMP (4)

6 -0.033509 -3.157826 -1.130264
6 0.936485 -4.240469 -0.670144
6 0.936485 -4.240469 0.670144
6 -0.033509 -3.157826 1.130264
6 0.669780 -1.792485 0.775396
6 0.669780 -1.792485 -0.775396
6 -0.148179 -0.567962 -1.169282
7 -0.565292 0.071701 -0.000000
6 -0.148179 -0.567962 1.169282
8 -0.423467 -0.193525 2.292055
6 -1.384410 1.288993 -0.000000
6 -0.557474 2.559907 -0.000000
6 -0.166500 3.150331 1.208261
6 0.600336 4.316240 1.207931
6 0.984631 4.901726 -0.000000
6 0.600336 4.316240 -1.207931
6 -0.166500 3.150331 -1.208261
1 -0.455738 2.684571 -2.146904
1 0.898847 4.766083 -2.151412
1 1.578909 5.811774 -0.000000
1 0.898847 4.766083 2.151412
1 -0.455738 2.684571 2.146904
1 -2.015057 1.238185 -0.890854
1 -2.015057 1.238185 0.890854
8 -0.423467 -0.193525 -2.292055
1 1.657119 -1.719611 -1.237789
1 1.657119 -1.719611 1.237789
6 -1.087099 -3.245110 0.000000
1 -1.619493 -4.199751 0.000000

1 -1.815895 -2.426618 0.000000
1 -0.383609 -3.210376 2.162665
1 1.575520 -4.817829 1.330900
1 1.575520 -4.817829 -1.330900
1 -0.383609 -3.210376 -2.162665

Anchor Group $xx-IM_6$ (5)

6 -3.591025 -1.143134 0.183821
6 -4.800537 -0.702320 -0.633460
6 -4.814472 0.638064 -0.644965
6 -3.614542 1.117996 0.164376
6 -2.355043 0.768136 -0.715106
6 -2.339011 -0.782407 -0.701751
6 -1.009330 -1.156369 -0.056270
7 -0.330542 0.022223 0.262669
6 -1.033650 1.181081 -0.076556
8 -0.636080 2.310328 0.131120
6 0.980909 0.040335 0.906681
6 2.135150 0.002738 -0.102160
6 3.505628 0.021840 0.585793
6 4.678556 -0.014551 -0.402241
6 6.052574 0.004292 0.279683
6 7.219200 -0.031082 -0.712675
1 8.185328 -0.016036 -0.195482
1 7.186607 -0.936570 -1.331168
1 7.190272 0.831842 -1.389453
1 6.132756 0.903418 0.907090
1 6.128148 -0.852022 0.964882
1 4.597285 -0.914595 -1.029561
1 4.602488 0.842088 -1.088251
1 3.586487 0.922522 1.212123
1 3.581246 -0.835488 1.270832
1 2.038550 -0.901914 -0.716208
1 2.044388 0.863991 -0.776828
1 1.025291 0.952557 1.508479
1 1.023048 -0.828819 1.569662
8 -0.587695 -2.273175 0.170853
1 -2.397923 -1.253558 -1.686366
1 -2.423690 1.220831 -1.707713
6 -3.546357 -0.002934 1.230007
1 -4.419759 -0.006396 1.887380
1 -2.636755 0.011826 1.841079
1 -3.629707 2.152515 0.511019
1 -5.480676 1.287189 -1.204000
1 -5.452976 -1.374627 -1.181211
1 -3.584727 -2.171647 0.548156

Anchor Group xx -IMEM₂E'P (6)
6 4.907716 0.856068 -0.727647
6 6.233410 0.180148 -1.243439
6 7.359763 1.091283 -0.767446
6 7.452222 0.959537 0.563251
6 6.389187 -0.041776 1.002024
6 5.014146 0.704116 0.813396
6 3.804746 -0.130614 1.214485
7 3.094053 -0.444742 0.051199
6 3.644658 0.098011 -1.114255
8 3.173713 -0.055706 -2.221932
6 1.838697 -1.153169 0.062770
1 1.815840 -1.811984 0.935315
1 1.752394 -1.755411 -0.845294
6 0.660555 -0.183777 0.136060
8 0.746482 1.014803 0.251965
8 -0.498189 -0.867976 0.057025
6 -1.699275 -0.072167 0.115586
6 -2.854877 -1.048115 -0.019256
8 -4.046737 -0.248756 0.033263
6 -5.213986 -0.930885 -0.100438
8 -5.255084 -2.135292 -0.251077
6 -6.404860 -0.039663 -0.041375
6 -7.668573 -0.631823 -0.173697
6 -8.816291 0.154925 -0.126403
6 -8.708784 1.536657 0.053592
6 -7.451108 2.130150 0.186076
6 -6.299386 1.346742 0.139165
1 -5.320775 1.801934 0.241732
1 -7.367665 3.204306 0.326010
1 -9.604770 2.150642 0.090520
1 -9.794160 -0.307037 -0.229619
1 -7.727353 -1.706336 -0.312412
1 -2.809725 -1.593216 -0.966667
1 -2.858227 -1.780716 0.793439
1 -1.738044 0.468746 1.065531
1 -1.696167 0.660252 -0.696552
8 3.488452 -0.500630 2.325952
1 4.987914 1.643719 1.370844
6 6.383333 -0.980710 -0.229349
1 7.327905 -1.517746 -0.348024
1 5.556501 -1.699969 -0.242635
1 6.508422 -0.493148 1.988284
1 8.083687 1.524744 1.241002
1 7.900035 1.786385 -1.401855

1 6.211143 -0.068855 -2.305602
1 4.817824 1.885731 -1.082577

Anchor Group *xx*-IMEMP (7)

6 3.631101 -0.775316 -0.705132
6 4.117652 -1.130336 0.751945
6 5.569724 -0.670294 0.809561
6 5.569355 0.670220 0.810930
6 4.117031 1.129585 0.754285
6 3.630620 0.777324 -0.703505
6 2.184755 1.173459 -0.971192
7 1.440770 0.000779 -1.138896
6 2.185501 -1.171792 -0.973732
8 1.717151 -2.289220 -1.044832
6 0.009247 0.000498 -1.308759
1 -0.282216 0.891619 -1.870848
1 -0.281625 -0.889701 -1.872617
6 -0.720714 -0.001110 0.034184
8 -0.188966 -0.001918 1.121787
8 -2.046510 -0.000885 -0.174100
6 -2.877332 -0.001908 1.025593
6 -4.316907 -0.000762 0.593864
6 -4.995477 -1.206788 0.380961
6 -6.325138 -1.207603 -0.040163
6 -6.990726 0.001418 -0.252438
6 -6.322685 1.209367 -0.041656
6 -4.993058 1.206387 0.379505
1 -4.473627 2.147647 0.543888
1 -6.837591 2.152673 -0.202276
1 -8.027682 0.002266 -0.577509
1 -6.841941 -2.150067 -0.199625
1 -4.477947 -2.148898 0.546470
1 -2.623335 -0.887746 1.614371
1 -2.622486 0.882334 1.616400
8 1.715716 2.290744 -1.039990
1 4.269326 1.238700 -1.461293
6 3.440454 -0.001404 1.567598
1 3.759054 -0.002397 2.613506
1 2.346410 -0.001655 1.521694
1 3.909626 2.161204 1.043156
1 6.428706 1.330846 0.755427
1 6.429438 -1.330332 0.752706
1 3.910808 -2.162667 1.038667
1 4.270137 -1.234709 -1.463845

Anchor Group xx -IM₂E'P (8)

6 3.765994 -0.633903 0.815045
6 4.314047 0.818473 1.086102
6 5.769520 0.787633 0.633321
6 5.775655 0.706990 -0.704673
6 4.324437 0.682990 -1.171465
6 3.773149 -0.727051 -0.733642
6 2.318870 -0.962939 -1.122761
7 1.557512 -1.016181 0.050805
6 2.307824 -0.820985 1.215935
8 1.836975 -0.805094 2.334911
6 0.117743 -1.235627 0.058427
1 -0.129962 -1.848221 -0.811523
1 -0.133239 -1.776962 0.973724
6 -0.645561 0.085601 0.004969
8 -2.041013 -0.258399 0.016769
6 -2.901877 0.789401 -0.030133
8 -2.528859 1.944662 -0.078443
6 -4.327379 0.358196 -0.015876
6 -5.310684 1.356186 -0.059653
6 -6.658975 1.008817 -0.049710
6 -7.032759 -0.336691 0.003840
6 -6.055533 -1.334008 0.047675
6 -4.704714 -0.990916 0.038095
1 -3.941560 -1.760179 0.071932
1 -6.346506 -2.379987 0.089436
1 -8.085171 -0.607986 0.011505
1 -7.418592 1.784815 -0.083697
1 -4.996291 2.393832 -0.101289
1 -0.413145 0.713785 0.869997
1 -0.410957 0.643365 -0.906689
8 1.859332 -1.084148 -2.239859
1 4.380770 -1.537854 -1.143858
6 3.683104 1.593562 -0.096202
1 4.040535 2.624635 -0.156479
1 2.587116 1.593862 -0.101217
1 4.135044 0.918375 -2.219923
1 6.634555 0.576651 -1.354944
1 6.622332 0.736766 1.302407
1 4.114756 1.177300 2.097066
1 4.369087 -1.389493 1.325144

Anchor Group 9

6 4.335565 -0.512511 0.606694
6 4.494655 -1.355378 -0.655491
6 3.279726 -1.810848 -0.991659

6 2.287832 -1.260453 0.024877
6 2.212200 0.284316 -0.315959
6 3.593858 0.803513 0.195082
1 4.131243 1.366465 -0.573218
1 3.488330 1.457828 1.066170
7 1.035136 1.002829 0.200765
6 -0.096332 0.921902 -0.590984
7 -1.169158 1.769506 -0.225626
6 -2.447864 1.407662 -0.865511
6 -3.041271 0.124094 -0.318660
6 -3.064891 -1.045290 -1.085934
6 -3.632241 -2.216428 -0.579660
6 -4.178290 -2.233338 0.704309
6 -4.154277 -1.072337 1.481207
6 -3.590715 0.096235 0.970245
1 -3.575128 0.999588 1.576551
1 -4.579274 -1.076734 2.481841
1 -4.620014 -3.144841 1.098838
1 -3.642511 -3.117192 -1.188039
1 -2.617718 -1.036700 -2.075172
1 -3.134192 2.235949 -0.656493
1 -2.329273 1.338505 -1.954486
6 -0.905439 3.212675 -0.245778
1 0.087992 3.426324 0.149394
1 -0.958987 3.624388 -1.266492
1 -1.642656 3.734077 0.374469
8 -0.170111 0.152470 -1.547106
6 0.977783 1.488535 1.574778
1 1.416633 0.759208 2.261351
1 1.507136 2.441780 1.709734
1 -0.067105 1.626335 1.853343
1 2.142028 0.382774 -1.397815
6 3.179368 -1.279782 1.290605
1 3.462555 -2.294128 1.587879
1 2.758579 -0.756930 2.156375
1 1.310208 -1.741298 0.065053
1 3.002345 -2.356004 -1.888149
1 5.419168 -1.465722 -1.213940
1 5.241673 -0.345175 1.194717

Anchor Group 10

6 -4.658126 0.349982 0.900482
6 -5.305584 -0.591621 -0.110975
6 -4.534042 -0.597917 -1.206250
6 -3.349660 0.323584 -0.937261
6 -2.480658 -0.469777 0.121800

6 -3.359249 -0.354693 1.412405
1 -3.558211 -1.333125 1.858337
1 -2.868200 0.257608 2.176484
7 -1.080880 -0.046026 0.270661
6 -0.119911 -0.941743 -0.129319
8 1.135311 -0.428257 0.026028
6 2.204343 -1.330475 -0.346334
6 3.508633 -0.602219 -0.159891
6 4.232350 -0.728829 1.031359
6 5.434820 -0.043631 1.210118
6 5.926198 0.779636 0.195503
6 5.211565 0.913590 -0.997054
6 4.011239 0.225340 -1.171856
1 3.457381 0.327337 -2.102381
1 5.591918 1.549860 -1.791801
1 6.864117 1.311625 0.331271
1 5.988442 -0.154479 2.138720
1 3.851126 -1.370852 1.822212
1 2.147309 -2.225732 0.279935
1 2.055681 -1.641438 -1.384487
8 -0.324424 -2.064433 -0.566581
6 -0.702125 1.291167 0.746321
6 -0.411622 2.302974 -0.367555
1 -0.131600 3.269292 0.069037
1 0.419872 1.958778 -0.989123
1 -1.284591 2.460701 -1.008996
1 -1.512496 1.656346 1.381997
1 0.178065 1.189916 1.385007
1 -2.406347 -1.506960 -0.195655
6 -4.047873 1.394834 -0.064880
1 -4.807618 1.955687 -0.617615
1 -3.367826 2.098394 0.427053
1 -2.784568 0.655405 -1.810496
1 -4.634071 -1.231698 -2.081712
1 -6.174885 -1.211141 0.086569
1 -5.306226 0.726957 1.695761

Anchor Group 11

6 4.719898 0.392349 -0.801966
6 5.306688 -0.359158 0.389487
6 4.454994 -0.218861 1.414247
6 3.275754 0.610133 0.917825
6 2.508894 -0.367903 -0.060611
6 3.477303 -0.422861 -1.289147
1 3.727253 -1.450801 -1.565559
1 3.028507 0.052037 -2.168603

7 1.122052 0.002516 -0.371134
6 0.137425 -0.846714 0.069744
8 -1.109827 -0.347854 -0.171832
6 -2.195973 -1.215357 0.217785
6 -3.481613 -0.433483 0.133478
6 -4.554232 -0.909274 -0.626630
6 -5.761485 -0.207997 -0.672983
6 -5.902974 0.985080 0.034990
6 -4.833399 1.472320 0.791795
6 -3.633578 0.765775 0.843252
1 -2.801717 1.146398 1.430005
1 -4.937306 2.402000 1.345223
1 -6.839904 1.534493 -0.002111
1 -6.586590 -0.591825 -1.267112
1 -4.445057 -1.835383 -1.186475
1 -2.216768 -2.088397 -0.442836
1 -2.002978 -1.577783 1.232431
8 0.323401 -1.927888 0.607660
6 0.809810 1.303501 -0.951574
1 1.470530 1.502173 -1.800925
1 -0.217905 1.306107 -1.307251
1 0.930413 2.117117 -0.223801
1 2.425907 -1.346748 0.404905
6 4.016133 1.554304 -0.061118
1 4.718753 2.218727 0.450761
1 3.359977 2.147715 -0.705791
1 2.639793 1.058246 1.684869
1 4.501276 -0.704612 2.383773
1 6.201319 -0.973102 0.355818
1 5.419674 0.660836 -1.597466

Anchor Group 12

6 4.244896 -0.507401 0.415253
6 4.456454 -1.242437 -0.905035
6 3.295727 -1.827407 -1.229534
6 2.284861 -1.477515 -0.142390
6 1.993363 0.059047 -0.379040
6 3.325443 0.720577 0.112408
1 3.749670 1.389391 -0.641982
1 3.168876 1.310922 1.021914
7 0.761452 0.612387 0.215537
6 -0.178002 1.093152 -0.663329
7 -1.311888 1.774251 -0.055047
6 -2.575702 1.327202 -0.696739
6 -2.922780 -0.117920 -0.408861
6 -2.531187 -1.141453 -1.282379

6 -2.862874 -2.471119 -1.014037
6 -3.595762 -2.795799 0.128646
6 -3.995540 -1.783234 1.003863
6 -3.659750 -0.456108 0.734553
1 -3.974697 0.330528 1.416924
1 -4.572588 -2.026423 1.892454
1 -3.859191 -3.830158 0.333899
1 -2.552866 -3.253188 -1.702482
1 -1.957049 -0.888635 -2.169093
1 -3.363521 1.971202 -0.291326
1 -2.533379 1.493025 -1.783035
6 -1.173636 3.240940 -0.251223
6 0.035017 3.863675 0.445069
1 0.042439 4.943238 0.257400
1 -0.001598 3.710202 1.528468
1 0.979993 3.457336 0.070842
1 -1.139448 3.478231 -1.328017
1 -2.088527 3.692134 0.150133
8 -0.077978 0.992423 -1.883797
6 0.539206 0.592141 1.670721
6 -0.108802 -0.690412 2.203428
1 -0.249260 -0.601748 3.288057
1 -1.088706 -0.845621 1.745014
1 0.502867 -1.577156 2.017229
1 1.504532 0.759849 2.158385
1 -0.100975 1.435512 1.919169
1 1.860216 0.223092 -1.444751
6 3.225440 -1.457808 1.087468
1 3.646342 -2.443068 1.309507
1 2.778763 -1.041643 1.996263
1 1.387663 -2.097132 -0.100419
1 3.051552 -2.345467 -2.151569
1 5.361655 -1.196645 -1.502580
1 5.145885 -0.262348 0.983497

Anchor Group 13

6 4.482446 1.360118 0.107049
6 5.427063 0.290142 -0.431901
6 4.951013 -0.899976 -0.042824
6 3.682318 -0.646546 0.760034
6 2.602604 -0.169168 -0.281793
6 3.156802 1.233135 -0.711667
1 3.319618 1.307182 -1.790288
1 2.450212 2.024488 -0.431885
7 1.259377 -0.116775 0.280707
6 0.195525 -0.752534 -0.332745

7 -1.034955 -0.458802 0.239873
6 -2.218823 -1.213295 -0.152745
6 -3.487208 -0.391478 -0.032444
6 -4.622776 -0.927193 0.584438
6 -5.806308 -0.190172 0.669384
6 -5.865193 1.099613 0.141862
6 -4.734639 1.646225 -0.471694
6 -3.556356 0.906369 -0.558129
1 -2.675905 1.332947 -1.031060
1 -4.772799 2.650596 -0.885913
1 -6.783453 1.676998 0.209402
1 -6.678407 -0.622805 1.152861
1 -4.580793 -1.931043 1.002060
1 -2.044502 -1.522448 -1.187770
1 -2.320976 -2.137472 0.436062
1 -1.034703 -0.106693 1.189042
8 0.317255 -1.497980 -1.299271
1 1.046377 0.657551 0.895584
1 2.534540 -0.861886 -1.120110
6 4.053911 0.694307 1.437663
1 4.875766 0.598021 2.153397
1 3.207628 1.196999 1.925854
1 3.332033 -1.461869 1.396017
1 5.312126 -1.881868 -0.331761
1 6.260359 0.480937 -1.101008
1 4.881594 2.375962 0.162687

Anchor Group 14

6 -3.740210 0.363629 0.821398
6 -4.432963 -0.477416 -0.244060
6 -3.609900 -0.546723 -1.299476
6 -2.350295 0.238123 -0.948373
6 -1.611705 -0.648077 0.131210
6 -2.549700 -0.489555 1.373678
1 -2.877343 -1.452676 1.777588
1 -2.036408 0.059046 2.170300
6 -0.142909 -0.305042 0.424396
6 0.791305 -0.580114 -0.779477
6 2.243808 -0.302914 -0.458585
6 2.778636 0.986765 -0.606888
6 4.104193 1.259434 -0.260339
6 4.920052 0.244617 0.240995
6 4.401816 -1.043584 0.392302
6 3.077027 -1.311583 0.047601
1 2.682783 -2.318748 0.165946
1 5.031487 -1.842011 0.776499

1 5.952799 0.453297 0.506891
1 4.499406 2.263791 -0.389098
1 2.151499 1.778398 -1.010769
1 0.668757 -1.627589 -1.082294
1 0.469882 0.043360 -1.621247
8 -0.050788 1.056129 0.839753
1 0.877330 1.225353 1.070270
1 0.183801 -0.961420 1.250498
1 -1.608283 -1.690756 -0.208473
6 -2.965729 1.358193 -0.074808
1 -3.629442 2.014178 -0.647499
1 -2.217985 1.945498 0.462962
1 -1.729441 0.549734 -1.791316
1 -3.736483 -1.146307 -2.196258
1 -5.373477 -1.002900 -0.107480
1 -4.383138 0.786203 1.598011

Anchor Group 15

6 2.662075 -1.407858 -0.059606
6 3.450958 -0.765158 1.074380
6 3.278944 0.560764 0.981097
6 2.369754 0.824045 -0.212096
6 0.943452 0.318157 0.232995
6 1.144674 -1.230716 0.285885
1 0.884056 -1.655128 1.259430
1 0.527771 -1.738471 -0.464774
6 -0.181145 0.774980 -0.712902
6 -1.553069 0.265345 -0.296850
6 -2.181206 -0.774274 -0.992496
6 -3.433742 -1.246904 -0.594862
6 -4.079703 -0.675676 0.502050
6 -3.467279 0.371314 1.195943
6 -2.214975 0.838235 0.799060
1 -1.743993 1.662227 1.327850
1 -3.968124 0.825808 2.047031
1 -5.056450 -1.038520 0.810946
1 -3.906745 -2.054809 -1.147201
1 -1.688481 -1.214212 -1.857289
8 -0.140806 2.207136 -0.708332
1 -0.901140 2.519005 -1.224320
1 0.033190 0.398678 -1.726984
1 0.704130 0.719921 1.223146
6 2.819316 -0.322054 -1.149774
1 3.851831 -0.206097 -1.493448
1 2.163177 -0.474056 -2.015831
1 2.367950 1.838676 -0.610846

1 3.611166 1.320089 1.682518
1 3.957159 -1.310973 1.864798
1 2.942626 -2.430427 -0.325321

Anchor Group 16

6 -2.955750 -1.698819 -0.254587
6 -4.255380 -0.900230 -0.236654
6 -4.004965 0.261977 0.381570
6 -2.537766 0.259221 0.784621
6 -1.727183 0.395938 -0.561319
6 -2.003116 -0.971520 -1.261271
1 -2.451127 -0.851988 -2.251168
1 -1.073383 -1.540473 -1.390544
7 -0.301101 0.616011 -0.353770
6 0.200479 1.846372 -0.058313
6 1.727789 1.940374 0.143946
6 2.520544 0.654204 0.106826
6 2.711255 -0.106737 1.270408
6 3.420966 -1.307757 1.234037
6 3.953192 -1.771286 0.029187
6 3.770860 -1.025573 -1.136909
6 3.060291 0.175104 -1.096398
1 2.926070 0.753938 -2.007629
1 4.186082 -1.375156 -2.078526
1 4.509412 -2.704296 0.000195
1 3.562368 -1.878800 2.147921
1 2.303841 0.251049 2.213541
1 2.084683 2.635807 -0.624845
1 1.865773 2.454321 1.101755
8 -0.497039 2.850790 0.028669
1 0.330395 -0.172493 -0.364723
1 -2.098616 1.247415 -1.134250
6 -2.337922 -1.243340 1.089760
1 -2.909489 -1.581469 1.959159
1 -1.285912 -1.532457 1.210063
1 -2.234343 0.987704 1.537508
1 -4.671469 1.112198 0.484932
1 -5.170641 -1.197344 -0.739344
1 -3.049390 -2.773923 -0.426426

Anchor Group 17

6 4.675549 -0.035508 -1.031619
6 5.457973 -0.123076 0.271376
6 4.701061 0.422947 1.233530
6 3.402041 0.881949 0.588281
6 2.610563 -0.449565 0.242349

6 3.488569 -1.050645 -0.911511
1 3.823514 -2.066588 -0.684747
1 2.926968 -1.091556 -1.852540
6 1.194296 -0.191326 -0.170424
7 0.230246 -0.687350 0.505828
8 -1.010339 -0.298088 -0.032352
6 -2.058646 -0.966015 0.679571
6 -3.375536 -0.348729 0.277957
6 -4.453273 -1.154712 -0.101662
6 -5.686241 -0.587419 -0.431356
6 -5.848641 0.797417 -0.396414
6 -4.773692 1.611174 -0.028100
6 -3.547418 1.041927 0.310268
1 -2.709539 1.673992 0.590212
1 -4.892998 2.691308 -0.002807
1 -6.805347 1.242095 -0.657613
1 -6.514858 -1.227508 -0.722874
1 -4.327098 -2.234397 -0.140899
1 -2.044592 -2.039863 0.450406
1 -1.877824 -0.852791 1.756932
1 0.989936 0.432305 -1.046603
1 2.584507 -1.107625 1.114581
6 3.919813 1.295610 -0.808814
1 4.585116 2.163374 -0.770230
1 3.126404 1.476750 -1.544499
1 2.811649 1.610953 1.147812
1 4.897898 0.437214 2.300949
1 6.404246 -0.641265 0.392408
1 5.254510 -0.134409 -1.953064

Anchor Group 18

6 -4.444332 0.869104 0.547588
6 -4.277103 1.956951 -0.506740
6 -2.994256 1.945667 -0.894642
6 -2.286526 0.848066 -0.109977
6 -2.834636 -0.509128 -0.690643
6 -4.320307 -0.501737 -0.199886
1 -5.037979 -0.595462 -1.020522
1 -4.507213 -1.328812 0.497512
6 -2.066674 -1.748471 -0.205773
7 -0.694316 -1.806732 -0.694735
6 0.382681 -1.754424 0.164508
7 1.607116 -1.974725 -0.453173
6 2.845896 -1.731959 0.289201
6 3.380533 -0.316661 0.161188
6 4.528379 -0.051917 -0.593732

6 5.011021 1.252259 -0.729324
6 4.345447 2.308752 -0.108165
6 3.198535 2.054539 0.649932
6 2.719006 0.752587 0.785316
1 1.831095 0.549253 1.377854
1 2.680288 2.873630 1.142138
1 4.718883 3.324450 -0.209441
1 5.905644 1.440159 -1.317578
1 5.053635 -0.874359 -1.076102
1 2.619000 -1.965983 1.331582
1 3.597937 -2.447869 -0.061815
1 1.653258 -1.761507 -1.442510
8 0.268701 -1.548055 1.371124
1 -0.545135 -2.185873 -1.619543
1 -2.599772 -2.656216 -0.521463
1 -2.006484 -1.768243 0.885031
1 -2.786681 -0.486849 -1.786374
6 -3.057440 0.933951 1.228909
1 -2.883861 1.877990 1.754146
1 -2.858153 0.098476 1.909734
1 -1.197280 0.904671 -0.065918
1 -2.544435 2.519013 -1.699817
1 -5.088726 2.542715 -0.927694
1 -5.324568 0.949967 1.190594

Anchor Group 19

6 3.539566 -0.408171 -0.558003
6 3.443831 -1.549714 0.449163
6 2.567590 -1.181656 1.393514
6 2.061749 0.208182 1.032466
6 1.143200 0.010771 -0.237191
6 2.184303 -0.386906 -1.337075
1 1.955493 -1.348058 -1.806280
1 2.198591 0.372822 -2.126446
7 0.391493 1.213931 -0.597487
6 -0.904413 1.536201 -0.247639
6 -1.912620 0.429032 -0.116335
6 -1.949228 -0.675527 -0.978971
6 -2.960225 -1.629897 -0.857984
6 -3.936570 -1.493644 0.130376
6 -3.912274 -0.388421 0.985170
6 -2.914380 0.574474 0.852819
1 -2.899383 1.454017 1.488617
1 -4.677713 -0.272974 1.747854
1 -4.719930 -2.240646 0.227914
1 -2.988194 -2.475931 -1.539484

1 -1.204192 -0.772310 -1.763415
8 -1.241022 2.708243 -0.102817
1 0.947801 2.060332 -0.679858
1 0.420142 -0.781636 -0.053590
6 3.335740 0.802260 0.385622
1 4.152493 0.932520 1.101347
1 3.170878 1.748131 -0.147326
1 1.579475 0.777465 1.830242
1 2.182904 -1.785025 2.209618
1 3.926729 -2.515590 0.338154
1 4.425022 -0.398483 -1.197988

Anchor Group 20

6 -3.304695 0.005761 -0.396497
6 -3.443063 -0.155131 1.112613
6 -2.272968 -0.615468 1.575890
6 -1.333527 -0.763626 0.385632
6 -0.972874 0.704964 -0.056584
6 -2.336511 1.213439 -0.633589
1 -2.686726 2.128840 -0.146777
1 -2.251446 1.422577 -1.707473
6 0.186250 0.798873 -1.075754
6 1.530407 0.373065 -0.521856
6 2.242035 1.211134 0.349596
6 3.469970 0.819440 0.882263
6 4.014426 -0.423439 0.550641
6 3.321169 -1.266287 -0.318365
6 2.091870 -0.868511 -0.848475
1 1.561638 -1.529313 -1.531028
1 3.737532 -2.233502 -0.588412
1 4.972554 -0.728883 0.962678
1 4.005250 1.487023 1.552866
1 1.829942 2.184587 0.608388
1 -0.053681 0.196856 -1.961517
1 0.249818 1.839768 -1.422229
1 -0.686605 1.286944 0.826614
6 -2.349812 -1.170698 -0.708651
1 -2.801759 -2.149760 -0.522064
1 -1.944347 -1.145672 -1.727599
1 -0.466271 -1.410329 0.534548
1 -1.980505 -0.749572 2.612929
1 -4.304747 0.160221 1.693137
1 -4.236713 0.059123 -0.965257

Anchor Group 21

6 -4.478026 1.083406 0.708384

6 -5.359033 0.148837 -0.114599
6 -4.594844 -0.376837 -1.081521
6 -3.193633 0.194153 -0.918730
6 -2.613841 -0.471939 0.388733
6 -3.490934 0.171571 1.509359
1 -4.007160 -0.575866 2.117174
1 -2.872952 0.773093 2.187740
7 -1.197064 -0.213463 0.604123
6 -0.233603 -0.956157 -0.009360
8 0.999236 -0.442690 0.274951
6 2.108297 -1.175612 -0.286527
6 3.357305 -0.345394 -0.137088
6 4.496041 -0.880560 0.472461
6 5.669010 -0.129122 0.575698
6 5.709798 1.172666 0.077323
6 4.573704 1.718605 -0.527036
6 3.407992 0.963268 -0.636643
1 2.524256 1.389759 -1.103728
1 4.598829 2.733136 -0.916257
1 6.619856 1.760952 0.159682
1 6.546210 -0.559759 1.051287
1 4.465507 -1.892407 0.870219
1 2.206645 -2.135663 0.231354
1 1.884928 -1.392417 -1.336471
8 -0.428963 -1.943942 -0.696437
1 -0.900464 0.630536 1.072884
1 -2.726590 -1.555818 0.338396
6 -3.531944 1.610167 -0.398066
1 -4.044059 2.227163 -1.142140
1 -2.663822 2.157296 -0.007781
1 -2.524383 0.103154 -1.775999
1 -4.865533 -1.155325 -1.787556
1 -6.385112 -0.108197 0.129506
1 -4.996602 1.825354 1.320390

Anchor Group 22

6 -4.683387 -2.345657 -0.254576
6 -6.118197 -1.835652 -0.168134
6 -6.090430 -0.664446 0.481926
6 -4.639984 -0.372389 0.838410
6 -3.927605 -0.032429 -0.527221
6 -3.940516 -1.408619 -1.264195
1 -4.438882 -1.358413 -2.235752
1 -2.918212 -1.767520 -1.441533
7 -2.571241 0.478564 -0.361289
6 -2.328495 1.795414 -0.083870

6 -0.870048 2.221655 0.102682
6 0.220207 1.173662 -0.128706
6 1.619521 1.750537 0.018036
8 2.543468 0.766701 -0.031936
6 3.928872 1.200735 0.077594
6 4.803677 -0.022157 0.051499
6 5.352385 -0.480565 -1.151831
6 6.149601 -1.625319 -1.178742
6 6.405387 -2.325374 0.001647
6 5.862643 -1.876034 1.207573
6 5.067725 -0.730519 1.230410
1 4.647652 -0.380074 2.170420
1 6.062442 -2.415066 2.129743
1 7.028885 -3.215238 -0.016953
1 6.572697 -1.968403 -2.119026
1 5.154646 0.064445 -2.072008
1 4.146184 1.878139 -0.753429
1 4.039168 1.765822 1.007628
8 1.886644 2.924615 0.151972
1 0.139321 0.330826 0.569794
1 0.153588 0.744095 -1.137655
1 -0.709572 3.077180 -0.560671
1 -0.788532 2.629363 1.116697
8 -3.231430 2.619942 0.006361
1 -1.807859 -0.180925 -0.357500
1 -4.486701 0.738933 -1.058351
6 -4.122890 -1.808744 1.084752
1 -4.577619 -2.281967 1.959945
1 -3.029738 -1.878170 1.161665
1 -4.465972 0.381423 1.607374
1 -6.913791 0.025538 0.635716
1 -6.970490 -2.302993 -0.651560
1 -4.558793 -3.411603 -0.460227

Anchor Group 23

6 -4.010807 -1.085497 -0.024088
6 -4.630659 -0.112133 -1.017503
6 -3.987037 1.056826 -0.892670
6 -2.930643 0.880247 0.188376
6 -1.818742 -0.069154 -0.440372
6 -2.576821 -1.425606 -0.557389
1 -2.595465 -1.797934 -1.585789
1 -2.098554 -2.173184 0.079373
6 -0.591328 -0.151744 0.473090
7 0.344842 0.853264 0.370057
6 1.544902 0.774291 1.215124

6 2.762845 0.221725 0.495712
6 2.802628 -1.127568 0.111740
6 3.913936 -1.639909 -0.555555
6 5.003562 -0.813937 -0.847408
6 4.974706 0.527228 -0.466567
6 3.858514 1.039473 0.199884
1 3.842392 2.085990 0.498437
1 5.818421 1.176247 -0.686832
1 5.870219 -1.216174 -1.365452
1 3.933956 -2.687860 -0.843731
1 1.958333 -1.769383 0.348430
1 1.760422 1.782145 1.590469
1 1.280953 0.139213 2.062100
6 0.355721 1.871780 -0.673033
1 -0.656431 2.184311 -0.931052
1 0.886610 2.751988 -0.296466
1 0.869075 1.533952 -1.583603
8 -0.468058 -1.051699 1.306433
1 -1.526489 0.301008 -1.425359
6 -3.649619 -0.117524 1.126596
1 -4.528685 0.323214 1.606857
1 -2.989226 -0.563012 1.877115
1 -2.536246 1.794523 0.638944
1 -4.097777 1.942102 -1.511700
1 -5.378540 -0.373988 -1.759897
1 -4.609343 -1.963396 0.230677

Anchor Group 24

6 -3.883033 -1.452901 -0.277159
6 -4.688476 -0.312373 -0.883821
6 -4.199668 0.833963 -0.389676
6 -3.059763 0.472359 0.551655
6 -1.883920 -0.032100 -0.397876
6 -2.453588 -1.390786 -0.918331
1 -2.484973 -1.432126 -2.011183
1 -1.841588 -2.219419 -0.553345
6 -0.585342 -0.199706 0.389917
7 0.402616 0.747964 0.250930
6 1.572044 0.660042 1.142217
6 2.794410 0.045041 0.486242
6 2.787093 -1.306390 0.107225
6 3.906746 -1.876099 -0.495714
6 5.051219 -1.106937 -0.728460
6 5.069187 0.235377 -0.352252
6 3.944865 0.805703 0.251232
1 3.965996 1.852159 0.550001

1 5.955246 0.840418 -0.526602
1 5.923642 -1.554502 -1.197373
1 3.890330 -2.924994 -0.780777
1 1.898746 -1.901794 0.298388
1 1.808653 1.672456 1.491266
1 1.262303 0.065499 2.003036
6 0.431321 1.831545 -0.736313
6 -0.205231 3.135411 -0.244081
1 -0.083990 3.926024 -0.993842
1 -1.275765 3.006682 -0.053752
1 0.263142 3.477035 0.685727
1 1.484773 2.000522 -0.985594
1 -0.041914 1.501690 -1.664111
8 -0.450714 -1.140479 1.178252
1 -1.765587 0.678971 -1.214765
6 -3.577482 -0.868051 1.121139
1 -4.476176 -0.737514 1.732168
1 -2.813696 -1.423905 1.670221
1 -2.754922 1.239949 1.267343
1 -4.465959 1.845777 -0.680610
1 -5.441134 -0.425605 -1.658318
1 -4.342016 -2.443828 -0.316063

Anchor Group 25

6 -5.101020 0.229734 0.330656
6 -4.950004 1.733040 0.129822
6 -3.642676 2.018812 0.203219
6 -2.899804 0.711206 0.447124
6 -3.004679 -0.091324 -0.904886
6 -4.525594 -0.455653 -0.954385
1 -5.014828 -0.107355 -1.868961
1 -4.669517 -1.542513 -0.896816
6 -2.105012 -1.336634 -0.968927
7 -0.681735 -1.038209 -1.024609
6 0.137551 -1.143817 0.057269
8 1.407241 -0.782944 -0.289601
6 2.384028 -0.885668 0.769705
6 3.626727 -0.147297 0.344927
6 4.849202 -0.815476 0.228408
6 6.006989 -0.124873 -0.137647
6 5.949137 1.243558 -0.399771
6 4.729947 1.919073 -0.292172
6 3.578772 1.228512 0.080664
1 2.631033 1.754669 0.162643
1 4.679110 2.985683 -0.494867
1 6.847793 1.783126 -0.686771

1 6.950302 -0.657886 -0.222042
1 4.896154 -1.884075 0.425460
1 1.950196 -0.466836 1.683040
1 2.596715 -1.942963 0.960609
8 -0.195788 -1.509926 1.172004
1 -0.274753 -0.684342 -1.878512
1 -2.365956 -1.931986 -1.853744
1 -2.257612 -1.970731 -0.091745
1 -2.734453 0.561905 -1.743628
6 -3.940327 -0.031464 1.318774
1 -4.090239 0.446605 2.291318
1 -3.716026 -1.093906 1.468648
1 -1.886834 0.789994 0.845029
1 -3.165604 2.975058 0.010204
1 -5.759333 2.408066 -0.131509
1 -6.095049 -0.122472 0.617992

Anchor Group 26

6 3.689995 0.021703 -1.026503
6 4.454052 -0.173420 0.277435
6 3.649943 0.215860 1.276133
6 2.334813 0.670806 0.655163
6 1.626099 -0.641030 0.138196
6 2.557166 -1.057446 -1.051133
1 2.948527 -2.073932 -0.945177
1 2.013950 -1.010652 -2.003273
6 0.158892 -0.454082 -0.282074
6 -0.808626 -0.218256 0.896758
6 -2.248049 -0.062906 0.452996
6 -2.769800 1.198062 0.133484
6 -4.084861 1.341201 -0.310862
6 -4.905217 0.219451 -0.443591
6 -4.399782 -1.042946 -0.127645
6 -3.083897 -1.179664 0.316302
1 -2.699400 -2.166654 0.566012
1 -5.032024 -1.922299 -0.222001
1 -5.930941 0.328582 -0.785795
1 -4.470144 2.329561 -0.548654
1 -2.138093 2.077927 0.239408
1 -0.500752 0.676020 1.452773
1 -0.726814 -1.061839 1.595519
1 -0.172332 -1.348311 -0.828242
1 0.072811 0.379355 -0.993047
1 1.656613 -1.401763 0.928017
6 2.858744 1.276245 -0.669694
1 3.474346 2.167266 -0.512248

1 2.072035 1.500747 -1.400159
1 1.707950 1.310337 1.281475
1 3.829379 0.120117 2.342797
1 5.426597 -0.648918 0.361105
1 4.291459 0.062990 -1.938294

Anchor Group 27

6 -4.450035 -0.312314 -0.019353
6 -4.693571 0.980735 -0.784293
6 -3.634048 1.776163 -0.580416
6 -2.671485 1.026200 0.327646
6 -2.065410 -0.143996 -0.572572
6 -3.300973 -1.071526 -0.770134
1 -3.530151 -1.232834 -1.827364
1 -3.118772 -2.042116 -0.299985
6 -0.892908 -0.805536 0.143425
6 0.490986 -0.261644 -0.193252
6 1.615144 -0.837460 0.681491
6 2.976434 -0.294841 0.302298
6 3.739409 -0.906045 -0.702373
6 4.979466 -0.388501 -1.078435
6 5.480921 0.754144 -0.452205
6 4.733792 1.371558 0.552381
6 3.493921 0.849689 0.924005
1 2.920801 1.332344 1.713306
1 5.118510 2.257209 1.051755
1 6.448301 1.156626 -0.740688
1 5.556776 -0.881127 -1.856762
1 3.359088 -1.801463 -1.190240
1 1.395948 -0.613297 1.731517
1 1.600003 -1.929400 0.596200
1 0.683202 -0.473573 -1.256142
1 0.465522 0.835849 -0.126771
8 -1.044234 -1.696252 0.962933
1 -1.705646 0.280193 -1.515468
6 -3.665788 0.226311 1.199640
1 -4.268405 0.875431 1.842297
1 -3.190479 -0.560315 1.793459
1 -1.919995 1.630968 0.842170
1 -3.419657 2.729150 -1.054144
1 -5.526979 1.156990 -1.457430
1 -5.329317 -0.928248 0.183707

Anchor Group 28

6 -4.345963 -0.798703 0.155374
6 -4.881265 0.617193 -0.033462

6 -3.902554 1.466220 0.307831
6 -2.698983 0.634314 0.726653
6 -2.152369 -0.015753 -0.603230
6 -3.285466 -1.025835 -0.972026
1 -3.691358 -0.852773 -1.972044
1 -2.908604 -2.056125 -0.947883
7 -0.865758 -0.691067 -0.461426
6 0.298505 0.057388 -0.402957
7 1.423300 -0.716558 -0.140418
6 2.764461 -0.300959 -0.022980
6 3.731005 -1.302842 0.165876
6 5.076654 -0.973629 0.301912
6 5.483741 0.360593 0.254276
6 4.522070 1.354347 0.067479
6 3.169631 1.042364 -0.072021
1 2.429569 1.814659 -0.226141
1 4.823177 2.398075 0.025907
1 6.533100 0.620348 0.359939
1 5.806581 -1.765987 0.445805
1 3.422926 -2.346539 0.206940
1 1.295272 -1.719247 -0.158003
8 0.318479 1.267059 -0.596193
1 -0.876463 -1.580959 0.020689
1 -2.010148 0.751743 -1.363912
6 -3.414142 -0.575666 1.371306
1 -3.955033 -0.314424 2.285474
1 -2.751111 -1.427419 1.575970
1 -1.925837 1.147383 1.300368
1 -3.897892 2.546273 0.202355
1 -5.844475 0.860758 -0.470915
1 -5.092280 -1.593047 0.233717

Anchor Group 29

6 -6.398588 1.400080 0.377764
6 -6.157606 2.250589 -0.863797
6 -4.872960 2.096413 -1.213324
6 -4.237501 1.136277 -0.215537
6 -4.857090 -0.275947 -0.536997
6 -6.343730 -0.095328 -0.083761
1 -7.058780 -0.312966 -0.882836
1 -6.579658 -0.757931 0.759165
6 -4.165257 -1.443672 0.185146
7 -2.809406 -1.705734 -0.284043
6 -1.692614 -1.345394 0.413638
6 -0.371127 -1.803595 -0.203853
6 0.777765 -0.870960 0.174061

6 2.134768 -1.506634 -0.044721
8 3.110912 -0.571699 -0.043001
6 4.462346 -1.076536 -0.175021
6 5.421193 0.082083 -0.089139
6 5.345250 0.998563 0.968477
6 6.258540 2.046962 1.061831
6 7.266513 2.188354 0.104012
6 7.350402 1.279426 -0.950387
6 6.427703 0.235517 -1.047654
1 6.490713 -0.465981 -1.876528
1 8.127692 1.384923 -1.702524
1 7.979888 3.004679 0.179424
1 6.186125 2.753998 1.884031
1 4.559261 0.893579 1.711243
1 4.631949 -1.809159 0.622382
1 4.555566 -1.606329 -1.127863
8 2.344792 -2.693765 -0.184347
1 0.734071 0.077733 -0.371135
1 0.683669 -0.610582 1.235825
1 -0.147362 -2.808809 0.174559
1 -0.457126 -1.898723 -1.293322
8 -1.739928 -0.731018 1.475587
1 -2.691693 -2.190155 -1.162859
1 -4.757139 -2.359169 0.055330
1 -4.089022 -1.247039 1.257328
1 -4.801632 -0.466353 -1.616018
6 -5.017700 1.521635 1.063992
1 -4.794839 2.538541 1.400266
1 -4.873517 0.824965 1.897813
1 -3.148352 1.143502 -0.151898
1 -4.382354 2.478289 -2.103728
1 -6.929718 2.786180 -1.407855
1 -7.279946 1.651806 0.973213

Anchor Group 30

6 -3.435751 -1.619234 -0.218083
6 -4.641488 -0.707710 -0.040088
6 -4.250825 0.337540 0.702982
6 -2.777979 0.142243 1.027529
6 -2.008251 0.385937 -0.345494
6 -2.443682 -0.875402 -1.175026
1 -2.903880 -0.601087 -2.128715
1 -1.581728 -1.515744 -1.396711
6 -0.523922 0.484009 -0.158923
6 0.270684 1.560150 -0.343254
6 1.716710 1.503715 0.047829

6 2.492015 0.214536 0.017989
6 3.547242 0.065947 0.932029
6 4.339884 -1.077958 0.918137
6 4.108313 -2.078464 -0.030791
6 3.080332 -1.928125 -0.962531
6 2.271391 -0.791074 -0.935370
1 1.482719 -0.671094 -1.671201
1 2.909103 -2.694289 -1.714037
1 4.732565 -2.968034 -0.047722
1 5.144382 -1.188551 1.640352
1 3.730818 0.864131 1.644187
8 2.283387 2.533131 0.405157
6 -0.190620 2.929774 -0.778559
1 -1.241818 2.945974 -1.072359
1 -0.040429 3.650544 0.032115
1 0.410058 3.289443 -1.622256
1 -0.053023 -0.424284 0.213816
1 -2.391894 1.297449 -0.807101
6 -2.722632 -1.398951 1.136778
1 -3.296024 -1.779347 1.987467
1 -1.706405 -1.809732 1.169723
1 -2.379975 0.724830 1.861025
1 -4.822123 1.229840 0.939556
1 -5.600747 -0.846086 -0.529278
1 -3.647216 -2.650623 -0.511039

Anchor Group 31

6 3.879416 1.127025 0.016931
6 4.549442 0.335332 -1.097133
6 4.035838 -0.902758 -1.077428
6 3.015921 -0.953214 0.051003
6 1.791602 -0.072134 -0.449375
6 2.394753 1.366180 -0.427268
1 2.324276 1.859431 -1.401036
1 1.873381 1.978104 0.313850
6 0.587220 -0.228611 0.475580
8 0.513255 0.314457 1.576951
7 -0.384779 -1.075212 0.014412
6 -1.615959 -1.337348 0.756790
6 -2.802290 -0.522425 0.274870
6 -3.880784 -1.134623 -0.371320
6 -4.965839 -0.378326 -0.822305
6 -4.979652 1.002882 -0.630679
6 -3.906408 1.623507 0.015825
6 -2.825957 0.867291 0.466354
1 -1.992546 1.345220 0.974719

1 -3.915358 2.698940 0.173659
1 -5.822431 1.594023 -0.979228
1 -5.797329 -0.869145 -1.321547
1 -3.875542 -2.212841 -0.520087
1 -1.842669 -2.407695 0.689982
1 -1.387078 -1.103908 1.799611
1 -0.344488 -1.372218 -0.950649
1 1.514349 -0.378077 -1.464075
6 3.669663 0.011172 1.067497
1 4.610888 -0.380957 1.465161
1 2.998306 0.298554 1.881239
1 2.728676 -1.945954 0.405943
1 4.207010 -1.701342 -1.792992
1 5.231919 0.751716 -1.831957
1 4.394262 2.033283 0.344864

Anchor Group 32

6 4.138472 -0.531000 -1.013450
6 4.819456 -0.811817 0.320478
6 4.164507 -0.116641 1.260105
6 3.032477 0.634287 0.569735
6 1.977763 -0.465602 0.160809
6 2.744538 -1.240501 -0.964735
1 2.829074 -2.311536 -0.756545
1 2.232674 -1.130966 -1.929014
6 0.621792 0.084330 -0.313096
6 -0.214093 0.731328 0.813858
6 -1.543135 1.257182 0.285093
6 -2.717510 0.330556 0.149623
6 -3.901585 0.850207 -0.399273
6 -5.025116 0.044658 -0.552297
6 -4.982415 -1.296945 -0.160025
6 -3.811709 -1.825723 0.385528
6 -2.685583 -1.016938 0.540910
1 -1.784476 -1.444616 0.968636
1 -3.774783 -2.867539 0.692064
1 -5.859678 -1.927441 -0.278893
1 -5.935687 0.458445 -0.977250
1 -3.910942 1.893552 -0.697098
8 -1.636915 2.425879 -0.064051
1 0.315978 1.594521 1.225944
1 -0.362357 0.010015 1.626326
1 0.046755 -0.736879 -0.761986
1 0.769186 0.824579 -1.110322
1 1.792813 -1.124853 1.018071
6 3.701126 0.936172 -0.793074

1 4.545317 1.626615 -0.704478
1 3.006895 1.305439 -1.557354
1 2.617187 1.482296 1.119404
1 4.314169 -0.156550 2.334845
1 5.616791 -1.533474 0.469893
1 4.722502 -0.749973 -1.910971

Anchor Group 33

6 4.814539 -0.574424 -0.439059
6 5.201628 0.885854 -0.639731
6 4.069370 1.581096 -0.814696
6 2.908765 0.597765 -0.727369
6 2.824303 0.173837 0.786258
6 4.130573 -0.668284 0.967095
1 4.771953 -0.289348 1.768315
1 3.892667 -1.713718 1.201671
6 1.564061 -0.626242 1.141958
7 0.348106 0.169926 1.019165
6 -0.811892 -0.379876 0.500547
7 -1.901595 0.478495 0.593244
6 -3.224463 0.263225 0.157916
6 -4.120051 1.339120 0.276237
6 -5.448038 1.203364 -0.118251
6 -5.908544 -0.007582 -0.637519
6 -5.017525 -1.075155 -0.754133
6 -3.683561 -0.956644 -0.363926
1 -2.995395 -1.783920 -0.463005
1 -5.359906 -2.024619 -1.157920
1 -6.944139 -0.116061 -0.946642
1 -6.122229 2.049978 -0.018036
1 -3.771145 2.287874 0.681263
1 -1.711763 1.421919 0.902952
8 -0.853780 -1.494327 -0.005863
1 0.260386 0.953036 1.653789
1 1.659365 -1.025446 2.163760
1 1.434654 -1.482782 0.477232
1 2.853383 1.069164 1.420979
6 3.568884 -0.654450 -1.352973
1 3.806466 -0.519685 -2.412334
1 2.988280 -1.575510 -1.225156
1 1.956641 0.928327 -1.147242
1 3.962970 2.659317 -0.888141
1 6.209177 1.278998 -0.544008
1 5.604995 -1.311466 -0.601559

Anchor Group 34

6 5.241597 -0.001379 -0.700984
6 5.742757 0.874197 0.442985
6 4.702306 1.592592 0.886557
6 3.491588 1.208733 0.048193
6 3.117591 -0.259601 0.489737
6 4.322695 -1.090722 -0.055037
1 4.828841 -1.656316 0.731515
1 3.984735 -1.810504 -0.810579
7 1.849372 -0.715256 -0.057955
6 0.676839 -0.613191 0.597255
6 -0.501542 -1.137261 -0.252516
7 -1.669503 -1.064777 0.415972
6 -2.949635 -1.469434 -0.145844
6 -3.986504 -0.362301 -0.112135
6 -5.214748 -0.557529 0.527101
6 -6.178405 0.453709 0.545874
6 -5.918662 1.676098 -0.072840
6 -4.692500 1.881704 -0.711772
6 -3.734511 0.869846 -0.731456
1 -2.781750 1.033325 -1.229054
1 -4.484243 2.831736 -1.196859
1 -6.664982 2.465828 -0.057489
1 -7.127726 0.285893 1.047632
1 -5.420128 -1.508603 1.013926
1 -2.737185 -1.782339 -1.173227
1 -3.328336 -2.347608 0.392653
1 -1.610915 -0.670145 1.349316
8 -0.339608 -1.554529 -1.398981
8 0.509769 -0.174738 1.734864
1 1.780636 -1.078433 -1.003035
1 3.017373 -0.315822 1.574685
6 4.172668 0.936413 -1.313086
1 4.599965 1.837908 -1.761606
1 3.520978 0.440894 -2.044230
1 2.640985 1.892432 0.071362
1 4.670581 2.244265 1.753770
1 6.739135 0.822533 0.870805
1 6.002442 -0.401920 -1.374966

Anchor Group 35

6 -5.239765 1.129179 0.584250
6 -5.101070 1.999954 -0.658703
6 -3.825168 1.925586 -1.061682
6 -3.093676 0.998515 -0.098933
6 -3.640674 -0.445154 -0.409114
6 -5.115171 -0.357598 0.107603

1 -5.848329 -0.612759 -0.663244
1 -5.275682 -1.038557 0.953544
6 -2.850154 -1.575244 0.270659
7 -1.498832 -1.726052 -0.247287
6 -0.390305 -1.361294 0.424822
6 0.890981 -1.632975 -0.394532
7 2.001238 -1.283904 0.284951
6 3.348986 -1.417693 -0.247013
6 4.164517 -0.146061 -0.109746
6 5.423265 -0.174313 0.499045
6 6.189620 0.988344 0.608127
6 5.699205 2.196336 0.113041
6 4.440548 2.235452 -0.493227
6 3.680039 1.072734 -0.604373
1 2.700577 1.107518 -1.074727
1 4.052156 3.173402 -0.881296
1 6.291446 3.103296 0.199921
1 7.165520 0.949118 1.084775
1 5.807499 -1.113526 0.891203
1 3.868085 -2.245223 0.254264
1 3.227954 -1.701637 -1.297788
1 1.841976 -0.901136 1.211383
8 0.846798 -2.106595 -1.529240
8 -0.343837 -0.870394 1.552399
1 -1.331800 -2.096640 -1.177097
1 -3.380616 -2.527114 0.138779
1 -2.753628 -1.395474 1.344783
1 -3.618528 -0.623733 -1.490900
6 -3.841662 1.328935 1.215033
1 -3.666055 2.355256 1.550580
1 -3.624143 0.636996 2.036951
1 -2.004674 1.072640 -0.084223
1 -3.394638 2.339944 -1.968273
1 -5.925514 2.491313 -1.166363
1 -6.109239 1.323703 1.217261

Anchor Group 36

6 -4.536566 0.215628 0.754044
6 -4.645423 1.502831 -0.054828
6 -3.402785 1.867089 -0.400062
6 -2.445032 0.825693 0.165567
6 -2.680383 -0.472478 -0.695744
6 -4.114160 -0.910890 -0.247708
1 -4.808496 -1.006707 -1.087868
1 -4.085082 -1.880112 0.267239
6 -1.636802 -1.578981 -0.470197

7 -0.308985 -1.253042 -0.972230
6 0.695516 -0.820372 -0.166224
8 1.800839 -0.557561 -0.950791
6 2.987522 -0.114687 -0.372268
6 3.651812 0.905224 -1.052407
6 4.888985 1.349240 -0.585917
6 5.453846 0.779904 0.556689
6 4.775935 -0.240735 1.226207
6 3.541184 -0.700978 0.766623
1 3.009836 -1.486731 1.287731
1 5.209900 -0.689462 2.115692
1 6.415707 1.127957 0.922503
1 5.408120 2.142662 -1.116699
1 3.193532 1.334070 -1.938146
8 0.642519 -0.688900 1.040050
1 -0.135721 -1.250995 -1.967350
1 -1.968241 -2.502489 -0.962033
1 -1.524413 -1.797919 0.594737
1 -2.669955 -0.214603 -1.761910
6 -3.188228 0.457736 1.472061
1 -3.223722 1.289152 2.182071
1 -2.788537 -0.430560 1.974825
1 -1.399081 1.122154 0.258128
1 -3.113307 2.680890 -1.058138
1 -5.578536 1.959813 -0.370073
1 -5.398518 -0.039474 1.375817

Anchor Group 37

6 5.007984 -1.818396 0.442238
6 6.211616 -0.949356 0.778740
6 6.110406 0.175956 0.057297
6 4.838342 0.071653 -0.771201
6 3.645315 0.212529 0.270696
6 3.755014 -1.119391 1.074414
1 3.870655 -0.946945 2.148354
1 2.860794 -1.727248 0.911487
6 2.306129 0.369635 -0.443693
8 1.698462 -0.572677 -0.953486
7 1.847688 1.653224 -0.544756
6 0.555477 1.946238 -1.167095
6 -0.623381 1.663367 -0.282146
7 -1.290980 2.657507 0.374549
7 -2.245960 2.132475 1.093980
7 -2.198018 0.790137 0.911623
6 -1.203106 0.456849 0.054473
1 -0.971982 -0.556847 -0.232958

6 -3.187624 -0.065509 1.563614
6 -4.279293 -0.547327 0.627266
6 -5.062227 0.375538 -0.079279
6 -6.078621 -0.066637 -0.923780
6 -6.327289 -1.434638 -1.068888
6 -5.552374 -2.357774 -0.367586
6 -4.530346 -1.913863 0.474969
1 -3.925596 -2.636754 1.018485
1 -5.737405 -3.422910 -0.477400
1 -7.121217 -1.777277 -1.726972
1 -6.679625 0.656530 -1.468468
1 -4.865392 1.438883 0.032185
1 -2.664609 -0.914301 2.014763
1 -3.599902 0.545271 2.372021
1 0.543648 3.004667 -1.439911
1 0.498116 1.349827 -2.080618
1 2.262689 2.366058 0.038837
1 3.821698 1.086276 0.907326
6 4.801968 -1.449471 -1.045445
1 5.629263 -1.776003 -1.683126
1 3.845922 -1.791367 -1.451774
1 4.755654 0.744627 -1.627938
1 6.736458 1.060841 0.120494
1 6.942932 -1.172007 1.549829
1 5.093141 -2.879715 0.687933

Anchor Group 38

6 -5.554604 -1.082075 -0.120421
6 -5.718130 -0.829777 1.373792
6 -4.501866 -0.571707 1.873637
6 -3.508330 -0.640788 0.720661
6 -3.800071 0.632182 -0.160347
6 -5.200063 0.296168 -0.773556
1 -5.949042 1.064885 -0.561676
1 -5.135452 0.190002 -1.864238
6 -2.741004 0.905613 -1.240684
7 -1.457041 1.323444 -0.696707
6 -0.350963 0.542175 -0.708149
6 0.839815 1.271350 -0.045613
8 1.943488 0.531966 -0.095469
6 3.129295 1.105526 0.489369
6 4.291692 0.164863 0.274574
6 5.553104 0.543432 0.752432
6 6.655608 -0.290774 0.577844
6 6.509218 -1.515419 -0.078591
6 5.255135 -1.895442 -0.555422

6 4.147791 -1.061349 -0.381196
1 3.172914 -1.357533 -0.752820
1 5.132282 -2.846100 -1.067566
1 7.368019 -2.166818 -0.216441
1 7.628494 0.015298 0.953260
1 5.674253 1.496616 1.264013
1 3.308145 2.084079 0.029128
1 2.940374 1.281370 1.555063
8 0.754929 2.378020 0.451659
8 -0.261041 -0.585593 -1.169517
1 -1.360578 2.227616 -0.250110
1 -3.101443 1.688985 -1.920247
1 -2.548322 0.010896 -1.838344
1 -3.861783 1.519402 0.481597
6 -4.161477 -1.753722 -0.133140
1 -4.150494 -2.726515 0.367013
1 -3.729646 -1.857161 -1.135558
1 -2.458050 -0.769993 0.989311
1 -4.257084 -0.253670 2.882523
1 -6.670544 -0.769343 1.891507
1 -6.372652 -1.612804 -0.613987

Anchor Group 39

6 -5.408492 -0.551227 -0.031500
6 -5.881717 0.897782 -0.083145
6 -4.905631 1.659332 0.429419
6 -3.765932 0.733644 0.829151
6 -3.141328 0.225007 -0.528495
6 -4.273165 -0.685716 -1.100008
1 -4.593952 -0.375672 -2.097760
1 -3.933476 -1.726332 -1.173740
7 -1.895222 -0.506245 -0.350352
6 -0.688233 0.107331 -0.324675
6 0.444198 -0.915356 -0.085393
8 1.636613 -0.327680 -0.116500
6 2.778656 -1.174830 0.118630
6 4.033352 -0.334322 0.080934
6 5.273473 -0.980569 0.164881
6 6.457188 -0.245100 0.151887
6 6.414286 1.147670 0.050941
6 5.181694 1.794106 -0.035967
6 3.993386 1.059509 -0.020358
1 3.035441 1.562892 -0.092580
1 5.139179 2.877034 -0.117325
1 7.336328 1.722631 0.038440
1 7.412439 -0.759226 0.217484

1 5.313995 -2.065725 0.240373
1 2.649208 -1.669337 1.088729
1 2.794824 -1.962158 -0.643701
8 0.247606 -2.099630 0.110780
8 -0.482545 1.302536 -0.474688
1 -1.897129 -1.502849 -0.170220
1 -2.909688 1.072223 -1.176092
6 -4.564844 -0.516210 1.265930
1 -5.166161 -0.343158 2.163043
1 -3.944925 -1.410385 1.410821
1 -3.021649 1.138647 1.516888
1 -4.858770 2.743116 0.458372
1 -6.800613 1.231871 -0.554754
1 -6.183232 -1.317968 -0.105632

Anchor Group 40

6 -4.950604 0.261685 0.019814
6 -5.308559 -1.168664 -0.364475
6 -4.198849 -1.744988 -0.846398
6 -3.081862 -0.710822 -0.786325
6 -2.747596 -0.542545 0.743109
6 -4.031528 0.168135 1.285588
1 -4.501857 -0.383889 2.104051
1 -3.800612 1.174740 1.658213
6 -1.490584 0.270520 1.023062
8 -0.346660 -0.446611 0.496522
15 1.149887 0.003096 0.967096
8 1.395653 0.136833 2.434276
6 2.130964 -1.304183 0.178208
6 1.798212 -1.870805 -1.061119
6 2.611363 -2.855636 -1.620190
6 3.760224 -3.280609 -0.947936
6 4.091782 -2.725484 0.288963
6 3.279760 -1.740689 0.852611
1 3.518318 -1.315586 1.822919
1 4.979269 -3.062375 0.817772
1 4.392337 -4.048323 -1.386529
1 2.346660 -3.295773 -2.577944
1 0.896321 -1.557215 -1.577390
6 1.444144 1.576637 0.091664
6 2.121231 2.596656 0.774133
6 2.378789 3.813859 0.141924
6 1.960427 4.020435 -1.173680
6 1.280408 3.009749 -1.858486
6 1.023029 1.792300 -1.229421
1 0.487429 1.012644 -1.763930

1 0.949366 3.171867 -2.880854
1 2.160868 4.968622 -1.665674
1 2.902886 4.601142 0.677163
1 2.429497 2.426553 1.801234
1 -1.355483 0.410597 2.101200
1 -1.535725 1.259628 0.549725
1 -2.610257 -1.525381 1.204960
6 -3.892465 0.577856 -1.063557
1 -4.310844 0.604011 -2.074300
1 -3.338136 1.505737 -0.876226
1 -2.207960 -0.905582 -1.410989
1 -4.061364 -2.786764 -1.119160
1 -6.265227 -1.642327 -0.166791
1 -5.785453 0.959017 0.124792

Anchor Group 41

6 4.087007 -0.583232 0.826825
6 4.303151 -1.469489 -0.393565
6 3.107573 -1.663055 -0.967165
6 2.075327 -0.903145 -0.144122
6 2.355369 0.621551 -0.424696
6 3.729430 0.844235 0.289944
1 4.493359 1.241743 -0.384286
1 3.631468 1.547102 1.127506
6 1.276029 1.552711 0.107675
8 0.065059 1.298941 -0.644090
6 -1.042781 1.945292 -0.226378
6 -2.260561 1.522169 -1.035278
6 -2.867878 0.249645 -0.465800
6 -2.765429 -0.966072 -1.150744
6 -3.314435 -2.132745 -0.614810
6 -3.969441 -2.096854 0.616621
6 -4.071426 -0.888206 1.309599
6 -3.523317 0.276277 0.772808
1 -3.594710 1.214608 1.317161
1 -4.579364 -0.851633 2.269774
1 -4.398930 -3.003770 1.033729
1 -3.230629 -3.068393 -1.161549
1 -2.256595 -0.998868 -2.111218
1 -2.978686 2.346093 -0.988724
1 -1.968924 1.367716 -2.078002
8 -1.064441 2.727716 0.699467
1 1.552607 2.605374 -0.020446
1 1.070402 1.393033 1.170990
1 2.439216 0.791915 -1.503236
6 2.685649 -1.065722 1.269385

1 2.679411 -2.104199 1.613573
1 2.224118 -0.427954 2.033204
1 1.031912 -1.192732 -0.282871
1 2.900922 -2.161388 -1.909344
1 5.273083 -1.781060 -0.768967
1 4.880803 -0.591001 1.577894

Anchor Group 42

6 -5.303377 0.105974 0.370070
6 -5.364862 1.565525 -0.062861
6 -4.130490 2.073278 0.058048
6 -3.223862 0.959594 0.566840
6 -3.073549 -0.040726 -0.640830
6 -4.507327 -0.658991 -0.741457
1 -4.949314 -0.533531 -1.733912
1 -4.492110 -1.734446 -0.521351
6 -2.011820 -1.110074 -0.432517
8 -0.726641 -0.447732 -0.366984
6 0.324889 -1.260703 -0.196689
8 1.430547 -0.500088 -0.137005
6 2.663641 -1.239742 0.024408
6 3.810596 -0.262978 0.043076
6 4.805583 -0.370012 1.019661
6 5.900219 0.497049 1.018185
6 6.002342 1.489458 0.043616
6 5.007398 1.608499 -0.930578
6 3.921262 0.735161 -0.934163
1 3.144593 0.833497 -1.687237
1 5.079191 2.382779 -1.689862
1 6.849869 2.169667 0.043563
1 6.665959 0.401408 1.783341
1 4.723920 -1.135614 1.787922
1 2.616678 -1.821082 0.950167
1 2.746750 -1.951557 -0.805166
8 0.288206 -2.469503 -0.109272
1 -1.996864 -1.826990 -1.260454
1 -2.165052 -1.675152 0.492959
1 -2.814646 0.511222 -1.550333
6 -4.220101 0.194026 1.470665
1 -4.538381 0.780535 2.337617
1 -3.858837 -0.784964 1.808833
1 -2.273160 1.268731 1.004922
1 -3.786392 3.054265 -0.254643
1 -6.237819 2.048410 -0.491186
1 -6.254535 -0.360614 0.638062

Anchor Group 43

6 3.023537 2.225276 0.319236
6 4.491603 2.625282 0.268908
6 5.218303 1.515527 0.462005
6 4.245547 0.360254 0.646377
6 3.617532 0.121930 -0.797225
6 2.738612 1.399638 -0.983992
1 3.009368 1.949020 -1.890219
1 1.678276 1.141277 -1.045365
6 2.903441 -1.213503 -0.883902
8 3.403207 -2.221614 -1.339435
8 1.653294 -1.186601 -0.357978
6 0.950269 -2.456714 -0.353977
6 -0.445351 -2.220383 0.108160
7 -0.826245 -2.455396 1.399508
7 -2.087881 -2.162390 1.537051
7 -2.539575 -1.731143 0.332681
6 -1.543576 -1.751035 -0.584129
1 -1.685589 -1.436427 -1.606927
6 -3.927815 -1.294144 0.190273
6 -4.067607 0.203826 0.000033
6 -3.508741 1.090010 0.930796
6 -3.655293 2.465939 0.766863
6 -4.365451 2.972238 -0.325650
6 -4.925625 2.095549 -1.254240
6 -4.773334 0.716304 -1.092345
1 -5.209863 0.035216 -1.819898
1 -5.477116 2.481492 -2.107248
1 -4.479871 4.045485 -0.450964
1 -3.217349 3.144797 1.493536
1 -2.955472 0.696087 1.779702
1 -4.379705 -1.833638 -0.648276
1 -4.419507 -1.628256 1.108506
1 0.989545 -2.878634 -1.361654
1 1.459440 -3.144610 0.325583
1 4.420508 0.058152 -1.534015
6 3.082851 1.084601 1.362312
1 3.365943 1.436491 2.358964
1 2.165128 0.492358 1.419912
1 4.646200 -0.545603 1.106411
1 6.295624 1.407079 0.384914
1 4.857682 3.613364 0.007209
1 2.307247 3.030993 0.497437

Anchor Group 44

6 5.674470 0.878103 -0.621625

6 6.144082 0.674692 0.813527
6 5.052783 0.609564 1.588496
6 3.837340 0.762764 0.683791
6 3.760271 -0.577024 -0.141749
6 5.013870 -0.468993 -1.072394
1 5.689414 -1.322384 -0.966134
1 4.721578 -0.410926 -2.129068
6 2.476801 -0.734256 -0.942238
8 1.375134 -0.817643 -0.000314
6 0.161359 -0.938554 -0.526914
6 -0.929501 -0.996928 0.566859
7 -2.158952 -1.129198 0.009733
6 -3.383582 -1.189607 0.794205
6 -4.422929 -0.181478 0.341864
6 -5.716305 -0.596340 0.008856
6 -6.683169 0.330337 -0.388325
6 -6.362030 1.685372 -0.462243
6 -5.071019 2.109279 -0.134777
6 -4.109697 1.182749 0.264944
1 -3.106607 1.516264 0.518972
1 -4.814439 3.164027 -0.188540
1 -7.111038 2.408324 -0.774025
1 -7.683472 -0.008910 -0.644124
1 -5.969826 -1.653063 0.060843
1 -3.805803 -2.202061 0.748917
1 -3.080264 -1.010716 1.830909
1 -2.199013 -1.158084 -1.002180
8 -0.680929 -0.924968 1.760168
8 -0.090807 -0.995642 -1.715977
1 2.483151 -1.646990 -1.547795
1 2.292813 0.109492 -1.615606
1 3.838141 -1.435226 0.533369
6 4.410168 1.734949 -0.375747
1 4.636588 2.722237 0.037488
1 3.779832 1.851095 -1.266220
1 2.899660 1.033836 1.172060
1 5.006569 0.372937 2.646856
1 7.174748 0.505455 1.109641
1 6.415983 1.267334 -1.323692

Anchor Group 45

6 3.793160 -0.687414 0.244140
6 4.384203 0.705143 0.074952
6 3.496890 1.439645 -0.610771
6 2.301916 0.545781 -0.908964
6 1.576758 0.331342 0.490790

6 2.604725 -0.555316 1.257841
1 2.911309 -0.104427 2.205935
1 2.170533 -1.537814 1.461971
6 0.221175 -0.350284 0.308085
8 0.103652 -1.556013 0.118603
7 -0.844968 0.523744 0.328749
6 -2.219303 0.266856 0.131670
6 -3.095163 1.360915 0.221331
6 -4.463904 1.187743 0.037462
6 -4.981688 -0.079116 -0.238297
6 -4.109632 -1.164764 -0.326493
6 -2.735123 -1.008883 -0.145083
1 -2.061109 -1.850817 -0.212277
1 -4.499311 -2.156615 -0.540525
1 -6.049504 -0.216909 -0.381928
1 -5.124996 2.047152 0.110840
1 -2.698823 2.351861 0.436561
1 -0.618069 1.492183 0.509651
1 1.438730 1.300941 0.981799
6 3.004858 -0.820518 -1.079946
1 3.653131 -0.845245 -1.961203
1 2.310904 -1.665540 -1.091271
1 1.632894 0.874735 -1.708089
1 3.542313 2.503291 -0.824178
1 5.307393 1.048302 0.532002
1 4.496932 -1.485993 0.490350

Anchor Group 46

6 -4.297705 -0.726486 0.385140
6 -4.855660 0.488483 -0.348829
6 -3.911662 1.439090 -0.329784
6 -2.709560 0.874917 0.413270
6 -2.092737 -0.214489 -0.546529
6 -3.186277 -1.328775 -0.537118
1 -3.552258 -1.563157 -1.539870
1 -2.791039 -2.258540 -0.108741
7 -0.804922 -0.728515 -0.097680
6 0.355008 -0.065820 -0.347240
8 1.390193 -0.752191 0.257484
6 2.700855 -0.295248 0.150480
6 3.669367 -1.276011 -0.060899
6 5.016084 -0.915270 -0.096915
6 5.390032 0.419112 0.071566
6 4.408269 1.389281 0.282117
6 3.057273 1.042277 0.328800
1 2.293895 1.793460 0.483818

1 4.691862 2.429857 0.415070
1 6.438632 0.701238 0.039806
1 5.771111 -1.679586 -0.259795
1 3.355484 -2.307011 -0.191015
8 0.469417 0.948694 -1.004190
1 -0.760676 -1.529456 0.515548
1 -1.932698 0.207381 -1.539922
6 -3.421873 -0.023206 1.450712
1 -4.007003 0.547133 2.177824
1 -2.745731 -0.705120 1.982611
1 -1.971506 1.594923 0.770701
1 -3.927524 2.396469 -0.840492
1 -5.804952 0.510854 -0.874892
1 -5.028513 -1.457982 0.738135

Anchor Group 47

6 4.217301 -1.775309 0.197292
6 5.423983 -0.852599 0.076747
6 4.999852 0.294080 -0.471854
6 3.503265 0.158663 -0.721420
6 2.839898 0.188630 0.705688
6 3.302356 -1.174184 1.318454
1 3.830917 -1.050309 2.267837
1 2.447617 -1.838828 1.502022
6 1.321535 0.321492 0.673491
8 1.005643 1.606423 0.119418
6 -0.277568 1.974283 -0.165933
8 -0.486591 3.009914 -0.762719
7 -1.264378 1.105148 0.231920
6 -2.669741 1.478114 0.085307
6 -3.562647 0.257668 0.001137
6 -4.640784 0.103103 0.878684
6 -5.481054 -1.009446 0.790135
6 -5.246163 -1.985991 -0.177238
6 -4.168696 -1.843596 -1.056334
6 -3.334605 -0.730511 -0.967732
1 -2.496858 -0.621051 -1.651790
1 -3.981559 -2.599714 -1.814431
1 -5.896809 -2.853553 -0.247606
1 -6.314972 -1.112675 1.479386
1 -4.826531 0.861363 1.636258
1 -2.994183 2.123344 0.914112
1 -2.732564 2.082112 -0.824459
1 -1.056899 0.389376 0.913098
1 0.922822 0.244548 1.697115
1 0.864614 -0.469677 0.064214

1 3.226522 1.036977 1.279051
6 3.422905 -1.349855 -1.060013
1 3.934379 -1.599535 -1.994225
1 2.401668 -1.750299 -1.089186
1 3.060826 0.864960 -1.425580
1 5.567410 1.208420 -0.613786
1 6.411431 -1.069549 0.472302
1 4.431375 -2.839896 0.320166

Anchor Group 48

6 -4.884265 -0.310713 0.529115
6 -5.293313 0.740170 -0.495127
6 -4.221140 1.507320 -0.735234
6 -3.076761 0.975891 0.118112
6 -2.675977 -0.401701 -0.533804
6 -3.914081 -1.299282 -0.202571
1 -4.361963 -1.741639 -1.096863
1 -3.639513 -2.122731 0.469504
6 -1.386398 -0.994981 0.012237
8 -0.301714 -0.112407 -0.368099
6 0.916636 -0.512211 0.012645
8 1.787857 0.429280 -0.425794
6 3.157898 0.286553 -0.189721
6 3.826490 1.449241 0.187196
6 5.209816 1.414824 0.362247
6 5.913532 0.225800 0.162483
6 5.226718 -0.928461 -0.218678
6 3.843374 -0.908699 -0.402924
1 3.307409 -1.803694 -0.691792
1 5.768567 -1.856644 -0.378159
1 6.990561 0.198771 0.301251
1 5.734842 2.319547 0.655888
1 3.257413 2.361695 0.333718
8 1.180793 -1.517172 0.628943
1 -1.191234 -1.988457 -0.405287
1 -1.397177 -1.088198 1.103245
1 -2.552526 -0.279869 -1.614840
6 -3.865941 0.502272 1.362619
1 -4.325219 1.330590 1.910172
1 -3.280772 -0.111526 2.058434
1 -2.233632 1.650883 0.276231
1 -4.122458 2.289524 -1.481465
1 -6.252812 0.770323 -1.002138
1 -5.696507 -0.802313 1.070122

Anchor Group 49

6 -5.975707 -0.650282 0.131479
6 -6.371434 0.746348 -0.331438
6 -5.320776 1.551856 -0.123928
6 -4.204780 0.705901 0.474760
6 -3.709204 -0.220809 -0.699554
6 -4.924906 -1.184806 -0.900679
1 -5.302626 -1.173623 -1.926860
1 -4.654735 -2.221457 -0.660494
6 -2.429989 -0.981759 -0.387919
8 -1.363452 -0.008336 -0.236463
6 -0.151715 -0.505611 0.019359
6 0.860023 0.644672 0.188498
8 2.103445 0.175492 0.044962
6 3.164439 1.140692 0.242153
6 4.491367 0.446811 0.070274
6 5.570758 1.150395 -0.474953
6 6.825112 0.548979 -0.587862
6 7.007612 -0.768783 -0.166985
6 5.930895 -1.479477 0.368042
6 4.679830 -0.875441 0.491012
1 3.840228 -1.432819 0.894576
1 6.064477 -2.508742 0.690226
1 7.981470 -1.241801 -0.260596
1 7.654695 1.106926 -1.013773
1 5.430305 2.174274 -0.814903
1 3.038391 1.960068 -0.472591
1 3.048687 1.565628 1.246571
8 0.558328 1.789003 0.432910
8 0.130601 -1.676048 0.127157
1 -2.157528 -1.670002 -1.195247
1 -2.498763 -1.564868 0.536581
1 -3.527036 0.380269 -1.596292
6 -5.041660 -0.292094 1.311186
1 -5.566331 0.190291 2.141095
1 -4.470248 -1.147492 1.692241
1 -3.401740 1.247145 0.978371
1 -5.213335 2.589028 -0.425641
1 -7.301435 0.991517 -0.835002
1 -6.795043 -1.344780 0.332544

Anchor Group 50

6 -4.926638 -0.419021 0.396247
6 -5.308138 0.951249 -0.149905
6 -4.213759 1.723008 -0.100677
6 -3.082673 0.878350 0.471266
6 -2.724586 -0.163329 -0.655326

6 -3.990748 -1.082823 -0.670231
1 -4.456557 -1.139708 -1.658087
1 -3.739679 -2.106974 -0.365173
6 -1.454304 -0.957812 -0.387516
8 -0.341060 -0.038205 -0.421231
6 0.878763 -0.594968 -0.190019
7 1.827760 0.395044 -0.251686
6 3.221449 0.286228 -0.075559
6 3.975146 1.466114 -0.177278
6 5.357459 1.435811 -0.015542
6 6.010033 0.230656 0.249772
6 5.257434 -0.940062 0.350095
6 3.871626 -0.928004 0.190898
1 3.292096 -1.837379 0.269939
1 5.751406 -1.886128 0.555994
1 7.088494 0.205421 0.376193
1 5.923399 2.359936 -0.097722
1 3.473016 2.409487 -0.383482
1 1.466511 1.318621 -0.447559
8 1.064492 -1.776524 0.031096
1 -1.298775 -1.729287 -1.149616
1 -1.473337 -1.456781 0.587213
1 -2.598733 0.352718 -1.613029
6 -3.880120 -0.007923 1.458430
1 -4.311069 0.564613 2.285120
1 -3.309510 -0.853639 1.861000
1 -2.219542 1.421084 0.861741
1 -4.095463 2.725900 -0.499345
1 -6.268483 1.196165 -0.593061
1 -5.751204 -1.056374 0.724839

Anchor Group 51

6 5.467122 -2.074167 0.354855
6 4.761500 -3.075074 -0.551408
6 3.472642 -2.715204 -0.622114
6 3.299140 -1.463950 0.228902
6 4.026769 -0.312170 -0.562451
6 5.531593 -0.720997 -0.432520
1 6.022899 -0.824878 -1.404067
1 6.096253 0.023165 0.143990
6 3.765734 1.079822 -0.005496
8 2.370737 1.397121 -0.228285
6 1.929774 2.554708 0.317934
6 0.475686 2.818903 -0.023686
6 -0.436179 1.595341 0.108694
6 -1.850127 1.891001 -0.356485

8 -2.675839 0.864736 -0.060362
6 -4.056625 1.028293 -0.490115
6 -4.802665 -0.234897 -0.159775
6 -5.464753 -0.372156 1.065976
6 -6.143925 -1.549981 1.378656
6 -6.167474 -2.605609 0.465248
6 -5.510377 -2.478521 -0.760452
6 -4.833114 -1.299130 -1.069345
1 -4.323649 -1.200319 -2.025171
1 -5.529016 -3.295737 -1.476496
1 -6.699189 -3.522358 0.705727
1 -6.656640 -1.642430 2.332302
1 -5.448736 0.449884 1.777945
1 -4.476570 1.898343 0.023418
1 -4.061665 1.239287 -1.563324
8 -2.203711 2.898750 -0.931522
1 -0.050889 0.760896 -0.488004
1 -0.477890 1.231833 1.142018
1 0.136223 3.637447 0.614857
1 0.431358 3.187675 -1.055910
8 2.631876 3.295172 0.971299
1 4.377661 1.835846 -0.510483
1 3.977070 1.149272 1.066246
1 3.705032 -0.318451 -1.609193
6 4.326397 -1.754975 1.349570
1 4.044526 -2.612997 1.967144
1 4.538795 -0.895944 1.997541
1 2.278440 -1.218204 0.528900
1 2.701609 -3.143536 -1.255106
1 5.258519 -3.860707 -1.112134
1 6.424651 -2.391746 0.774842

Anchor Group 52

6 -5.737936 0.773256 0.571322
6 -6.320407 0.021741 -0.619300
6 -5.313411 -0.233434 -1.465869
6 -4.041437 0.336420 -0.850897
6 -3.716505 -0.599814 0.373049
6 -4.870047 -0.257522 1.371901
1 -5.440819 -1.140490 1.672882
1 -4.480009 0.208838 2.286369
6 -2.340988 -0.360378 0.980003
8 -1.352302 -0.706131 -0.003940
6 -0.078421 -0.409824 0.320010
7 0.864047 -0.833545 -0.427785
8 2.098294 -0.347002 0.065065

6 3.154445 -0.965310 -0.676248
6 4.449475 -0.285268 -0.306775
6 5.563636 -1.035123 0.082409
6 6.774603 -0.408274 0.384833
6 6.878191 0.980751 0.312721
6 5.766692 1.739054 -0.065689
6 4.562598 1.110172 -0.376863
1 3.696699 1.698822 -0.666386
1 5.840555 2.822163 -0.120790
1 7.817875 1.471683 0.552056
1 7.632352 -1.005268 0.683516
1 5.483434 -2.117754 0.149795
1 3.197104 -2.039278 -0.450210
1 2.939470 -0.858781 -1.748230
1 0.092833 0.204809 1.207885
1 -2.199781 -0.984855 1.873445
1 -2.212495 0.690524 1.276330
1 -3.756471 -1.648244 0.060850
6 -4.622595 1.579321 -0.134685
1 -5.010994 2.325228 -0.834349
1 -3.926131 2.064509 0.560592
1 -3.197633 0.484799 -1.526656
1 -5.345373 -0.836076 -2.368154
1 -7.346349 -0.326089 -0.690217
1 -6.447903 1.330719 1.187237

Anchor Group 53

6 3.062832 1.299234 0.219564
6 4.260480 0.363119 0.139177
6 3.827474 -0.872243 0.427771
6 2.332856 -0.777818 0.699580
6 1.685322 -0.497388 -0.728133
6 2.146974 0.968657 -1.010450
1 2.680975 1.047807 -1.961475
1 1.293560 1.651316 -1.041994
6 0.193488 -0.758390 -0.747320
8 -0.320254 -1.743235 -1.221441
8 -0.515165 0.240308 -0.121991
6 -1.904674 0.156164 0.003314
6 -2.626865 1.291174 -0.358825
6 -4.010646 1.306944 -0.181796
6 -4.662597 0.193524 0.350915
6 -3.923248 -0.935496 0.710022
6 -2.538325 -0.963139 0.542165
1 -1.962050 -1.838788 0.814245
1 -4.424890 -1.805030 1.125768

1 -5.740350 0.205089 0.486362
1 -4.576681 2.191019 -0.462022
1 -2.098910 2.145958 -0.769992
1 2.094076 -1.202787 -1.453642
6 2.257476 0.621487 1.352231
1 2.773319 0.654597 2.316547
1 1.238900 1.005133 1.457764
1 1.881373 -1.617062 1.233369
1 4.384365 -1.801731 0.364022
1 5.250782 0.649783 -0.200936
1 3.285598 2.363135 0.330141

Anchor Group 54

6 3.295726 -1.442675 0.078488
6 4.187057 -0.528717 -0.753728
6 3.407194 0.428643 -1.273738
6 1.984126 0.173031 -0.792475
6 1.986694 0.523966 0.743017
6 2.868407 -0.621895 1.342198
1 3.727503 -0.243334 1.903684
1 2.282913 -1.253472 2.023048
6 0.587856 0.581839 1.380149
7 -0.216350 1.697120 0.879304
6 -1.269313 1.660668 -0.009829
6 -2.158943 0.448813 -0.021909
6 -2.720431 0.067503 -1.248229
6 -3.600141 -1.010211 -1.316040
6 -3.951458 -1.701652 -0.153404
6 -3.420708 -1.308820 1.076378
6 -2.524174 -0.241227 1.142468
1 -2.131013 0.075583 2.104150
1 -3.708665 -1.829028 1.986032
1 -4.644489 -2.537232 -0.204985
1 -4.020473 -1.305967 -2.273499
1 -2.461878 0.634435 -2.136899
8 -1.506936 2.618576 -0.740803
1 0.275358 2.582754 0.805786
1 0.692334 0.672693 2.470602
1 0.045003 -0.345916 1.190030
1 2.465643 1.499274 0.897789
6 1.989061 -1.374253 -0.746159
1 2.085226 -1.824201 -1.738678
1 1.122881 -1.810105 -0.233542
1 1.189744 0.659416 -1.362915
1 3.719929 1.301870 -1.837886
1 5.268938 -0.600702 -0.808491

1 3.695261 -2.434603 0.303943

Anchor Group 55

6 -1.650905 2.830419 -0.348421
6 -1.308596 4.068696 -1.168559
6 -0.114445 4.507468 -0.748926
6 0.349032 3.582982 0.367055
6 0.733170 2.220903 -0.305366
6 -0.669900 1.711160 -0.863385
6 -0.998781 0.255145 -0.532751
8 -0.496364 -0.655031 -1.200028
7 -1.834832 0.014371 0.511196
6 -2.243946 -1.334239 0.904047
6 -3.622963 -1.717728 0.400358
6 -4.694080 -1.871807 1.285993
6 -5.963631 -2.218124 0.816236
6 -6.172232 -2.412007 -0.548950
6 -5.106663 -2.261179 -1.441494
6 -3.840611 -1.917597 -0.970998
1 -3.008344 -1.806094 -1.661336
1 -5.262674 -2.417762 -2.505719
1 -7.158183 -2.682638 -0.917381
1 -6.786059 -2.336149 1.516938
1 -4.534600 -1.724564 2.352465
1 -1.484881 -2.006876 0.497568
1 -2.208309 -1.399480 1.997033
1 -2.278925 0.796231 0.970476
1 -0.634571 1.720664 -1.955343
6 1.463729 1.297070 0.688728
7 1.989918 0.166684 0.129559
6 2.637142 -0.863085 0.935029
6 3.945422 -1.343741 0.336514
6 4.187179 -2.709816 0.160037
6 5.403564 -3.160031 -0.358917
6 6.393101 -2.243599 -0.713374
6 6.159370 -0.875735 -0.545485
6 4.945651 -0.430643 -0.024724
1 4.764345 0.633629 0.101341
1 6.925997 -0.155360 -0.819514
1 7.339463 -2.590260 -1.120087
1 5.573320 -4.225567 -0.490488
1 3.416007 -3.428352 0.429853
1 2.797729 -0.414884 1.920209
1 1.958324 -1.716025 1.069325
1 1.608496 -0.126490 -0.764193
8 1.616647 1.597386 1.869891

1 1.410537 2.378013 -1.150952
6 -1.008603 3.216282 1.007558
1 -1.501180 4.073689 1.475337
1 -0.918480 2.400251 1.731611
1 1.121985 3.956168 1.037652
1 0.478012 5.311566 -1.173995
1 -1.892891 4.431058 -2.008409
1 -2.705010 2.538239 -0.357808

Anchor Group 56

6 1.753471 2.780047 0.744429
6 1.330054 4.243735 0.727154
6 0.590699 4.437757 -0.373546
6 0.509578 3.104832 -1.105439
6 -0.438854 2.203015 -0.221282
6 0.450898 1.967162 1.072484
6 0.625657 0.492916 1.417180
8 -0.299260 -0.211696 1.773340
8 1.897239 0.070375 1.304574
6 2.153816 -1.343860 1.530811
6 3.177691 -1.822712 0.536050
6 4.412680 -2.316570 0.966659
6 5.351115 -2.785959 0.044755
6 5.062167 -2.754957 -1.319254
6 3.831622 -2.256631 -1.757312
6 2.891442 -1.796710 -0.837008
1 1.936584 -1.406040 -1.179667
1 3.602518 -2.230293 -2.819398
1 5.791554 -3.116372 -2.039448
1 6.306518 -3.169517 0.392964
1 4.642676 -2.335026 2.029801
1 2.513821 -1.452889 2.558669
1 1.203285 -1.874183 1.438938
1 -0.074943 2.391836 1.932813
6 -0.843464 0.925287 -0.933961
8 -2.182837 0.781344 -0.930503
6 -2.727134 -0.444625 -1.483843
6 -3.868588 -0.912714 -0.618308
6 -5.103044 -1.235150 -1.189720
6 -6.148516 -1.715278 -0.397802
6 -5.968153 -1.865048 0.977017
6 -4.738752 -1.535516 1.555103
6 -3.691592 -1.065413 0.764361
1 -2.737627 -0.805324 1.215961
1 -4.594164 -1.648083 2.626442
1 -6.781300 -2.233698 1.596871

1 -7.102941 -1.963306 -0.854775
1 -5.249333 -1.110502 -2.260623
1 -3.062246 -0.230650 -2.503996
1 -1.918328 -1.178310 -1.535836
8 -0.074632 0.138617 -1.454280
1 -1.352173 2.737209 0.041684
6 1.897036 2.512856 -0.770815
1 2.711581 3.088587 -1.220070
1 1.995456 1.456256 -1.025414
1 0.217819 3.141989 -2.157359
1 0.049178 5.334493 -0.657798
1 1.518589 4.952179 1.527875
1 2.600421 2.523739 1.381040

Anchor Group 57

6 -2.652561 -1.151164 0.254047
6 -3.893665 -0.723038 -0.521567
6 -3.919290 0.617114 -0.536493
6 -2.695896 1.109880 0.228758
6 -1.465163 0.767597 -0.692880
6 -1.435696 -0.782621 -0.675507
6 -0.080568 -1.143279 -0.077011
7 0.600010 0.041730 0.212227
6 -0.124979 1.193805 -0.104160
8 0.270107 2.327074 0.085012
6 1.935543 0.071513 0.804172
6 3.048691 -0.011947 -0.247041
6 4.446208 0.019726 0.383884
6 5.569604 -0.065758 -0.654190
1 6.555387 -0.041567 -0.176431
1 5.502577 -0.993904 -1.234602
1 5.520585 0.771737 -1.360693
1 4.559501 0.941934 0.971000
1 4.541857 -0.811750 1.096305
1 2.921828 -0.937278 -0.823569
1 2.938365 0.825235 -0.948909
1 2.008357 1.004321 1.370371
1 1.999329 -0.773543 1.496198
8 0.358434 -2.255695 0.138764
1 -1.525109 -1.257030 -1.656278
1 -1.572737 1.216187 -1.683923
6 -2.581194 -0.007181 1.295107
1 -3.431242 -0.015820 1.982317
1 -1.650923 0.017225 1.873924
1 -2.707935 2.145342 0.572710
1 -4.610297 1.258802 -1.073570

1 -4.559299 -1.402434 -1.044112
1 -2.624833 -2.178483 0.620738

Anchor Group 58

6 5.911691 1.085636 0.265331
6 7.134438 0.570502 -0.486003
6 7.092550 -0.769035 -0.457986
6 5.840684 -1.174336 0.312550
6 4.635325 -0.800324 -0.629811
6 4.683163 0.749146 -0.661427
6 3.344106 1.196450 -0.085795
7 2.603587 0.055928 0.236215
6 3.271791 -1.139676 -0.038257
8 2.817699 -2.244844 0.183338
6 1.264249 0.106073 0.818087
6 0.158688 0.043094 -0.242669
6 -1.243078 0.078023 0.378581
6 -2.366093 0.020889 -0.665195
6 -3.769884 0.031803 -0.047871
6 -4.895012 -0.011442 -1.101452
6 -6.280379 -0.018636 -0.490536
6 -6.924934 1.180474 -0.156325
6 -8.185824 1.176696 0.441217
6 -8.827891 -0.032542 0.714801
6 -8.199179 -1.234518 0.385689
6 -6.937729 -1.224364 -0.211352
1 -6.456460 -2.165530 -0.469946
1 -8.692757 -2.181529 0.589115
1 -9.811823 -0.037780 1.176291
1 -8.669188 2.118480 0.688669
1 -6.433972 2.127570 -0.371728
1 -4.790348 0.853995 -1.769794
1 -4.763790 -0.904509 -1.726918
1 -3.881683 -0.825066 0.631050
1 -3.894692 0.929990 0.572966
1 -2.263981 0.871634 -1.355065
1 -2.245518 -0.884351 -1.278349
1 -1.352628 -0.764955 1.076505
1 -1.353655 0.991415 0.981213
1 0.282302 0.886703 -0.934332
1 0.283525 -0.877096 -0.827663
1 1.182138 -0.740117 1.506692
1 1.201256 1.038069 1.386781
8 2.960672 2.335870 0.090093
1 4.802564 1.187108 -1.655871
1 4.726689 -1.285190 -1.605266

6 5.775797 -0.019357 1.341864
1 6.620844 -0.031535 2.035148
1 4.841872 0.022177 1.913771
1 5.797663 -2.197595 0.688998
1 7.753705 -1.461572 -0.968833
1 7.837126 1.198404 -1.024226
1 5.933867 2.124234 0.599184

Anchor Group 59

6 -4.769624 -1.144606 0.376299
6 -6.034926 -0.781028 -0.392820
6 -6.074523 0.554726 -0.498768
6 -4.836842 1.108998 0.198262
6 -3.626588 0.714447 -0.730911
6 -3.581046 -0.830613 -0.609438
6 -2.207437 -1.138435 -0.024864
7 -1.532048 0.069619 0.168133
6 -2.276882 1.191504 -0.206247
8 -1.889658 2.338485 -0.103590
6 -0.182014 0.147419 0.721055
6 0.902280 -0.003119 -0.353496
6 2.314703 0.063971 0.240508
6 3.402480 -0.095980 -0.827509
6 4.844376 -0.046659 -0.345258
6 5.878123 -0.169030 -1.287746
6 7.216180 -0.133818 -0.902791
6 7.553912 0.025713 0.443998
6 6.539703 0.148884 1.391360
6 5.197914 0.113217 0.999439
1 4.426658 0.210962 1.757254
1 6.787506 0.273709 2.442435
1 8.596704 0.053540 0.748454
1 7.996665 -0.231039 -1.653223
1 5.625350 -0.293920 -2.339129
1 3.263071 0.682233 -1.592221
1 3.242057 -1.049060 -1.352655
1 2.424635 -0.721796 1.000677
1 2.445125 1.022578 0.761588
1 0.772692 0.789874 -1.101453
1 0.758067 -0.961852 -0.867466
1 -0.099486 1.117146 1.219757
1 -0.093605 -0.647975 1.466797
8 -1.749468 -2.229842 0.250705
1 -3.692097 -1.371628 -1.552571
1 -3.763442 1.093191 -1.747043
6 -4.682479 0.068514 1.334617

1 -5.514307 0.099061 2.043007
1 -3.737685 0.140428 1.884998
1 -4.849745 2.165433 0.470521
1 -6.785665 1.152211 -1.059865
1 -6.707206 -1.500179 -0.849316
1 -4.721796 -2.144022 0.811467

Anchor Group 60

6 -4.599041 -1.458978 0.130917
6 -5.959760 -1.091115 -0.450155
6 -6.167492 0.209858 -0.202790
6 -4.949611 0.735921 0.548400
6 -3.784518 0.757148 -0.511605
6 -3.545238 -0.747240 -0.799635
6 -2.099475 -1.001338 -0.388479
7 -1.559658 0.198756 0.081580
6 -2.463196 1.266265 0.052198
8 -2.210052 2.390671 0.435405
6 -0.195171 0.316491 0.586745
6 0.824298 0.448432 -0.556150
7 2.189917 0.541174 -0.046175
6 3.185853 0.120713 -1.036271
6 4.552013 -0.149720 -0.431541
6 5.714676 0.320001 -1.051167
6 6.974908 0.024672 -0.525760
6 7.085091 -0.740421 0.635268
6 5.928774 -1.207731 1.266299
6 4.672933 -0.916050 0.736010
1 3.770074 -1.266789 1.227744
1 6.006949 -1.802244 2.173135
1 8.063885 -0.968974 1.048851
1 7.867745 0.398458 -1.020468
1 5.633239 0.922664 -1.953461
1 2.814603 -0.804094 -1.496624
1 3.291030 0.857959 -1.856874
6 2.495385 1.866502 0.488397
1 3.503296 1.866771 0.911452
1 1.796967 2.127767 1.288269
1 2.442335 2.657711 -0.284423
1 0.745664 -0.451691 -1.173933
1 0.551130 1.312037 -1.192656
1 -0.184085 1.190448 1.240870
1 0.033051 -0.578157 1.171175
8 -1.492226 -2.052864 -0.434411
1 -3.671831 -1.044036 -1.843995
1 -4.050715 1.358137 -1.385030

6 -4.575801 -0.525286 1.366191
1 -5.342102 -0.787410 2.100264
1 -3.603235 -0.465333 1.867764
1 -5.065421 1.678072 1.086471
1 -6.990590 0.825389 -0.551063
1 -6.578078 -1.758011 -1.042275
1 -4.395270 -2.519395 0.287790

Anchor Group 61

6 -4.684871 -1.198801 0.077859
6 -5.983563 -0.606845 -0.458852
6 -6.008761 0.689349 -0.118067
6 -4.727460 0.987651 0.652949
6 -3.573734 0.924150 -0.418178
6 -3.546307 -0.574801 -0.814600
6 -2.148643 -1.056150 -0.442673
7 -1.445628 0.022466 0.102568
6 -2.191407 1.203797 0.160133
8 -1.779328 2.252510 0.614330
6 -0.072740 -0.080558 0.584311
6 0.949888 0.128607 -0.538922
7 2.300317 0.049790 0.004384
6 3.345024 0.101525 -1.020143
6 4.731433 0.024847 -0.412410
6 5.755587 0.866642 -0.859981
6 7.041563 0.776565 -0.322727
6 7.316246 -0.155678 0.678075
6 6.298272 -0.995801 1.137002
6 5.016421 -0.907045 0.595457
1 4.218957 -1.550675 0.954847
1 6.504580 -1.722980 1.918359
1 8.315180 -0.225890 1.100619
1 7.824864 1.439111 -0.681979
1 5.544571 1.599857 -1.635752
1 3.183926 -0.758738 -1.686321
1 3.277453 1.000846 -1.661245
1 2.449144 0.816985 0.659793
1 0.830272 -0.673230 -1.277319
1 0.735607 1.082970 -1.055532
1 0.047978 0.680786 1.360664
1 0.061313 -1.071276 1.023985
8 -1.694072 -2.175122 -0.570898
1 -3.717309 -0.774966 -1.875462
1 -3.756786 1.617107 -1.243561
6 -4.528635 -0.367626 1.374630
1 -5.320730 -0.573904 2.099066

1 -3.554967 -0.477152 1.865655
1 -4.710726 1.895730 1.257711
1 -6.739811 1.435716 -0.411590
1 -6.689700 -1.138503 -1.088413
1 -4.629324 -2.285659 0.157166

2.9 Supporting Information References

1. Au – Liu, J.; Au – Gao, A. X.; Au – Johnson, J. A., Particles without a Box: Brush–first Synthesis of Photodegradable PEG Star Polymers under Ambient Conditions. *JoVE* **2013**, e50874.
2. Love, J. A.; Morgan, J. P.; Trnka, T. M.; Grubbs, R. H., A Practical and Highly Active Ruthenium-based Catalyst that Effects the Cross Metathesis of Acrylonitrile. *Angew. Chem* **2002**, *41*, 4035–4037.
3. Frisch, M. J.; Trucks, G. W.; Schlegel, H. B.; Scuseria, G. E.; Robb, M. A.; Cheeseman, J. R.; Scalmani, G.; Barone, V.; Petersson, G. A.; Nakatsuji, H.; Li, X.; Caricato, M.; Marenich, A. V.; Bloino, J.; Janesko, B. G.; Gomperts, R.; Mennucci, B.; Hratchian, H. P.; Ortiz, J. V.; Izmaylov, A. F.; Sonnenberg, J. L.; Williams; Ding, F.; Lipparini, F.; Egidi, F.; Goings, J.; Peng, B.; Petrone, A.; Henderson, T.; Ranasinghe, D.; Zakrzewski, V. G.; Gao, J.; Rega, N.; Zheng, G.; Liang, W.; Hada, M.; Ehara, M.; Toyota, K.; Fukuda, R.; Hasegawa, J.; Ishida, M.; Nakajima, T.; Honda, Y.; Kitao, O.; Nakai, H.; Vreven, T.; Throssell, K.; Montgomery Jr., J. A.; Peralta, J. E.; Ogliaro, F.; Bearpark, M. J.; Heyd, J. J.; Brothers, E. N.; Kudin, K. N.; Staroverov, V. N.; Keith, T. A.; Kobayashi, R.; Normand, J.; Raghavachari, K.; Rendell, A. P.; Burant, J. C.; Iyengar, S. S.; Tomasi, J.; Cossi, M.; Millam, J. M.; Klene, M.; Adamo, C.; Cammi, R.; Ochterski, J. W.; Martin, R. L.; Morokuma, K.; Farkas, O.; Foresman, J. B.; Fox, D. J. *Gaussian 16 Rev. C.01*, Wallingford, CT, 2016.

4. Radzinski, S. C.; Foster, J. C.; Matson, J. B., Preparation of Bottlebrush Polymers via a One-pot Ring-opening Polymerization (ROP) and Ring-opening Metathesis Polymerization (ROMP) Grafting-through Strategy. *Macromol. Rapid Commun.* **2016**, *37*, 616–621.
5. Alaboalirat, M.; Qi, L.; Arrington, K. J.; Qian, S.; Keum, J. K.; Mei, H.; Littrell, K. C.; Sumpter, B. G.; Carrillo, J.-M. Y.; Verduzco, R.; Matson, J. B., Amphiphilic Bottlebrush Block Copolymers: Analysis of Aqueous Self-Assembly by Small-Angle Neutron Scattering and Surface Tension Measurements. *Macromolecules* **2019**, *52*, 465–476.
6. Driver, T. G.; Franz, A. K.; Woerpel, K. A., Diastereoselective Silacyclopropanations of Functionalized Chiral Alkenes. *J. Am. Chem. Soc.* **2002**, *124*, 6524–6525.
7. Abd-El-Aziz, A. S.; Edel, A. L.; May, L. J.; Epp, K. M.; Hutton, H. M., Controlled molecular design of ether- and ester-bridged norbornenes and their ring-opening metathesis polymerizations. *Can. J. Chem.* **1999**, *77*, 1797–1809.
8. Kumar, S. N.; Yu, I. F.; Chein, R.-J., Oxathiaborolium: A Type of Chiral Lewis Acid Catalyst and Its Application in Catalytic and Highly Enantioselective Diels–Alder Reactions. *Org. Lett.* **2017**, *19*, 22–25.
9. Radzinski, S. C.; Foster, J. C.; Matson, J. B., Synthesis of bottlebrush polymers via transfer-to and grafting-through approaches using a RAFT chain transfer agent with a ROMP-active Z-group. *Polym. Chem.* **2015**, *6*, 5643–5652.
10. Ku, T.-H.; Chien, M.-P.; Thompson, M. P.; Sinkovits, R. S.; Olson, N. H.; Baker, T. S.; Gianneschi, N. C., Controlling and Switching the Morphology of Micellar Nanoparticles with Enzymes. *J. Am. Chem. Soc.* **2011**, *133*, 8392–8395.
11. Conrad, R. M.; Grubbs, R. H., Tunable, Temperature-Responsive Polynorbornenes with Side Chains Based on an Elastin Peptide Sequence. *Angew. Chem* **2009**, *48*, 8328–8330.

12. Radzinski, S. C.; Foster, J. C.; Chapleski, R. C.; Troya, D.; Matson, J. B., Bottlebrush Polymer Synthesis by Ring-opening Metathesis Polymerization: The Significance of the Anchor Group. *J. Am. Chem. Soc.* **2016**, *138*, 6998–7004.
13. Reynard, G.; Joseph-Valcin, E.-M.; Lebel, H., Protecting-group-free synthesis of hydroxyesters from amino alcohols. *Chem. Comm.* **2020**, *56*, 10938–10941.
14. Moatsou, D.; Nagarkar, A.; Kilbinger, A. F. M.; O'Reilly, R. K., Degradable precision polynorbornenes via ring-opening metathesis polymerization. *J. Polym. Sci., Part A: Polym. Chem.* **2016**, *54*, 1236–1242.

Chapter 3: The influence of the norbornene anchor group in Ru-mediated ring-opening metathesis polymerization: Synthesis of bottlebrush polymers

3.1 Authors

Samantha J. Scannelli, Mohammed Alaboalirat, Diego Troya, and John B. Matson*

Department of Chemistry, Virginia Tech, Blacksburg, VA 24061, United States

Macromolecules Innovation Institute, Virginia Tech, Blacksburg, VA 24061, United States

3.2 Abstract

Ring-opening metathesis polymerization (ROMP) mediated by Grubbs' third-generation catalyst [G3, (H₂IMes)(Cl)₂(pyr)₂RuCHPh] is widely used to make bottlebrush polymers by polymerization of a macromonomer (MM), typically a low molecular weight polymer functionalized with a norbornene. Termed the grafting-through method, this strategy requires a high degree of living character ("livingness") to form well-defined bottlebrush polymers. Here we studied how various anchor groups, the series of atoms connecting the polymerizable norbornene unit to the polymer side-chain, affect livingness in ROMP in a series of *exo*-norbornene polystyrene MMs. First, we calculated the HOMO and HOMO/LUMO gap energies of MM structures containing five different anchor groups using density functional theory methods, finding that these energies spanned a range of 10 kcal/mol. We then performed kinetics experiments on each MM with target backbone degrees of polymerization (N_{bb}) of 100 to measure the propagation rate constant ($k_{p,obs}$) under identical conditions. A positive correlation between the HOMO energy and measured $k_{p,obs}$ values emerged, revealing a 7-fold variation in

$k_{p,obs}$ values across the five MMs, suggesting different degrees of livingness among the anchor groups. A series of studies targeting N_{bb} values ranging from 100 to 2000 further highlighted these differences: The MMs with high $k_{p,obs}$ values reached higher conversions at high target N_{bb} values with lower dispersities (D) than the MMs with lower $k_{p,obs}$ values. Finally, we evaluated the synthesis of bottlebrush pentablock copolymers using the MMs at the two extremes by injecting an MM aliquot into a catalyst solution five consecutive times, allowing for polymerization of each block before the next injection. MM conversion at each step was higher, and the D values for each block were lower, for the MM with the highest k_p anchor group compared to the lowest k_p anchor group. Taken together, these studies highlight how the anchor group dramatically affects both k_p and livingness in ROMP, which is crucial for the synthesis of precise bottlebrush (co)polymers.

3.3 Introduction

Complex synthetic polymer architectures (topologies) have garnered interest over the years due to their ability to capture intricate properties found in nature. A particularly interesting one is bottlebrush polymers, which contain polymer backbones with densely grafted polymeric side-chains, similar to the topology of proteoglycans.¹⁻⁵ The densely packed side-chains prevent entanglement of these macromolecules, influencing properties such as elasticity and domain size in solid state materials, and nanoscopic size and shape in solution.⁵⁻¹⁰ As a result, bottlebrush polymers have many potential applications including as elastomers with unusual properties,¹¹⁻¹⁶ as carriers in biomedicine/drug delivery,¹⁷⁻¹⁹ and as photonic crystals,²⁰⁻²² and semiconductors.²³⁻²⁷ Tuning properties in these materials is achieved through adjusting the backbone and side-chain degree of polymerization (N_{bb} and N_{sc} , respectively), as well as grafting

density (z , the fraction of monomer units that contain side-chains).⁶ However, control over these structural features of the resulting polymers is sometimes lost at high N_{bb} or N_{sc} , especially when z is near 1. Therefore, living polymerizations are vital for the synthesis of bottlebrush polymers as they allow for control over molecular weight, molecular weight distribution, and retention of chain end functionalities on the side-chains and backbone.^{28–29}

Living polymerizations are chain polymerizations that lack chain termination and irreversible chain transfer, and in most cases, a fast initiation process enables them to maintain a constant number of kinetic-chain carriers throughout the polymerization.³⁰ Historically, anionic polymerization was preferred for synthesizing bottlebrush polymers,^{31–33} although they were simply referred to as densely grafted polymers until the mid-1990s.³⁴ More recently, many other polymerization methods that exhibit living characteristics (i.e., “livingness”) have been used to synthesize either the backbones or side-chains of bottlebrush polymers, such as atom-transfer radical polymerization (ATRP) and reversible addition-fragmentation chain transfer (RAFT) polymerization.^{35–37} Since Bowden’s seminal work in 2004,¹ ring-opening metathesis polymerization (ROMP) is also commonly used due to its high propagation rates (k_p), high functional group tolerance, and relative insensitivity to air and water.³⁸ Mediated by a transition metal catalyst such as Grubbs’ third-generation catalyst [G3, $(H_2IMes)(Cl)_2(py)_2RuCHPh$], ROMP typically has high propagation rates and even higher initiation rates, enabling living characteristics.³⁹ Low termination rates (k_t) are also critical in polymerizations with a high degree of living character, where livingness is defined as k_p/k_t . In the context of ROMP, termination occurs primarily through catalyst decomposition,⁴⁰ with a rate that is generally low, making it a well-suited method for the synthesis of complex architectures such as bottlebrush polymers.

In most cases, ROMP enables the synthesis of well-defined bottlebrush polymers via the polymerization of norbornene-functionalized macromonomers (MMs).^{8–9} The collective synthesis of MMs followed by ROMP is referred to as the grafting-through technique, and it enables control over N_{sc} and N_{bb} , with the capacity for perfect grafting density ($z = 1$).⁴¹ However, despite the popularity of ROMP for making complex polymer topologies, bottlebrush polymers prepared by ROMP grafting-through tend to be fairly small due to the loss of living character when polymerizing even moderately sized MMs ($N_{sc} = 50–100$) to moderate degrees of polymerization ($N_{bb} = 100–200$). This is because k_p is lower in MMs than in small molecule monomers.^{42–44} It is worth noting that this phenomenon is not limited to ROMP—Sheiko and coworkers recently described similar rate decreases between monomers and MMs in ATRP.⁴⁵ In contrast to k_p , k_t in ROMP is unlikely to be affected by the length of MM side-chains because it is a function of catalyst decomposition, which primarily (although not entirely) occurs through an intramolecular C–H activation pathway that does not depend heavily on monomer type.^{46–47} Therefore, while ATRP and RAFT achieve high livingness (as quantified by high k_p/k_t ratios)⁴⁸ by reducing k_t , this option is not available in ROMP using G3 catalyst. Instead, one needs to enhance k_p to increase livingness in ROMP.

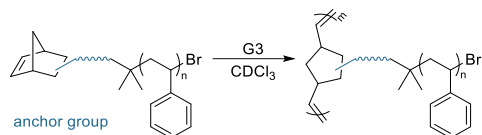
In 2016 we enhanced the k_p of ROMP mediated by G3 catalyst by tuning MM reactivity.⁴⁹ In a recent paper, we presented a thorough investigation of this phenomenon through a combined computational and experimental approach, measuring propagation and termination rates of small molecule monomers in the synthesis of linear polymers.⁵⁰ In this recent work, we monitored the polymerization of eight different monomers mediated by G3 catalyst as well as the less active Grubbs 1st generation catalyst [G1, (PCy₃)₂(Cl)₂RuCHPh]. The monomers had varying anchor groups, which is the series of atoms directly connected to the polymerizable unit

used in ROMP (norbornene here).⁵¹ We found that the anchor group influenced the energy of the HOMO localized on the norbornene olefin and that an increasing HOMO energy increased k_p but did not substantially affect k_t . However, when using the highly active G3 catalyst, the effect on k_p reached a plateau for the three monomers with the highest HOMO energies, where k_p remained flat despite a continued increase in the HOMO energy. Interestingly, when using G1 catalyst, where k_p values were 10–20-fold lower than in G3 catalyst, we saw larger variations in k_p for the three monomers that plateaued in rate with G3 catalyst. Therefore, we hypothesized that adding a side-chain (i.e., using an MM instead of a small molecule norbornene) would slow down polymerization enough for the HOMO energy to influence k_p in MMs with these three anchor groups. In other words, we envisioned that adding a side-chain would allow us to observe differences among these “fast” (i.e., high k_p) anchor groups that were unobservable in small molecule norbornenes.

Here we focus on the ROMP of MMs, quantitatively investigating how the anchor group affects k_p and livingness in the synthesis of bottlebrush polymers (Scheme 3.1). We set out to study five anchor groups of interest, specifically those suitable for attaching a polymer chain to the norbornene as well as easily comparable to equivalent structures in our recent paper.⁵⁰ Through the use of computational methods to determine HOMO energy values and experimental methods to measure k_p values, we investigated the effects of the anchor group in ROMP of MMs. Additionally, we aimed to study how k_p affects livingness in ROMP by monitoring MM conversion and maximum obtainable bottlebrush polymer N_{bb} at high [MM]/[G3] ratios (up to 2000). We also anticipated that livingness could be assessed by synthesizing bottlebrush pentablock copolymers in a sequential addition of MMs approach by following molecular weight evolution and increases in dispersity (D) upon the addition of each new block. Overall, we

envisioned that these studies could reveal how the anchor group can be tuned to yield maximum (macro)monomer conversion and livingness when synthesizing complex polymer topologies by ROMP.

Scheme 3.1. Representative scheme of grafting-through ROMP of norbornene MMs with various anchor groups where $n = N_{sc}$ and $m = N_{bb}$



3.4 Results and Discussion

In the recent paper mentioned in the introduction, we calculated the HOMO and HOMO/LUMO gap energies of 61 monomers with different anchor groups for the synthesis of linear polymers via ROMP.⁵⁰ All HOMOs were centered on the norbornene alkene, which interacts with the Ru center in the rate-determining metallacyclobutane formation step in ROMP.⁵² Of these 61 monomers, we selected eight anchor groups to synthesize and study experimentally with the goal of identifying the effects of the anchor group on k_p and livingness in ROMP. Here we focus on five of these eight anchor groups, including the three that showed the highest k_p in the ROMP of small molecule norbornenes, in the form of MMs to investigate the effects of the anchor group on livingness in bottlebrush polymer synthesis.

3.4.1 HOMO Energy Calculations

We first calculated the HOMO energies of the five selected anchor groups attached to a polystyrene (PS) side-chain (MMs **1–5**) (Figure 3.1A). In these computational studies, only one styrene repeat unit, representing the PS side-chain, was used to calculate the molecular orbital energies because we aimed to investigate the HOMO localized on the reactive olefin, which should not be influenced by the side-chain beyond the first repeat unit. The HOMO energies were calculated from optimized geometries of the five monomer structures using density functional theory (DFT) (M06–2X method and def2–TZVP basis set).^{53–54} Coordinates of the five monomer structures and the HOMO energies are shown in the Supporting Information. Our goal was to investigate the π bonding orbital of the olefin, as these electrons are involved in the rate-determining step of norbornenyl ROMP, which corresponds formation of the metallocyclobutane intermediate from the olefin and metal carbene.⁵² In MMs *x*-MOM₂E'-PS (**1**) and *x*-ME'-PS (**2**), the π bonding orbital was the absolute HOMO (HOMO–0), but in some monomers, this orbital did not correspond to the absolute HOMO. For the anchor group in MM *x*-EM₂E'-PS (**3**), the olefin-centered HOMO was HOMO–1, for MMs *xx*-IMEM₂E'-PS (**4**) and *xx*-IM₂E'-PS (**5**), it was HOMO–2. For the sake of simplicity, we use the term HOMO to refer to "olefin-centered HOMO" in the rest of this paper.

The HOMOs localized on the reactive olefins span energies in the –197 to –187 kcal/mol range, similar to analogous small molecule structures in our related paper.⁵⁰ In this related paper,⁵⁰ we also calculated the HOMO/LUMO energy gap for each monomer based on the concept that multiple orbital interactions occur during the formation of the metallocyclobutane ring, as suggested by Suresh and Koha.⁵⁵ Here, we hypothesized that MMs with higher norbornene HOMO energies and lower LUMO olefin energies would exhibit faster

polymerization rates (k_p values) and higher livingness in general, as measured in maximum obtainable N_{bb} studies and bottlebrush pentablock copolymer chain extension studies.

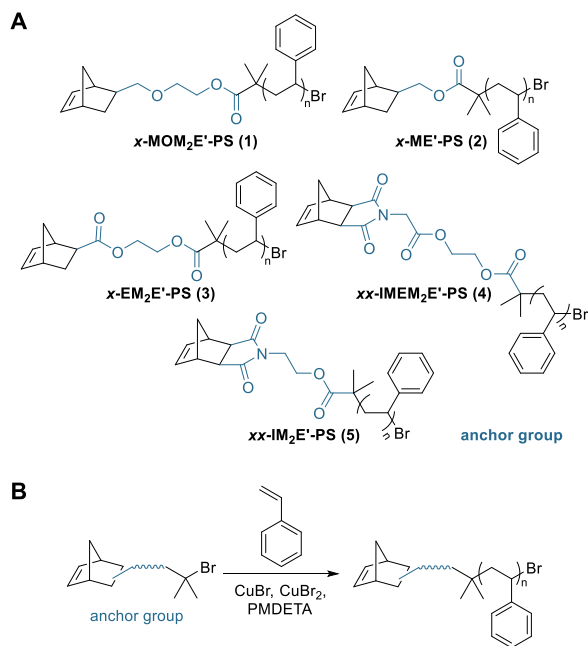


Figure 3.1. (A) Norbornene MMs with various anchor groups (blue) computationally and experimentally investigated where $n = N_{sc}$. For computations, $N_{sc} = 1$ and the Br end group was replaced with H; for experiments, $N_{sc} = 24\text{--}28$. All monomers exhibited *exo* (x prefix) or *exo-Exo* (xx prefix) stereochemistry. Letters identify structural components of the anchor group from left to right (M = methylene, O = oxygen, E = ester with carbonyl on the left, E' = ester with carbonyl on the right, I = imide); all MM side-chains are polystyrene (PS). Subscripts indicate the number of times that component is repeated. (B) Representative synthesis of PS MMs via ATRP. Polymerizations were conducted at 90 °C for 3 h targeting 10% conversion of styrene.

3.4.2 Macromonomer synthesis and analysis

We employed ATRP to synthesize five PS MMs (Figure 3.1B), all with number-average molecular weight values (M_n) near 3 kg/mol. We designed these MMs to have the same polymer

side-chain and M_n to isolate the contributions of the anchor group on k_p . Each was synthesized using the direct-growth approach from five different norbornene-derived initiators (Table 3.1). Standard conditions of Cu(I)Br, Cu(II)Br, and *N,N,N',N'',N''*-pentamethyldiethylenetriamine (PMDETA) were used in all cases and polymerizations were conducted at 90 °C for 3 h. We targeted 10% monomer conversion in the ATRP reactions to avoid termination by coupling, which would result in MMs with norbornene groups on both chain ends.⁵⁶

Because any residual impurities, in particular styrene monomer but also Cu catalyst or ligand, could detrimentally affect the rate of ROMP,⁵⁷⁻⁵⁹ we extensively purified each MM. In brief, crude MMs were diluted with water and extracted with ethyl acetate to remove Cu species, then purified by automated silica gel chromatography using an ethyl acetate/hexane gradient as the mobile phase. After solvent removal, each MM was passed through basic alumina in tetrahydrofuran (THF), and finally precipitated into methanol. Automated flash chromatography, which monitors UV absorbance throughout the separation (Figures S15–S19), provided confidence in the removal of all residual monomer through the clear separation between the styrene peak that elutes first and the broad MM peak that elutes later, as we showed previously.⁵⁶ Passage of the polymer solution through an alumina plug after column purification presumably removed trace catalyst and/or ligand that remained; we observed lower conversion to bottlebrush polymer when this step was not carried out. A final precipitation step into methanol afforded the final MM products as white powders, making them easy to work with for the subsequent ROMP step.

Table 3.1. Characterization of PS MMs

MM	$M_{n,SEC}^a$ (kg/mol)	$M_{n,NMR}^b$ (kg/mol)	D^a
<i>x</i> -MOM ₂ E'-PS (1)	3.2	2.9	1.06
<i>x</i> -ME'-PS (2)	3.2	3.3	1.08
<i>x</i> -EM ₂ E'-PS (3)	2.9	3.2	1.07
<i>xx</i> -IMEM ₂ E'-PS (4)	2.9	3.3	1.09
<i>xx</i> -IM ₂ E'-PS (5)	2.9	3.4	1.06

^aMeasured by SEC in THF at 30 °C with multiangle light scattering. ^bMeasured by end-group analysis via ¹H NMR spectroscopy. See Figures S20–S29.

Each MM was next polymerized via ROMP to investigate the differences in $k_{p,obs}$ based on the anchor group. Polymerizations of all MMs were mediated by G3 catalyst with a targeted N_{bb} of 100 at a concentration of 20 mM in CDCl₃, under air and at room temperature. Aliquots were removed and terminated with an excess of ethyl vinyl ether at predetermined time intervals, the solvent was removed, and each aliquot was then analyzed by size exclusion chromatography (SEC). MM conversion at each time point was measured by comparing the areas of the MM peak and bottlebrush polymer peak. Average $k_{p,obs}$ values and half-lives were calculated from first-order kinetics plots for at least three polymerizations per MM. The conversion versus time data and first-order fits are shown in Figure 3.2 for a representative MM, *x*-MOM₂E'-PS (1). Similar graphs for the other four MMs are included in the Supporting Information (Figures S30–S39).

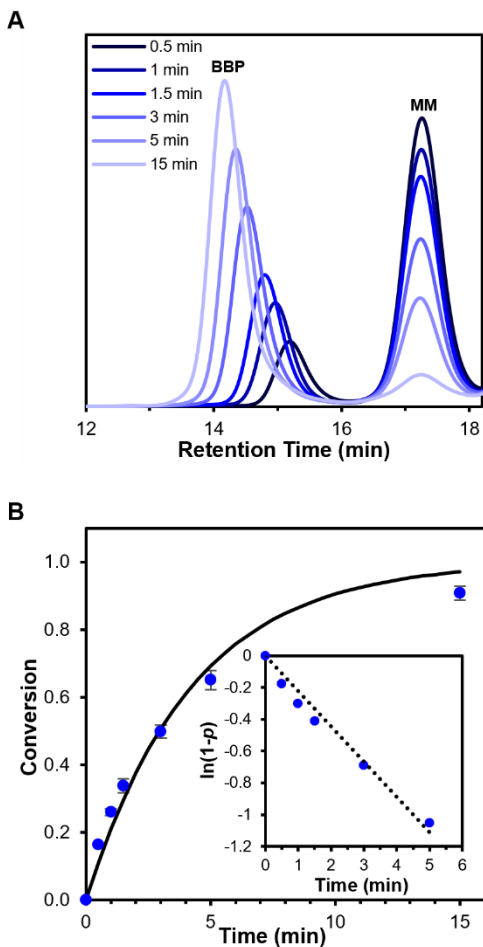


Figure 3.2. (A) Representative SEC traces (dRI signal) of the ROMP of MM *x*-MOM₂E'-PS (**1**) at an [MM]/[G3] ratio of 100:1. As the polymerization proceeds, the MM signal at 17.2 min decreases in intensity and the bottlebrush polymer signal increases in intensity and shifts in retention time from 15.2 min to 14 min. (B) Kinetic analysis of the ROMP of MM *x*-MOM₂E'-PS (**1**) in CDCl₃ at an [MM]/[G3] ratio of 100:1 and [MM] = 20 mM. The solid line represents the fit to the averaged conversion data based on the equation $p = 1 - e^{(-k_{obs}t)}$ where p = fractional conversion.

As expected, each MM polymerized slower, by approximately an order of magnitude, compared with analogue small molecule monomer structures,⁵⁰ where the only difference lies in

the presence of the PS side-chain. MM *x*-ME'-PS (**2**) had the highest $k_{p,obs}$ out of all the MMs tested and polymerized 7-fold faster than the MM with the lowest $k_{p,obs}$ [*xx*-IM₂E'-PS (**5**)]. MMs **1–3** all had half-lives under 4 min, whereas the imide-based MMs (**4–5**) had half-lives over 13 min. Relatively low dispersities and good agreement between expected and measured M_n values for the resulting bottlebrush polymers suggest high livingness in all of these polymerizations (Table 3.2).

Table 3.2. HOMO energies, HOMO/LUMO gap energies, polymerization kinetics, and bottlebrush polymer characterization for ROMP of MMs **1–5**

MM	HOMO Energy ^a (kcal/mol)	HOMO/LUMO Gap (kcal/mol) ^a	$k_{p,obs}$ ^b (min ⁻¹)	$t_{1/2}$ (min)	% conv ^c	BB $M_{n,expected}$ ^d (kg/mol)	BB $M_{n,SEC}$ ^e (kg/mol)	BB D ^e
<i>x</i> -MOM ₂ E'-PS (1)	-187	214	0.23 ± 0.02	3.0 ± 0.2	98	320	325	1.06
<i>x</i> -ME'-PS (2)	-187	214	0.31 ± 0.03	2.3 ± 0.2	98	320	295	1.04
<i>x</i> -EM ₂ E'-PS (3)	-191	211	0.19 ± 0.01	3.7 ± 0.1	98	290	296	1.05
<i>xx</i> -IMEM ₂ E'-PS (4)	-196	217	0.052 ± 0.01	13.4 ± 0.3	98	290	251	1.07
<i>xx</i> -IM ₂ E'-PS (5)	-197	218	0.040 ± 0.003	17 ± 1	98	290	302	1.07

^aCalculated using M06-2X method and def2-TZVP basis set.⁵³⁻⁵⁴ ^bCalculated from conversions measured by SEC on aliquots removed at specific time points during the polymerizations. A minimum of three polymerizations were run for each MM. ^cMeasured on the final sample of the kinetics runs using SEC by comparing the areas of the bottlebrush polymer and MM peaks in the dRI trace. ^dDetermined using the equation $M_{n,expected} = M_{n,MM} * ([MM]/[G3])_0$. ^eMeasured on the final sample of the kinetics runs by SEC in THF at 30 °C with multiangle light scattering using the known dn/dc for PS of 0.185 mL/g.

We next examined how HOMO energy influenced k_p . By plotting the HOMO energies calculated for the MMs versus the experimentally measured $k_{p,obs}$ values, we found a positive correlation between HOMO energy and $k_{p,obs}$ for these five MMs (Figure 3.3). We found an inverse correlation for the HOMO/LUMO energy gaps and the $k_{p,obs}$ values for each MM (Figure S40). Evidently, multiple orbital interactions are important during the rate-determining step, but we focus here on the HOMO energy as a simple predictor for relative k_p values. Both trends were similar to the eight different anchor groups in analogous molecule monomers,⁵⁰ with MMs *x*-MOM₂E'-PS (**1**), *x*-ME'-PS (**2**), and *x*-EM₂E'-PS (**3**) with the highest HOMO energies exhibiting the highest $k_{p,obs}$ values and the MMs *xx*-IMEM₂E'-PS (**4**) and *xx*-IM₂E'-PS (**5**) with lower HOMO energies undergoing slower polymerization. In the small molecule norbornene monomers, there were no measurable differences in $k_{p,obs}$ among monomers polymerized using G3 catalyst with anchor groups similar to those in MMs **1–3**.⁵⁰ In this MM study, however, $k_{p,obs}$ values were different among these three anchor groups. Interestingly, MM *x*-ME'-PS (**2**) showed the highest $k_{p,obs}$ value even though MM *x*-MOM₂E'-PS (**1**) had a slightly higher HOMO energy, although the 0.8 kcal/mol difference between these two MMs is likely within the accuracy of the methods used.

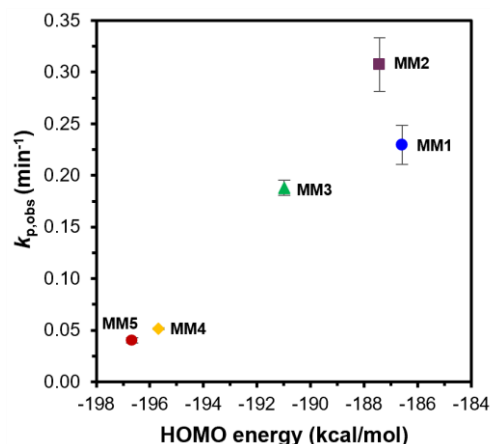


Figure 3.3. Measured $k_{p,obs}$ values versus HOMO energy for MMs 1–5.

3.4.3 Effects of the Anchor Group on Livingness in High Target N_{bb} Bottlebrush Polymers

Polymerizations that exhibit living characteristics have high k_p/k_t ratios, enabling the synthesis of polymers with high degrees of polymerization while maintaining low D values.⁴⁸ High livingness in ROMP grafting-through of MMs is critical for the synthesis of precise bottlebrush polymers. Control over M_n and D of the resulting bottlebrush polymers can be lost when targeting high N_{bb} values due to the increased number of required successful catalyst turnovers compared to polymerizations targeting low N_{bb} values. Therefore, as a method of evaluating livingness, we designed a series of experiments examining grafting-through ROMP with high [MM]/[G3] ratios (i.e., target N_{bb} values ranging from 100 to 2000). By comparing the experimentally observed N_{bb} values (as estimated by the equation $N_{bb} = M_{n,bottlebrush}/M_{n,MM}$) to their target N_{bb} values across the five MMs studied here, we envisioned that this set of experiments would reveal the most living anchor groups, i.e., those with the highest k_p/k_t ratios. We hypothesized that MM *x*-ME'-PS (**2**), which had the highest k_p , would exhibit the highest livingness in these experiments because anchor group choice did not substantially affect k_t in small molecule norbornenes.⁵⁰

The high target N_{bb} experiments were prepared at an MM concentration of 20 mM in $CDCl_3$, under air and at room temperature, similar to the kinetics experiments described above. We set the target N_{bb} (i.e., $[MM]/[G3]$ ratio) to 100, 250, 500, 750, 1000, 1500, and 2000 for each of the MMs. Each ROMP reaction was terminated after 24 h with an excess of ethyl vinyl ether to ensure maximum conversion was reached. The solvent was removed and the residual polymer was redissolved in THF for SEC analysis. All polymerizations were run at least three times.

MM conversion versus target N_{bb} (Figure 3.4A) and measured N_{bb} versus target N_{bb} (Figure 3.4B) were plotted for all five MMs (error bars were not included in the graphs for the sake of clarity and are provided in Tables S1–S5). All MMs reached high conversion (>90%) and showed measured N_{bb} values matching target values when with an $[MM]/[G3]$ ratio of 100:1, similar to the kinetics experiments. However, even at a modest $[MM]/[G3]$ ratio of 250:1, MMs *xx*-IMEM₂E'-PS (**4**) and *xx*-IM₂E'-PS (**5**) failed to exceed 90% conversion and did not reach target N_{bb} values. These two MMs showed even lower conversion (<60%) and significant deviation from targeted N_{bb} with $D \sim 1.4$ at an $[MM]/[G3]$ ratio of 500:1. Less than 3% MM conversion was observed for MM *xx*-IM₂E'-PS (**5**) at target $N_{bb} = 1000$ and higher, and MM *xx*-IMEM₂E'-PS (**4**) barely polymerized to form bottlebrush polymer at or above target $N_{bb} = 1500$. Thus, these two imide-based anchor groups only exhibited a high degree of livingness up to $N_{bb} = 100$, consistent with the lower livingness for imide-based anchor groups in small molecule norbornenes.⁵⁰

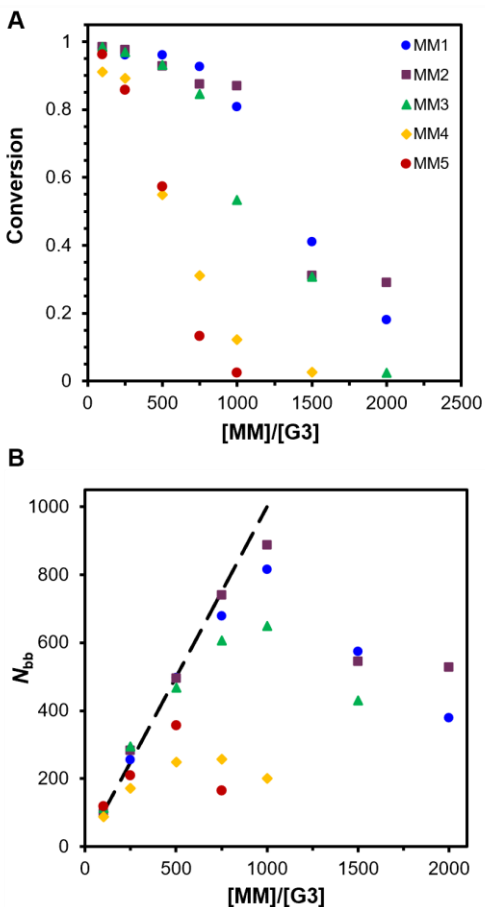


Figure 3.4. (A) Fractional MM conversion to bottlebrush polymer after 24 h versus target N_{bb} values, referred to as [MM]/[G3] ratio, for grafting-through ROMP of the five MMs studied here. Reactions were conducted at 20 mM in MM in $CDCl_3$ under air at rt. Conversion was measured using SEC by comparing the areas of the bottlebrush polymer and MM peaks in the dRI trace. (B) Measured N_{bb} versus target N_{bb} values, referred to as [MM]/[G3] ratio. The black dashed line refers to expected N_{bb} as [MM]/[G3] increases. Measured N_{bb} values were determined from $M_{n,bottlebrush}$ obtained by SEC in THF at 30 °C with multiangle light scattering, calculated based on the equation $N_{bb} = M_{n,bottlebrush}/M_{n,MM}$. In both graphs, error bars were removed for better visualization of the data but can be found in Tables S1–S5.

The three MMs with higher k_p values (**1–3**) showed high livingness out to higher target N_{bb} values than MMs xx -IMEM₂E'-PS (**4**) and xx -IM₂E'-PS (**5**). MM x -EM₂E'-PS (**3**) showed >90% conversion and N_{bb} matching expected values out to a target $N_{bb} = 500$, but experienced lower conversion and large deviations from target N_{bb} values at 750 and higher, with <3% conversion to bottlebrush polymer observed at $N_{bb} = 2000$. MMs x -MOM₂E'-PS (**1**) and x -ME'-PS (**2**), those with the highest $k_{p,obs}$ and HOMO energies, maintained high conversion (>90%) up to an [MM]/[G3] ratio of 500:1 with D values <1.2. They both reached very good conversion (>80%) with N_{bb} matching expected values out to a target $N_{bb} = 1000$, although D values increased to 1.5–1.6. A substantial drop in conversion when targeting $N_{bb} = 1500$ and higher was observed for both MMs, but some conversion was still observed even at target $N_{bb} = 2000$. Therefore, MMs x -MOM₂E'-PS (**1**) and x -ME'-PS (**2**) maintained the most livingness of all five MMs during the grafting-through ROMP process with the highest MM conversion, best control over M_n (i.e., experimentally observed N_{bb}), and lowest D values out all the MMs investigated.

It is worth noting that MM x -ME'-PS (**2**) had the highest conversion and highest observed N_{bb} when targeting $N_{bb} = 2000$ out of MMs **1–5**, even though it was not highly living at this high target N_{bb} . These results, combined with the $k_{p,obs}$ results (Table 2), suggest that the anchor group in MM x -ME'-PS (**2**) was the most living anchor group studied here. In contrast, MM xx -IM₂E'-PS (**5**) had the lowest $k_{p,obs}$ and performed the worst in the high target N_{bb} studies, making MM xx -IM₂E'-PS (**5**) the least living anchor group out of the five MMs tested. Therefore, we decided to further compare the livingness of these two MMs in chain extension studies using the sequential addition of MMs ROMP (SAM-ROMP) process.

3.4.4 Effects of the Anchor Group on Livingness in Bottlebrush Pentablock Copolymer Synthesis

Multiblock bottlebrush copolymers with three or more blocks have been recently used to make electronic materials,⁶⁰ injectable hydrogels,⁶¹⁻⁶² solid electrolytes,⁶³ and nanostructures with unusual shapes.⁶⁴⁻⁶⁵ High livingness in block copolymer synthesis is critical for complete chain extension, so in order to evaluate the effect of the anchor group on chain extension, we conducted a series of studies on the synthesis of bottlebrush pseudo-pentablock copolymers. In these SAM-ROMP studies, we aimed to follow evolution of molecular weight and D over the course of five consecutive additions of the same MM with a target $N_{bb} = 20$ for each addition. This strategy of consecutive additions of the same MM allowed us to remove any potential variable reactivity of different MMs, but we expect that the results would be useful in making complex structures with up to five different MMs.

The first step was to determine the time required for each MM to reach near-complete conversion (>95%) at a target $N_{bb} = 20$; therefore, we conducted kinetics experiments for MM x -ME'-PS (**2**) and xx -IM₂E'-PS (**5**) with an [MM]/[G3] ratio of 20:1. Polymerizations were carried out and monitored under the same conditions and using the same methods as the other polymerizations described here. In these experiments, MM x -ME'-PS (**2**) had a propagation half-life of 1.4 min and MM xx -IM₂E'-PS (**5**) had a propagation half-life of 13.4 min, with both MMs reaching near-complete conversion based on SEC analysis at very close to 7 half-lives [10 min for MM x -ME'-PS (**2**) and 90 min for MM xx -IM₂E'-PS (**5**)].

We then set out to compare bottlebrush pentablock copolymer synthesis for the two MMs. The pentablock polymerizations via the SAM-ROMP method were conducted under the same conditions as described above, injecting 20 equiv of the same MM five times at intervals of

either 10 min [MM *x*-ME'-PS (**2**)] or 90 min [MM *xx*-IM₂E'-PS (**5**)] (Figure 3.5A and 3.5E). Aliquots were removed right before each MM injection to determine conversion, M_n , and \bar{D} of each block (Table 3.3).

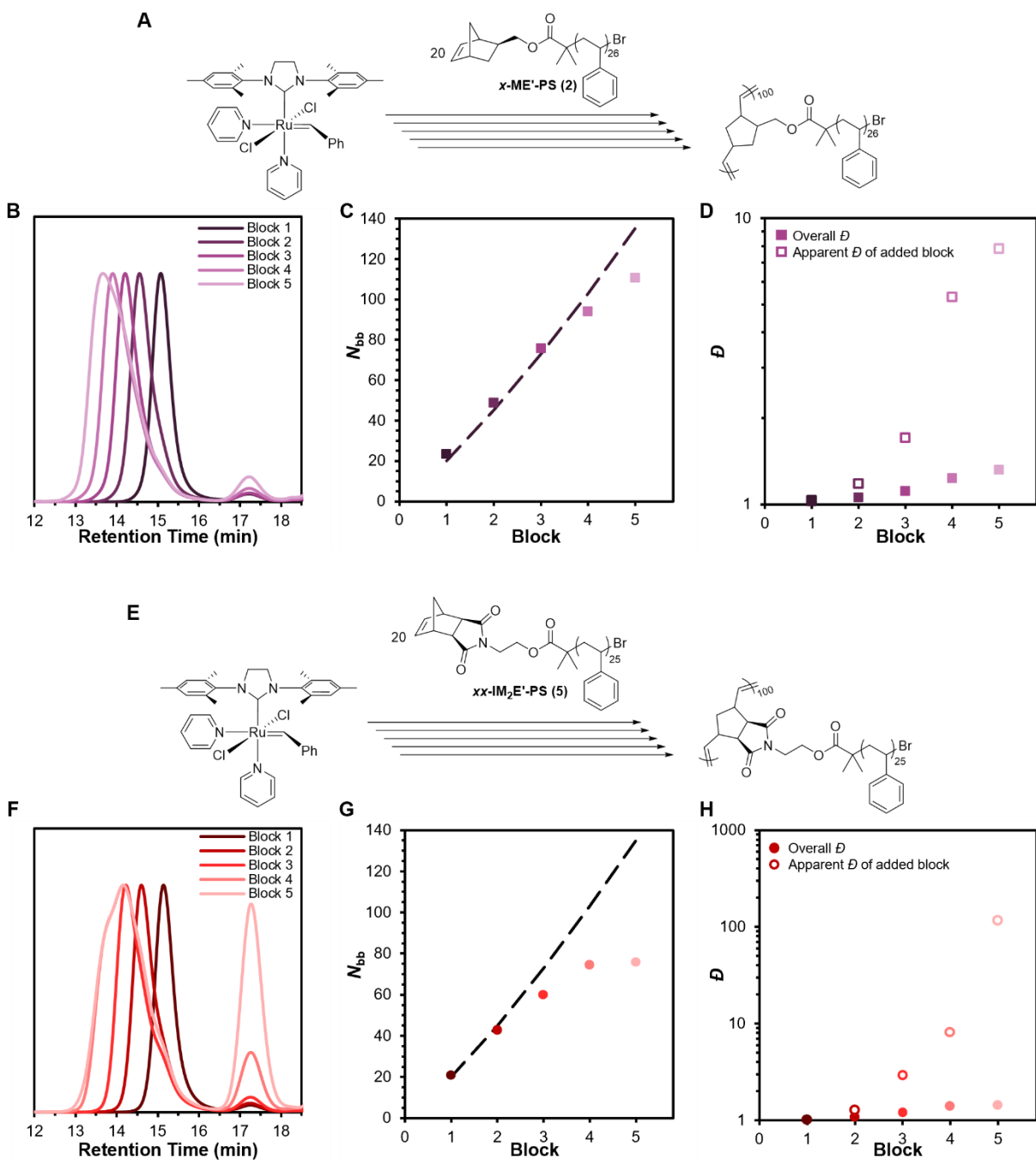


Figure 3.5. A and E): Schemes for bottlebrush pentablock copolymer syntheses for the ROMP of MMs *x*-ME'-PS (**2**) (A) and *xx*-IM₂E'-PS (**5**) (E). Reactions were run at a total MM

concentration of 20 mM in CDCl₃ under air at rt. B and F): SEC traces (dRI signal) for the ROMP of MM *x*-ME'-PS (**2**) (B) and *xx*-IM₂E'-PS (**5**) (F) showing a decrease in retention time after each block addition. C and G): Measured N_{bb} value versus block number for the ROMP of MM *x*-ME'-PS (**2**) (C) and *xx*-IM₂E'-PS (**5**) (G). Measured N_{bb} values were determined from $M_{n,bottlebrush}$ measured by SEC in THF at 30 °C with multiangle light scattering, estimated based on the equation $N_{bb} = M_{n,bottlebrush}/M_{n,MM}$. The dashed line refers to expected N_{bb} as block number increases. D and H): Overall \mathcal{D} and apparent \mathcal{D} of each added block for the ROMP of MM *x*-ME'-PS (**2**) (D) and *xx*-IM₂E'-PS (**5**) (H). Apparent \mathcal{D} refers to the estimated dispersity of each specific block as calculated by the method developed by Harrison using the formula $\mathcal{D}_2 = 1 + \frac{\mu_{1+2}^2(\mathcal{D}_{1+2} - 1) - \mu_1^2(\mathcal{D}_1 - 1)}{(\mu_{1+2} - \mu_1)^2}$ where \mathcal{D}_2 is the apparent dispersity in terms of the number-average molar masses of the initial (μ_1) and final (μ_{1+2}) polymers and the overall dispersity of the initial (\mathcal{D}_1) and final (\mathcal{D}_{1+2}) polymers.⁶⁶

Table 3.3. Characterization of Bottlebrush Pentablock Copolymers Prepared by SAM-ROMP

MM	Block	%	BB $M_{n,expected}^b$	BB $M_{n,SEC}^c$	Total	Total	BB	Apparent
	#	conv ^a	(kg/mol)	(kg/mol)	Target N_{bb}	$N_{bb, SEC}^d$	D^e	D^e
<i>x</i> -ME'-PS (2)	1	97	64	70	20	23	1.03	1.03
	2	97	128	147	40	48	1.06	1.18
	3	97	192	227	60	76	1.11	1.71
	4	96	256	282	80	94	1.23	5.3
	5	95	320	332	100	110	1.32	7.8
<i>xx</i> -IM ₂ E'-PS (5)	1	97	58	60	20	21	1.02	1.02
	2	97	116	124	40	43	1.08	1.27
	3	96	174	174	60	60	1.20	2.9
	4	89	232	216	80	74	1.40	8.1
	5	71	290	220	100	75	1.43	116

^aMeasured using SEC by comparing the areas of the bottlebrush polymer and MM peaks in the dRI trace. ^bDetermined using the equation $M_{n,expected} = M_{n,MM} * ([MM]/[G3])_0$. ^cMeasured by SEC in THF at 30 °C with multiangle light scattering using the known dn/dc for PS of 0.185 mL/g. ^dDetermined using the equation $N_{bb,expected} = M_{n,bottlebrush}/M_{n,MM}$. ^eDetermined using the method developed by Harrison.⁶⁶

For both MM *x*-ME'-PS (**2**) and MM *xx*-IM₂E'-PS (**5**), we saw a decrease in the retention time of the main SEC peak upon polymerization of each additional block, indicating an increase in molecular weight of the bottlebrush polymer (Figures 3.5B and 3.5F). As expected, the first block for both MMs reached near-complete conversion (>97%) while maintaining low D . However, MM conversion generally decreased after each block addition, with MM *x*-ME'-PS (**2**) dropping to 95% conversion and MM *xx*-IM₂E'-PS (**5**) dropping to just 71% conversion after the

addition of all five blocks. A small residual MM peak at 17.2 min was observed in the final SEC trace for the ROMP of MM *x*-ME'-PS (**2**), while a much more prominent MM peak remained for MM *xx*-IM₂E'-PS (**5**).

We also observed an increase in N_{bb} after each block addition, as determined by SEC, for both MMs, as expected (Figure 3.5C and 3.5G). After each injection of MM *x*-ME'-PS (**2**), a linear increase in N_{bb} was observed. All N_{bb} values generally matched target values for this MM as well, with a final estimated $N_{bb} = 110$ for the bottlebrush pentablock copolymer, close to the target N_{bb} value of 100. The small deviations from the expected values are likely due to small errors in injected monomer amount or catalyst loading. In contrast, this close agreement between target N_{bb} and measured N_{bb} values was not the case for the bottlebrush polymer derived from MM *xx*-IM₂E'-PS (**5**). A linear increase in N_{bb} matching target values was found for the first three MM injections, but blocks 4 and 5 did not reach target N_{bb} values. For this imide-based anchor group, we observed a maximum $N_{bb} = 75$, where only very little polymerization was observed for the fifth MM injection.

Comparing the bottlebrush polymer D values and the shapes of the SEC curves after every block addition for both MMs also revealed valuable insights regarding livingness. For the bottlebrush polymer derived from MM *x*-ME'-PS (**2**), D values reached 1.3, but they increased to 1.4 for the bottlebrush polymer derived from MM *xx*-IM₂E'-PS (**5**) (Table 3.3). Furthermore, the bottlebrush polymers with a final target $N_{bb} = 100$ for both MMs made by the SAM-ROMP method exhibited higher D values than those synthesized directly to a target N_{bb} value of 100 (1.04 for MM *x*-ME'-PS (**2**) and 1.07 for MM *xx*-IM₂E'-PS (**5**), from the kinetics data in Table 3.2). Additionally, low molecular weight shoulders were present in the SEC traces for blocks 4 and 5 for the ROMP of MM *x*-ME'-PS (**2**) and blocks 3 through 5 for the ROMP of MM *xx*-

IM₂E'-PS (5), suggesting some amount of chain termination in both ROMP experiments before all five blocks had been added. However, the shoulders in the SEC traces of the bottlebrush polymers derived from MM *xx*-IM₂E'-PS (5) were drastically larger than in those derived from MM *x*-ME'-PS (2), clearly indicating a lower degree of livingness for MM *xx*-IM₂E'-PS (5) compared with MM *x*-ME'-PS (2). This reduced livingness for MM *xx*-IM₂E'-PS (5) was not as readily apparent in the high target N_{bb} studies, where this MM reached a total N_{bb} of 100, matching the target N_{bb} value, with high conversion and low \bar{D} ; however, these SAM-ROMP studies make clear that the relatively low $k_{p,obs}$ for MM *xx*-IM₂E'-PS (5) leads to low livingness when challenging the catalyst with multiple MM injections.

Only a small difference in \bar{D} values (1.3 versus 1.4) between the final polymers in these two SAM-ROMP experiments was found, but we were interested in estimating the \bar{D} values of each individual bottlebrush polymer block in these pentablock copolymers. Harrisson recently reported a mathematical method of estimating the apparent \bar{D} of each individual block in a linear multiblock copolymer synthesis.⁶⁶ His results in a study of a 24-block copolymer made by RAFT⁶⁷ suggested that the individual substructures of complex macromolecules may be highly disperse even though the overall \bar{D} remains relatively low. Using this method, we estimated the apparent \bar{D} of each individual block in both bottlebrush pentablock copolymer syntheses (Figure 3.5D and 3.5H). For both MMs, the apparent \bar{D} of each block increased roughly exponentially, consistent with Harrisson's analysis, but with very different outcomes between the two SAM-ROMP experiments: The final block of MM *x*-ME'-PS (2) reached an apparent \bar{D} of 7.8, whereas the final block of MM *xx*-IM₂E'-PS (5) had an apparent \bar{D} of 116. This order of magnitude difference between the two anchor groups dramatically demonstrates the higher degree of livingness for MM *x*-ME'-PS (2) compared with MM *xx*-IM₂E'-PS (5). The data also

suggest that even with MM *x*-ME'-PS (**2**), the most living anchor group studied here, there is still significant chain termination when making bottlebrush pentablock copolymers. Overall, we conclude that high k_p is critical in the ROMP of MMs to control molecular weight, maintain low dispersity, and retain high chain end fidelity when synthesizing multiblock bottlebrush copolymers, but that even for the best anchor group studied here, structural heterogeneities arise.

3.5 Conclusions

We investigated the relationship between HOMO energies localized on the norbornene olefin and livingness in the ROMP of a series of five MMs with PS side-chains of similar molecular weights but different anchor groups. DFT calculations showed that the choice of anchor group affects the norbornene HOMO energy of these MMs, and experimental results suggested that a higher HOMO energy increases the reactivity of the norbornene and increases k_p in grafting-through ROMP. Further investigation into the livingness of grafting-through ROMP through high target N_{bb} studies demonstrated that high k_p values are critical to synthesize macromolecules with precise molecular weights and low D values. MMs with lower HOMO energies (those with imide-containing anchor groups), and lower $k_{p,obs}$ values in our ROMP experiments, showed lower livingness at target $N_{bb} = 250$ and above than the other MMs. However, the two MMs with the highest HOMO energies and $k_{p,obs}$ values reached high conversion and maintained control over molecular weight when targeting N_{bb} values up to 1000. Therefore, MMs with anchor groups that lead to higher k_p values increase livingness in grafting-through ROMP compared with MMs with lower k_p values, allowing for better-defined bottlebrush polymer structures. The effect of the anchor group on livingness was further evidenced in SAM-ROMP experiments synthesizing bottlebrush pentablock copolymers using

the MMs with the highest and lowest $k_{p,obs}$ values (MMs *x*-ME'-PS (**2**) and *xx*-IM₂E'-PS (**5**), respectively). Each block addition of MM *xx*-IM₂E'-PS (**5**) exhibited an increase in the \mathcal{D} value of both the overall polymer structure and the apparent \mathcal{D} of each additional block, where the final block had a staggering apparent \mathcal{D} of 116. A similar effect was seen for the SAM-ROMP of MM *x*-ME'-PS (**2**) to make a bottlebrush pentablock copolymer; however, the increase in apparent \mathcal{D} was significantly lower, only reaching 7.8 for the final block.

In sum, these experiments indicate that high k_p values in ROMP are critical to maintain high livingness for the synthesis of complex macromolecules such as bottlebrush polymers, and that anchor group selection has a substantial effect on k_p . Our studies were designed to evaluate the effect of the anchor group on k_p in a defined set of MMs of similar molecular weights, but we expect that these results will suggest straightforward methods to enhance livingness and control in a wide variety of polymer topologies made by ROMP. These experiments also underscore the need to develop better anchor groups that increase k_p and better catalysts that decrease k_t in ROMP, as well as improved methods that increase the k_p/k_t ratio, to continue to expand the synthetic boundaries of complex polymer architectures.

3.6 Acknowledgments

This work was supported by a joint grant between the National Science Foundation and the Binational Science Foundation (DMR-2104602). We thank Dr. Santu Sarkar, Tamalika Paul, and Ishani Sarkar for critical reading of the manuscript. The authors acknowledge Advanced Research Computing at Virginia Tech for providing computational resources and technical support that have contributed to the results reported within this paper. We also acknowledge the

Virginia Tech Mass Spectrometry Research Incubator for high-resolution mass spectrometry analysis.

3.7 References

1. Jha, S.; Dutta, S.; Bowden, N. B., Synthesis of Ultralarge Molecular Weight Bottlebrush Polymers Using Grubbs' Catalysts. *Macromolecules* **2004**, *37*, 4365–4374.
2. Wintermantel, M.; Gerle, M.; Fischer, K.; Schmidt, M.; Wataoka, I.; Urakawa, H.; Kajiwara, K.; Tsukahara, Y., Molecular Bottlebrushes. *Macromolecules* **1996**, *29*, 978–983.
3. Xie, G.; Martinez, M. R.; Olszewski, M.; Sheiko, S. S.; Matyjaszewski, K., Molecular Bottlebrushes as Novel Materials. *Biomacromolecules* **2019**, *20*, 27–54.
4. Li, Z.; Tang, M.; Liang, S.; Zhang, M.; Biesold, G. M.; He, Y.; Hao, S.-M.; Choi, W.; Liu, Y.; Peng, J.; Lin, Z., Bottlebrush polymers: From controlled synthesis, self-assembly, properties to applications. *Prog. Polym. Sci.* **2021**, *116*, 101387.
5. Sheiko, S. S.; Sumerlin, B. S.; Matyjaszewski, K., Cylindrical molecular brushes: Synthesis, characterization, and properties. *Prog. Polym. Sci.* **2008**, *33*, 759–785.
6. Verduzco, R.; Li, X.; Pesek, S. L.; Stein, G. E., Structure, function, self-assembly, and applications of bottlebrush copolymers. *Chem. Soc. Rev.* **2015**, *44*, 2405–2420.
7. Zhulina, E. B.; Sheiko, S. S.; Borisov, O. V., Theoretical advances in molecular bottlebrushes and comblike (co)polymers: solutions, gels, and self-assembly. *Soft Matter* **2022**, *18*, 8714–8732.
8. Walsh, D. J.; Guironnet, D., Macromolecules with programmable shape, size, and chemistry. *Proc. Natl. Acad. Sci. U.S.A* **2019**, *116*, 1538–1542.

9. Dearman, M.; Ogbonna, N. D.; Amofa, C. A.; Peters, A. J.; Lawrence, J., Versatile strategies to tailor the glass transition temperatures of bottlebrush polymers. *Polym. Chem.* **2022**, *13*, 4901–4907.
10. Kamble, Y. L.; Walsh, D. J.; Guironnet, D., Precision of Architecture–Controlled Bottlebrush Polymer Synthesis: A Monte Carlo Analysis. *Macromolecules* **2022**, *55*, 10255–10263.
11. Maw, M.; Morgan, B. J.; Dashtimoghadam, E.; Tian, Y.; Bersenev, E. A.; Maryasevskaya, A. V.; Ivanov, D. A.; Matyjaszewski, K.; Dobrynin, A. V.; Sheiko, S. S., Brush Architecture and Network Elasticity: Path to the Design of Mechanically Diverse Elastomers. *Macromolecules* **2022**, *55*, 2940–2951.
12. Self, J. L.; Sample, C. S.; Levi, A. E.; Li, K.; Xie, R.; de Alaniz, J. R.; Bates, C. M., Dynamic Bottlebrush Polymer Networks: Self-Healing in Super–Soft Materials. *J. Am. Chem. Soc.* **2020**, *142*, 7567–7573.
13. Sarapas, J. M.; Chan, E. P.; Rettner, E. M.; Beers, K. L., Compressing and Swelling To Study the Structure of Extremely Soft Bottlebrush Networks Prepared by ROMP. *Macromolecules* **2018**, *51*, 2359–2366.
14. Cushman, K.; Keith, A.; Tanaka, J.; Sheiko, S. S.; You, W., Investigating the Stress–Strain Behavior in Ring-opening Metathesis Polymerization-based Brush Elastomers. *Macromolecules* **2021**, *54*, 8365–8371.
15. Arrington, K. J.; Radzinski, S. C.; Drummey, K. J.; Long, T. E.; Matson, J. B., Reversibly Cross–linkable Bottlebrush Polymers as Pressure–Sensitive Adhesives. *ACS Appl. Mater. Interfaces* **2018**, *10*, 26662–26668.

16. Neary, W. J.; Fultz, B. A.; Kennemur, J. G., Well-Defined and Precision-Grafted Bottlebrush Polypentenamers from Variable Temperature ROMP and ATRP. *ACS Macro Lett.* **2018**, *7*, 1080–1086.
17. Ramamurthi, P.; Zhao, Z.; Burke, E.; Steinmetz, N. F.; Müllner, M., Tuning the Hydrophilic–Hydrophobic Balance of Molecular Polymer Bottlebrushes Enhances their Tumor Homing Properties. *Adv. Healthc. Mater.* **2022**, *11*, 2200163.
18. Nguyen, H. V. T.; Jiang, Y.; Mohapatra, S.; Wang, W.; Barnes, J. C.; Oldenhuis, N. J.; Chen, K. K.; Axelrod, S.; Huang, Z.; Chen, Q.; Golder, M. R.; Young, K.; Suvlu, D.; Shen, Y.; Willard, A. P.; Hore, M. J. A.; Gómez–Bombarelli, R.; Johnson, J. A., Bottlebrush polymers with flexible enantiomeric side chains display differential biological properties. *Nat. Chem.* **2022**, *14*, 85–93.
19. Sowers, M. A.; McCombs, J. R.; Wang, Y.; Paletta, J. T.; Morton, S. W.; Dreaden, E. C.; Boska, M. D.; Ottaviani, M. F.; Hammond, P. T.; Rajca, A.; Johnson, J. A., Redox–responsive branched–bottlebrush polymers for in vivo MRI and fluorescence imaging. *Nat. Commun.* **2014**, *5*, 5460.
20. Miyake, G. M.; Piunova, V. A.; Weitekamp, R. A.; Grubbs, R. H., Precisely Tunable Photonic Crystals From Rapidly Self-Assembling Brush Block Copolymer Blends. *Angew. Chem* **2012**, *51*, 11246–11248.
21. Liberman-Martin, A. L.; Chang, A. B.; Chu, C. K.; Siddique, R. H.; Lee, B.; Grubbs, R. H., Processing Effects on the Self-Assembly of Brush Block Polymer Photonic Crystals. *ACS Macro Lett.* **2021**, *10*, 1480–1486.

22. Boyle, B. M.; French, T. A.; Pearson, R. M.; McCarthy, B. G.; Miyake, G. M., Structural Color for Additive Manufacturing: 3D-Printed Photonic Crystals from Block Copolymers. *ACS Nano* **2017**, *11*, 3052–3058.
23. van As, D.; Subbiah, J.; Jones, D. J.; Wong, W. W. H., Controlled Synthesis of Well-Defined Semiconducting Brush Polymers. *Macromol. Chem. Phys.* **2016**, *217*, 403–413.
24. Tonge, C. M.; Sauv e, E. R.; Cheng, S.; Howard, T. A.; Hudson, Z. M., Multiblock Bottlebrush Nanofibers from Organic Electronic Materials. *J. Am. Chem. Soc.* **2018**, *140*, 11599–11603.
25. Sauv e, E. R.; Tonge, C. M.; Hudson, Z. M., Aggregation-Induced Energy Transfer in Color-Tunable Multiblock Bottlebrush Nanofibers. *J. Am. Chem. Soc.* **2019**, *141*, 16422–16431.
26. Obhi, N. K.; Peda, D. M.; Kynaston, E. L.; Seferos, D. S., Exploring the Graft-To Synthesis of All-Conjugated Comb Copolymers Using Azide-Alkyne Click Chemistry. *Macromolecules* **2018**, *51*, 2969–2978.
27. Pelras, T.; Nonappa; Mahon, C. S.; M ullner, M., Cylindrical Zwitterionic Particles via Interpolyelectrolyte Complexation on Molecular Polymer Brushes. *Macromol. Rapid Commun.* **2021**, *42*, 2000401.
28. Szwarc, M., Living polymers. Their discovery, characterization, and properties. *J. Polym. Sci., Part A: Polym. Chem.* **1998**, *36*, IX–XV.
29. Stenzel, M. H.; Barner-Kowollik, C., The living dead – common misconceptions about reversible deactivation radical polymerization. *Mater. Horiz.* **2016**, *3*, 471–477.
30. Jenkins, A. D.; Kratochv l, P.; Stepto, R. F. T.; Suter, U. W., Glossary of basic terms in polymer science (IUPAC Recommendations 1996). *Pure Appl. Chem.* **1996**, *68*, 2287–2311.

31. Desimone, J. M.; Hellstern, A. M.; Siochi, E. J.; Smith, S. D.; Ward, T. C.; McGrath, J. E.; Gallagher, P. M.; Krukonis, V. J., Homogeneous and multiphase poly(methyl methacrylate) graft polymers via the macromonomer method. *Makromol. Chem. Macromol. Symp.* **1990**, *32*, 21–45.
32. Rahlwes, D.; Roovers, J. E. L.; Bywater, S., Synthesis and Characterization of Poly(styrene-g-Isoprene) Copolymers. *Macromolecules* **1977**, *10*, 604–609.
33. Hadjichristidis, N.; Iatrou, H.; Pitsikalis, M.; Mays, J., Macromolecular architectures by living and controlled/living polymerizations. *Prog. Polym. Sci.* **2006**, *31*, 1068–1132.
34. Wintermantel, M.; Fischer, K.; Gerle, M.; Ries, R.; Schmidt, M.; Kajiwara, K.; Urakawa, H.; Wataoka, I., Lyotropic Phases Formed by “Molecular Bottlebrushes”. *Angew. Chem., Int. Ed. Engl.* **1995**, *34*, 1472–1474.
35. Matyjaszewski, K., Atom Transfer Radical Polymerization: From Mechanisms to Applications. *Isr. J. Chem.* **2012**, *52*, 206–220.
36. Keddie, D. J.; Moad, G.; Rizzardo, E.; Thang, S. H., RAFT Agent Design and Synthesis. *Macromolecules* **2012**, *45*, 5321–5342.
37. Cheng, C.; Khoshdel, E.; Wooley, K. L., ATRP from a Norbornenyl-Functionalized Initiator: Balancing of Complementary Reactivity for the Preparation of α -Norbornenyl Macromonomers/ ω -Haloalkyl Macroinitiators. *Macromolecules* **2005**, *38*, 9455–9465.
38. Bielawski, C. W.; Grubbs, R. H., Living ring-opening metathesis polymerization. *Prog. Polym. Sci.* **2007**, *32*, 1–29.
39. Choi, T.-L.; Grubbs, R. H., Controlled Living Ring-opening-Metathesis Polymerization by a Fast-Initiating Ruthenium Catalyst. *Angew. Chem* **2003**, *42*, 1743–1746.

40. Trnka, T. M.; Grubbs, R. H., The Development of L₂X₂RuCHR Olefin Metathesis Catalysts: An Organometallic Success Story. *Acc. Chem. Res.* **2001**, *34*, 18–29.
41. Bloch, S. E.; Scannelli, S. J.; Alaboalirat, M.; Matson, J. B., Complex Polymer Architectures Using Ring-opening Metathesis Polymerization: Synthesis, Applications, and Practical Considerations. *Macromolecules* **2022**, *55*, 4200–4227.
42. Ren, N.; Yu, C.; Zhu, X., Topological Effect on Macromonomer Polymerization. *Macromolecules* **2021**, *54*, 6101–6108.
43. Ogbonna, N. D.; Dearman, M.; Cho, C.-T.; Bharti, B.; Peters, A. J.; Lawrence, J., Topologically Precise and Discrete Bottlebrush Polymers: Synthesis, Characterization, and Structure–Property Relationships. *JACS Au* **2022**, *2*, 898–905.
44. Walsh, D. J.; Guironnet, D., Macromolecules with programmable shape, size, and chemistry. *Proc. Natl. Acad. Sci.* **2019**, *116*, 1538–1542.
45. Cong, Y.; Vatankhah–Varnosfaderani, M.; Karimkhani, V.; Keith, A. N.; Leibfarth, F. A.; Martinez, M. R.; Matyjaszewski, K.; Sheiko, S. S., Understanding the Synthesis of Linear–Bottlebrush–Linear Block Copolymers: Toward Elastomers with Well-Defined Mechanical Properties. *Macromolecules* **2020**, *53*, 8324–8332.
46. Hong, S. H.; Wenzel, A. G.; Salguero, T. T.; Day, M. W.; Grubbs, R. H., Decomposition of Ruthenium Olefin Metathesis Catalysts. *J. Am. Chem. Soc.* **2007**, *129*, 7961–7968.
47. Bailey, G. A.; Foscatto, M.; Higman, C. S.; Day, C. S.; Jensen, V. R.; Fogg, D. E., Bimolecular Coupling as a Vector for Decomposition of Fast-Initiating Olefin Metathesis Catalysts. *J. Am. Chem. Soc.* **2018**, *140*, 6931–6944.
48. Matyjaszewski, K., Ranking living systems. *Macromolecules* **1993**, *26*, 1787–1788.

49. Radzinski, S. C.; Foster, J. C.; Chapleski, R. C.; Troya, D.; Matson, J. B., Bottlebrush Polymer Synthesis by Ring-opening Metathesis Polymerization: The Significance of the Anchor Group. *J. Am. Chem. Soc.* **2016**, *138*, 6998–7004.
50. Scannelli, S. J.; Paripati, A.; Weaver, J. R.; Alaboalirat, M.; Troya, D.; Matson, J. B., The influence of the anchor group in ring-opening metathesis polymerization: Synthesis of linear polymers. *Macromolecules* **2023**, *Submitted*, ma-2023-001729.
51. Slugovc, C.; Demel, S.; Riegler, S.; Hobisch, J.; Stelzer, F., The Resting State Makes the Difference: The Influence of the Anchor Group in the ROMP of Norbornene Derivatives. *Macromol. Rapid Commun.* **2004**, *25*, 475–480.
52. Hyatt, M. G.; Walsh, D. J.; Lord, R. L.; Andino Martinez, J. G.; Guironnet, D., Mechanistic and Kinetic Studies of the Ring Opening Metathesis Polymerization of Norbornenyl Monomers by a Grubbs Third Generation Catalyst. *J. Am. Chem. Soc.* **2019**, *141*, 17918–17925.
53. Zhao, Y.; Truhlar, D. G., The M06 suite of density functionals for main group thermochemistry, thermochemical kinetics, noncovalent interactions, excited states, and transition elements: two new functionals and systematic testing of four M06-class functionals and 12 other functionals. *Theor. Chem. Acc.* **2008**, *120*, 215–241.
54. Weigend, F.; Ahlrichs, R., Balanced basis sets of split valence, triple zeta valence and quadruple zeta valence quality for H to Rn: Design and assessment of accuracy. *Phys. Chem. Chem. Phys.* **2005**, *7*, 3297–3305.
55. Suresh, C. H.; Koga, N., Orbital Interactions in the Ruthenium Olefin Metathesis Catalysts. *Organometallics* **2004**, *23*, 76–80.

56. Alaboalirat, M.; Vu, C.; Matson, J. B., Radical–radical coupling effects in the direct-growth grafting-through synthesis of bottlebrush polymers using RAFT and ROMP. *Polym. Chem.* **2022**, *13*, 5841–5851.
57. Lexer, C.; Saf, R.; Slugovc, C., Acrylates as termination reagent for the preparation of semi–telechelic polymers made by ring opening metathesis polymerization. *J. Polym. Sci., Part A: Polym. Chem.* **2009**, *47*, 299–305.
58. Choi, J.; Kim, H.; Do, T.; Moon, J.; Choe, Y.; Kim, J. G.; Bang, J., Influence of residual impurities on ring-opening metathesis polymerization after copper(I)-catalyzed alkyne–azide cycloaddition click reaction. *J. Polym. Sci., Part A: Polym. Chem.* **2019**, *57*, 726–737.
59. Teo, Y. C.; Xia, Y., Importance of Macromonomer Quality in the Ring-opening Metathesis Polymerization of Macromonomers. *Macromolecules* **2015**, *48*, 5656–5662.
60. Polgar, A. M.; Poisson, J.; Christopherson, C. J.; Hudson, Z. M., Enhancement of Red Thermally Assisted Fluorescence in Bottlebrush Block Copolymers. *Macromolecules* **2021**, *54*, 7880–7889.
61. Nakagawa, Y.; Oki, Y.; Da, X.; Singh Chandel, A. K.; Ohta, S.; Ito, T., Injectable bottlebrush triblock copolymer hydrogel crosslinked with ferric ions. *Polymer* **2022**, *240*, 124519.
62. Vohidov, F.; Milling, L. E.; Chen, Q.; Zhang, W.; Bhagchandani, S.; Nguyen, Hung V. T.; Irvine, D. J.; Johnson, J. A., ABC triblock bottlebrush copolymer-based injectable hydrogels: design, synthesis, and application to expanding the therapeutic index of cancer immunochemotherapy. *Chem. Sci.* **2020**, *11*, 5974–5986.

63. Bates, C. M.; Chang, A. B.; Momčilović, N.; Jones, S. C.; Grubbs, R. H., ABA Triblock Brush Polymers: Synthesis, Self-Assembly, Conductivity, and Rheological Properties. *Macromolecules* **2015**, *48*, 4967–4973.
64. Radzinski, S. C.; Foster, J. C.; Scannelli, S. J.; Weaver, J. R.; Arrington, K. J.; Matson, J. B., Tapered Bottlebrush Polymers: Cone-shaped Nanostructures by Sequential Addition of Macromonomers. *ACS Macro Lett.* **2017**, *6*, 1175–1179.
65. Li, A.; Li, Z.; Zhang, S.; Sun, G.; Policarpio, D. M.; Wooley, K. L., Synthesis and Direct Visualization of Dumbbell-shaped Molecular Brushes. *ACS Macro Lett.* **2012**, *1*, 241–245.
66. Harrisson, S., The downside of dispersity: why the standard deviation is a better measure of dispersion in precision polymerization. *Polym. Chem.* **2018**, *9*, 1366–1370.
67. Engelis, N. G.; Anastasaki, A.; Nurumbetov, G.; Truong, N. P.; Nikolaou, V.; Shegiwal, A.; Whittaker, M. R.; Davis, T. P.; Haddleton, D. M., Sequence-controlled methacrylic multiblock copolymers via sulfur-free RAFT emulsion polymerization. *Nat. Chem.* **2017**, *9*, 171–178.

3.8 Supporting Information

Materials and Methods

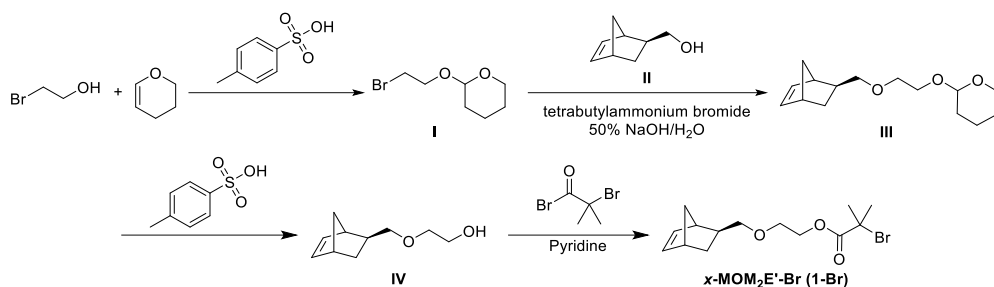
All reagents and solvents were obtained from commercial vendors and used as received unless otherwise stated. ^1H NMR spectra were measured on either an Agilent 400 MHz or Bruker 600 MHz spectrometer with a high ^1H sensitivity TCI Prodigy probe. ^1H and ^{13}C NMR chemical shifts are reported in ppm relative to internal solvent resonances unless otherwise stated. Yields refer to compounds as isolated after requisite purification unless otherwise stated. A Biotage Selekt flash purification system was used for automated silica gel column purification. Silica

used for automated flash chromatography purifications was ZEOCHEM ZEOprep 60 HYD 40–63 μM pore size. Thin-layer chromatography (TLC) was performed on glass-backed silica plates and visualized by UV unless otherwise stated. High-resolution mass spectra were analyzed by flow injection analysis using a Shimadzu 9030 QTOF mass spectrometer interfaced with a Shimadzu 40 series UPLC. Size exclusion chromatography (SEC) was carried out in tetrahydrofuran at 1 mL min^{-1} at $30 \text{ }^\circ\text{C}$ on two Agilent PLgel $10 \text{ }\mu\text{m}$ MIXED-B columns connected in series with a Wyatt Dawn Heleos 2 light scattering detector and a Wyatt Optilab Rex refractive index detector. No calibration standards were used, and the known dn/dc for PS of 0.185 mL/g was used for all samples.

Preparation of Grubbs' 3rd generation catalyst (G3)

Grubbs' 3rd generation catalyst (G3) was prepared freshly and used within 2 days following a modified version of published methods.^{1–2} First, pyridine and pentane were purified via passage through a short column of basic alumina. A one dram vial was charged with a stir bar and 20 mg of Grubbs' 2nd generation catalyst ($\text{H}_2\text{Imes})(\text{Pcy}_3)(\text{Cl})_2\text{Ru}=\text{CHPh}$). Next, purified pyridine (20 μL) was added to the vial, and the reaction mixture was stirred vigorously for 20–30 min until it had turned a vivid lime-green color. If the reaction mixture dried to a solid, additional pyridine (10 μL increments) was added and solids were broken up manually with a spatula to allow for more stirring. Next, purified pentane (3 mL) was added to the vial to precipitate the catalyst. The pentane was decanted, and the solids were washed with additional purified pentane (3 mL). Once again, the pentane was decanted and the remaining solids were dried by blowing air over the vial for 1 min, then transferred to a clean vial, and then dried under vacuum overnight.

Synthesis of compound *x*-MOM₂E'-Br (1-Br)



Compound I

A round-bottom flask was charged with bromoethanol (5.00 mL, 70.5 mmol), 3,4-dihydropyran (7.72 mL, 84.6 mmol), *p*-toluenesulfonic acid (1.21 g, 7.05 mmol), CH₂Cl₂ (200 mL), and a stir bar. The reaction mixture was stirred at rt for 16 h, and reaction progress was monitored by TLC (CH₂Cl₂, visualization by I₂) until bromoethanol was completely consumed. The reaction mixture was concentrated by rotary evaporation, and the crude product was purified by automated flash chromatography on silica with CH₂Cl₂ as the mobile phase to give the pure product as a colorless oil (10.0 g, 70% yield). ¹H NMR (CDCl₃): δ 4.65 (m, 1H), 4.03–3.97 (m, 1H), 3.90–3.84 (m, 1H), 3.78–3.72 (m, 1H), 3.53–3.44 (m, 3H), 1.86–1.47 (m, 6H). ¹³C NMR (CDCl₃): δ 98.91, 67.50, 62.25, 30.82, 30.40, 25.33, 19.23. Both ¹H and ¹³C NMR spectra matched literature values.³

Exo-5-norbornene-2-Methanol (II)

Compound II, *exo*-5-norbornene-2-Methanol was prepared according to a previously reported procedure.⁴ ¹H NMR (CDCl₃): δ 6.08 (m, 2H), 3.70 (m, 1H), 3.54 (m, 1H), 2.82 (s, 1H), 2.74 (s,

1H), 1.64 (m, 1H), 1.30 (m, 3H), 1.11 (m, 1H). ¹³C NMR (CDCl₃): δ 136.91, 136.57, 67.65, 45.08, 43.38, 41.99, 41.63, 29.64. Both ¹H and ¹³C NMR spectra matched literature values.

Compound III

A round-bottom flask was charged with NaOH (4.8 g, 120 mmol) and water (4.8 mL). A second round-bottom flask was charged with compound **II** (0.5 g, 4.0 mmol), compound **I** (1.7 g, 8.1 mmol), and hexanes (4.8 mL). Once dissolved, the solution containing compound **II** was added all at once to the NaOH solution, followed by the addition of tetrabutylammonium bromide (0.13 g, 0.40 mmol). The reaction mixture was stirred while heating at reflux for 24 h with reaction progress monitored by TLC (CH₂Cl₂, visualization by a potassium permanganate stain). The reaction mixture was cooled and diluted with water (20 mL). The organic layer was removed in a separatory funnel, and then the aqueous layer was extracted with CH₂Cl₂ (2 x 30 mL). The organic layers were combined and washed with brine (10 mL), dried over Na₂SO₄, and concentrated by rotary evaporation. The crude product was purified by automated flash chromatography on silica with a hexanes/CH₂Cl₂ gradient as the mobile phase to give the pure product as a colorless oil (0.72 g, 71% yield). ¹H NMR (CDCl₃): δ 6.09 (m, 2H), 4.68 (m, 1H), 3.95–3.82 (m, 2H), 3.73–3.48 (m, 5H), 3.40 (m, 1H), 2.80 (m, 2H), 1.93–1.79 (m, 1H), 1.79–1.48 (m, 6H), 1.38–1.29 (m, 2H), 1.28–1.06 (m, 2H). ¹³C NMR (CDCl₃): δ 136.76, 99.01, 76.08, 70.29, 66.73, 62.33, 45.11, 43.74, 41.64, 38.91, 30.70, 29.78, 25.58, 19.58. HR-MS calculated for C₁₅H₂₄O₃ [M + Na]⁺ 275.1618; found 275.1619.

Compound IV

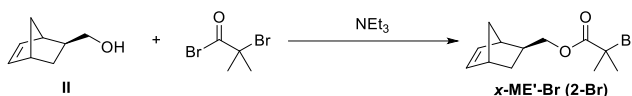
A round-bottom flask was charged with compound **III** (0.76 g, 3.0 mmol), *p*-toluenesulfonic acid (0.052 g, 0.30 mmol), methanol (100 mL), and a stir bar. The reaction mixture was stirred for about 1 h, and monitored by TLC (CH₂Cl₂, visualization by a potassium permanganate stain) and then concentrated by rotary evaporation. The crude product was purified by automated flash chromatography on silica with CH₂Cl₂ as the mobile phase to give pure compound **IV** as a colorless oil (0.49 g, 97% yield). ¹H NMR (CDCl₃): δ 6.12–6.03 (m, 2H), 3.78–3.70 (m, 2H), 3.59–3.50 (m, 3H), 3.38 (t, *J* = 9.1 Hz, 1H), 2.83–2.71 (m, 2H), 2.10 (s, 1H), 1.70 (m, 1H), 1.35–1.21 (3H), 1.10 (m, 1H). ¹³C NMR (CDCl₃): δ 136.83, 136.62, 76.09, 72.07, 61.98, 45.14, 43.79, 41.65, 38.96, 29.83. HR-MS calculated for C₁₀H₁₆O₂ [M + Na]⁺ 191.1043; found 191.1034.

Compound *x*-MOM₂E'-Br (**1-Br**)

A flame-dried, two-neck round-bottom flask equipped with a stir bar, septum, and an adapter for N₂ was charged with compound **IV** (0.49 g, 2.9 mmol), pyridine (0.41 mL, 5.2 mmol), and dry tetrahydrofuran (15 mL). The flask was placed in an ice bath. Once cooled, α-bromoisobutyryl bromide (0.43 mL, 3.5 mmol) was added dropwise by a syringe and needle under N₂ atmosphere. The reaction mixture was stirred overnight, allowing the ice to melt and the contents of the flask to warm to rt. The reaction mixture was monitored by TLC (CH₂Cl₂, visualization by a potassium permanganate stain) until compound **IV** was completely consumed. Next, the reaction mixture was filtered, and then the filtrate was concentrated by rotary evaporation and then the crude product was purified by automated flash chromatography on silica with CH₂Cl₂ as the mobile phase. Pure product *x*-MOM₂E'-Br (**1-Br**) was obtained as a colorless oil (0.36 g, 39%

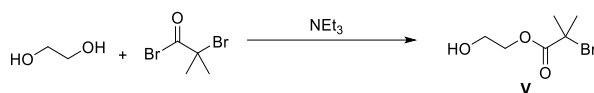
yield). ^1H NMR (CDCl_3): δ 6.13–6.02 (m, 2H), 4.33 (t, $J = 4.9$ Hz, 2H), 3.75–3.64 (m, 2H), 3.55 (m, 1H), 3.44–3.36 (m, 1H), 2.80 (s, 1H), 2.74 (m, 1H), 1.95 (s, 6H), 1.75–1.63 (m, 1H), 1.36–1.19 (m, 3H), 1.11 (m, 1H). ^{13}C NMR (CDCl_3): δ 171.82, 136.85, 136.70, 76.13, 68.50, 65.31, 55.86, 45.16, 43.77, 41.69, 38.97, 30.93, 29.75. HR-MS calculated for $\text{C}_{14}\text{H}_{21}\text{BrO}_3$ [$\text{M} + \text{H}$] $^+$ 317.0747; found 317.0768.

Compound *x*-ME'-Br (2-Br)



Compound *x*-ME'-Br (2-Br) was synthesized as previously reported.⁴ ^1H NMR (CDCl_3): δ 6.13–6.06 (m, 2H), 4.24 (m, 1H), 4.08 (m, 1H), 2.85 (m, 1H), 2.74 (m, 1H), 1.95 (s, 6H), 1.85–1.73 (m, 1H), 1.40–1.26 (m, 3H), 1.20 (m, 1H). ^{13}C NMR (CDCl_3): δ 171.85, 137.11, 136.31, 70.16, 56.14, 45.14, 43.71, 41.75, 37.96, 30.94, 29.58. Both ^1H and ^{13}C NMR spectra matched literature values.

Compound V



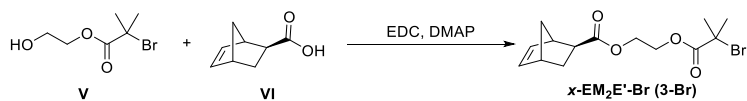
A flame-dried, two-neck round-bottom flask equipped with a stir bar, septum, and adapter for N_2 was charged with ethylene glycol (9.05 mL, 162 mmol), NEt_3 (2.37 mL, 17.0 mmol), and dry tetrahydrofuran (100 mL). The flask was placed in an ice bath. Once cooled, α -bromoisobutyryl bromide (2.00 mL, 16.2 mmol) was added dropwise under N_2 atmosphere. The reaction mixture was stirred overnight, allowing the ice to melt and the contents of the flask to warm to rt.

Reaction progress was monitored by TLC (CH₂Cl₂, visualization by I₂) until α-bromoisobutyryl bromide was completely consumed. Once complete, the reaction mixture was filtered, and the filtrate was concentrated by rotary evaporation. The crude product was purified by automated flash chromatography on silica with 5% methanol in CH₂Cl₂ as the mobile phase. Pure compound **V** was obtained as a colorless oil (2.8 g, 83% yield). ¹H NMR (CDCl₃): δ 4.33–4.27 (m, 2H), 3.89–3.84 (m, 2H), 2.12 (s, 1H), 1.94 (s, 6H). ¹³C NMR (CDCl₃): δ 172.06, 67.56, 61.03, 55.93, 30.85. Both ¹H and ¹³C NMR spectra matched literature values.⁵

***Exo*-5-norbornene-2-carboxylic acid (VI)**

Compound **VI**, *exo*-5-norbornene-2-carboxylic acid, was prepared according to a previously reported procedure.⁶ ¹H NMR (CDCl₃): δ 6.13 (m, 2H), 3.11 (s, 1H), 2.94 (s, 1H), 2.27 (m, 1H), 1.95 (m, 1H), 1.54 (d, *J* = 8 Hz, 1H), 1.41 (m, 2H). ¹³C NMR (CDCl₃): δ 182.77, 138.28, 135.85, 46.84, 46.54, 43.26, 41.81, 30.47. Both ¹H and ¹³C NMR spectra matched literature values.

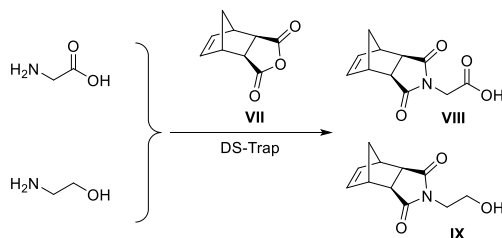
Synthesis of compound *x*-EM₂E'-Br (3-Br)



Compound **VI** (0.60 g, 4.34 mmol) and EDC (0.876 g, 5.65 mmol) were dissolved in CH₂Cl₂ (25 mL) in a round-bottom flask equipped with a stir bar. The reaction mixture was stirred until the solids had completely dissolved (~5 min). Meanwhile, a second flask was charged with compound **V** (1.10 g, 5.21 mmol), DMAP (0.265 g, 2.17 mmol) and CH₂Cl₂ (25 mL). This second solution was added dropwise to the flask containing compound **VI** via an addition funnel while stirring. The reaction mixture was stirred at rt, and reaction progress was monitored by

TLC (CH₂Cl₂, visualization by a potassium permanganate stain), around 12 h. The reaction mixture was then transferred to a separatory funnel, washed with water (2 x 20 mL) and brine (20 mL), dried over Na₂SO₄, and concentrated by rotary evaporation. The concentrated crude product was purified by automated flash chromatography on silica with 2.5% ethyl acetate in hexanes to give the pure product as a colorless oil (3.7 g, 72% yield). ¹H NMR (CDCl₃): δ 6.16–6.08 (m, 2H), 4.42–4.31 (m, 4H), 3.05 (m, 1H), 2.96–2.89 (m, 1H), 2.29 – 2.19 (m, 1H), 1.93 (m, 7H), 1.53–1.48 (m, 1H), 1.41–1.34 (m, 2H). ¹³C NMR (CDCl₃): δ 176.1, 171.6, 138.3, 135.8, 63.9, 61.8, 55.5, 46.7, 46.5, 43.2, 41.8, 30.8, 30.48. HR-MS calculated for C₁₄H₁₉BrO₄ [M + Na]⁺ 353.0359; found 353.0383.

Synthesis of compounds *xx*-IMEM₂E'-Br (4-Br) and *xx*-IM₂E'-Br (5-Br)



Exo-Carbic anhydride (VII)

Compound VII, *exo*-norbornene anhydride (carbic anhydride) was prepared from *endo*-carbic anhydride according to a previously reported procedure.⁷ ¹H NMR (CDCl₃): δ 6.33 (t, *J* = 1.9 Hz, 2H), 3.26 (m, 2H), 3.06 (d, *J* = 1.6 Hz, 2H), 1.49 (m, 1H), 1.28 (m, 1H). ¹³C NMR (CDCl₃): δ 179.02, 137.83, 49.34, 45.22, 43.01. Both ¹H and ¹³C NMR spectra matched literature values.

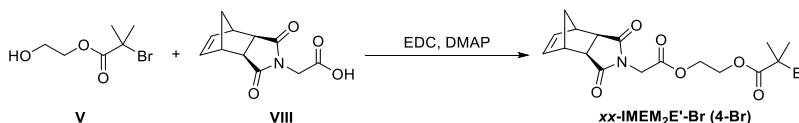
Compound VIII

Compound **VIII** was prepared according to a previously reported procedure.⁸ ¹H NMR (CDCl₃): δ 8.80 (s, 1H), 6.30 (t, *J* = 1.9 Hz, 2H), 4.26 (s, 2H), 3.30 (m, 2H), 2.76 (d, *J* = 1.4 Hz, 2H), 1.6–1.57 (m, 1H), 1.50 (m, 1H). ¹³C NMR (CDCl₃): δ 177.54, 172.28, 138.32, 48.37, 45.75, 43.18, 39.45. Both ¹H and ¹³C NMR spectra matched literature values.

Compound IX

Compound **IX** was prepared according to a previously reported procedure.⁹ ¹H NMR (CDCl₃): δ 6.27 (m, 2H), 3.74 (m, 2H), 3.67 (m, 2H), 3.25 (s, 2H), 2.69 (s, 2H), 2.45 (s, 1H), 1.49 (m, 1H), 1.33 (m, 1H). ¹³C NMR (CDCl₃): δ 178.71, 137.76, 59.85, 47.84, 45.26, 42.79, 41.21. Both ¹H and ¹³C NMR spectra matched literature values.

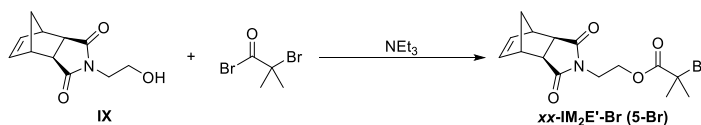
Compound *xx*-IMEM₂E'-Br (4-Br)



Compound **VIII** (1.00 g, 4.52 mmol) and EDC (0.737 g, 4.75 mmol) were dissolved in CH₂Cl₂ (10 mL) in a round-bottom flask equipped with a stir bar. The reaction mixture was stirred until the solids had completely dissolved (5 min). Meanwhile, a second flask was charged with compound **V** (1.14 g, 5.42 mmol), DMAP (0.276 g, 2.26 mmol) and CH₂Cl₂ (10 mL). This second solution was added dropwise to the flask containing compound **VIII** via an addition funnel while stirring. The reaction mixture was stirred at rt and monitored by TLC (CH₂Cl₂, visualization by a potassium permanganate stain), around 12 h. The reaction mixture was then

transferred to a separatory funnel, washed with water (2 x 20 mL) and brine (20 mL), dried over Na₂SO₄, and concentrated by rotary evaporation. The concentrated crude product was purified by automated flash chromatography on silica with 2.5% ethyl acetate in hexanes as the mobile phase to give the pure product as a colorless oil (0.92 g, 55% yield). ¹H NMR (CDCl₃): δ 6.33–6.28 (m, 2H), 4.44–4.35 (m, 4H), 4.26 (s, 2H), 3.34–3.29 (m, 2H), 2.76 (d, J = 1.4 Hz, 2H), 1.94 (s, 6H), 1.68 (m, 1H), 1.53 (m, 1H). ¹³C NMR (CDCl₃): δ 177.21, 171.60, 166.93, 138.13, 63.27, 63.19, 55.45, 48.18, 45.58, 42.99, 39.42, 30.76. HR-MS calculated for C₁₇H₂₀BrNO₆ [M + H]⁺ 414.0547; found 414.0554.

Compound *xx-IM₂E'*-Br (5-Br)



Compound *xx-IM₂E'*-Br (5-Br)

A flame-dried, two-neck round-bottom flask equipped with a septum, stir bar, and an adapter for N₂ was charged with compound **IX** (1.00 g, 4.83 mmol), NEt₃ (1.01 mL, 7.23 mmol), and dry tetrahydrofuran (30 mL). The flask was placed in an ice bath. Once cool, α -bromoisobutyryl bromide (0.775 mL, 6.27 mmol) was added dropwise via syringe under N₂ atmosphere. The reaction mixture was stirred overnight, allowing the ice to melt and the contents of the flask to warm to rt. Reaction progress was monitored by TLC (CH₂Cl₂, visualization by a potassium permanganate stain) until compound **IX** was consumed. The reaction mixture was then filtered, the filtrate was concentrated by rotary evaporation, and then the crude product was purified by automated flash chromatography on silica with a hexanes/CH₂Cl₂ gradient as the mobile phase.

The product was obtained as a white solid (1.2 g, 70% yield). ^1H NMR (CDCl_3): δ 6.29 (m, 2H), 4.35–4.29 (m, 2H), 3.81 (m, 2H) 3.28 (m, 2H), 2.70 (m, 2H), 1.89 (s, 6H), 1.52 (m, 1H), 1.32 (m, 1H). ^{13}C NMR (CDCl_3): δ 177.84, 171.51, 137.95, 62.71, 55.60, 47.99, 45.34, 43.06, 37.48, 30.75. Both ^1H and ^{13}C NMR spectra matched literature values.¹⁰

Synthesis of polystyrene macromonomers (MMs)

A typical styrene polymerization procedure is as follows: Initiator $x\text{-ME}'\text{-Br}$ (**2-Br**) (0.082 g, 0.30 mmol), styrene (9.3 mL, 81 mmol), CuBr (22 mg, 0.15 mmol), and CuBr₂ (34 mg, 0.15 mmol) were added to a 100 mL Schlenk tube equipped with a stir bar. The mixture in the Schlenk tube was deoxygenated by three freeze-pump-thaw cycles and then backfilled with N₂. The reaction mixture was submerged in an oil bath at 90 °C and after ~10 min, N,N,N',N'',N'' -pentamethyldiethylenetriamine (PMDETA) (0.063 mL, 0.30 mmol) was injected under N₂ flow. The reaction mixture was heated in an oil bath maintained at 90 °C for about 3 h. An aliquot was removed via an N₂-purged syringe and analyzed via ^1H NMR spectroscopy to ensure that ~10% monomer conversion had been reached. At this point, the reaction was terminated by exposing the contents of the Schlenk tube to air. The reaction mixture was diluted with ethyl acetate (50 mL) and washed with water (3 x 20 mL) in a separatory funnel, and then the ethyl acetate layer was concentrated by rotary evaporation. The crude product was loaded onto a column by either dry loading onto silica or liquid loading using a small amount of CH₂Cl₂. The crude product was then purified by automated flash chromatography on silica with a gradient of 0% to 40 % ethyl acetate in hexanes as the mobile phase, similar to previous descriptions of this procedure (Figures S15–S19).¹¹ The MM-containing fractions were concentrated by rotary evaporation, and then the product was purified further via passage through a short column of basic alumina using

tetrahydrofuran as the mobile phase. The resulting MM solution was then concentrated by rotary evaporation, redissolved in a small volume of tetrahydrofuran, and then precipitated once into methanol. After precipitation, the polymer was recovered via filtration and then dried under vacuum overnight to yield a white solid. The molar ratios of reagents for the ATRP reaction were [styrene]/[Initiator]/[CuBr]/[CuBr₂]/[PMDETA] 270:1:0.5:0.5:1 when targeting 3 kg/mol.

SEC kinetic experiments on polystyrene MMs

A representative synthesis is as follows: MM *x*-ME'-PS (**2**) (25 mg, 100 equiv) was dissolved in CDCl₃ (0.317 mL) in a vial equipped with a stir bar. A stock solution of **G3** in CDCl₃ at a concentration of 0.61 mg/mL was prepared, and 100 μL of this solution (to achieve 0.061 mg of **G3**, 1 equiv) was then added rapidly to the first vial to make the final concentration of MM = 20 mM. Aliquots (45 μL) were withdrawn periodically via micropipette at predetermined timepoints and added to 1.5 mL Eppendorf microcentrifuge tubes containing 0.1 mL CDCl₃ and ethyl vinyl ether (2 μL) to terminate the polymerizations. Polymerizations were conducted under air with capping of vials in between aliquots to minimize solvent evaporation. Each aliquot was then analyzed by SEC after evaporation of CDCl₃ by blowing air over the aliquots for about 15 min (Figures S30–S39). This procedure was also used to determine the kinetics when targeting an $N_{bb} = 20$ by adjusting the MM equiv to 20, used in the synthesis of bottlebrush pentablock copolymers from MM *x*-ME'-PS (**2**) and MM *xx*-IM₂E'-PS (**5**) (Figures S45–S48).

ROMP of polystyrene MMs targeting various N_{bb} values

A representative synthesis is as follows: MM *x*-ME'-PS (**2**) (10.0 mg, 100 equiv) was dissolved in CDCl₃ (0.157 mL) in a vial equipped with a stir bar. A stock solution of **G3** in CDCl₃ at a

concentration of 2.42 mg/mL was prepared, and 10 μ L of this solution (to achieve 0.0242 mg of G3, 1 equiv) was then added rapidly to the first vial to make the final concentration of MM = 20 mM. Polymerizations were conducted under air in capped vials after catalyst addition and then terminated with excess ethyl vinyl ether after 24 h. Each polymerization was then analyzed by SEC after evaporation of CDCl_3 by blowing air over the aliquots for about 15 min (Figures S40–S44). This procedure was used to target N_{bb} values of 100–2000 by reducing the amount of catalyst added to target the desired N_{bb} value.

Bottlebrush pentablock copolymer synthesis

A representative synthesis is as follows: MM *x*-ME'-PS (**2**) (5 mg, 20 equiv) was weighed out five times in separate vials. One vial containing MM was equipped with a stir bar and dissolved in CDCl_3 (73.4 μ L). The other four vials containing MM were dissolved in CDCl_3 (83.4 μ L per vial). A stock solution of **G3** in CDCl_3 at a concentration of 6.10 mg/mL was prepared, and 10 μ L of this solution (to achieve 0.0606 mg of G3, 1 equiv) was then added rapidly to the first vial containing a stir bar. The reaction mixture was stirred for a predetermined amount of time [10 min for MM *x*-ME'-PS (**2**)] at which point an aliquot (17 μ L) was withdrawn via micropipette and added to an SEC vial containing excess ethyl vinyl ether to terminate the polymerization. Immediately following aliquot removal, another injection of a MM solution (vial 2) was added rapidly to the stirring polymerization. This second injection of MM was allowed to polymerize for the same amount of time as the first before the removal of an aliquot and the third injection of the MM solution. The procedure continued until all MM solutions were added to the reaction mixture and the final aliquot was removed. Polymerizations were conducted under air with capping of vials in between aliquot removals and injections to minimize solvent evaporation.

Each aliquot was then analyzed by SEC after evaporation of CDCl_3 by blowing air over the aliquots for about 15 min (Figure 5). This procedure was also used for the synthesis of bottlebrush pentablock copolymers from MM $\alpha\alpha$ - $\text{IM}_2\text{E}'$ -PS (**5**) allowing for 90 min between each aliquot and monomer addition.

Characterization of ATRP Initiators and Precursors:

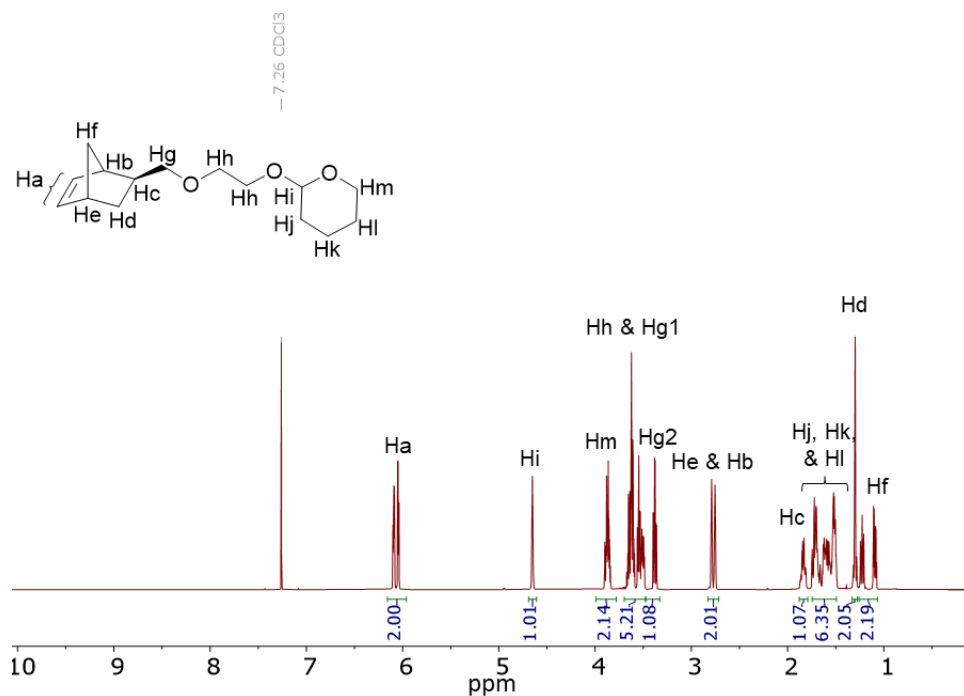


Figure S1. ^1H NMR spectrum of compound **III**.

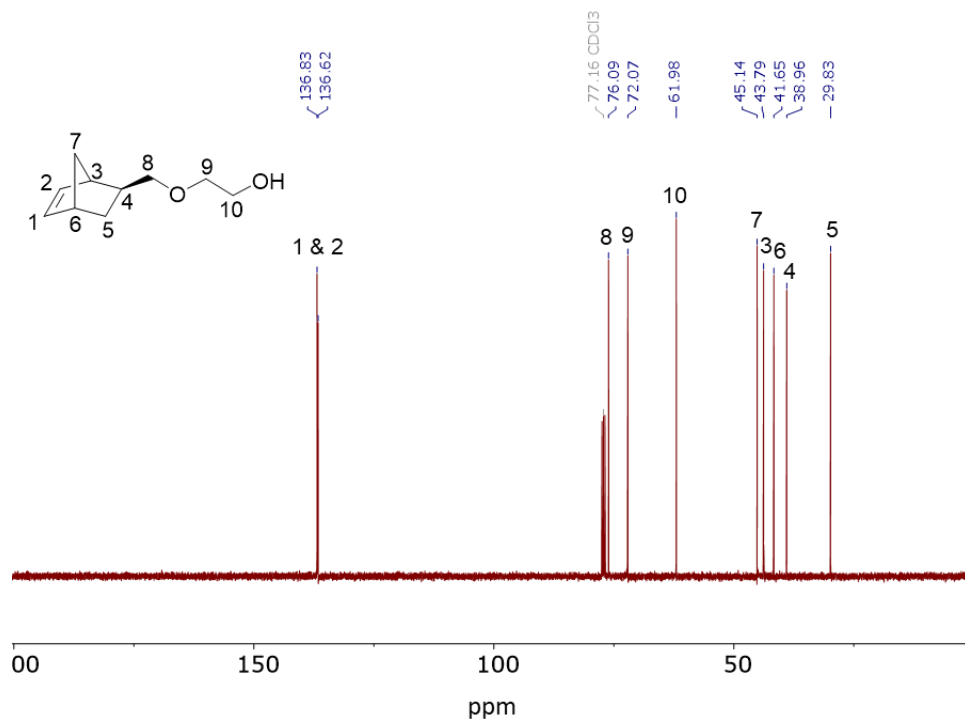


Figure S4. ^{13}C NMR spectrum of compound **IV**.

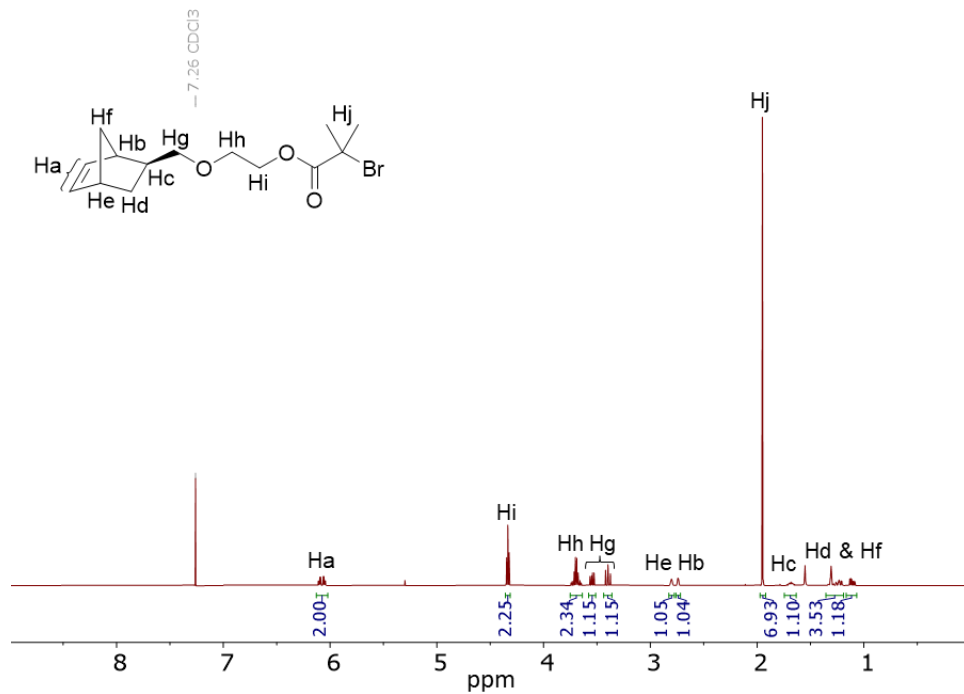


Figure S5. ^1H NMR spectrum of compound *x*-MOM₂E'-Br (**1-Br**).

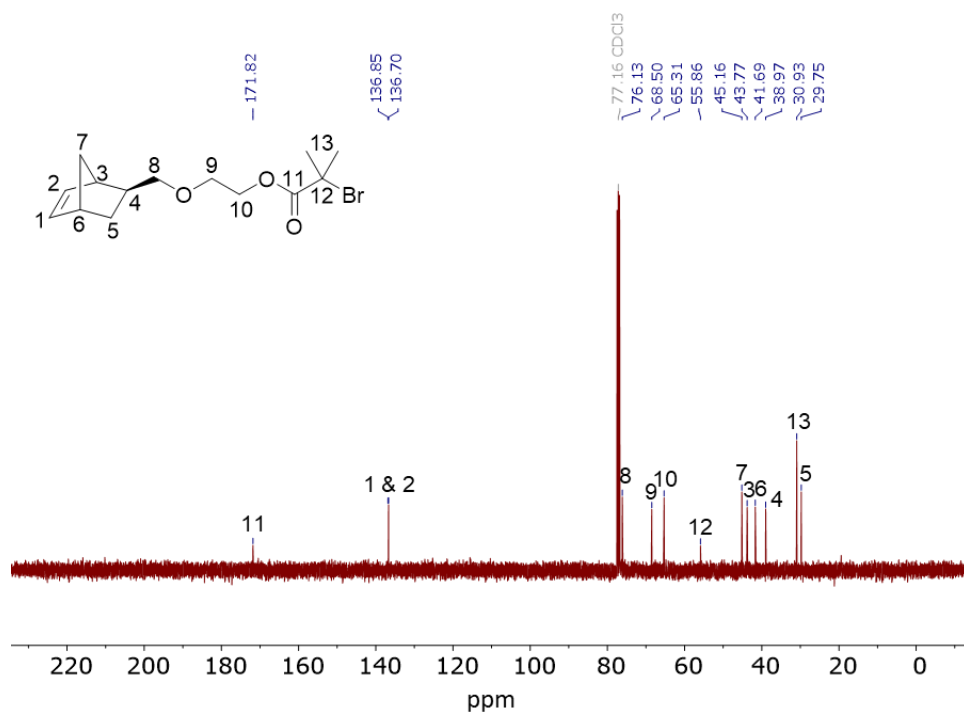


Figure S6. ¹³C NMR spectrum of compound *x*-MOM₂E'-Br (**1-Br**).

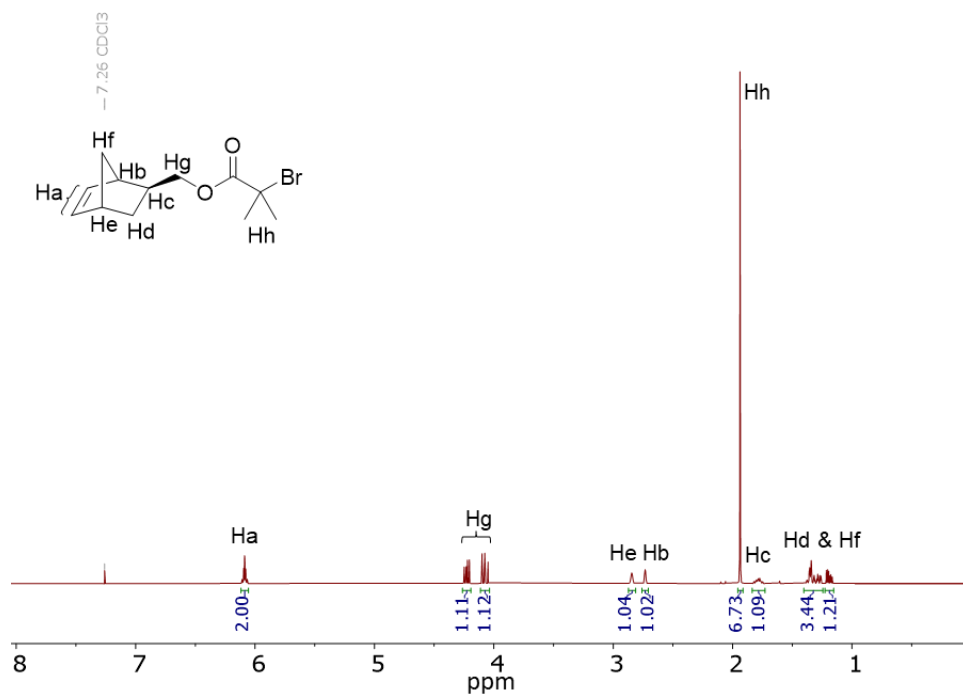


Figure S7. ¹H NMR spectrum of compound *x*-ME'-Br (**2-Br**).

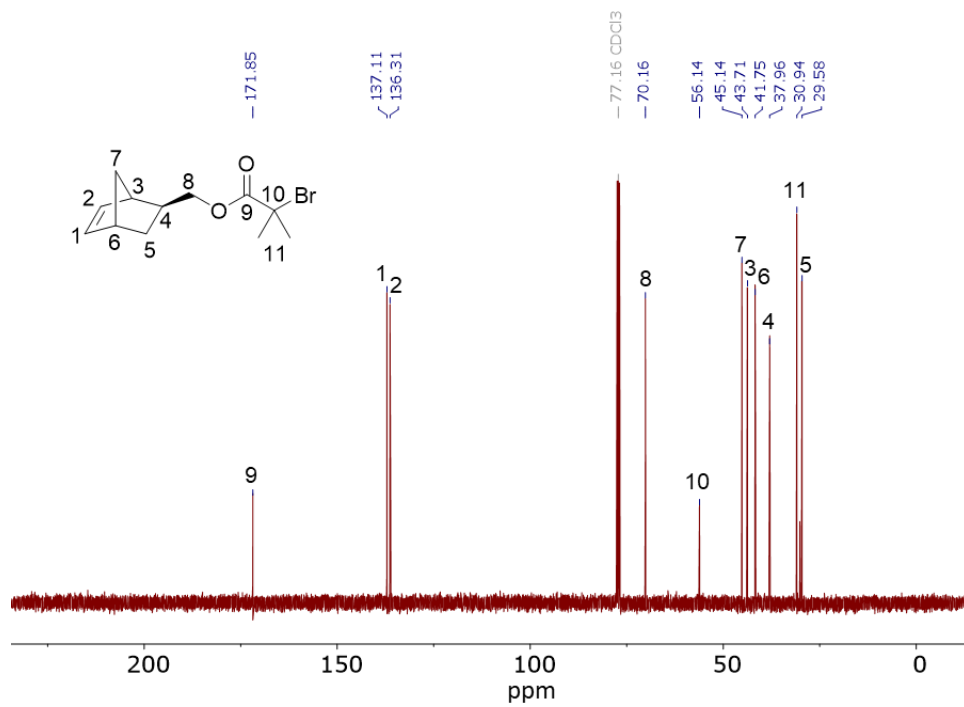


Figure S8. ¹³C NMR spectrum of compound *x*-ME'-Br (**2-Br**).

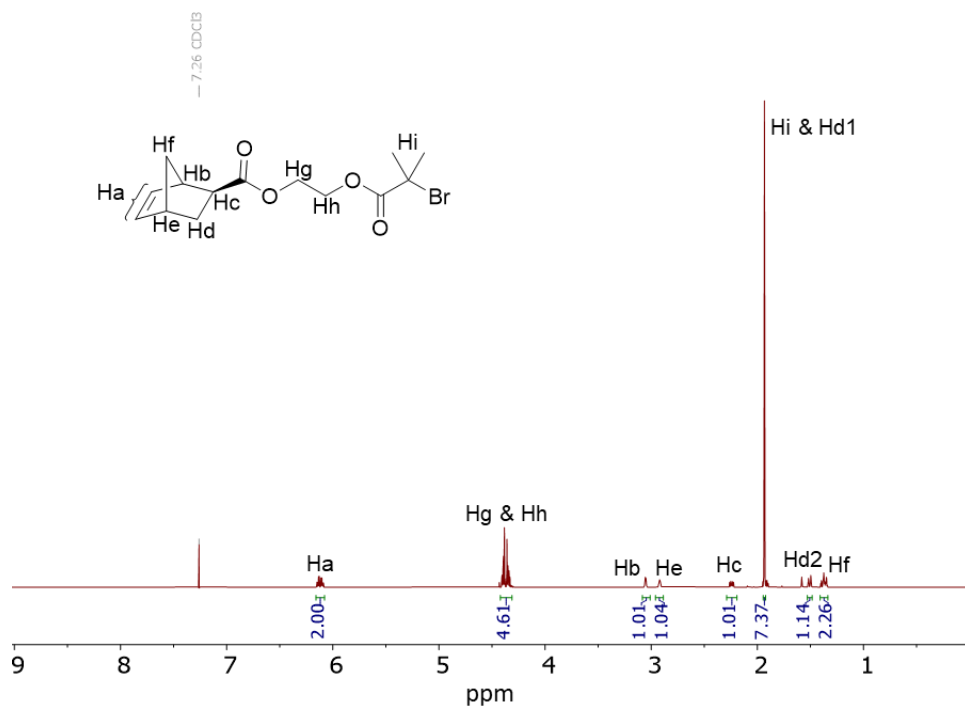


Figure S9. ¹H NMR spectrum of compound *x*-EM₂E'-Br (**3-Br**).

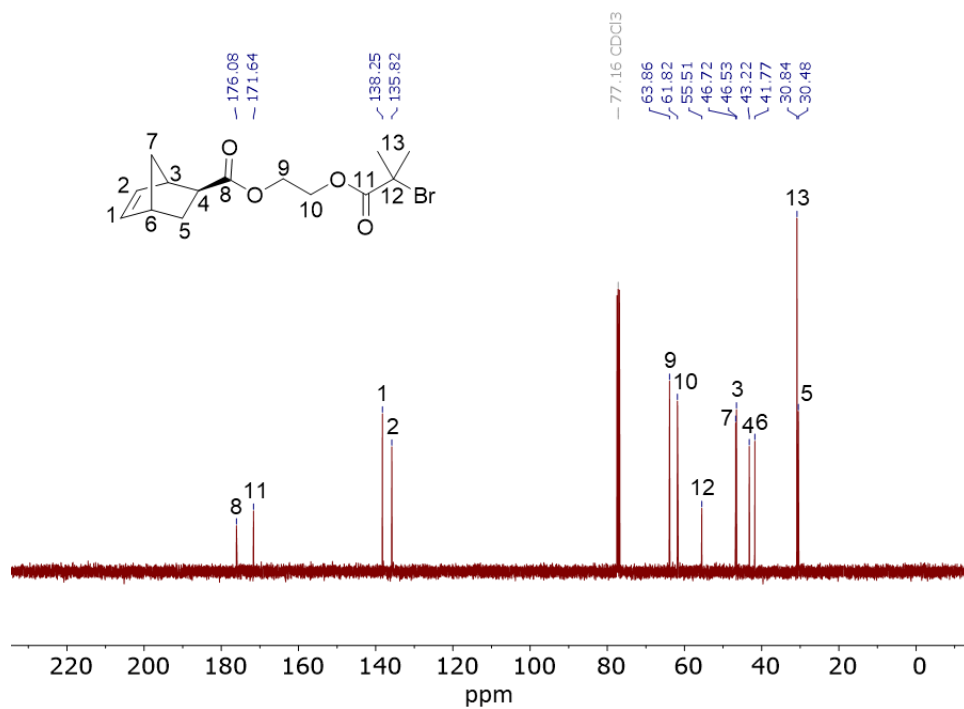


Figure S10. ¹³C NMR spectrum of compound *x*-EM₂E'-Br (**3-Br**).

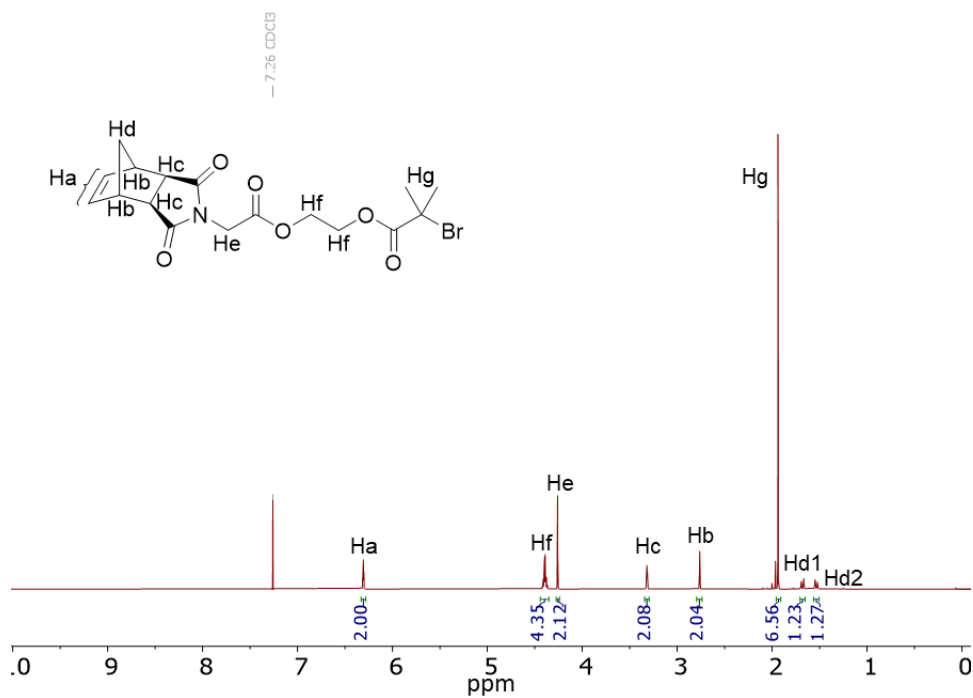


Figure S11. ¹H NMR spectrum of compound *xx*-IMEM₂E'-Br (**4-Br**).

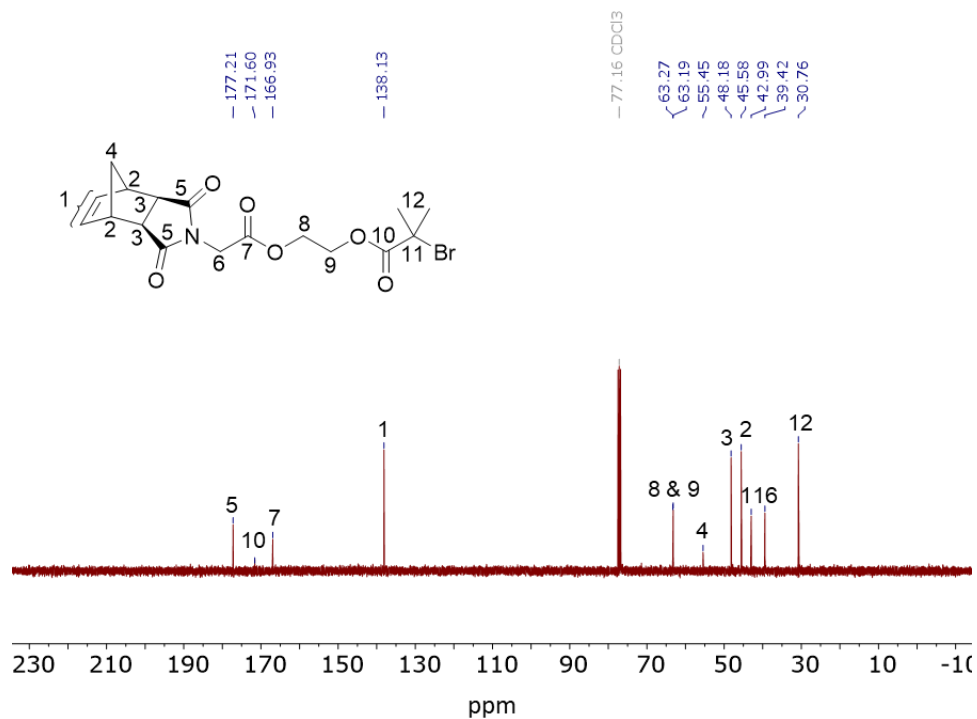


Figure S12. ¹³C NMR spectrum of compound *xx*-IMEM₂E'-Br (**4-Br**).

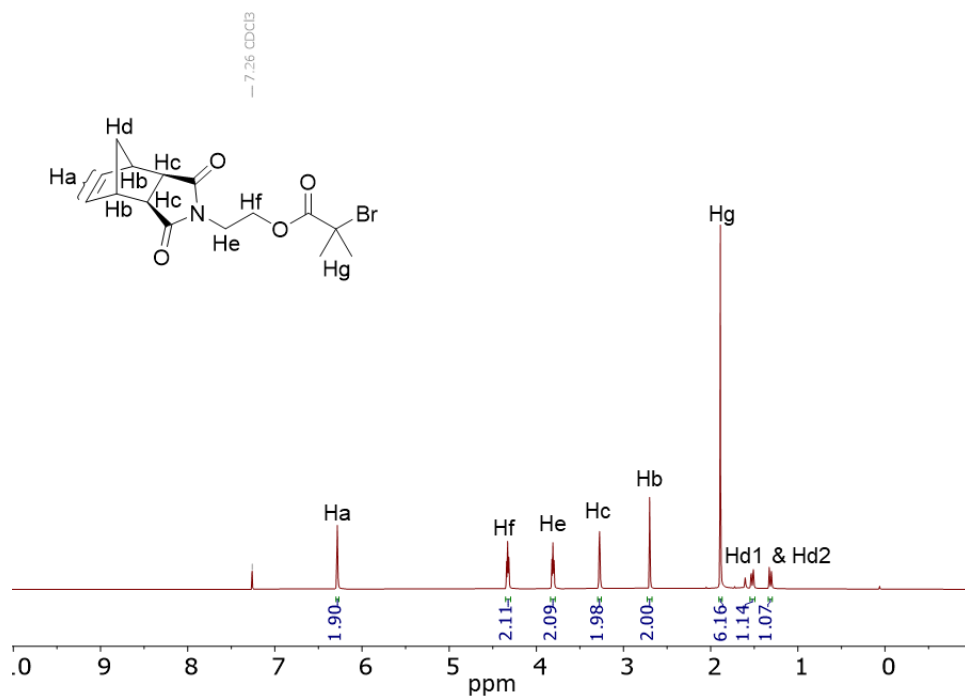


Figure S13. ¹H NMR spectrum of compound *xx*-IM₂E'-Br (**5-Br**).

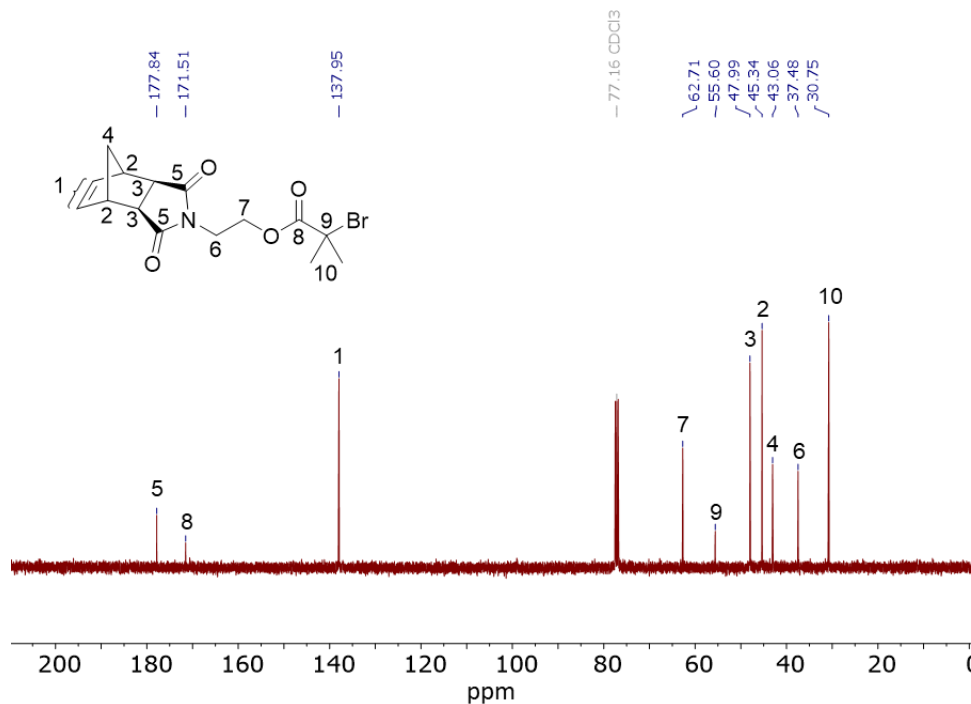


Figure S14. ^{13}C NMR spectrum of compound $xx\text{-IM}_2\text{E}'\text{-Br}$ (5-Br).

Biotage purification of MMs

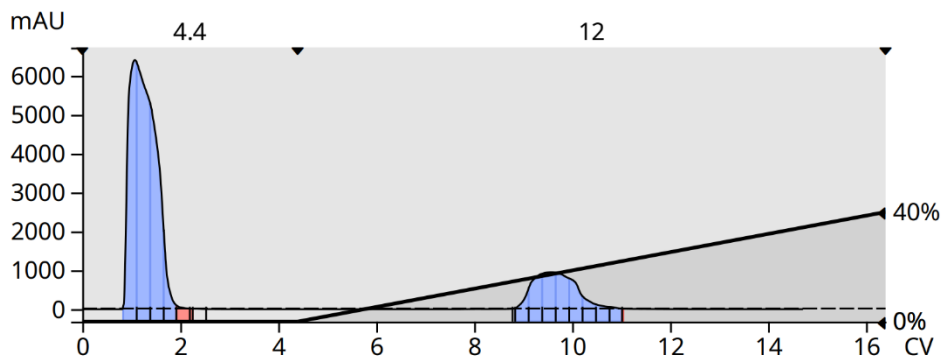


Figure S15. UV-vis trace (complete UV-vis range) of MM $x\text{-MOM}_2\text{E}'\text{-PS}$ (1) from purification via automated column chromatography. The black line indicates the solvent gradient from 0% ethyl acetate to 40% ethyl acetate in hexanes. The first peak eluting at 0% ethyl acetate in hexanes is excess styrene and the second peak eluting at about 18% ethyl acetate in hexanes is the desired MM $x\text{-MOM}_2\text{E}'\text{-PS}$ (1) peak.

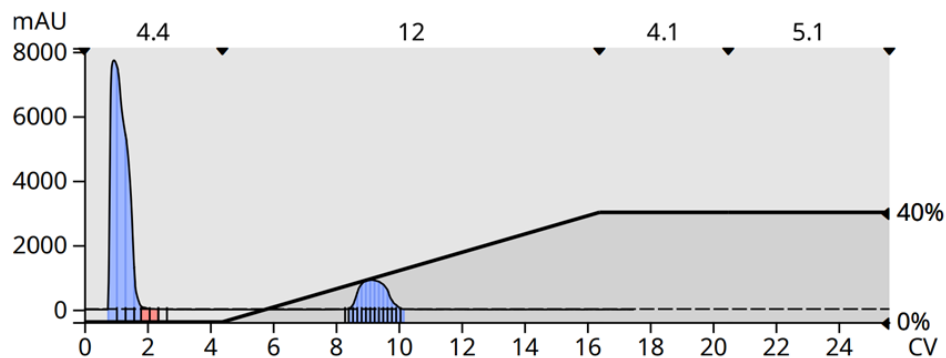


Figure S16. UV-vis trace (complete UV-vis range) of MM x -ME'-PS (**2**) from purification via automated column chromatography. The black line indicates the solvent gradient from 0% ethyl acetate to 40% ethyl acetate in hexanes. The first peak eluting at 0% ethyl acetate in hexanes is excess styrene and the second peak eluting at about 18% ethyl acetate in hexanes is the desired MM x -ME'-PS (**2**) peak.

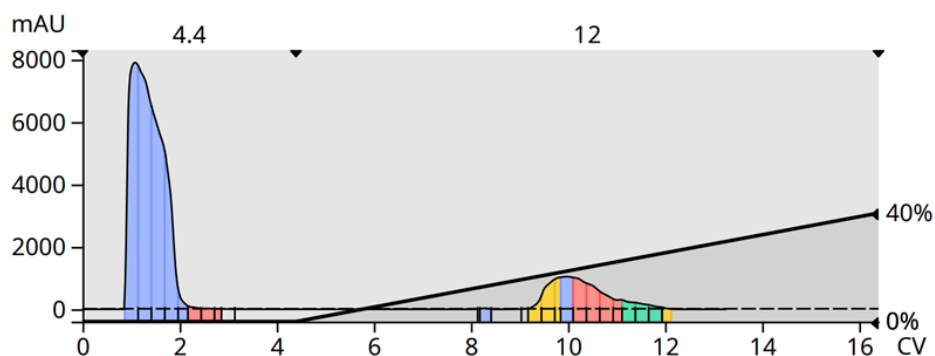


Figure S17. UV-vis trace (complete UV-vis range) of MM x -EM₂E'-PS (**3**) from purification via automated column chromatography. The black line indicates the solvent gradient from 0% ethyl acetate to 40% ethyl acetate in hexanes. The first peak eluting at 0% ethyl acetate in hexanes is excess styrene and the second peak eluting at about 18% ethyl acetate in hexanes is the desired MM x -EM₂E'-PS (**3**) peak.

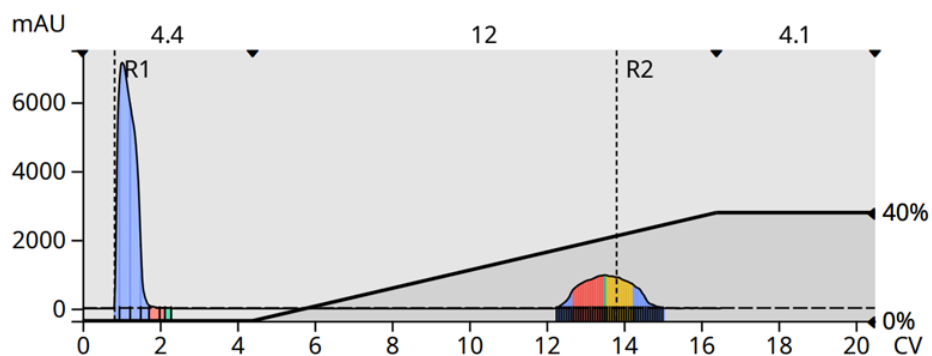


Figure S18. UV-vis trace (complete UV-vis range) of MM xx -IMEM₂E'-PS (**4**) from purification via automated column chromatography. The black line indicates the solvent gradient

from 0% ethyl acetate to 40% ethyl acetate in hexanes. The first peak eluting at 0% ethyl acetate in hexanes is excess styrene and the second peak eluting at about 30% ethyl acetate in hexanes is the desired MM *xx*-IMEM₂E'-PS (**4**) peak.

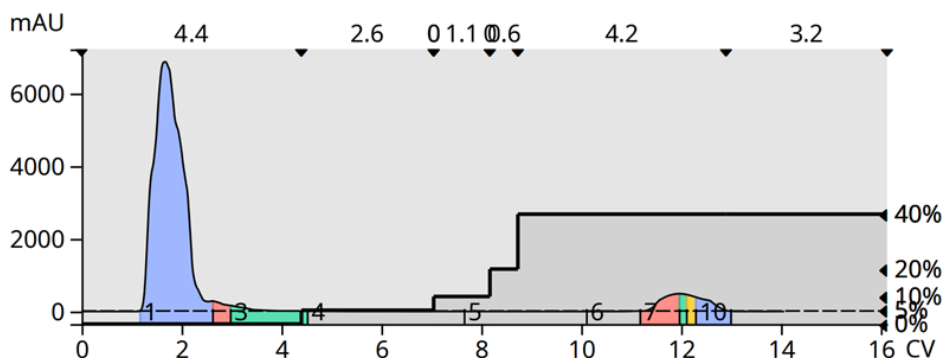


Figure S19. UV-vis trace (complete UV-vis range) of MM *xx*-IM₂E'-PS (**5**) from purification via automated column chromatography. The black line indicates the solvent gradient from 0% ethyl acetate to 40% ethyl acetate in hexanes. The first peak eluting at 0% ethyl acetate in hexanes is excess styrene and the second peak eluting at about 40% ethyl acetate in hexanes is the desired MM *xx*-IM₂E'-PS (**5**) peak.

¹H NMR and SEC Analysis of MMs

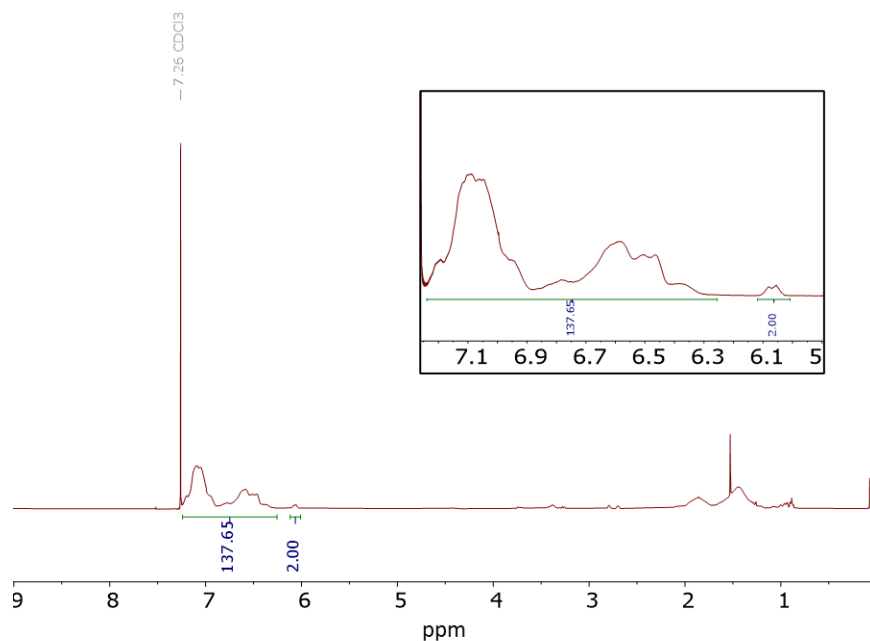


Figure S20. ¹H NMR spectrum of MM *x*-MOM₂E'-PS (**1**).

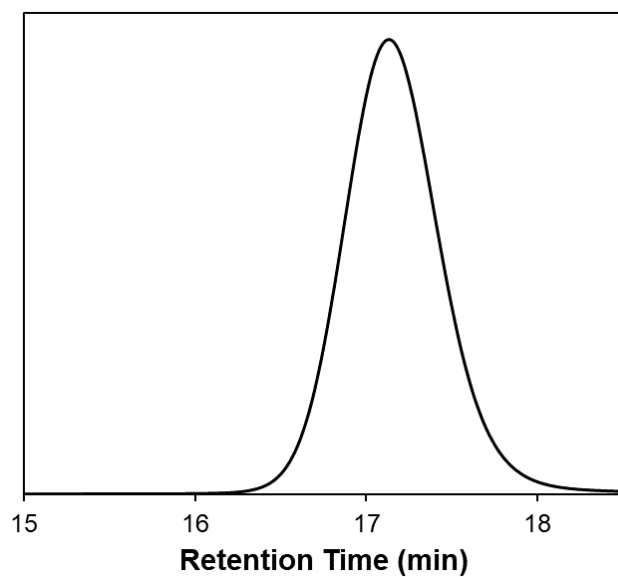


Figure S21. SEC trace (dRI signal) of MM x -MOM₂E'-PS (**1**).

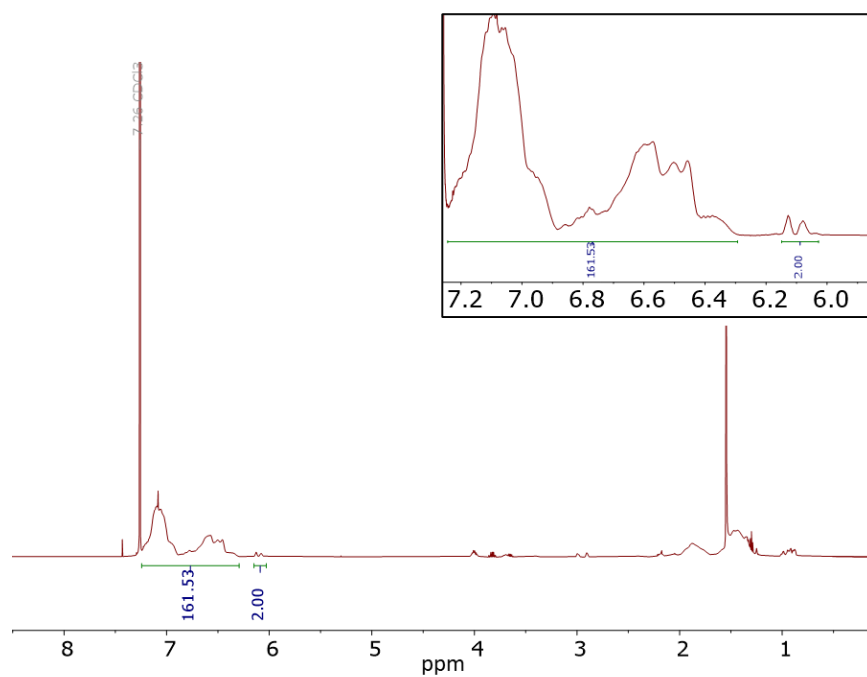


Figure S22. ¹H NMR spectrum of MM x -ME'-PS (**2**).

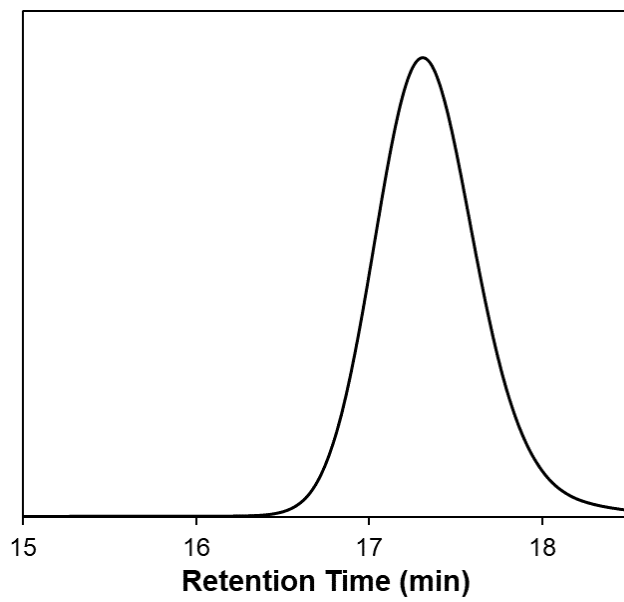


Figure S23. SEC trace (dRI signal) of MM x -ME'-PS (2).

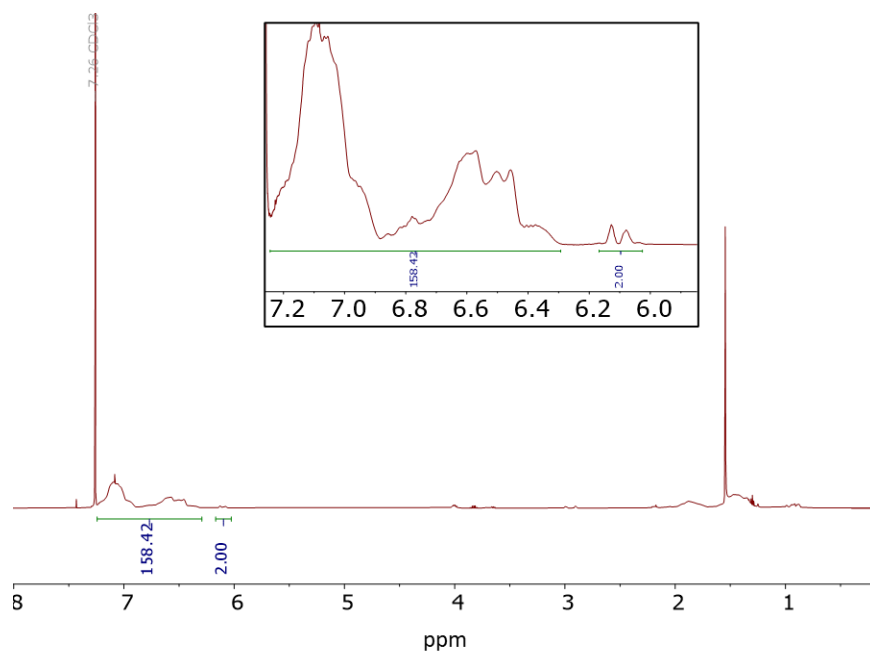


Figure S24. ^1H NMR spectrum of MM x -EM₂E'-PS (3).

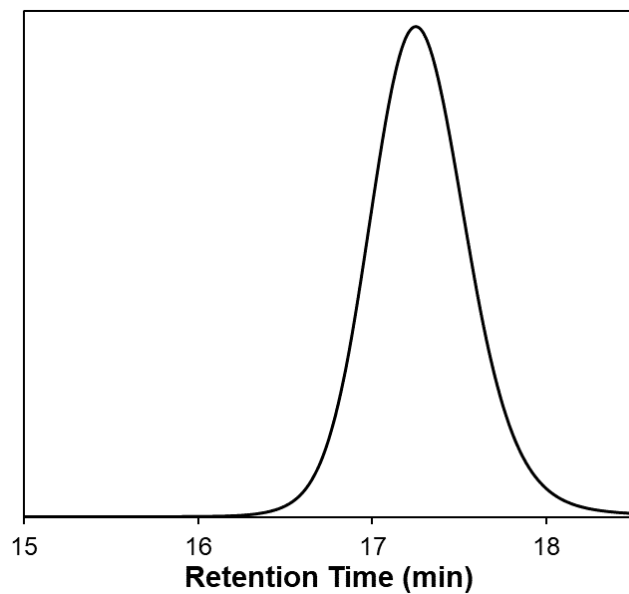


Figure S25. SEC trace (dRI signal) of MM x -EM₂E'-PS (3).

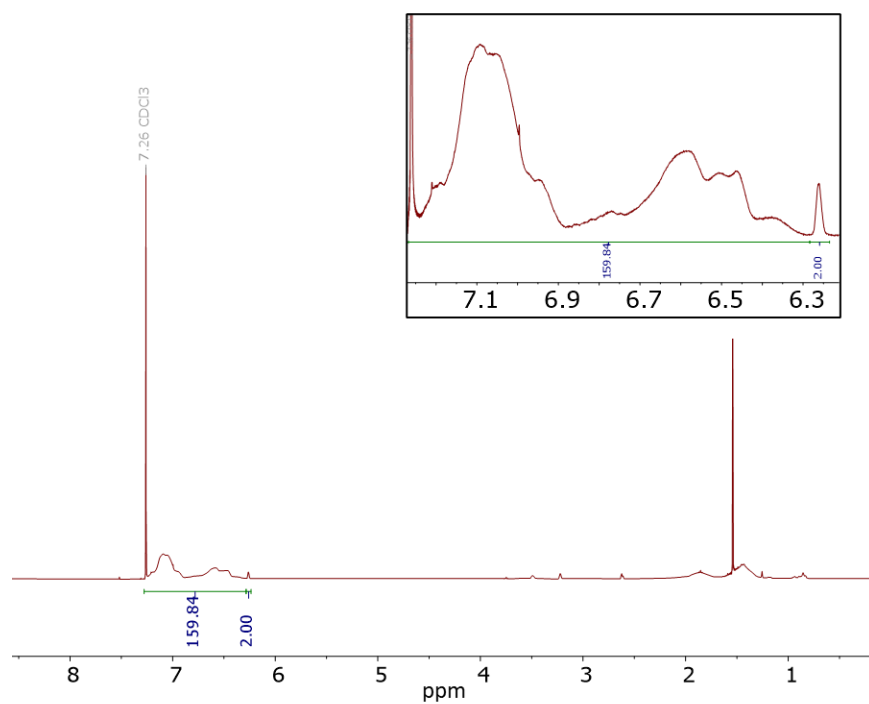


Figure S26. ¹H NMR spectrum of MM xx -IMEM₂E'-PS (4).

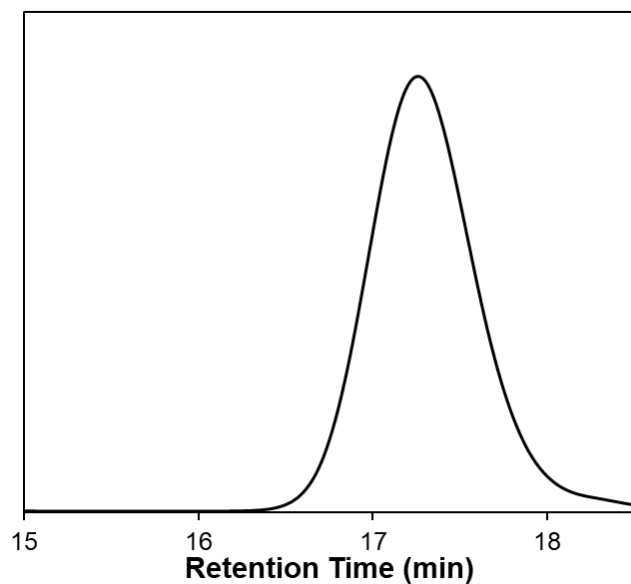


Figure S27. SEC trace (dRI signal) of MM *xx*-IMEM₂E'-PS (**4**).

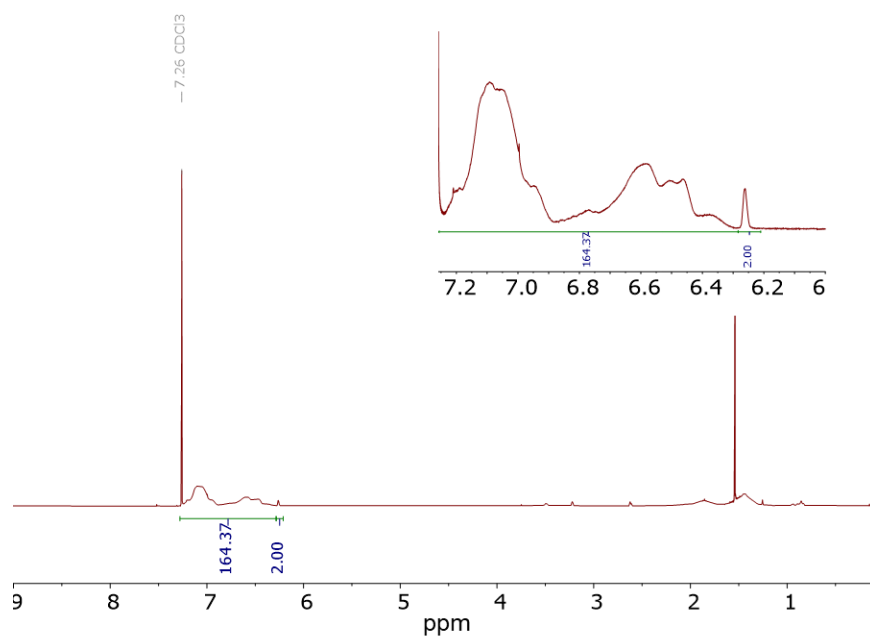


Figure S28. ¹H NMR spectrum of MM *xx*-IM₂E'-PS (**5**).

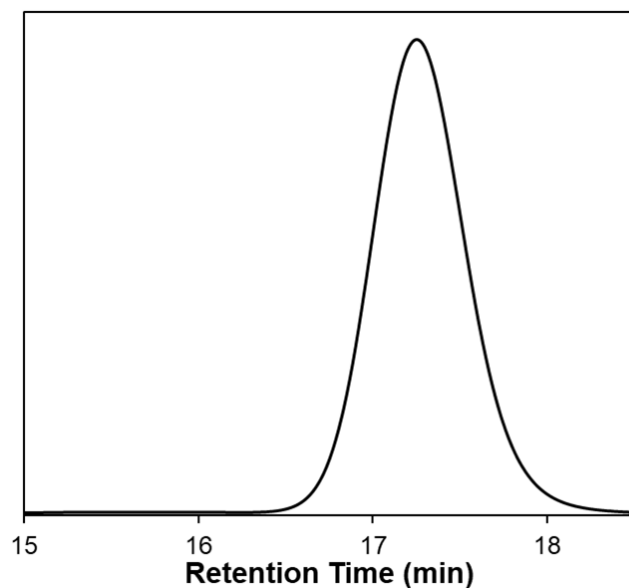


Figure S29. SEC trace (dRI signal) of MM x -IM₂E'-PS (**5**).

Kinetic Analysis of MMs

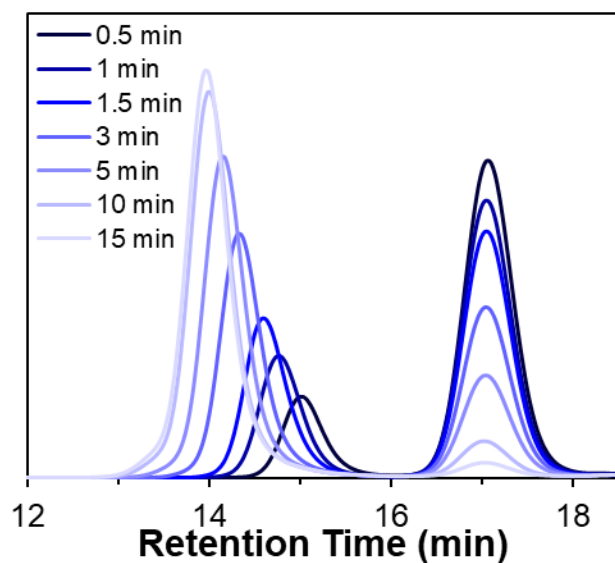


Figure S30. Representative SEC traces (dRI signal) of the ROMP of MM x -MOM₂E'-PS (**1**) at an [MM]/[G3] ratio of 100:1. As the polymerization proceeds, the MM signal at 17.2 min decreases in intensity and the bottlebrush polymer signal increases in intensity and shifts in retention time from 15.2 min to 14 min.

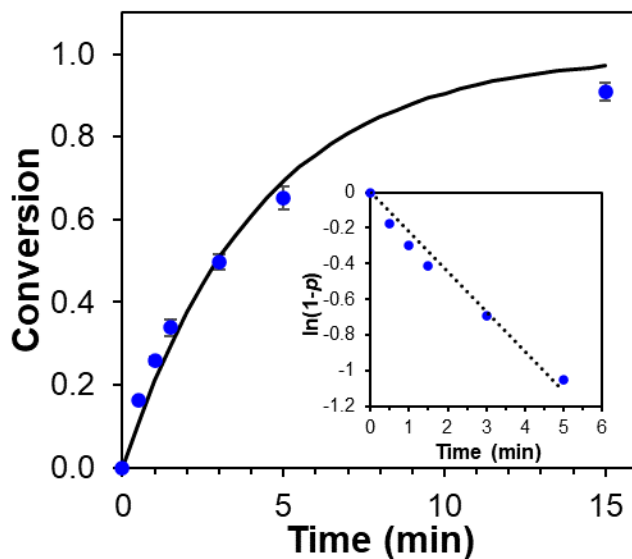


Figure S31. Kinetic analysis of the ROMP of MM *x*-MOM₂E'-PS (**1**) in CDCl₃ at a [MM]/[G3] ratio of 100:1 and [MM] = 20 mM. The solid line represents the fit to the averaged conversion data based on the equation $p = 1 - e^{(-k_{obs}t)}$ where p = fractional conversion.

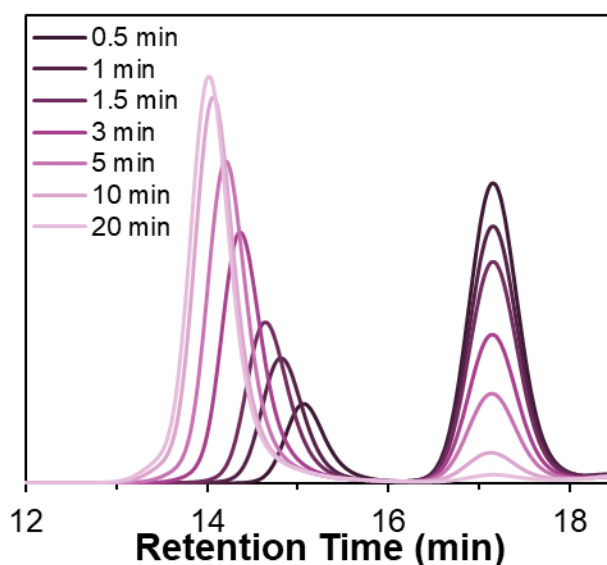


Figure S32. Representative SEC traces (dRI signal) of the ROMP of MM *x*-ME'-PS (**2**) at an [MM]/[G3] ratio of 100:1. As the polymerization proceeds, the MM signal at 17.2 min decreases in intensity and the bottlebrush polymer signal increases in intensity and shifts in retention time from 15.2 min to 14 min.

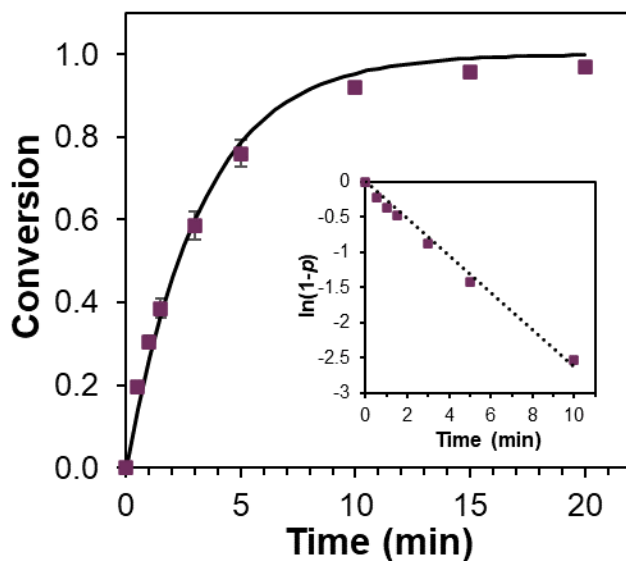


Figure S33. Kinetic analysis of the ROMP of MM x -ME'-PS (**2**) in CDCl_3 at a [MM]/[G3] ratio of 100:1 and [MM] = 20 mM. The solid line represents the fit to the averaged conversion data based on the equation $p = 1 - e^{-k_{obs}t}$ where p = fractional conversion.

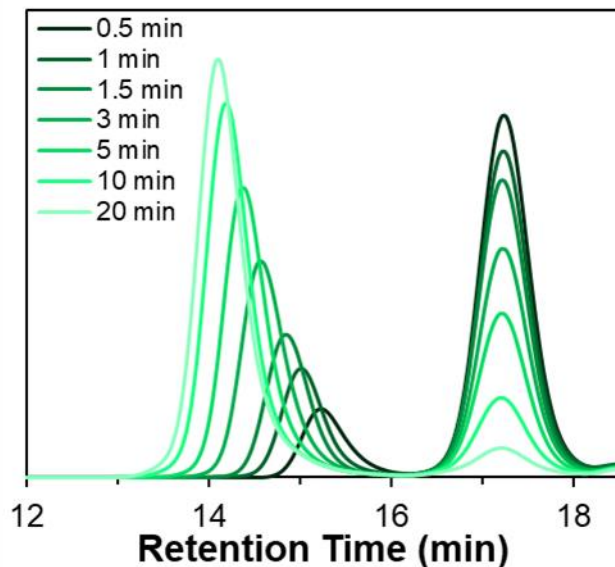


Figure S34. Representative SEC traces (dRI signal) of the ROMP of MM x -EM₂E'-PS (**3**) at an [MM]/[G3] ratio of 100:1. As the polymerization proceeds, the MM signal at 17.2 min decreases in intensity and the bottlebrush polymer signal increases in intensity and shifts in retention time from 15.2 min to 14 min.

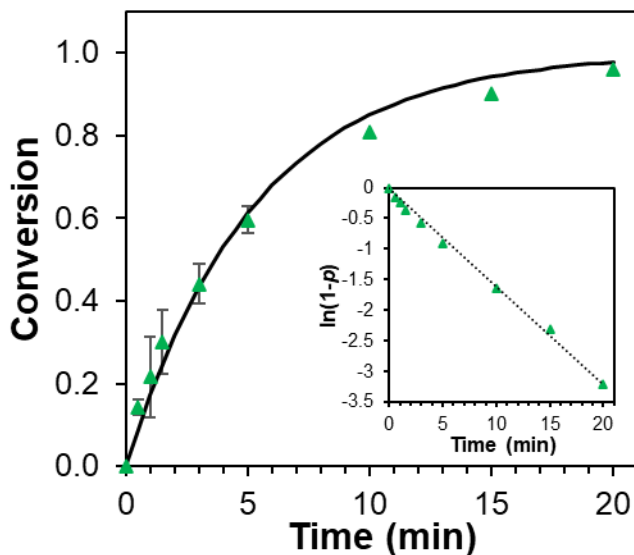


Figure S35. Kinetic analysis of the ROMP of MM x -EM₂E'-PS (**3**) in CDCl₃ at a [MM]/[G3] ratio of 100:1 and [MM] = 20 mM. The solid line represents the fit to the averaged conversion data based on the equation $p = 1 - e^{-k_{obs}t}$ where p = fractional conversion.

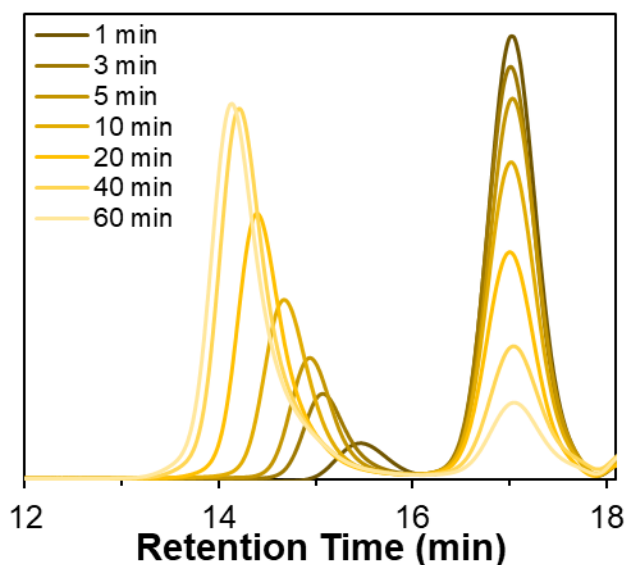


Figure S36. Representative SEC traces (dRI signal) of the ROMP of MM xx -IMEM₂E'-PS (**4**) at an [MM]/[G3] ratio of 100:1. As the polymerization proceeds, the MM signal at 17.2 min decreases in intensity and the bottlebrush polymer signal increases in intensity and shifts in retention time from 15.5 min to 14 min.

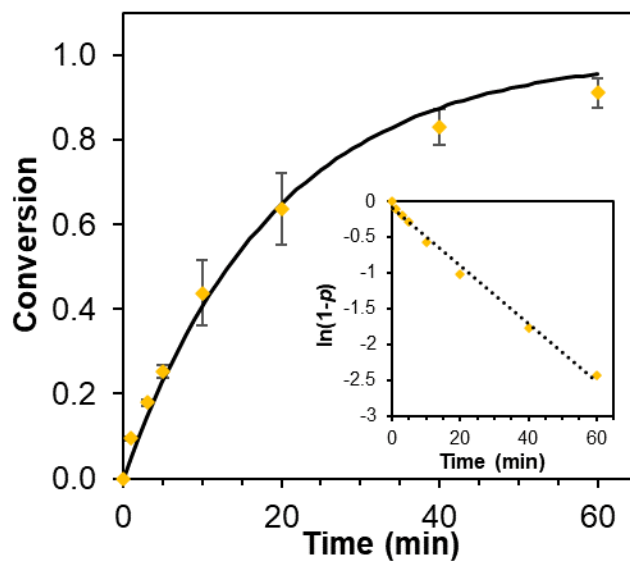


Figure S37. Kinetic analysis of the ROMP of MM xx -IMEM₂E'-PS (**4**) in CDCl₃ at a [MM]/[G3] ratio of 100:1 and [MM] = 20 mM. The solid line represents the fit to the averaged conversion data based on the equation $p = 1 - e^{-k_{obs}t}$ where p = fractional conversion.

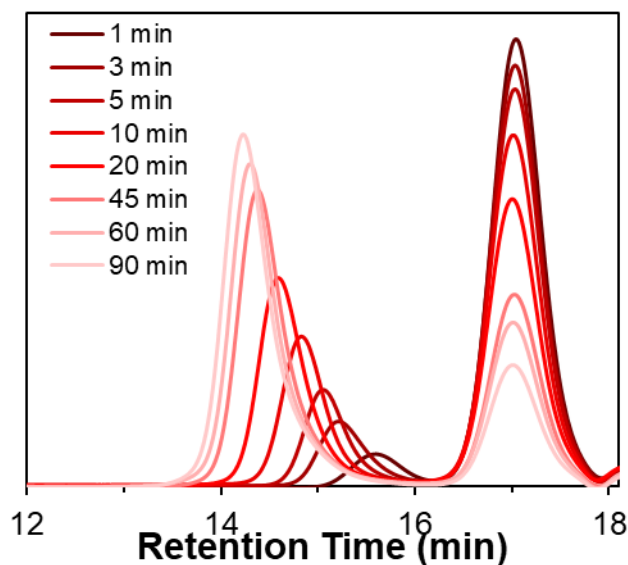


Figure S38. Representative SEC traces (dRI signal) of the ROMP of MM xx -IM₂E'-PS (**5**) at an [MM]/[G3] ratio of 100:1. As the polymerization proceeds, the MM signal at 17.2 min decreases in intensity and the bottlebrush polymer signal increases in intensity and shifts in retention time from 15.8 min to 14.2 min.

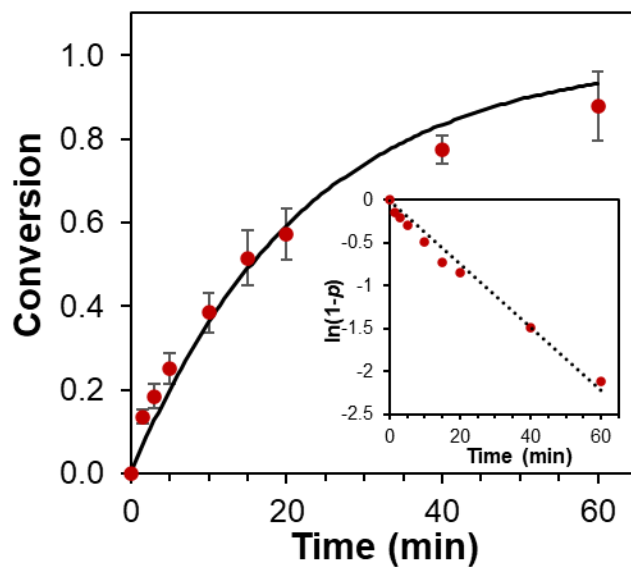


Figure S39. Kinetic analysis of the ROMP of MM *xx*-IM₂E²-PS (**5**) in CDCl₃ at a [MM]/[G3] ratio of 100:1 and [MM] = 20 mM. The solid line represents the fit to the averaged conversion data based on the equation $p = 1 - e^{(-k_{obs}t)}$ where p = fractional conversion.

HOMO/LUMO Energy Gap

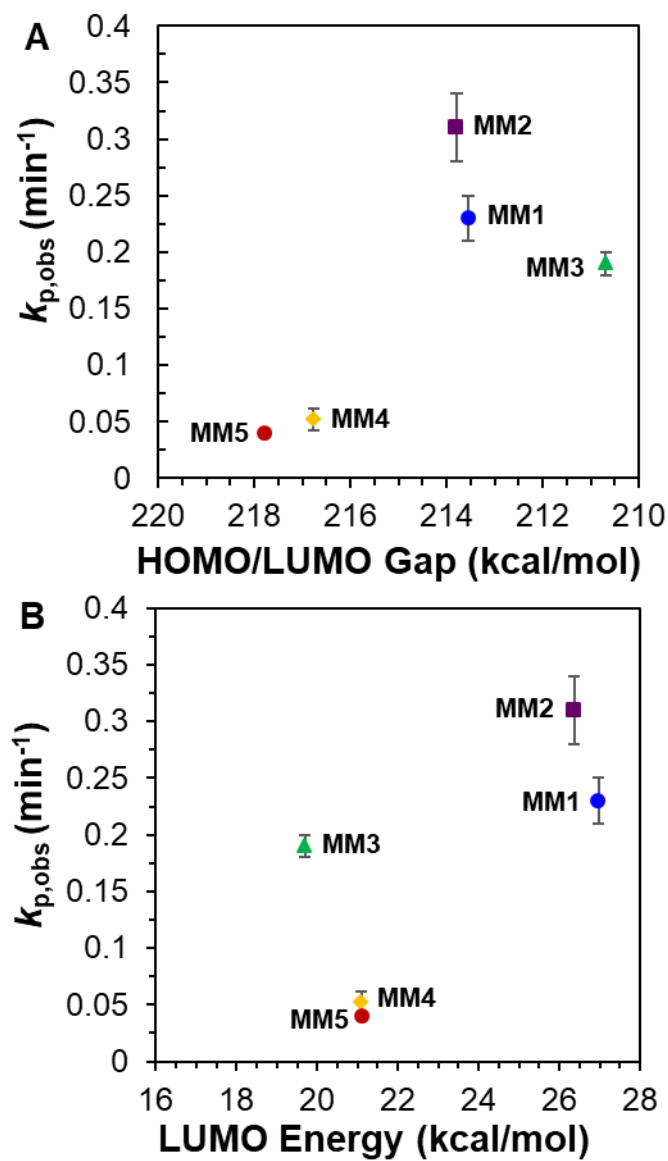


Figure S40. (A) Measured $k_{p,obs}$ versus HOMO/LUMO energy gap for MMs 1–5 with G3 catalyst. (B) Measured $k_{p,obs}$ versus LUMO energy for MMs 1–5 with G3 catalyst.

Conversion and N_{bb} Data for ROMPs of Various Target N_{bb} Values

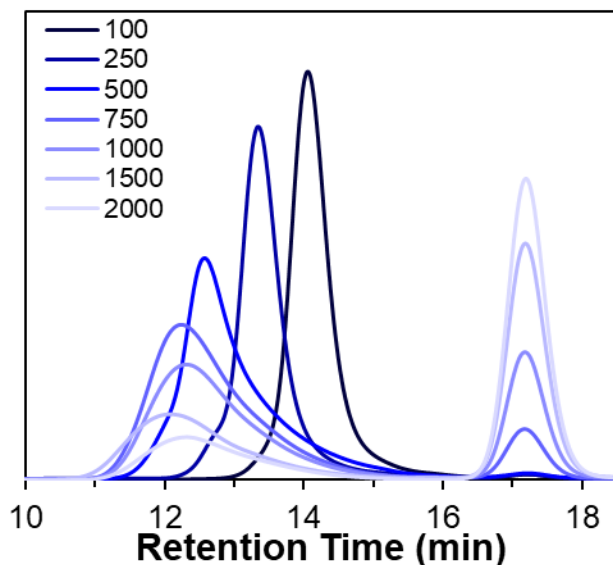


Figure S41. Representative SEC traces (dRI signal) of the ROMP of MM x -MOM₂E'-PS (**1**) targeting various N_{bb} values. Each trace is a separate polymerization targeting a different N_{bb} value noted in the legend.

Table S1. ROMPs of MM x -MOM₂E'-PS (**1**) to various target N_{bb} values.

[MM]/[G3]	% conv ^a	BB M_n , expected ^b (kg/mol)	BB M_n , SEC ^c (kg/mol)	N_{bb} , SEC ^d	BB Đ ^c
100	98.1 ± 0.4	320	320 ± 40	100 ± 10	1.06
250	96 ± 3	800	800 ± 100	260 ± 30	1.09
500	96 ± 2	1600	1600 ± 200	500 ± 70	1.13
750	93 ± 4	2400	2170 ± 80	680 ± 30	1.59
1000	80 ± 10	3200	2600 ± 500	800 ± 200	1.61
1500	41 ± 1	4800	2200 ± 300	700 ± 90	1.70
2000	18 ± 7	6400	1200 ± 600	400 ± 200	1.90

^aMeasured on an aliquot removed after 24 h using SEC by comparing the areas of the bottlebrush polymer and MM peaks in the dRI trace using the known dn/dc for PS of 0.185 mL/g.

^bDetermined using the equation $M_{n,expected} = M_{n,MM} * ([MM]/[G3])_0$. ^cMeasured by SEC in tetrahydrofuran at 30 °C with multiangle light scattering. ^dMeasured N_{bb} calculated based on the equation $N_{bb} = M_{n,bottlebrush}/M_{n,MM}$.

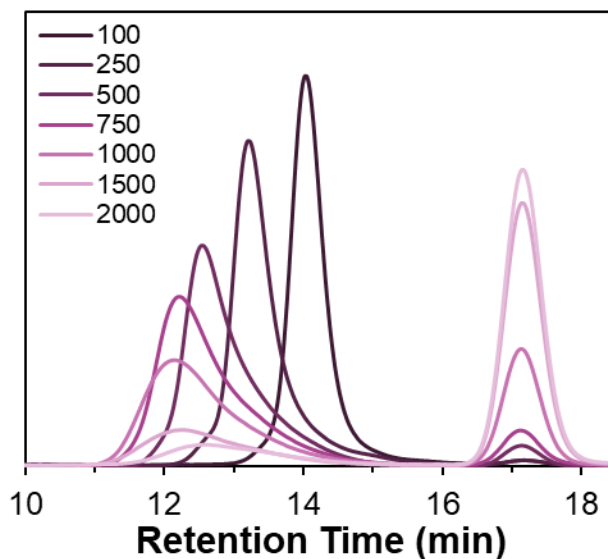


Figure S42. Representative SEC traces (dRI signal) of the ROMP of MM *x*-ME'-PS (**2**) targeting various N_{bb} . Each trace is a separate polymerization targeting a different N_{bb} value noted in the legend.

Table S2. ROMPs of MM *x*-ME'-PS (**2**) to various target N_{bb} values.

[MM]/[G3]	% conv ^a	BB M_n , expected ^b (kg/mol)	BB M_n , SEC ^c (kg/mol)	N_{bb} , SEC ^d	BB \bar{D} ^c
100	98.5 ± 0.1	320	290 ± 10	100 ± 5	1.04
250	97 ± 1	800	840 ± 80	280 ± 30	1.08
500	93 ± 4	1600	1500 ± 100	500 ± 40	1.27
750	88 ± 2	2400	2200 ± 500	700 ± 200	1.46
1000	87 ± 5	3200	2600 ± 500	900 ± 200	1.63
1500	30 ± 10	4800	1500 ± 200	550 ± 70	1.72
2000	29 ± 7	6400	1560 ± 60	530 ± 30	1.75

^aMeasured on an aliquot removed after 24 h using SEC by comparing the areas of the bottlebrush polymer and MM peaks in the dRI trace using the known dn/dc for PS of 0.185 mL/g.

^bDetermined using the equation $M_{n,expected} = M_{n,MM} * ([MM]/[G3])_0$. ^cMeasured by SEC in tetrahydrofuran at 30 °C with multiangle light scattering. ^dMeasured N_{bb} calculated based on the equation $N_{bb} = M_{n,bottlebrush}/M_{n,MM}$.

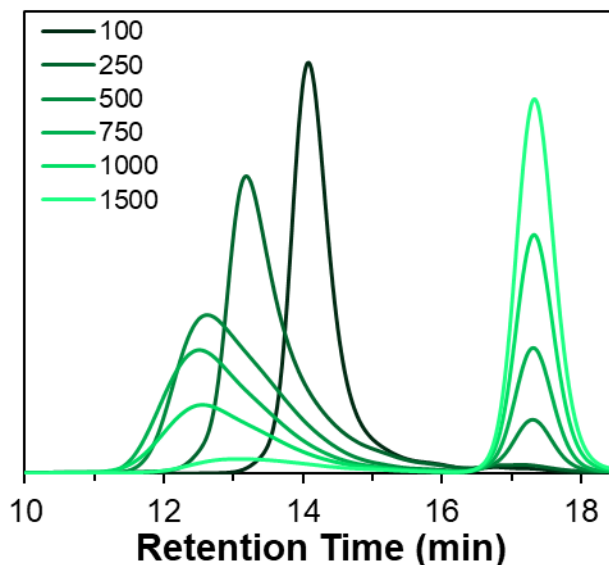


Figure S43. Representative SEC traces (dRI signal) of the ROMP of MM x -EM₂E'-PS (**3**) targeting various N_{bb} . Each trace is a separate polymerization targeting a different N_{bb} value noted in the legend.

Table S3. ROMPs of MM x -EM₂E'-PS (**3**) to various target N_{bb} values

[MM]/[G3]	% conv ^a	BB M_n , expected ^b (kg/mol)	BB M_n , SEC ^c (kg/mol)	N_{bb} , SEC ^d	BB \bar{D} ^c
100	98 ± 1	290	330 ± 30	110 ± 10	1.05
250	96.8 ± 0.8	725	860 ± 80	290 ± 30	1.07
500	93 ± 5	1450	1400 ± 100	470 ± 40	1.25
750	90 ± 10	2175	1800 ± 400	600 ± 100	1.47
1000	53 ± 8	2900	1900 ± 500	600 ± 200	1.60
1500	30 ± 10	4350	1200 ± 400	400 ± 100	1.69
2000	<3%	5800	—	—	—

^aMeasured on an aliquot removed after 24 h using SEC by comparing the areas of the bottlebrush polymer and MM peaks in the dRI trace using the known dn/dc for PS of 0.185 mL/g.

^bDetermined using the equation $M_{n,expected} = M_{n,MM} * ([MM]/[G3])_0$. ^cMeasured by SEC in tetrahydrofuran at 30 °C with multiangle light scattering. ^dMeasured N_{bb} calculated based on the equation $N_{bb} = M_{n,bottlebrush}/M_{n,MM}$.

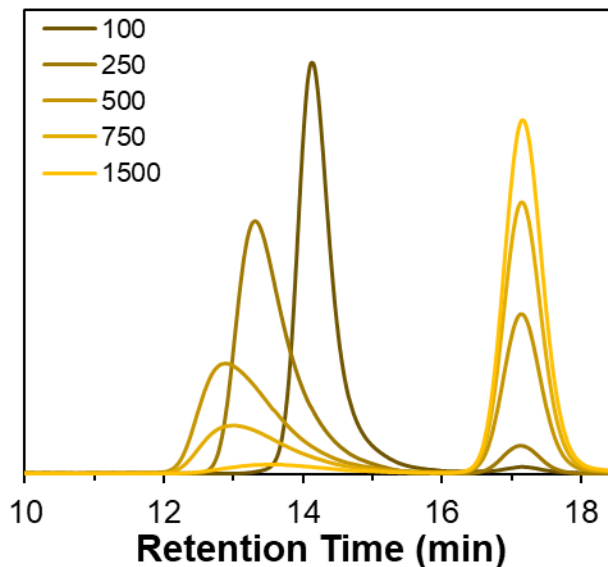


Figure S44. Representative SEC traces (dRI signal) of the ROMP of MM xx -IMEM₂E'-PS (**4**) targeting various N_{bb} . Each trace is a separate polymerization targeting a different N_{bb} value noted in the legend.

Table S4. ROMPs of MM xx -IMEM₂E'-PS (**4**) to various target N_{bb} values

[MM]/[G3]	% conv ^a	BB M_n , expected ^b (kg/mol)	BB M_n , SEC ^c (kg/mol)	N_{bb} , SEC ^d	BB \bar{D} ^c
100	91 ± 7	290	260 ± 20	88 ± 8	1.07
250	89 ± 3	725	500 ± 50	170 ± 20	1.21
500	55 ± 6	1450	720 ± 40	250 ± 10	1.38
750	31 ± 6	2175	700 ± 100	260 ± 50	1.50
1000	10 ± 20	2900	580 ± 50	200 ± 70	1.50
1500	<3%	4350	—	—	—

^aMeasured on an aliquot removed after 24 h using SEC by comparing the areas of the bottlebrush polymer and MM peaks in the dRI trace using the known dn/dc for PS of 0.185 mL/g.

^bDetermined using the equation $M_{n,expected} = M_{n,MM} * ([MM]/[G3])_0$. ^cMeasured by SEC in tetrahydrofuran at 30 °C with multiangle light scattering. ^dMeasured N_{bb} calculated based on the equation $N_{bb} = M_{n,bottlebrush}/M_{n,MM}$.

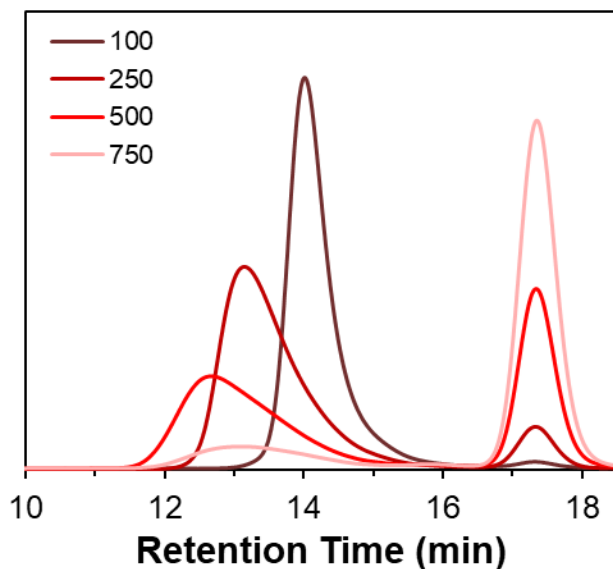


Figure S45. Representative SEC traces (dRI signal) of the ROMP of MM xx -IM₂E'-PS (**5**) targeting various N_{bb} . Each trace is a separate polymerization targeting a different N_{bb} value noted in the legend.

Table S5. ROMPs of MM xx -IM₂E'-PS (**5**) to various target N_{bb} values

[MM]/[G3]	% conv ^a	BB M_n , expected ^b (kg/mol)	BB M_n , SEC ^c (kg/mol)	N_{bb} , SEC ^d	BB \bar{D} ^c
100	96 ± 3	290	340 ± 40	120 ± 10	1.07
250	86 ± 4	725	600 ± 100	210 ± 40	1.29
500	57 ± 6	1450	1030 ± 40	360 ± 10	1.49
750	13 ± 6	2175	500 ± 200	170 ± 60	1.80
1000	<3%	2900	—	—	—

^aMeasured on an aliquot removed after 24 h using SEC by comparing the areas of the bottlebrush polymer and MM peaks in the dRI trace using the known dn/dc for PS of 0.185 mL/g.

^bDetermined using the equation $M_{n,expected} = M_{n,MM} * ([MM]/[G3])_0$. ^cMeasured by SEC in tetrahydrofuran at 30 °C with multiangle light scattering. ^dMeasured N_{bb} calculated based on the equation $N_{bb} = M_{n,bottlebrush}/M_{n,MM}$.

Kinetic Analysis of MMs Targeting $N_{bb} = 20$ for Each Block for Bottlebrush Pentablock Copolymer Synthesis

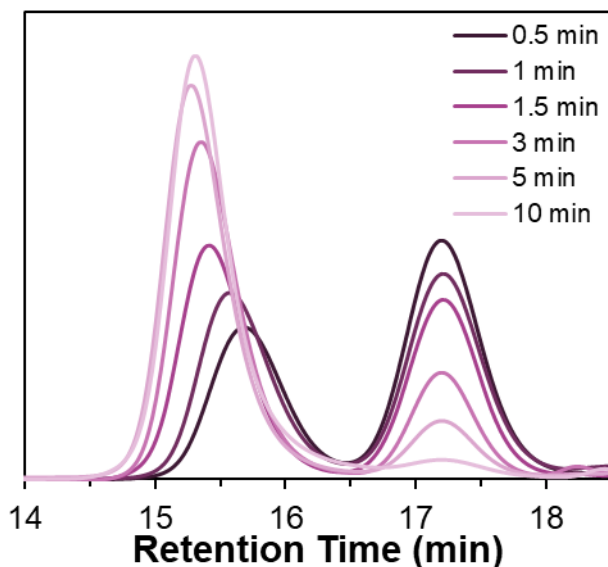


Figure S46. SEC traces (dRI signal) of the ROMP of MM x -ME'-PS (**2**) at an [MM]/[G3] ratio of 20:1. As the polymerization proceeds, the MM signal at 17.2 min decreases in intensity and the bottlebrush polymer signal increases in intensity and shifts in retention time from 15.8 min to 15.2 min.

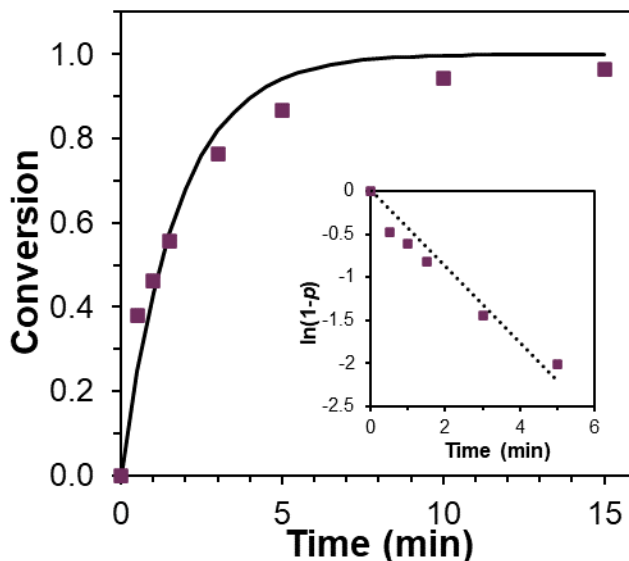


Figure S47. Kinetic analysis of the ROMP of MM x -ME'-PS (**2**) in CDCl_3 at a [MM]/[G3] ratio of 20:1 and [MM] = 20 mM. The solid line represents the fit to the averaged conversion data based on the equation $p = 1 - e^{-k_{\text{obs}}t}$ where p = fractional conversion. Measured $k_{\text{p,obs}} = 0.57 \text{ min}^{-1}$ and $t_{1/2} = 1.2 \text{ min}$.

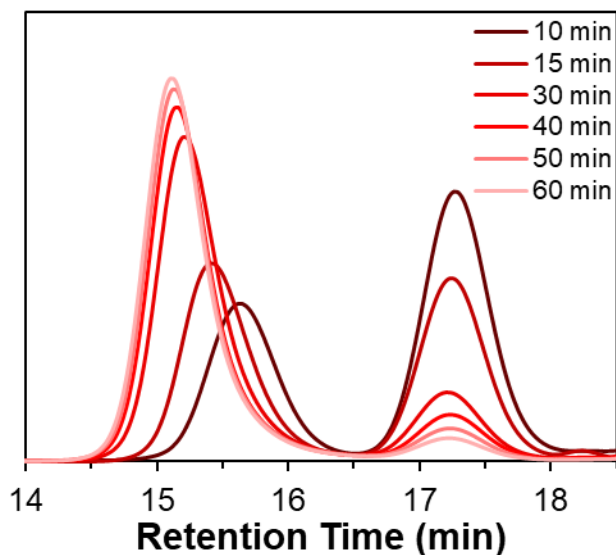


Figure S48. SEC traces (dRI signal) of the ROMP of MM xx -IM₂E'-PS (**5**) at an [MM]/[G3] ratio of 20:1. As the polymerization proceeds, the MM signal at 17.2 min decreases in intensity and the bottlebrush polymer signal increases in intensity and shifts in retention time from 15.8 min to 15.2 min.

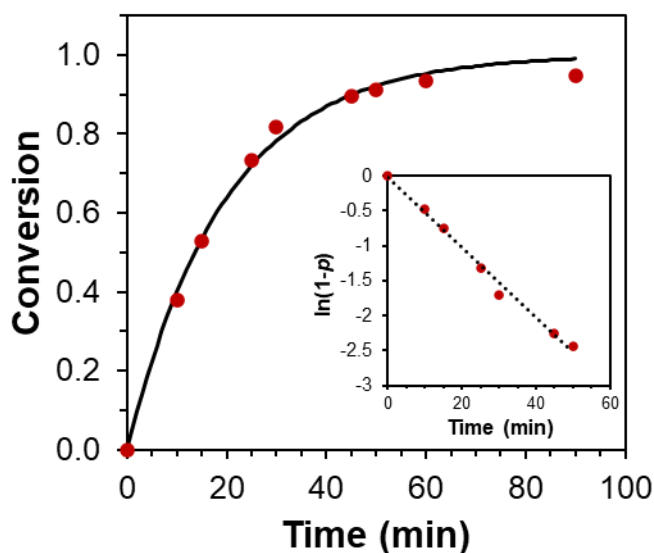


Figure S49. Kinetic analysis of the ROMP of MM xx -IM₂E'-PS (**5**) in CDCl₃ at a [MM]/[G3] ratio of 20:1 and [MM] = 20 mM. The solid line represents the fit to the averaged conversion data based on the equation $p = 1 - e^{-k_{obs}t}$ where p = fractional conversion. Measured $k_{p,obs} = 0.051 \text{ min}^{-1}$ and $t_{1/2} = 14 \text{ min}$.

Theoretical Calculations

All density functional theory calculations were performed using the Gaussian 09¹² suite of software. The M06-2X functional and def2-TZVP basis set were used to optimize the geometries

with PCM solvation (chloroform) and an ultrafine integration grid. HOMO energies were obtained with the optimum structures.

MM *x*-MOM₂E'-PS (1)

HOMO: -186.5838 kcal/mol

C	-4.687519	1.759704	1.088401
C	-3.948556	1.338386	-0.194142
C	-4.356784	-0.166229	-0.296954
C	-5.805664	-0.159738	0.259438
C	-6.067225	1.347307	0.549013
C	-6.052578	2.045370	-0.797709
C	-4.794848	2.044941	-1.235764
C	-3.451492	-1.086328	0.493605
H	-6.933150	2.371122	-1.334388
H	-4.437901	2.365733	-2.204897
H	-4.609519	2.828282	1.283513
H	-4.388458	1.198382	1.974984
H	-4.328096	-0.490373	-1.337939
H	-5.866413	-0.732715	1.188117
H	-6.526533	-0.578544	-0.440388
H	-2.876267	1.507291	-0.241554
H	-6.929784	1.537990	1.182193
O	-2.157575	-1.061501	-0.084788
H	-3.393457	-0.771343	1.543817
H	-3.845405	-2.110663	0.474789
C	-1.275838	-1.894018	0.584184
O	-0.047353	-1.741394	-0.104089
H	-1.149130	-1.594758	1.630793
H	-1.593512	-2.941724	0.539573
C	0.976760	-2.466831	0.364854
O	0.858055	-3.212679	1.303061
C	2.265128	-2.204680	-0.399850
C	2.693849	-0.767522	-0.025836
C	3.304799	-3.230517	0.042670
C	1.995809	-2.331501	-1.904088
C	4.012153	-0.307512	-0.655382
H	1.902173	-0.075427	-0.322743
H	2.786050	-0.699963	1.063132
C	4.333482	1.105902	-0.245810
H	4.824614	-0.966263	-0.344790
H	3.941964	-0.361566	-1.743414

H	4.216807	-3.115561	-0.542022
H	3.547568	-3.114522	1.099083
H	2.931024	-4.243484	-0.107528
H	2.931805	-2.254858	-2.456853
H	1.553755	-3.302386	-2.134687
H	1.317989	-1.553098	-2.252445
C	5.097028	1.361474	0.890539
C	5.358106	2.663918	1.295091
C	4.855228	3.733483	0.565997
C	4.090879	3.490925	-0.568268
C	3.832896	2.186814	-0.968036
H	5.493530	0.529157	1.461548
H	5.957364	2.843712	2.178649
H	5.059811	4.749469	0.877788
H	3.697435	4.318813	-1.144374
H	3.237044	2.001805	-1.855132

MM.x-ME'-PS (2)

HOMO: -187.43096 kcal/mol

C	-9.268148	-1.909792	-1.873788
C	-10.309712	-0.828068	-1.440231
C	-10.468790	0.070108	-2.651959
C	-11.125363	-0.622780	-3.580659
C	-11.425086	-1.992512	-3.002068
C	-10.060982	-2.737923	-2.920808
C	-11.620723	-1.629863	-1.520628
C	-8.790156	-2.772385	-0.727598
H	-11.318686	-0.327894	-4.602991
H	-10.012206	1.044352	-2.760976
H	-12.499520	-1.010662	-1.346963
H	-11.646184	-2.501904	-0.865394
H	-8.395894	-1.431275	-2.320941
H	-10.216821	-3.760625	-2.568902
H	-9.557251	-2.788077	-3.884329
H	-10.073055	-0.337420	-0.499276
H	-12.215514	-2.558994	-3.487239
O	-8.045835	-1.937592	0.170732
H	-9.620676	-3.225372	-0.182234
H	-8.141527	-3.577296	-1.079084
C	-7.579147	-2.517803	1.280393
O	-7.751340	-3.684638	1.526287
C	-6.842072	-1.529901	2.175417
C	-6.237272	-2.294557	3.348826
C	-5.736279	-0.850729	1.357488
C	-7.895344	-0.504494	2.649893

H	-5.133899	-0.210326	2.001565
H	-5.071360	-1.596459	0.917821
H	-6.154875	-0.245552	0.554130
H	-5.630803	-1.625857	3.959087
H	-7.014614	-2.732788	3.975530
H	-5.598930	-3.102033	2.990667
C	-7.380431	0.526331	3.659141
H	-8.290311	0.021331	1.777441
H	-8.734532	-1.042887	3.103113
C	-8.459760	1.518230	4.005067
H	-7.047739	0.023067	4.568329
H	-6.521108	1.056923	3.244250
C	-9.339437	1.274844	5.057144
C	-10.364006	2.165329	5.349409
C	-10.524385	3.316456	4.589162
C	-9.654024	3.569383	3.536647
C	-8.631767	2.675270	3.248587
H	-9.216286	0.378544	5.655082
H	-11.035949	1.961637	6.173484
H	-11.320293	4.013451	4.817247
H	-9.769486	4.466022	2.940985
H	-7.953006	2.877638	2.427299

MM.x-EM₂E'-PS (3)

HOMO: -190.9889 kcal/mol

C	5.046245	-0.650228	-0.811602
C	5.120124	-1.648009	0.409515
C	6.597320	-1.961819	0.538349
C	7.197464	-0.868340	1.004918
C	6.131702	0.191235	1.200077
C	5.687957	0.634454	-0.226612
C	4.933762	-0.687210	1.595280
C	3.633962	-0.525686	-1.317402
H	8.260214	-0.705456	1.119925
H	7.063709	-2.871500	0.186606
H	5.075315	-1.187354	2.552117
H	3.985098	-0.152601	1.580357
H	5.612628	-1.055388	-1.646412
H	4.957640	1.439065	-0.157127
H	6.524232	0.978237	-0.831905
H	4.447386	-2.497985	0.327277
H	6.385378	1.016425	1.859731
O	2.860187	0.273807	-0.568492
O	3.207223	-1.114753	-2.277573
C	1.492845	0.372516	-0.963154

C	0.839433	1.295418	0.037849
H	1.426564	0.774962	-1.974322
H	1.030262	-0.614758	-0.951935
O	-0.527160	1.397394	-0.355883
H	0.906166	0.891654	1.048802
H	1.304184	2.281830	0.027589
C	-1.304682	2.179239	0.408814
O	-0.876937	2.769403	1.365755
C	-2.748395	2.195182	-0.071233
C	-3.518854	3.224756	0.750106
C	-2.774798	2.573078	-1.557794
C	-3.295089	0.767464	0.153354
C	-4.780275	0.590610	-0.176771
H	-2.713306	0.069050	-0.452523
H	-3.137542	0.488889	1.200602
H	-4.536758	3.318013	0.373061
H	-3.558959	2.939666	1.801760
H	-3.040891	4.202017	0.684006
H	-3.804489	2.693648	-1.893214
H	-2.260792	3.521877	-1.721913
H	-2.294579	1.809964	-2.169145
C	-5.200795	-0.843304	0.012698
H	-5.384038	1.231856	0.467279
H	-4.970215	0.889566	-1.209418
C	-5.661168	-1.292284	1.248241
C	-6.007112	-2.623520	1.438324
C	-5.895958	-3.528306	0.390614
C	-5.436895	-3.092496	-0.845786
C	-5.091818	-1.760433	-1.030031
H	-5.752483	-0.588399	2.068148
H	-6.367018	-2.954027	2.404413
H	-6.168017	-4.565722	0.535660
H	-5.350272	-3.790435	-1.668852
H	-4.735763	-1.423808	-1.997548

MM *xx*-IMEM₂E'-PS (4)

HOMO: -195.6764 kcal/mol

C	-7.074753	-0.458198	-0.650785
C	-7.214482	0.997343	-1.204221
C	-8.585711	1.456968	-0.742975
C	-8.526676	1.640468	0.574201
C	-7.114779	1.307390	1.021128
C	-7.006508	-0.245517	0.875578
C	-6.317867	1.763431	-0.214608
C	-5.749330	-1.089378	-1.014684

H	-9.342454	1.877556	1.242365
H	-9.459751	1.512862	-1.376275
H	-6.370322	2.839980	-0.362197
H	-5.275236	1.439757	-0.215816
H	-7.880483	-1.105219	-0.991613
C	-5.646762	-0.769527	1.279596
H	-7.771292	-0.765144	1.449234
H	-6.994196	1.083114	-2.264088
H	-6.803345	1.676209	1.993850
N	-5.021188	-1.279976	0.151219
O	-5.143192	-0.759086	2.373502
O	-5.345422	-1.383769	-2.110250
C	-3.678475	-1.783322	0.165329
H	-3.548581	-2.486696	-0.656608
H	-3.492209	-2.299042	1.106614
C	-2.671138	-0.660413	0.012402
O	-2.949817	0.495628	-0.139849
O	-1.430207	-1.136531	0.068313
C	-0.381765	-0.171975	-0.064257
C	0.909024	-0.947431	0.049302
H	-0.462417	0.327273	-1.029809
H	-0.467297	0.573534	0.726224
O	1.952111	0.016029	-0.075737
H	0.981949	-1.452465	1.012727
H	0.993502	-1.692852	-0.741873
C	3.200348	-0.462961	0.010647
O	3.437746	-1.630990	0.180781
C	4.235114	0.597045	-0.124913
C	5.571404	0.216519	-0.040325
C	6.616522	1.213776	-0.165653
C	7.912080	0.574140	-0.043612
H	6.541111	1.698412	-1.137951
H	6.503842	1.958504	0.620861
C	8.562931	0.088024	-1.183824
C	9.813815	-0.529556	-1.065990
C	10.413848	-0.661020	0.192055
C	9.762996	-0.174903	1.332266
C	8.512113	0.442677	1.214433
H	8.096191	0.190284	-2.162403
H	10.320084	-0.907686	-1.952913
H	11.386856	-1.141408	0.283712
H	10.229736	-0.277162	2.310846
H	8.005844	0.820806	2.101356
H	5.646815	-0.268116	0.931972
H	5.684083	-0.528209	-0.826840
C	3.953202	1.599433	0.884168

C	4.001426	1.262890	-1.391617
H	2.955999	1.560589	-1.457793
H	4.635292	2.145759	-1.460001
H	4.237479	0.582396	-2.208396
H	2.907776	1.897131	0.817992
H	4.151018	1.185794	1.871940
H	4.589090	2.468200	0.720427

MM.xx-IM₂E'-PS (5)

HOMO: -196.6679 kcal/mol

C	5.427301	-0.162686	0.768450
C	5.542319	1.355674	1.124320
C	6.932873	1.756180	0.665415
C	6.932972	1.757661	-0.665636
C	5.542487	1.358177	-1.125638
C	5.427422	-0.160970	-0.773163
C	4.694853	1.977768	-0.000032
C	4.086640	-0.747169	1.154991
H	7.777209	1.906698	-1.323646
H	7.777013	1.903750	1.323879
H	4.740367	3.064388	0.001180
H	3.650736	1.657575	-0.000462
H	6.216980	-0.751021	1.230996
C	4.086826	-0.744596	-1.161212
H	6.217174	-0.748273	-1.236893
H	5.275153	1.585230	2.151494
H	5.275477	1.590014	-2.152341
N	3.396170	-1.072124	-0.003529
O	3.646107	-0.900758	-2.271681
O	3.645747	-0.905790	2.265040
C	2.056989	-1.622103	-0.004258
H	1.944339	-2.237978	-0.895056
H	1.944081	-2.239657	0.885345
C	1.033959	-0.501334	-0.003354
O	-0.247882	-1.125534	-0.004122
H	1.139745	0.123503	0.884989
H	1.139999	0.125150	-0.890506
C	-1.300826	-0.298120	-0.003493
O	-1.186788	0.900706	-0.002337
C	-2.601523	-1.020577	-0.004389
C	-3.768813	-0.262321	-0.003964
C	-5.059799	-0.922514	-0.004828
C	-6.112564	0.074574	-0.004167
H	-5.149064	-1.544061	-0.894566
H	-5.149444	-1.545644	0.883764
C	-6.620536	0.557005	-1.216283

C	-7.636999	1.519711	-1.215644
C	-8.145490	1.999986	-0.002889
C	-7.637519	1.517553	1.209227
C	-6.621055	0.554848	1.208587
H	-6.225001	0.183421	-2.159632
H	-8.032128	1.894974	-2.158497
H	-8.936153	2.748833	-0.002393
H	-8.033052	1.891138	2.152576
H	-6.225925	0.179585	2.151440
H	-3.679166	0.360808	-0.892556
H	-3.679547	0.359226	0.885773
C	-2.598168	-1.902033	-1.155703
C	-2.538129	-1.810931	1.209622
H	-1.684932	-2.495261	-1.156035
H	-3.461275	-2.564393	-1.108283
H	-2.645780	-1.308450	-2.067467
H	-1.624893	-2.404159	1.209290
H	-2.540649	-1.148927	2.074299
H	-3.401236	-2.473290	1.257042

3.9 Supporting Information References

1. Au – Liu, J.; Au – Gao, A. X.; Au – Johnson, J. A., Particles without a Box: Brush–first Synthesis of Photodegradable PEG Star Polymers under Ambient Conditions. *JoVE* **2013**, e50874.
2. Love, J. A.; Morgan, J. P.; Trnka, T. M.; Grubbs, R. H., A Practical and Highly Active Ruthenium-based Catalyst that Effects the Cross Metathesis of Acrylonitrile. *Angew. Chem* **2002**, *41*, 4035–4037.
3. Witiak, D. T.; Poochikian, G. K.; Feller, D. R.; Kenfield, N. A.; Newman, H. A. I., 9–Chloro–2,3–dihydro–5H–1,4–dioxepino[6,5–b]benzofuran, a novel antilipidemic agent structurally related to clofibrate. *J. Med. Chem.* **1975**, *18*, 992–996.
4. Alaboalirat, M.; Qi, L.; Arrington, K. J.; Qian, S.; Keum, J. K.; Mei, H.; Littrell, K. C.; Sumpter, B. G.; Carrillo, J.-M. Y.; Verduzco, R.; Matson, J. B., Amphiphilic Bottlebrush Block

Copolymers: Analysis of Aqueous Self-Assembly by Small-Angle Neutron Scattering and Surface Tension Measurements. *Macromolecules* **2019**, *52*, 465–476.

5. White, M. A.; Johnson, J. A.; Koberstein, J. T.; Turro, N. J., Toward the Syntheses of Universal Ligands for Metal Oxide Surfaces: Controlling Surface Functionality through Click Chemistry. *J. Am. Chem. Soc.* **2006**, *128*, 11356–11357.

6. Radzinski, S. C.; Foster, J. C.; Matson, J. B., Preparation of Bottlebrush Polymers via a One-pot Ring-opening Polymerization (ROP) and Ring-opening Metathesis Polymerization (ROMP) Grafting-through Strategy. *Macromol. Rapid Commun.* **2016**, *37*, 616–621.

7. Radzinski, S. C.; Foster, J. C.; Matson, J. B., Synthesis of bottlebrush polymers via transfer-to and grafting-through approaches using a RAFT chain transfer agent with a ROMP-active Z-group. *Polym. Chem.* **2015**, *6*, 5643–5652.

8. Conrad, R. M.; Grubbs, R. H., Tunable, Temperature-Responsive Polynorbornenes with Side Chains Based on an Elastin Peptide Sequence. *Angew. Chem* **2009**, *48*, 8328–8330.

9. Radzinski, S. C.; Foster, J. C.; Chapleski, R. C.; Troya, D.; Matson, J. B., Bottlebrush Polymer Synthesis by Ring-opening Metathesis Polymerization: The Significance of the Anchor Group. *J. Am. Chem. Soc.* **2016**, *138*, 6998–7004.

10. Qiao, Y.; Ping, J.; Tian, H.; Zhang, Q.; Zhou, S.; Shen, Z.; Zheng, S.; Fan, X., Synthesis and phase behavior of a polynorbornene-based molecular brush with dual “jacketing” effects. *J. Polym. Sci., Part A: Polym. Chem.* **2015**, *53*, 2116–2123.

11. Alaboalirat, M.; Vu, C.; Matson, J. B., Radical-radical coupling effects in the direct-growth grafting-through synthesis of bottlebrush polymers using RAFT and ROMP. *Polym. Chem.* **2022**, *13*, 5841–5851.

12. Frisch, M. J.; Trucks, G. W.; Schlegel, H. B.; Scuseria, G. E.; Robb, M. A.; Cheeseman, J. R.; Scalmani, G.; Barone, V.; Petersson, G. A.; Nakatsuji, H.; Li, X.; Caricato, M.; Marenich, A. V.; Bloino, J.; Janesko, B. G.; Gomperts, R.; Mennucci, B.; Hratchian, H. P.; Ortiz, J. V.; Izmaylov, A. F.; Sonnenberg, J. L.; Williams; Ding, F.; Lipparini, F.; Egidi, F.; Goings, J.; Peng, B.; Petrone, A.; Henderson, T.; Ranasinghe, D.; Zakrzewski, V. G.; Gao, J.; Rega, N.; Zheng, G.; Liang, W.; Hada, M.; Ehara, M.; Toyota, K.; Fukuda, R.; Hasegawa, J.; Ishida, M.; Nakajima, T.; Honda, Y.; Kitao, O.; Nakai, H.; Vreven, T.; Throssell, K.; Montgomery Jr., J. A.; Peralta, J. E.; Ogliaro, F.; Bearpark, M. J.; Heyd, J. J.; Brothers, E. N.; Kudin, K. N.; Staroverov, V. N.; Keith, T. A.; Kobayashi, R.; Normand, J.; Raghavachari, K.; Rendell, A. P.; Burant, J. C.; Iyengar, S. S.; Tomasi, J.; Cossi, M.; Millam, J. M.; Klene, M.; Adamo, C.; Cammi, R.; Ochterski, J. W.; Martin, R. L.; Morokuma, K.; Farkas, O.; Foresman, J. B.; Fox, D. J. *Gaussian 16 Rev. C.01*, Wallingford, CT, 2016.

Chapter 4: Ring-opening metathesis polymerization of norbornene–benzoladderene (macro)monomers

4.1 Authors

Samantha J. Scannelli, Mohammed Alaboalirat, Diego Troya, and John B. Matson*

Department of Chemistry, Virginia Tech, Blacksburg, VA 24061, United States

Macromolecules Innovation Institute, Virginia Tech, Blacksburg, VA 24061, United States

4.2 Abstract

Ring-opening metathesis polymerization (ROMP) utilizes highly active metal catalysts such as Grubbs' third-generation catalyst $(\text{H}_2\text{IMes})(\text{pyr})_2(\text{Cl})_2\text{Ru}=\text{CHPh}$ for the synthesis of well-defined linear and bottlebrush polymers. Recent interest is in the development of novel (macro)monomers for use in ROMP for the synthesis of interesting polymer structures. In this work, we introduce a new anchor group, the unit that attaches a polymer side-chain to the polymerizable unit, the *exo* norbornene–benzoladderene structure for use in ROMP. We synthesized one monomer and two macromonomers, containing polystyrene side-chains, varying the position where the side-chain attached to the anchor group. Then we evaluated propagation rate (k_p) and calculated HOMO energies for all three (macro)monomers. The norbornene–benzoladderene anchor group had HOMO energies higher than (macro)monomers previously reported, but only two of the (macro)monomers synthesized here had k_p values that aligned with the HOMO energies. When the side-chain was positioned closer to the reactive olefin, in the *ortho* position, k_p was significantly lower than expected, suggesting the HOMO energy was no

longer the only factor affecting the rate-determining step. We anticipate that when the side-chain is in closer proximity to the reactive chain end, *ortho* versus *meta*, there is more interference between the side-chains and the addition of new macromonomer units resulting in a lower, k_p . Ultimately, the introduction of the norbornene–benzoladderene structure as an anchor group broadens the scope of (macro)monomer structures available for ROMP.

4.3 Introduction

Ring-opening metathesis polymerization (ROMP) has garnered interest in recent years as a robust method to synthesize complex polymer architectures, such as bottlebrush polymers.¹ Specifically, ROMP is widely utilized to polymerize macromonomers (MMs), in a technique called the grafting-through approach, resulting in bottlebrush polymers with 100% side-chain grafting density ($z = 1$) along the backbone.^{1–4} Mediated by highly active Ru catalysts, such as Grubbs' third-generation catalyst [G3, (H₂IMes)(Cl)₂(pyr)₂RuCHPh], ROMP exhibits living characteristics.^{5–6} High livingness in ROMP allows for control over the molecular weight and dispersity (D) of the resulting polymers, which is particularly useful in the synthesis of well-defined bottlebrush polymers.^{7–8}

Unlike many other polymerization techniques, ROMP has relatively low sensitivity to air and water, enabling its use on the benchtop in many cases. ROMP also has high functional group tolerance, allowing for the direct polymerization of functional monomers and MMs.^{9–12} In recent years there has been interest in broadening the scope of (macro)monomers used in ROMP to achieve faster polymerizations, as well as larger and better defined polymers.^{13–16} A common cyclic olefin used in ROMP is norbornene, often with substituents, due to its high ring strain providing high propagation rates (k_p) and its facile functionalization with various side-chains to

make MMs.^{17–18} By tuning the side-chain identities and sizes to match specific applications, researchers have turned to ROMP to synthesize various bottlebrush polymers for use as templates for nanomaterials,^{19–21} photonic crystals,^{22–24} organic electronic materials,^{25–27} elastomers,^{28–30} and drug delivery systems.^{31–35} Monomers with bulky side-chains and side-chains containing functional groups with the ability to coordinate with the catalyst (i.e., oligosaccharides^{9–10} and polypeptides^{11–12}) have also been successfully polymerized via ROMP to moderate degrees of polymerization (DPs). However, continued development of (macro)monomer structures and their successful ROMP is needed for the synthesis of novel bottlebrush polymer materials to continue to expand potential applications of this polymer class.

Design of new bottlebrush polymers mostly focuses on the inclusion of diverse polymer side-chains along the backbone to achieve unique properties or behavior in the resultant bottlebrush polymer. However, development of the anchor group, the series of atoms used to connect a side-chain directly to the polymerizable unit,³⁶ can also help improve bottlebrush polymer reproducibility and structural integrity in bottlebrush (multi)block copolymers. Not only is the anchor group important as the linker between the backbone and side-chains of bottlebrush polymers, it also greatly affects the reactivity of the norbornene unit.^{18, 37–38} Our group has studied the effects of the anchor group in ROMP and found that HOMO energy of various (macro)monomer structures was a reasonable predictor for olefin reactivity and showed positive correlation with k_p values.^{39–40} Therefore, development and characterization of new anchor groups broadens the scope of bottlebrush polymer materials by increasing (macro)monomer structural diversity and allowing for tunability of monomer olefin reactivity.

Here, we designed an *exo*-norbornene–benzoladderene (NBL) anchor group for use in ROMP of (macro)monomers. This anchor group was inspired by work from Xia and coworkers,

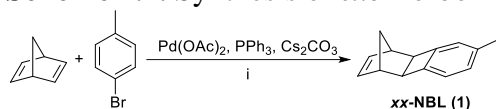
who developed the efficient catalytic arene-norbornene annulation (CANAL) method to synthesize ladder polymers.⁴¹⁻⁴³ Their interest was in expanding the synthetic methods used to generate rigid ladder polymers and in developing a new class of ladder polymers from easily accessible monomers.⁴⁴ In this work, we envisioned CANAL could be used to synthesize novel norbornene-based (macro)monomers with a rigid anchor group. We synthesized and evaluated three related NBL compounds, one small molecule monomer and two MMs, to be used in ROMP for the synthesis of linear and bottlebrush polymers, respectively. Between the two MMs, we envisioned that varying the position where the side-chain was attached to the anchor group would allow us to probe how regiochemistry on the ring influenced k_p . Additionally, we aimed to compare k_p values for these NBL compounds to other more commonly used (macro)monomers to highlight the importance of continued development of anchor group structures.

4.4 Results and Discussion

First, we aimed to synthesize an NBL monomer for use in ROMP of linear polymers. Anchor groups in the *exo* configuration have superior ROMP kinetics to norbornenes in the *endo* configuration with generally higher k_p values for *exo* monomers than *endo* monomers.⁴⁵⁻⁴⁶ Therefore, it was important to study this new anchor group in the *exo* configuration for enhanced propagation rates. We utilized a method reported by Xia and coworkers for the synthesis of NBL compounds where *exo* (abbreviated *xx* to indicate *exo* stereochemistry at the 5 and 6 positions) was the only product.⁴³ Scheme 4.1 depicts the synthesis of monomer *xx*-NBL (**1**). In brief, an annulation reaction between norbornadiene and 4-bromotoluene, mediated by a Pd catalyst, afforded the desired product. CANAL has largely been used as a polymerization technique between norbornadiene and dibromoarene monomers; therefore consideration of reactant

equivalents and choice was important. An excess of norbornadiene was required to minimize annulation on both sides of the norbornadiene ring, and we used mono-brominated compounds to avoid polymerization. Despite these efforts, inevitable disubstitution on norbornadiene led to poor yields, suggesting that the second annulation reaction is faster than the first. However, we envision that more optimized conditions that reduce the rate of the second reaction, for example by coordinating one of the alkenes with a Lewis acid, could improve yields.

Scheme 4.1. Synthesis of *exo*-norbornene benzoladderene monomer [*xx*-NBL (**1**)]^a

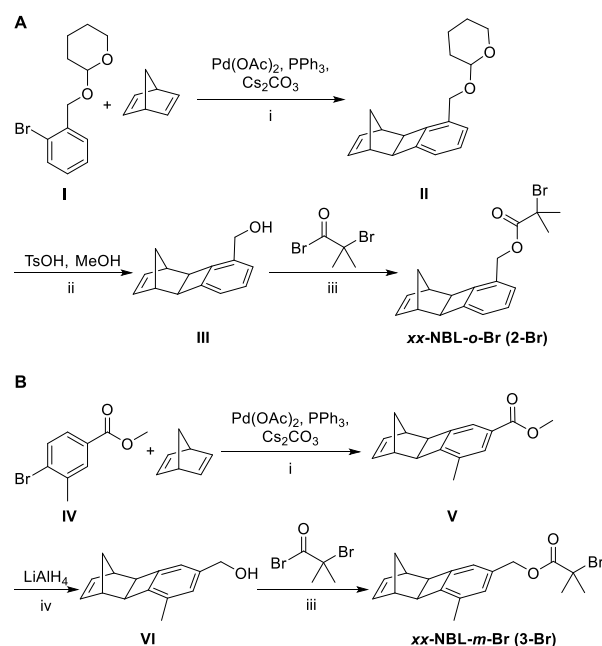


^aConditions: (i) Dioxane, reflux, 12 h. Norbornene benzoladderene (NBL) monomer with *exo*-*exo* (*xx* prefix) stereochemistry.

This general CANAL reaction, under similar conditions, was also used to synthesize two MM structures for use in ROMP of bottlebrush polymers. We designed two *xx*-NBL structures to be used as initiators in atom transfer radical polymerization (ATRP). The position of the α -bromoester initiator varied on the aromatic ring (Scheme 4.2). CANAL of 2-bromobenzyl alcohol protected with tetrahydro-2*H*-pyran (compound **I**) formed the precursor *xx*-NBL structure (compound **II**) used to synthesize *xx*-NBL-*o*-Br (Scheme 2A). The *ortho* positioning of the two functionalities on the benzene ring in compound **I** forced annulation to occur at only one position, eliminating isomeric products. To place the α -bromoester in the meta position, methyl 4-bromo-3-methylbenzoate (compound **IV**) was used in the CANAL reaction (Scheme 2B). The methyl substituent was necessary to force annulation to occur at only one position on the ring, avoiding difficult isolation of the desired isomer that occurred when the methyl group was

omitted. Reduction of the methyl ester followed by installation of the α -bromoester group afforded ATRP initiator *xx*-NBL-*m*-Br.

Scheme 4.2. Synthesis of *xx*-NBL ATRP initiator compounds^a

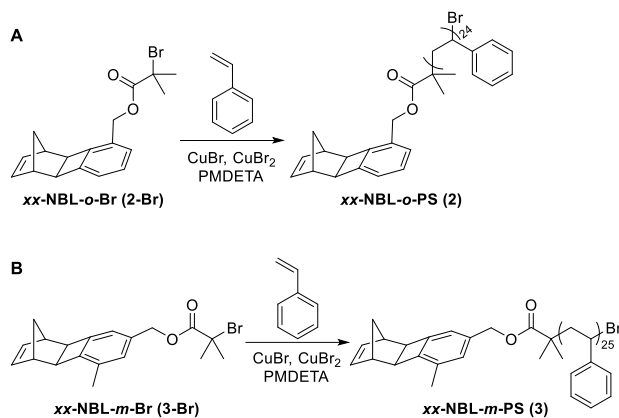


^aConditions: (i) Dioxane, reflux, 12h; (ii) MeOH, rt, 2 h; (iii) THF, rt, 12 h; (iv) THF, reflux, 16 h. All NBL compounds exhibited *exo-Exo* (*xx* prefix) stereochemistry. Italicized letters identify the position of substitution on the benzene ring starting from the top left carbon of the benzene ring (*o* = *ortho* and *m* = *meta*).

Next, we employed ATRP to add a polystyrene (PS) side-chain to both MMs. We targeted number-average molecular weight values (M_n) of approximately 3 kg/mol for both MMs. All ATRP reactions were performed under typical conditions for styrene at 90 °C for 3 h. PS can copolymerize with norbornene and can easily terminate by combination at high monomer conversion; therefore, we targeted low monomer conversion (10%) to avoid branched and coupled bottlebrush polymer products.^{47–48} The resulting crude MMs were then diluted with water and extracted with ethyl acetate before precipitation into methanol four times to yield the pure MM products as white powders. The final MM products were then analyzed by size

exclusion chromatography (SEC) to determine M_n and dispersity (D); MM *xx*-NBL-*o*-PS (**2**) had an M_n value of 2.9 kg/mol with a D of 1.04 and MM *xx*-NBL-*m*-PS (**3**) had an M_n of 3.0 kg/mol and a D of 1.06 (Scheme 4.3).

Scheme 4.3. ATRP of PS side-chains from *xx*-NBL initiators^a



xx-NBL-*o*-PS (**2**): $M_n = 2.9$ kg/mol, $D = 1.04$
xx-NBL-*m*-PS (**3**): $M_n = 3.0$ kg/mol, $D = 1.06$

^aAll (macro)monomers exhibited *exo-exo* (*xx* prefix) stereochemistry. Italicized letters identify the position of the polystyrene (PS) side-chain on the benzene ring starting from the top left carbon of the benzene ring (*o* = *ortho* and *m* = *meta*).

With the three (macro)monomers in hand, we studied the kinetics of ROMP for each in the synthesis of either linear or bottlebrush polymers. All polymerizations were initiated by G3 catalyst at rt and open to air, at a monomer concentration of 20 mM in CDCl₃. Additionally, the catalyst to (macro)monomer ratio was controlled to target a DP of 100 for each polymerization. Aliquots were removed from all polymerizations at predetermined time intervals and terminated with ethyl vinyl ether. For monomer *xx*-NBL (**1**), aliquots were then analyzed by ¹H NMR spectroscopy to measure monomer conversion by comparing the integration of the polymer backbone olefin protons to the monomer olefin protons. The final aliquot was also analyzed by SEC to determine M_n and D values. For the two MMs, the solvent in each aliquot was evaporated quickly under a stream of air, and the residue was dissolved in tetrahydrofuran (THF) for SEC

analysis. MM conversion was determined at each time point by comparing the areas under the MM and bottlebrush polymer peaks in the dRI traces. The conversion data were then used to fit first-order kinetics plots for each of the three polymerizations (Figure 4.1).

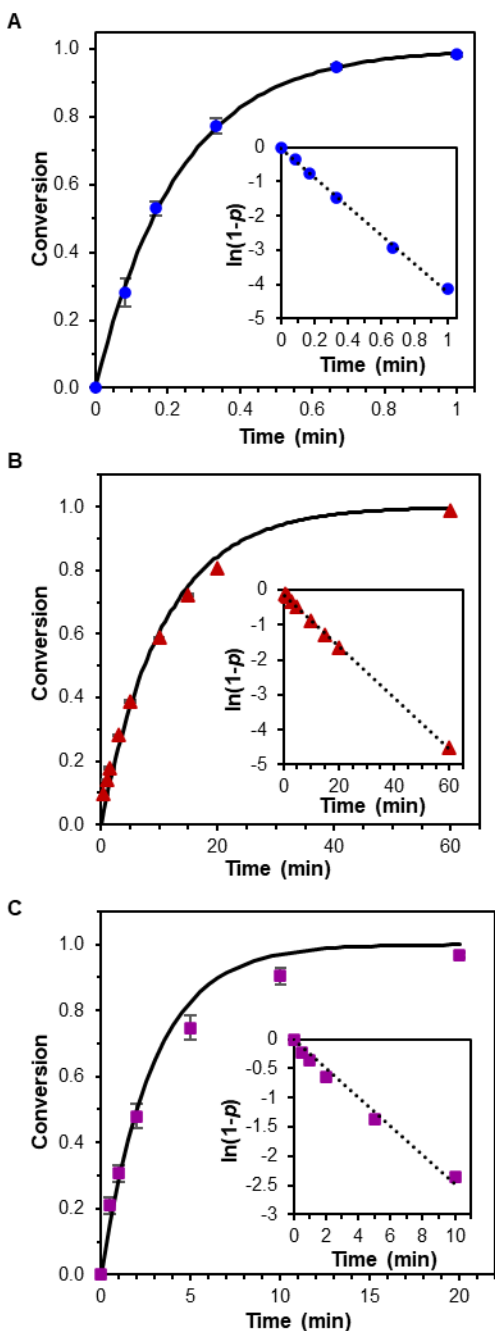


Figure 4.1. First-order kinetics analysis of (A) monomer *xx*-NBL (1), (B) MM *xx*-NBL-*o*-PS (2), and (C) MM *xx*-NBL-*m*-PS (3) in CDCl_3 at a [(macro)monomer]/[G3] ratio of 100:1 and [(macro)monomer] = 20 mM. The solid line represents the fit to the averaged conversion data based on the equation $p = 1 - e^{-k_{obs}t}$ where p = fractional conversion.

All three (macro)monomers showed relatively good agreement between the conversion data and the first-order fits, although some deviation from the fit lines at high conversion was observed for the two MMs. Additionally, instead of reaching ~98–99% conversion, both MMs leveled off at 95% conversion based on SEC, even though ¹H NMR spectroscopy confirmed complete consumption of the norbornene. This phenomenon was previously observed in other norbornene MMs made by ATRP and is attributed to the presence of ~5% MM species that lack a norbornene end group.⁴⁹ Therefore, we adjusted the conversion data for MMs *xx*-NBL-*o*-PS (**2**) and *xx*-NBL-*m*-PS (**3**) to account for 5% MM species that lacked a norbornene (Figure 1B and 1C). Average $k_{p,obs}$ and propagation half-lives were calculated from the conversion versus time plots and are shown in Table 4.1.

Table 4.1. Summary of ROMP Kinetic Analysis of (Macro)Monomers

(Macro)monomer	$k_{p,obs}^a$ (min ⁻¹)	$t_{1/2}$ (min)	% conv ^b	Final $M_{n,expected}^c$ (kg/mol)	Final $M_{n,SEC}^d$ (kg/mol)	Final \bar{D}^d
<i>xx</i> -NBL (1)	4.4 ± 0.3	0.16 ± 0.01	98	22	20	1.04
<i>xx</i> -NBL- <i>o</i> -PS (2)	0.094 ± 0.002	7.4 ± 0.2	95	276	244	1.06
<i>xx</i> -NBL- <i>m</i> -PS (3)	0.31 ± 0.04	2.3 ± 0.3	95	285	220	1.09

^aCalculated from conversions measured by ¹H NMR spectroscopy (**1**) or SEC (**2–3**) on aliquots removed at specific time points during the polymerizations. A minimum of three polymerizations were run for each MM. ^bMeasured on the final sample of the kinetics runs using ¹H NMR spectroscopy (**1**) by comparing the integrations of the polymer backbone olefin protons to the monomer olefin protons or using SEC (**2–3**) by comparing the areas of the bottlebrush polymer and MM peaks in the dRI trace (95% represents near-complete conversion for MMs **2–3** based on complete disappearance of the norbornene signal by ¹H NMR spectroscopy). ^cDetermined using the equation $M_{n,expected} = M_{n,initial} * conv * ([MM]/[G3])_0$ where $M_{n,initial}$ is either the molecular weight of the monomer (**1**) or the $M_{n,SEC}$ measured for the MMs (**2–3**). ^dMeasured on the final sample of the kinetics runs by SEC in THF at 30 °C with multiangle light scattering, using either the 100% mass recovery method to estimate dn/dc (**1**) or using the known dn/dc for PS of 0.185 mL/g (**2–3**).

All (macro)monomers reached near-complete conversion ($\geq 95\%$), and M_n values matched expected values while maintaining relatively low \bar{D} values for the final linear or

bottlebrush polymer products. As expected, monomer *xx*-NBL (**1**) had a significantly higher $k_{p,obs}$ than both MMs; the $k_{p,obs}$ of monomer *xx*-NBL (**1**) was 14-fold higher than *xx*-NBL-*m*-PS (**3**) and almost 50-fold higher than *xx*-NBL-*o*-PS (**2**). This result is consistent with observations that k_p decreases with increasing side-chain molecular weight in MMs.^{8, 50–51} Interestingly, the $k_{p,obs}$ values for the two MMs differed by a factor of 3.3, with MM *xx*-NBL-*m*-PS (**3**) polymerizing faster than MM *xx*-NBL-*o*-PS (**2**). This was surprising because the anchor group structure and M_n values of the side-chains were the same; only the regiochemistry on the aromatic ring differed.

The anchor group in these NBL compounds is quite rigid, which prevents mobility of the structural units close to the reactive norbornene olefin. We expected the rigidity of the anchor group to enhance k_p in ROMP compared with more common imide and ester-based anchor groups, because there would be less potential for steric interactions between the anchor group and the metal center. Additionally, we expected no chelation to the Ru center due to its fully hydrocarbon structure. These expectations were consistent for monomer *xx*-NBL (**1**) and MM *xx*-NBL-*m*-PS (**3**) which both exhibited high k_p values compared to other anchor groups.^{39–40} This expectation did not hold true for MM *xx*-NBL-*o*-PS (**2**), which exhibited an unexpectedly low k_p .^{39–40} Therefore, we conclude that the position of the PS side-chain affected the rate-determining step in grafting-through ROMP of *exo*-NBL MMs.

Guironnet and coworkers found that the rate-determining step in ROMP is the formation of the metallocyclobutane ring.³⁷ In our previous work, we showed that HOMO energy was a reasonable predictor of k_p because the rate-determining step employs the π electrons of the olefin substrate, corresponding to the HOMO, to form a bond with the catalyst.^{38–40} Therefore, we investigated the HOMO energies of the three *exo*-NBL (macro)monomers. The HOMO energy

for each (macro)monomer was calculated from optimized geometries using density functional theory (M06-2X method and def2-TZVP basis set).⁵²⁻⁵³ For MMs *xx*-NBL-*o*-PS (**2**) and *xx*-NBL-*m*-PS (**3**), we used only one styrene unit to represent the entire PS side-chain. Our goal was to investigate the effects of the position of the side-chain in relation to the reactive norbornene olefin on the HOMO, which should not be influenced by the side-chain beyond the first repeat unit. From these calculations, we found HOMO energies in the range of -178 to -174 kcal/mol. We then compared these HOMO energies to the measured $k_{p,obs}$ values, including in the graphs several published norbornenes with various anchor groups, where HOMO energies were calculated using the same method and $k_{p,obs}$ values were measured under identical conditions (Figure 4.2).

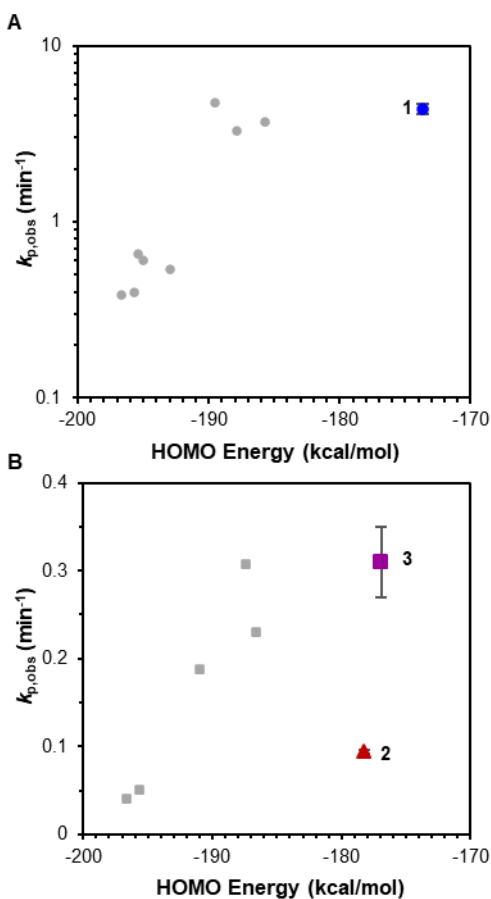


Figure 4.2. Measured $k_{p,obs}$ values versus HOMO energy for (A) monomer *xx*-NBL (**1**) (blue circle) compared to published small molecule *exo*-norbornene monomers with various anchor groups (grey circles);³⁹ and (B) for MM *xx*-NBL-*o*-PS (**2**) (red triangle) and MM *xx*-NBL-*m*-PS (**3**) (purple square) compared to published MMs (grey squares).⁴⁰

Similar to previous results, (macro)monomers with higher HOMO energies had higher $k_{p,obs}$ values than (macro)monomers with lower HOMO energies. Monomer *xx*-NBL (**1**) had a HOMO energy of -174 kcal/mol alongside a high $k_{p,obs}$ value. In comparison to monomers in our previous report,³⁹ the $k_{p,obs}$ value of monomer *xx*-NBL (**1**) aligns with monomers with high k_p anchor groups (i.e., *exo*-norbornene ester and ether anchor groups) suggesting that the *exo*-NBL anchor group is a “fast” anchor group for ROMP of linear polymers. Monomer *xx*-NBL (**1**) had a higher HOMO energy than the previously reported monomers by 10 kcal/mol and a $k_{p,obs}$ value similar to the fastest previously reported monomer. In other words, despite the much higher HOMO energy of *xx*-NBL (**1**), k_p did not increase compared to other norbornene monomers, consistent with the plateau in k_p observed for monomers with HOMO energies above -190 kcal/mol in our previous study.³⁹

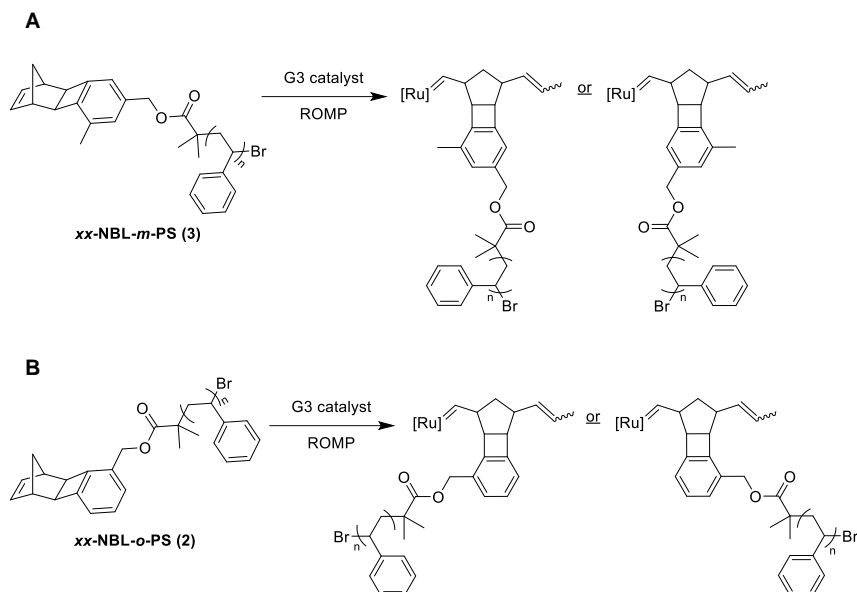
MMs *xx*-NBL-*o*-PS (**2**) and *xx*-NBL-*m*-PS (**3**) also had high HOMO energies, -178 and -177 kcal/mol respectively. When compared to MMs previously studied, MM *xx*-NBL-*m*-PS (**3**) had the highest HOMO energy and one of the highest $k_{p,obs}$ values, consistent with the positive correlation between HOMO energy and k_p . MM *xx*-NBL-*o*-PS (**2**) also had a higher HOMO energy than all previous MMs studied; however, the $k_{p,obs}$ of *xx*-NBL-*o*-PS (**2**) was unexpectedly low, aligning with MMs with low k_p anchor groups reported in the literature (i.e., *exo*-norbornene imide anchor groups).⁴⁰ This major discrepancy drew our attention to other potential factors affecting ROMP kinetics.

When comparing the three NBL (macro)monomers, we noticed that the addition of the ATRP initiator with one styrene unit on the MM structures decreased the HOMO energy by ~5 kcal/mol compared to monomer *xx*-NBL (**1**). This significant decrease in HOMO energy between the small molecule monomer and the MM structures was surprising as previous studies showed very little difference, about 1 kcal/mol, in the HOMO energy when comparing monomer and MM structures containing the same anchor group. Thus, the addition of the polymer side-chain onto the *exo* NBL anchor group changed the electronics of the MM structures more so than other anchor groups previously studied. Additionally, the MM with the lowest $k_{p,obs}$, MM *xx*-NBL-*o*-PS (**2**), had the lowest HOMO energy, but it was only 1 kcal/mol lower than the HOMO energy for MM *xx*-NBL-*m*-PS (**3**). A difference of 1 kcal/mol in HOMO energy is within the error of the calculations and does not predict a large change in k_p between the two MMs, but we observed a 3.3-fold difference. This suggests that HOMO energy is not the only factor affecting the rate-determining step for MMs *xx*-NBL-*o*-PS (**2**) and *xx*-NBL-*m*-PS (**3**), further implying the importance of the orientation of the PS side-chain during propagation.

We hypothesize that the difference in propagation rates between MMs *xx*-NBL-*o*-PS (**2**) and *xx*-NBL-*m*-PS (**3**) may be explained by an effect of the orientation of the side-chains along the backbone. MMs experience steric effects during ROMP caused by the side-chains attached to the growing bottlebrush segment, hindering unreacted MMs from approaching the Ru-center.⁵⁰ Therefore, changing the position of the side-chains could lead to varying steric effects, resulting in the variable k_p values observed in MMs *xx*-NBL-*o*-PS (**2**) and *xx*-NBL-*m*-PS (**3**). Thus, we envisioned that the rate differences could be explained by examining the position of the side-chains relative to the reactive chain end.

An analysis of the propagating alkylidenes during ROMP of MM *xx*-NBL-*m*-PS (**3**) reveals that the number of bonds between the PS side-chain and the reactive chain end only changes by 1 for the two possible regioisomers (Scheme 4.4A). Therefore, during propagation, interactions between the PS side-chain and the Ru-center likely remain low regardless of which direction MM addition occurs. In contrast, the *ortho* position of the PS side-chain in MM *xx*-NBL-*o*-PS (**2**) makes the number of bonds between the reactive chain end and the side-chain less than for MM *xx*-NBL-*m*-PS (**3**); when MM adds in one direction the side-chain is only 5 bonds away for the Ru-center (Scheme 4.4B). In this propagating alkylidene structure, the side-chain is more likely to sterically hinder the addition of new MM units, resulting in a lower k_p , than when the side-chain is positioned in the other orientation, farther away from the Ru-center. Thus, during propagation the steric hinderance of MM addition for MM *xx*-NBL-*o*-PS (**2**) is likely higher than for MM *xx*-NBL-*m*-PS (**3**) because the *ortho* positioning causes the side-chains to be in closer proximity to the Ru-center than the *meta* positioning. Ultimately, we envisioned that the lower $k_{p,obs}$ found for MM *xx*-NBL-*o*-PS (**2**) compared to MM *xx*-NBL-*m*-PS (**3**) was likely due to a greater steric effect for MM *xx*-NBL-*o*-PS (**2**), posed by the *ortho* positioning of the side-chain, than that of MM *xx*-NBL-*m*-PS (**3**).

Scheme 4.4. Propagating alkylidene structures for MM *xx*-NBL-*m*-PS (**3**) (A) and MM *xx*-NBL-*o*-PS (**2**) (B).



To test this hypothesis, we copolymerized each MM with a small molecule monomer to decrease the grafting density of the final bottlebrush polymer. We predicted that spacing out the PS side-chains using a diluent monomer would lessen the steric interactions between the side-chains and Ru-center for both MMs, resulting in equal k_p values for the two MMs. We chose a diluent monomer, *xx*-IM₂E'P, with a similar rate to MM *xx*-NBL-*m*-PS (**3**) to avoid blocky compositions, with the expectation that the k_p of MM *xx*-NBL-*o*-PS (**2**) would increase when polymerized with diluent monomer compared to without diluent monomer. We polymerized both MMs at room temperature and open to air, at a total norbornene concentration of 20 mM in CDCl₃. Again, the catalyst to MM ratio was controlled to target a DP of 100, but 500 equiv of diluent monomer *xx*-IM₂E'P was included at the start of both polymerizations. Thus, the target grafting density (z) was 0.16. Aliquots were removed from polymerizations at predetermined time intervals and terminated with ethyl vinyl ether before SEC analysis. MM conversion was determined at each time point by comparing the areas under the MM peak in the dRI traces

normalized to an initial dRI trace before catalyst addition. The conversion data were then used to fit first-order kinetics plots.

Keeping the norbornene concentration at 20 mM during the copolymerization resulted in a lower catalyst concentration than the homopolymerizations but was necessary to ensure proper stirring during the polymerization. Therefore, we used second-order rate constants (k_{MM}), which account for the difference in catalyst concentration, to compare the rate of MM addition during homopolymerization ($k_{MM(\text{homo})}$) and copolymerization ($k_{MM(\text{copo})}$) seen in Figure 4.3. In comparing the k_{MM} values, we expected $k_{MM(\text{copo})}$ to be higher than $k_{MM(\text{homo})}$ for both MMs due to the lower steric hinderance on MM addition when $z = 0.16$, during copolymerization, then when $z = 1$ during homopolymerization.

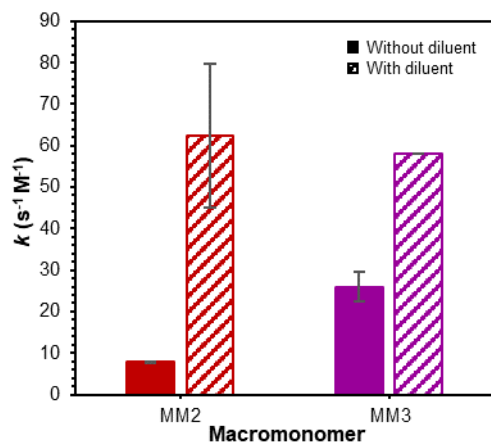


Figure 4.3. Measured k_{MM} values for MMs *xx*-NBL-*o*-PS (**2**) and *xx*-NBL-*m*-PS (**3**) without, $k_{MM(\text{homo})}$, and with diluent, $k_{MM(\text{copo})}$, (solid and patterned bars, respectively).

The $k_{MM(\text{homo})}$ of MM *xx*-NBL-*o*-PS (**2**) was 3.3-fold lower than that of MM *xx*-NBL-*m*-PS (**3**) under the same conditions. With the addition of diluent monomer, the $k_{MM(\text{copo})}$ of both MMs *xx*-NBL-*o*-PS (**2**) and *xx*-NBL-*m*-PS (**3**) increased, consistent with less side-chain interference during propagation when $z \ll 1$. Interestingly, the $k_{MM(\text{copo})}$ of MM *xx*-NBL-*o*-PS (**2**) was only 0.9-fold lower than that of MM *xx*-NBL-*m*-PS (**3**). This difference being closer to 1

than the rate difference found for the homopolymerizations suggests the k_{MM} of MMs *xx*-NBL-*o*-PS (**2**) and *xx*-NBL-*m*-PS (**3**) are similar with $z \ll 1$. In other words, MMs *xx*-NBL-*o*-PS (**2**) and *xx*-NBL-*m*-PS (**3**) polymerize at similar rates when $z \ll 1$ because the side-chain interactions during propagation are similar regardless of the positioning of the side-chains. Therefore, $k_{MM(\text{homo})}$ of MM *xx*-NBL-*o*-PS (**2**) is affected by the steric hinderance of the PS side-chains when $z = 1$, resulting in a lower $k_{MM(\text{homo})}$ than MM *xx*-NBL-*m*-PS (**3**).

4.5 Conclusions

In summary, we successfully synthesized a new anchor group in the form of a small molecule monomer and two PS MMs. The NBL structures all had *exo* stereochemistry in efforts to maintain high k_p values. The small molecule monomer structure had the highest HOMO energy and one of the highest k_p values compared to monomers previously reported. Interestingly, we found a large change in k_p for MMs due to the change in positioning of the polymer side-chain. We determined that the reactivity of these MM structures, predicted by HOMO energy, varied slightly due to the position of the side-chain, but not enough to explain such large variation in k_p . We suspected the positioning of the side-chain changed the steric effects in ROMP and when side-chains were positioned closer to the reactive olefin of the norbornene, they hindered the addition of new MM units, slowing down polymerization. When copolymerized with a diluent monomer, the difference in k_{MM} between the two MMs was less than when polymerized without a diluent. The copolymerization resulting in a $z \ll 1$ reduced the steric hinderance experienced by MM *xx*-NBL-*o*-PS (**2**) and increased the $k_{MM(\text{copo})}$ value compared to the $k_{MM(\text{homo})}$ value. Ultimately, the synthesis of *exo*-NBL (macro)monomers further

broadens the scope of anchor group structures available for the synthesis of bottlebrush polymers.

4.6 Acknowledgments

This work was supported by the National Science Foundation and the Binational Science Foundation (DMR-2104602). The authors acknowledge Advanced Research Computing at Virginia Tech for providing computational resources and technical support that have contributed to the results reported within this paper. We also acknowledge the Virginia Tech Mass Spectrometry Research Incubator for high-resolution mass spectrometry analysis.

4.7 References

1. Bloch, S. E.; Scannelli, S. J.; Alaboalirat, M.; Matson, J. B., Complex Polymer Architectures Using Ring-opening Metathesis Polymerization: Synthesis, Applications, and Practical Considerations. *Macromolecules* **2022**, *55*, 4200–4227.
2. Jha, S.; Dutta, S.; Bowden, N. B., Synthesis of Ultralarge Molecular Weight Bottlebrush Polymers Using Grubbs' Catalysts. *Macromolecules* **2004**, *37*, 4365–4374.
3. Sheiko, S. S.; Sumerlin, B. S.; Matyjaszewski, K., Cylindrical molecular brushes: Synthesis, characterization, and properties. *Prog. Polym. Sci.* **2008**, *33*, 759–785.
4. Verduzco, R.; Li, X.; Pesek, S. L.; Stein, G. E., Structure, function, self-assembly, and applications of bottlebrush copolymers. *Chem. Soc. Rev.* **2015**, *44*, 2405–2420.
5. Choi, T.-L.; Grubbs, R. H., Controlled Living Ring-opening-Metathesis Polymerization by a Fast-Initiating Ruthenium Catalyst. *Angew. Chem* **2003**, *42*, 1743–1746.

6. Bielawski, C. W.; Grubbs, R. H., Living ring-opening metathesis polymerization. *Prog. Polym. Sci.* **2007**, *32*, 1–29.
7. Walsh, D. J.; Guironnet, D., Macromolecules with programmable shape, size, and chemistry. *Proc. Natl. Acad. Sci. U.S.A* **2019**, *116*, 1538–1542.
8. Ogbonna, N. D.; Dearman, M.; Cho, C.-T.; Bharti, B.; Peters, A. J.; Lawrence, J., Topologically Precise and Discrete Bottlebrush Polymers: Synthesis, Characterization, and Structure–Property Relationships. *JACS Au* **2022**, *2*, 898–905.
9. Nomura, K.; Schrock, R. R., Preparation of “Sugar–Coated” Homopolymers and Multiblock ROMP Copolymers. *Macromolecules* **1996**, *29*, 540–545.
10. Murphy, J. J.; Furusho, H.; Paton, R. M.; Nomura, K., Precise Synthesis of Poly(macromonomer)s Containing Sugars by Repetitive ROMP and Their Attachments to Poly(ethylene glycol): Synthesis, TEM Analysis and Their Properties as Amphiphilic Block Fragments. *Chemistry – A European Journal* **2007**, *13*, 8985–8997.
11. Kammeyer, J. K.; Blum, A. P.; Adamiak, L.; Hahn, M. E.; Gianneschi, N. C., Polymerization of protecting–group–free peptides via ROMP. *Polym. Chem.* **2013**, *4*, 3929–3933.
12. Sutthasupa, S.; Sanda, F.; Masuda, T., ROMP of Norbornene Monomers Carrying Nonprotected Amino Groups with Ruthenium Catalyst. *Macromolecules* **2009**, *42*, 1519–1525.
13. Medina, J. M.; Ko, J. H.; Maynard, H. D.; Garg, N. K., Expanding the ROMP Toolbox: Synthesis of Air–Stable Benzonorbornadiene Polymers by Aryne Chemistry. *Macromolecules* **2017**, *50*, 580–586.

14. Hancock, S. N.; Yuntawattana, N.; Valdez, S. M.; Michaudel, Q., Expedient synthesis and ring-opening metathesis polymerization of pyridinonorbornenes. *Polym. Chem.* **2022**, *13*, 5530–5535.
15. Nguyen, H. V. T.; Gallagher, N. M.; Vohidov, F.; Jiang, Y.; Kawamoto, K.; Zhang, H.; Park, J. V.; Huang, Z.; Ottaviani, M. F.; Rajca, A.; Johnson, J. A., Scalable Synthesis of Multivalent Macromonomers for ROMP. *ACS Macro Lett.* **2018**, *7*, 472–476.
16. Dutertre, F.; Bang, K.-T.; Vereroudakis, E.; Loppinet, B.; Yang, S.; Kang, S.-Y.; Fytas, G.; Choi, T.-L., Conformation of Tunable Nanocylinders: Up to Sixth-generation Dendronized Polymers via Graft-Through Approach by ROMP. *Macromolecules* **2019**, *52*, 3342–3350.
17. Yu, H.; Lin, S.; Sun, D.; Pan, Q., Synthesis of norbornene derivatives and their polymers via ROMP of norbornene derivatives. *High Performance Polymers* **2020**, *32*, 729–737.
18. Wolf, W. J.; Lin, T.-P.; Grubbs, R. H., Examining the Effects of Monomer and Catalyst Structure on the Mechanism of Ruthenium-catalyzed Ring-opening Metathesis Polymerization. *J. Am. Chem. Soc.* **2019**, *141*, 17796–17808.
19. Xiao, L.; Qu, L.; Zhu, W.; Wu, Y.; Liu, Z.; Zhang, K., Donut-shaped Nanoparticles Templated by Cyclic Bottlebrush Polymers. *Macromolecules* **2017**, *50*, 6762–6770.
20. Müllner, M.; Lunkenbein, T.; Schieder, M.; Gröschel, A. H.; Miyajima, N.; Förtsch, M.; Breu, J.; Caruso, F.; Müller, A. H. E., Template-Directed Mild Synthesis of Anatase Hybrid Nanotubes within Cylindrical Core-Shell-Corona Polymer Brushes. *Macromolecules* **2012**, *45*, 6981–6988.
21. Aviv, Y.; Altay, E.; Fink, L.; Raviv, U.; Rzayev, J.; Shenhar, R., Quasi-Two-Dimensional Assembly of Bottlebrush Block Copolymers with Nanoparticles in Ultrathin Films:

Combined Effect of Graft Asymmetry and Nanoparticle Size. *Macromolecules* **2019**, *52*, 196–207.

22. Miyake, G. M.; Weitekamp, R. A.; Piunova, V. A.; Grubbs, R. H., Synthesis of Isocyanate-based Brush Block Copolymers and Their Rapid Self-Assembly to Infrared-Reflecting Photonic Crystals. *J. Am. Chem. Soc.* **2012**, *134*, 14249–14254.

23. Macfarlane, R. J.; Kim, B.; Lee, B.; Weitekamp, R. A.; Bates, C. M.; Lee, S. F.; Chang, A. B.; Delaney, K. T.; Fredrickson, G. H.; Atwater, H. A.; Grubbs, R. H., Improving Brush Polymer Infrared One-Dimensional Photonic Crystals via Linear Polymer Additives. *J. Am. Chem. Soc.* **2014**, *136*, 17374–17377.

24. Boyle, B. M.; French, T. A.; Pearson, R. M.; McCarthy, B. G.; Miyake, G. M., Structural Color for Additive Manufacturing: 3D-Printed Photonic Crystals from Block Copolymers. *ACS Nano* **2017**, *11*, 3052–3058.

25. Thompson, K. A.; Mayder, D. M.; Tonge, C. M.; Sauvé, E. R.; Lefeaux, H. R.; Hudson, Z. M., A grafting-from strategy for the synthesis of bottlebrush nanofibers from organic semiconductors. *Can. J. Chem.* **2023**, *101*, 118–125.

26. Yin, X.; Qiao, Y.; Gadinski, M. R.; Wang, Q.; Tang, C., Flexible thiophene polymers: a concerted macromolecular architecture for dielectrics. *Polym. Chem.* **2016**, *7*, 2929–2933.

27. Tonge, C. M.; Sauvé, E. R.; Cheng, S.; Howard, T. A.; Hudson, Z. M., Multiblock Bottlebrush Nanofibers from Organic Electronic Materials. *J. Am. Chem. Soc.* **2018**, *140*, 11599–11603.

28. Self, J. L.; Sample, C. S.; Levi, A. E.; Li, K.; Xie, R.; de Alaniz, J. R.; Bates, C. M., Dynamic Bottlebrush Polymer Networks: Self-Healing in Super-Soft Materials. *J. Am. Chem. Soc.* **2020**, *142*, 7567–7573.

29. Arrington, K. J.; Radzinski, S. C.; Drummey, K. J.; Long, T. E.; Matson, J. B., Reversibly Cross-linkable Bottlebrush Polymers as Pressure-Sensitive Adhesives. *ACS Appl. Mater. Interfaces* **2018**, *10*, 26662–26668.
30. Fournier, L.; Rivera Mirabal, D. M.; Hillmyer, M. A., Toward Sustainable Elastomers from the Grafting-through Polymerization of Lactone-containing Polyester Macromonomers. *Macromolecules* **2022**, *55*, 1003–1014.
31. Lienkamp, K.; Madkour, A. E.; Musante, A.; Nelson, C. F.; Nüsslein, K.; Tew, G. N., Antimicrobial Polymers Prepared by ROMP with Unprecedented Selectivity: A Molecular Construction Kit Approach. *J. Am. Chem. Soc.* **2008**, *130*, 9836–9843.
32. Zhao, P.; Liu, L.; Feng, X.; Wang, C.; Shuai, X.; Chen, Y., Molecular Nanoworm with PCL Core and PEO Shell as a Non-spherical Carrier for Drug Delivery. *Macromol. Rapid Commun.* **2012**, *33*, 1351–1355.
33. Miki, K.; Kimura, A.; Oride, K.; Kuramochi, Y.; Matsuoka, H.; Harada, H.; Hiraoka, M.; Ohe, K., High-Contrast Fluorescence Imaging of Tumors In Vivo Using Nanoparticles of Amphiphilic Brush-Like Copolymers Produced by ROMP. *Angew. Chem* **2011**, *50*, 6567–6570.
34. Vohidov, F.; Milling, L. E.; Chen, Q.; Zhang, W.; Bhagchandani, S.; Nguyen, Hung V. T.; Irvine, D. J.; Johnson, J. A., ABC triblock bottlebrush copolymer-based injectable hydrogels: design, synthesis, and application to expanding the therapeutic index of cancer immunochemotherapy. *Chem. Sci.* **2020**, *11*, 5974–5986.
35. Detappe, A.; Nguyen, H. V. T.; Jiang, Y.; Agius, M. P.; Wang, W.; Mathieu, C.; Su, N. K.; Kristufek, S. L.; Lundberg, D. J.; Bhagchandani, S.; Ghobrial, I. M.; Ghoroghchian, P. P.; Johnson, J. A., Molecular bottlebrush prodrugs as mono- and triplex combination therapies for multiple myeloma. *Nature Nanotechnology* **2023**, *18*, 184–192.

36. Slugovc, C.; Demel, S.; Riegler, S.; Hobisch, J.; Stelzer, F., The Resting State Makes the Difference: The Influence of the Anchor Group in the ROMP of Norbornene Derivatives. *Macromol. Rapid Commun.* **2004**, *25*, 475–480.
37. Hyatt, M. G.; Walsh, D. J.; Lord, R. L.; Andino Martinez, J. G.; Guironnet, D., Mechanistic and Kinetic Studies of the Ring Opening Metathesis Polymerization of Norbornenyl Monomers by a Grubbs Third Generation Catalyst. *J. Am. Chem. Soc.* **2019**, *141*, 17918–17925.
38. Radzinski, S. C.; Foster, J. C.; Chapleski, R. C.; Troya, D.; Matson, J. B., Bottlebrush Polymer Synthesis by Ring-opening Metathesis Polymerization: The Significance of the Anchor Group. *J. Am. Chem. Soc.* **2016**, *138*, 6998–7004.
39. Scannelli, S. J.; Paripati, A.; Weaver, J. R.; Vu, C.; Alaboalirat, M.; Troya, D.; Matson, J. B., The influence of the norbornene anchor group in Ru-mediated ring-opening metathesis polymerization: Synthesis of linear polymers. *Macromolecules* **2023**, *Submitted*, ma–2023–001729.
40. Scannelli, S. J.; Alaboalirat, M.; Troya, D.; Matson, J. B., The influence of the norbornene anchor group in Ru-mediated ring-opening metathesis polymerization: Synthesis of bottlebrush polymers. *Macromolecules* **2023**, ma–2023–00214b.
41. Jin, Z.; Teo, Y. C.; Zulaybar, N. G.; Smith, M. D.; Xia, Y., Streamlined Synthesis of Polycyclic Conjugated Hydrocarbons Containing Cyclobutadienoids via C–H Activated Annulation and Aromatization. *J. Am. Chem. Soc.* **2017**, *139*, 1806–1809.
42. Hazazi, K.; Wang, Y.; Bettahalli, N. M. S.; Ma, X.; Xia, Y.; Pinnau, I., Catalytic arene-norbornene annulation (CANAL) ladder polymer derived carbon membranes with unparalleled hydrogen/carbon dioxide size-sieving capability. *Journal of Membrane Science* **2022**, *654*, 120548.

43. Lai, H. W. H.; Teo, Y. C.; Xia, Y., Functionalized Rigid Ladder Polymers from Catalytic Arene-norbornene Annulation Polymerization. *ACS Macro Lett.* **2017**, *6*, 1357–1361.
44. Lai, H. W. H.; Liu, S.; Xia, Y., Norbornyl benzocyclobutene ladder polymers: Conformation and microporosity. *J. Polym. Sci., Part A: Polym. Chem.* **2017**, *55*, 3075–3081.
45. Rule, J. D.; Moore, J. S., ROMP Reactivity of endo- and exo-Dicyclopentadiene. *Macromolecules* **2002**, *35*, 7878–7882.
46. Ivin, K. J.; Mol, J. C., 11 – Ring-opening Metathesis Polymerization: General Aspects. In *Olefin Metathesis and Metathesis Polymerization (Second Edition)*, Ivin, K. J.; Mol, J. C., Eds. Academic Press: London, 1997; pp 224–259.
47. Alaboalirat, M.; Vu, C.; Matson, J. B., Radical–radical coupling effects in the direct-growth grafting-through synthesis of bottlebrush polymers using RAFT and ROMP. *Polym. Chem.* **2022**, *13*, 5841–5851.
48. Naguib, M.; Nixon, K. L.; Keddie, D. J., Effect of radical copolymerization of the (oxa)norbornene end-group of RAFT-prepared macromonomers on bottlebrush copolymer synthesis via ROMP. *Polym. Chem.* **2022**, *13*, 1401–1410.
49. Bloch, S. E.; Alaboalirat, M.; Eades, C. B.; Scannelli, S. J.; Matson, J. B., Solvent Effects in Grafting-through Ring-opening Metathesis Polymerization. *Macromolecules* **2022**, *55*, 3522–3532.
50. Ren, N.; Yu, C.; Zhu, X., Topological Effect on Macromonomer Polymerization. *Macromolecules* **2021**, *54*, 6101–6108.
51. Zografos, A.; Lynd, N. A.; Bates, F. S.; Hillmyer, M. A., Impact of Macromonomer Molar Mass and Feed Composition on Branch Distributions in Model Graft Copolymerizations. *ACS Macro Lett.* **2021**, *10*, 1622–1628.

52. Zhao, Y.; Truhlar, D. G., The M06 suite of density functionals for main group thermochemistry, thermochemical kinetics, noncovalent interactions, excited states, and transition elements: two new functionals and systematic testing of four M06–class functionals and 12 other functionals. *Theor. Chem. Acc*, **2008**, *120*, 215–241.
53. Weigend, F.; Ahlrichs, R., Balanced basis sets of split valence, triple zeta valence and quadruple zeta valence quality for H to Rn: Design and assessment of accuracy. *Phys. Chem. Chem. Phys.* **2005**, *7*, 3297–3305.

4.8 Supporting Information

Materials

All reagents and solvents were obtained from commercial vendors and used as received unless otherwise stated. ^1H NMR spectra were measured on an Agilent 400 MHz. ^1H and ^{13}C NMR chemical shifts are reported in ppm relative to internal solvent resonances unless otherwise stated. Yields refer to compounds as isolated after requisite purification unless otherwise stated. A Biotage Selekt flash purification system was used for automated silica gel column purification. Silica used for automated flash chromatography purifications was ZEOCHEM ZEOprep 60 HYD 40–63 μm pore size. Thin-layer chromatography (TLC) was performed on glass-backed silica plates and visualized by UV unless otherwise stated. High-resolution mass spectra were analyzed by flow injection analysis using a Shimadzu 9030 QTOF mass spectrometer interfaced with a Shimadzu 40 series UPLC. Size exclusion chromatography (SEC) was carried out in tetrahydrofuran (THF) at 1 mL min^{-1} at $30\text{ }^\circ\text{C}$ on two Agilent PLgel 10 μm MIXED–B columns connected in series with a Wyatt Dawn Heleos 2 light scattering detector and a Wyatt Optilab Rex refractive index detector. No calibration standards were used, and dn/dc values were

obtained by assuming 100% mass elution from the columns. The known dn/dc for PS of 0.185 mL/g was used for all macromonomer and bottlebrush polymer samples.

Preparation of Grubbs' 3rd generation catalyst (G3)

Grubbs' 3rd generation catalyst (G3) was prepared freshly and used within 2 days following a modified version of published methods.¹⁻² First, pyridine and pentane were purified via passage through a short column of basic alumina. A one dram vial was charged with a stir bar and 20 mg of Grubbs' 2nd generation catalyst (H₂Imes)(Pcy₃)(Cl)₂Ru=CHPh). Next, purified pyridine (20 μ L) was added to the vial, and the reaction mixture was stirred vigorously for 20–30 min until it had turned a vivid lime–green color. If the reaction mixture dried to a solid, additional pyridine (10 μ L increments) was added and solids were broken up manually with a spatula to allow for more stirring. Next, purified pentane (3 mL) was added to the vial to precipitate the catalyst. The pentane was decanted off, and the solids were washed with additional purified pentane (3 mL). Once again, the pentane was decanted off and the remaining solids were dried by blowing air over the vial for 1 min, then transferred to a clean vial, and then dried under vacuum overnight.

Monomer *exo*-norbornene benzoladderene [*xx*-NBL (1)]

Monomer *exo*-norbornene benzoladderene [*xx*-NBL (1)] was synthesized based on adaptations of a literature procedure.³ To a flame dried two–neck round-bottom flask equipped with a stir bar and an adapter for N₂, dioxane (65 mL) was added and degassed. Next, cesium carbonate (10 g, 33 mmol), norbornadiene (30 g, 330 mmol), and 4–bromotoluene (5.6 g, 33 mmol) were added followed by palladium acetate (0.28 g, 1.2 mmol) and triphenylphosphine

(0.66 g, 2.5 mmol). The reaction mixture was stirred at rt for 5 min and then refluxed for 24 h. The reaction mixture was cooled to rt, filtered, and the filtrate was concentrated by rotary evaporation. The crude product was purified by automated flash chromatography on silica with hexanes as the mobile phase to yield a colorless oil. (1.4 g, 24 % yield). ¹H NMR (CDCl₃): δ 7.02 (m, 1H), 6.96 (m, 1H), 6.91 (m, 1H), 6.24–6.19 (m, 2H), 3.13–3.08 (m, 2H), 2.78–2.74 (m, 2H), 2.34 (s, 3H), 1.28 (m, 1H), 0.89 (m, 1H). ¹³C NMR (CDCl₃): 146.12, 142.89, 136.67, 136.61, 127.68, 122.52, 121.45, 47.17, 46.99, 41.60, 41.53, 41.34, 22.01.

Compound 2–(2′–bromobenzyloxy)tetrahydropyran (I)

A round-bottom flask equipped with a stir bar was charged with 2–bromobenzyl alcohol (8.00 g, 42.8 mmol), 3,4–dihydro–2*H*–pyran (4.00 mL, 43.8 mmol), *p*–toluenesulfonic acid (0.20 g, 1.2 mmol), and CH₂Cl₂ (70 mL). The reaction mixture was stirred at rt for 16 h and then concentrated by rotary evaporation. The crude product was purified by automated flash chromatography on silica a hexanes/EtOAc gradient as the mobile phase to give compound **I** as a colorless oil (9.50 g, 82 % yield). ¹H NMR (CDCl₃): δ 7.56–7.46 (m, 2H), 7.30 (m, 1H), 7.13 (m, 1H), 4.81 (m, 1H), 4.76 (m, 1H), 4.56 (m, 1H), 3.96–3.86 (m, 1H), 3.60–3.52 (m, 1H), 1.88–1.55 (m, 6H). ¹³C NMR (CDCl₃): δ 138.4, 133.0, 129.4, 129.3, 127.9, 123.5, 98.9, 69.3, 62.5, 31.2, 26.0, 19.8. Both ¹H and ¹³C NMR spectra matched literature values.⁴

Compound *exo*-norbornene benzoladderene–*ortho*-Methoxytetrahydropyran (II)

Compound **I** (9.5 g, 35 mmol) was added to a flame dried two–neck round-bottom flask equipped with a stir bar, and adapter for N₂, along with degassed dioxane (100 mL). Cesium carbonate (11 g, 35 mmol) and norbornadiene (32 g, 350 mmol) were added to the round-bottom

flask. Palladium acetate (390 mg, 1.8 mmol) and triphenylphosphine (920 mg, 3.5 mmol) were then added to the reaction mixture. The reaction mixture was stirred at rt for 5 min and then refluxed for 24 h. The reaction mixture was cooled to rt, filtered and the filtrate was concentrated by rotary evaporation. The crude product was purified by automated flash chromatography on silica with 2% EtOAc in hexanes as the mobile phase to yield a yellow oil. The oil was then distilled under reduced pressure to give compound **II** as a colorless oil (1.50 g, 15.2 % yield). ¹H NMR (CDCl₃): δ 7.20–7.11 (m, 2H), 6.97 (m, 1H), 6.23–6.19 (m, 2H), 4.74 (m, 1H), 4.68 (m, 1H), 4.47 (m, 1H), 3.96–3.84 (m, 1H), 3.54 (m, 1H), 3.16 (m, 1H), 3.13–3.08 (m, 1H), 2.87–2.79 (m, 1H), 2.76 (m, 1H), 1.86–1.54 (m, 6H).

Compound *exo*-norbornene benzoladderene–ortho–2–bromo–2-Methylpropanoate (2–Br)

Compound **II** (1.5 g, 5.3 mmol) was dissolved in methanol (50 mL) in a round-bottom flask equipped with a stir bar. Next, *p*-toluenesulfonic acid (0.20 g, 1.2 mmol) was added and the reaction mixture was monitored until compound **II** was gone, about 2 h. The reaction mixture was concentrated by rotary evaporation, redissolved in CH₂Cl₂ (100 mL) and transferred to a separatory funnel. The organic solution was washed with saturated NaHCO₃ (3 x 20 mL) and brine (20 mL), dried over Na₂SO₄, and concentrated by rotary evaporation. Crude compound **III** (1.05 g, >99 % yield) was used immediately in the following step.

A flame dried two-neck round-bottom flask containing a stir bar and an N₂ adapter was charged with compound **III** (1.05 g, 5.31 mmol), NEt₃ (1.18 mL, 8.47 mmol), and dry THF (30 mL). The flask was placed in an ice bath and once cooled, α-bromoisobutyryl bromide (1.83 mL, 14.8 mmol) was added dropwise under N₂ atmosphere. The reaction mixture was stirred overnight, allowing the ice to melt and the contents of the flask to warm to rt. The reaction

mixture was filtered, the filtrate was concentrated by rotary evaporation, and the crude product was purified by automated flash chromatography on silica with an EtOAc/hexanes gradient as the mobile phase. The product was obtained as a colorless oil (0.77 g, 42 % yield). ¹H NMR (CDCl₃): δ 7.24–7.16 (m, 2H), 7.05 (m, 1H), 6.23 (t, *J* = 1.8 Hz, 2H), 5.24–5.09 (m, 2H), 3.24–3.14 (m, 2H), 2.84 (m, 2H), 1.95 (m, 6H), 1.30 (m, 1H), 0.86 (m, 1H). ¹³C NMR (CDCl₃): δ 171.98, 146.87, 145.31, 137.09, 129.62, 128.13, 127.01, 122.35, 98.85, 65.19, 56.13, 47.90, 47.35, 41.91, 41.85, 41.76, 31.29, 31.27.

Compound *exo*-norbornene benzoladderene-*Meta*-Methoxycarbonyl (IV)

To a flame dried two-neck round-bottom flask equipped with a stir bar and an adapter for N₂, dioxane (40 mL) was added and degassed. Cesium carbonate (4.2 g, 13 mmol), norbornadiene (13 mL, 130 mmol), and methyl 4-bromo-3-methylbenzoate (3.0 g, 13 mmol) were added to the round-bottom flask. Palladium acetate (0.15 g, 0.67 mmol) and triphenylphosphine (0.35 g, 1.3 mmol) were then added to the reaction mixture. The mixture was stirred at rt for 5 min and then refluxed for 24 h. The reaction mixture was cooled to rt and the solids were filtered off. The mixture was concentrated by rotary evaporation and the crude product was purified by automated flash chromatography on silica, eluting with 2% EtOAc in hexanes to yield a yellow oil. The oil was then distilled to yield compound **IV** as a colorless oil (1.25 g, 40 % yield).

Synthesis of *exo*-norbornene benzoladderene-*Meta*-Methanol (V)

LiAlH₄ (0.22 g) was dissolved in dry THF (5 mL) at 0 °C in a flame dried two-neck round-bottom flask equipped with a stir bar, an adapter for N₂, and an addition funnel. Compound **IV** (1.25g, 5.20 mmol) was dissolved in dry THF (5 mL) and added dropwise to the

LiAlH₄ suspension via addition funnel. The reaction was brought to rt and the addition funnel was replaced with a condenser. The reaction mixture was heated to reflux in an oil bath for 12 h then cooled to rt and placed in an ice bath again. Once cooled to 0 °C, 1N HCl was added dropwise slowly until no more foaming was observed. Brine was added to the solution until two separate layers formed and then the mixture was transferred to a separatory funnel. The top organic layer was collected and dried over Na₂SO₄ and was concentrated by rotary evaporation. The product was purified by automated flash chromatography on silica, eluting with 5% EtOAc in hexanes to yield compound **V** as a colorless oil (0.7 g, 60 % yield). ¹H NMR (CDCl₃): δ 6.99 (m, 1H), 6.94–6.90 (m, 1H), 6.24–6.21 (m, 2H), 4.62 (d, *J* = 5.5 Hz, 2H), 3.12–3.06 (m, 2H), 2.83–2.74 (m, 2H), 2.22 (s, 3H), 1.58 (m, 1H), 1.28 (m, 1H), 0.86 (m, 1H).

Compound *exo*-norbornene benzoladderene-*Meta*-2-bromo-2-Methylpropanoate (3-Br)

An oven-dried, two-neck round-bottom flask containing a stir bar and an adapter for N₂ was charged with compound **V** (0.70 g, 3.3 mmol), NEt₃ (1.0 mL, 7.2 mmol), and dry THF (16 mL). The flask was placed in an ice bath. Once cooled, α-bromoisobutyryl bromide (0.6 mL, 4.9 mmol) was added dropwise under N₂ atmosphere. The reaction mixture was stirred overnight, allowing the ice to melt and the contents of the flask to warm to rt. The reaction mixture was concentrated by rotary evaporation and the crude product was purified by automated flash chromatography on silica eluting with CH₂Cl₂ as the mobile phase. The product was obtained as a colorless oil (0.48 g, 40 % yield). ¹H NMR (CDCl₃): δ 6.99 (m, 1H), 6.92 (m, 1H), 6.22 (m, 2H), 5.15–5.12 (m, 2H), 3.09 (d, *J* = 1.1 Hz, 2H), 2.82–2.74 (m, 2H), 2.22 (m, 3H), 1.94 (s, 6H), 1.28 (m, 1H), 0.85 (m, 1H).

Synthesis of Polystyrene Macromonomers

A typical styrene polymerization procedure is as follows: Initiator (0.085 g, x mmol), styrene (7 mL, x mmol), CuBr (17 mg, x mmol), and CuBr₂ (26 mg, x mmol) were added to a 100 mL Schlenk tube equipped with a stir bar. The mixture in the Schlenk tube was deoxygenated by three freeze-pump-thaw cycles and then backfilled with N₂. The reaction mixture was submerged in an oil bath at 90 °C and after ~10 min, *N,N,N',N'',N''*-pentamethyldiethylenetriamine (PMDETA) (0.050 mL, x mmol) was injected under N₂ flow. The reaction mixture was heated in an oil bath maintained at 90 °C for about 3 h. An aliquot was removed via N₂-purged syringe and analyzed via ¹H NMR spectroscopy to ensure that ~10% conversion had been reached. At this point, the reaction was terminated by exposing the contents of the Schlenk tube to air. The reaction mixture was diluted with ethyl acetate (50 mL) and washed with water (3 x 20 mL) in a separatory funnel, and then the ethyl acetate layer was concentrated by rotary evaporation. The resultant PS-MM was dissolved in a small volume of THF and then purified by four successive precipitations into MeOH. Before the final precipitation, the product was purified further via passage through a short column of basic alumina using THF as the mobile phase. After the last precipitation, the polymer was recovered via filtration and then dried under vacuum overnight. The molar ratios of reagents for the ATRP reaction were [styrene]/[Initiator]/[CuBr]/[CuBr₂]/[PMDETA] 270:1:0.5:0.5:1 when targeting 3 kg/mol.

Evaluation of Propagation Rates of ROMP

A representative synthesis is as follows: Monomer/MM (40 mg, 100 equiv) was dissolved in CDCl₃ in a vial equipped with a stir bar. A stock solution of **G3** in CDCl₃ was made,

and 0.1 mL of this solution (to achieve 1 equiv with respect to monomer) was then added rapidly to the first vial to make the final concentration of monomer = 20 mmol. Polymerizations were conducted under air with capping of the vials in between aliquots. Aliquots (0.50 mL) were withdrawn periodically via micropipette at pre-determined timepoints and added to 1.5 mL Eppendorf microcentrifuge tubes containing 0.1 mL CDCl₃ and ethyl vinyl ether (2 μL) to terminate the polymerizations. Each aliquot was then analyzed by ¹H NMR spectroscopy or SEC.

Monomer Characterization:

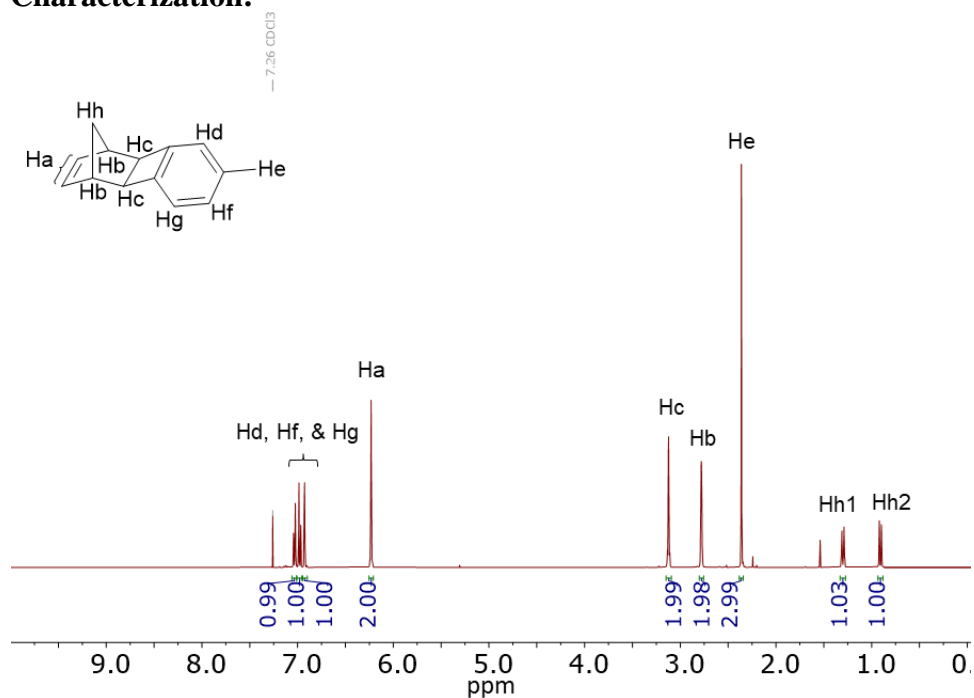


Figure S1. ¹H NMR spectrum of compound *xx*-NBL (**1**).

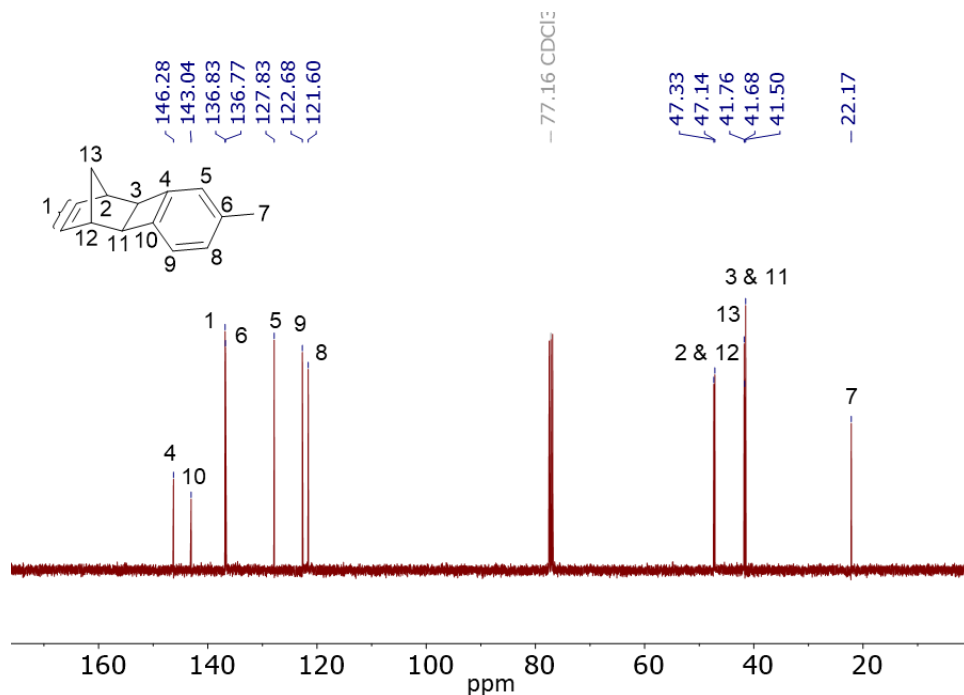


Figure S2. ¹³C NMR spectrum of compound *xx*-NBL (**1**).

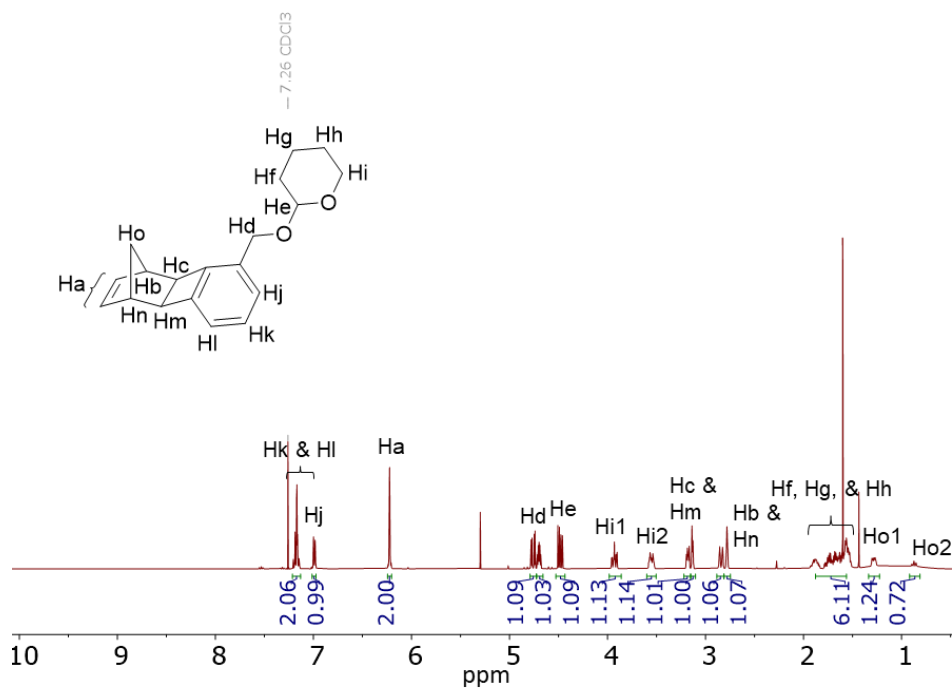


Figure S3. ¹H NMR spectrum of compound **II**.

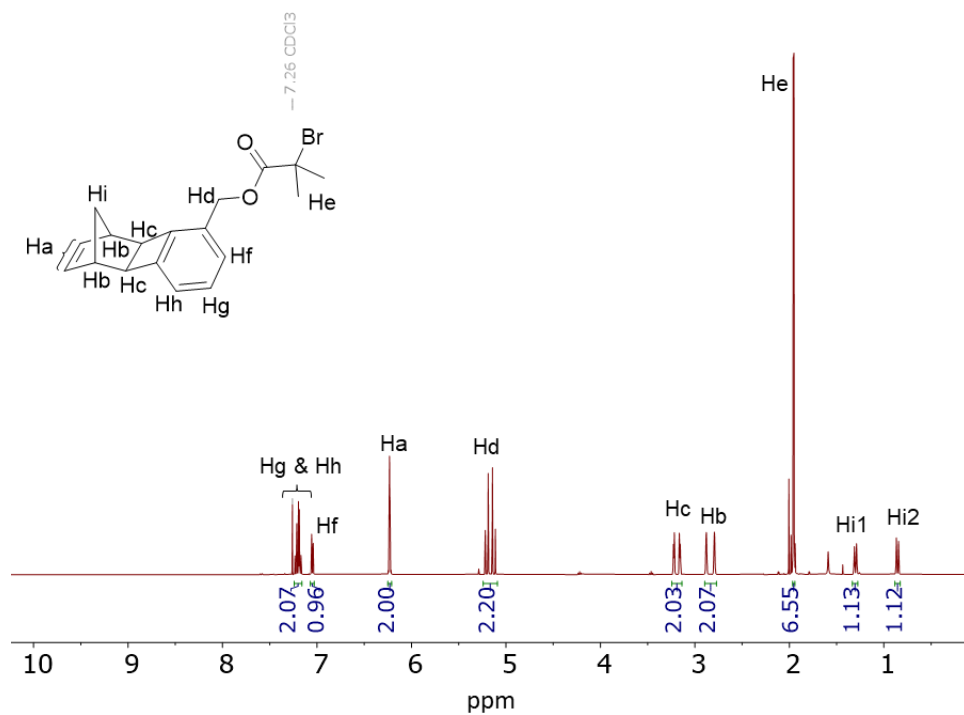


Figure S4. ¹H NMR spectrum of compound *xx*-NBL-*o*-Br (**2-Br**).

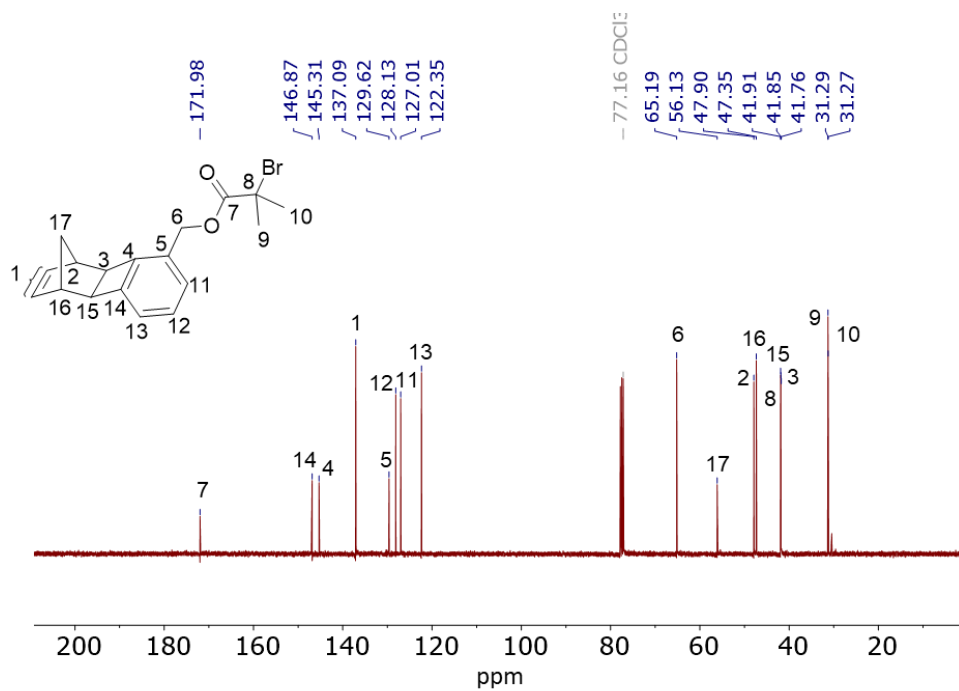


Figure S5. ¹³C NMR spectrum of compound *xx*-NBL-*o*-Br (**2-Br**).

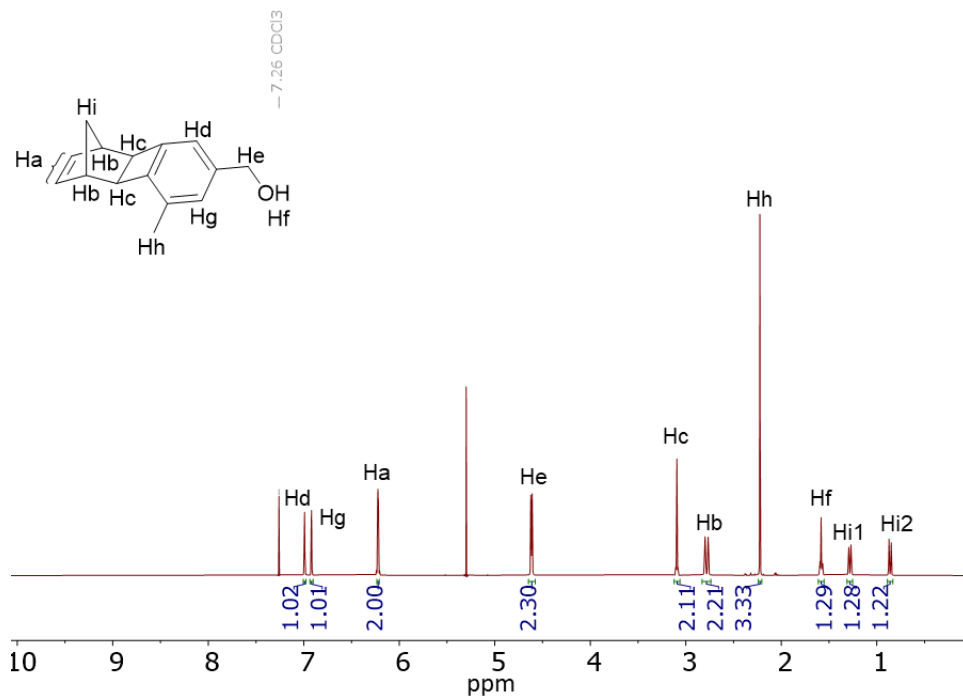


Figure S6. ^1H NMR spectrum of compound V.

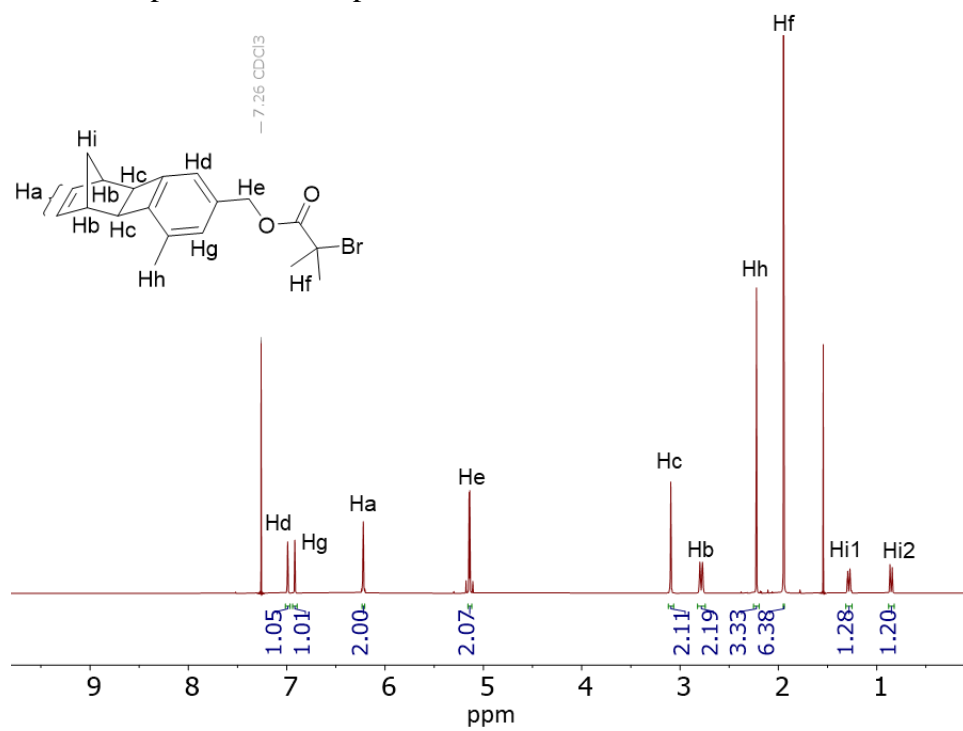


Figure S7. ^1H NMR spectrum of compound xx-NBL-M-Br (**3-Br**).

ROMP Kinetic Analysis

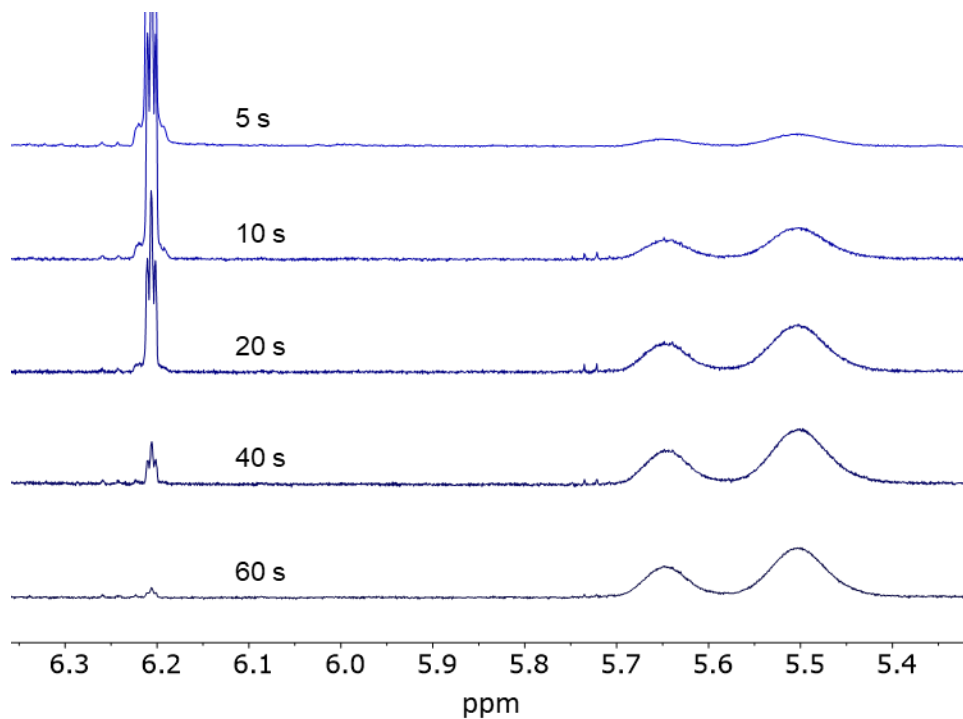


Figure S8. Representative spectra for H^1 NMR kinetics experiment of the ROMP of monomer *xx*-NBL (**1**). As the polymerization proceeds, the norbornene olefin resonance at ~ 6.2 ppm decreases in intensity and the polymer backbone resonance at 5.4–5.7 ppm increases in intensity.

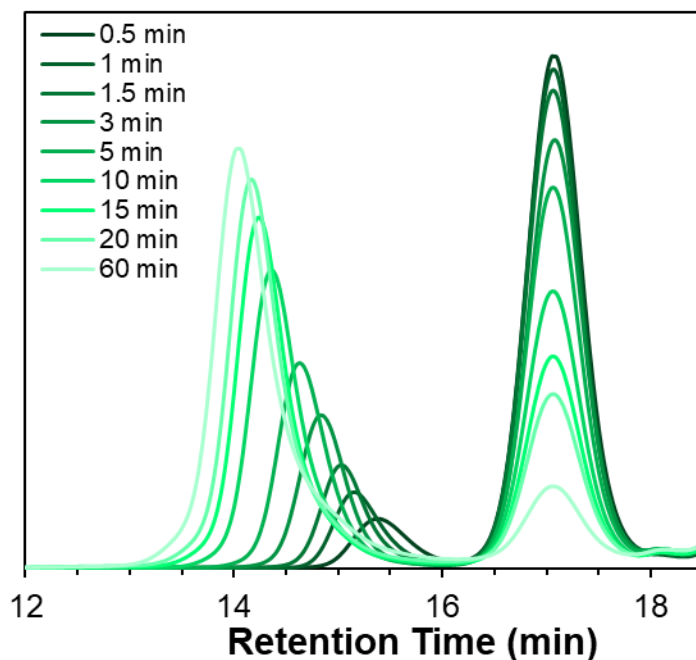


Figure S9. Representative SEC traces (dRI signal) of the ROMP of MM *xx*-NBL-*o*-PS (**2**) at an $[MM]/[G3]$ ratio of 100:1. As the polymerization proceeds, the MM signal at 17.2 min decreases

in intensity and the bottlebrush polymer signal increases in intensity and shifts in retention time from 15.2 min to 14 min.

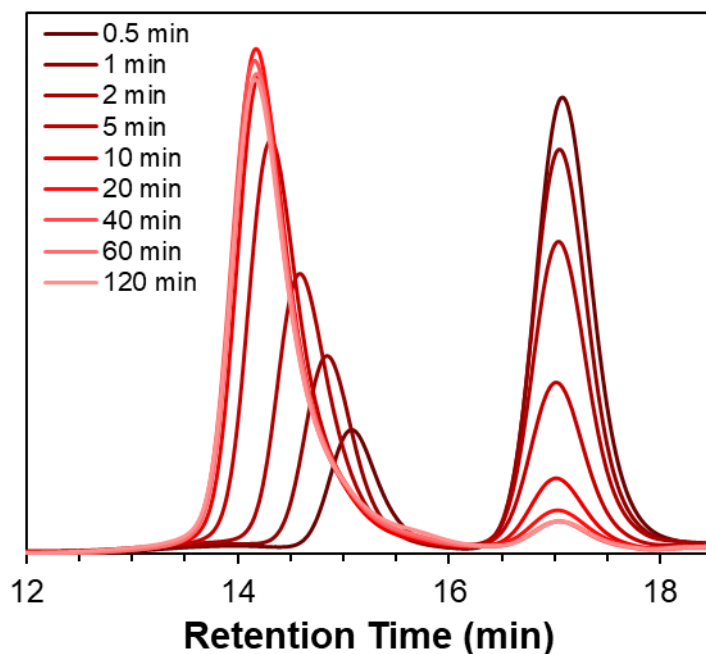


Figure S10. Representative SEC traces (dRI signal) of the ROMP of MM *xx*-NBL-*m*-PS (**3**) at an [MM]/[G3] ratio of 100:1. As the polymerization proceeds, the MM signal at 17.2 min decreases in intensity and the bottlebrush polymer signal increases in intensity and shifts in retention time from 15.2 min to 14 min.

Theoretical Calculations

All density functional theory calculations were performed using the Gaussian 09⁵ suite of software. The M06-2X functional and def2-TZVP basis set were used to optimize the geometries

with PCM solvation (chloroform) and an ultrafine integration grid. HOMO energies were obtained with the optimum structures.

Monomer *xx*-NBL (**1**)

Pi Energy (homo): -0.27673 Pi* energy (lumo+1): 0.02947

C	-7.848675	-2.677772	-0.056966
C	-8.665584	-2.316980	-1.107189
C	-8.803345	-3.096618	-2.246480
C	-8.127229	-4.289203	-2.396608
C	-7.294592	-4.661935	-1.336526
C	-7.144728	-3.884708	-0.184975
C	-9.650763	-1.266377	-1.590012
C	-11.087009	-1.281667	-0.995539
C	-11.557303	-2.707738	-1.336440

C	-11.310692	-2.549773	-2.848280
C	-9.807550	-2.155906	-2.889140
C	-12.036848	-1.236403	-3.096913
C	-11.904631	-0.487555	-2.003058
C	-6.213699	-4.326114	0.913304
H	-12.473155	-0.942362	-4.041622
H	-12.210874	0.541494	-1.874288
H	-12.611182	-2.855545	-1.107878
H	-10.962578	-3.492588	-0.871202
H	-9.258167	-0.259401	-1.723283
H	-9.513765	-1.705355	-3.836054
H	-11.155468	-0.967923	0.043083
H	-11.582106	-3.385519	-3.488386
H	-8.217933	-4.918312	-3.273555
H	-6.739677	-5.590771	-1.403871
H	-7.736179	-2.074810	0.837485
H	-5.302314	-3.724318	0.913654
H	-6.679770	-4.210394	1.892494
H	-5.925289	-5.369298	0.791821

MM *xx*-NBL-*o*-PS₁ (2)

Pi energy (homo): -0.28408 Pi* energy (lumo+3): 0.02207

C	-3.984952	-0.431662	-1.593606
C	-2.472298	-0.226770	-1.797990
C	-1.890061	-0.768266	-0.463106
C	-2.865003	-1.965399	-0.121762
C	-3.859113	-1.940930	-1.316760
C	-3.005629	-2.354990	-2.506816
C	-2.188358	-1.342157	-2.792272
C	-2.372150	-0.132656	0.824977
H	-3.003544	-3.341490	-2.949578
H	-1.383560	-1.334318	-3.514890
H	-4.549790	-0.228583	-2.501533
H	-4.400708	0.137522	-0.763323
H	-0.825900	-0.993306	-0.518782
H	-2.413609	-2.943663	0.035740
H	-2.136068	0.771162	-2.068898
H	-4.778777	-2.498878	-1.159848
C	-3.228863	-1.181544	1.128544
C	-4.030573	-1.180965	2.251317
C	-3.923067	-0.054057	3.072567
C	-3.062132	0.996854	2.767724
C	-2.258182	0.990091	1.621471
H	-4.703327	-1.990825	2.503325
H	-4.518256	0.007055	3.974975
C	-1.373424	2.157141	1.302583

O	-0.381094	1.730577	0.366528
H	-1.945083	2.977716	0.862051
H	-0.884904	2.541694	2.199315
C	0.526766	2.647586	0.008432
O	0.504914	3.776799	0.425214
C	1.564467	2.079061	-0.950073
C	2.323680	0.979712	-0.175569
C	0.839791	1.493421	-2.169262
C	2.495279	3.208434	-1.380571
C	3.464399	0.318167	-0.954581
H	2.733995	1.411075	0.743471
H	1.610197	0.209595	0.127171
H	3.204164	2.846323	-2.124533
H	1.925766	4.025943	-1.822364
H	3.050822	3.606041	-0.530776
H	1.563345	1.206884	-2.932196
H	0.254476	0.615780	-1.895070
H	0.168050	2.232023	-2.611252
C	4.092612	-0.786013	-0.145448
H	3.083755	-0.093254	-1.891627
H	4.224620	1.059190	-1.206429
C	5.187307	-0.533723	0.677460
C	5.739150	-1.541562	1.457537
C	5.200295	-2.820880	1.425556
C	4.107207	-3.084259	0.609562
C	3.559418	-2.073044	-0.167588
H	5.612928	0.463295	0.703339
H	6.592583	-1.328109	2.088555
H	5.630373	-3.608485	2.030534
H	3.682600	-4.079591	0.576575
H	2.706935	-2.283278	-0.804629
H	-3.011029	1.843932	3.442772

MM *xx*-NBL-*m*-PS₁ (3)

Pi energy (homo): -0.28194 Pi* energy (lumo+3): 0.02287

C	-3.250997	1.715444	1.335284
C	-2.879550	2.417370	0.015902
C	-3.239599	1.333473	-1.038416
C	-4.520910	0.652975	-0.406561
C	-4.708593	1.449237	0.915558
C	-5.105381	2.841377	0.447761
C	-4.025553	3.412989	-0.083177
C	-2.575220	-0.026684	-0.916804
H	-6.114979	3.228601	0.451889
H	-3.974951	4.361159	-0.600496
H	-3.188394	2.389624	2.187485

H	-2.674924	0.812513	1.533184
H	-3.337171	1.736436	-2.045173
H	-5.422045	0.627878	-1.018104
H	-1.873647	2.820959	-0.069299
H	-5.360667	0.976636	1.646070
C	-3.697870	-0.621953	-0.361848
C	-3.737699	-1.948647	0.025212
C	-2.544346	-2.651633	-0.188495
C	-1.408665	-2.066445	-0.748743
C	-1.403329	-0.718716	-1.131696
C	-4.949675	-2.585805	0.639877
H	-2.498723	-3.698844	0.092584
C	-0.167621	-2.885929	-0.949259
H	-0.515473	-0.274784	-1.567425
O	0.872499	-2.314513	-0.137510
H	-0.317877	-3.925015	-0.656092
H	0.162499	-2.868472	-1.989097
H	-4.834072	-3.666120	0.715636
H	-5.125083	-2.192135	1.643271
H	-5.841692	-2.373496	0.048658
C	2.101641	-2.814903	-0.302530
O	2.338935	-3.722080	-1.058516
C	3.127938	-2.090361	0.559494
C	3.135904	-0.618315	0.093051
C	2.695802	-2.204975	2.027567
C	4.487614	-2.751320	0.356651
C	4.177622	0.270109	0.779692
H	3.314684	-0.589534	-0.987213
H	2.144114	-0.192761	0.261364
H	5.223501	-2.306643	1.026132
H	4.430489	-3.817880	0.572905
H	4.833137	-2.634234	-0.671147
H	3.461817	-1.782007	2.677176
H	1.757101	-1.680964	2.204389
H	2.566171	-3.251906	2.307990
C	4.048330	1.696267	0.312627
H	4.043369	0.231016	1.862594
H	5.182856	-0.092801	0.560128
C	4.787968	2.162485	-0.771221
C	4.633829	3.463635	-1.232039
C	3.732635	4.319569	-0.612940
C	2.988141	3.865405	0.468609
C	3.146011	2.563970	0.924673
H	5.494540	1.498195	-1.256409
H	5.220346	3.810031	-2.073534
H	3.613138	5.334753	-0.968511

H 2.285957 4.527180 0.959742
H 2.563941 2.213660 1.770147

4.9 Supporting Information References

- 1 Au – Liu, J.; Au – Gao, A. X.; Au – Johnson, J. A., Particles without a Box: Brush–first Synthesis of Photodegradable PEG Star Polymers under Ambient Conditions. *JoVE* 2013, e50874.
- 2 Love, J. A.; Morgan, J. P.; Trnka, T. M.; Grubbs, R. H., A Practical and Highly Active Ruthenium-based Catalyst that Effects the Cross Metathesis of Acrylonitrile. *Angew. Chem* 2002, 41, 4035–4037.
- 3 Liu, S.; Jin, Z.; Teo, Y. C.; Xia, Y., Efficient Synthesis of Rigid Ladder Polymers via Palladium Catalyzed Annulation. *J. Am. Chem. Soc.* 2014, 136, 17434–17437.
- 4 Park, H. J.; Choi, J. H.; Park, B. N.; Yoon, U. C.; Cho, D. W.; Mariano, P. S., A strategy for the preparation of cyclic polyarenes based on single electron transfer–promoted photocyclization reactions. *Research on Chemical Intermediates* 2012, 38, 847–862.

Chapter 5: Effects of reaction atmosphere in Ru-mediated ring-opening metathesis polymerization

5.1 Authors

Samantha J. Scannelli, Daniela Samaniego Gonzalez, Clark Vu, and John B. Matson*

Department of Chemistry, Virginia Tech, Blacksburg, VA 24061, United States

Macromolecules Innovation Institute, Virginia Tech, Blacksburg, VA 24061, United States

5.2 Abstract

Ring-opening metathesis polymerization (ROMP) mediated by Grubbs' third generation catalyst, $(\text{H}_2\text{IMes})(\text{Cl})_2(\text{pyr})_2\text{RuCHPh}$, exhibits living characteristics for many (macro)monomers. However, decomposition of the catalyst chain end limits the maximum achievable degree of polymerization, especially for sterically demanding macromonomers (MM). Catalyst decomposition also limits chain extension efficiency in multiblock copolymers. Here we systematically measured how polymerization atmosphere affects livingness in ROMP of four different norbornene-based (macro)monomers with variable polymerization rates. We synthesized pseudo-pentablock copolymers in CH_2Cl_2 using two small molecule monomers and two polystyrene MMs under three different atmospheres: open to air, under N_2 on a Schlenk line, and in an N_2 -filled glovebox. Following the evolution of molecular weight and dispersity (D) values throughout the pseudo-pentablock copolymer synthesis, we found little improvement in block extension efficiency due to the change in atmosphere, regardless of propagation rate. Polymerization atmosphere condition did not change the molecular weight values reached or the

D of the overall polymer structures. Inert atmosphere did lower the apparent D values of the individual blocks but only for the bottlebrush pseudo-pentablock copolymers. Nevertheless, inert atmosphere did not improve livingness in ROMP for these chain-Extension studies.

5.3 Introduction

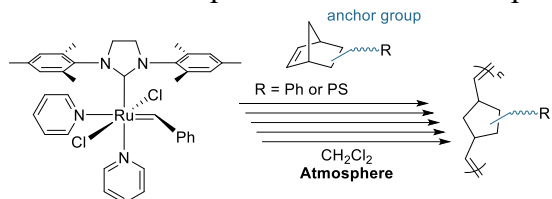
Ring-opening metathesis polymerization (ROMP) has emerged as a useful method for polymer synthesis, particularly for the synthesis of complex polymer structures.¹ ROMP utilizes fast-Initiating catalysts (initiators), the most popular based on ruthenium, to polymerize high-strain, cyclic olefin monomers at relatively high propagation rates (k_p).² Along with high k_p , ROMP in most cases experiences low termination rates (k_t), which permits ROMP to exhibit living characteristics (i.e., livingness).³⁻⁴ Livingness describes chain polymerizations where termination and chain transfer are absent and is particularly important for maintaining control over molecular weight and dispersity (D) of the resulting polymers.⁵⁻⁷ High livingness in ROMP allows for the synthesis of well-defined bottlebrush polymers, through the polymerization of macromonomers (MMs) known as the grafting-through technique.⁸⁻⁹ However, bottlebrush polymers generated by ROMP grafting-through tend to be small due to the loss of living character when polymerizing even moderately sized MMs (5–10 kg/mol) to moderate degrees of polymerization ($DP = 100$ – 200) as a result of lower k_p values typically observed for MMs than for small molecule monomers.¹⁰ Because the ROMP catalyst must remain active for longer durations when polymerizing lower k_p MMs compared to higher k_p MMs, the ongoing polymerization experiences a greater amount of chain termination, which reduces the overall livingness in ROMP. Thus, further optimization of the factors that affect livingness in ROMP is needed.

Many reaction conditions affect the efficiency of ROMP.¹¹ Our group has previously shown that both solvent and (macro)monomer structure greatly impact k_p in ROMP and that enhancing k_p can improve livingness as well.^{12–14} Specifically, solvent choice not only increased k_p of different MMs, but also affected catalyst decomposition significantly. Therefore, choosing a solvent that provides high k_p and low k_t enhanced the livingness in ROMP of various MMs.¹² Another common experimental condition that affects a wide range of polymerizations is reaction atmosphere. The presence of oxygen is detrimental for reversible deactivation radical polymerizations (RDRPs), such as atom–transfer radical polymerization (ATRP), as AIR reacts with active radicals to generate dead chains.¹⁵ In ROMP, the choice of atmosphere is often dictated by the catalyst. Initially, tungsten and molybdenum catalysts developed by Schrock dominated ROMP for their high living character.^{16–17} However, these catalysts are restricted by their low functional group tolerance along with sensitivity to air and protic solvents. The introduction of Ru-based catalysts developed by Grubbs,¹⁸ broadened the scope of ROMP due to the higher functional group tolerance than W– and Mo-based catalysts and the relative insensitivity to air and water of Ru complexes.^{19–20} Even though Ru-based catalysts are more tolerant of various atmospheres than W– or Mo-based catalysts, many researchers continue to perform ROMP under inert atmospheres. To our knowledge, no systematic study exists reporting the difference in the living character of Ru-mediated ROMP based on reaction atmosphere.

Here our goal was to evaluate differences in livingness in ROMP under three reaction atmospheres through the synthesis of pseudo-pentablock copolymers (Scheme 5.1), with the hypothesis that inert atmospheres would lead to higher livingness in ROMP. High livingness in block copolymer synthesis is critical for complete chain extension, so to evaluate the effect of atmosphere on chain extension, we conducted a series of studies on the synthesis of linear and

bottlebrush pseudo-pentablock copolymers. A recent report by Harrison suggested that the individual substructures of complex polymer structures may be more disperse than the overall polymer structure even if the overall D remains low.²¹ Using this mathematical method of estimating the apparent D of each individual block in a linear multiblock copolymer synthesis, we aimed to compare chain extension in ROMP under ambient and inert atmospheres by following the evolution of molecular weight and D for each block.

Scheme 5.1. Representative scheme of pseudo-pentablock copolymer synthesis via ROMP



5.4 Results and Discussion

5.4.1 Atmosphere Choice

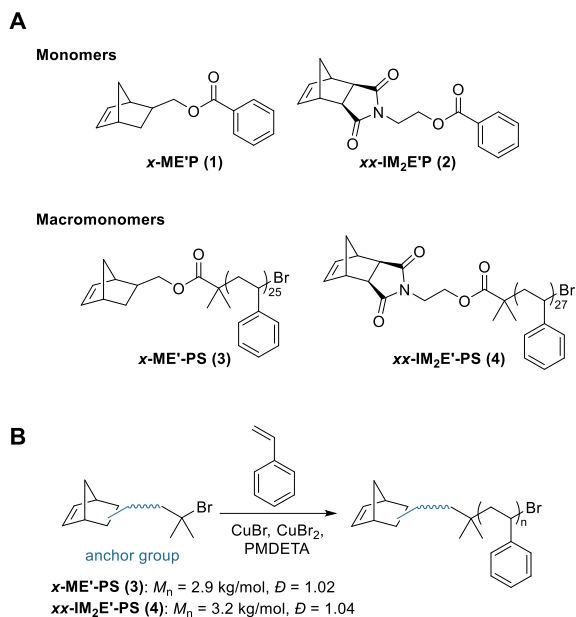
We set out to investigate the effects of three reaction atmospheres on Ru-mediated ROMP: air, N_2 on the Schlenk line, and in an N_2 -filled glovebox. Although G3 catalyst generally tolerates air and water, many researchers perform ROMP in gloveboxes. Therefore, we chose to compare ROMP polymers synthesized in an N_2 -filled glovebox to those synthesized open to air and those synthesized under N_2 using Schlenk line techniques. We envisioned that the N_2 -filled glovebox would provide an atmosphere with the lowest level of oxygen and that the Schlenk line would provide a similarly inert atmosphere. For N_2 atmospheres, we used standard Schlenk line procedures for drying and glassware along with the use of degassed solvent. We used degassed CH_2Cl_2 from solvent drying columns, charged with activated alumina, for all atmospheres. For polymerizations on the Schlenk line or in the glovebox, solvent was stored in a Strauss flask and

used directly from the flask or was transferred into the glovebox. Under ambient conditions, we used the solvent immediately after removal from the columns.

5.4.2 (Macro)monomer Design and Synthesis

To investigate the effects of reaction atmosphere on the livingness in ROMP, we designed a series of (macro)monomers containing two different anchor groups, the series of atoms directly attached to the polymerizable norbornene.²²⁻²³ We chose an *exo* ester-based group and an *exo* imide-based group to use in both monomer and MM form (Scheme 5.2A). In previous work, we reported that these two anchor groups had significantly different k_p values in both monomers and MMs, which greatly impacted the livingness in ROMP.¹³⁻¹⁴ Therefore, using different anchor groups allows us to probe the effects of atmospheric conditions on ROMP at high k_p and low k_p values. Here we studied two monomer structures [*x*-ME'P (**1**) and *xx*-IM₂E'P (**2**)] and two polystyrene (PS) MM structures [*x*-ME'-PS (**3**) and *xx*-IM₂E'-PS (**4**)] to compare the livingness under ambient and inert atmospheres for the synthesis of linear and bottlebrush polymers.

Scheme 5.2. Norbornene (macro)monomers with different anchor groups used in ROMP (A). Representative ATRP synthesis of PS MMs (B).



^a(A) All monomers exhibited *exo* (*x* prefix) or *exo-Exo* (*xx* prefix) stereochemistry. Letters identify structural components of the anchor group from left to right (M = methylene, E' = ester with carbonyl on the right, I = imide); all MM side-chains are polystyrene (PS). Subscripts indicate the number of times that component is repeated. (B) ATRP reactions were conducted at 90 °C for 3 h.

Monomers *x*-ME'P (**1**) and *xx*-IM₂E'P (**2**) were synthesized according to previously reported procedures.^{13–14} Two PS MMs with number-average molecular weight values (M_n) close to 3 kg/mol were synthesized through the use of two norbornene initiators and ATRP (Scheme 5.2B). Polymerizations were carried out under typical conditions for PS at 90 °C for 3 h. Following ATRP, the crude MMs were dissolved in ethyl acetate and stirred with water to remove residual Cu species. Next, we used automated silica gel chromatography with an ethyl acetate/hexane gradient as the mobile phase for further purification. After isolating the MM from

the column and the removal of solvent, the MMs were passed through basic alumina in tetrahydrofuran (THF) and then precipitated into methanol to afford the final MM products as white powders. Both MMs were then analyzed by size exclusion chromatography (SEC) to determine M_n and dispersity (D); MM x -ME'-PS (**3**) had an M_n value of 2.9 kg/mol with a D of 1.02 and MM xx -IM₂E'-PS (**4**) had an M_n of 3.2 kg/mol and a D of 1.04.

5.4.3 Kinetic Analysis of ROMP

Our goal was to measure any differences in livingness among the three atmospheres by following the evolution of molecular weight and D in the synthesis of linear and bottlebrush pseudo-pentablock copolymers. We envisioned that five consecutive injections of (macro)monomer would provide a clean comparison by following molecular weight evolution over time as compared with expected values, as well as evolution of D values. This pseudo-pentablock synthesis strategy mimics the synthesis of complex bottlebrush polymer topologies while avoiding complications introduced by adding different types of monomers with variable k_p values, functionalities, and potential trace contaminants.

Prior to the pentablock synthesis, we conducted kinetics experiments for each (macro)monomer to determine the time required to reach near-complete conversion (>95%) for each block. Polymerizations of all (macro)monomers were mediated by G3 catalyst with a concentration of 20 mM in CH₂Cl₂ at room temperature. We chose CH₂Cl₂ for its high relatively k_p and low k_t which provides high livingness in ROMP. For these kinetics experiments, we used a (macro)monomer/G3 ratio equal to the DP we targeted for each block in the subsequent pseudo-pentablock syntheses. Therefore, we targeted a DP = 100 for monomers x -ME'P (**1**) and xx -IM₂E'P (**2**) and a DP = 50 for MMs x -ME'-PS (**3**) and xx -IM₂E'-PS (**4**). We targeted DPs that

would challenge the catalyst during pentablock synthesis, resulting in lower than expected M_n values and large D values, to ensure any improvement in the living chain end would be observed.

All kinetics experiments were performed under ambient conditions (under air at room temperature) with the assumption that k_p in each atmosphere would be comparable, ensuring that all polymerizations would have adequate time to reach 95% conversion for each injection. Aliquots were removed throughout the polymerizations and terminated with excess ethyl vinyl ether at predetermined time intervals. Solvent was removed by evaporation under air from all aliquots before analysis. Aliquots for small molecule monomers x -ME'P (**1**) and xx -IM₂E'P (**2**) were analyzed by ¹H NMR spectroscopy, and monomer conversion was determined by comparing the integration of the polymer backbone olefins to the olefin protons of the monomer. Aliquots for MMs x -ME'-PS (**3**) and xx -IM₂E'-PS (**4**) were analyzed by SEC. Small molecular measuring conversion at each time point by comparing the areas of the MM peak and bottlebrush polymer peak in the dRI trace. Conversion versus time data are shown in Figure 5.1 for (macro)monomers **1–4**.

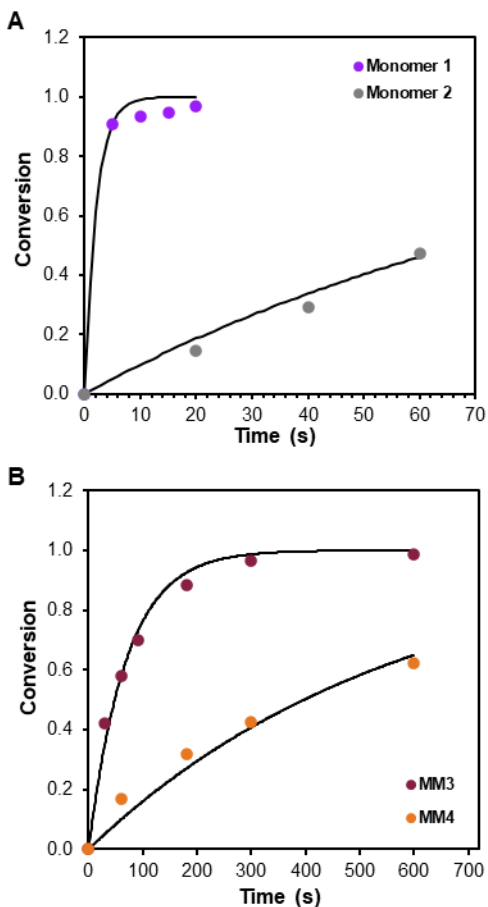


Figure 5.1. (A) Kinetic analysis of monomers *x*-ME'P (**1**) and *xx*-IM₂E'P (**2**) in CH₂Cl₂ with G3 catalyst at a [monomer]/[G3] ratio of 100:1 and [monomer] = 20 mM. The solid line represents the fit to the averaged conversion data based on the equation $p = 1 - e^{(-k_p t)}$ where p = fractional conversion. (B) Kinetic analysis of the ROMP of MMs *x*-ME'-PS (**3**) and *xx*-IM₂E'-PS (**4**) in CH₂Cl₂ at an [MM]/[G3] ratio of 50:1 and [MM] = 20 mM. The solid line represents the fit to the averaged conversion data based on the equation $p = 1 - e^{(-k_p t)}$ where p = fractional conversion.

Based on a previous report, ROMP generally exhibits a high k_p and high livingness in CH₂Cl₂,¹² making it difficult to obtain proper kinetics experiments for monomer *x*-ME'P (**1**). Monomer *x*-ME'P (**1**) reached 90% conversion in the first 5 s of the polymerization in CH₂Cl₂,

therefore, we assumed a half-life of <3 s for monomer *x*-ME'P (**1**). Consistent with our previous study,¹³ monomer *xx*-IM₂E'P (**2**) showed a lower $k_{p,obs}$ value compared to monomer *x*-ME'P (**1**). MM *xx*-IM₂E'-PS (**4**) had a $k_{p,obs}$ six times lower than MM *x*-ME'-PS (**3**). Ultimately, monomers containing the anchor group *x*-ME' (**1** and **3**) had significantly higher k_p values than monomers with the anchor group *xx*-IM₂E' (**2** and **4**), as expected (Table 5.1). Additionally, both MMs were significantly slower than the analogous monomer containing the same anchor group. These results were expected as k_p decreases with increasing molecular weight.¹⁰ Regardless of k_p , all (macro)monomers reached high conversion and with M_n values determined by SEC matching targeted M_n values while maintaining low dispersities, which is crucial for proper chain extension of at least one block in the pentablock copolymer synthesis.

Table 5.1. Polymerization kinetics and polymer characterization for ROMP of (macro)monomers **1–4**

MM	$k_{p,obs}^a$ (s ⁻¹)	$t_{1/2}$ (s)	% conv ^b	Final $M_{n,expected}^c$ (kg/mol)	Final $M_{n,SEC}^d$ (kg/mol)	Final \bar{D}^d
<i>x</i> -ME'P (1)	>0.4	<3	>99	23	26	1.02
<i>xx</i> -IM ₂ E'P (2)	0.010	67	>99	31	32	1.01
<i>x</i> -ME'-PS (3)	0.014	48	97	145	148	1.02
<i>xx</i> -IM ₂ E'-PS (4)	0.002	288	95	160	150	1.01

^aCalculated from conversions measured by ¹H NMR spectroscopy (**2**) or SEC (**3–4**) on aliquots removed at specific time points during the polymerizations. ^bMeasured on the final sample of the kinetics runs using ¹H NMR spectroscopy (**1–2**) by comparing the integrations of the polymer backbone olefin protons to the monomer olefin protons or SEC (**3–4**) by comparing the areas of the bottlebrush polymer and MM peaks in the dRI trace. ^cDetermined using the equation $M_{n,expected} = M_{n,initial} * \text{conv} * ([MM]/[G3])_0$ where $M_{n,initial}$ is either the molecular weight of the monomer (**1–2**) or the $M_{n,SEC}$ measured for the MM structure (**3–4**). ^dMeasured on the final sample of the kinetics runs by SEC in THF at 30 °C with multiangle light scattering either by mass recovery (**1–2**) or using the known dn/dc for PS of 0.185 mL/g (**3–4**).

5.4.4 Pentablock Copolymer Synthesis and Analysis

Block copolymer synthesis requires high livingness for complete chain extension; therefore, we analyzed the synthesis of linear and bottlebrush pseudo-pentablock copolymers under the three different conditions noted above—air, Schlenk line under N₂ and an in N₂-filled glovebox. Using five consecutive additions of the same (macro)monomer, in a process termed sequential addition of (macro)monomers ROMP (SAM-ROMP), we synthesized linear or bottlebrush pentablock copolymers of (macro)monomers **1–4** separately. We envisioned that removing an aliquot of the reaction mixture before each injection of new (macro)monomer would allow us to follow the evolution of molecular weight and \bar{D} over the course of each block addition. This systematic study would allow us to determine which atmosphere provided the most living chain end during ROMP.

All SAM-ROMP experiments were conducted at room temperature and with the same initial (macro)monomer concentration (20 mM). For linear pentablock copolymers, we targeted a DP of 100 for each monomer addition. We allowed each block addition to polymerize for ≥ 6 propagation half-lives before the next addition of monomer (1 and 10 min for monomers **1** and **2**, respectively). Aliquots were removed and terminated right before the next monomer addition to determine monomer conversion by ¹H NMR spectroscopy and M_n and \bar{D} by SEC (Table 5.2).

Table 5.2. Characterization of Linear Pentablock Copolymers Prepared by SAM-ROMP

Monomer	Atmosphere	Block #	% conv ^a	$M_{n,expected}^b$ (kg/mol)	$M_{n,SEC}^c$ (kg/mol)	\bar{D}^c	Apparent \bar{D}^d
<i>x</i> -ME'P (1)	air	1	>99	23	23 ± 2	1.02 ± 0.004	1.02 ± 0.004
		2	>99	51	49 ± 3	1.04 ± 0.02	1.13 ± 0.06
		3	>99	84	72 ± 3	1.09 ± 0.04	1.70 ± 0.3
		4	>99	119	93 ± 5	1.15 ± 0.06	2.9 ± 0.9
		5	>99	156	110 ± 6	1.22 ± 0.08	5.9 ± 2
	N ₂ (Schlenk line)	1	>99	23	24 ± 1	1.01 ± 0.001	1.01 ± 0.002
		2	>99	51	52 ± 3	1.03 ± 0.005	1.07 ± 0.02
		3	>99	84	82 ± 3	1.04 ± 0.001	1.23 ± 0.03
		4	>99	119	103 ± 8	1.11 ± 0.02	3.2 ± 1
		5	>99	156	120 ± 10	1.16 ± 0.01	6.0 ± 1
	N ₂ (Glovebox)	1	>99	23	19	1.05	1.05
		2	>99	51	41	1.06	1.17
		3	>99	84	61	1.09	1.59
		4	>99	119	79	1.16	3.18
		5	>99	156	91	1.25	8.74
<i>xx</i> -IM ₂ E'P (2)	air	1	>99	31	32 ± 1	1.01 ± 0.001	1.01 ± 0.002
		2	>99	70	63 ± 8	1.05 ± 0.03	1.21 ± 0.2
		3	>99	113	95 ± 10	1.10 ± 0.05	1.72 ± 0.4
		4	>99	160	120 ± 20	1.17 ± 0.04	4.0 ± 0.3
		5	>99	210	130 ± 20	1.22 ± 0.03	6.1 ± 0.6
	N ₂ (Schlenk line)	1	>99	31	37	1.01	1.01
		2	>99	70	62	1.04	1.22
		3	>99	113	82	1.10	2.37
		4	>99	160	104	1.19	3.75
		5	>99	210	121	1.24	6.25
	N ₂ (Glovebox)	1	>99	31	26	1.01	1.01
		2	>99	70	58	1.02	1.06
		3	>99	113	90	1.06	1.40
		4	>99	160	120	1.12	2.46
		5	>99	210	147	1.18	3.96

^aMeasured using ¹H NMR spectroscopy by comparing the integrations of the polymer backbone olefin protons to the monomer olefin protons. ^bDetermined using the equation $M_{n,expected} = MW_{mon} * ([MM]/[G3])_0$. ^cDispersity value for the aliquot as measured using SEC in THF at 30 °C with multiangle light scattering by mass recovery. ^dDispersity value for the individual block as estimated using the method developed by Harrisson using the formula $\bar{D}_2 = 1 + \frac{\mu_{1+2}^2(\bar{D}_{1+2} - 1) - \mu_1^2(\bar{D}_1 - 1)}{(\mu_{1+2} - \mu_1)^2}$ where \bar{D}_2 is the apparent dispersity in terms of the number-average molar masses of the initial (μ_1) and final (μ_{1+2}) polymers and the overall dispersity of the initial (\bar{D}_1) and final (\bar{D}_{1+2}) polymers.²¹

Both monomers reached >99% conversion for each block addition, based on ^1H NMR spectroscopy, under all three atmospheres. We observed a decrease in the retention time of the primary SEC peak with the polymerization of each additional block for both monomers. The first block addition for both monomers also reached targeted M_n values while maintaining low \mathcal{D} values (≤ 1.05), as expected based on our kinetics experiments. However, we observed low molecular weight tails in the SEC traces, indicative of chain termination, of later block additions (blocks three, four, or five) in many cases (Figure 5.2). Monomer *x*-ME'P (**1**) experienced low molecular weight tails for blocks four and five when polymerized open to air. This was expected because we targeted a DP where chain termination occurred under ambient conditions to ensure any decrease in chain death due to the change in atmosphere could be visualized by SEC. While we expected the low molecular weight tails to decrease in area for SAM-ROMP reactions run in the other two conditions, the SEC traces for the fourth and fifth block additions of monomer *x*-ME'P (**1**) looked similar when reactions were conducted under an N_2 atmosphere on both a Schlenk line and in a glovebox. Monomer *xx*-IM₂E'P (**2**) also experienced low molecular weight tails, but in all blocks except for the first when polymerized open to air. The size of these tails seemed to decrease when monomer *xx*-IM₂E'P (**2**) was polymerized under N_2 atmosphere on both a Schlenk line and in a glovebox, but to a marginal degree. Therefore, further analysis of M_n and \mathcal{D} values was needed.

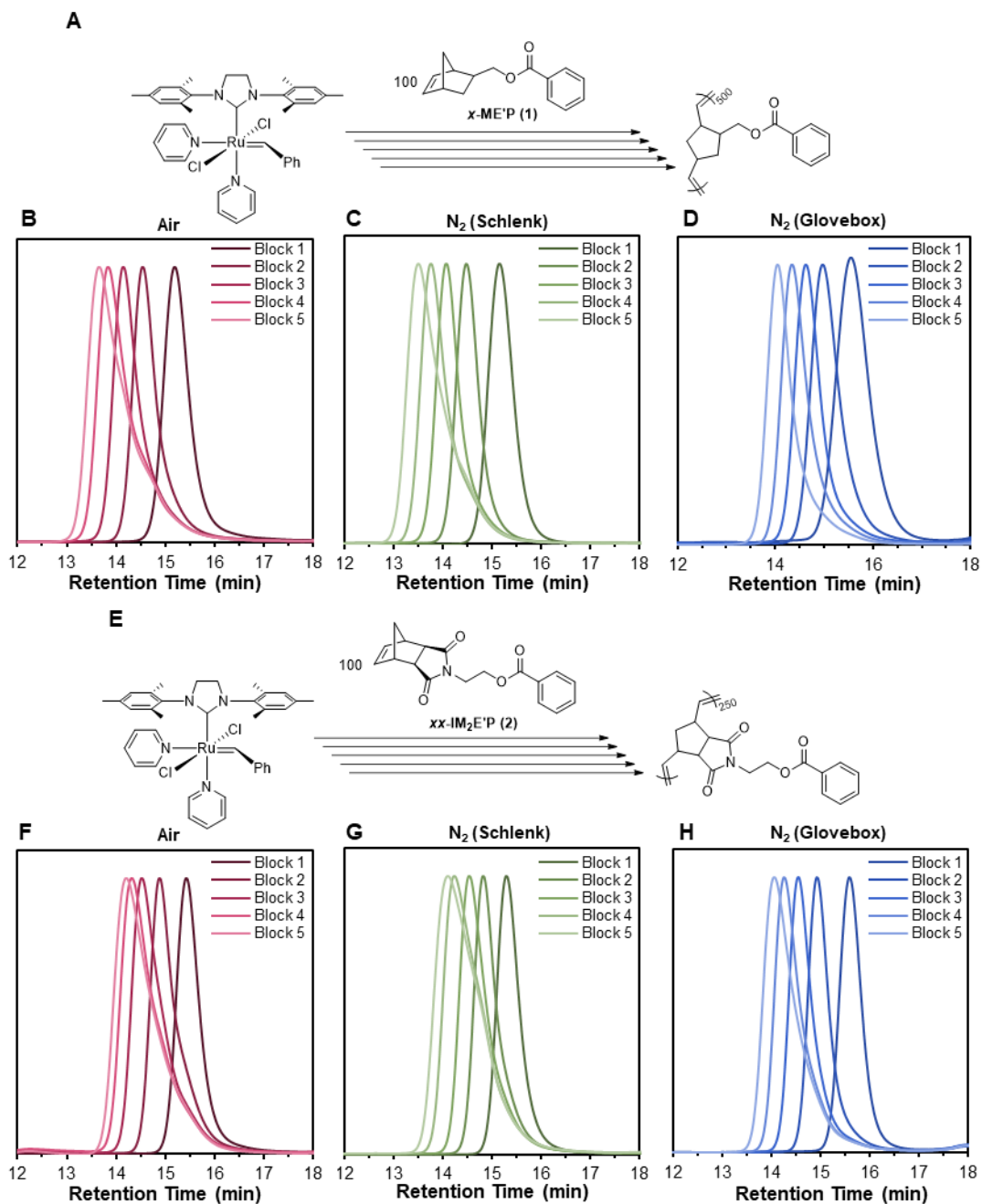


Figure 5.2. A and E) Scheme for the synthesis of linear pseudo-pentablock copolymers for the SAM-ROMP of monomers *x*-ME'P (**1**) (A) and *xx*-IM₂E'P (**2**) (E). Reactions were run at a total monomer concentration of 20 mM in CH₂Cl₂ at rt. B–D): SEC traces (dRI signal) for the ROMP of monomer *x*-ME'P (**1**) either open to air (B), on a Schlenk line under N₂ (C), or in an N₂-filled glovebox (D), showing a decrease in retention time after each block addition. F–H): SEC traces (dRI signal) for the ROMP of monomer *x*-IM₂E'P (**2**) either open to air (F), on a Schlenk line

under N₂ (G), or in an N₂-filled glovebox (H), showing a decrease in retention time after each block addition.

We observed a general increase in M_n over the course of all five monomer additions for both monomers under all atmospheres, confirming that at least some chain extension occurred in all cases (Figure 5.3A and 5.3C). A linear increase in M_n was observed for monomer *x*-ME'P (**1**) under all three atmospheres. Monomer *x*-ME'P (**1**) also experienced good agreement between expected and observed M_n values for all three atmospheres, with slight deviations attributed to some catalyst decomposition. On the other hand, more significant deviations from expected M_n were observed for monomer *xx*-IM₂E'P (**2**) than monomer *x*-ME'P (**1**). The third, fourth, and fifth block additions of monomer *xx*-IM₂E'P (**2**) fell below expected M_n values when polymerized under all three atmospheres. Thus, for monomers *x*-ME'P (**1**) and *xx*-IM₂E'P (**2**), change in atmosphere did little to improve M_n values of linear pseudo-pentablock polymers.

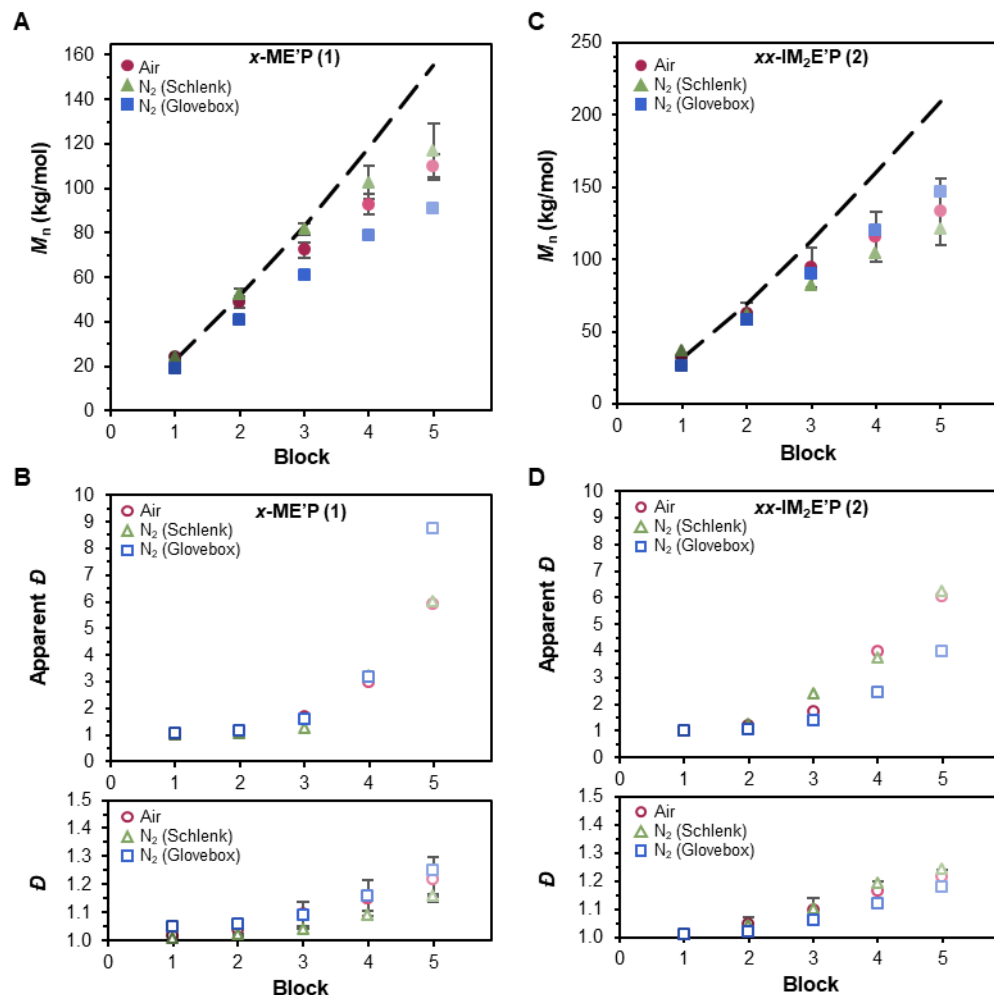


Figure 5.3. A and C): Measured M_n versus block number for the ROMP of monomers $x\text{-ME}'\text{P}$ (1) (A) and $xx\text{-IM}_2\text{E}'\text{P}$ (2) (C). Determined by SEC in THF at 30 °C with multiangle light scattering using 100% mass recovery. The dashed line refers to expected M_n as block number increases. B and D): Overall \bar{D} and apparent \bar{D} for the ROMP of monomers $x\text{-ME}'\text{P}$ (1) (B) and $xx\text{-IM}_2\text{E}'\text{P}$ (2) (D). Apparent \bar{D} refers to the dispersity value for each individual block estimated by the method developed by Harrison.²¹

Changes in \bar{D} values upon each block addition in these SAM-ROMP experiments, for both the overall polymer and each individual block, also provided useful information on the livingness in ROMP. There was very little difference in the \bar{D} values of the final polymers

synthesized from monomer *x*-ME'P (**1**) in all three atmospheres (all ~ 1.2). We observed small increases in \bar{D} values for the last two blocks of monomer *x*-ME'P (**1**) under all three atmospheres, consistent with the shapes of the SEC curves. Using the method reported by Harrison discussed earlier, the apparent \bar{D} values increased exponentially for SAM-ROMP of monomer *x*-ME'P (**1**) in all three atmospheres. This exponential behavior is consistent with Harrison's analysis of a polymer made by RAFT and our recent work on bottlebrush polymers made by SAM-ROMP. Monomer *xx*-IM₂E'P (**2**) showed very similar results to monomer *x*-ME'P (**1**) in most cases. The overall \bar{D} values of the third, fourth, and fifth blocks of monomer *xx*-IM₂E'P (**2**) increased slightly with little improvement based on atmosphere and the overall \bar{D} values of the same blocks increased exponentially in all three atmospheres. The apparent \bar{D} values for the polymerizations open to air or on the Schlenk line were comparable and reached ~ 6 for the final block under both atmospheres. However, when polymerized in the glovebox, the apparent \bar{D} value of the final block addition of monomer *xx*-IM₂E'P (**2**) (apparent $\bar{D} = 4$) was less than that of the apparent \bar{D} of the same block when polymerized only under N₂ on the Schlenk line or open to AIR. It is worth noting that there is substantial variability in the apparent \bar{D} values, especially in the fourth and fifth blocks in these experiments, but the final apparent \bar{D} value was consistently lower in the glovebox SAM-ROMP experiments for monomer *xx*-IM₂E'P (**2**). This decrease in apparent \bar{D} and good agreement in expected and measured M_n for monomer *xx*-IM₂E'P (**2**) when polymerized in a glovebox suggests slightly higher livingness for these polymerizations in the glovebox, but to a marginal degree.

Although inert atmosphere did not enhance livingness in ROMP of small molecule monomers, we were curious about the effects of atmosphere on ROMP grafting-through. The k_p of small molecule monomers is generally high, which makes the synthesis of linear polymers

relatively straightforward. However, in polymerizations that experience low k_p (i.e., ROMP of MMs) chain termination becomes more prevalent. Thus, we also investigated the effects of reaction atmosphere on the synthesis of bottlebrush pseudo-pentablock copolymers. These SAM-ROMP experiments were conducted using the same methods as the linear polymers, but we targeted a DP = 50 for each MM addition. The lower k_p for MMs compared to monomers along with the bulky side-chain makes targeting high DP values more challenging for MMs than monomers. Therefore, we expect chain termination to effect MMs when targeting a lower DP than the monomers. Again, we allowed each MM addition to polymerize for 6 propagation half-lives before the next addition of MM (5 and 30 min for monomers **3** and **4** respectively). Aliquots were removed and terminated right before the next monomer addition to determine conversion, M_n , and D by SEC (Table 5.3).

Table 5.3. Characterization of Bottlebrush Pentablock Copolymers Prepared by SAM-ROMP

MM	Atmosphere	Block #	% conv ^a	$M_{n,expected}^b$ (kg/mol)	BB $M_{n,SEC}^c$ (kg/mol)	BB D^c	Apparent D^d
<i>x</i> -ME'-PS (3)	Air	1	97	145	146 ± 6	1.03 ± 0.004	1.03 ± 0.001
		2	98	325	340 ± 30	1.04 ± 0.01	1.08 ± 0.03
		3	98	528	550 ± 60	1.07 ± 0.02	1.36 ± 0.2
		4	98	751	710 ± 70	1.16 ± 0.06	3.7 ± 2
		5	98	983	830 ± 140	1.24 ± 0.08	14.2 ± 10
	N ₂ (Schlenk line)	1	93	145	140 ± 10	1.02 ± 0.005	1.02 ± 0.01
		2	96	325	310 ± 80	1.03 ± 0.002	1.09 ± 0.01
		3	96	528	500 ± 140	1.07 ± 0.005	1.40 ± 0.08
		4	95	751	700 ± 100	1.15 ± 0.01	3.6 ± 2
		5	96	983	750 ± 80	1.22 ± 0.03	7.5 ± 2
	N ₂ (Glovebox)	1	97	145	134	1.03	1.03
		2	97	325	287	1.04	1.08
		3	98	528	460	1.06	1.23
		4	98	751	616	1.09	2.08
		5	98	983	755	1.16	3.88
<i>xx</i> -IM ₂ E'-PS (4)	Air	1	94	160	166 ± 6	1.01 ± 0.001	1.01 ± 0.01
		2	94	359	330 ± 40	1.09 ± 0.04	1.45 ± 0.3
		3	94	579	470 ± 80	1.21 ± 0.06	3.3 ± 1
		4	93	819	580 ± 150	1.31 ± 0.08	15.3 ± 14
		5	95	1072	700 ± 200	1.41 ± 0.08	27.6 ± 20
	N ₂ (Schlenk line)	1	88	160	110	1.02	1.02
		2	91	359	204	1.07	1.30
		3	92	579	277	1.21	3.54
		4	92	819	341	1.30	5.55
		5	91	1072	368	1.43	32.8
	N ₂ (Glovebox)	1	93	160	177	1.01	1.01
		2	93	359	368	1.05	1.17
		3	93	579	551	1.11	1.83
		4	91	819	705	1.20	3.78
		5	86	1072	824	1.29	7.98

^aMeasured using SEC by comparing the areas of the bottlebrush polymer and MM peaks in the dRI trace. ^bDetermined using the equation $M_{n,expected} = M_{n,MM} * ([MM]/[G3])_0$. ^cDispersity value for the aliquot as measured using SEC in THF at 30 °C with multiangle light scattering using the known dn/dc for PS of 0.185 mL/g. ^dDispersity value for the individual block as estimated using the method developed by Harrison.²¹

MM conversion was generally high (>85%) for both MMs under all three atmospheric conditions. Again, we observed a decrease in the retention time of the main SEC peak with the polymerization of each additional block for both MMs, along with the first block addition for

both MMs reaching targeted M_n values while maintaining low D values. The ROMP of MM *x*-ME'-PS (**3**) experienced low molecular weight tails in the SEC traces for blocks three, four, and five when polymerized open to air (Figure 5.4). The low molecular weight tails decreased in area when MM *x*-ME'-PS (**3**) was polymerized under inert atmospheres; a low molecular weight tail was observed for only the last block for MM *x*-ME'-PS (**3**) when polymerized in an N₂-filled glovebox. The ROMP of MM *xx*-IM₂E'-PS (**4**) experienced the most chain termination out of all four (macro)monomers as evidenced by having the largest low molecular weight tails and residual MM peak observed in the SEC curves. Similar to MM *x*-ME'-PS (**3**), the ROMP of MM *xx*-IM₂E'-PS (**4**) experienced low molecular weight tails in the dRI traces of blocks three through five under ambient condition. Again, the low molecular weight tails decreased in area when *xx*-IM₂E'-PS (**4**) was polymerized in an N₂-filled glovebox.

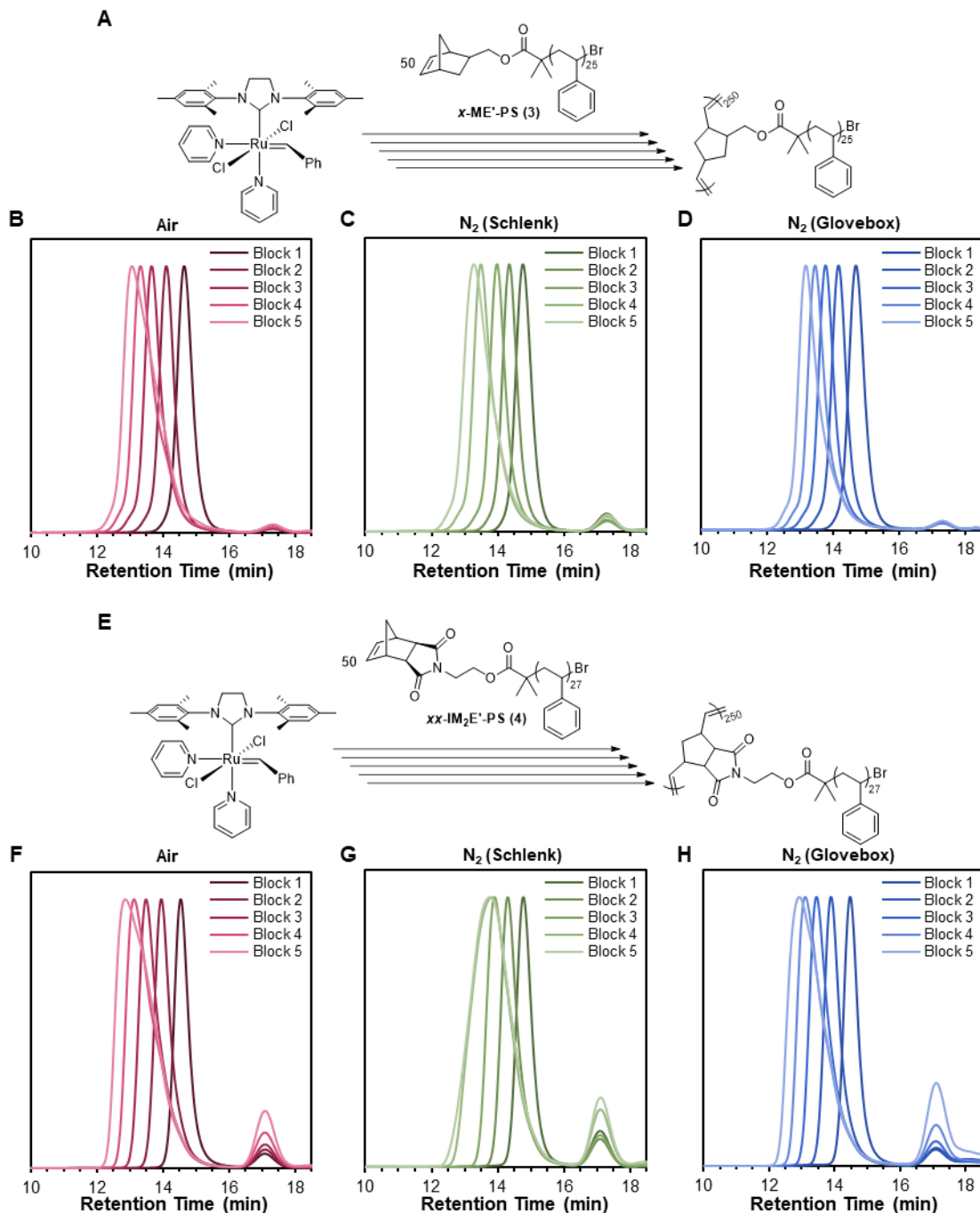


Figure 5.4. A and E): Scheme for the synthesis of bottlebrush pentablock copolymers from the ROMP of MMs *x*-ME'-PS (**3**) (A) and *xx*-IM₂E'-PS (**4**) (E). Reactions were run at a total MM concentration of 20 mM in CH₂Cl₂ at rt. B–D): SEC traces (dRI signal) for the ROMP of MM *x*-ME'-PS (**3**) either open to air (B), on a Schlenk line under N₂ (C), or in an N₂-filled glovebox (D), showing a decrease in retention time after each block addition. F–H): SEC traces (dRI

signal) for the ROMP of MM *xx*-IM₂E'-PS (**4**) either open to air (F), on a Schlenk line under N₂ (G), or in an N₂-filled glovebox (H), showing a decrease in retention time after each block addition.

We observed a linear increase in M_n over the course of all five monomer additions for MM *x*-ME'-PS (**3**) under all three atmospheric conditions (Figure 5.5A). MM *x*-ME'-PS (**3**) experienced good agreement between expected and observed M_n values for all three atmospheres, with slight deviations observed for the fourth and fifth blocks consistent with some chain termination. In contrast, significant deviations from expected M_n were observed for MM *xx*-IM₂E'-PS (**4**) when polymerized open to air and under N₂ on a Schlenk line. The M_n of the bottlebrush polymers made from MM *xx*-IM₂E'-PS (**4**) open to air reached 700 kg/mol on average. When polymerized in a glovebox, MM *xx*-IM₂E'-PS (**4**) reached an M_n value of 824 kg/mol for the final bottlebrush polymer.

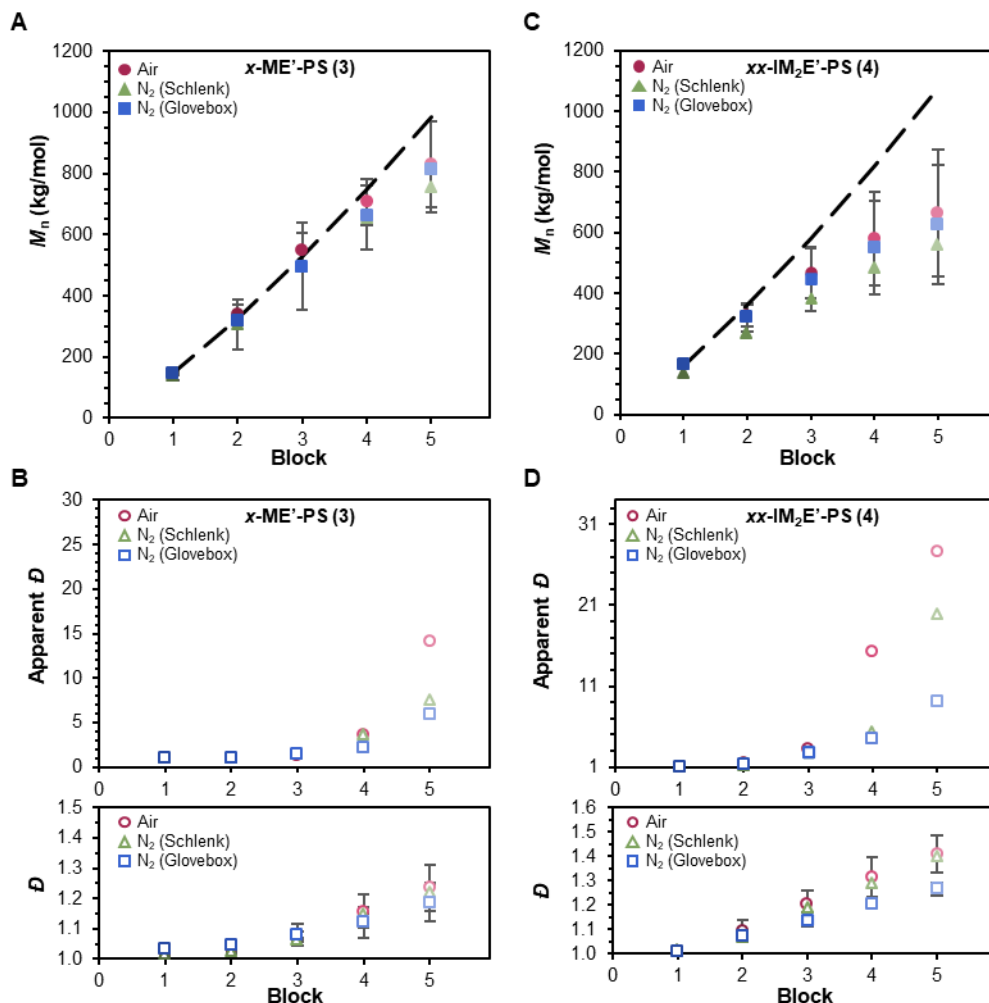


Figure 5.5. A and C): Measured M_n versus block number for the ROMP of MMs $x\text{-ME}'\text{-PS (3)}$ (A) and $xx\text{-IM}_2\text{E}'\text{-PS (4)}$ (C). Determined by SEC in THF at 30 °C with multiangle light scattering using the known dn/dc for PS of 0.185 mL/g. The dashed line refers to expected M_n as block number increases. B and D): Overall D and apparent D for the ROMP of MMs $x\text{-ME}'\text{-PS (3)}$ (B) and $xx\text{-IM}_2\text{E}'\text{-PS (4)}$ (D). Apparent D refers to the dispersity value for each individual block estimated by the method developed by Harrison.²¹

Once again, changes in D values upon each block addition in these SAM-ROMP experiments for the overall bottlebrush polymer structures synthesized from MMs $x\text{-ME}'\text{-PS (3)}$ and $xx\text{-IM}_2\text{E}'\text{-PS (4)}$ provided little insight into the differences in livingness in ROMP due to

atmosphere (Figure 4.5B and 4.5D). There was very little difference in the D values of the final polymers synthesized from MM x -ME'-PS (**3**) in all three atmospheres (~ 1.2). We observed small increases in D values for the last two blocks of MM x -ME'-PS (**3**) under all three atmospheres, consistent with the shapes of the SEC curves. Again, the apparent D values increased exponentially for the last two block additions of MM x -ME'-PS (**3**) in all three atmospheric conditions, but the final block when polymerized open to air had the highest apparent D compared to the final blocks under the other two atmosphere conditions. The overall D values for MM xx -IM₂E'-PS (**4**) were relatively similar between the three atmospheres. Although this MM had the highest increase in overall D compared to the other (macro)monomers, atmosphere did not affect the overall D values significantly with all final bottlebrush polymers reaching $D = 1.3$ – 1.4 . Open to air, the apparent D of the final block addition of MM xx -IM₂E'-PS (**4**) reached ~ 30 , higher than all other (macro)monomers. The final bottlebrush polymer made from MM xx -IM₂E'-PS (**4**) had the highest overall D value out of all other final polymer structures, which likely caused the significant increase in apparent D . In contrast, the apparent D of the final block addition of MM xx -IM₂E'-PS (**4**) dropped to 8 when polymerized in a glovebox, almost 4-fold less than the final block addition of MM xx -IM₂E'-PS (**4**) open to air. Out of all parameters studied here, apparent D changed the most based on atmosphere, suggesting slight improvement in livingness in ROMP when under inert atmospheres.

5.5 Conclusions

In summary, we studied the effects of atmosphere on the livingness in ROMP through the synthesis of pseudo-pentablock copolymers. We found that atmosphere had little effect on the

livingness in ROMP of monomers for the synthesis of linear polymers. Only small improvements in M_n , overall \mathcal{D} , and apparent \mathcal{D} were observed for both N_2 and glovebox atmospheres for monomers **1–2**. However, this improvement was marginal and suggests little change in the number of dead chains between atmospheres during the polymerizations of small molecule monomers. Therefore, inert atmospheres are not necessary to maintain high livingness in ROMP for the synthesis of linear pseudo-pentablock copolymers.

The effects of polymerization atmosphere were slightly greater for the ROMP of MMs than small molecule monomers. With higher molecular weights than the monomers, MMs had lower k_p values which gave rise to higher amounts of dead chains during polymerization than the small molecule monomers. Polymerizations open to air provided the highest apparent \mathcal{D} values out of the three atmospheres for both MMs. However, MM *xx*-ME'-PS (**3**) maintained high enough livingness when open to air to reach close to expected M_n values with relatively low \mathcal{D} values, even though apparent \mathcal{D} was high. MM *xx*-IM₂E'-PS (**4**) reached the highest M_n value with the lowest apparent \mathcal{D} value for the final block addition when polymerized in the glovebox compared to the other atmosphere conditions. It is worth noting that the ROMP of MM *xx*-IM₂E'-PS (**4**) open to air maintained high enough livingness to reach relatively high M_n values with low \mathcal{D} values. Therefore, when working with low k_p MMs, inert atmosphere may improve livingness in ROMP but is not essential for successful polymerization. Overall, it is important to maintain high livingness to achieve complex polymer architectures and polymerization atmosphere does not drastically affect the livingness in ROMP.

5.6 Acknowledgments

This work was supported by a joint grant between the National Science Foundation and the Binational Science Foundation (DMR–2104602). We thank Professor Diana Thornton for providing the glovebox and Matthew Williams for assistance with the glovebox.

4.7 References

1. Bloch, S. E.; Scannelli, S. J.; Alaboalirat, M.; Matson, J. B., Complex Polymer Architectures Using Ring-opening Metathesis Polymerization: Synthesis, Applications, and Practical Considerations. *Macromolecules* **2022**, *55*, 4200–4227.
2. Choi, T.–L.; Grubbs, R. H., Controlled Living Ring-opening-Metathesis Polymerization by a Fast-Initiating Ruthenium Catalyst. *Angew. Chem* **2003**, *42*, 1743–1746.
3. Jawiczuk, M.; Marczyk, A.; Trzaskowski, B., Decomposition of Ruthenium Olefin Metathesis Catalyst. *Catalysts* **2020**, *10*, 887.
4. Hong, S. H.; Wenzel, A. G.; Salguero, T. T.; Day, M. W.; Grubbs, R. H., Decomposition of Ruthenium Olefin Metathesis Catalysts. *J. Am. Chem. Soc.* **2007**, *129*, 7961–7968.
5. Walsh, D. J.; Guironnet, D., Macromolecules with programmable shape, size, and chemistry. *Proc. Natl. Acad. Sci.* **2019**, *116*, 1538–1542.
6. Ogbonna, N. D.; Dearman, M.; Cho, C.–T.; Bharti, B.; Peters, A. J.; Lawrence, J., Topologically Precise and Discrete Bottlebrush Polymers: Synthesis, Characterization, and Structure–Property Relationships. *JACS Au* **2022**, *2*, 898–905.
7. Jenkins, A. D.; Kratochvíl, P.; Stepto, R. F. T.; Suter, U. W., Glossary of basic terms in polymer science (IUPAC Recommendations 1996). *Pure Appl. Chem.* **1996**, *68*, 2287–2311.

8. Jha, S.; Dutta, S.; Bowden, N. B., Synthesis of Ultralarge Molecular Weight Bottlebrush Polymers Using Grubbs' Catalysts. *Macromolecules* **2004**, *37*, 4365–4374.
9. Sheiko, S. S.; Sumerlin, B. S.; Matyjaszewski, K., Cylindrical molecular brushes: Synthesis, characterization, and properties. *Prog. Polym. Sci.* **2008**, *33*, 759–785.
10. Ren, N.; Yu, C.; Zhu, X., Topological Effect on Macromonomer Polymerization. *Macromolecules* **2021**, *54*, 6101–6108.
11. Slugovc, C., The Ring Opening Metathesis Polymerisation Toolbox. *Macromol. Rapid Commun.* **2004**, *25*, 1283–1297.
12. Bloch, S. E.; Alaboalirat, M.; Eades, C. B.; Scannelli, S. J.; Matson, J. B., Solvent Effects in Grafting-through Ring-opening Metathesis Polymerization. *Macromolecules* **2022**, *55*, 3522–3532.
13. Scannelli, S. J.; Paripati, A.; Weaver, J. R.; Vu, C.; Alaboalirat, M.; Troya, D.; Matson, J. B., The influence of the norbornene anchor group in Ru-mediated ring-opening metathesis polymerization: Synthesis of linear polymers. *Macromolecules* **2023**, *Submitted*, ma–2023–001729.
14. Scannelli, S. J.; Alaboalirat, M.; Troya, D.; Matson, J. B., The influence of the norbornene anchor group in Ru-mediated ring-opening metathesis polymerization: Synthesis of bottlebrush polymers. *Macromolecules* **2023**, ma–2023–00214b.
15. Bhanu, V. A.; Kishore, K., Role of oxygen in polymerization reactions. *Chem. Rev.* **1991**, *91*, 99–117.
16. Schrock, R. R.; Hoveyda, A. H., Molybdenum and Tungsten Imido Alkylidene Complexes as Efficient Olefin-Metathesis Catalysts. *Angew. Chem* **2003**, *42*, 4592–4633.

17. Schrock, R. R., Olefin metathesis by molybdenum imido alkylidene catalysts. *Tetrahedron* **1999**, *55*, 8141–8153.
18. Bielawski, C. W.; Grubbs, R. H., Highly Efficient Ring-opening Metathesis Polymerization (ROMP) Using New Ruthenium Catalysts Containing N-Heterocyclic Carbene Ligands. *Angew. Chem* **2000**, *39*, 2903–2906.
19. Choinopoulos, I., Grubbs' and Schrock's Catalysts, Ring Opening Metathesis Polymerization and Molecular Brushes—Synthesis, Characterization, Properties and Applications. *Polymers* **2019**, *11*, 298.
20. Ogba, O. M.; Warner, N. C.; O'Leary, D. J.; Grubbs, R. H., Recent advances in ruthenium-based olefin metathesis. *Chem. Soc. Rev.* **2018**, *47*, 4510–4544.
21. Harrison, S., The downside of dispersity: why the standard deviation is a better measure of dispersion in precision polymerization. *Polym. Chem.* **2018**, *9*, 1366–1370.
22. Slugovc, C.; Demel, S.; Riegler, S.; Hobisch, J.; Stelzer, F., The Resting State Makes the Difference: The Influence of the Anchor Group in the ROMP of Norbornene Derivatives. *Macromol. Rapid Commun.* **2004**, *25*, 475–480.
23. Radzinski, S. C.; Foster, J. C.; Chapleski, R. C.; Troya, D.; Matson, J. B., Bottlebrush Polymer Synthesis by Ring-opening Metathesis Polymerization: The Significance of the Anchor Group. *J. Am. Chem. Soc.* **2016**, *138*, 6998–7004.

5.8 Supporting Information

Materials and Methods:

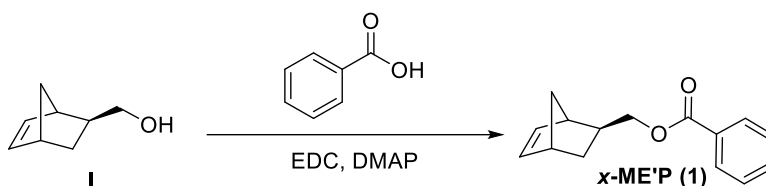
All reagents and solvents were obtained from commercial vendors and used as received unless otherwise stated. ^1H NMR spectra were measured on either an Agilent 400 MHz or Bruker 600 MHz spectrometer with a high ^1H sensitivity TCI Prodigy probe. ^1H and ^{13}C NMR chemical shifts are reported in ppm relative to internal solvent resonances unless otherwise stated. A Biotage Selekt flash purification system was used for automated silica gel column purification. Silica used for automated flash chromatography purifications was ZEOCHEM ZEOprep 60 HYD 40–63 μM pore size. Size exclusion chromatography (SEC) was carried out in tetrahydrofuran at 1 mL min^{-1} at $30\text{ }^\circ\text{C}$ on two Agilent PLgel $10\text{ }\mu\text{m}$ MIXED–B columns connected in series with a Wyatt Dawn Heleos 2 light scattering detector and a Wyatt Optilab Rex refractive index detector. No calibration standards were used, and the known dn/dc for PS of 0.185 mL/g was used for macromonomer samples. AIR levels in the glovebox were monitored constantly and remained at $<3\text{ ppm}$.

Preparation of Grubbs' 3rd generation catalyst (G3)

Grubbs' 3rd generation catalyst (G3) was prepared freshly and used within 2 days following a modified version of published methods.^{1–2} First, pyridine and pentane were purified via passage through a short column of basic alumina. A one dram vial was charged with a stir bar and 20 mg of Grubbs' 2nd generation catalyst $(\text{H}_2\text{Imes})(\text{Pcy}_3)(\text{Cl})_2\text{Ru}=\text{CHPh}$. Next, purified pyridine (20 μL) was added to the vial, and the reaction mixture was stirred vigorously for 20–30 min until it had turned a vivid lime–green color. If the reaction mixture dried to a solid, additional pyridine (10 μL increments) was added and solids were broken up manually with a spatula to

allow for more stirring. Next, purified pentane (3 mL) was added to the vial to precipitate the catalyst. The pentane was decanted, and the solids were washed with additional purified pentane (3 mL). Once again, the pentane was decanted and the remaining solids were dried by blowing air over the vial for 1 min, then transferred to a clean vial, and then dried under vacuum overnight.

Monomer *x*-ME'P (1)



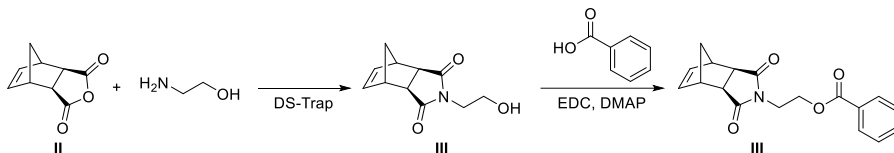
Exo-5-norbornene-2-Methanol (**II**)

Compound **II**, *exo*-5-norbornene-2-Methanol was prepared according to a previously reported procedure.³ ¹H NMR (CDCl₃): δ 6.08 (m, 2H), 3.70 (m, 1H), 3.54 (m, 1H), 2.82 (s, 1H), 2.74 (s, 1H), 1.64 (m, 1H), 1.30 (m, 3H), 1.11 (m, 1H). ¹³C NMR (CDCl₃): δ 136.91, 136.57, 67.65, 45.08, 43.38, 41.99, 41.63, 29.64. Both ¹H and ¹³C NMR spectra matched literature values.

Monomer *x*-ME'P (1)

Monomer *x*-ME'P (**2**) was synthesized according to a previously reported procedure.⁴ ¹H NMR (CDCl₃): δ 8.11–8.02 (m, 2H), 7.60–7.53 (m, 1H), 7.49–7.40 (m, 2H), 6.12 (m, 2H), 4.42 (m, 1H), 4.22 (m, 1H), 2.91–2.78 (m, 2H), 1.96–1.83 (m, 1H), 1.45–1.22 (m, 5H). ¹³C NMR (CDCl₃): δ 166.38, 136.72, 135.98, 132.58, 130.21, 129.31, 128.08, 68.74, 44.75, 43.46, 41.37, 37.84, 29.33. Both ¹H and ¹³C NMR spectra matched literature values.

Monomer *xx-IM*₂*E*'*P* (**8**)



Exo-Carbic anhydride (**II**)

Compound **II**, *exo*-norbornene anhydride (carbic anhydride) was prepared from *endo*-carbic anhydride according to a previously reported procedure.⁵ ¹H NMR (CDCl₃): δ 6.33 (t, *J* = 1.9 Hz, 2H), 3.26 (m, 2H), 3.06 (d, *J* = 1.6 Hz, 2H), 1.49 (m, 1H), 1.28 (m, 1H). ¹³C NMR (CDCl₃): δ 179.02, 137.83, 49.34, 45.22, 43.01. Both ¹H and ¹³C NMR spectra matched literature values.

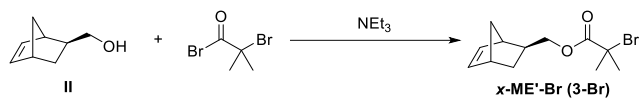
Compound **III**

Compound **III** was prepared according to a previously reported procedure.⁶ ¹H NMR (CDCl₃): δ 6.27 (m, 2H), 3.74 (m, 2H), 3.67 (m, 2H), 3.25 (s, 2H), 2.69 (s, 2H), 2.45 (s, 1H), 1.49 (m, 1H), 1.33 (m, 1H). ¹³C NMR (CDCl₃): δ 178.71, 137.76, 59.85, 47.84, 45.26, 42.79, 41.21. Both ¹H and ¹³C NMR spectra matched literature values.

Monomer *xx-IM*₂*E*'*P* (**8**)

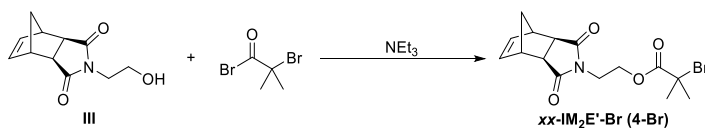
Monomer *xx-IM*₂*E*'*P* (**8**) was synthesized according to a previously reported procedure.⁴ ¹H NMR (CDCl₃): δ 7.99–7.94 (m, 2H), 7.58–7.52 (m, 1H), 7.43 (m, 2H), 6.27 (t, *J* = 1.9 Hz, 2H), 4.48–4.43 (m, 2H), 3.92 (m, 2H), 3.25 (m, 2H), 2.71 (d, *J* = 1.4 Hz, 2H), 1.43 (m, 1H), 1.27 (m, 1H). ¹³C NMR (CDCl₃): δ 177.46, 165.92, 137.51, 132.85, 129.40, 128.12, 128.04, 61.25, 47.56, 44.98, 42.38, 37.22.

Compound *x*-ME'-Br (3-Br)



Compound *x*-ME'-Br (3-Br) was synthesized as previously reported.³ ¹H NMR (CDCl₃): δ 6.13 – 6.06 (m, 2H), 4.24 (m, 1H), 4.08 (m, 1H), 2.85 (m, 1H), 2.74 (m, 1H), 1.95 (s, 6H), 1.85 – 1.73 (m, 1H), 1.40 – 1.26 (m, 3H), 1.20 (m, 1H). ¹³C NMR (CDCl₃): δ 171.85, 137.11, 136.31, 70.16, 56.14, 45.14, 43.71, 41.75, 37.96, 30.94, 29.58. Both ¹H and ¹³C NMR spectra matched literature values.

Compound *xx*-IM₂E'-Br (4-Br)



Compound *xx*-IM₂E'-Br (4-Br)

Compound *xx*-IM₂E'-Br (4-Br) was synthesized as previously reported procedure.⁷ ¹H NMR (CDCl₃): δ 6.29 (m, 2H), 4.35 – 4.29 (m, 2H), 3.81 (m, 2H) 3.28 (m, 2H), 2.70 (m, 2H), 1.89 (s, 6H), 1.52 (m, 1H), 1.32 (m, 1H). ¹³C NMR (CDCl₃): δ 177.84, 171.51, 137.95, 62.71, 55.60, 47.99, 45.34, 43.06, 37.48, 30.75. Both ¹H and ¹³C NMR spectra matched literature values.

Synthesis of polystyrene macromonomers (MMs)

A typical styrene polymerization procedure is as follows: Initiator *x*-ME'-Br (3-Br) (0.082 g, 0.30 mmol), styrene (9.3 mL, 81 mmol), CuBr (22 mg, 0.15 mmol), and CuBr₂ (34 mg, 0.15 mmol) were added to a 100 mL Schlenk tube equipped with a stir bar. The mixture in the

Schlenk tube was deoxygenated by three freeze-pump-thaw cycles and then backfilled with N₂. The reaction mixture was submerged in an oil bath at 90 °C and after ~10 min, *N,N,N',N'',N'''*-pentamethyldiethylenetriamine (PMDETA) (0.063 mL, 0.30 mmol) was injected under N₂ flow. The reaction mixture was heated in an oil bath maintained at 90 °C for about 3 h. An aliquot was removed via an N₂-purged syringe and analyzed via ¹H NMR spectroscopy to ensure that ~10% monomer conversion had been reached. At this point, the reaction was terminated by exposing the contents of the Schlenk tube to air. The reaction mixture was diluted with ethyl acetate (50 mL) and washed with water (3 x 20 mL) in a separatory funnel, and then the ethyl acetate layer was concentrated by rotary evaporation. The crude product was loaded onto a column by either dry loading onto silica or liquid loading using a small amount of CH₂Cl₂. The crude product was then purified by automated flash chromatography on silica with a gradient of 0% to 40 % ethyl acetate in hexanes as the mobile phase, similar to previous descriptions of this procedure (Figures S15–S19).⁸ The MM-containing fractions were concentrated by rotary evaporation, and then the product was purified further via passage through a short column of basic alumina using tetrahydrofuran as the mobile phase. The resulting MM solution was then concentrated by rotary evaporation, redissolved in a small volume of tetrahydrofuran, and then precipitated once into methanol. After precipitation, the polymer was recovered via filtration and then dried under vacuum overnight to yield a white solid. The molar ratios of reagents for the ATRP reaction were [styrene]/[Initiator]/[CuBr]/[CuBr₂]/[PMDETA] 270:1:0.5:0.5:1 when targeting 3 kg/mol.

NMR Kinetic experiments on anchor group monomers

A representative synthesis is as follows: Monomer (40 mg) was dissolved in CDCl₃ in a vial equipped with a stir bar. A stock solution of **G3** in CDCl₃ was made, and 0.1 mL of this solution

(to achieve 1 equiv with respect to monomer) was then added rapidly to the first vial to make the final concentration of monomer = 20 mM. Polymerizations were conducted under air with capping of the vials in between aliquot removal steps. Aliquots (0.50 mL) were withdrawn periodically via micropipette at pre-determined timepoints and added to 1.5 mL Eppendorf microcentrifuge tubes containing 0.1 mL CDCl₃ and ethyl vinyl ether (2 μL) to terminate the polymerizations. Each aliquot was then analyzed by ¹H NMR spectroscopy. Kinetic parameters were obtained from a conversion vs. time plot.

SEC kinetic experiments on polystyrene MMs

A representative synthesis is as follows: MM *x*-ME'-PS (**2**) (25 mg, 100 equiv) was dissolved in CDCl₃ (0.317 mL) in a vial equipped with a stir bar. A stock solution of **G3** in CDCl₃ at a concentration of 0.61 mg/mL was prepared, and 100 μL of this solution (to achieve 0.061 mg of **G3**, 1 equiv) was then added rapidly to the first vial to make the final concentration of MM = 20 mM. Aliquots (45 μL) were withdrawn periodically via micropipette at predetermined timepoints and added to 1.5 mL Eppendorf microcentrifuge tubes containing 0.1 mL CDCl₃ and ethyl vinyl ether (2 μL) to terminate the polymerizations. Polymerizations were conducted under air with capping of vials in between aliquots to minimize solvent evaporation. Each aliquot was then analyzed by SEC after evaporation of CDCl₃ by blowing air over the aliquots for about 15 min (Figures S30–S39). This procedure was also used to determine the kinetics when targeting an $N_{bb} = 20$ by adjusting the MM equiv to 20, used in the synthesis of bottlebrush pentablock copolymers from MM *x*-ME'-PS (**2**) and MM *xx*-IM₂E'-PS (**5**) (Figures S45–S48).

Linear or bottlebrush pentablock copolymer synthesis in presence of oxygen or in a glove box

A representative synthesis is as follows: MM *x*-ME'-PS (**3**) (5 mg, 50 equiv) was weighed out in a vial equipped with a stir bar and dissolved in CH₂Cl₂ (76 μ L). MM *x*-ME'-PS (**3**) (20 mg) was weighed out in a separate vial and dissolved in CH₂Cl₂ (340 μ L) as a stock solution of MM. A stock solution of **G3** in CH₂Cl₂ at a concentration of 2.50 mg/mL was prepared, and 10 μ L of this solution (to achieve 0.0251 mg of G3, 1 equiv) was then added rapidly to the first vial containing a stir bar. The reaction mixture was stirred for a predetermined amount of time [5 min for MM *x*-ME'-PS (**3**)] at which point an aliquot (17 μ L) was withdrawn via glass syringe and added to an SEC vial containing excess ethyl vinyl ether to terminate the polymerization. Immediately following aliquot removal, another injection of a MM solution (86 μ L) was added rapidly to the stirring polymerization. This second injection of MM was allowed to polymerize for the same amount of time as the first before the removal of an aliquot and the third injection of the MM solution. The procedure continued until all of the MM stock solution was added to the reaction mixture and the final aliquot was removed. Polymerizations were conducted under air or in a glove box with capping of vials in between aliquot removals and injections to minimize solvent evaporation. Each aliquot was then analyzed by SEC after evaporation of CH₂Cl₂ by blowing air over the aliquots for about 2 min. This procedure was also used for the synthesis of linear pentablock copolymers from monomers *x*-ME'P (**1**) and *xx*-IM₂E'P (**2**) and bottlebrush pentablock copolymers from MM *xx*-IM₂E'-PS (**4**) allowing for 1.5 min, 7 min, or 30 min respectively between each aliquot and monomer addition.

Linear or bottlebrush pentablock copolymer synthesis on a Schlenk line

A representative synthesis is as follows: MM *x*-ME'-PS (**3**) (5 mg, 50 equiv) was added to a flame-dried 10 mL Schlenk tube equipped with a stir bar followed by dry CH₂Cl₂ (76 uL) from a Strauss flask. MM *x*-ME'-PS (**3**) (25 mg) was added to a second flame-dried Schlenk tube and dissolved in dry CH₂Cl₂ (430 μL) as a stock solution of MM. A stock solution of **G3** in dry CH₂Cl₂ at a concentration of 2.50 mg/mL was prepared in a 10 mL two-neck round-bottom flask, and 10 μL of this solution (to achieve 0.0251 mg of G3, 1 equiv) was then added rapidly to the first Schlenk tube containing a stir bar. The reaction mixture was stirred for a predetermined amount of time [5 min for MM *x*-ME'-PS (**3**)] at which point an aliquot (17 μL) was withdrawn via glass syringe and added to an SEC vial containing excess ethyl vinyl ether to terminate the polymerization. Immediately following aliquot removal, another injection of a MM solution (86 uL) was added rapidly to the stirring polymerization. This second injection of MM was allowed to polymerize for the same amount of time as the first before the removal of an aliquot and the third injection of the MM solution. The procedure continued until four injections of the MM stock solution were added to the reaction mixture, for a total of five blocks, and the final aliquot was removed. Each aliquot was then analyzed by SEC after evaporation of CH₂Cl₂ by blowing air over the aliquots for about 2 min. This procedure was also used for the synthesis of linear pentablock copolymers from monomers *x*-ME'P (**1**) and *xx*-IM₂E'P (**2**) and bottlebrush pentablock copolymers from MM *xx*-IM₂E'-PS (**4**) allowing for 1.5 min, 7 min, or 30 min respectively between each aliquot and monomer addition.

^1H NMR and SEC analysis of MMs

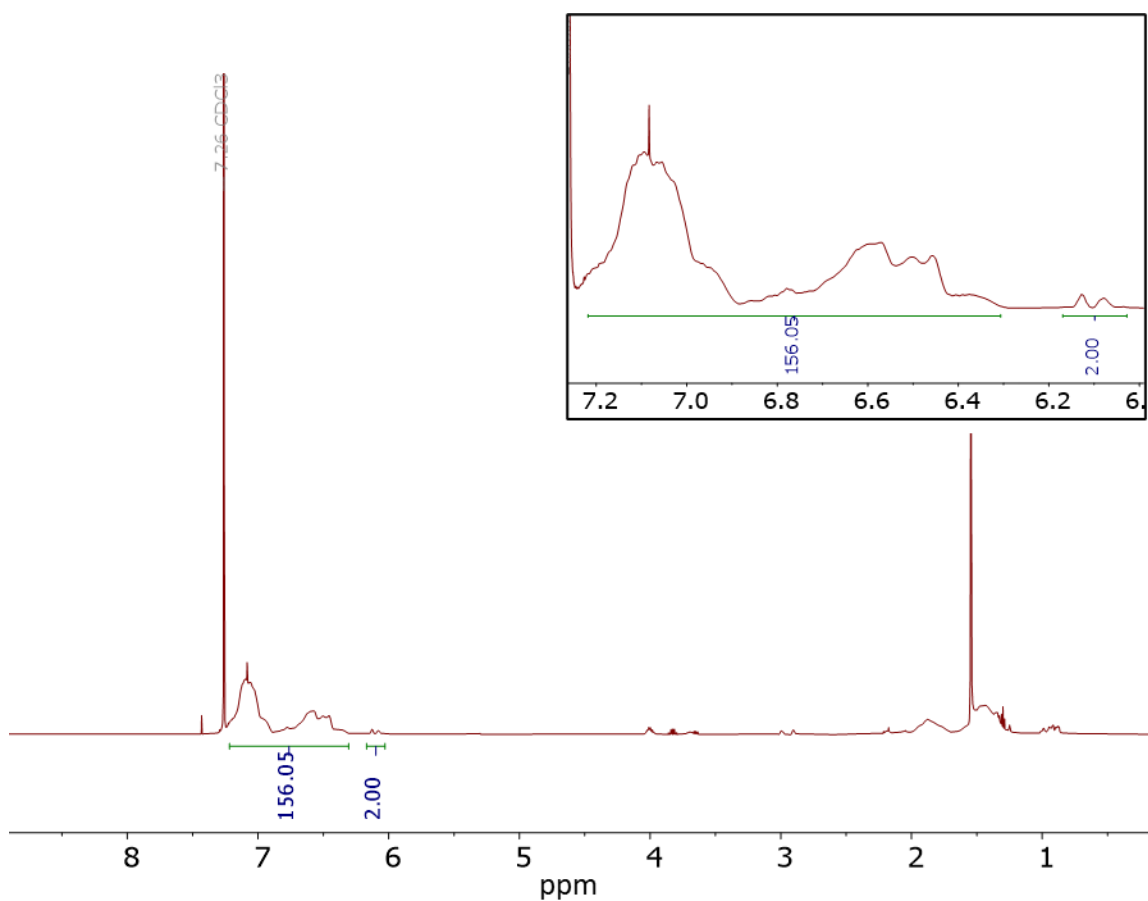


Figure S1. ^1H NMR spectrum of MM x -ME 2 -PS (3).

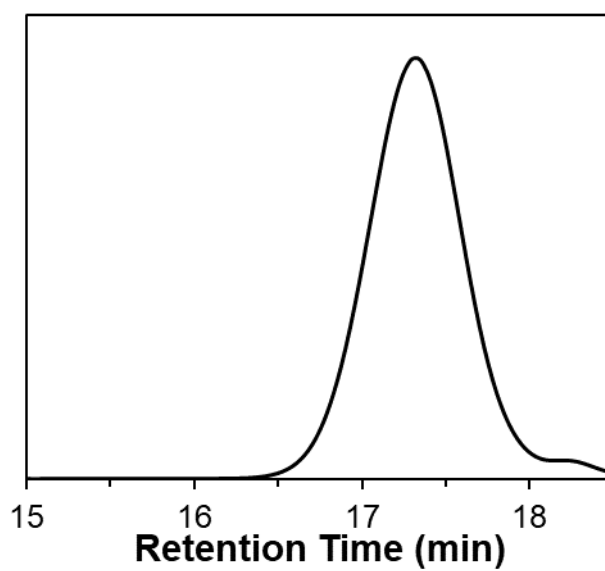


Figure S2. SEC trace (dRI signal) of MM *x*-ME'-PS (3).

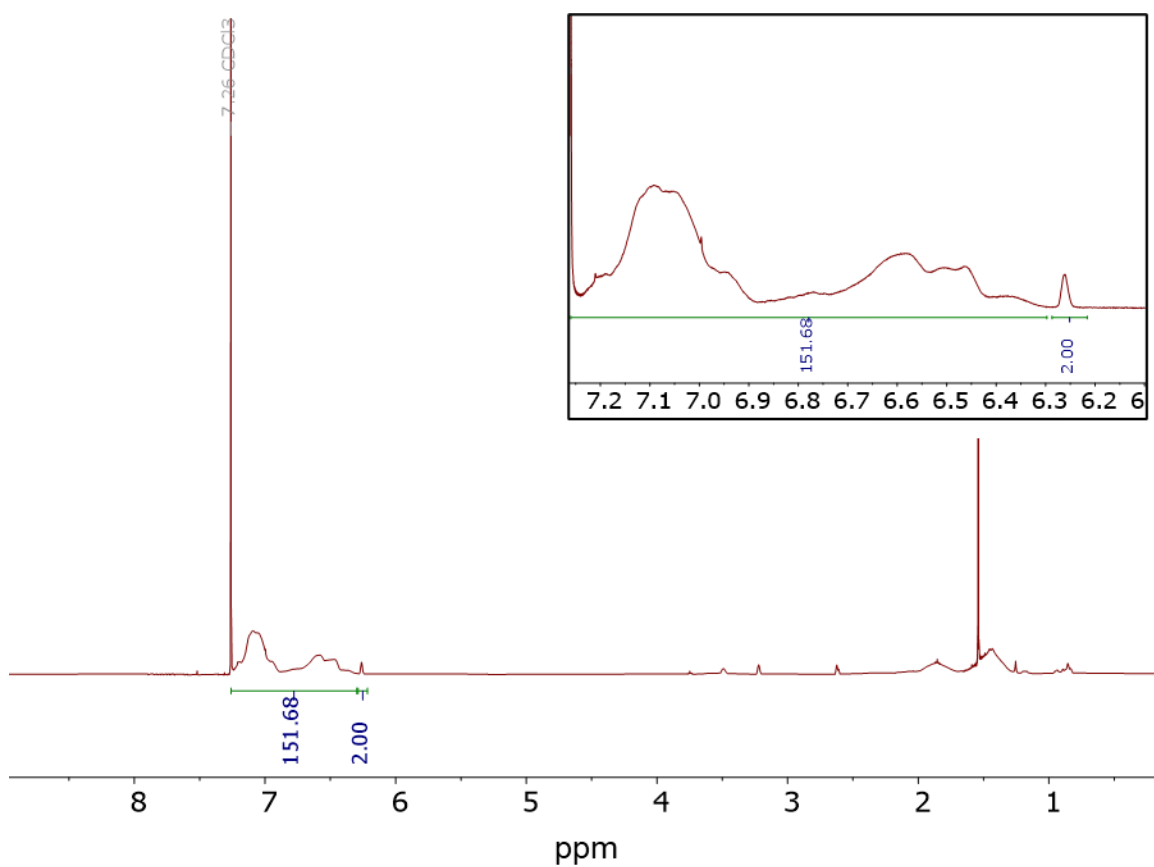


Figure S3. ¹H NMR spectrum of MM *xx*-IM₂E'-PS (4).

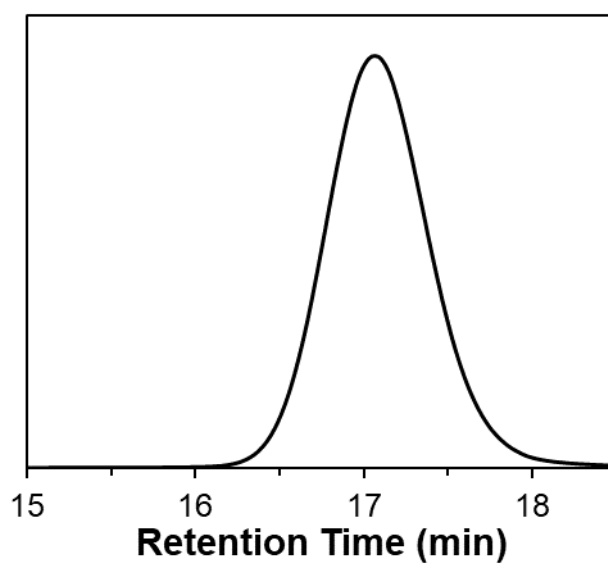


Figure S4. SEC trace (dRI signal) of MM *xx*-IM₂E'-PS (4).

Kinetic analysis of monomers and MMs

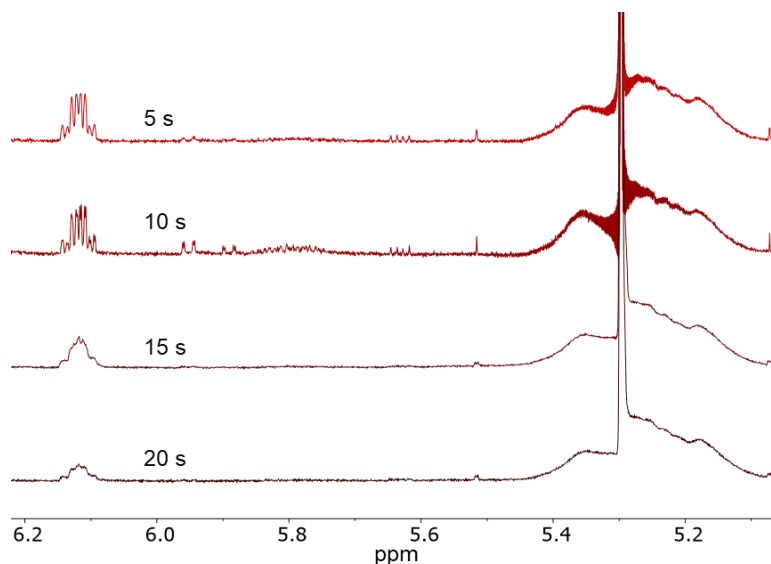


Figure S5. Representative spectra for ^1H NMR kinetics experiment of the ROMP of monomer *x*-ME'P (**1**) with G3. As the polymerization proceeds, the norbornene olefin resonance at ~ 6.1 ppm decreases in intensity, and the polymer backbone resonance at 5.2–5.4 ppm increases in intensity

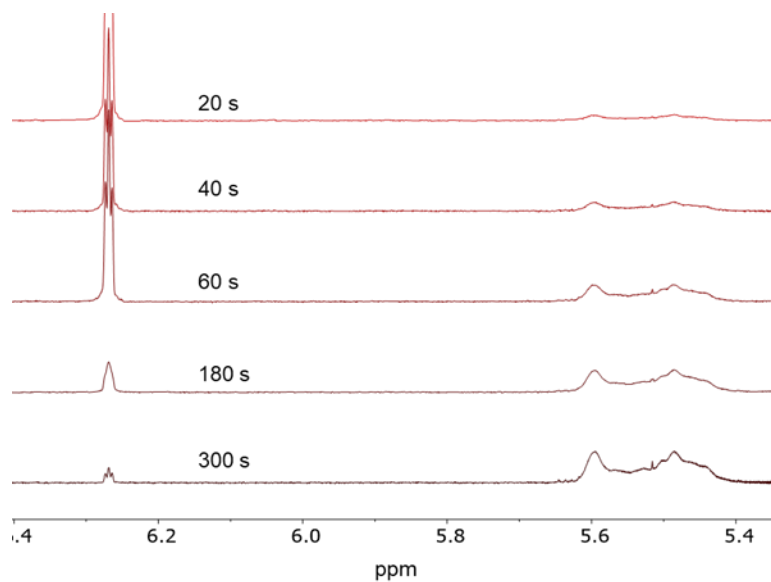


Figure S6. Representative spectra for ^1H NMR kinetics experiment of the ROMP of monomer *xx*-IM₂E'P (**2**) with G3. As the polymerization proceeds, the norbornene olefin resonance at ~ 6.25 ppm decreases in intensity, and the polymer backbone resonance at 5.4–5.6 ppm increases in intensity.

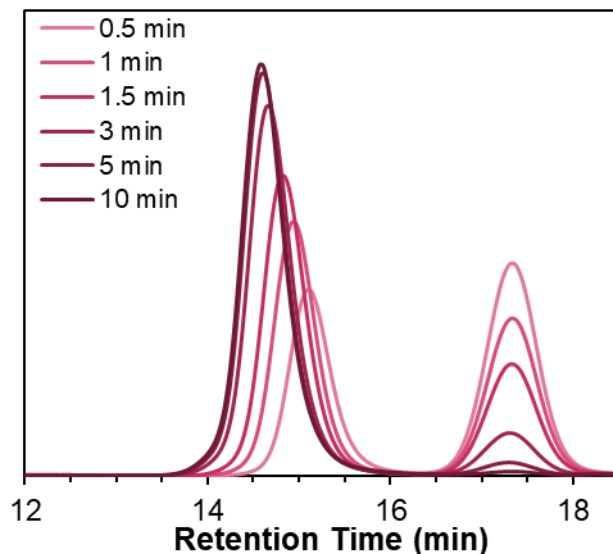


Figure S7. Representative SEC traces (dRI signal) of the ROMP of MM x -ME'-PS (**3**) at an [MM]/[G3] ratio of 50:1. As the polymerization proceeds, the MM signal at 17.2 min decreases in intensity and the bottlebrush polymer signal increases in intensity and shifts in retention time from 15.2 min to 14 min.

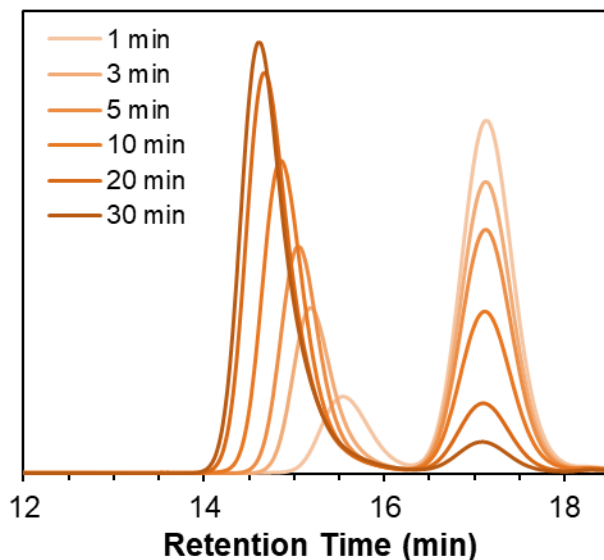


Figure S8. Representative SEC traces (dRI signal) of the ROMP of MM xx -IM₂E'-PS (**4**) at an [MM]/[G3] ratio of 50:1. As the polymerization proceeds, the MM signal at 17.2 min decreases in intensity and the bottlebrush polymer signal increases in intensity and shifts in retention time from 15.8 min to 14.2 min.

5.9 Supporting Information References

1. Au – Liu, J.; Au – Gao, A. X.; Au – Johnson, J. A., Particles without a Box: Brush–first Synthesis of Photodegradable PEG Star Polymers under Ambient Conditions. *JoVE* **2013**, e50874.
2. Love, J. A.; Morgan, J. P.; Trnka, T. M.; Grubbs, R. H., A Practical and Highly Active Ruthenium-based Catalyst that Effects the Cross Metathesis of Acrylonitrile. *Angew. Chem* **2002**, *41*, 4035–4037.
3. Alaboalirat, M.; Qi, L.; Arrington, K. J.; Qian, S.; Keum, J. K.; Mei, H.; Littrell, K. C.; Sumpter, B. G.; Carrillo, J.-M. Y.; Verduzco, R.; Matson, J. B., Amphiphilic Bottlebrush Block Copolymers: Analysis of Aqueous Self-Assembly by Small–Angle Neutron Scattering and Surface Tension Measurements. *Macromolecules* **2019**, *52*, 465–476.
4. Scannelli, S. J.; Paripati, A.; Weaver, J. R.; Vu, C.; Alaboalirat, M.; Troya, D.; Matson, J. B., The influence of the norbornene anchor group in Ru-mediated ring-opening metathesis polymerization: Synthesis of linear polymers. *Macromolecules* **2023**, *Submitted*, ma–2023–001729.
5. Radzinski, S. C.; Foster, J. C.; Matson, J. B., Synthesis of bottlebrush polymers via transfer–to and grafting-through approaches using a RAFT chain transfer agent with a ROMP–active Z–group. *Polym. Chem.* **2015**, *6*, 5643–5652.
6. Radzinski, S. C.; Foster, J. C.; Chapleski, R. C.; Troya, D.; Matson, J. B., Bottlebrush Polymer Synthesis by Ring-opening Metathesis Polymerization: The Significance of the Anchor Group. *J. Am. Chem. Soc.* **2016**, *138*, 6998–7004.

7. Scannelli, S. J.; Alaboalirat, M.; Troya, D.; Matson, J. B., The influence of the norbornene anchor group in Ru-mediated ring-opening metathesis polymerization: Synthesis of bottlebrush polymers. *Macromolecules* **2023**, ma–2023–00214b.
8. Alaboalirat, M.; Vu, C.; Matson, J. B., Radical–radical coupling effects in the direct-growth grafting-through synthesis of bottlebrush polymers using RAFT and ROMP. *Polym. Chem.* **2022**, *13*, 5841–5851.

Chapter 6: Conclusions and Future Outlooks

Chapter 2

In this chapter we thoroughly studied the norbornene anchor group effect on Ru-mediated ring-opening metathesis polymerization (ROMP). We calculated the HOMO energy of over 60 different norbornene monomers and experimentally measured the $k_{p,obs}$, catalyst decomposition (as a proxy for k_t), and the livingness in ROMP of eight different monomers. We found that the anchor group significantly affected k_p , and we found a positive correlation between HOMO energy and $k_{p,obs}$ with both Grubbs' first generation (G1) and Grubbs' 3rd generation (G3) catalysts. The rate-determining step of ROMP is the formation of the metallocyclobutane ring, suggesting the HOMO energy should influence the reactivity of monomers and therefore the k_p . A similar trend was found with the HOMO/LUMO energy gap as well for the eight monomers studied, suggesting the influence of multiple orbital interactions on k_p . However, we found a plateau in k_p for monomers with HOMO energies above -190 kcal/mol, suggesting the anchor group no longer affected the rate-determining step.

Additionally, we found that the anchor group had little effect on catalyst decomposition, or k_t , with the use of either G1 or G3 catalysts. Therefore, differences in livingness in ROMP of the various monomers were attributed to the large variations in k_p . We measured livingness by generating k_p/k_t ratios using the $k_{p,obs}$ values from kinetics experiments and the estimated $k_{t,obs}$ from catalyst decomposition measurements. For polymerizations mediated by G1, we found at least a 10-fold difference in the k_p/k_t ratios between two groups of monomers: 1) monomers *x*-MOMP (**1**) and *x*-ME'P (**2**) with high $k_{p,obs}$ and, 2) monomers **3–8** with low $k_{p,obs}$ values. Polymerizations with G3 also showed two distinct groups between monomers with high $k_{p,obs}$

and monomers with low $k_{p,obs}$, with a 4-fold difference in k_p/k_t ratio between the two groups. Ultimately, monomer *x*-ME'P (**2**) had the highest k_p/k_t ratio and was the most living monomer when polymerized with G1 catalyst. With G3 catalyst, monomers **1–3** all had similar k_p/k_t ratios and therefore had similar levels of livingness. In summary, anchor group choice greatly influenced the rate and livingness of ROMP with both G1 and G3 catalysts.

This work was expanded on in chapter 3 to study the anchor group effect in more complex polymer systems than linear polymers. The synthesis of linear polymers via ROMP is relatively straightforward, but the use of small molecule monomers provided an easy approach to study a wide selection of monomers computationally and experimentally. The high livingness of ROMP makes it well-suited for the synthesis of complex polymer architectures (i.e., bottlebrush polymers); therefore, fundamental studies on enhancing livingness in ROMP are important for improving the synthesis of large and well-defined bottlebrush polymers.

Many opportunities for the expansion of the anchor group effect exist. First, experimentally investigating more anchor groups is needed. We generated a library of monomer HOMO energies, but solubility limited this study to eight monomers. It would be interesting to investigate the rates of monomers we were unable to polymerize in $CDCl_3$, especially those with higher HOMO energies than the ones we studied. We did not experimentally study any anchor groups containing amide bonds, which may require more polar solvents, such as DMF, to obtain proper kinetics. Furthermore, researchers could expand on the anchor group by studying different cyclic olefins. In addition to norbornene, oxanorbornene is also commonly used in ROMP and it would be interesting to compare the trends of HOMO energy and k_p across various cyclic monomer systems.

Chapter 3

Expanding on chapter 2, we further studied the norbornene anchor group effect in Ru-mediated ROMP for the synthesis of bottlebrush polymers. Using five of the eight anchor groups studied in chapter 2, we designed five polystyrene (PS) macromonomers (MMs) to investigate in a combined computational and experimental approach. We calculated the HOMO energies of five structures containing the norbornene anchor group and one styrene unit attached to resemble to PS side-chain, and we hypothesized that MMs with high HOMO energy would have high k_p values. We found a positive correlation between HOMO energy and $k_{p,obs}$, even for the MMs with HOMO energies above -190 kcal/mol.

Similar to Chapter 2, we aimed to evaluate the livingness in ROMP. Unfortunately, measuring k_t during the polymerization of MMs proved challenging; therefore, we opted to evaluate livingness in ROMP through a series of polymerizations targeting large backbone degrees of polymerization (N_{bb}). We observed higher MM conversion and lower dispersities (\mathcal{D}) at higher target N_{bb} values for MMs with higher $k_{p,obs}$ values than MMs with lower $k_{p,obs}$ values. Ultimately, MM x -ME'-PS (**2**) had the highest MM conversion and lowest \mathcal{D} when targeting an $N_{bb} = 2000$. Along with having the highest $k_{p,obs}$ out of all the MMs studies, the anchor group in MM x -ME'-PS (**2**) experienced the highest livingness in ROMP.

The final evaluation of livingness in this chapter was studying the synthesis of bottlebrush pentablock copolymers made by using either the MM with the highest k_p anchor group or the MM with the lowest k_p anchor group (x -ME'-PS (**2**) and xx -IM₂E'-PS (**5**), respectively). High livingness is crucial for maintaining high MM conversion and low \mathcal{D} polymers during polymerizations with multiple injections of MM. In this study, the ROMP of MM x -ME'-PS (**2**) produced well-defined and more precise bottlebrush pentablock copolymers

than MM *xx*-IM₂E'-PS (**5**). Both MMs experienced an increase in \bar{D} after each block addition for the overall polymer structure, but when isolating the \bar{D} of each individual block, the apparent \bar{D} of the fifth block of MM *xx*-IM₂E'-PS (**5**) was significantly higher than the fifth block of MM *x*-ME'-PS (**2**), 116 compared to 7.8, respectively. This dramatic increase in the apparent dispersity of the final block addition emphasizes the importance of continuing to find methods that enhance the livingness in ROMP for complex polymer architectures, as even the most living MM produced bottlebrush polymers containing highly disperse substructures.

Expansion on the anchor group study in MMs would entail studying different polymer side-chain composition and size for a broader understanding of the anchor group effect on bottlebrush polymer synthesis. Additionally, tuning monomer reactivity through the anchor group has potential use in a copolymerization when targeting a gradient distribution of side-chains. It would be interesting to use MMs with different anchor groups to synthesize gradient bottlebrush polymers.

Chapter 4

In this chapter, we designed a novel anchor group structure for use in small molecule monomers and MMs. We synthesized an *exo*-norbornene benzoladderene (*xx*-NBL) monomer, measured ROMP kinetics mediated by G3 catalyst, and calculated the HOMO energy of this anchor group to compare to the previously reported anchor groups. Interestingly, *xx*-NBL had the highest HOMO energy out of all monomers previously studied and had one of the highest k_p values. Even though the HOMO energy of *xx*-NBL (**1**) was 10 kcal/mol higher than monomers previously studied, the k_p was not higher than the other monomers with high k_p values. This

result further supports the idea that at above a certain level, HOMO energy no longer affects the rate-determining step in ROMP.

When synthesizing MMs, the *exo*-norbornene benzoladderene anchor group allowed us to vary the position of PS side-chains on the ring and probe differences in k_p based on side-chain position. We observed a 3-fold difference in k_p between the MMs with *ortho* and *meta* positioned side-chains with the MM with *meta* positioned side-chains polymerizing faster than the MM with *ortho* side-chains. Again, the HOMO energy of this anchor group, regardless of side-chain position) was higher than all other MMs previously studied, but *xx*-NBL-*o*-PS had a $k_{p,obs}$ significantly lower than expected. This suggests there are more factors affecting k_p of the MM with *ortho* side-chains than just HOMO energy. We attribute the low $k_{p,obs}$ to a greater steric effect generated by the *ortho* side-chains than the *meta* side-chains. When the side-chains are in the *ortho* position, they are in closer proximity to the reactive chain end than the *meta* side-chain, hindering MM addition and slowing down propagation. Nevertheless, the synthesis of *exo* NBL (macro)monomers further broadens the scope of anchor group structures with high HOMO energy and generally high k_p available for the synthesis of bottlebrush polymers.

Development of an anchor group with a higher HOMO energy than monomers previously studied supported the idea that HOMO energy impacts the rate-determining step only below a certain HOMO energy value. MMs are not affected by the plateau in k_p at high HOMO energies, but are susceptible to other factors that affect polymerization rate in ROMP, such as steric effects. It would be interesting to model these steric effects to investigate interactions the side-chains have on incoming MM units and compare the *ortho* and

Chapter 5

In this final chapter, we build upon our previous work by comparing the livingness in Ru-mediated ROMP in different reaction atmosphere conditions. To accomplish this goal, we evaluated the synthesis of linear and bottlebrush pseudo-pentablock copolymers made from four various (macro)monomer structures, including two small molecule monomers and two PS MMs, either open to air, under N₂ atmosphere using Schlenk line techniques, or in a glovebox. We chose two anchor group structures previously studied, one with high k_p and one with low k_p , to use in the (macro)monomers. Additionally, we targeted degrees of polymerizations at which chain termination occurred when polymerized under ambient conditions to ensure any improvement in the living chain end would be observed.

In the synthesis of linear pentablock copolymers, little change in the livingness in ROMP was observed between inert and ambient atmosphere. Near-complete conversion to polymer was observed for both monomers, regardless of k_p , but M_n values of the final polymer structures fell below expected M_n values under all three atmosphere conditions. Livingness in ROMP of MMs was enhanced slightly when under inert conditions compared to ambient conditions, only evidenced by lower apparent D values of the final block additions when polymerized in the glovebox compared to ambient conditions. However, measured M_n values were lower than expected M_n and overall D values of the resulting bottlebrush polymers remained the same for both MMs regardless of atmosphere. Therefore, reaction atmosphere does not affect ROMP of (macro)monomers in these chain extension studies. This is an important result because many researchers perform ROMP in a glovebox and the inert atmosphere may not be needed.

Future work related to improving livingness in ROMP through atmospheric conditions would entail investigating the impacts of an argon atmosphere on ROMP. It would also be interesting to study catalyst stability in different atmospheres for long amounts of time.

Currently, our lab only uses G3 catalyst for two days after synthesis because we observe lower MM conversion and M_n values for bottlebrush polymers made with G3 catalyst stored for more than 2 days. Even though inert atmosphere did not affect the livingness in our ROMP study, it is possible that inert atmosphere affects the longevity of the catalyst.

Appendix A. Solution Self-Assembly of 30mer Homopolymers

The dense packing of polymer side-chains and large overall size of bottlebrush polymers causes unique structure properties. Our group has been interested in synthesizing bottlebrush polymers of various size and architecture made using grafting-through ring-opening metathesis polymerization (ROMP). By tuning the addition of macromonomers (MMs) of various side-chain length (N_{sc}), we can alter the bottlebrush polymer architecture, cylindrical when N_{sc} remains constant or tapered when N_{sc} varies in an increasing or decreasing order. To achieve tapered bottlebrush polymers, we use the sequential addition of macromonomers (SAM) approach to polymerize blocks of various N_{sc} values along the backbone. Our group recently studied tapered bottlebrush polymers with poly(*tert*-butyl acrylate) (PtBA) side-chains and a polynorbornene backbone using small angle neutron scattering (SANS). Here we further that analysis by studying individual segments of the tapered bottlebrush polymer.

The N_{sc} in a series of tapered bottlebrush polymers in the original study ranged from 1 to 5 kg/mol and the degree of polymerization of the backbone (N_{bb}) of each block was 30 units. The SANS data was fit to the flexible cylinder model, with relative good agreement with the data, mostly in the low q range with deviation in the high q range. To further analyze the solution properties, we synthesized each segment of the tapered bottlebrush polymer separately for use in SANS measurements. The MMs were synthesized using the direct-growth approach using a norbornene initiator in atom transfer radical polymerization (ATRP). Standard conditions of Cu(I)Br, Cu(II)Br, and N,N,N',N'',N''' -pentamethyldiethylenetriamine (PMDETA) were used in all cases and polymerizations were conducted at 60 °C for 5 h targeting 50% monomer conversion. The resultant PtBA MM was dissolved in ethyl acetate and was washed with NH₄Cl saturated water and brine, then was dried, filtered, and evaporated. The crude MM product was

passed through a plug of neutral alumina in benzene. Dimethylformamide was added to the eluate and the mixture was evaporated under air flow overnight, removing benzene and residual *t*BA monomer and most of the DMF. The dried product was redissolved in benzene and lyophilized on a Schlenk line to afford a fluffy white powder as the product. Pure MM samples were analyzed by ¹H NMR and size exclusion chromatography (SEC).

Table A.1 Characterization of Macromonomers

Notebook #	Macromonomer ^a	$M_{n,NMR}$ (kg/mol) ^b	$M_{n,SEC}$ (kg/mol) ^c	\bar{D} ^c
MAA-2765	T^{2k}	2.3	2.0	1.04
VU-524	T^{3k}	3.3	3.1	1.03
MAA-2283	T^{4k}	4.0	3.8	1.04
MAA-2775	T^{5k}	5.3	5.0	1.05

^aTargeted macromonomer structure represented by X^y where X is the macromonomer type [T = poly(*t*-butyl acrylate)] and y is the targeted N_{sc} . ^bMeasured by ¹H NMR spectroscopy.

^cMeasured by SEC in THF at 30 °C using light scattering and refractive index detectors.

Each MM was then polymerized via ROMP to afford 30mer homopolymers. Grubbs' third generation catalyst [G3, (H₂IMes)(Cl)₂(pyr)₂RuCHPh] was used to mediate polymerizations with a targeted $N_{bb} = 30$ at a MM concentration of 25 mM in ethyl acetate. Polymerizations were terminated with excess ethyl vinyl ether after 1 h and solvent was evaporated. The crude bottlebrush polymers were redissolved in a 1:1 mixture of hexanes and CH₂Cl₂ and passed through a silica plug to remove catalyst and unreacted MM. The solution was evaporated and then dried under vacuum to afford the pure bottlebrush polymer samples. The bottlebrush homopolymer were then analyzed by SEC before running SANS measurements.

Table A.2 Characterization of Bottlebrush 30-Mer Homopolymers

Notebook #	Bottlebrush Polymer ^a	$M_{n, \text{expected}}$ (kg/mol)	$M_{n, \text{SEC}}$ (kg/mol) ^b	\bar{D} ^c
SJS-1308	T_{30}^{2k}	60	75	1.03
SJS-1309	T_{30}^{3k}	93	92	1.01
SJS-1310	T_{30}^{4k}	114	140	1.01
SJS-1311	T_{30}^{5k}	150	203	1.05

^aTargeted bottlebrush polymer structure represented by X_n^y where X is the macromonomer type [T = poly(*t-butyl* acrylate)], y is the targeted N_{sc} , and n is the bottlebrush polymer N_{bb} . ^b M_n of the bottlebrush polymer as measured by SEC in THF at 30 °C, determined by removing an aliquot from the reaction after termination. ^cMeasured by SEC in THF at 30 °C using light scattering and refractive index detectors.

Appendix B. Ring-opening metathesis polymerization of peptide and sugar monomers

Previous studies from our group showed ROMP in DMF was improved with the addition of various acid additives, specifically CF_3COOH . Therefore, our goal was to investigate the effects of acid additives in ROMP of particularly challenging monomers that require polar solvents like DMF. One class of monomers that is typically only soluble in DMF (not EtOAc or toluene) is peptide-based monomers. ROMP of peptide-based monomers, especially unprotected peptides, is often limited to low N_{bb} due to the need for polar solvents such as DMF.¹ Additionally, cyclic oligosaccharides typically require polar solvents, especially in the un-acetylated form. Here, we hypothesized that CF_3COOH could improve the ROMP of a peptide-based and sugar-based monomers.

In order to test this hypothesis, we designed several norbornene-functionalized peptide or sugar monomers and performed ROMP reactions in DMF with and without an acid additive. To study peptide monomers, we chose Tyr-Ile-Gly-Ser-Arg (YIGSR) and Val-Pro-Gly-Val-Gly (VPGVG) as the peptide sequences to attach to our norbornene monomer. YIGSR is a pentapeptide derived from laminin that improves cell adhesion and promotes cell spreading,² and VPGVG is an elastin-Mimetic peptide.³ We synthesized both peptide monomers using Fmoc-based solid-phase peptide synthesis (SPPS), adding the norbornene to the N-terminus on-resin, and finally cleaving the peptide monomer from the resin and removing all protecting groups under acidic conditions. Purification by preparative-scale HPLC afforded the desired unprotected peptide monomers (**Nb-YIGSR-NH₂** and **Nb-VPGVG-NH₂**) which were both soluble in DMF but not EtOAc or toluene.

All polymerizations were conducted at a $[\text{MM}] = 10 \text{ mg/mL}$ in DMF at a $[\text{peptide}]/[\text{G3}]$ ratio of 25:1 with 20 equiv of CF_3COOH . For MM **Nb-YIGSR-NH₂**, conversion did not change

when CF₃COOH was added (Table B.1). We hypothesize that the charged peptide sequence limits the maximum conversion attainable for this peptide MM. Therefore, we used a neutral peptide sequence to test this hypothesis. MM **Nb-VPGVG-NH₂** reached higher conversion than MM **Nb-YIGSR-NH₂**; however, added CF₃COOH also did not improve conversion for this neutral peptide sequence.

Table B.1. MM conversion for different peptide MMs with various amounts of acid additives

Monomer	Additive	Additive equiv	% conv
Nb-YIGSR-NH ₂	CF ₃ COOH	0	27
		20	27
Nb-VPGVG-NH ₂	CF ₃ COOH	0	49
		20	47
	H ₃ PO ₄	0	48
		20	55

^aMeasured after polymerizing for 24 h using SEC by comparing the areas of the bottlebrush polymer and MM peaks in the dRI trace.

Although added CF₃COOH in DMF had the highest MM conversion out of all additives previously tested, it showed lower MM conversions in EtOAc and toluene compared to the other acid additives. Added H₃PO₄ showed high MM conversion in all three solvents, therefore we tested the effects of added H₃PO₄ on the ROMP of MM **Nb1-VPGVG-NH₂**. 20 equiv of H₃PO₄ gave a MM conversion of 55% compared to 47% without added acid, however, this difference is attributed to errors in the baseline dRI trace baseline. There were no obvious differences in conversion when looking at the dRI traces of the ROMP of MM **Nb1-VPGVG-NH₂** with or without added H₃PO₄ (Figure B.1); therefore, changing the additive did not improve MM

conversion either. We plan on furthering this study by changing the norbornene attached to the peptide sequences and testing the ROMP of a norbornene-oligosaccharide MM as well.

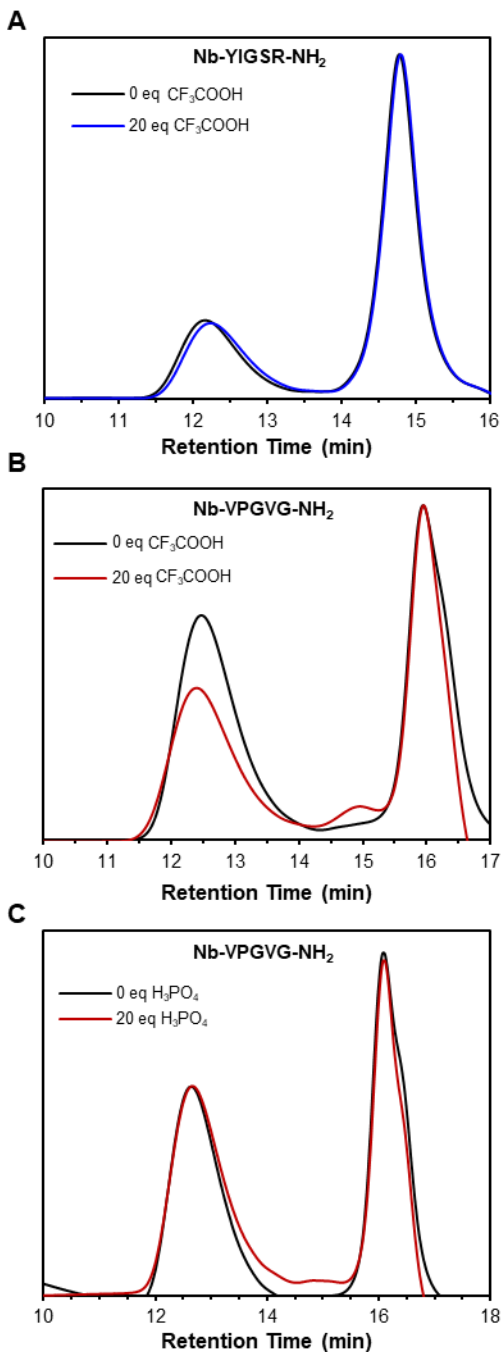


Figure B.1. SEC traces (dRI signal) of the ROMP of peptide MMs at an [MM]/[G3] ratio of 25:1 in DMF. (A) 0 and 20 equiv of CF₃COOH added to the ROMPs of MM Nb-YIGSR-NH₂.

(B) 0 and 20 equiv of CF_3COOH added to the ROMPs of MM **Nb-VPGVG-NH₂**. (C) 0 and 20 equiv of H_3PO_4 added to the ROMPs of MM **Nb-VPGVG-NH₂**.

References

1. Hahn, M. E.; Randolph, L. M.; Adamiak, L.; Thompson, M. P.; Gianneschi, N. C., Polymerization of a peptide-based enzyme substrate. *Chem. Commun.* **2013**, *49*, 2873–2875.
2. Boateng, S. Y.; Lateef, S. S.; Mosley, W.; Hartman, T. J.; Hanley, L.; Russell, B., RGD and YIGSR synthetic peptides facilitate cellular adhesion identical to that of laminin and fibronectin but alter the physiology of neonatal cardiac myocytes. *Am. J. Physiol. Cell Physiol.* **2005**, *288*, C30–C38.
3. Yao, X. L.; Hong, M., Structure distribution in an elastin-mimetic peptide (VPGVG)₃ investigated by solid-state NMR. *J. Am. Chem. Soc.* **2004**, *126*, 4199–4210.